Thomas Henning
Editor

LECTURE NOTES IN PHYSICS 815

Astromineralogy

Second Revised and Extended Edition

Lecture Notes in Physics

The Lecture Notes in Physics

The series Lecture Notes in Physics (LNP), founded in 1969, reports new developments in physics research and teaching – quickly and informally, but with a high quality and the explicit aim to summarize and communicate current knowledge in an accessible way. Books published in this series are conceived as bridging material between advanced graduate textbooks and the forefront of research and to serve three purposes:

- to be a compact and modern up-to-date source of reference on a well-defined topic
- to serve as an accessible introduction to the field to postgraduate students and nonspecialist researchers from related areas
- to be a source of advanced teaching material for specialized seminars, courses and schools

Both monographs and multi-author volumes will be considered for publication. Edited volumes should, however, consist of a very limited number of contributions only. Proceedings will not be considered for LNP.

Volumes published in LNP are disseminated both in print and in electronic formats, the electronic archive being available at springerlink.com. The series content is indexed, abstracted and referenced by many abstracting and information services, bibliographic networks, subscription agencies, library networks, and consortia.

Proposals should be sent to a member of the Editorial Board, or directly to the managing editor at Springer:

Christian Caron
Springer Heidelberg
Physics Editorial Department I
Tiergartenstrasse 17
69121 Heidelberg / Germany
christian.caron@springer.com

Thomas Henning (Ed.)

Astromineralogy

Second Edition

Springer

Thomas Henning
MPI für Astronomie
Königstuhl 17
69117 Heidelberg
Germany
henning@mpia-hd.mpg.de

Henning, T. (Ed.): *Astromineralogy*, Lect. Notes Physics 815, (Springer-Verlag Berlin Heidelberg 2010), DOI 10.1007/978-3-642-13259-9

Lecture Notes in Physics ISSN 0075-8450 e-ISSN 1616-6361
ISBN 978-3-642-13258-2 e-ISBN 978-3-642-13259-9
DOI 10.1007/978-3-642-13259-9
Springer Heidelberg Dordrecht London New York

Library of Congress Control Number: 2010931086

Cover design: Integra Software Services Pvt. Ltd., Pondicherry

Printed on acid-free paper

Springer is part of Springer Science+Business Media (www.springer.com)

Preface

The space between the stars is not empty, but filled with interstellar matter, mostly composed of atomic, ionized or molecular hydrogen, depending on the temperature and density of the various phases of this medium. About 1% of the total mass of interstellar matter in our galaxy is contained in small solid particles, ranging in size from a few nanometers to many microns and even millimeters in planet-forming disks around young stars. This cosmic dust undergoes a complicated life cycle, with fresh material produced in the outflows of evolved stars and supernovae, modified by shocks and cosmic rays in the diffuse interstellar medium and providing the surface for the formation of molecular ices in cold and relatively dense molecular clouds.

Although elemental abundances, formation routes, extinction curves, and early infrared and ultraviolet spectroscopy pointed to the presence of silicates, carbides, and graphitic material in space, it was only recently that a new field – astromineralogy – emerged from astronomical observations. The unprecedented spectral resolution and wavelength coverage provided by the *Infrared Space Observatory* together with dedicated experimental work in the field of laboratory astrophysics provided the unambiguous identification of minerals in space, ranging from olivines and pyroxenes to various carbides.

Cosmic mineralogy already provided earlier results on minerals in space by the in-situ study of minerals which entered the solar system. Meanwhile, we see a bridge between astronomically identified minerals and stardust minerals found by their isotopic signatures in meteorites and interplanetary dust. This may lead to a wider definition of astromineralogy that includes these investigations. A comprehensive study in this field should certainly include the comparative investigation of cometary dust material.

First seminars on astromineralogy were held at the University of Amsterdam and the University of Heidelberg. They showed the large interest of astronomers, physicists, chemists, and mineralogists in this new field and encouraged the publication of the first edition of this book in 2003. Meanwhile, a flood of new dust data arrived from the *Spitzer Infrared Space Telescope* which provided unprecedented sensitivity in the field of astronomical infrared spectroscopy. In addition, the *Stardust Mission* returned material from the comet 81P/Wild 2 to Earth for in-situ analysis. These new data together with progress in ground-based observations and laboratory astrophysics led to the idea for a second revised edition of this book.

The publication of this second edition comes at a time where the cryogenic part of the *Spitzer* mission just came to its end. With the launch of the *Herschel Observatory* during the final editing of this book, a new era of the exploration of the cold dusty universe just started. On the horizon is the *James Webb Space Telescope* which will allow to extend astromineralogy to even fainter objects and will provide information on the spatial distribution of minerals in protoplanetary disks and other environments. In a planning stage, there are other missions to bring back interstellar grains to Earth for their in-situ analysis.

I would like to thank all authors for their contributions to this book and their willingness to revise their chapters and to follow my recommendations. In addition, I thank my former colleagues Drs. J. Dorschner, J. Gürtler, C. Jäger and H. Mutschke for many years of fruitful collaboration in the experimental characterization of cosmic dust analogues in our Jena dust group, which paved the way for the identification of minerals in space. This work is now continued in the laboratory astrophysics facility of the Max Planck Institute for Astronomy at the University of Jena under the leadership of Drs. F. Huisken and C. Jäger.

Finally, I would like to thank J. Weiprecht and C. Schnupp. Without their technical help, the production of this book would not have been possible.

Heidelberg, Germany Thomas Henning
December 2009

Contents

From Dust Astrophysics Towards Dust Mineralogy – A Historical Review

J. Dorschner

Abstract Via meteorite research, mineralogy became the first discipline among the earth sciences that developed a cosmic branch. The current link connecting astronomy and mineralogy is the dust in the Galaxy. Interstellar dust reached astrophysical topicality around 1930. In their first dust models astrophysicists took the assumption for granted that the grains consist of minerals related to those of the solar system. An exception formed the "ice" model prevailing in the decade 1950–1960. Scrutinizing discussions of the weak points of this model and new observations in the UV spectral range paved the way for considering refractory materials as grain constituents and stars and planetary systems as the main suppliers of such dust grains. In the decade 1960–1970 many refractory dust materials heuristically came into discussion, e.g. graphite and meteoritic silicates.

The strong solid-state band detected at 217 nm in the interstellar extinction curves was commonly assigned to graphite grains. Beginning in 1968, observations of the vibrational bands of the SiO_4 group in circumstellar as well as in interstellar dust provided ample evidence for the ubiquitous occurrence of silicate grains in the Galaxy. Bands of silicates and of some other solids opened the new era of dust diagnostics resting on IR spectroscopy and laboratory simulation experiments. In most cases, the observed spectral features indicated heavily distorted structures of the grain material.

In 1996–1998 the Infrared Space Observatory (ISO) surprisingly discovered stardust bands of crystalline silicates. This opened the chance of unambiguously identifying dust minerals via astronomical spectroscopy in the combination with laboratory data of dust analogues. The term "astromineralogy" was coined.

In the last two decades, mineralogists have discovered "fossil" dust grains in primitive meteorites, which had been preserved from the parent cloud of the solar system. This way, cosmic mineralogy could directly contribute to astrophysical dust research, and confirm astromineralogical conclusions.

J. Dorschner (✉)
University of Jena, Astrophysical Institute and University Observatory, Schillergässchen 2-3, 07745 Jena, Germany
e-mail: dorsch@astro.uni-jena.de

Dorschner, J.: *From Dust Astrophysics Towards Dust Mineralogy – A Historical Review*. Lect. Notes Phys. **815**, 1–60 (2010)
DOI 10.1007/978-3-642-13259-9_1

New ways of experimental research are on the horizon that could advance our understanding of interstellar dust. Promising results have been attained in detecting dust grains of the local interstellar medium that traverse the solar system. The interstellar meteors as messengers from other planetary systems could likewise become an important information source in the future.

Intensified collaboration between astrophysicists and mineralogists should enclose discussions on the applicability of the traditional mineral definition on cosmic particulates and on a subdivision of the field of astromineralogy.

1 Astrophysics and Cosmic Mineralogy

For centuries, astronomy and mineralogy have been well separated science disciplines that, for a long time, had nothing in common with each other. It is self-evident that in former times mineralogists devoted little interest to the material of other celestial bodies because samples of them were not attainable to practical inspection. Astronomers, who were familiar with studying unattainable phenomena, had focused since antiquity their scientific interests to the mathematical description of the observable movements on the sky. They, at the best, had speculative views on the nature of celestial bodies, which vigorously flourished after the invention of the telescope. However, before the emergence of the astrophysics there was no base for the scientific approach to such questions.

Mineralogists have got much earlier the chance to make scientific statements on extraterrestrial material, because it fell down from the sky as meteorites. However, in the time of Enlightenment leading scientific authorities refused reports on the fall of meteorites as products of superstition and required removal of meteorites from the collections. The turnaround occurred, when the well-witnessed meteorite rain of L'Aigle in 1803 convinced the authorities of Paris academy that the arguments for the cosmic origin of meteorites published at that time in a series of startling publications by the physicist E. F. F. Chladni [1] deserve attention. From that time the way towards the systematic chemical and mineralogical study of meteorites was open, and mineralogy became already in the nineteenth century the first discipline among the earth sciences that developed a "cosmic branch".

However, only in 1962 this development found its official expression, when the International Mineralogical Association (IMA) formed the working group "Cosmic Mineralogy" [2]. In the 1960s, the meteorites ceased being the only type of achievable extraterrestrial material that could be studied by mineralogical techniques. Systematic collection of interplanetary dust particles in the stratosphere by airplanes and in space by rockets had been taken up. At the end of this decade, first rock samples from the moon were recovered and lunar mineralogy was established. First in-situ soil analyses by soft-landed spacecraft on Venus and Mars opened the era of planetary mineralogy in 1975 and 1976. In 1986 in-situ research by mass spectrometry of coma dust of comet P1/Halley yielded first experimental results on comet mineralogy. At the end of the last century, comprehensive monographs on extraterrestrial materials were available (cf., e.g., [3]).

When astronomers and astrophysicists became aware of the existence of solid particles in interstellar space, already the earliest speculations on the composition of these solids took minerals into account. In the present historical overview, we sketch the troublesome way of the astrophysical efforts to understand the nature of the cosmic dust particles. However, as long as observations of phenomena attributed to interstellar dust only rested on measurements of continuous light, such as interstellar extinction measurements and albedo determination on reflection nebulae, there was no chance to identify dust minerals.

However, astronomers got their chance. Over the same period in which direct analytical methods of cosmic mineralogy were applied to growing extent to solar system solids astronomy gained its own access to mineralogy of such solids by spectroscopy. As soon as detectors and spectral devices were available for wavelength regions containing diagnostic mineral features, solid state bands were detected in reflection spectra of asteroids and thermal emission of cometary comae. This spectroscopic approach could be extended step by step to particulates beyond the solar system. The new era began in the 1960s by spectacular discoveries in spectral regions that became accessible by the progress of ultraviolet and infrared astronomy. The first discovery concerned the detection of an ubiquitous strong absorption band centered at 217 nm in the interstellar extinction curves, which was attributed to an electronic transition in interstellar carbon grains. Even if graphite was commonly proposed to be the carrier, this assignment was not without problems. By no means, it was a reliable mineral identification.

The second detection was a broad emission band at 10 μm in late-type giants and supergiants. This band proved to be a genuine mineral feature due to Si—O vibrations of circumstellar silicate grains. The handicap preventing the band from authentic mineralogical identification was its large width and structureless profile pointing to distorted silicate structure. Nevertheless, its detection confirmed the suspicion that cool stellar atmospheres and circumstellar envelopes could be "hatcheries" of mineral-like dust grains.

The discovery of spectral "fingerprints" changed the epistemological situation in the astrophysical dust research because the findings restricted the number of the hitherto existing speculative assumptions on dust composition and showed new ways in getting information on dust chemistry and mineralogy. Carbon and silicates began to play a dominant role in interstellar dust modelling. In the strict sense, this preference has been maintained up to the present time (cf. Table 2). As a matter of fact, the new spectral features did not suffice for an exact mineral identification, they solely proved reliably the presence of particular chemical bonds of the corresponding dust materials that could be energetically changed by photon absorption. In the case of carbon the excitation concerned delocalized π electrons in a graphitic sheet structure ($\pi \longrightarrow \pi^*$ transition). Concerning silicates, Si—O stretching modes of the SiO_4 tetrahedra in a silicatic structure were responsible for the observed 10 μm bands. Nevertheless, the term "interstellar mineralogy" enjoyed increasing popularity among astrophysicists. Further, primitive meteorite and interplanetary dust mineralogy began to play an important role as guide to the solids beyond the solar system. The progress of dust spectroscopy made the whole field more complex

and revealed new cosmogonic relations. It was necessary to discriminate between different dust populations in the Galaxy (for review see [4, 5]).

Correct identification of observed spectral features required targeted laboratory work on analogue materials to be adopted in the dust models. In the 1970s the necessary connection between astrophysics and laboratory work got its institutionalization in the new branch of "laboratory astrophysics". This lead to more realistic dust modelling. However, as a matter of principle, laboratory material simulation of the heavily disordered or totally amorphous interstellar dust materials cannot provide ultimate clarity on the identity of the cosmic solids with their laboratory analogues. Nevertheless, experience won by the comparison of spectra of laboratory analogues with observed cosmic dust spectra laid the base of what could be called "interstellar material science".

Great support to the astrophysical efforts to understand the nature of cosmic dust was given by an unexpected discovery in the field of cosmic mineralogy: From primitive meteorites and interplanetary dust particles (IDP) components could be isolated that turned out to be "fossil" dust grains from the parent cloud of the solar system. Such presolar solids opened the possibility to subject intrinsic interstellar material to laboratory analyses. This amazing development will even be surpassed, when in the future interplanetary spacecraft succeed in collecting dust grains from the local ISM that just pass through the solar system. All of these new possibilities are treated in special chapters of the present book.

All of these developments paved the way to a close collaboration between astrophysics and cosmic mineralogy with great mutual use. From the analyses of stardust grains in meteorites, astrophysics gets improved knowledge on the processes around circumstellar dust formation, even on nucleosynthesis in evolved stars. On the other hand, astrophysical dust modelling does not become dispensable because the cosmic grains available to laboratory research are restricted only to few species of refractory dust solids, not to the main stream dust involved in the manifold evolutionary processes in the Galaxy. Improved astrophysical mineral identification via spectroscopy will give the cosmic mineralogy the chance to widen its scope over the whole Galaxy.

The break-through in reliable identification of some common circumstellar dust minerals via spectroscopy occurred by the measurements of the Infrared Space Observatory (ISO, operating 1995–1998). This most successful space observatory, the spectrometers of which covered the whole IR range, detected bands that could reliably be attributed to well-known silicate minerals. This discovery was characterized by the phrase "crystalline revolution"(cf. [6]) and manifests the coronation of the hitherto astrophysical efforts to investigate cosmic dust mineralogy. It puts signs that unambiguous mineral diagnosis of cosmic dust grains via spectroscopic observations in combination with targeted laboratory work is possible, at least in the circumstellar environment, mostly in AGB and Post-AGB stars. The intensifying contact of astrophysics to mineralogy found its expression in coining the term "astromineralogy". It is not quite clear, who used it first. However, it certainly arose as a consequence of the "ISO revolution" (cf. the papers enclosed in the Ph.D. dissertation by F. J. Molster [7]). "Astromineralogy" is definitely an adequate term

and this new field can be considered in legitimate analogy to such designations as astrophysics and astrochemistry. As the chapters of the present book convincingly demonstrate in great detail, minerals have been confidently detected in circumstellar and interstellar particulates in the Universe. There are other scientific fields that adorned themselves with the prefix name "astro", which, however, are not in the lucky situation that their central research subject has actually been found out of the earth.

The need for using mineralogical expertise in dust astrophysics is clearly underscored by the increasing significance of projects based on current or planned data acquisition with the help of spaceborne IR spectroscopy (Spitzer Space Telescope, Herschel Space Telecope, airborne observatory SOFIA, James Webb Space Telescope). This growth of the mineralogical dimension of the solid-state astrophysics should also be of influence on leading international organizations of mineralogists. As a matter of fact, in 2003 the Internationale Mineralogical Association established a Working Group "Astromineralogy". Apparently, the interest in this cosmic topic was limited so that the WG "Astromineralogy" ceased its work in 2008 [8]. However, among astrophysicists studying dust grains laboratory simulation experiments with mineral grains and optical data of minerals of cosmic importance are an essential requirement of their current work and of the expectations for future observations (see, e.g., [9–11]).

2 Interstellar Dust on the Way to Astrophysical Topicality

2.1 Light Extinction Between the Stars

Interstellar dust research articulated itself as a field of astrophysics around 1930. Interaction of small grains with starlight turned out to be the most plausible explanation of the accumulating observational evidence in favour of selective light extinction in space. Speculations on the occurrence of a general cosmic light extinction have a long history. In 1744 Loys de Chéseaux [12] proposed an absorbing fluid or ether in the space between the stars in order to settle the old problem that in an infinite universe, uniformly filled with stars, the night sky could never be dark. A century later this paradox of dark night sky was named after Olbers, who had proposed a similar solution [13]. However, dust extinction has proved to be unable to solve this cosmological problem.

At the end of the nineteenth century, light extinction (then commonly addressed as "light absorption") in the interstellar space anew attained astronomical topicality. One impact was given by the enigmatic starvoids visible in the Milky Way, the investigation of which flourished by applying celestial photography. The realization that these voids are simply pretended by obscuring dust clouds in front of the starfield, was by no means a matter of course, mainly because W. Herschel's opinion was still dominating. In his report "On the Construction of the Heavens" to the Royal Society in London in 1785 Herschel [14] had described such a starvoid as an *"opening in*

the heavens" formed by collection of stars in a nearby cluster, which had left the observed vacancy. For Herschel's often quoted anecdotal exclamation on the "hole in the sky", see [15]. In particular E. E. Barnard, one of the pioneers of photographic techniques, usually denoted the starvoid as "holes", sometimes also "black holes" (see, e.g., [16, 17]). He never used the term "dark nebulae". Admittedly, in his large catalogue [18] that contained 182 such objects he more cautiously called them "dark markings" (for details of his curious reluctance to accept the explanation by obscuring clouds, see [19]). It is not clear, whether he did not know or refused to take notice of the view of prominent astronomers, e.g. A. Secchi who already in 1853 had parted with the picture of the holey Milky Way and accepted obscuring nebulous matter as the simplest explanation [15, 19].

Another pioneer of Milky Way photography, Max Wolf, also used misleading terms, such as "dunkle Höhlen" (dark caves) or "Sternleeren" (star voids), but already in his early papers, e.g. [20], he was open for the obscuring cloud explanation. In Wolf's famous paper [21] on the statistical method for estimating total absorptions, distances and spatial extensions of such dark clouds, he also presented morphological evidence for a close connection between dark and bright nebulosity. Wolf was convinced that the obscuring medium is dust, however, speculations on the nature of the dust grains were out of his scope.

Extinction of starlight was also suggested by stellar-statistical investigations that resulted in a systematic decrease of the star density in the Galaxy with increasing distance. The state of the knowledge on interstellar extinction reached around 1920 was critically reviewed by Kienle [22], who summarized that claims of observed interstellar light dispersion (dependence of phase velocity on wavelength) had no longer a serious base, that the interstellar light absorption should be smaller than 0.002 mag/pc, and that there are only qualitative indications, but no convincing evidence for the selectivity (wavelength dependence) of this absorption. Kienle concluded that the light absorption should be due to inhomogeneously distributed non-luminous gas masses and dark dust clouds, whereby he stressed that cosmic dust is quite different from terrestrial one because the former should also contain large rocks, apparently in analogy to the meteorites.

Kienle [22] probably did not know Pannekoek's [23] paper, who in 1920 had rejected obscuration due to Rayleigh scattering by gas because this mechanism yielded unrealistically high masses of the dark nebulae. Pannekoek [23] quoted a suggestion by de Sitter that the cloud mass problem vanishes if the extinction is due to dust grains. However, de Sitter's suggestion was "obscured" by the wrong assumption that dust extinction is always neutral. This combination of the right mechanism with the wrong dust model confused in the following time observers that had found clear evidence of selective extinction. They again reverted to Rayleigh scattering.

Still at the end of the 1920s leading astrophysicists had very different opinions on the role of dust. Even capacities as A. S. Eddington underestimated the role of dust. In the review of Eddington's famous book "The Internal Constitution of the Stars" (1926) H. N. Russell [24] critically annotated to the last chapter on diffuse matter in space: "The fact that . . . fine dust is enormously the most effective obscuring

agent, appears to be more important than any a priori impression. The allied fact that such dust, if smaller than the wavelength will produce selective scattering, following Rayleigh's law, but vastly greater per unit mass than in the case of gas, is not mentioned."

2.2 Interstellar Dust Gets a Physical Face

Pannekoek's [23] hope that scrutinized photometric work would settle the questions on the interstellar extinction could be fulfilled not earlier than about 1929/1930. Conclusive measurements of the interstellar extinction coefficient were not only handicapped by the low accuracy of the photographic photometry and the problems of distance determination, but also by the (unknown) distribution of the absorbing medium in the Galaxy. This latter fact explains why the apparently best suited objects for extinction determination, namely the most remote ones, i.e. globular clusters and spiral nebulae, failed to give the expected success because they simply were not observable in low galactic latitudes where the dust was concentrated.

In 1929 Schalén [25] from observations in Cepheus and Cassiopeia determined the mean interstellar extinction to be 0.5 mag/kpc. The values towards Cygnus were much larger and led to an upper limit of 2 mag/kpc. Schalén [25] was the first to speculate on the nature of the dust grains. Based on Hoffmeister's [26] results on the statistics of meteors, which, at that time, were assumed to contain a considerable proportion of interstellar particles, he suggested that the absorber in the dark nebulae is "meteoric dust", the spatial density in the clouds he estimated to be about 10^{-23} g/cm^3.

Schalén's [25] extinction values were confirmed by Trümpler's [27] extensive study of distances, dimensions, and space distribution of open star clusters. These objects turned out to be the best possible test objects for extinction determinations. They are concentrated in low galactic latitudes, where the dust accumulates, and cover all longitudes, and they allow accurate distance determination. Trümpler's [27] investigation proved the occurrence of a general interstellar extinction at low galactic latitudes with a mean photographic coefficient of 0.67 mag/kpc towards all directions. He also found evidence that the brightest cluster stars showed growing discrepancy between colour equivalents and spectral types with increasing distance and, thus, indicated selective extinction that reddened the stars. Trümpler's [27] paper manifests the breakthrough to the final proof of a general selective interstellar extinction "landscape", out of which the dark clouds loom as the "summits".

At the same time, Öhman [28] published a spectrophotometric study of 882 B, A and F type stars. Most of the B stars showed colour equivalents too large to be in agreement with the temperatures corresponding to the spectral type. This disagreement between stellar continuum and lines led some astrophysicists, e.g. Gerasimovič [29] and Unsöld [30], to the premature definition of a "superexcitation" of these atmospheres due to a UV excess radiation. However, Öhman [28] proposed an alternative explanation and considered the low colour temperatures of the observed

stellar continuum as a spurious effect caused by the reddening of the star light due to selective interstellar extinction. Figure 1 shows Öhman's [28] Fig. 25 indicating the tight correlation of the colour equivalents C (precursor of colour excess) for early B stars near the galactic plane with their distances. The extinction coefficient derived from the C-values was in satisfactory agreement with Trümplers results. From his results, Öhman also concluded that the interstellar extinction increases less steeply with decreasing wavelength than Rayleigh scattering would require. This trend was confirmed by later observers and, finally, resulted in a λ^{-1}-law. At the end of that decade, Stebbins et al. [31] could demonstrate the approximative validity of the λ^{-1}-law for the whole optical wavelength range from 380 to 800 nm.

In 1931 Öpik [32] used Öhman's [28] spectrophotometric results for a thorough theoretical analysis of the observed colour-temperature discrepancy. He concluded

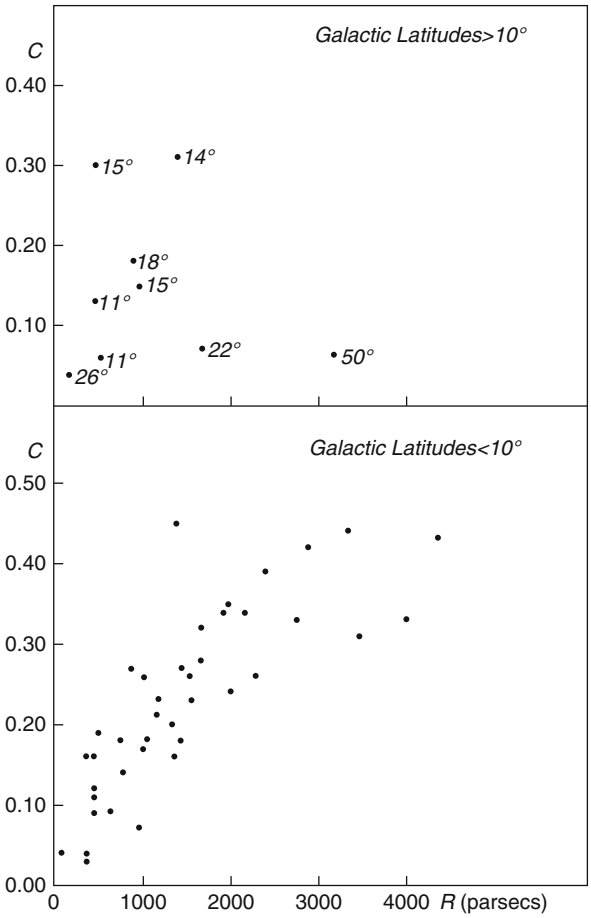

Fig. 1 Öhman's [28] colour-equivalent C as function of stellar distances for early B stars, clear evidence for selective interstellar extinction

that the hypothesis of dust extinction is "the most probable, being at the same time the simplest and well under control of our present physical knowledge". The last phrase referred to the light scattering theory developed by Mie [33] in 1908 that had apparently escaped the attention of the astronomers for more than two decades. Öpik learned this theory from papers by Blumer [34–37] who had painstakingly bothered to compute scattering functions for spherical dielectric particles (refractive indices $m = 1.25$, 1.333, 1,466, 1.5, and ∞) for the characteristic Mie parameter $x = 2\pi a/\lambda$ (a being the particle radius) in the range from 0.1 to 10. From Blumer's substantial computational work Öpik [32] recognized the key role of the particle size distribution for the mathematical shape of the wavelength dependence of the extinction coefficient. Since the refractive index of the particle material was apparently of minor influence (dielectric grains!), he concluded that the explanation of the observed reddening law is primarily a question of finding the suitable particle size distribution function. Power laws as derived from meteor observations seemed to solve the problem. Öpik [32] excluded Rayleigh scattering and presented arguments for a λ^{-1}-dependence. Even if he did not explicitly address the chemical nature of interstellar dust, it can be assumed that he thought of "meteoric grains", not only because he preferred a "meteoric" size distribution. In the following years, he became an outstanding advocator of the interstellar origin of the sporadic meteors.

The first who explicitly applied the Mie theory to extinction observations have been Schalén [38] and Schoenberg and Jung [39], probably without knowing Öpik's [32] paper, for they focussed their attention to metal grains. The iron-nickel alloy of the meteorites and the wavelength dependence of the absorption coefficient of small metal grains ($\propto 1/\lambda$) seemed to have triggered this orientation. Schalén [38] calculated absorption coefficients for small iron spheres (diameters in the range 10^{-6} to 10^{-5} cm) at the wavelengths $\lambda = 395$ and 440 nm and compared the theoretical colour differences with the observed ones derived from objective prism spectra of stars in obscured regions of Auriga, Cygnus, and Cepheus. The result was that the particles in this range could reproduce the observations. The total cloud masses got realistic values and the mass density of the dust clouds resulted in values of the order of 10^{-26} g/cm^3, which was absolutely compatible with Oort's [40] mass limit of interstellar matter near the sun. Similar conclusions were drawn by Schoenberg and Jung [39]. In later papers the calculations were also extended to other metals [41, 42].

2.3 Renunciation from Meteor/Meteorite Analogy

As already mentioned, the iron dust model was merely based on analogy considerations from iron meteorites and on the suitable wavelength dependence of the absorption coefficient of metal particles. Further support could be derived from the interstellar meteors. Observations seemed to confirm that more than 60% of the sporadic meteors and fireballs had hyperbolic heliocentric velocities. Even

if some astrophysical authorities drastically expressed their doubts on this view (Eddington was alleged to have declared in 1932 *that he would as lief believe in ghosts as in hyperbolic meteors* (cf. [43]), the experts of meteor research could point to confirming observational facts in favour of hyperbolic velocities, e.g. the results of Harvard Meteor Expedition to Arizona in 1931–1933. During the whole decade from 1930 to 1940 the "hardliners" of the concept of hyperbolic meteors, Hoffmeister and Öpik, though entangled in violent debates and mutual criticism of their data reduction procedures, agreed with the interstellar origin (for review see [43–45]).

The criticism of the interstellar meteors was steadily increasing and culminated in 1943/1944 with Porter's [46] clear statement based on the analyses of the British meteor data: "There is no direct evidence for the existence of an excess of hyperbolic velocities. With a few doubtful exceptions, all meteors are members of the solar system . . . The hyperbolic theory has hindered the progress of meteoric astronomy for many years, and in the opinion of the writer should be abandoned". For the review of fallacies leading to the overestimated meteor velocities see Lovell's monograph "Meteor Astronomy" [47]. Because of the rejection of the hypothesis of interstellar meteors analogy arguments connecting meteorites and interstellar solids lost their weight.

The other argument supporting metal grains because of the λ^{-1} dependence of the absorption coefficient is absolutely not cogent. The efficiency factor of extinction (being the sum of absorption and scattering efficiency) of small spheres according to the Mie theory can be expanded as a power series of the characteristic parameter $x = 2\pi a/\lambda$ (this was the approach to the problem by Schoenberg and Jung [39, 42]). The first term in this series, which is the decisive term for grains with $x \ll 1$, is $\propto \lambda^{-1}$ for absorbing and $\propto \lambda^{-4}$ for dielectric grains. For somewhat larger grains, terms with higher powers of x also become significant. Apart from this, the coefficients of the terms contain the refractive index of the material, which in the case of metals is strongly wavelength-dependent so that the wavelength dependence of relative small metal particles leaves the simple $1/\lambda$-law. Already Öpik [32] in his early paper had called attention to the fact that dielectric grains can also reproduce the observed interstellar reddening law if combined with a suitable particle size distribution function.

As a matter of fact, after 1938 dielectric grains plaid an increasing role in the discussions, in particular in connection with theoretical studies of reflection nebulae and the diffuse galactic light [48–50], which lead to the realization that the albedo of interstellar grains (the ratio of scattering to extinction cross-section) had to be assumed larger than that of metal grains. However, alone on the basis of extinction and albedo observations in comparison with Mie calculations a final decision between dielectric and metallic grains was not possible (cf. the analysis by Güttler [51]). After the break-down of the interstellar meteor hypothesis, finding plausible mechanisms of grain formation became a new important key for the evaluation of grain models. This "cosmogonic" criterion was applied in dust modelling only after World War II.

2.4 Early Approaches to Dust Formation

In 1935 Lindblad [52] confronted the dust community with the idea of condensation processes in interstellar gas leading to the formation of the meteoric matter in the interstellar clouds. His estimate intended to show that in the age of meteorites (adopted to be about 10^9 years) the condensation of the metal content of the interstellar gas could explain the growth of particles up to the size required. The interstellar particles should continuously grow because the metals in the hot gas ($T \approx 10000$ K) must precipitate on the cool particle surfaces ($T \approx 3$ K). The paper found little resonance with the dust activists. The only immediate response was given by Jung [53] who discussed objections because of charging effects on the grains and found Lindblad's timescale for the present interstellar conditions too optimistic.

Nevertheless, it was Lindblad's apparently unexciting note that revolutionized the dust picture. This approach, originally thought to give a physical explanation for the formation of refractory solids in space, a decade later, entirely ruled out the early speculations on mineral dust and focussed the attention to non-mineralic volatiles as the significant dust constituents. Before this new dust model dominated the dust astrophysics some other points in connection with dust condensation have to be briefly reported.

In 1933 Wildt [54] discussed the possibility of condensation of solid grains and their effect as opacity source in the atmospheres of very cool stars. The motivation to this study was the longstanding claim that the variability of Mira stars could be caused by periodical condensation and resublimation of aerosols in their atmospheres (veil theory, see, e.g., Merrill [55]). By the discussion of the vapor pressure curves for selected elements and oxides and the thermal properties of some carbides and nitrides, Wildt draw the conclusion that solid particles of carbon, Al_2O_3, CaO, and several highly refractory carbides (SiC, TiC, ZrC) and nitrides (TiN, ZrN) might form in N stars. He excluded SiO_2 and did also not consider highly refractory silicates.

Wildt's paper was the first approach to the formation of mineral grains in stellar environment. Some of his candidates today are among the dust materials that have been detected in presolar grains with an isotope signature pointing to their stellar origin (see Sect. 5.2). However, at Wildt's time it was not imaginable that stellar aerosol particles could be conveyed out of the star and, thus, contribute to the interstellar dust.

Another impact to stellar condensation hypotheses was given by the light curves of R CrB stars. In 1935 Loreta [56] suggested that the irregular deep minima of these variables could be caused by eruptions of "dark matter" transiently obscuring the star. The lacking chemical precision of Loreta's hypothesis was appended by O'Keefe [57], who concluded from the exceptionally high carbon abundance of these stars that the aerosol particles should be graphite crystallites. The sharp drop to the minimum should be caused by the fast graphite formation, whereas the slow recovery to the normal light reflects the dissipation of the ejected soot cloud.

Estimates of the expected optical properties and the formation time of the grains showed rough agreement with the observations. However, also O'Keefe's considerations did not include any interstellar significance of the stellar graphite grains.

2.5 The Cold Way to Interstellar Dust

While Wildt's [54] and O'Keefes [57] stellar mineral grains did not inspire the interstellar dust researchers for more than two decades, Lindblad's [52] condensation idea did it already some years after its publication. During World War II in the Netherlands Lindblad's [52] suggestion has provoked intensive studies of interstellar condensation culminating in a new dust model founded by Oort and van de Hulst [58]. In his Ph.D. thesis, van de Hulst [59] had thoroughly studied the optics of small grains. This laid the basis for some improvements of the original model [58], which appeared in 1949 [60], as well as for van de Hulst's famous monograph "Light Scattering by Small Grains" [61] used for about three decades as a standard book by astrophysicists, meteorologists and other people occupied with any sorts of small droplets or grains.

In contrast to Lindblad's [52] note, the Oort–van de Hulst model [58, 60] aimed at the formation of volatile grains consisting of what was later commonly called "dirty ice". The ice grains should grow in HI regions (according to Strömgren's [62] new classification) by gas accretion. The equilibrium temperature ($T \approx 10$–20 K) of the dust grains in the interstellar radiation field was low enough that gas species like C, N, O and some metals could really condense onto the cool grain surfaces, however, it was too high for the condensation of hydrogen. Oort and van de Hulst [58] assumed that the impinging hydrogen atoms are involved in chemical reactions with the condensed species and are bonded in hydrogen-saturated compounds like H_2O, CH_4, NH_3, and metal hydrides. Thus, the resulting ice conglomerate roughly reflected the interstellar gas composition. A critical point remained the question of the seeds for the start of the grain growth according to this concept.

A further innovation in this dust model was the elegant explanation of the grain size distribution. The authors [58] assumed that the continuous grain growth by gas accretion and hydrogenation of condensed species was controlled by mutual grain destructions due to grain–grain collisions as a consequence of interstellar cloud encounters. From the assumption of the equilibrium between both processes the average particle size distribution function could be derived that together with Mie cross sections of the icy grains allowed a satisfactory representation of the observed interstellar reddening law and other observed dust properties. It also gave a plausible explanation for the apparent universality of interstellar dust. Deviations of the observed extinction curve towards certain galactic direction, e.g. the Orion region, could be attributed to peculiar local effects.

The theoretical elegance of this model and obvious success lead to honestly name it "classical dust model". The model had a great lobby within the Commission 34 ("Interstellar Matter and Galactic Nebulae") of the International Astronomical Union, which had been formed in 1938 on the IAU General Assembly at Stockholm.

For about two decades, the cold way to the formation of interstellar grains in HI clouds dominated the astrophysical considerations on interstellar dust in the textbooks. Speculations on mineral grains in interstellar dust and dust formation in stellar atmospheres seemed to be untimely.

3 Heuristic Dust Modelling with Refractory Grains

3.1 Interstellar Polarization and the Come-Back of Minerals

In the 1950s the discussion on the material properties of interstellar dust was considerably influenced by the detection of the interstellar polarization. In 1949 independently of each other Hiltner [63], Hall [64], and Dombrovski [65] discovered that the light of reddened stars shows a slight linear polarization that could be explained as a result of the interaction of interstellar dust grains with the starlight.

The discovery had two far-reaching consequences:

1. The assumption that all interstellar dust grains are roughly spherical and optically isotropic had to be considerably modified. In order to polarize the transmitting light, a significant part of the particles must be non-spherical or optically anisotropic or both, and, in addition, the grain axes had to get a preferential orientation. This requires the action of a mechanism that permanently exerts a torque damping the irregular tumbling of the grains due to impinging gas atoms and, thus, providing the necessary degree of alignment.
2. Special requirements of the orientation mechanism and/or the fact that non-spherical dirty ice grains of the prevailing classical dust model proved to be very inefficient polarizers focussed again the attention to refractory grains that are much better polarizers. After the era of meteoritic grains in the 1930s, this was the second time that minerals arouse the interests of astrophysicists.

Accurately measuring interstellar polarization was a great challenge to the observers because the small intensity differences to be measured through a polarization filter at different position angles required outstanding photometric accuracy. This especially held for the determination of the wavelength dependence, the "polarization law"; such data became available not until 1959 [66, 67].

The challenge for the theorists was similarly great. One important handicap was the lack of a general light scattering theory for non-spherical grains. Up to now, the only exact solution of light scattering by non-spherical particles is the case of infinite circular cylinders (needles) of arbitrary diameters. Light scattering by spheroids could and can be treated only by approximations for very small particles (cf. [61]). In 1937 Wellmann [68] had the right feeling that the interstellar absorption coefficient should be influenced not only by the grain radii and the refraction of the dust material, but also by the shape of the grains. For this reason, he solved the Maxwell equations for the case of light scattering by cylindrical particles for oblique

incidence. He was aware that the absorption coefficient depends on the orientation of the cylinder axis relative to the electrical light vector, but his efforts were strictly directed to answering the question if metal cylinders mixed with spheres could reproduce the observed λ^{-1}-law of interstellar extinction. He got a positive result, even if cylinders were much more abundant than spheres, and was contended with it. That aligned cylinders could produce interstellar polarization was not imaginable at this time.

The second challenge of theorists was the grain alignment. This task was first tackled by Spitzer and Tukey [69]. They proposed a static alignment of ferromagnetic grains in a large-scale galactic magnetic field in analogy to compass needles. Concerning the ferromagnetic behaviour of the grain material, already in 1949 Spitzer and Schatzman [70] had suggested that such grain properties could be expected as a consequence of mutual collisions of dirty ice grains. Collisions should support the formation of elongated aggregates as well as the accumulation of Fe and Mg in the refractory collisional remnants. The energy release of chemical reactions should support the formation of ferromagnetic mineral domains in iron oxides of spinel type (maghemite: γ-Fe_2O_3; magnetite: Fe_3O_4) as well as mixed Mg-Fe-oxide (magnesio ferrite: $MgFe_2O_4$).

The dust model [69] had the advantage that ferromagnetic grains would be effective polarizers, and the alignment mechanism the disadvantage that a very strong magnetic field (10^{-3} G) was necessary, having lines perpendicular to the spiral arms contrary to the expectations. Some years later, laboratory experiments by Fick [71, 72] with elongated γ-Fe_2O_3-smoke particles, which were produced by an iron arc in a chamber and had average dimensions of 4 μm in length and 0.5 μm in diameter, demonstrated that the mechanism by Spitzer and Tukey [69] also operates with fields of about 10^{-5} G. With these grains Fick could also reproduce the interstellar λ^{-1}-law and the observed ratio between polarization and extinction. However, these experiments did apparently not meet much interest in the dust community, mainly because in the meantime the discussion on grain alignment had stroke the other path pointed by the dynamical mechanism proposed by Davis and Greenstein [73] (D–G mechanism). Nevertheless, Fick's experiments are among the "early birds" in the field that today is called "laboratory astrophysics" and does not deserve to be completely ignored.

The D–G mechanism was superior to that of Spitzer-Tukey. It used paramagnetic grains and a magnetic field of only 10^{-5} G with lines parallel to the spiral arms of the Galaxy. The paramagnetism of the particles was explained by ferromagnetic impurities in the ice conglomerate of the classical grains (see also, [70]; later the term "dirty ice" was introduced). The energy dissipation due to paramagnetic relaxation of the grains in the galactic magnetic field resulted in gradually swivelling the angular momentum vectors of the spinning and tumbling grains in the direction of the magnetic field. This way, the rotating grains should be beaded along the magnetic field lines with their long figure axes perpendicular to the field lines.

Later improvement and generalization made the D–G mechanism to an astrophysical standard theory that could be applied to paramagnetic and ferromagnetic

as well as diamagnetic grain materials [74, 75]. The expectations that polarization measurements would clearly define the magnetic grain properties did not fulfil, but instead of this the improved D–G mechanism turned out to be an effective tool to trace the magnetic field lines in the Galaxy by polarization measurements.

However, the discovery of the interstellar polarization presented a basic problem to the classical ice model: the inefficient polarization of ice needles. In order to reproduce the observed ratios of polarization to extinction improbable conditions were necessary, namely infinite cylinders (the case of maximum elongated shape) in perfect alignment. Already in 1950, before the problem of the grain orientation was promisingly solved, van de Hulst [76] on the base of his profound knowledge of grain optics had foreseen this weak point of the ice model: "The conclusion is that interstellar grains of the ordinary size as indicated by reddening measurements, may give a barely sufficient amount of polarization . . . We hope that partly absorbing grains will leave a better margin by giving a stronger polarization". However, the interstellar extinction sets narrow limits for the enlargement of the imaginary part of the refractive index of ice. Abandoning ices at all and using dust models of refractory solids should become the final solution of this problem. However, for this radical procedure, the time was not yet ripe.

It is, however, noteworthy that already in 1954 Cayrel and Schatzman [77] tentatively considered interstellar graphite grains as a potential candidate that could help out of the polarization worry. Because of their strong optical anisotropy aligned graphite particles would be a very efficient interstellar polarizer. The authors demonstrated this by laboratory measurements of extinction and polarization of oriented coloidal graphite grains smaller than 0.1 μm. They further pointed out that the Davis–Greenstein mechanism, in principle, should also operate with diamagnetic grains like graphite. Concerning the formation of graphite grains, the authors were less enterprising. Apparently they did not know the paper by Rosen and Swings [78], who in 1953 had stated "The atmosphere of a late N-star should be pictured as containing, probably on its outskirts, solid carbon particles. There is some kind of smoke veil around the star causing a reddening by absorption of the ultraviolet.

A veiling effect by smoke has been occasionally envisaged to interpret various astronomical phenomena, even in the case of novae. A late N-star would be a striking example. The smoke veil would vary in variable N-stars". Although in [77] a comment by P. Swings on soot grains in N stars was quoted the authors could not link these ideas to propose stars as the proper source of graphite dust. Not even Struve's [79] extended review paper on "Dust and related phenomena in stars", presented at the same congress (6th International Astrophysics Colloquium in Liège), on which Cayrel and Schatzman [77] discussed their new idea, was suggestive in this direction. The time was not yet ripe for a synthesis of the observational evidence of "stardust" that confirmed the old speculations [54, 56, 57] with the new requirements of dust astrophysics. On the other hand, at that time the attraction of the ice model was unbroken and could not be seriously endangered by the polarization problems.

3.2 From Cold to Hot Dust Formation

Apart from the objections due to inefficient polarization [76, 69, 77, 80] the ice model met additional criticism. Important counterarguments accumulated during more than two decades have been:

1. The grain formation in usual HI clouds turned out to be much less efficient than it was originally suggested [81]. Additional problems were presented by the search for plausible explanations of the formation of long ice needles.
2. A lot of processes eroding and chemically altering ice grains in the diffuse interstellar medium (ISM) have turned out to be much more destructive than the original mechanism of cloud collisions assumed by Oort and van de Hulst [58], e.g. suprathermal comic rays [82], sputtering in HII regions and shock fronts [83–85], enrichment of radicals [81, 86] leading to grain explosions [87], photolytic processing transforming volatiles to refractories [88].
3. Some of the observed extinction curves significantly deviated from the theoretical expectations (curve No. 15 in [60]) in the infrared range (see, e.g., [89]).
4. The search for the strong vibrational band of H_2O ice at 3 μm in the diffuse ISM was not successful [90, 91]. When it had finally been detected [92] the carrier ice turned out to occur only in special environments (young stellar objects in molecular clouds and star-forming regions) representing a dust population different from that in the diffuse ISM.
5. Generally, all observed UV extinction curves strongly deviated from the model predictions of ices. Extraterrestrial observations [93–95] revealed continuing rise of the extinction toward UV, superposed by a strong solid-state band at 217 nm (the extinction "bump"), while (curve No. 15 in [60]) showed a broad flat plateau there and decreasing extinction in the far UV (cf. Fig. 2).
6. Shortly after its detection, the band at 217 nm was attributed to graphite [96].

Affected by the growing number of objections against the ice model, in the decade 1960–1970 intensive theoretical efforts were undertaken to study alternative dust models consisting of refractory grains. The idea was to reach better reproduction of the observations and to find suitable environments in which such grains could be efficiently formed and ejected in a sufficiently large quantity to the interstellar space. These environments could be the expanding outer layers of evolved stars, e.g. giant stars and cataclysmic variables, but also planetary systems. In any case, the formation place of the grains was relocated from the cold interstellar clouds to much hotter environments, and, consequently, the new models defined the "hot way" of dust formation.

The new approach did not follow a uniform strategy. At the beginning of the 1960s dust modelling was very ambitious, and the model "designers" claimed to offer the perfect alternative to the classical dust. The expectation was to reproduce, with only one type of dust material, as many observations as possible better and without meeting the objections against the cold way. However, in the course of this decade, the condition of chemical uniformity was more and more dropped, and the strategy only aimed to guarantee the best possible compatibility with the obser-

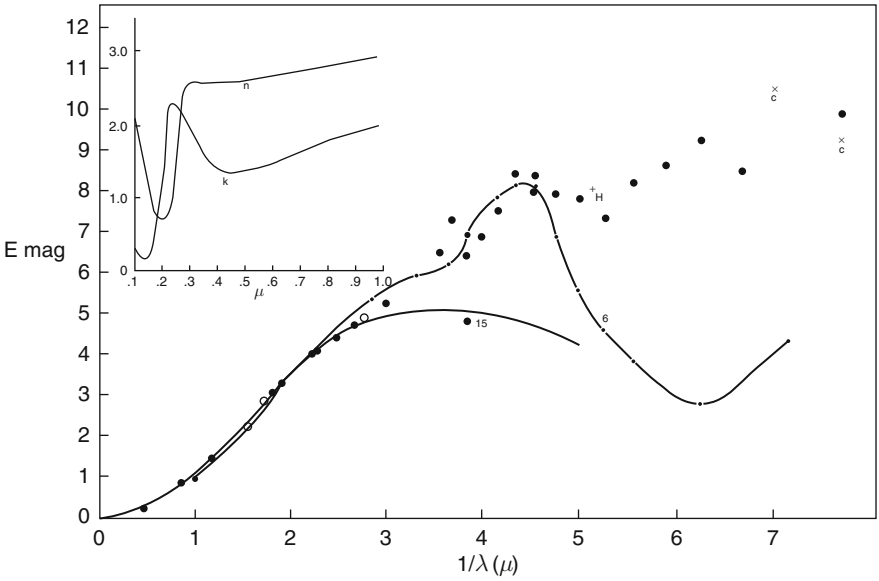

Fig. 2 Early UV rocket measurements of interstellar extinction compared with van de Hulst's curve No. 15 and calculated absorption coefficients of graphite grains (optical constants in the insert). The figure was published in 1965 by Stecher and Donn [96]

vations. The new compromises consisted in the proposal of layered grains (core-mantle up to multi-layer grains) and also grain mixtures. The latter case considered the ISM clouds as "catchment basin" of all possible dust sorts coming from the different circumstellar sources and forming a more or less uniform mixture. Some authors restricted their contribution to propose only single components that could be significant constituents of the interstellar mixture.

3.3 The Revolutionizing Graphite Model

The hot way of dust formation was opened in 1962/1963 with the graphite model by Hoyle and Wickramasinghe [97] and N. C. Wickramasinghe [98]. The authors, who explicitly referred to the old ideas [57, 77], could reproduce the main observational facts on interstellar dust, which were known at that time, with graphite grains having diameters of $10^{-6} - 10^{-5}$ cm. As source of these particles N stars were assumed, in which the excess carbon should condense to graphite grains in the low-temperature phase of the pulsation cycle of these stars. The grains should be subsequently driven out of the atmospheres by the radiation pressure. Estimates showed that the number of N stars in the Galaxy could account for the necessary quantity of graphite dust. The details of this new dust model, its comparison with the observations and its astrophysical advantages, e.g. in connection with molecule formation, can be found in Wickramasinghe's monograph [83].

The new dust model [97] greatly impacted the theoretical discussion on interstellar dust. However, contrary to the early optimism of the authors, the model did not solve all of the problems and, in particular, could not completely rule out ices. For improving the compatibility with the observations, mainly to get higher grain albedo, composite grains (graphite core + dirty-ice mantle [99, 100]) were introduced. Friedemann and Schmidt [101] pointed to a possible problem of graphite grains with observable consequences. Because of the large grain velocities ($\approx 1000\,\mathrm{km/s}$!) sputtering by impinging interstellar gas atoms should destroy many of them and increase the carbon abundance in the vicinity of N stars.

However, an obvious advantage of the graphite dust was that this model could explain the UV extinction observed by Boggess and Borgman [93] and by Stecher [94]. The interstellar extinction curve showed continuing rise for for $\lambda^{-1} > 3.0\,\mu\mathrm{m}^{-1}$, which, however, was interrupted by a big "bump" at about $\lambda^{-1} = 4.6\,\mu\mathrm{m}^{-1}$, the first diagnostic solid-state band of interstellar dust. Stecher and Donn [96] assigned it to graphite grains according to the model [97] (Fig. 2).

3.4 The Revival of Iron Grains

In two papers in 1965 and 1967 Cernuschi et al. [102, 103] focused the attention to the adiabatically expanding supernova explosion shells as a possible grain-forming environment. In the first paper [102], they studied the condensation of iron grains. Due to the relatively strong magnetic fields in the SN-shell, the grains should consist of single magnetic domains and stick together, forming elongated particle aggregates that could act as effective interstellar polarizers. The theory had some flaws, as the authors self-critically conceded in their second paper [103]. However, the idea that supernova explosion shells are a dust-forming medium has found confirmation, e.g. by presolar grains (cf. Sect. 5.2).

Independent of the papers [102, 103] Schalén [104], too, revived his old idea and included iron grains in his extinction analysis. At the end of this creative dust modelling phase Hoyle and Wickramasinghe [105] seized the supernova origin of dust grains and extended their suggestions not only to iron grains, but also to graphite and silicates. Iron grains were later occasionally included in the dust models (see, e.g., [106]), and today there are more arguments in favour of than against their interstellar occurrence.

3.5 The Disregarded Case: Silicate Grains

For the first time, silicon compounds in the context of interstellar dust emerged in the literature in 1963. Like Hoyle and Wickramasinghe, Kamijo [107] reverted to old stellar condensation speculations [55, 54] and included them in modern models. In the third part of a series of papers on long-period M variables, Kamijo came to the conclusion that nanometre-sized droplets or particles of fused silica (vitreous

SiO_2) should be the most abundant species that condensed primarily in the extended envelopes of these stars. The blown out particles were suggested to be condensation seeds in the interstellar gas, i.e., Kamijo [107] understood his result as a contribution to improved condensation conditions for ice grains rather than as a new refractory dust model. Anyhow, mineral grains as potential interstellar dust components must have been in the air at that time. Without giving any reasons, Gaustad [108] in the same year enclosed grains of enstatite ((Mg, Fe)SiO_3), hematite (Fe_2O_3) and α-quartz (SiO_2) in his paper "The opacity of diffuse cosmic matter and the early stages of star formation".

In 1968 the present author [109] suggested that all planetary systems present in the Galaxy could be subjected to similar disintegration processes of interplanetary bodies like the solar system. This way, fine-grained debris of Mg-Fe-silicates grains mixtured with minor portions of, e.g., the meteoritic Fe-Ni-alloy and troilite (FeS) would be permanently released into the interstellar space. Consequently, meteoritic silicates should be a substantial constituent of interstellar dust. Working out in detail the dust model of meteoritic silicates formed the base of the author's Ph.D. thesis [110].

The innovational character of this approach was not only that silicates like olivine and pyroxenes with their favourable optical properties (FUV extinction rise, efficient polarizer, high grain albedo) were included in the dust modelling, but mainly that the evolutionary concept "that at least part of the interstellar dust is a by-product of the phenomenon of stellar evolution" (formulation by Herbig [111] on the 16th Astrophysics Colloquium in 1969 in Liège) entered for the first time the stage of dust theory. Herbig [111] improved this concept by adding, among others, the conclusion that young planetary systems in the clear-off phase of their "solar nebulae" should release much more dust than the "evolved systems" like ours, on which the first estimates in [109, 110] were based.

In reference to a preprinted abstract of [109], distributed on the IAU General Assembly in Prague in 1967, Knacke [112] calculated extinction cross-sections for grains of quartz and vitreous silica and concluded that particles with the radius 0.2 μm were within 15% in agreement with the extinction measurements by Boggess and Borgman [93]. However, Knacke's [112] paper contained a very important hint to IR observers that such grains should show strong spectral features in the 8–14 μm atmospheric window. It does not matter that he misinterpreted Dorschner's [109] *silicates* as silica, for both solids show IR features in this window.

Still in 1968 Gillett et al. [113] had found a broad spectral feature in some giant stars in the 8–13 μm atmospheric window, but did not give any assignment because they were not sure if it was an absorption band at 8 μm or an emission band at 10 μm (Fig. 3). This problem was settled on the 2nd IAU Colloquium on Interstellar Dust (Jena 1969). From the comparison of the observed spectra [113] with the silicate spectra contained in the atlas by Moenke [114] Dorschner [115] concluded that Gillett et al. [113] had observed the 10 μm emission band due to the stretching vibrations of the SiO_4 tetrahedra of circumstellar silicates. As possible carriers enstatite ($MgSiO_3$) and related pyroxenes as well as mixtures of pyroxenes and olivines ($(Mg, Fe)_2SiO_4$) were suggested, whereas quartz was ruled out. As a

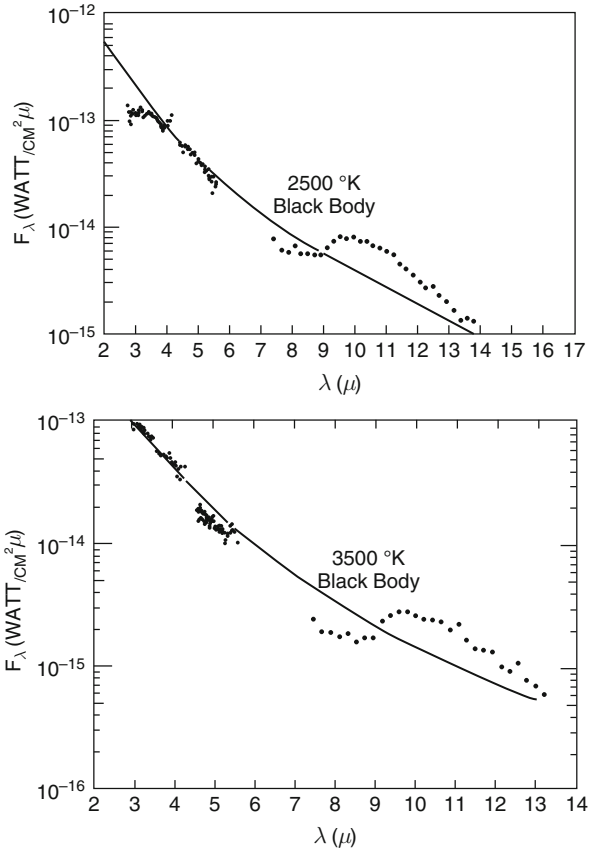

Fig. 3 First spectral indications for an unknown solid state band in the 10 μm-region detected by Gillett et al. [113], which in 1969 was identified as the silicate dust fingerprint. *Bottom*: μ Cep, *top*: o Cet

crucial test for the silicate identification the search for the second fundamental band at about 20 μm was recommended.

Since the manuscripts of the Proceedings of the Jena IAU Colloquium were very ill-fated in the hands of the American editor, they could be published only in 1971 after their return from the USA. In the meantime, the identification discussion around the 10 μm band was successfully closed. Already in 1969, Woolf and Ney [116] had published an analog proposal, and, since that time, are commonly quoted in the literature for the successful identification of the circumstellar silicate dust.

3.6 Silicon Carbide and Diamond

In 1969 two more minerals have been suggested to contribute to the interstellar dust: silicon carbide (SiC) and diamond. Friedemann [117], independently of Gilman's [118] thermochemical conclusions published in the same year, calculated

the growth of SiC grains in the atmospheres of carbon stars and showed that such grains could leave the star. Carrying out estimates of the total mass of SiC that could be injected this way in the interstellar space, Friedemann [117] was aware that SiC grains should be only a minor dust component.

The Jena dust group at that time favoured the mixture concept of interstellar dust (see, e.g., [119, 109, 117]) that paved the way to the later picture of the "multi-component" interstellar dust. In perfect analogy to the silicate story, SiC grains have been detected already few years later as a common circumstellar dust species in C-rich evolved stars.

In the same year 1969, Saslaw and Gaustad [120] came to the conclusion that "none of the classical models for the interstellar dust grains fit in with all the modern observations", and they presented diamonds as an alternative worth of being studied. They argued that diamond in contrast to graphite could reproduce the steep extinction rise in the FUV, for which first indications had just been found. A second supporting point was the occurrence of diamonds in some types of meteorites. However at that time only the diamonds in shock-metamorphosed achondrites were known, not to be mixed up with the presolar nanodiamonds detected in 1987 [121] in chondrites.

The recommendation of optical studies given by Saslaw and Gaustad [120] was seized by Wickramasinghe [122], who came to the disillusive conclusion that the diamond hypothesis was in serious conflict with the observations because the calculated extinction curves showed too little IR extinction and a much too high ratio of total to selective extinction, $R = A_V / E_{B_V}$. However, his conclusion was weakened by Landau [123], who showed that a modification of Wickramasinghe's [122] particle radii distribution would much improve the match. Landau commented his realization with the warning that often the choice of a suitable size distribution function can formally provide apparent agreement between calculations and observations for different materials. This way, he had rediscovered the basic "uncertainty principle" of interstellar extinction theory of which already Öpik [32] had taken notice 40 years ago.

Table 1 Refractory dust materials proposed in the models during 1962–1969, which later found confirmation by spectral observations and/or detection in meteorites and IDPs

Material	Year/Lit.	Formation environment	Spectral evidence	Fossil dust
Graphite	1962/[97]	C stars	SD[a], IS[a], V[a]	MET
Silica	1963/[107]	M stars	–	–
Iron	1965/[102]	Supernovae	–	IDP
Silicate	1968/[109]	Planet. Systems	SD, IS, DY, V	IDP, MET
SiC	1969/[117]	C stars	SD	MET
Diamond	1969/[120]		IS?, DY	MET

The symbols mean:
SD, stardust; IS, interstellar dust; DY, disks of young stars; V, Vega objects;

MET, isolated presolar grains in meteorites; IDP, components from IDPs.
[a]soot-like carbon, not exactly graphite, as in the original model adopted.

Shortly after this debate, diamonds have been forgotten and did not play any longer a role in theoretical dust models. It is one of the wryly traits in the development of interstellar dust research that about 20 years later diamonds [121] turned out to be by far the most abundant (≈1000 ppm per mass!) presolar grains preserved in primitive meteorites.

3.7 New Positioning of the Points in Dust Astrophysics

Although the dust models proposed in the decade 1960–1970 were mostly based on speculative assumptions, they were very helpful in formulating important principles of dust research and provided deep insights into the role of dust in stellar as well as galactic evolution. The dust researchers learned that it is "forlorn hope" to strive for a universal "standard dust model" accounting for all observational facts and resting on a unique type of material formed in one cosmic environment. The mixture concept more and more gained ground and prepared the modern "multi-component" or "multi-modal" picture of interstellar dust (Table 1).

From the standpoint of theoretical modelling, dust mixtures simplified the procedure of reproducing the observations, if the constituents and their size distributions were suitably chosen. Further, regionally different extinction and polarization curves could easily be explained by variations of the mixture ratios. The disadvantage of the mixture philosophy was that a larger number of free parameters entered the problem and this meant increasing arbitrariness, at least, as long as for the processes fixing the parameters no plausible theories were available.

An important realization was that the whole supply of different types of dust observations, not only the extinction curve, must be included in dust modelling. Such comprehensive models were often denoted as "unified dust models" [124, 100]. A consequent (and very eloquent) proponent of such improved dust modelling has been the late Mayo Greenberg (see, e.g., the reviews [86, 84, 125]). However, since continuous dust spectra, e.g. extinction, polarization and albedo, as a matter of principle, cannot result in non-ambiguous identification of dust components, striking progress in dust theory could occur not until spectral "fingerprints" of the components were discovered. Progress towards this direction was connected with IR and UV spectroscopy. It is most impressive to see how near the heuristic dust modelling in the 1960s came to reality, and how short the temporal distance between the model proposal and the detection of the respective spectral evidence was. For graphite [97], silicate [109] and silicon carbide [117] this distance amounted only 2–3 years each.

The observational detection of these three dust species confirmed the mixture concept. In 1971 Gilra [126] draw a balance and optimistically concluded "a mixture of meteoritic silicate, silicon carbide, and graphite particles can explain all the observed properties of interstellar grains". However, this mixture could not claim to be the only one that is compatible with the observations (see, e.g., [127]).

The exclusion of ices was a correct decision that has permanently endured (see Table 2). However, the ice problem transiently provided some confusion, after in

1973 strong H_2O ice bands in IR sources had been found [92]. During the 1970s, it became clear that this ice belonged to a special dust population typical of molecular clouds and the dense dust cocoons around young massive stars. In contrast to the diffuse ISM, in cool regions that are screened by strong dust extinction against dissociating UV radiation, H_2O ice can form grain mantles. The existence of different dust populations and evolutionary connections between them represented the next step in modifying the cosmic dust picture in the 1980s (see [4, 5]).

Because of the exciting developments in dust astrophysics in the late 1960s Greenberg agitated for holding an international meeting of higher rank than the Jena Colloquium and found resonance in the IAU administration as well as in the dust community. The first IAU symposium completely devoted to interstellar dust was the very successful Symposium No. 52, held 1972 in Albany, NY. Its proceedings [128] positioned the points for the next decade of astrophysical dust research.

4 Dust Mineralogy via Spectral Analysis

4.1 The Impact by the Interstellar UV Band

Even if carbon was the most abundant cosmic element that could form solids, graphite as dust material according to the model [97] looked somewhat too exotic in order to be promptly accepted. It was an unprecedented case of luck in the dust research that useful observational evidence followed the provocative proposal within only three years. Similarly as in 1930 [28] spectral observations of early-type stars anew played the role of the messengers of key information. The UV extinction derived from the spectra of these stars exhibited indications of a "bump" at $\lambda^{-1} = 4.6\,\mu\mathrm{m}^{-1}$. Being the first true solid-state band, this feature opened the way towards spectral analysis of interstellar dust. Stecher and Donn [96] did not hesitate to assume a connection with graphite grains (cf. Fig. 2), even if the absorption curves calculated with the optical constants of graphite available at that time did not show striking similarity with the measured UV extinction course. Anyway, graphite grains of the right size provided an absorption peak at the observed position.

The extinction curves derived from the spectra of the first astronomical satellite observatory, OAO-2, over the whole UV range up to $\lambda^{-1} = 9\,\mu\mathrm{m}^{-1}$ (see Fig. 4) convincingly showed that the "bump" with its peak at $\lambda_0 = 217.5$ nm was the result of the superposition of a strong solid-state band over a monotonously rising continuous extinction, which continued the optical extinction curve. The band could be exactly reproduced by a Lorentzian profile, the position, oscillator strength and damping constant pointed to an electronic transition of an abundant solid carrier. From the measurements of the diffuse galactic light obtained by the same satellite OAO-2 the UV albedo curve of the interstellar dust could be derived. It had a deep minimum at the bump peak, indicating that the 217.5 nm feature was due to almost pure absorption ([129]; see Fig. 5). This pointed to carrier particles very small compared with the wavelength. The equivalent widths of the 217.5 nm band

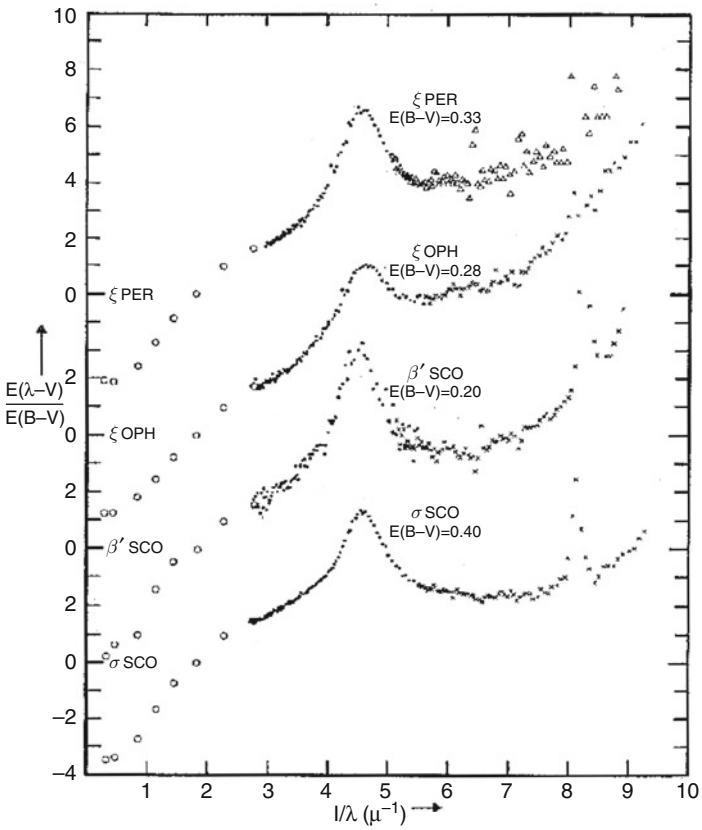

Fig. 4 UV extinction curves derived by Bless and Savage [95] from spectra obtained with the Orbiting Astronomical Observatory (OAO-2)

towards different lines of sight turned out to be tightly correlated with the visual extinction E_{B-V}, however, not with the FUV extinction slope [130]. This fact, too, could be interpreted as an indication for different components responsible for the whole course of the extinction curve.

An important step was Greenberg's [131] attempt to decompose the extinction curve. The simple sketch, first presented on IAU Symposium No. 52 (see Fig. 6), became a kind of trade mark of the new era of multi-component dust modelling. It is noteworthy that this procedure could be done without special assumptions on the chemical nature of the components. Of course, it was tempting to attribute the partial curves (2)–(4) (Fig. 6) to hitherto used model components. The visual part (2) was attributed to dielectric grains with radii in the order of 0.1 μm (first ice grains according to van de Hulst's curve No. 15 and/or composite grains with refractory cores and ice mantles; later, after abandoning the ice model, silicate grains). The superimposed band profile (3) was assumed to be due to very small graphite grains. For the FUV extinction nm-sized dielectric grains (mostly silicates) were proposed.

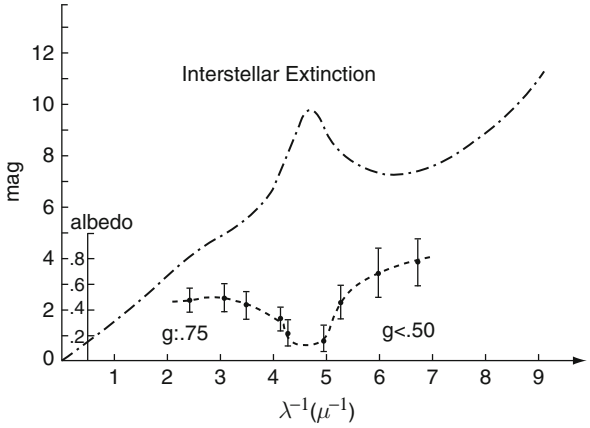

Fig. 5 The band at $\lambda_0 = 217.5\,\text{nm}$ is due to pure absorption. The *upper curve* is the average interstellar extinction curve [95], the *lower curve* shows the dust albedo derived from observations of the diffuse galactic light [132]

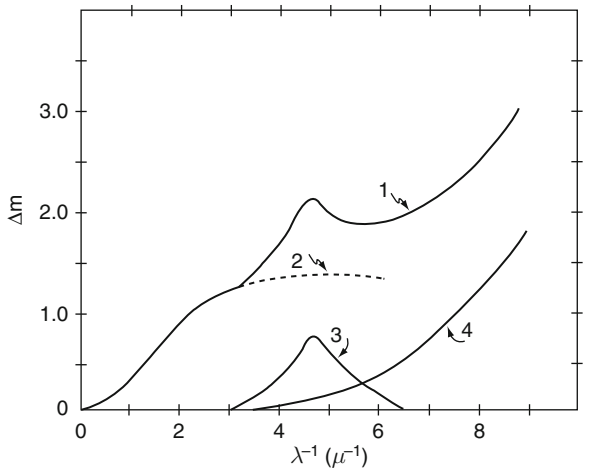

Fig. 6 The decomposition of the extinction curve (*1*) in three partial curves responsible for the visual and NIR extinction (*2*), the superimposed UV band (*3*) and the FUV extinction (*4*). After [131]

Much observational and laboratory work was concentrated to studies of the UV band in order to get it correctly identified. On the observational side, further space observatories (OAO 3 (1972–1981), TD-1A (1974–1978), IUE (1978–1996!)) confirmed the band's interstellar ubiquity, its invariant position ($\lambda_0 = 217.5 \pm 1\,\text{nm}$) in contrast to the remarkable scatter of the width along different lines of sight (FWHM $= 48 \pm 12\,\text{nm}$). It turned out to be a typical interstellar solid without a circumstellar counterpart. Spectroscopic evidence for graphite (in the mineralogical sense) was not found in the spectra of carbon stars [133, 134]. From the chemical

standpoint, it was not implausible that in a hydrogen-dominated environment pure graphite grains could not be formed. Spectral evidence for the presence of carbon grains in hydrogen-deficient stars were found, e.g. in WC stars [135] and in R CrB stars [136]. However, the strong UV absorption band of the latter was positioned at about 240 nm instead of 217 nm! This was in agreement with spectral data of different soots.

From the theoretical standpoint (inclusive laboratory experiments for obtaining optical constants of different forms of carbonaceous solids) an interesting splitting of opinions occurred in the time between the two large IAU dust symposia (No. 52 in 1973 and No. 135 in 1988). Even if graphite was the initial point for the interpretation of the UV bump, more sophisticated modelling and aspects of grain formation suggested that "graphite" as used in the astrophysical literature is not identical with the mineral graphite. Apart from the intensive search for the right soot type as the band carrier, some dust experts entertained suspicion that carbon could be the wrong track, at all, and searched for alternative explanations of the UV band. On IAU Symposium 135, Draine [137], critically summarizing the identification proposals for the UV band, came to the conclusion that two hypotheses "stand out as being well-defined, based on at least some laboratory data, and not obviously ruled out by the known observational constraints: 1. graphite grains; and 2. OH^- absorption on the surface of small silicate grains (Steel and Duley, 1987 [138])".

The widespread graphite-silicate dualism that had emerged after the silicate discovery and the general acceptance of "graphite" (see, e.g., [133, 139]) was transiently replaced by a "silicate monism" represented by a minority on IAU Symposium No. 135, who pleaded in favour of a silicate origin of the UV band. However, this idea was quickly abandoned, and the same fate had Draine's [137] exclusion of "nongraphitic carbonaceous solids". Amorphous (a-C) and hydrogenated amorphous carbon (a-C:H, HAC) found increasing interest among dust model designers (for review see [140], and cf. also Table 2). One decade later, hydrogenation of soot-like carbon turned out to play the key role in shifting the UV band of small soot grains towards the interstellar position. The multi-face interstellar carbon and its various problems have been reviewed in [5, 141].

4.2 Silicates – The Ubiquitous Dust Constituent

In 1989 Gürtler et al. [142] started their review article on circumstellar silicate dust with the apposite statement "In the hindsight, it seems rather surprising that silicate particles entered the stage only 20 years ago, because meteorites, asteroids, and the terrestrial planets should have been clear enough evidence for the condensation of silicates taking place whenever and wherever stars and planetary systems are being formed. However, the solar system was generally treated as a special case and links between it and the chemical evolution of the Galaxy or interstellar matter were then not envisaged". With the interstellar meteors, every vision of a potential relationship between meteorites and the ISM died away. The reanimation up to the

general acceptance of solar system solids as guide to interstellar dust composition [143, 144] was a procedure of several decades, in spite of the meteoritic dust model [109], the detection of interstellar silicate bands [145], and stimulating suggestions to learn to know interstellar mineralogy by the investigation of primitive meteorites (cf. [146–148]).

In what follows we briefly report the most important events in the discovery story of the silicate bands and some consequences of this second step towards quantitative spectral analysis of cosmic dust.

In 1969 Woolf and Ney [116] considered the feature observed by Gillett et al. [113] in the 8–13 μm atmospheric window as emission band due to circumstellar silicate grains and compared its profile with that of olivine grains in Gaustad's [108] old mineral mixture. As we already mentioned, analogous conclusions drawn at about the same time on the IAU Colloquium on Interstellar Dust at Jena found its way in the literature only in 1971 [115] (see Sect. 3.5).

In the early 1970s impressive progress in circumstellar dust research was reached. The detection of the second vibrational band at about 20 μm [149] (bending vibrations of the SiO_4 group) strikingly confirmed the silicate identification. Copious evidence for dust formation in evolved stars [150] established the prevailing view that such stars are the main sources of virgin dust in the Galaxy. Simultaneously, dust formation offered a plausible explanation of the dynamical background of stellar mass loss (see [151]). Mass loss was already a well-known, but insufficiently understood phenomenon (cf. [152]). Now an interesting feedback became obvious: Via momentum coupling between radiation-pressure driven grains and the gas, dust formation supports stellar mass loss, and the outflowing and cooling gas fuels the dust production. The ultimate fate of the "stardust" was to become interstellar dust. The figurative term "stardust" was successfully introduced in the literature by Ney [153]. Already in 1969, Gilman [118] by simple equilibrium calculations of the condensation of solids in late-type giants had shown that the O/C abundance ratio in the stellar atmospheres was the key parameter for the dust production: oxygen-rich stars (O/C > 1) supply silicates, carbon-rich (O/C < 1) carbon (soot), and stars with O/C ≈ 1 silicon carbide.

Silicate bands were not restricted to circumstellar environments. Still in 1969 Stein and Gillett [154] discovered the 10 μm emission band in the Orion Trapezium nebula, an infrared nebulosity discovered by Ney and Allen [155]. Few months after this first interstellar evidence for silicate dust, Hackwell, Gehrz and Woolf [145] found the silicate bands in absorption along the line of sight towards the IR sources in the Galactic Centre.

In the first time after the discovery of 10 μm band, the silicate dust was naturally considered to be crystalline, i.e. consisting of mineral grains (cf. [115, 116]). At that time, this idea appeared obvious rather than devious, since the silicates even in the most primitive meteorites were also crystalline and could be mineralogically classified. In case of need, the observed wide and structureless profiles could be explained as the result of the superposition of many different mineral profiles resulting in wiping out diagnostic profile structure. In this "mineralogically saturated" period, silicate minerals were even used to solve the longstanding problem of the

diffuse interstellar bands (DIBs). Several authors, among them also mineralogists, proposed crystal-field transitions of 3d-elements (Ti, Cr, Mn, Fe) as potential cause of the strongest DIBs [156–159]. However, most of the proposed transitions showed oscillator strengths too low to be compatible with the observed DIBs and the cosmic abundance constraints (see, e.g., [160]). The idea had to be dropped after the structure of the silicates turned out to be amorphous.

In 1983 the low-resolution spectrometer data (LRS, spectral range 8–22 μm) of the IRAS satellite drastically increased the number of circumstellar silicate sources. The yield of the IRAS spectroscopy included more than 1800 spectra of evolved stars with the silicate emission features at 10 and 18 μm and about 300 sources with the same features in absorption [161].

As in the case of the "graphite" story, also with the silicates between the publication of the speculative dust model proposal and the discovery of confirming spectral evidence only few years elapsed. However, both stories also showed remarkable differences that are worth of mentioning:

1. The silicate interpretation, which was based on two observed bands, let less space for other identifications. A certain alternative explanation of some transient significance was the oxide model by Duley et al. [162], which, however, used the same chemical elements as the silicate model.
2. The silicates grains revealed a striking environmental ubiquity. They were detected almost simultaneously in circumstellar envelopes, in planetary nebulae, in HII regions, in interstellar HI clouds and in molecular clouds, and, also via IR spectroscopy, in interplanetary dust (still in 1969 the 10 μm band was found in the spectrum of comet Bennett [163]).
3. The silicate bands, except the "trough" between them, could be observed from the ground.

Unfortunately, the IR silicate bands have also one big problem in common with the UV carbon feature: Like the great variety among the soots, silicates, too, exhibit greatest structural variety nullifying the possibility of accurate "mineralogical diagnosis" of the observed bands. The bands merely prove that there are IR-active Si—O bonds in a spatial (tetrahedral) arrangement that allows bending vibrations and, thus, indicate short-range order. However, their wide and smooth profiles point to lacking translational symmetry in the arrangements of the SiO_4 groups, i.e. long-range order typical of crystallinity is absent. These silicates, therefore, are considered amorphous; basic mineralogical information is not available. For instance, we do not know

– whether the "amorphous silicate" contains complete SiO_4-tetrahedra or whether they are oxygens deficient;
– to which extent silicon is substituted by other ions;
– how large the average number of non-bridging oxygens (NBO number) is;
– which cations with which average coordination are incorporated, etc.

The much evoked "striking spectral resemblance" of laboratory spectra that has been emphasized in many experimental papers of the 1970s was certainly per se very impressive, but unfortunately not of ultimate conclusiveness because of lacking unambiguity (cf. [164]). The way to the retrieval of theoretical band profiles was tedious, because exact optical constants in the range of the band profile were needed as input of a scattering theory for small grains. These data had to be measured from artificially amorphized silicates, the laboratory analogues. The fabrication of such simulation products was the task of the new branch of "laboratory astrophysics" that will be treated in Sect. 5.1. The calculations stressed the importance of the grain size for the width of the profile.

The amorphousness concept had to be somewhat modified for stardust in evolved stars and also for dust in disks around young stellar objects (YSO) and Vega phenomenon stars. The IRAS LRS spectra displayed profile variations from source to source, indicating structural diversity among the silicates and potential contributions of crystalline silicates. Such variations were used to introduce classification schemes (cf., e.g., [165–169]). "Fine-structure" peaks at constant positions within the 10 μm emission profiles gave reason to look for the presence of particular mineral "fingerprint" bands superposed on the amorphous background profile. Interesting cases had been the peaks at 11 and 13 μm of the "three-component feature" studied by [165–167]. The 13-μm peak will be discussed in the next section, here we consider the 11-μm peak tentatively assigned to crystalline olivine.

Support for the identification of a secondary peak at 11.2 μm with olivine came first from cometary spectra [170]. The analogous subfeature was also found in the spectra of main-sequence stars with the so-called Vega phenomenon [171, 172]. The latter consisted in a conspicuous FIR excess due to thermal dust emission of a disk around the star. Indications pointing to the formation of a planetary system and striking relationship to interplanetary phenomena of our solar system were found (see, e.g., [173]). A particularly interesting case was presented by the Vega phenomenon star β Pictoris, which not only showed indications for crystalline silicates but also for the presence of an extended cloud of cometary planetesimals and for the presence of planets. It became the paradigm for a main-sequence star where planetary formation is going on. We will get back to β Pic in connection with the new evidence to interstellar meteors in Sect. 5.3.

Crystallinity peaks superposed to the broad features of amorphous silicates have been the first weak indications for the presence of circumstellar minerals, justifying the speech of "stardust mineralogy" (for review see [174]). The "ISO revolution" has strikingly confirmed these cautious expectations by the discovery of many highly diagnostic mineral bands in the hitherto not available spectral range beyond the silicate fundamentals (cf. Molster et al. in this book and also Figs. 11 and 12).

It is, however, noteworthy that neither the "ISO revolution" nor subsequent space-bound telescopes did give upper limits of the fraction of crystalline silicates within the diffuse ISM above 5% (see, e.g., [175]). Much larger percentages of crystalline silicates, i.e. silicate minerals in the strict sense, have been found in numerous studies of disks around young stars, e.g. [176–178]. Altogether, the contribution of crystalline particles to the total mass of silicate dust in the Galaxy is very small.

This could mean, that the crystallized stardust ejected into the interstellar space must have been completely amorphized by interstellar processing and/or that amorphous silicate grains are effectively formed in interstellar environments themselves [11].

4.3 Other Oxygen-Bearing Dust Minerals

Already in the era of heuristic dust modelling, iron oxides were discussed as interstellar dust constituents, e.g. maghemite (γ-Fe_2O_3), magnetite (Fe_3O_4) and magnesio-ferrite ($MgFe_2O_4$) in the context of interstellar polarization [69] and hematite (α-Fe_2O_3) in Gaustad's [108] opacity mixture for protostars. Huffman [179] counted magnetite (Fe_3O_4) to the "solids of possible interstellar importance". The detection of the very broad structures (VBS) in the interstellar extinction curve [180] formed an important application field for magnetite grains [181–183]. Cox [184] called attention to IRAS LRS spectra of HII-regions showing a band-like excess beyond 15 μm. He proposed iron oxides (Fe_3O_4, γ-Fe_2O_3) as carrier material and pointed to the presence of magnetite in carbonaceous chondrites, the most primitive meteorites, to its possible significance for the VBS explanation, and to the advantages offered by these oxides for grain alignment.

In the context of this section, we briefly revert to the aforementioned mixed oxide dust model by Duley et al. [162]. It was conceived in order to give an alternative explanation of the vibrational bands commonly attributed to silicates. The grains were adopted to consist of diatomic oxides with NaCl-type lattice structure (except SiO, which was considered amorphous), i.e., each metal ion M^{2+} (M = Mg, Fe, Ca, Ni . . .) is coordinated by six O^{2-} ions. They are formed by kinetic processes in the interstellar environment and can concomitantly explain the observed dust properties as well as the depletion pattern of elements in the interstellar gas. According to this model, the UV feature at 217.5 nm is produced by coordinatively unsaturated O^{2-} ions at the grains' surfaces as proposed in an earlier paper [185]. The 10 μm feature is assumed to be due to the vibrational band of SiO grains, whereas the 18 μm band is caused as a cumulative effect of MgO and FeO. Today the oxide model is no longer of significance in competition to silicates. However, metal oxides, especially those of Fe, still play a role as potential minor ingredients of the multi-component dust (see Table 2).

As a matter of fact, so far non-ambiguous spectral evidence for refractory oxides in one of the dust populations is still lacking, anyhow, there is, at least, one debatable feature in oxygen-rich stars. In IRAS LRS spectra of Miras and SR variables, a weak, but distinct narrow emission band at 13.1 μm was found, which rides on the "red wings" of the strong 10-μm silicate emission bands. As mentioned in the preceding section, in their IR-classification of M stars Little-Marenin and coworkers [165–167] used the "three-component feature" consisting of two main peaks at 10 and 11 μm and a third one at 13.1 μm. In the literature, Vardya et al. [186] are commonly quoted as the discoverers of the 13-μm band and Onaka et al. [187] as those who identified it as being due to Al_2O_3 grains. Both of these statements deserve

some clarification. The paper [186] contains only the lapidary statement "Among the LRS spectra those of M-type Mira variables are particularly interesting because some show strong silicate emission features at 9.7 and 20 μm, usually attributed to silicate dust, while others show a rather flat spectrum with weaker broad emission features at 12 and 20 μm, whose origin is unknown at present." The band that Onaka et al. [187] assigned to Al_2O_3 grains was this "weaker broad emission", which can hardly be identical with the much narrower 13.1 μm feature. The identification in [187] was based on optical constants of partially amorphized γ-Al_2O_3 measured by Eriksson et al. [188], which has indeed a band around 12 μm. Corundum (α-Al_2O_3) was excluded in [187] because the authors erroneously assumed the position of the corundum band at 15 μm. Anyhow, the authors of [187] had focussed the attention to aluminium oxide.

Glaccum [189] attributed the 13-μm feature to grains of sapphire, the blue gemstone variety of corundum (α-Al_2O_3). This identification also found some indirect support by the just managed isolation of presolar corundum grains from meteorites [190]. Moreover, Aluminium-containing minerals play a basic role in the high-temperature condensates CAI (Ca-Al inclusions) in primitive meteorites. However, the derivation of the accurate 13-μm profile from IRAS LRS spectra met some difficulties resulting in different shapes (cf. [191, 192]). The profile problems settled when the much better resolved ISO-SWS spectra became available. However, the ISO-spectra did not show the second band of corundum grains expected at about 21 μm. Based on ISO-SWS spectra and extended laboratory work, Posch et al. [193] and Fabian et al. [194] have recently shown that the Al–O vibrations of spinel grains ($MgAl_2O_4$) would give a better reproduction of the observed 13-μm band than corundum; they also got additional support for this attribution.

Among the potential oxygen-bearing dust constituents two additional identification proposals must be mentioned: carbonates and carbonyles. Carbonate grains have been repeatedly proposed as a dust component. The first assignment was made by Gillett et al. [195] who considered magnesite ($MgCO_3$) as carrier of a band at 11.3 μm in 8–13 μm spectra of the planetary nebulae NGC 7027 and BD+30°3639. They already pointed out that the crucial test of the carbonate hypothesis could be the search for the strong vibration band of the CO_3-group at 6.9 μm. However, at that time this wavelength region was not yet available and the carbonate identification was followed up in the 1970s. After carbonate (braunerite and magnesiosiderite) had been found in IDPs [196, 197] that showed additionally a band at 6.8 μm with some resemblance to that found in protostellar sources, the carbonate hypothesis remained debatable. However, convincing spectral evidence for circumstellar or interstellar carbonate grains could not be detected. In ISO-LWS spectra of the planetary nebula NGC 6302 Kemper et al. [198] attributed a band at 92 μm in ISO-LWS to calcite ($CaCO_3$) and a second component in the emission complex around 62 μm to dolomite ($CaMgCO_3$). In a study of ISO spectra of protostars, Chiavassa et al. [199] found emission features peaking between 90 and 110 μm, which they again suggested to be due to calcite. In a thorough discussion of the carbonate problem, which was based on new laboratory measurements of calcite and dolomite and particularly considered the significant dependence of the absorption efficiency

on grain shapes and temperatures Posch et al. [200] concluded that the identification of carbonates in dust beyond the solar system still meets important criticism.

Metal carbonyles like $Fe(CO)_5$ have been tentatively proposed by Tielens et al. [201] in order to explain some interstellar absorption bands toward the Galactic Centre (cf. Table 1 in [5]).

4.4 Non-oxidic Dust Minerals

The main species of non-oxidic interstellar dust consists of carbon grains, for many years simply designated as "graphite" (cf. Sect. 4.1). During the 1990s, "graphite" was more and more replaced by more adequate carbon solids, and, finally, the profile of the 217.5-nm feature could be satisfactorily reproduced by laboratory analogues. Pioneering experimental work was done by Mennella et al. [202] and Schnaiter et al. [203] in the laboratory astrophysics groups in Neapels and Jena, respectively. For reviews of laboratory work on carbon dust (see, e.g., [204, 205]). According to this successful experimental simulation, the interstellar carbon dust should consist of a special type of hydrogenated soot that contains structural units of graphene sheets (aromatically bonded carbon) embedded in an amorphous carbon network structure containing hydrogen heteroatoms. However, although such laboratory products confidently reproduced the profile of the 217.5-nm feature, a persistent problem remained: The amount of carbon needed in order to explain the strength of the interstellar band was too large to be compatible with the cosmic carbon abundance.

There also were some further open questions. The UV spectra of the grains of carbon-rich stars differ clearly from those of the interstellar particles. In interplanetary carbon grains the λ217.5 carrier is lacking. The only exception found by Bradley et al. [206] concerns presolar grains embedded within interplanetary dust particles. The presolar graphite grains found in meteorites (cf. Sect. 5.2) have nothing to do with the carbon grains that are responsible for the interstellar UV extinction. The λ217.5 carrier obviously is a solid formed by processing in interstellar space. The particles must be very small (nanoparticles). More than a decade ago suspicion was expressed that there could be a narrow relationship between interstellar carbon grains and polycyclic aromatic hydrocarbons. An early representative of this line of argumentation among the laboratory experimenters was W. W. Duley (cf. [207]). In some respects a very sympathetic solution of the interstellar carbon problem could be if the enigmatic carrier of the 217.5 nm band would belong to the same chemical group that is also discussed as being responsible for the so called UIR bands (Unidentified Infrared Bands) and probably also for the DIB (Diffuse Interstellar Bands), the most durable interstellar mystery. This way a consistent theory of the puzzling interstellar carbon phenomena would come in sight. Nobody can predict when the breakthrough to such a unified carbon theory will occur.

Carbon probably is not the only elemental solid in interstellar dust. A recent approach to explain so-called Extended Red Emission (ERE), a galactic photoluminescence phenomenon, is based on nanocrystals of silicon in the ISM. ERE is a band-like excess radiation (FWHM≈100 nm) in the red and NIR, whose peak shifts

with increasing radiation field density from 610 to 820 nm. It was detected in reflection nebulae, planetary nebulae, HII regions, dark clouds, galactic cirrus clouds, and finally in the diffuse galactic light (see [208, 209]). The prevailing interpretation was, for a long time, based on a carbonaceous carrier material (see [210]). In some strong ERE sources sharp features have been detected [211, 212]; it is unclear if they are connected with the ERE carrier. Ledoux et al. [213] and Witt et al. [214] independently proposed Si nanograins as the alternative hypothesis. If confirmed silicon crystals could represent a hitherto unknown mineral species spread over the whole ISM.

Another non-oxidic dust component is silicon carbide, which has been proposed first as a possible constituent of the multi-component dust (cf. [117, 118]) and, in amazing analogy to "graphite" and silicate dust, has been identified via spectroscopy few years later, however, only as a stardust solid. The SiC-discovery story was initiated by the Ph.D. thesis of Hackwell [215], who performed a comparative study of IR spectra of M, S, and C stars. Deviating from M and S stars with their typical two silicate peaks, C stars contained only one hump in the 10 μm region, which was distinctly different from the 10-μm silicate band. More resolved spectra of the carbon stars V Hydrae and CIT 6 ([216], Fig. 7) showed that the peak position was 11.3 μm. Having been aware that he had detected a different circumstellar dust species, Hackwell did not offer any assignment of the new band.

Gilra [217] correctly identified this band with the fundamental vibration of circumstellar SiC grains. His paper contained an utmost important conclusion: "For about a tenth of a micron radius particles the shape of the particle is the most important parameter . . . Depending on the shape, the emission band(s) should appear between about 10.2 μ and 12.8 μ". Based on high-resolution spectra of carbon stars and detailed profile calculations for different shapes, Treffers and Cohen [218] could confirm Gilra's [217] conclusions on the sensitive shape dependence of the SiC

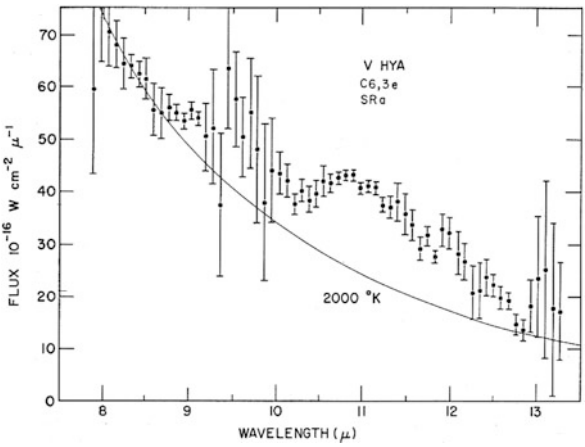

Fig. 7 Infrared excess of V Hya, a C6.3e variable observed by Hackwell [216], the first spectral indication of SiC dust

profile due to surface modes (Fröhlich modes). They occur, at the wavelength λ_F fulfilling the condition $\epsilon(\lambda_F) = -2\epsilon_m(\lambda_F)$, where $\epsilon(\lambda_F)$ and ϵ_m are the dielectric functions of the grain material at λ_F and of the surrounding medium, respectively. SiC is a paradigmatic case of the influence of such modes (see [219]).

At that time, many representatives of the dust community were not yet very familiar with grains shape effects on band profiles, and Gilra's proposal met disbelief. Because of the apparent wavelength disagreement of calculated Mie-cross-sections with the observations, Woolf [150] rejected SiC and proposed instead of this silicon nitride (Si_3N_4) as the carrier material. In the following time, much work of the beginning laboratory astrophysics – mainly with size-separated grains obtained from commercial mixtures of α-SiC polytypes (hexagonal or rhombohedral), more rarely on β-SiC (cubic) – was devoted to the spectrum of submicrometre-sized SiC grains in the band region [220–222] and generally supported Gilra's identification with SiC. Critically must be annotated that the experimenters' conclusions often disregarded shape and matrix effects on the band's position and shape. This explains why different authors came sometimes to different conclusions which SiC modification dominates. The whole problem α-vs. β-SiC has been later discussed from the observational and the experimental standpoint by Speck et al. [223].

The IRAS LRS spectral atlas [161] contained more than 500 stars with the SiC band. The profiles showed variations of peak positions and widths from source to source, which impacted first classification work [224]. In this time of commencement, mixing up the SiC feature with one of the UIR bands at about the same wavelength played a certain role. However, since the Unidentified IR (UIR) bands commonly attributed to polycyclic aromatic hydrocarbon (PAH) molecules always occur as a series with characteristic wavelengths, mix-up of the 11.3 μm bands of different origin could be excluded later.

The few SiC absorption features [223] are probably due to the optical thickness of the corresponding circumstellar shells rather than to interstellar SiC absorption. Whittet et al. [225] have conjectured that SiC could be destroyed in interstellar space by oxidation. A very weak SiC absorption feature could also be hidden within the strong silicate absorption.

Apart from SiC another oxygen-free silicon compound has maintained its position in the list of circumstellar dust minerals: silicon nitride (Si_3N_4). Already in 1989 Russell et al. [226] pointed to this potential dust component by presenting emissivity measurements of crystalline (mixture of α- and β-Si_3N_4) and amorphous samples of silicon nitride. According to these results, grains of Si_3N_4 would be expected to produce observable effects by slightly modifying the SiC profile (cf. [174]). However, there could be additional weak bands at longer wavelengths that should help to unambiguously identify silicon nitride. The detection of silicon nitride grains among the presolar inclusions in primitive meteorites (see Sect. 5.2) has justified the search for spectral indications in carbon-rich IR sources. Clément et al. [227] have taken first steps in this direction and studied absorption spectra of submicrometre-sized particles of α-, β- and amorphous Si_3N_4 and compared them with ISO spectra of the extreme carbon stars AFGL 2477 and IRAS 21318+563. Clear positive evidence was found in the spectrum of IRAS 21318+563, whereas

AFGL 2477 showed less definite indications. Further laboratory and observational work is necessary in order get clear conclusions in which carbon stars, at all, Si_3N_4 occurs and which modification is dominating in circumstellar dust. Important is the question how the spectral investigations matches with the mineralogical results on presolar Si_3N_4 grains isolated from meteorites.

A long-standing question concerns the occurrence of sulfides among the circumstellar solids. In 1981, in their 16–30 μm spectrometry of carbon-rich objects, Forrest et al. [228] could confirm early IR observations by Low et al. [229], who in 1973 had found an excess radiation of the carbon star IRC +10 216 at 34 μm. Kuiper Airborne Observatory spectra [230, 231] finally created clarity that the excess is due to a wide solid-state band peaking at about 30 μm. Following the early MgS assignment [232, 233], Begemann et al. [234] could show that the observations are indeed compatible with magnesium sulfide (MgS). Moreover, based on laboratory work, they suggested the existence of a whole series of mixed Mg-Fe sulfides. In contrast to Mg-rich sulfide grains, the Fe-rich members and pure FeS have sufficient chemical stability to survive the stay in interstellar space and to be included in primitive Solar System solids. The sulfide-bearing GEMS (see Sect. 5.2) give some support to this expectation.

In the last decade, new contributions to the sulfide discussion were made. The strong depletion of sulfur in dense molecular clouds awoke the suspicion that it could reside in solid grains. Based on laboratory data on troilite (FeS) and pyrrhotite ($[Fe,\ Ni]_{(1-x)}S$), Keller et al. [235] studied ISO spectra of young stellar objects and assigned a broad band at 23.5 μm to iron sulfide grains. At about the same time, Hony et al. [236] announced the detection of iron sulfides in carbon-rich planetary nebulae. The assignment was based on the broad spectral feature at 23 μm and additional weak features at 34, 38, and 44 μm. These bands had been found in laboratory spectra of troilite (FeS) by Begemann et al. [234]. The occurrence of sulfides as troilite, pyrrhotite, and pentlandite in circumstellar environment has been stressed by the mineralogical analyses of the grains recovered from the comet 81P/Wild 2 (cf. [237]).

For the sake of completeness in reporting we briefly refer to a sideline of the sulfide discussion. A connection with sulfides was also supposed for the strong emission band at 21 μm detected in 1989 by Kwok et al. [238] in IRAS LRS spectra of four carbon-rich post-AGB stars. Goebel's [239] proposal that silicon disulfide (SiS_2) could be a candidate for the identification got some support by laboratory work with amorphous SiS_2 prepared by Begemann et al. [240]. KAO observations by [241] confirmed that the 21-μm band occurs only in the post-AGB stadium, probably as a transient phenomenon. These authors, however, joined the opinion by Buss et al. [242] who pleaded in favour of a carbonaceous instead of sulfidic carrier material. Following a qualitative suggestion by Koike et al. [243] and the relatively large abundance of presolar diamonds (see Sect. 5.2), Hill et al. [244] reproduced the 21-μm profile by nitrogen-rich diamonds with lattice defects due to irradiation by fast neutrons. Later tentative identification proposals supposed carbides (titanium carbide [245], silicon carbide with impurities [246]). However, convincing identification of this band is still lacking.

5 The Laboratory Base of Cosmic Dust Mineralogy

5.1 The Approach by Laboratory Astrophysics

The preceding chapter has shown that laboratory measurements are the inevitable condition of reliable identifications of cosmic solids. After 1970 laboratory work, aiming at experimental simulation of cosmic dust materials and processes, became more and more a new institutional astrophysical branch called "laboratory astrophysics". Experimental work in astrophysics was, of course, not restricted to solids, but dust problems have been the first to demonstrate its inevitability for reaching progress. The search for optical properties of many of the "exotic" materials, which have been supposed as dust constituents, in the data collections of the physical, chemical, mineralogical, and technological literature often ended with a "nil return", or they were published only for a insufficient wavelength range. To gradually overcome this *material problem* astrophysicists initiated the determination of optical constants of solids of "possible interstellar importance" [179] over the whole wavelength range of interest in astrophysics.

The wide and smooth band profiles of cosmic dust silicates, which revealed heavily disturbed crystal structure, virtually excluded the direct comparison with mineral spectra. An exception formed indications of "fine-structure" in the profiles of stardust bands as discussed in Sect. 4.2. In the early years of laboratory work on silicate problems, many different attempts have been undertaken to gain sufficiently amorphized laboratory analogues (cf. [164]). Despite the often emphasized "striking resemblance" of the laboratory spectra with the observations, there was little conclusiveness that the structure of the laboratory products was exactly the same as that of the carrier of the observed features. Nevertheless, in this phase of heuristic experimentalizing important insights on structure and composition of the interstellar silicates were gained (for overview, see the Proceedings of the OAC2-workshop [247]). The title of the latter in 1987 successfully introduced the term "cosmic dust analogues" for laboratory products prepared for better understanding chemistry and structure of dust solids.

Except the material problem, dust research met other serious problems. There was a basic *morphology problem*: The real dust grains could not be expected to exhibit such canonical shapes as spheres, infinite cylinders, and small spheroids, for which the light scattering theory offered exact solutions. It is an interesting fact that just the experimental approach to overcome this restriction formed the background for the early development of what gave rise to coin the term "laboratory astrophysics". Its first user probably was J. M. Greenberg in connection with his microwave analogy experiments that he started at the Rensselaer Polytechnic Institute in Troy, NY, in 1960 [248, 249]. Similar experiments were also carried out at about the same time in the Tübingen University Observatory by Giese and Siedentopf [250]. Later such experiments were continued with improved equipment at the University of Bochum, Germany, where light scattering by the fluffy cometary grains detected among the IDPs was simulated (see [251, 252], Fig. 8). A more

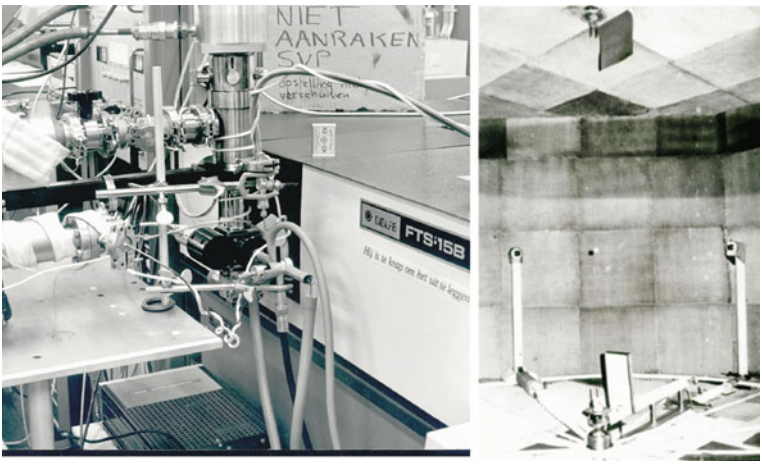

Fig. 8 Laboratory astrophysics in the beginning. *Left picture*: the experimental setup for the photolysis experiments in Leiden transforming ice mixtures to refractory organic material (RO in Table 2, photo credit: J. M. Greenberg, 1979). *Right picture*: Microwave scattering setup of the Bochum group. The "particle" is suspended on a nylon threat, transmitter (*right*) and swivel-mounted receiver (*left*) are positioned on columns (photo credit: R. H. Giese, 1979)

sophisticated version of such analogy techniques working with millimetre waves was developed at the University of Florida [253].

The designation "laboratory astrophysics" was also used in a wider sense. On the first "International Conference on Laboratory Astrophysics", held 1968 in Lunteren, Holland, gas experiments, too, were included in the program. However, the term only slowly gained ground, for in 1973 on IAU Symposium No. 52 [254], where 14% of the contributions concerned experimental work, and also on the first European (sponsored by the EAS) dust symposium, held in 1974 in Cardiff, UK, with the interesting title "Solid-state Astrophysics" [255], the term "laboratory astrophysics" did not yet find official emphasis. Optical measurement of real-sized particulates produced by grinding raised a *consistency problem* since the measured absorption coefficient in many cases was not compatible with the absorption coefficients calculated with the optical constants of bulk material. Special awareness of this problem and its causes was repeatedly recollected on dust meetings by Huffman and collaborators [179, 256], who formulated important (but often insufficiently observed) warnings of the "pitfalls in calculating scattering by small particles" [257]. These concerned the role of surface modes, shape and anisotropy effects, and clumping of particles in matrices. The ample laboratory experience gained by Huffman is reflected by the monograph "Absorption and Scattering of Light by Small Particles" [219] that became a standard work successfully replacing [61]. The method of CDE calculations used there turned out to be a useful criterion whether shape effects play a role or not.

Experimental simulation was also inevitable for the investigation of grain formation and modification by environmental influences. Classical nucleation theory and

equilibrium condensation could give, at the best, rough orientation. Experimental simulation and comparison with kinetic calculations proved to be the adequate tools for treating dust formation. One of the first advocates of this type of approach to the *formation problem* was Bertram Donn (for review and literature see [258]).

Finally, much laboratory simulation work has been and will be in future devoted to the *galactic ecology problem*, i.e. dust evolution and its significance in the galactic ecosystem. Here, the manifold questions of the close connections between cloud and grain evolution ([259, 260], Fig. 9) of the 'life-cycle of dust" (cf. [261]) and the "dust metamorphosis" [4] occurring when the dust passes through different dust populations and acts as an agent in the galactic "dust metabolism" [277]. It attests Greenberg's visionary foresight, when he tackled such problems already in 1975, the foundation year of the "Laboratory Astrophysics Group" at the Huygens Laboratory of the University of Leiden, Holland. This group had a lasting effect to the further development of laboratory astrophysics in Europe and in USA; well-known activists, e.g. L. Allamandola and L. d'Hendecourt, started their scientific career in the Leiden laboratory and were involved in the famous experiments simulating dust evolution by photolytic processing of mantle ices in the molecular cloud dust, transforming C-bearing ices to the refractory organic material of the diffuse ISM dust (for details see [4], Fig. 9). The experiments played a basic role in the development of the coupled evolutionary concept of clouds and grains which characterize the galactic dust "metabolism".

In the modern population concept of the cosmic dust (see [4]) the term "interstellar dust" lost its original universality, which existed still at the time of the laboratory-based dust research. In the strict sense, each population has its own characteristic dust model. Nevertheless, the diffuse ISM dust plays a central role since it represents the dusty debris coming from the different sources. This interstellar "catchment basin" contains stardust from evolved stars, disk dust from protoplanetary discs, refractory dust remnants and modified solids from molecular clouds dissolved by star formation, and "interplanetary dust" from planetary systems. The discovery avalanche of planetary systems around main-sequence stars (cf. [278, 279]) underscores that the contributions of planetary systems to the interstellar dust budget must no longer be neglected (cf. Sect. 5.3).

In the harsh physical conditions of the interstellar space only sufficiently robust materials survive or are modified to form typical interstellar dust materials. There are manifold modifications. Grains composed of different constituents lose their ingredients according to the degree of the volatility. Ice-like organics are transformed to refractory carbonaceous material. Even highly refractory grains suffer from significant structural disorder by ion irradiation and implantation of foreign atoms. Crystalline matter becomes amorphized to a large extent. For a review of processes modifying grains in the diffuse ISM see [4] (general review), [205] (laboratory simulation of processing carbonaceous dust), [280, 281] (laboratory simulation of processing silicate grains).

Probably, this heavy interstellar processing generates a trend to the unification of the material properties that, for instance, explains the relative uniformity of interstellar extinction. In this connection, the question deserves attention if

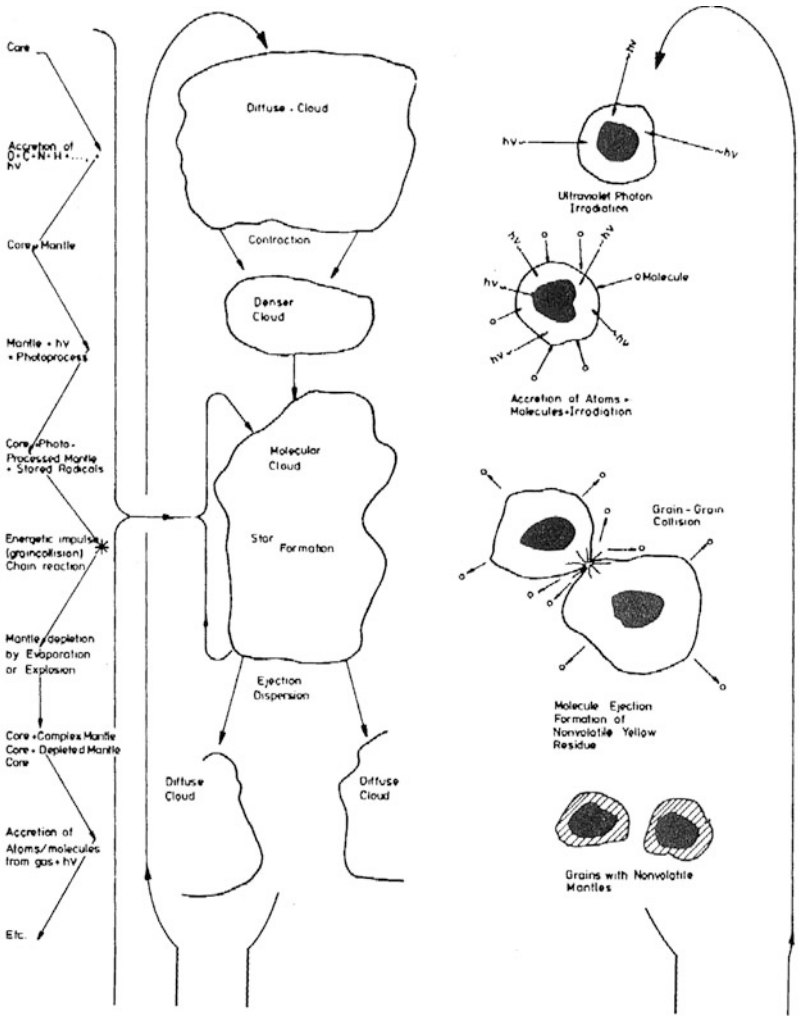

Fig. 9 Schematic diagram of the coupled evolution of clouds and grains. For detailed explanation see Greenberg [260]

such highly processed solids represent a kind of galactic minerals or mineraloids within an advanced mineral definition widened by the new comic requirements (cf. Sect. 6).

We conclude this laboratory-devoted section by a listing of the dust models of the last decades (Table 2) that reflect the laboratory efforts on understanding particulates of the diffuse ISM that are the main dust mass in the Galaxy. They can be classified in three categories of oxidized (silicate) and reduced (carbon-dominated) solids: (1) Mixtures of homogenous grains: Silicate + Graphite (+ PAH); (2) Core-mantle grains: Silicate core + carbonaceous mantle; (3) Composite grains of silicates, carbonaceous solids, and vacuum (holes).

Table 2 Advanced grain modelling for the diffuse ISM

Authors, reference	Grain type (species)	Size	UV band
Draine and Lee [262]	b (aSIL, GRA)	p	GRA
Chlewicki and Laureijs [106]	c-m(aSIL-RO) + b (GRA, FE, PAH)	exp, d	GRA
Greenberg [263]	c-m(aSIL-RO)+b(GRA)	exp, d	GRA
Williams [264]	c-m(aSIL-haC)+b(aSIL)	p, vs	SIL
Mathis and Whiffen [265]	co (aSIL,GRA,haC,VAC) + b(GRA)	p	GRA
Désert et al. [266]	c-m (aSIL-RO)+ b (aC, PAH)	p, vs	CAR
Sorrell [267]	b (aSIL, aC, GRA)	d	GRA
Rowan-Robinson [268]	b (aSIL, aC, GRA)	d, g	GRA
Siebenmorgen and Krügel [269]	b (aSIL, aC, GRA, PAH)	p	GRA
Mathis [270]	co (aC, haC, GRA, aSIL, MOX, VAC) + b (GRA, aSIL, MOX)	p	GRA
Li and Greenberg [271]	c-m (aSIL-RO) + b (CAR, PAH)	exp, p	CAR
Zubko et al. [272]	c-m (aSIL-RO) + ml (aSIL,RO,WI) + b (GRA, SI)	d	GRA
Weingartner and Draine [273]	b(CAR, PAH)	pf	PAH
Zubko et al. [274]	b(PAH, aSIL, GRA, aC) + co(aSIL, RO, WI, VAC)	pf	GRA
Draine and Li [275]	b(aSIL, GRA, PAH)	pf	GRA

Meaning of the abbreviations:
Grain types: c-m, core-mantle; co, composite; ml, multi-layered; b, bare.
Chemical species: aC, amorphous carbon; haC, hydrogenated amorphous carbon; GRA, graphite; CAR, carbonaceous material; PAH, polycyclic aromatic hydrocarbons; RO, refractory organics; MOX, metal oxides; aSIL, amorphous silicate; SI, silicon; FE, iron; VAC, vacuum; WI, water ice.
Size distribution function: d, discrete size or narrow interval; exp, exponential law ($n(a) \propto \exp(-Ca^3)$ [276]); g, giant grains $\geq 10\,\mu$m; p, power law (MRN-distribution $n(a) \propto a^{-3.5}$[139] or related); pf, parameterized function (parameters determined by optimisation techniques, such as maximum entropy or regularization); vs, very small grains.

5.2 Interstellar Dust "Fossils" in the Laboratory

After its death in 1930s, the idea of a relationship between interstellar and interplanetary solids resurrected, when silicates entered the stage, first as a heuristic model, then by observational evidence (cf. [109, 146, 147]). However, hardly anybody among the "early birds" in dust laboratory simulation work would have dared to hope that, some day, real interstellar dust grains would be available for laboratory analyses. Today this possibility is almost a matter of course.

In this historic overview, it is not possible to represent the whole development of mineralogic and isotopic microprobing techniques, which does not only allow identifying minerals of tiny inclusions in meteoritic grains but also unravels the cosmic sources of the grains by the anomalies in the isotopic signature of some key elements. Longstanding puzzles of the search for the carriers of exotic isotopic patterns in primitive meteorites could be solved, e.g. Ne-E and Xe-HL. The meteoriticists and cosmochemists improved their painstaking laboratory techniques up to the successful identification and isolation of the carrier materials. The latter turned out to be, as a rule, grains of highly refractory stardust minerals. We point to review articles by the pioneers of this exciting field [282–285].

Apart from the astromineralogical viewpoints, deep insights in the mechanisms of nuclear astrophysics in late stages of stellar evolution (RGB-, AGB-stars, supernovae, novae, WR-stars) could be obtained. In the last decade, breath-taking progress has occurred especially in the Secondary Ion Mass Spectrometry (SIMS) which is ideally suited for the study of isotopic compositions of small samples (nanoSIMS).

A detailed review of these new ways of dust research is contained within this volume. Here, we briefly report on the incipiencies of these exciting developments. Since 1987 meteoriticists succeeded in isolating presolar grains from primitive meteorites. Their isotope signatures proved the extrasolar origin. They are indeed "fossil" interstellar grains embedded 4.6×10^9 years ago in the meteorite parent bodies of the forming solar system. Being sufficiently resistant, they survived almost unchanged the formation of the solar system and the stay within the meteoritic rock (see Fig. 10).

The discovery of presolar grains is the highlight of the second "grand encounter" between astrophysics and meteoritics. In the first one, in the 1950s, the new table of accurate meteoritic elemental abundances by Suess and Urey [286] turned out to be the challenge that triggered the pioneering work by Burbidge et al. [287] (B^2FH-theory) and Cameron [288], who founded the modern theory of nucleosynthesis. In the second "grand encounter" about 20 years later, astrophysicists began to decode the "cosmic chemical memory" [289] of meteoritic matter. "The consequence of this is that today meteoriticists realize that they are also doing astronomy, that they are finding in these falling stones unique memories of events that predated our solar system formation . . ." reported D. D. Clayton [290] in the "Leonard Medal Address" presented in 1991. In 1982 Clayton [289] in an idiosyncratic but highly original paper with the title "Cosmic chemical memory: a new astronomy" drew a symbolic picture of this "new astronomical science" that he preferentially called "astrochemistry". The "telescopes" are the technological means of the laboratory work providing the "astrochemical" data, i.e. mass spectrometry (investigating the isotopic composition), microanalytics (studying single meteoritic grains, e.g., micron-sized Fremdlinge entirely encapsulated in a different mineral environment), and acid-dissolution techniques (providing insoluble residues, from which the carriers of the extreme isotopic anomalies can be extracted).

Clayton's astrochemical "telescopes" have indeed revealed most surprising things. The detection story of astrophysically highly relevant isotope anomalies

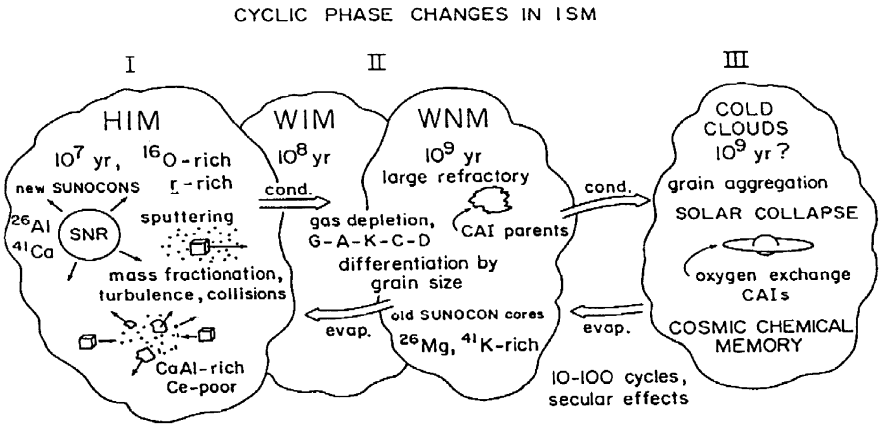

Fig. 10 The cyclic phase changes of ISM, the galactic "generator of chemical memory" [289]. The historical witnesses are the preserved solids (Stardust, SUNOCONS, CAIs, NEBCONS). SUNOCONS (supernova condensates) and NEBCONS (solar nebula condensates) are terms by Clayton that did not generally be accepted by the community. The abbreviations HIM (hot ionized matter), WIM (warm ionized matter), and WNM (warm neutral matter) are the ISM phases according to the generally accepted and meanwhile much improved model by McKee and Ostriker [293]

began already in the 1960s, when Reynolds and Turner [291] became attentive to isotopically anomalous Xe in the Renazzo meteorite. Continuing the "xenology" (coined by Reynolds) showed that not only the heavy (H: ^{134}Xe, ^{136}Xe), but also the light (L: ^{124}Xe, ^{126}Xe) Xe-isotopes were greatly overabundant relative to the solar system values. Since Xe-H and Xe-L were correlated with each other, later the designation was contracted to Xe-HL. Black and Pepin [292] in their isotopic study of carbonaceous chondrites found another noble gas anomaly. Hidden among large amounts of isotopically normal Ne, they detected a small component greatly enriched in the isotope ^{22}Ne. The anomalous neon component was later called neon-E and split in two components, Ne-E(H) and Ne-E(L).

In Table 3 we give a list of the presolar grain species detected up to now and also include some IDP components that show isotopic anomalies pointing to extrasolar origin. The table shows the dominance of thermally and chemically utmost resistant minerals in the stardust mineralogy. This is the result of the incisive selection by the acid-dissolution techniques that was used to extract the presolar grains from the main mass of meteorites. This chemical approach consisted in "burning down the [meteoritic] haystack to find the [interstellar] needle" [285]. Interstellar silicate, sulfide, iron... grains were dissolved in this radical isolation procedure.

In the IDP investigation such material-wasting technology could not be applied. The detection of silicate particles of extrasolar origin in IDPs began with the discovery of the Glasses with Embedded Metall and Sulfide (GEMS, see Table 3). The properties of these amorphous silicates match well with those postulated in the interstellar dust models (Table 2), and their metal inclusions are favourable for the

Table 3 Presolar grains in meteorites and possible pre-accretional grains in IDPs

Species	Formula structure	Abundance (ppm)	Size μm	Proposed origin	Detected by (year), References
Meteorites:					
Diamond	β-C fc-cubic	≈1400	0.0026	SN	Lewis et al. (1987) [121]
Silicon carbide	β-SiC fc-cubic	≈14	0.3–20	AGB, SN	Bernatowicz et al. (1987) [295]
Graphite	graphitic spherules[a]	≈10	0.8–20	AGB, SN,WR	Amari et al. (1990) [296]
Titanium carbide (carbide alloys)	TiC (Ti,Zr,Mo)C	[b]	0.005–0.2		Bernatowicz et al. (1991) [297]
Corundum	α-Al_2O_3 rhomboh.	≈0.01	0.5–5	RGB, AGB	Nittler et al., Hutcheon et al. (1994) [190, 298]
Silicon nitride	Si_3N_4	> 0.002	0.8–5	SN	Nittler et al. (1995) [299]
Spinel	$MgAl_2O_4$	[c]		AGB	Nittler et al. (1997) [300]
Hibonite	$CaAl_{12}O_{19}$	[c]		RGB, AGB	Choi et al. (1999) [301]
Rutile (?)	TiO_2	[c]			Nittler and Alexander (1999) [302]
IDPs:					
Silicate glass	GEMS	[d]			Bradley (1994) [303]
Forsterite	Mg_2SiO_4	[e]	0,3	ISM	Messenger et al. (2002) [304]

Notes:
[a] Composite structure: core of nanocrystalline C, surrounded by a mantle of well-graphitized C.
[b] Nanometre-sized crystallites within μm-sized graphite spherules ("grains within grains" [297]), illustrating details of the grain formation.
[c] Only a few particles.
[d] Glass with embedded metal and sulfide: non-stoichiometric silicate glass (depleted in Mg and Si relative to O) with inclusions of FeNi metal and Fe-Ni-sulfides.
[e] One particle only; the other ones of this cluster IDP were too tiny for mineral diagnostics.

alignment mechanism necessary for the explanation of the interstellar polarization [294]. The suspicion that they are interstellar silicate grains has been confirmed (see the contribution of the chapter “The Astromineralogy of Interplanetary Dust Particles" by J. Bradley, this volume). Some years ago single crystalline extrasolar silicate grains have been identified (Table 3), among them also for the first time a presolar olivine grain of probable supernova origin.

Today the time of unrecognized presolar silicates in primitive meteorites is over, too. The recent development of advanced ion probe imaging techniques led to their discovery. Silicates turned out to be the most abundant presolar minerals [305, 306].

From the astrophysical side, the expectation to find interstellar material in IDPs had been implied by modelling comets as samples of interstellar dust. Greenberg [307] first elaborated this idea in form of a cometary nucleus model and presented it on high ranked meetings in the run-up of the comet Halley encounter (see, e.g., [259]). The problem was that the comet dust mineralogy and morphology derived from the IDPs (that, at that time, were accepted as mainly coming from the disintegration of cometary nuclei) seemed to be very different from that derived from an interstellar dust model [259].

5.3 “Dust Astronomy” – A Promising Experimental Approach

In the 2002 Kuiper prize lecture Grün et al. [308] introduced a new possibility for carrying out experimental research of cosmic dust. They called it “Dust Astronomy” and sketched the picture of special equipment to be developed in future, such as dust telescopes and dust observatories in space and on the lunar surface. The rationale of this proposal rested on the realization that interstellar dust grains traversing our planetary system from beyond carry information on other galactic environments, especially of their galactic birthplaces. Part of this information (trajectory direction, speed, e/m ratio, elemental composition by mass spectrometry) could be retrieved already in near future with the help of presently available well proven hardware (see [309]). The first spacecraft succeeding in detection of interstellar grains passing through the solar system was the solar polar mission Ulysses [310, 311]. The results were confirmed by the Jupiter spacecraft Galileo. From these data the mass distribution of the interstellar grains was derived and compared with the distributions used in interstellar dust models [312]. It turned out, that the mass distributions of the particles impacting the dust detectors aboard Ulysses and Galileo differ from that derived from astronomical observations of interstellar extinction as used in the dust models of Table 2. Apparently these particles are representative for the dust in the local interstellar cloud rather than for that of the average diffuse interstellar medium. This is confirmed by the speed and the approach path of this particle stream which are in agreement with those of the neutral He atoms of the Local Interstellar Cloud (LIC) that penetrate the solar heliosphere.

The successful detection of extrasolar dust in the planetary system opens up an additional direct information source of galactic dust, and the “Dust Astronomy”

concept activated the development of improved dust detectors for the equipment of the proposed dust telescopes in more sophisticated spacecraft for the combined study of interstellar and interplanetary dust in Earth orbit, e.g. DuneXpress [313], and on the lunar surface. If this line should turn out to be promising, in more distant future collecting and recovering of interstellar grains penetrating the solar system seem to be feasible. Such expectations are justified since the successful recovery and mineralogical examination of dust collected in the coma of comet 81P/Wild2 by the spacecraft "Stardust"(see [314] and this book).

In the 1990s another possibility for the direct investigation of extrasolar solids was found. The interstellar meteors that had been buried in the 1940s did resurge half a century later in radar astronomy. In 1996 Taylor et al. [315] conducting a survey of orbits of very faint radar meteors using AMOR (Advanced Meteor Orbit Radar [316]) in New Zealand found indications for the extrasolar origin. Further centers of this new research branch are the NAIC Arecibo [317] and the Canadian Meteor Orbit Radar (CMOR) [318]. A concise review of the hitherto results was given by Baggaley et al. [319]. In the light of these new developments the explanation given by Dubinin and Soberman [320] in order to unravel the mystery of the enigmatic meteoroid measurements of Pioneer 10 and 11 got further support.

These earth-impacting meteoroids with hyperbolic velocities are larger than the common interstellar dust grains and the dust particles detected by Ulysses and Galileo. For the AMOR facility the limiting particle radius amounts to about 20 μm. A further difference to the LIC particles is the significantly different influx direction of this meteoroids. The larger mass makes these particles less susceptible to galactic forces that could change their dynamical behaviour. For this reason there is some hope that such extrasolar particle streams coming from sources in the galactic neighbourhood of the sun could be used to identify these discrete sources. Source candidates for grains larger by at least a factor of ten compared with the common dust grains condensed in the extended atmospheres of evolved stars could be young stellar objects with dusty surroundings, stars with debris disks (Vega-type objects) and planetary systems. As a matter of fact, Baggaley [321] observed with AMOR a collimated stream of such meteor particles coming from southern galactic latitudes. His suggestion that the source could be the debris system of β Pictoris initiated scrutinized dynamical analyses. Krivova and Solanki [322] proposed that an ejection mechanism based on a Jupiter-like protoplanet in the disk of β Pictoris is compatible with Baggaley's meteor stream observations. Their estimates showed that debris disks like that of β Pictoris could contribute about 10% of the total dust injection rate by all sources of stardust in the Galaxy. The analysis of stream geometry and kinematics by Krivov et al. [323] confirmed that β Pic is the most likely source of the observed stream and suggested that an intense dust ejection took place $\approx$0.7 million years ago. They studied the planetary ejection scenario as well as a radiation pressure scenario for the ejection and found that the dust flux measured at Earth can be brought under realistic assumptions with both scenarios into reasonable agreement, provided that β Pic's disk recently passed through an intensive short-lasting ($\approx$0.1 million years) clearing stage by nascent giant planets.

6 Mineral Identification by Spectroscopy

6.1 Possibilities and Limits of the Classical Mineral Definition

Since more than twenty years, terms like "mineral" and "mineralogy" have been applied to interstellar and circumstellar solids (cf. [148, 324, 325]). We finally ask the crucial question: *Is this linguistic usage in astrophysics compatible with the mineral definition in mineralogy?* Improving collaboration would also require standardization of the terminology.

The IMA Commission on New Minerals and Mineral Names (CNMMN) published "Procedures and Guidelines on Mineral Nomenclature" [326] and, in this connection, the following definition is given (based on [327]): "A mineral substance is a naturally occurring solid formed by geological processes, either on earth or in extraterrestrial bodies. A mineral species is a mineral substance with well-defined chemical composition and crystallographic properties, and which merits a unique name". This definition is, of course, formulated in terms of traditional mineralogy working with (macroscopic) material samples that could be subjected to all available analytical techniques. However, the mineral classification has also been extended to the micrometre-sized presolar grains, since the modern micro-analytics admits classification of such tiny samples.

No principle problems in the conventional sense are raised by the paradigmatic cases revealed by the ISO "crystalline revolution" [6]. The multitude of sharp mid-IR bands at the positions calculated with laboratory optical data for forsterite and enstatite grains allowed the mineralogical assignment to Mg-rich silicates of the olivine and the pyroxene classes with a satisfying degree of certainty. We illustrate the facts of the case in Fig. 11.

In this context we remind a permanent residue of uncertainty connected with mineral identification of small grains by means of observed IR bands via comparison with laboratory analogs, especially if only one spectral feature is under consideration. Each band profile is modified by manifold effects: particle size, shape, and temperature. We have discussed the role of these effects in the historical context of the identification stories of special groups of interstellar and circumstellar solids (cf. Sect. 4). In consideration of these effects, Jones [11] has recently warned to use too specific mineral terms for spectral identifications. We add the warning that even greater caution is indicated if the mineral identification rests on laboratory measurements of particles embedded in tablets of IR-transparent media (KBr, CsI, PE). In most cases the changes of positions and profile shapes cannot be corrected exactly. Up to now, there are, however, only few endeavours to measure freely floating particles (aerosol method) [328].

Crystalline solids represent a small minority of some percent of the galactic dust mass. They are mainly restricted to stardust and to disk dust. The great mass of dust in the diffuse ISM and in molecular clouds does not fit the mineral definition in the classical sense as defined by [326], at least, at the first view. For cosmic dust problems some modifications of the term "mineral" would be desirable. It surely does not present problems to upgrade the term "geological processes" towards mineral

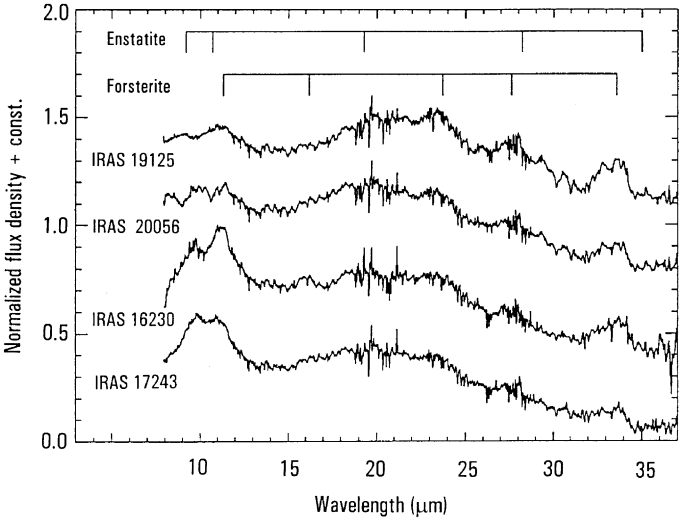

Fig. 11 A typical phenomenon in oxygen-rich post-AGB stars is the predominance of the Mg-rich endmembers of the mineral series of olivine and pyroxene, forsterite and enstatite. After Gielen and Van Winckel [329]

formation under conditions typical to cosmic dust grains, i.e. condensation out of the gas phase and subsequent processing of the grains. However, the widening of the scope of the mineral-forming processes is also significant towards an extension of the term "mineral substance". The adaptation of the temperature scale to low interstellar values could mean that a lot of substances that are volatiles in the conventional mineralogical sight now exist as crystalline solids within a definite compositional range. In this sense, it would be reasonable to considered them minerals according to the extended definition.

Few problems should be connected with metal grains (iron, silicon) among the analogues of Table 2. They are minerals. However, an open question is whether the widely spread nanograins that produce the 217.5 nm feature with its relatively uniform band profile can be incorporated in an extended new mineral definition. An objection could come from the fact that these particles fall below any acceptable size-limit. It is apparently a matter of debate among mineralogists, if there is a lower size-limit in the application of the term "mineral". The CMNNM-paper [326] expresses the following view: "... with the development of modern analytical techniques, it is now possible to perform complete chemical and crystal-structure analyses on nanometric volumes ... Should such submicroscopic domains be accepted as valid mineral species? There is a wide range of opinions on this subject. On the one hand it is argued that if a mineral substance can be characterized in terms of composition and crystallography, then it should be regarded as a valid mineral species. On the other hand, it is contended that the other properties traditionally reported for minerals such as colour, hardness, optical properties, etc., cannot be determined on an area of that size, and that the description is therefore incomplete.

Furthermore, the size of the described particle should be sufficiently large so that sufficient type material can be retained to enable a later independent examination to confirm the original characterization . . .. It has not been possible to reach agreement on a minimal acceptable size for a mineral substance to be regarded as a species, and therefore each case must be decided on its own merits."

The biggest case beyond the limits of the classical mineral definition should be solids that are commonly called "amorphous" because they are lacking a regular lattice. However, even in this case scrutinized examination if their well defined and homogeneous spectroscopic properties justifies to consider them mineral-like solids or mineraloids. Even among mineralogists there apparently was not drawn a clear "demarcation line" separating minerals from amorphous solids, so far. Since amorphous substances in interstellar context are of utmost importance (cf. Table 2) we quote the following lengthy passages in [326]: "Amorphous substances are non-crystalline and therefore do not meet the normal requirements for mineral species. The term 'crystalline', as generally used in mineralogy, means atomic ordering on a scale that can produce a regular array of diffraction spots when the substance is traversed by a wave of suitable wavelength (X-ray, electrons, neutrons, etc.). However, some geologically derived substances such as gels, glasses and bitumens are non-crystalline. Such substances can be divided into two categories:
amorphous – substances that have never been crystalline and do not diffract; and
metamict – those that were crystalline at one time, but whose crystallinity has been destroyed by ionizing radiation.
Some mineralogists are reluctant to accept amorphous substances as mineral species because of the difficulty of determining whether the substance is a true chemical compound or a mixture, and the impossibility of characterizing it completely; the term 'mineraloid' is sometimes applied to such substances. . . . With modern techniques it is possible to study amorphous phases more effectively than was possible in the past. Spectroscopic methods associated with a complete chemical analysis can often identify an amorphous phase unequivocally. In fact, appropriate spectroscopies (e.g., IR, NMR, Raman, EXAFS, Mössbauer) can reveal the three-dimensional short-range structural environment (chemical bonds) of each atom in the structure. Of course, without the possibility of obtaining a complete crystal structure analysis, which can give the coordinates and the nature of the atoms, the need for a complete chemical analysis is more stringent with amorphous material than with a crystalline phase.

The basis for accepting a naturally occurring amorphous phase as a mineral species could be a series of complete quantitative chemical analyses that are sufficient to reveal the homogeneous chemical composition of a substantial number of grains in the specimen, and physico-chemical data (normally spectroscopic) that prove the uniqueness of the phase.

Metamict substances, if formed by geological processes, are accepted as mineral species if it can be established with reasonable certainty that the original substance (before metamictization) was a crystalline mineral of the same bulk composition. Evidence for this includes the restoration of crystallinity by appropriate heat treat-

ment and the compatibility of the diffraction pattern of the heat-treated product with the external morphology (if any) of the original crystal . . ."

In principle, these statements offer the possibility to consider typical amorphous cosmic solids, e.g. interstellar dust silicates, as mineraloids if their composition is clearly defined and sufficiently uniform. The basic problem is that, at present, for the wide-spread interstellar silicates only insufficient structural and compositional characterization is available by the astronomical observations (see Sect. 4.2). The mineralogical information contained in the spectral "fingerprints" is hopelessly "blurred". However, the situation becomes much less hopeless, if attainable interplanetary solids, e.g. GEMS, should turn out to be indeed typical representatives of interstellar silicates. Their analyses are important not only for the characterization of the glass component, but also of the mineralic inclusions.

Thinkable is also the application of the passage "metamict substances" in [326]. Is transformation of stardust minerals by interstellar processing, e.g. the amorphization of originally crystalline circumstellar silicates by ion irradiation in the interstellar environment, a kind of cosmic metamictization? Even if such transformation is more complex than the corresponding processes in geology? In addition, many open questions remain: How, for instance, is the status of the organic (carbonaceous) materials among the dust analogues in Table 2? Comparable to the mineraloid bitumen in geology?

More clarity concerning all of these basic questions at the modern interface between astrophysical and mineralogical dust research will surely be reached if in future unchanged interstellar solids are successfully collected by spacecraft, recovered, and subjected to the improved methods of mineralogical and chemical microanalytics.

6.2 Beginning Classification in Astromineralogy

The dust in the Galaxy can be divided by phenomenological observational criteria into different populations which characterize typical environments: stardust, interstellar dust, molecular cloud dust and disk dust (cf. e.g. [4]). At the same time, these populations represent stages in the galactic dust evolution cycle. Chemistry and structure of particulates of solids, i.e. their "mineralogical status" in the broadest sense, are determined by the conditions in their formation environment and by secondary processing forces. The latter drastically change the original properties of the particles' structure and chemistry, they apparently could also provide substantial homogenization visible in the spectral appearance.

Due to the isolation of presolar grains from primitive meteorites and IDPs (including extrasolar components in recovered cometary grains) cosmic solids are available for laboratory investigation, and, thus, can be unambiguously classified in the mineralogical sense. This way, these stardust minerals represent the absolutely safe main pillar of astromineralogy. The detection of some of these minerals in

circumstellar spectra establishes the connection to the mineral identifications that are based on spectral methods only. Some experts in astromineralogy [330, 331] have introduced a conceptual sophistication. In analogy to the term “asteroseismology" they designated the stardust mineralogy in the strict sense as asteromineralogy. In this term, the difference in Greek between the two words *to astron*, the general notation for star or constellation, and *ho aster*, the single star, is stressed. Asteromineralogy concerns the stardust branch of astromineralogy with the richest mineral list. It is restricted to late stages of stellar evolution, red giants, AGB stars, post-AGB-stars, and supernovae. According to the chemical composition of the stellar environment asteromineralogy splits up in several branches, mainly an oxygen-rich and a carbon-rich branch.

Further subsystems within astromineralogy are thinkable. Here, we only point to the mineralisation processes within the disk-like configurations around main

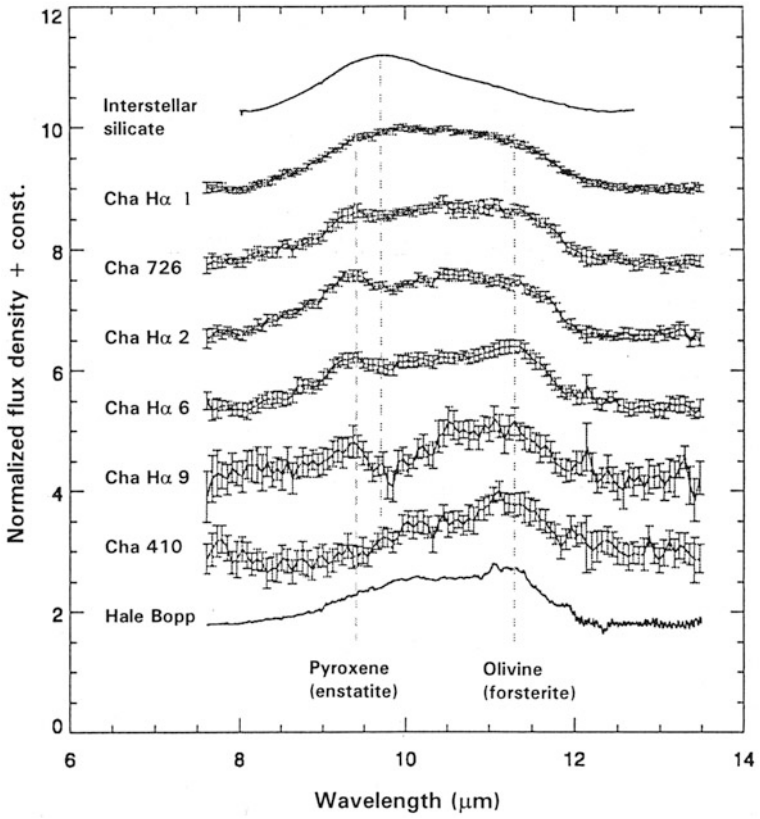

Fig. 12 Indications of mineralisation of silicate dust in the context of planet formation in 10 μm spectra of 6 brown dwarf disks in the star-forming region Chamaeleon I taken by Spitzer Space Telescope. The peaks at 9.3 and 11.2 μm are due to enstatite and forsterite. For comparison spectra of the diffuse ISM silicate and of the comet Hale-Bopp are plotted. After Apai et al. [332]

sequence stars and brown dwarfs. To this type the Vega-phenomenon objects with their debris disks belong. Here particulates are included that should be related to the interplanetary dust of our solar system. An adequate designation of the mineralogy could take reference to the disk-like configuration. Since the usually used word disk is directly derived from the Greek word *ho diskos* the word adequately formed as asteromineralogy would be diskomineralogy. Figure 12, illustrates how the mineral formation in disks around brown dwarfs becomes visible in spectra of the 10-μm band.

Since some decades astronomy and astrophysics have successfully assisted mineralogy to continue the way into cosmic environments, where mineral formation takes place. As a kind of return service mineralogy and isotope analytics have detected genuine extrasolar dust and revealed important information on nucleosynthetic processes in the stellar interior and on dust formation. The great number of planetary systems detected in the last decade promise a great field of research activity in astromineralogy in the future, which requires close collaboration between astrophysics and mineralogy.

Acknowledgments I should like to address my heartiest thanks to my colleagues of the Jena Laboratory Astrophysics Group with whom I had the pleasure to collaborate in the fields of dust astrophysics and astromineralogy from 1992 up to my retirement in 2004. I further gratefully acknowledge helpful discussions for updating this review by Harald Mutschke, Cornelia Jäger, and Alexander Krivov, Jena, and Thomas Posch, Vienna.

References

1. Chladni, E.F.F.: Über den Ursprung der von Pallas gefundenen und anderer Eisenmassen und über einige damit in Verbindung stehende Naturerscheinungen. Wittenberg 1794; Neues Verzeichnis der herabgefallenen Stein- und Eisenmassen: in chronologischer Ordnung. Gilberts Annalen der Physik 1815; Über Feuer-Meteore und über die mit denselben herabgefallenen Massen. Wien 1819 2
2. Engelhardt, W.v.: Probleme der kosmischen Mineralogie. In: *Tübinger Universitätsreden* No. 16 (1963) 2
3. Papike, J.J. (ed.): Planetary materials. Reviews in Mineralogy, vol. 36. Mineralogical Society of America, Washington, DC (1998) 2
4. Dorschner, J., Henning, T.: Astron. Astrophys. Rev. **6**, 271 (1995) 4, 23, 38, 49
5. Dorschner, J.: Interstellar dust and circumstellar dust disks. In: Grün, E., Gustafson, B.Å.S., Dermott, S., Fechtig, H. (eds.) Interplanetary Dust, pp. 727–786. Springer, Berlin (2001) 4, 23, 26, 32
6. Jäger, C., Molster, F., Dorschner, J., Henning, Th., Mutschke, H., Waters, L.B.F.M.: Astron. Astrophys. **339**, 904 (1998) 4, 46
7. Molster, F.J.: Crystalline silicates in circumstellar dust shells. Ph.D. Thesis, University of Amsterdam (2000) 4
8. Information by IMA secretary Maryse Ohnenstetter 5
9. Draine, B.T.: Interstellar dust grains. Annu. Rev. Astron. Astrophys. **41**, 241–289 (2003) 5
10. Posch, Th., Mutschke, H., Kerschbaum, F., Lebzeller, Th.: Progress and perspectives in solid state astrophysics from *ISO* to *Herschel*. Rev. Mod. Astron. **19**, 252–277 (2006) 5
11. Jones, A.P.: Eur. J. Mineral. **19**, 771 (2007) 5, 30, 46
12. Loys de Chéseaux, J.P.: Traité de la Comete qui a paru en Decembre 1743 and en Janvier, Fevrier and Mars 1744 (Lausanne and Geneve 1744), p. 213ff. (1744) 5

13. Olbers, W.: Über die Durchsichtigkeit des Weltraumes (1823). In: Schilling, C. (ed.) Wilhelm Olbers. Sein Leben und seine Werke, Bd. 1, pp. 133–141. Springer, Berlin (1894) 5
14. Herschel, W.: Philos. Trans. R. Soc. Lond. **85**, 213 (1785) 5
15. Hagen, J.G.: Die Geschichte des Nebels "Barnard 86". In: Specola Astron. Vaticana. Miscellanea Astronomica, vol. 2, pp. 61–64 (1929) 6
16. Barnard, E.E.: Astron. Nachr. **108**, 370 (1884) 6
17. Barnard, E.E.: Astrophys. J. **31**, 8 (1910) 6
18. Barnard, E.E.: Astrophys. J. **49**, 1 (1919) 6
19. Verschuur, G.L.: Interstellar Matters. Essays on Curiosity and Astronomical Discovery. Springer-Verlag, New York, NY (1989) 6
20. Wolf, M.: Mon. Not. R. Astron. Soc. **64**, 838 (1904) 6
21. Wolf, M.: Astron. Nachr. **219**, 109 (1923) 6
22. Kienle, H.: Die Absorption des Lichtes im interstellaren Raume. Jahrbuch der Radioaktivität und Elektronik **20**(1), 1–46 (1922) 6
23. Pannekoek, A.: Proc. Kon. Akad. Amsterdam **23**, No. 5, (1920) 6, 7
24. Russell, H.N.: Astrophys. J. **67**, 83 (1928) 6
25. Schalén, C.: Astron. Nachr. **236**, 249 (1929) 7
26. Hoffmeister, C.: Astrophys. J. **69**, 159 (1929) 7
27. Trümpler, R.J.: Lick Obs. Bull. **14**, 154 (No. 420; 1930) 7
28. Öhman, Y.: Meddel. Astron. Obs. Upsala No. 48 (1930) 7, 8, 23
29. Gerasimovič, B.P.: Harvard Obs. Circ. No. 339 (1929) 7
30. Unsöld, A.: Z. Astrophys. **1**, 1 (1930) 7
31. Stebbins, J., Huffer, C.M., Whitford, A.E.: Astrophys. J. **90**, 209 (1939) 8
32. Öpik, E.: Harvard Obs. Circ. No. 359 (1931) 8, 9, 10, 21
33. Mie, G.: Ann. Phys. **25**, 377 (1908) 9
34. Blumer, H.: Z. Phys. **32**, 119 (1925) 9
35. Blumer, H.: Z. Phys. **38**, 304 (1926) 9
36. Blumer, H.: Z. Phys. **38**, 920 (1926)
37. Blumer, H.: Z. Phys. **39**, 195 (1926) 9
38. Schalén, C.: Meddel. Astron. Obs. Upsala No. 58 (1934) 9
39. Schoenberg, E., Jung, B.: Astron. Nachr. **253**, 261 (1934) 9
40. Oort, J.H.: Bull. Astron. Inst. Netherlands **6**, 247 (1932) 9, 10
41. Schalén, C.: Meddel. Astron. Obs. Upsala No. 64 (1936) 9
42. Schoenberg, E., Jung, B.: Mitt. Univ.-Sternw. Breslau **4**, 61 (1937) 9
43. Whipple, F.L.: The incentive of a bold hypothesis – hyperbolic meteors and comets. The Collected Contributions of Fred L. Whipple, vol. 1. Smithsonian Astrophysical Observatory, Cambridge, MA (1972) 9, 10
44. Hoffmeister, C.: Die Meteore, ihre kosmischen und irdischen Beziehungen. Akadem. Verlagsgesellschaft, Leipzig (1937) 10
45. Öpik, E., Mon. Not. R. Astron. Soc. **100**, 315 (1940) 10
46. Porter, J.G.: Mon. Not. R. Astron. Soc. **104**, 257 (1944) 10
47. Lovell, A.C.B.: Meteor Astronomy. Clarendon Press, Oxford (1954) 10
48. Greenstein, J.L.: Harvard Obs. Circ. No. 422 (1938) 10
49. Henyey, L.G., Greenstein, J.L.: Astrophys. J. **88**, 580 (1938) 10
50. Henyey, L.G., Greenstein, J.L.: Astrophys. J. **93**, 70 (1941) 10
51. Güttler, A.: Z. Astrophys. **31**, 1 (1952) 10
52. Lindblad, B.: Nature **135**, 133 (1935) 10
53. Jung, B.: Astron. Nachr. **263**, 426 (1937) 11, 12
54. Wildt, R.: Z. Astrophys. **6**, 345 (1933) 11
55. Merrill, P.W.: Publ. Astron. Obs. Univ. Michigan **2**, 70 (1916) 11, 12, 15, 18
56. Loreta, E.: Astron. Nachr. **254**, 151 (1935) 11, 18
57. O'Keefe, J.A.: Astrophys. J. **90**, 294 (1939) 11, 15
58. Oort, J.H., van de Hulst, H.C.: Bull. Astron. Inst. Netherlands **10**(376), 294 (1946) 11, 12, 15, 17

59. van de Hulst, H.C.: Rech. Astron. Obs. Utrecht **11**(Pt 1), 10 (1946) 12, 16
60. van de Hulst, H.C.: Rech. Astron. Obs. Utrecht **11**(Pt 2) (1949) 12
61. van de Hulst, H.C.: Light Scattering by Small Grains. Wiley, New York, NY (1957) 12, 16
62. Strömgren, B.: Astrophys. J. **89**, 526 (1939) 12, 13, 37
63. Hiltner, W.A.: Astrophys. J. **109**, 471 (1949) 12
64. Hall, J.S.: Science **109**, 166 (1949) 13
65. Dombrovski, V.A. Doklady Akad. Nauk Armenia **10**, 199 (1949) 13
66. Behr, A.: Z. Astrophys. **47**, 54 (1959) 13
67. Gehrels, T.: Astron. J. **65**, 470 (1960) 13
68. Wellmann, P.: Z. Astrophys. **14**, 195 (1937) 13
69. Spitzer, L., Jr., Tukey, J.W.: Astrophys. J. **114**, 187 (1951) 13
70. Spitzer, L., Jr., Schatzman, E.: Astron. J. **54**, 195 (1949) 14, 16, 30
71. Fick, E.: Z. Phys. **138**, 183 (1954) 14
72. Fick, E.: Z. Phys. **140**, 308 (1955) 14
73. Davis, L., Jr., Greenstein, J.L.: Astrophys. J. **114**, 206 (1951) 14
74. Henry, J.: Astrophys. J. **128**, 497 (1958) 14
75. Jones, V.R., Spitzer, L.: Astrophys. J. **147**, 943 (1967) 15
76. van de Hulst, H.C.: Astrophys. J. **112**, 1 (1950) 15
77. Cayrel, R., Schatzman, E.: Ann. Astrophys. **17**, 555 (1954) 15, 16
78. Rosen, B., Swings, P.: Ann. Astrophys. **16**, 82 (1953) 15, 16, 17
79. Struve, O.: Dust and related phenomena in stars. Le particule solides dans les astres. Université de Liège, Liège (1954) 15
80. van de Hulst, H.C.: Publ. R. Obs. Edinburgh **4**, 13 (1964) 15
81. Donn, B.: Some chemical problems of interstellar grains. Le particule solides dans les astres. Université de Liège, Liège (1954) 16
82. Kimura, H.: Publ. Astron. Soc. Jpn. **14**, 374 (1962) 16
83. Wickramasinghe, N.C.: Interstellar Grains. Chapman and Hall Ltd, London (1967) 16
84. Greenberg, J.M.: Interstellar grains. In: Middlehurst, B.M., Aller, L.A. (eds.) Stars and Stellar Systems, vol. VII. University of Chicago, Chicago, IL (1968) 16, 17
85. Aannestad, P.A.: Destruction of dirty ice mantles by sputtering. In: Greenberg, J.M., van de Hulst, H.C. (eds.) Interstellar Dust and Related Objects. Proceedings IAU Symposium No. 52, pp. 341–344. Reidel, Dordrecht (1973) 16, 22
86. Greenberg, J.M.: Interstellar grains. In: Goldberg, L., Deutsch, A.J., Layzer, D. (eds.) Annual Review of Astronomy and Astrophysics, vol. 1. Annual Review, Inc., Palo Alto, CA (1963) 16
87. Greenberg, J.M., Yencha, A.J.: Exploding interstellar grains and complex molecules. In: Greenberg, J.M., van de Hulst, H.C. (eds.) Interstellar Dust and Related Objects. Proceedings IAU Symposium No. 52, pp. 369–373. Reidel, Dordrecht (1973) 16, 22
88. Hagen, W., Allamandola, L.J., Greenberg, J.M.: Astrophys. Space Sci. **65**, 215 (1979) 16
89. Johnson, H.L.: Astrophys. J. **141**, 923 (1965) 16
90. Danielson, R.E., Woolf, N.J., Gaustad, J.E.: Astrophys. J. **141**, 116 (1965) 16
91. Knacke, R.F., Cudaback, D., Gaustad, J.E.: Astrophys. J. **158**, 151 (1969) 16
92. Gillett, F.C., Forrest, W.J.: Astrophys. J. **179**, 483 (1973) 16
93. Boggess, A., III, Borgman, J.: Astrophys. J. **140**, 1636 (1964) 16, 23
94. Stecher, T.P.: Astrophys. J. **142**, 1683 (1965) 16, 18, 19
95. Bless, R.C., Savage, B.D.: Astrophys. J. **171**, 293 (1972) 16, 18
96. Stecher, T.P., Donn, B.: Astrophys. J. **142**, 1681 (1965) 16, 24, 25
97. Hoyle, F., Wickramasinghe, N.C.: Mon. Not. R. Astron. Soc. **124**, 417 (1962) 16, 17, 18, 23
98. Wickramasinghe, N.C.: Mon. Not. R. Astron. Soc. **125**, 87 (1963) 17, 18, 21, 22, 23
99. Wickramasinghe, N.C., Dharmawardhana, M.W.C., Wyld, C.: Mon. Not. R. Astron. Soc. **134**, 25 (1966) 17
100. Wickramasinghe, N.C., Krishna Swamy, K.S.: Nature **215**, 895 (1967) 18
101. Friedemann, Ch., Schmidt, K.-H.: Astron. Nachr. **290**, 233 (1968) 18, 22

102. Cernuschi, F., Marsicano, F.R., Kimel, I.: Ann. Astrophys. **28**, 860 (1965) 18
103. Cernuschi, F., Marsicano, F.R., Kimel, I.: Ann. Astrophys. **30**, 1039 (1967) 18, 21
104. Schalén, C.: Medd. Lunds Obs. Ser.1 Nr. 210 (1965) 18
105. Hoyle, F., Wickramasinghe, N.C.: Nature **226**, 62 (1970) 18
106. Chlewicki, G., Laureijs, R.J.: Astron. Astrophys. **207**, L11 (1988) 18
107. Kamijo, F.: Publ. Astron. Soc. Jpn. **15**, 440 (1963) 18, 40
108. Gaustad, J.E.: Astrophys. J. **138**, 1050 (1963) 18, 19, 21
109. Dorschner, J.: Astron. Nachr. **290**, 191 (1968) 19, 27, 30
110. Dorschner, J.: Thesis, University of Jena (1968) 19, 21, 22, 27, 40
111. Herbig, G.H.: Mém. Soc. Roy. Sci. Liège **19**, 13 (1970) 19
112. Knacke, R.F.: Nature **217**, 44 (1968) 19
113. Gillett, F.C., Low, F.J., Stein, W.A.: Astrophys. J. **154**, 677 (1968) 19
114. Moenke, H.: Mineralspektren. Akademie Verlag, Berlin (1962) 19, 20, 27
115. Dorschner, J.: Astron. Nachr. **293**, 53 (1971) 19
116. Woolf, N.J., Ney, E.P.: Astrophys. J. Lett. **155**, L181 (1969) 19, 27
117. Friedemann, Chr.: Astron. Nachr. **291**, 177 (1969) 20, 27
118. Gilman, R.C.: Astrophys. J. Lett. **155**, L185 (1969) 20, 21, 22, 33
119. Friedemann, Ch., Schmidt, K.-H.: Astron. Nachr. **290**, 65 (1967) 20, 27, 33
120. Saslaw, W.C., Gaustad, J.E.: Nature **221**, 160 (1969) 21
121. Lewis, R.S., Tang, M., Wacker, J.F., Anders, E., Steel, E.: Nature **326**, 160 (1987) 21
122. Wickramasinghe, N.C.: Nature **222**, 154 (1969) 21, 22, 43
123. Landau, R.: Nature **226**, 924 (1970) 21
124. Greenberg, J.M., Shah, G.: Astrophys. J. **145**, 63 (1966) 21
125. Greenberg, J.M.: Interstellar dust. In: McDonnell, J.A.M. (ed.) Cosmic DustWiley, Chichester (1978) 22
126. Gilra, D.P.: Nature **229**, 237 (1971) 22
127. Wickramasinghe, N.C., Nandy, K.: Mon. Not. R. Astron. Soc. **153**, 205 (1971) 22
128. Greenberg, J.M., van de Hulst H.C. (eds.): Interstellar Dust and Related Objects. Proceedings IAU Symposium No. 52. Reidel, Dordrecht (1973) 22
129. Witt, A.N., Lillie, C.F.: Astron. Astrophys. **25**,397 (1973) 23
130. Dorschner, J.: Astrophys. Space Sci. **25**, 405 (1973) 23
131. Greenberg, J.M.: Some scattering problems of interstellar grains. In: Greenberg, J.M., van de Hulst, H.C. (eds.) Interstellar Dust and Related Objects. Proceedings IAU Symposium No. 52, pp. 3–9. Reidel, Dordrecht (1973) 24
132. Witt, A.N.: Interstellar dust: observations in the ultraviolet and their interpretations. In: Greenberg, J.M., van de Hulst, H.C. (eds.) Interstellar Dust and Related Objects. Proceedings IAU Symposium No. 52, pp. 53–57. Reidel, Dordrecht (1973) 24, 25
133. Draine, B.T.: Astrophys. J. Lett. **277**, L71 (1984) 25
134. Glasse, A.C.H., Towlson, W.A., Aitken, D.K., Roche, P.F.: Mon. Not. R. Astron. Soc. **220**, 185 (1986) 25, 26
135. Cohen, M., Tielens, A.G.G.M., Bregman, J.D.: Astrophys. J. Lett. **344**, L13 (1989) 25
136. Hecht, J.H.: Astrophys. J. **367**, 635 (1991) 26
137. Draine, B.T.: On the interpretation of the λ2175Å feature. In: Allamandola, L.J., Tielens, A.G.D.M. (eds.) Interstellar Dust. Proceedings IAU Symposium No. 135, pp. 313–327. Kluwer, Dordrecht (1989) 26
138. Steel, T.M., Duley, W.W.: Astrophys. J. **315**, 337 (1987) 26
139. Mathis, J.S., Rumpl, W., Nordsieck, K.H.: Astrophys. J. **217**, 425 (1977) 26
140. Duley, W.W.: Carbonaceous grains. In: Millar, T.J., Williams, D.A. (eds.) Dust and Chemistry in Astronomy, pp. 71–101. Institute of Physics Publishing, Bristol, PA (1993) 26, 40
141. Henning, Th., Schnaiter, M.: Carbon – from space to laboratory. In: Ehrenfreund, P., Kraft, C., Kochan, H., Pirronello, V. (eds.) Laboratory Astrophysics and Space Research, pp. 249–277. Kluwer, Dordrecht (1999) 26
142. Gürtler, J., Henning, Th., Dorschner, J.: Astron. Nachr. **310**, 319 (1989) 26

143. Jones, A.P., Williams, D.A.: Mon. Not. R. Astron. Soc. **224**, 473 (1987) 26
144. McDonnell, J.A.M.: Solar system dust as a guide to interstellar matter. In: Bailey, M.E., Williams, D.A. (eds.) Dust in the Universe, pp. 169–181.Cambridge University Press, Cambridge, IL (1988) 27
145. Hackwell, J.A., Gehrz, R.D., Woolf, N.J.: Nature **227**, 822 (1970) 27
146. Cameron, A.G.W.: Interstellar grains in museums? In: Greenberg, J.M., van de Hulst, H.C. (eds.) Interstellar Dust and Related Objects. Proceedings IAU Symposium No. 52, pp. 545–547. Reidel, Dordrecht (1973) 27
147. Cameron, A.G.W.: The role of dust in cosmogony. In: Field, G.B., Cameron, A.G.W. (eds.) The Dusty Universe, pp. 1–31. Neale Watson Acadademic Publications, New York, NY (1975) 27, 40
148. Knacke, R.F.: Mineralogical similarities between interstellar dust and primitive solar system material. In: Gehrels, T., Mathews, M.S. (eds.) Protostars and Planets. Studies of Star Formation and of the Origin of the Solar System, pp. 112–133. University of Arizona Press, Tucson, AZ (1978) 27, 40
149. Low, F.J., Krishna Swamy, K.S.: Nature **227**, 1333 (1970) 27, 46
150. Woolf, N.J.: Circumstellar infrared emission. In: Greenberg, J.M., van de Hulst, H.C. (eds.) Interstellar Dust and Related Objects. Proceedings IAU Symposium No. 52, pp. 485–504. Reidel, Dordrecht (1973) 27
151. Gehrz, R.D., Woolf, N.J.: Astrophys. J. **165**, 285 (1971) 27, 34
152. Deutsch, A.J.: The mass loss from red giant stars. In: Greenstein, J.L. (ed.) Stars and Stellar Systems, vol. VI, pp. 543–568. University of Chicago Press, Chicago, IL (1960) 27
153. Ney, E.P.: Science **195**, 541 (1977) 27
154. Stein, W.A., Gillett, F.C.: Astrophys. J. Lett. **155**, L193 (1969) 27
155. Ney, E.P., Allen, D.A.: Astrophys. J. Lett. **155**, L197 (1969) 27
156. Dorschner, J.: Astron. Nachr. **292**, 107 (1970) 27
157. Manning, P.G.: Nature **226**, 829 (1970) 28
158. Huffman, D.R.: Astrophys. J. **161**, 1157 (1970) 28
159. Runciman, W.A.: Nature **228**, 843 (1970) 28
160. Dorschner, J.: Nature **231**, 124 (1971) 28
161. Olnon, F.M., Raimond, E. (eds.): IRAS catalogues and atlases. Atlas of low-resolution spectra. Astron. Astrophys. Suppl. Ser. **65**, 607–1065 (1986) 28
162. Duley, W.W., Millar, T.J., Williams, D.A.: Astrophys. Space Sci. **65**, 69 (1979) 28, 34
163. Maas, R.W., Ney, E.P., Woolf, N.J.: Astrophys. J. Lett. **160**, L101 (1969) 28, 30
164. Dorschner, J., Henning, Th.: Astrophys. Space Sci. **128**, 47 (1986) 28
165. Little-Marenin, I.R., Price, S.D.: The shapes of circumstellar "silicate" features. In: Hollenbach, D.J., Thronson, H.A. (eds.) Summer School on Interstellar Processes, pp. 137–138. NASA Tech. Memo. 88342, Washington, DC (1986) 29, 36
166. Little-Marenin, I.R., Little, S.J.: Astrophys. J. **333**, 305 (1988). 29, 30
167. Little-Marenin, I.R., Little, S.J.: Astron. J. **99**, 1173 (1990) 29, 30
168. Simpson, J.P.: Astrophys. J. **368**, 570 (1991) 29, 30
169. Sloan, G.C., Price, S.D.: Astrophys. J. **451**, 758 (1995) 29
170. Hanner, M.S., Lynch, D.K., Russell, R.W.: Astrophys. J. **425**, 274 (1994) 29
171. Knacke, R.F., Fajardo-Acosta, S.B., Telesco, C.M., Hackwell, J.A., Lynch, D.K., Russell, R.W.: Astrophys. J. **418**, 440 (1993) 29
172. Fajardo-Acosta, S.B., Knacke, R.F.: Astron. Astrophys. **295**, 767 (1995) 29
173. Backman, D.E., Paresce, F.: Main-sequence stars with circumstellar solid material: the Vega phenomenon. In: Levy, E.H., Lunine, J.I., Matthews, M.S. (eds.) Protostars and Planets III, pp. 1253–1304. University of Arizona Press, Tucson, AZ (1993) 29
174. Dorschner, J.: Stardust mineralogy. The laboratory approach. In: Greenberg, J.M., Li, A. (eds.) Formation and Evolution of Solids in Space, pp. 229–264. Kluwer, Dordrecht (1999) 29
175. Li, M.P., Zhao, G., Li, A.: Mon. Not. R. Astron. Soc. **382**, L26 (2007) 29, 34
176. Kessler-Silacc, J., Augerau, J.-Ch., Dullemond, C.P., et al.: Astrophys. J. **639**, 275 (2006) 29

177. Honda, M., Kataza, H., Okamoto, Y.K., et al.: Astrophys. J. **646**, 1024 (2006) 29
178. Sicilia-Aguilar, A., Hartmann, L.W., Watson, D., Bohac, Ch., Henning, Th., Bouwman, J.: Astrophys. J. **659**, 1637 (2007) 29
179. Huffman, D.R., Stapp, J.L.: Optical measurements on solids of possible interstellar importance. In: Greenberg, J.M., van de Hulst, H.C. (eds.) Interstellar Dust and Related Objects. Proceedings IAU Symposium No. 52, pp. 297–301. Reidel, Dordrecht (1973) 29
180. Hayes, D.S., Mavko, G.A., Radick, R.R., Rex, K.H., Greenberg, J.M.: Broadband structure in the interstellar extinction curve. In: Greenberg, J.M., van de Hulst, H.C. (eds.) Interstellar Dust and Related Objects. Proceedings IAU Symposium No. 52, pp. 83–90. Reidel, Dordrecht (1973) 30, 36, 37
181. Manning, P.G.: Nature **255**, 40 (1975) 30
182. Huffman, D.R.: Adv. Phys. **26**, 129 (1977) 30
183. van Breda, I.G., Whittet, D.C.B.: Mon. Not. R. Astron. Soc. **195**, 79 (1981) 30
184. Cox, P.: Astron. Astrophys. **236**, L29 (1990) 30
185. Duley, W.W.: Astrophys. Space Sci. **45**, 253 (1976) 30
186. Vardya, M.S., de Jong, T., Willems, F.J.: Astrophys. J. Lett. **304**, L29 (1986) 30
187. Onaka, T., de Jong, T., Willems, F.J.: Astron. Astrophys. **218**, 169 (1989) 30, 31
188. Eriksson, T.S., Hjortsberg, A., Niklasson, G.A., Granquist, C.G.: Appl. Opt. **20**, 2742 (1981) 30, 31
189. Glaccum, W.: Infrared dust features of late-type stars and planetary nebulae. In: Haas, M.R., Davidson, J.A., Erickson, E.F. (eds.) Airborne Astronomy Symposium on Galactic Ecosystem: From Gas to Stars to Dust. ASP Conf. Ser. vol. 73, p. 395. ASP, San Francisco, CA (1995) 31
190. Nittler, L.R., Alexander, C.M.O'D., Gao, X., Walker, R.M., Zinner, E.: Nature **370**, 443 (1994) 31
191. Sloan, G.C., LeVan, P.D., Little-Marenin, I.R.: Astrophys. J. **463**, 310 (1996) 31, 43
192. Begemann, B., Dorschner, J., Henning, Th., Mutschke, H., Gürtler, J., Kömpe, C., Nass, R.: Astrophys. J. **476**, 199 (1997) 31
193. Posch, T., Kerschbaum, F., Mutschke, H., Fabian, D., Dorschner, J., Hron, J.: Astron. Astrophys. **352**, 609 (1999) 31
194. Fabian, D., Posch, Th., Mutschke, H., Kerschbaum, F., Dorschner, J.: Astron. Astrophys. **373**, 1125 (2001) 31
195. Gillett, F.C., Forrest, W.J., Merrill, K.M.: Astrophys. J. **183**, 87 (1973) 31
196. Sandford, S.A.: Science **231**, 1540 (1986) 31
197. Tomeoka, K., Buseck, P.R.: Science **231**, 1544 (1986) 31
198. Kemper, F., Molster, F.J., Jäger, C., Waters, L.B.F.M.: Astron. Astrophys. **394**, 679 (2002) 31
199. Chiavassa, A., Ceccarelli, C., Tielens, A.G.G.M., Caux, E., Maret, S.: Astron. Astrophys. **432**, 547 (2005) 31
200. Posch, Th., Baier, A., Mutschke, H., Henning, Th.: Astrophys. J. **668**, 993 (2007) 31
201. Tielens, A.G.G.M., Wooden, D.H., Allamandola, L.J., Bregman, J., Witteborn, F.C.: Astrophys. J. **461**, 210 (1996) 32
202. Mennella, V., Colangeli, L., Bussoletti, E., Monaco, G., Palumbo, P., Rotundi, A.: Astrophys. J. Suppl. Ser. **100**, 149 (1995) 32
203. Schnaiter, M., Mutschke, H., Dorschner, J., Henning, Th., Salama, F.: Astrophys. J. **498**, 486 (1998) 32
204. Henning, Th., Jäger, C., Mutschke, H.: Laboratory studies of carbonaceous dust analogs. In: Witt, A.N., Clayton, G.C., Draine, B.T. (eds.) Astrophysics of Dust. ASP Conf. Ser. vol. 309, pp. 603–628. ASP, San Francisco, CA (2004) 32
205. Mennella, V.: Laboratory simulation of srocessing of grains. In: Witt, A.N., Clayton, G.C., Draine, B.T. (eds.) Astrophysics of Dust. ASP Conf. Ser. vol. 309, pp. 629–648. ASP, San Francisco, CA (2004) 32
206. Bradley, J., Dai, Z.R., Erni, R., et al.: Science **307**, 244 (2005) 32, 38
207. Duley, W.W., Seahra, S.: Astrophys. J. **507**, 874 (1998) 32

208. Witt, A.N.: Visible/UV scattering by interstellar dust. In: Allamandola, L.J., Tielens, A.G.D.M. (eds.) Interstellar Dust. Proceedings IAU Symposium No. 135, pp. 87–100. Kluwer, Dordrecht (1989) 32
209. Gordon, K.D., Witt, A.N., Friedmann, B.C.: Astrophys. J. **498**, 522 (1998) 33
210. Seahra, S.S., Duley, W.W.: Astrophys. J. **520**, 719 (1999) 33
211. Duley, W.W.: Astrophys. Space Sci. **150**, 387 (1988) 33
212. Gordon, K.D., Witt, A.N., Rudy, R.J., Puetter, R.C., Lynch, D.K., Mazuk, S., Misselt, K.A., Clayton, G.C., Smith, T.L.: Astrophys. J. **544**, 859 (2000) 33
213. Ledoux, G., Ehbrecht, M., Guillois, O., Huisken, F., Kohn, B., Laguna, M.A., Nenner, I., Paillard, V., Papoular, R., Porterat, D., Reynaud, C.: Astron. Astrophys. **333**, L39 (1998) 33
214. Witt, A.N., Gordon, K.D., Furton, D.G.: Astrophys. J. **501**, L111 (1998) 33
215. Hackwell, J.A.: Thesis, London University College (1971) 33
216. Hackwell, J.A.: Astron. Astrophys. **21**, 239 (1972) 33
217. Gilra, D.P.: Dust particles and molecules in the extended atmospheres of carbon stars. In: Greenberg, J.M., van de Hulst, H.C. (eds.) Interstellar Dust and Related Objects. Proceedings IAU Symposium No. 52, pp. 517–528. Reidel, Dordrecht (1973) 33
218. Treffers, R., Cohen, M.: Astrophys. J. **188**, 545 (1974) 33
219. Bohren, C.F., Huffman, D.R.: Absorption and Scattering of Light by Small Particles. Wiley, New York (1983) 33
220. Dorschner, J., Friedemann, C., Gürtler, J.: Astron. Nachr. **298**, 279 (1977) 34, 37
221. Friedemann, C., Gürtler, J., Schmidt, R., Dorschner, J.: Astrophys. Space Sci. **79**, 405 (1981) 34
222. Borghesi, A., Bussoletti, E., Colangeli, L., de Blasi, C.: Astron. Astrophys. **153**, 1 (1985) 34
223. Speck, A.K., Barlow, M.J., Skinner, C.J.: Mon. Not. R. Astron. Soc. **288**, 431 (1997) 34
224. Goebel, J.H., Cheeseman, P., Gerbault, F.: Astrophys. J. **449**, 246 (1995) 34
225. Whittet, D.C.B., Duley, W.W., Martin, P.G.: Mon. Not. R. Astron. Soc. **244**, 427 (1990) 34
226. Russell, R.W., Chatelain, M.A., Hecht, J.H., Stephens, J.R.: Si_3N_4 emissivity and the unidentified infrared bands. In: Tielens, A.G.G.M., Allamandola, L.J. (eds.) Interstellar Dust. Contributed Papers, pp. 157–162 NASA CP-3036 (1989) 34
227. Clément, D., Mutschke, H., Klein, R., Jäger, C., Dorschner, J., Sturm, E., Henning, Th.: Astrophys. J. **621**, 985 (2005) 34
228. Forrest, F.J., Houck, J.R., McCarthy, J.F.: Astrophys. J. **248**, 195 (1981) 34
229. Low, F.J., Rieke, G.H., Armstrong, K.R.: Astrophys. J. Lett. **183**, L105 (1973) 35
230. Cox, P.: Far-infrared spectroscopy of solid-state features. In: Kwok, S. (ed.) Astronomical Infrared Spectroscopy: Future Observational Directions. Astron. Soc. Pacific Conf. Ser. vol. 41, pp. 163–170. ASP, San Francisco, CA (1993) 35
231. Omont, A., Moseley, S.H., Cox, P., Glaccum, W., Casey, S., Forveille, T., Chan, K.-W., Szczerba, R., Loewenstein, R.F., Harvey, P.M., Kwok, S.: Astrophys. J. **454**, 819 (1995) 35
232. Goebel, J.H., Moseley, S.H.: Astrophys. J. Lett. **290**, L35 (1985) 35
233. Nuth, J.A., III, Moseley, S.H. , Silverberg, R.F., Goebel, J.H., Moore, W.J.: Astrophys. J. Lett. **290**, L41 (1985) 35
234. Begemann, B., Dorschner, J., Henning, Th., Mutschke, H., Thamm, E.: Astrophys. J. Lett. **423**, L71 (1994) 35
235. Keller, L.P., Hony, S., Bradley, J.P., et al.: Nature **417**, 148 (2002) 35
236. Hony, S., Bouwman, J., Keller, L.P., Waters, L.B.F.M.: Astron. Astrophys. **393**, L103 (2002) 35
237. Zolensky, M.E., Zega, T.J., Yano, H., et al.: Science **314**, 1735 (2006) 35
238. Kwok, S., Volk, K., Hrivnak, B.J.: Astrophys. J. **345**, L51 (1989) 35
239. Goebel, J.H.: Astron. Astrophys. **278**, 226 (1993) 35
240. Begemann, B., Dorschner, J., Henning, Th., Mutschke, H.: Astrophys. J. **464**, L195 (1996) 35
241. Omont, A., Cox, P., Moseley, S.H., Glaccum, W., Casey, S., Forveille, T., Szczerba, R., Chan, K.-W.: Mid- and far-infrared emission bands in C-rich protoplanetary nebulae. In: Haas, M.R., Davidson, J.A., Erickson, E.F. (eds.) Airborne Astronomy Symposium on Galactic Ecosystem: From Gas to Stars to Dust. ASP Conf. Ser. vol. 73, pp. 413–418. ASP, San Francisco, CA (1995) 35

242. Buss, R.H., Jr., Cohen, M., Tielens, A.G.G.M., Werner, M.W., Bregman, J.D., Witteborn, F.C., Rank, D., Sandford, S.A.: Astrophys. J. **365**, L23 (1990) 35
243. Koike, C., Wickramasinghe, N.C., Kano, N., Yamakoshi, K., Yamamoto, T., Kaito, C., Kimura, S., Okuda, H.: Mon. Not. R. Astron. Soc. **277**, 986 (1995) 35
244. Hill, H.G.M., Jones, A.P., d'Hendecourt, L.B.: Astron. Astrophys. **336**, L41 (1998) 35
245. Li, A.: Astrophys. J. **599**, L45 (2003) 35
246. Jiang, B.W., Zhang, K., Li, A.: Astrophys. J. **630**, L77 (2005) 35
247. Bussoletti, E., Fusco, C., Longo, G. (eds.): Experiments on cosmic dust analogues. In: Procedings of the Second International Workshop of the Astronomical Observatory of Capodimonte (OAC2), held at Capri, Italy, Septemper 8–12, 1987. Kluwer, Dordrecht (1988) 35
248. Greenberg, J.M.: Rensselaer Res. **5**(1) (1960) 36
249. Greenberg, J.M., Pedersen, N.E., Pedersen, J.C.: J. Appl. Phys. **32**, 233 (1961) 36
250. Giese, R.H., Siedentopf, H.: Z. Naturforsch. **17a**, 817 (1962) 36
251. Zerrull, R., Giese, R.H., Weiss, K.: Appl. Opt. **16**, 777 (1977) 36
252. Zerrull, R.H., Giese, R.H., Schwill, S., Weiss, K.: Scattering by particles of non-spherical shape. In: Schuerman, D.W. (ed.) Light Scattering by Irregularly Shaped Particles, pp. 273-282. Plenum Press, New York, NY (1980) 36
253. Gustafson, B.Å.S.: Optical properties of dust from laboratory scattering measurements. In: Gustafson, B.Å.S., Hanner, M.S. (eds.) Physics, Chemistry and Dynamics of Interplanetary Dust. ASP Conf. Ser. vol. 104, pp. 401–408. ASP, San Francisco, CA (1995) 36
254. Greenberg, J.M., van de Hulst, H.C. (eds.): Interstellar Dust and Related Objects. Proceedings IAU Symposium No. 52. Reidel, Dordrecht (1973) 37
255. Wickramasinghe, N.C., Morgan, D.J. (eds.): Solid State Astrophysics, Astrophysics and Space Science Library vol. 55. Reidel, Dordrecht (1976) 37
256. Huffman, D.R.: Astrophys. Space Sci. **34**, 175 (1975) 37
257. Huffman, D.R.: Pitfalls in calculating scattering by small particles. In: Allamandola, L.J., Tielens, A.G.D.M. (eds.) Interstellar Dust. Proceedings IAU Symposium No. 135, pp. 329–336. Kluwer, Dordrecht (1989) 37
258. Donn, B.: Experimental investigations relating to the properties and formation of cosmic grains. In: Nuth, J.A., III, Stencel, R.E. (eds.) Interrelationships Among Circumstellar, Interstellar, and Interplanetary Dust, pp. 109–134. NASA CP-2403 (1986) 37
259. Greenberg, J.M.: What are comets made of? A model based on interstellar dust. In: Wilkening, L.L. (ed.) Comets, pp. 131–163. University of Arizona Press, Tucson, AZ (1982) 38
260. Greenberg, J.M.: Occas. Rep. Roy. Obs. Edinb. **12**, 1 (1984) 38, 44
261. Jones, A.P.: The lifecycle of interstellar dust. In: Pendleton, Y.J., Tielens, A.G.G.M. (eds.) From Stardust to Planetesimals, pp. 97–106. ASP, San Francisco, CA (1997) 38, 39
262. Draine, B.T., Lee, H.M.: Astrophys. J. **285**, 89 (1984) 38
263. Greenberg, J.M.: The core-mantle model of interstellar grains and the cosmic dust connection. In: Allamandola, L.J., Tielens, A.G.D.M. (eds.) Interstellar Dust. Proceedings IAU Symposium No. 135, pp. 345–355. Kluwer, Dordrecht (1989) 40
264. Williams, D.A.: Grains in diffuse clouds: carbon-coated silicate cores. In: Allamandola, L.J., Tielens, A.G.D.M. (eds.) Interstellar Dust. Proceedings IAU Symposium No. 135, pp. 367–373. Kluwer, Dordrecht (1989) 40
265. Mathis, J.S., Whiffen, G.: Astrophys. J. **341**, 808 (1989) 40
266. Désert, F.J., Boulanger, F., Puget, J.: Interstellar dust models for extinction and emission. Astron. Astrophys. **237**, 215 (1990) 40
267. Sorrell, W.F.: Mon. Not. R. Astron. Soc. **243**, 570 (1990) 40
268. Rowan-Robinson, M.: Mon. Not. R. Astron. Soc. **258**, 787 (1992) 40
269. Siebenmorgen, R., Krügel, E.: Astron. Astrophys. **259**, 614 (1992) 40
270. Mathis, J.S.: Astrophys. J. **472**, 643 (1996) 40
271. Li, A., Greenberg, J.M.: Astron. Astrophys. **323**, 566 (1997) 40
272. Zubko, V.G., Smith, T.L., Witt, A.N.: Astrophys. J. **511**, L57 (1999) 40
273. Weingartner, J.S., Draine, B.T.: Astrophys. J. **548**, 296 (2001) 40

274. Zubko, V., Dwek, E., Arendt, R.G.: Astrophys. J. Suppl. Ser. **152**, 211 (2004) 40
275. Draine, B.T., Li, A.: Astrophys. J. **657**, 810 (2007) 40
276. Hong, S.S., Greenberg, J.M.: Astron. Astrophys. **70**, 695 (1978) 40
277. Dorschner, J.: Rev. Mod. Astron. **6**, 117 (1992) 40
278. Perryman, M.: Rep. Prog. Phys. **63**, 1209 (2000) 38
279. Schneider, J.: The extrasolar planets encyclopaedia. http://www.obspm.fr/encycl/encycl.html 38
280. Jäger, C., Fabian, D., Schrempel, F., Dorschner, J., Henning, Th., Wesch, W.: Astron. Astrophys. **401**, 57 (2003) 38
281. Demyk, K., d'Hendecourt, L., Jones, A., Leroux, H., Carrez, Ph., Cordier, P.: Laboratory studies of the ion-irradiation of dust analogs: application to the evolution of interstellar silicates. In: Witt, A.N., Clayton, G.C., Draine, B.T. (eds.) Astrophysics of Dust. ASP Conf. Ser. vol. 309, pp. 649–663. ASP, San Francisco, CA (2004) 38
282. Anders, E.: Annu. Rev. Astron. Astrophys. **9**, 1 (1971) 38
283. Anders, E.: Philos. Trans. R. Soc. Lond. **A323**, 287 (1987) 41
284. Anders, E., Zinner, E.: Meteoritics **28**, 490 (1993) 41
285. Zinner, E.: Presolar material in meteorites: an overview. In: Bernatowicz, T.J., Zinner, E.K. (eds.) Astrophysical Implications of the Laboratory Study of Presolar Materials. CP-402, pp. 3–57. American Institute of Physics, New York, NY (1997) 41
286. Suess, H.E., Urey, H.C.: Phys. Rev. **28**, 53 (1956) 41, 42
287. Burbidge, E.M., Burbidge, G.R., Fowler, W.A., Hoyle, F.: Rev. Mod. Phys. **29**, 547 (1957) 41
288. Cameron, A.G.W.: Chalk River Rep. AECL, CRL-41, Atomic Energy of Canada, Ltd., Chalk River (1957) 41
289. Clayton, D.D.: Quart. J. R. Astron. Soc. **23**, 174 (1982) 41
290. Clayton, D.D.: Meteoritics **27**, 5 (1992) 41, 42
291. Reynolds, J.H., Turner, G.: J. Geophys. Res. **69**, 3263 (1964) 41
292. Black, D.C., Pepin, R.O.: Earth Planet. Sci. Lett. **6**, 395 (1969) 42
293. McKee, C., Ostriker, J.P.: Astrophys. J. **218**, 148 (1977) 42
294. Martin, P.G.: Astrophys. J. **445**, L63 (1995) 42
295. Bernatowicz, T., Fraundorf, G., Ming, T., Anders, E., Wopenka, B., Zinner, E., Fraundorf, P.: Nature **330**, 728 (1987) 44
296. Amari, S., Anders, E., Viraq, A., Zinner, E.: Nature **345**, 238 (1990) 43
297. Bernatowicz, T.J., Amari, S., Zinner, E.K., Lewis, R.S.: Astrophys. J. **373**, L73 (1991) 43
298. Hutcheon, I.D., Huss, G.R., Fahey, A.J., Wasserburg, G.J.: Astrophys. J. **425**, L97 (1994) 43
299. Nittler, L.R., Hoppe, P., Alexander, C.M.O'D., et al.: Astrophys. J. Lett. **453**, L25 (1995) 43
300. Nittler, L.R., Alexander, C.M.O'D., Gao, X., Walker, R.M., Zinner, E.: Astrophys. J. **483**, 457 (1997) 43
301. Choi, B.G., Wasserburg, G.J., Huss, G.R.: Astrophys. J. **522**, L133 (1999) 43
302. Nittler, L.R., Alexander, C.M.O'D.: Lunar Planet. Sci. **30**, Abstr. 2041 (1999) 43
303. Bradley, J.P.: Science **265**, 925 (1994) 43
304. Messenger, S., Keller, L.P., Walker, R.M.: Lunar Planet. Sci. **33**, Abstr. 1887 (2002) 43
305. Vollmer, Ch., Hoppe, P., Brenker, F.E., Holzapfel, Ch.: Astrophys. J. **666**, L49 (2007) 43
306. Hoppe, P., Vollmer, Ch.: Presolar silicates in meteorites and interplanetary dust particles. In: IXth Torino Workshop on Evolution and Nucleosynthesis in AGB Stars and IInd Perugia Workshop on Nuclear Astrophysics, AIP Conference Proceedings **1001**, pp. 254–261 (2008) 44
307. Greenberg, J.M.: From interstellar dust to comets. In: Delsemme, A. (ed.) Comets, Asteroids and Meteorites, pp. 491–497. University of Toledo, Toledo, OH (1977) 44
308. Grün, E., Srama, R., Krüger, H., Kempf, S., Dikarev, V., Helfert, S., Moragas-Klostermeyer, G.: Icarus **174**, 1 (2005) 44
309. Grün, E., Srama, R., Helfert, S., Kempf, S., Moragas-Klostermeyer, G., Rachev, M., Srowik, A., Auer, S., Horanyi, M., Sternovsky, Z., Harris, D.: Dust in Planetary Systems. Proceeding Conference Kaua'i, Hawaii LPT Contr. No. 1280, p. 61 (2005) 44
310. Grün, E., Zook, H.A., Baguhl, M., et al.: Nature **362**, 428 (1993) 44

311. Grün, E., Gustafson, B., Mann, I., Baguhl, M., Morfill, G.E., Staubach, P., Taylor, A., Zook, H.A., et al.: Astron. Astrophys. **286**, 915 (1994) 44
312. Landgraf, M., Baggaley, W.J., Grün, E., Krüger, H., Linkert, G.: J. Geophys. Res. **105**(A5), 10343 (2000) 44
313. Grün, E., Srama, R., Altobelli, N., et al.: Exp. Astron. **23**, 981 44
314. Brownlee, D., Tsou, P., Aléon, J., et al.: Science **314**, 1711 (2006) 45
315. Taylor, A.D., Baggaley, W.J., Steel, D.I.: Nature **380**, 323 (1996) 45
316. Baggaley, W.J., Bennett, R.G.T., Steel, D., Taylor, A.D.: Quart. J. R. Astron. Soc. **35**, 293 (1994) 45
317. Meisel, D.D., Janches, D., Mathews, J.D.: Astrophys. J. **567**, 323 (2002) 45
318. Weryk, R.J., Brown, P.: Earth Moon Planets **95**, 221 (2004) 45
319. Baggaley, W.J., Marsh, S.H., Close, S.: Dust in Planetary Systems. Proceeding Conference Kaua'i, Hawaii ESA SP-643, p. 27 (2007) 45
320. Dubinin, M., Soberman, R.K.: Planet. Space Sci. **39**, 1573 (1991) 45
321. Baggaley, W.J.: J. Geophys. Res. **105**(A5), 10353 (2000) 45
322. Krivova, N.A., Solanki, S.K.: Astron. Astrophys. **402**, L5 (2003) 45
323. Krivov, A.V., Krivova, N.A., Solanki, S.K., Titov, V.B.: Astron. Astrophys. **417**, 341 (2004) 45
324. Dorschner, J., Gürtler, J., Henning, Th.: Steps toward interstellar silicate dust mineralogy. In: Tielens, A.G.G.M., Allamandola, L.J. (eds.) Interstellar Dust. Contributed Papers, pp. 369–370. NASA CP-3036 (1989) 45
325. Tielens, A.G.G.M.: Towards a circumstellar silicate mineralogy. In: Mennessier, M.O., Omont, A. (eds.) From Miras to Planetary Nebulae, pp. 186–200. Edition Frontieres, Gif sur Yvette (1990) 46
326. Nickel, E.N., Grice, J.D.: The IMA Commission on New Minerals and Mineral Names: Procedures and Guidelines on Mineral Nomenclature (1998) 46
327. Nickel, E.N.: Can. Mineral. **33**, 689 (1995) 46, 47, 48, 49
328. Tamanai, A., Mutschke, H., Blum, J., Meeus, G.: Astrophys. J. **648**, L147 (2006) 46
329. Gielen, C., Van Winckel, H.: Baltic Astron. **16**, 148 (2007) 46
330. Jena-Vienna Stardust Mineralogy Collaboration (Dorschner, J., Fabian, D., Jäger, C., Kerschbaum, F., Posch, Th.): Astron. Nachr. **324**(Suppl. 2), 74–75 (2003) 47
331. Van Winckel, H.: Post-AGB stars. Annu. Rev. Astron. Astrophys. **41**, 391–427 (2003) 50
332. Apai, D., Pascucci, I., Bouwman, J., Natta, A., Henning, Th., Dullemond, C.P.: Science **310**, 834 (2005) 50

Formation and Evolution of Minerals in Accretion Disks and Stellar Outflows

H.-P. Gail

Abstract The contribution discusses dust formation and dust processing in oxygen-rich stellar outflows under non-explosive conditions, and in circumstellar discs. The main topics are calculation of solid-gas chemical equilibria, the basic concepts for calculating dust growth under non-equilibrium conditions, dust processing by annealing and solid diffusion, a discussion of non-equilibrium dust formation in stellar winds, and in particular a discussion of the composition and evolution of the mineral mixture in protoplanetary accretion discs. An overview is given over the data on dust growth, annealing, and on solid diffusion for astrophysically relevant materials available so far from laboratory experiments.

1 Introduction

The existence of dust particles in the interstellar medium is known since nearly a century. Since the end of the 1960s we also know of the existence of dust in circumstellar shells around certain highly evolved stellar types that form dust in their stellar outflows, and at the end of the 1980s the first dusty circumstellar discs around young stellar objects have been detected. A lot of observational efforts have been undertaken since the beginning to establish the nature and composition of the dust in these different environments and remarkable progress has been achieved on the observational side (cf. Molster et al., this book), especially since infrared observations from satellites became available.

Parallel to the observational work a lot of theoretical efforts have been undertaken to explain the formation of dust particles and their composition and properties in interstellar space and in circumstellar environments. The success of the theoretical analysis has always been meagre, however, since this problem turned out to be particular difficult and unintelligible because of a complex interplay between a lot of different chemical, physical and mineralogical processes, most of which are

H.-P. Gail (✉)
Institute for Theoretical Astrophysics, Center for Astronomy, University of Heidelberg, Albert-Überle-Str. 2, 69120 Heidelberg, Germany
e-mail: gail@ita.uni-heidelberg.de

Gail, H.-P.: *Formation and Evolution of Minerals in Accretion Disks and Stellar Outflows*. Lect. Notes Phys. **815**, 61–141 (2010)
DOI 10.1007/978-3-642-13259-9_2

not well understood even under laboratory conditions. So presently we do not have a really complete picture of the processes that are responsible for dust formation, growth, and processing, and of the processes that ultimately determine the chemical composition and mineralogical structure of cosmic dust.

Some details of the general problem of dust formation and its chemical and mineralogical evolution, especially in protoplanetary discs, can already be solved, however. By laboratory investigations of dust-related processes by a number of groups, many phenomenological coefficients entering the basic equations for calculating formation, destruction, and chemical and physical processing of dust grains have been experimentally determined during the last two decades. Most of these investigations had the main purpose to study processes relevant for processing meteoritic material in the early Solar System, but the results can immediately be carried over to processes in the gas-dust-mixtures of protoplanetary accretion discs and of circumstellar dust shells. This allows to put theoretical calculations of dust formation and processing now on a much firmer basis than this was possible in the past. This contribution gives an overview over some of the major problems encountered in calculating compositions and properties of cosmic mineral mixtures and how this problem can be tackled.

2 Dust-Forming Objects and Their Element Abundances

Dust formation in cosmic environments is generally associated with phases of severe mass loss during late stages of stellar evolution or with stellar explosions. In the cooling outflow of stellar winds or of expelled mass shells, conditions become favourable for condensation of the heavy element content of the gas phase into solid particulates. During most of the life time of a star, with only minor exceptions, its photospheric element abundances reflects the standard cosmic element abundances of the interstellar matter at the time and location of birth of the star within a molecular cloud. The surface element abundances change if the stars evolve off from the main sequence and enter advanced stages of their evolution for two reasons:

(1) In low- and intermediate-mass stars, convective mixing between the nuclear burning interior and the stellar photosphere carries some fraction of the freshly synthesized heavy nuclei from the centre to the surface (cf. Herwig [1]). In rapidly rotating hot stars some mixing from the central region to the photosphere occurs by circulation currents.
(2) In evolved massive stars surface abundances change because the outer stellar zones are peeled off by massive stellar winds and initially deeply embedded zones are exposed to the surface which have formerly been subject to nuclear burning processes.

Dust formation in highly evolved stars, thus, may and in fact often does occur in matter with a composition considerably different from the standard cosmic element abundance.

Matter with unusual chemical composition also is expelled during nova and supernova explosions. Dust formation is observed to occur also in such environments, but the present contribution does not consider dust formation in element mixtures and environments originating from explosive processes.

As long as dust-forming stars show the standard cosmic element mixture in their photosphere, they mainly form silicate dust in their stellar outflows. With progressive change of the surface element mixture they start to form completely different dust mixtures. The best known example is the change of spectral type from M over S to C for stars of low and intermediate mass (initial mass $M \lesssim 8\mathrm{M}_{\odot}$) during their evolution on the thermally pulsing AGB. This results from the mixing of freshly produced carbon from He burning in the core region to the surface after each pulse. The change in chemistry and spectral type from being oxygen rich for M stars to carbon-rich for C stars is accompanied by a drastic change of the dust manufacturing processes, that turn from silicate to soot production.

Similarly, drastic changes of the elemental composition of stellar outflows occur for other types of stars. Such changes of the element mixture also result in drastic, but less well known, changes in the composition of the dust mixture formed in the outflow.

Table 1 lists the abundances of a number of elements, which may be important in some way or the other for the dust formation process, for different element mixtures appearing during different stages of non-explosive stellar evolution at the stellar surface. These are:

1. M stars on the AGB. Reduced C and slightly reduced O abundance, enhanced N abundance due to first and second dredge up of CNO processed material. Gradually increasing C abundance and increased *s*-Process element abundances after onset of thermal pulsing.
2. C stars on the AGB. Carbon enriched by third dredge up of products of He burning. Strongly increased abundances of *s*-Process elements.
3. CNO processed material. Material exposed by massive stellar winds of massive stars. C and O abundance strongly reduced, in advanced stages reduced below the abundances of Si, Mg, and Fe, strongly enhanced N (cf. Fig. 2). In its extreme form the material is (nearly) free of H which has been converted into He. Such material is encountered in Luminous Blue Variables and WN stars.
4. Products of He burning. If formerly H burning outer layers are peeled off by massive stellar winds of massive stars. Nearly pure He, C, and O, and some Ne (cf. Fig. 2). This material is encountered in WC stars and in the rare R Cor B stars (borne again AGB-stars).
5. Solar system abundances are shown for comparison in Table 1.

The abundances of the elements between Ne and the iron peak are essentially unchanged in these element mixtures since temperatures during H and He burning are insufficient for processing elements with nuclear charge $Z > 10$.

The dust formed from these different element mixtures has quite different chemical compositions. In mixtures (1) and (2) of Table 1 the standard silicate and carbon dust mixtures, respectively, are formed that are usually observed in circumstellar

Table 1 Estimated elemental abundances for the more important dust-forming stars with non-explosive mass ejection. Abundances for AGB stars are for models with $2\,M_\odot$, for massive stars for a model with $60\,M_\odot$ ($Z = 0.02$ in both cases). The abundances are particle densities with respect to the total particle density. The carbon-rich mixture on the AGB essentially equals the oxygen-rich one except for the indicated enhancements. The abundances of the elements heavier than Ne essentially equal solar system abundances in all cases

Element	AGB M-star	AGB C-star	CNO processed	He burning	Solar system
H	9.07×10^{-1}		4.34×10^{-1}	Consumed	9.09×10^{-1}
He	9.15×10^{-2}		5.66×10^{-1}	8.59×10^{-1}	8.89×10^{-2}
C	2.17×10^{-4}	$1 \ldots 2 \times \epsilon_O$	2.23×10^{-5}	1.22×10^{-1}	3.23×10^{-4}
N	1.91×10^{-4}		1.17×10^{-3}	Destroyed	8.49×10^{-5}
O	6.54×10^{-4}		2.95×10^{-5}	1.27×10^{-2}	6.74×10^{-4}
Ne	1.07×10^{-4}		1.07×10^{-4}	5.68×10^{-3}	1.07×10^{-4}
Mg					3.50×10^{-5}
Al					2.75×10^{-6}
Si					3.23×10^{-5}
S					1.69×10^{-5}
Ca					1.99×10^{-6}
Ti					7.82×10^{-8}
Fe					2.94×10^{-5}
Ni					1.62×10^{-6}
Zr		$\ldots 100\times$			3.72×10^{-10}
No.	(1)	(2)	(3)	(4)	(5)

References: (1) Boothroyd and Sackmann [2], Schaller et al. [3] (3)+(4): Meynet et al. [4] (5): Anders and Grevesse [5], Grevesse and Noels [6].

shells of AGB stars or Red Supergiants. In the transition case of S stars with $\varepsilon_C \approx \epsilon_O$ neither silicates nor carbon dust can be formed since C and O are blocked in the CO molecule. Some unusual type of dust is formed in this case (discussed in Sect. 6.1). From mixture (3) of Table 1 also unusual dust will be formed since only insufficient amounts of C and O are present for silicate or carbon dust formation, like in S stars. From mixture (4) carbon dust is formed, but its properties may be different from carbon dust in AGB star shells because the lack of H requires a different formation mechanism in this case.

The element abundances determined from analysis of stellar atmospheres show some scatter and a systematic variation with metallicity. The numbers given in Table 1 are only typical values for Pop I stars. These are subject to some variations in individual objects. In most cases this has no implications for the dust mixture that is formed, except for the case of the Mg/Si abundance ratio that is critical for the composition of the silicate dust mixture observed in part of the dust forming objects. Figure 1 shows this ratio as determined for several hundred stars from the solar vicinity. The most recent Solar System value is Mg/Si = 1.047 (Lodders et al. [8]), which exceeds unity. The scattering of observed values is significantly higher and part of the dust forming objects in space may have abundance ratios Mg/Si < 1, resulting in a somewhat different mineral mixture than for Mg/Si > 1.

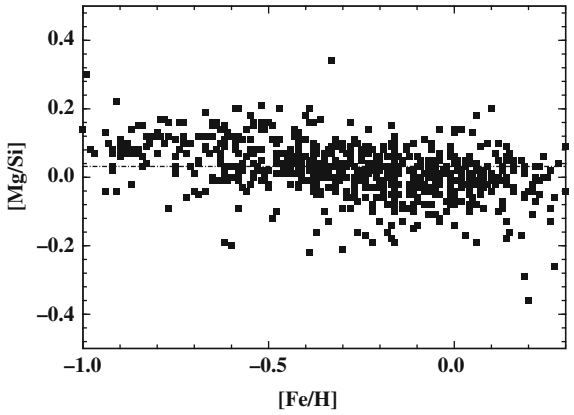

Fig. 1 Variation of the Mg/Si abundance ratio with metallicity for F and G dwarf stars from the solar vicinity. Data from Soubiran and Girard [7]

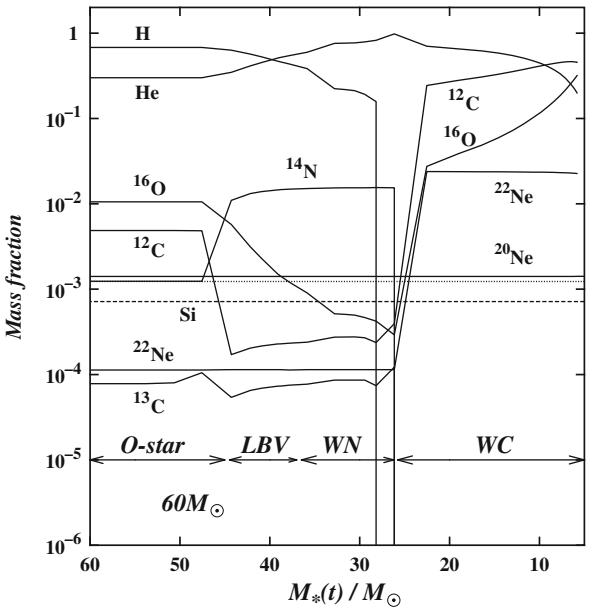

Fig. 2 Evolution of the surface abundances of a massive star with an initial mass of 60 $M_\odot$ on the main sequence due to mass loss (without rotation) according to Meynet et al. [4]. The mass scale $M_*(t)$ is the residual mass of the star. Indicated are the evolutionary stages where the surface abundances approximately correspond to the abundances of O-stars, LBV's, WN-, and WC-stars, respectively. The *dashed line* shows the initial abundance of the dust-forming element Si. The *dotted line* is the lower limit for the oxygen abundance where normal silicate dust can be formed

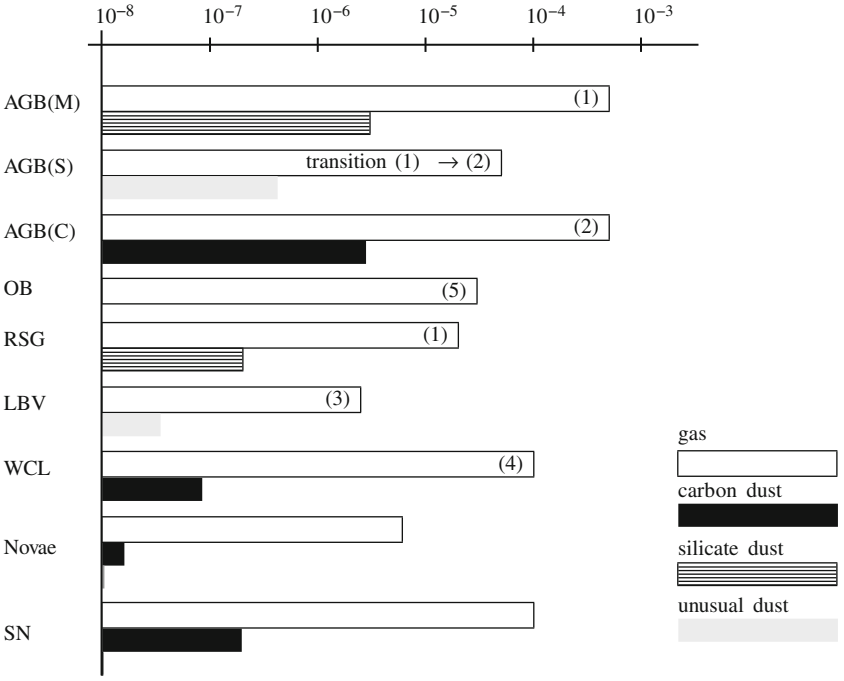

Fig. 3 Gas and dust injection rates (in $M_\odot$ kpc^{-2} a^{-1}) into the interstellar medium by the different stellar sources (data from Tielens [9]; Zhukovska et al. [10]). Stars produce mainly silicate or carbon dust; only in some cases a different kind of dust material is formed, probably iron or some iron alloy (unusual dust). Additionally, several minor dust components from less abundant elements are formed. The abbreviations for the dust sources are: AGB = asymptotic giant stars of spectral type M, S, or C, OB = massive stars on the upper main sequence, RSG = red supergiants, LBV = Luminous Blue Variables, WCL = Wolf-Rayet stars of spectral type WC8-11. The different compositions of the dust mixture formed in the different dust forming objects are simplified to the three basic types "silicate", "carbon", and "unsual". The numbers refer to the element mixtures in Table 1

Figure 2 shows how mixtures (3) and (4) occur during the course of stellar evolution of massive stars, and Fig. 3 presents a brief overview over the dust forming stellar types and the different kinds of dust produced in the different objects.

3 Equilibrium Condensation

Calculation of chemical equilibrium compositions of solid-gas-mixtures is an important tool for studying dust formation in space. Though in most dust-forming objects the gas-dust-mixture is not in a state of chemical equilibrium, the calculation of the hypothetical equilibrium state yields information on the most stable condensates probably existing in the element mixture under consideration and helps to find out the dust species that can be expected to exist in that environment. This concept

has been applied successfully to dust formation problems in circumstellar shells and accretion discs.

3.1 Theory: Pure Substances

The problem of determining the chemical equilibrium between several species in a mixture with given total pressure p and temperature T and a given total number of moles of the elements is a standard problem of thermodynamics, which is treated in almost every textbook. It is shown that for this problem the equilibrium state corresponds to the minimum of the Gibbs function $G(p, T, n_i)$ with respect to the variations of the mole fractions n_i of all gaseous and solid species i which may be formed from the elements contained in the system. Liquids usually need not to be considered in accretion discs and circumstellar shells because sublimation temperatures are generally below the melting point because of low pressures.

First, we consider, with respect to the possible solid phases, only *pure* substances, i.e., substances for which their composition can be characterized by a chemical formula for a stoichiometrically composed chemical compound. The case that solid materials are composed of more than one pure substance (solid solutions, alloys, incorporation of impurities) is considered later.

In thermodynamics it is shown (e.g. Atkins [11]; Smith and Missen [12]) that a chemical reaction of the type

$$i\mathrm{A} + j\mathrm{B} + k\mathrm{C} + \ldots \longrightarrow l\mathrm{D} + m\mathrm{E} + n\mathrm{F} + \ldots \tag{1}$$

between reactants A, B, C, ... with products D, E, F, ...[1] is in equilibrium if the following relation holds

$$\sum_i \nu_i \mu_i = 0. \tag{2}$$

The ν_i in (2) are the stoichiometric coefficients i, j, ... in (1) that are usually taken to be positive for the products and negative for the reactants. The μ_i are the chemical potentials of species i defined by

$$\mu_i = \left(\frac{\partial G}{\partial n_i} \right)_{p,T}. \tag{3}$$

[1] If necessary, other phases than gaseous ones are indicated by "s" for solids or "l" for liquid. In the present contribution we indicate this by adding a corresponding label in brackets after the chemical formula. E.g., the reaction corresponding to the sublimation of solid iron is written as follows: Fe(s) → Fe. Here Fe(s) denotes solid iron and Fe iron atoms in the gas phase

For astrophysical applications one is interested in most cases only in the special case of formation of some molecular compound or solid phase from free atoms in the gas phase. We consider only this case.

For an ideal mixture the Gibbs function is given by

$$G(p,T,n_j) = \sum_i n_i G_i(p,T) \tag{4}$$

where $G_i(p,T)$ is the partial free enthalpy of one mole of species i at temperature T and pressure p, which equals the chemical potential μ_i in this case. We denote by $\mu_0 = \mu(p_0,T)$ the chemical potential at temperature T and at standard pressure p_0 of one bar. The equilibrium condition (2) can then be written as

$$\sum_i \nu_i \left(\mu_i - \mu_{0,i}\right) = -\sum_i \nu_i G_i(p_0,T). \tag{5}$$

One defines the activity a_i of component i by

$$RT \ln a_i = \mu_i(p,T) - \mu_i(p_0,T), \tag{6}$$

with R being the gas constant. Then (5) may be written as

$$\sum_i \nu_i \ln a_i = -\Delta G/RT, \tag{7}$$

where

$$\Delta G = \sum_i \nu_i G_i(p_0,T). \tag{8}$$

3.1.1 Equilibrium Conditions for Gases and Solids

Consider a mixture of ideal gases and solids at the rather low pressures in circumstellar shells or protoplanetary accretion discs. The activities can be determined from the thermodynamic relation (see Atkins [11])

$$\partial G/\partial p = V\ . \tag{9}$$

Ideal gases: For n moles of an ideal gas at pressure p we substitute at the r.h.s. of Eq. (9) the equation of state $pV = nRT$ and integrate from p_0 to p

$$G(p,T) = G(p_0,T) + nRT \ln p/p_0\ . \tag{10}$$

From definition (3) we obtain for the pressure dependence of the chemical potential of an ideal gas

$$\mu(p, T) = \mu(p_0, T) + RT \ln p/p_0 \tag{11}$$

and from definition (6) for the activity of an ideal gas:

$$a = p/p_0 \quad \text{(ideal gas)}. \tag{12}$$

Solids: For n moles of a solid we have to substitute nV_{mol} at the r.h.s. of Eq. (9), where V_{mol} is the molar volume of the solid. In the low pressure regime for solids (pressure lower than ≈ 1 kbar) V_{mol} can be considered to be constant which yields

$$G(p, T) = G(p_0, T) + nV_{\text{mol}}\,(p - p_0) \tag{13}$$

and Eq. (3) shows

$$\mu(p, T) = \mu(p_0, T) + V_{\text{mol}}\,(p - p_0)\ . \tag{14}$$

The molar Gibbs function $G(p_0, T)$ of a solid is typically of the order of several hundred kJ/mole, while the product $V_{\text{mol}}\,(p - p_0)$ is of the order of only a few J/mol at low pressures. The p-V-work can be completely neglected in this case and (6) shows

$$a = 1 \quad \text{(pure solids)}\ . \tag{15}$$

At pressure low enough that solids can be considered as being essentially incompressible, the activities a_i of pure solids equal unity.

Law of mass-action: The equilibrium condition (7) for a chemical reaction involving gaseous species and condensed phases then reads as follows

$$\prod_{\substack{i \\ \text{all gases}}} \left(\frac{p_i}{p_0}\right)^{\nu_i} \prod_{\substack{i \\ \text{all solids}}} a_i^{\nu_i} = \mathrm{e}^{-\Delta G/RT}. \tag{16}$$

Equation (16) is the well-known law of mass action for heterogeneous reactions that involve gases and solid phases.

We need two special cases: If a molecule of composition $\mathrm{A}_i\mathrm{B}_j\mathrm{C}_k\ldots$ is formed from the free atoms A, B, C, ... from the gas phase, then according to (16) its partial pressure in chemical equilibrium is

$$p_{\mathrm{A}_i\mathrm{B}_j\mathrm{C}_k\ldots} = p_{\mathrm{A}}^i p_{\mathrm{B}}^j p_{\mathrm{C}}^k \ldots \mathrm{e}^{-\Delta G/RT} \quad \text{(for molecules)}, \tag{17}$$

where all pressures are in units of the standard pressure $p_0 = 1$ atm. If a solid with composition $\mathrm{A}_i\mathrm{B}_j\mathrm{C}_k\ldots$ is formed from the free atoms A, B, C, ... from the gas phase it is in chemical equilibrium with the gas phase if

$$a_{\mathrm{A}_i\mathrm{B}_j\mathrm{C}_k\ldots} = p_{\mathrm{A}}^i p_{\mathrm{B}}^j p_{\mathrm{C}}^k \ldots \mathrm{e}^{-\Delta G/RT} = 1 \quad \text{(for solids)}. \tag{18}$$

While for gas phase species Eq. (17) yields the partial pressure of a molecule in terms of the partial pressures of free atoms of the elements that form the molecule, for solids the corresponding Eq. (18) does not provide direct information on the abundances of the solids in the mixture. Instead it defines for each solid a condition for the partial pressures of the free atoms which has to be satisfied if the solid exists in equilibrium with the gas phase.

If we start with some arbitrary initial state of a solid gas-mixture and if there is chemical equilibrium between all the gas phase species, then the partial pressures of the free atoms $p_{\rm A}$, $p_{\rm B}$, $p_{\rm C}, \ldots$ can readily be determined for this state. The quantities $a_{{\rm A}_i{\rm B}_j{\rm C}_k\ldots}$ calculated from Eq. (18) can take any of the values $a > 1$, $a = 1$, or $a < 1$ if the solids are not in chemical equilibrium with the gas phase.

If we have $a > 1$ for some solid phase in the mixture, the number of moles of this solid in the mixture can be increased by condensing material from the gas phase into this solid until the associated reduction of the partial pressures of the gas phase species decreases the value of a determined by the l.h.s. of Eq. (18) to unity, from which point on the solid would be in equilibrium with the gas phase.

If we have $a < 1$ for some solid this solid can vaporise or can decompose by reactions with gas phase species until (i) either the solid disappears from the mixture or (ii) the associated increase of the partial pressures of the gas phase species increases a to unity, from which point on the solid exists in chemical equilibrium with the gas phase.

This shows: In a state of chemical equilibrium we have

- $a = 1$ for each of the solids present in the gas-solid-mixture, or
- $a < 1$ for all solids which do not exist in this mixture.

3.1.2 Constraints Set by Element Abundances

The partial pressures of the free atoms in a mixture and the fraction of the elements condensed into solids are determined by the element abundances ε_k in the mixture. Here and in the following we assume that abundances ε are given relative to hydrogen. For each solid one defines a degree of condensation f_j, for instance as the fraction of the least abundant of the elements forming this solid, which actually is condensed into the solid.[2] If a solid is present in the mixture then $f_j > 0$ and the corresponding a_j equals unity. If it is absent from the mixture then $f_j = 0$ and $a_j < 0$. For each element k one has the following condition for the partial pressures of the molecules and the condensation degrees f_j of solids containing element k

[2] For instance, for $MgSiO_3$ the least abundant of the elements Mg, Si, and O in the cosmic element mixture is Mg. Then it would be appropriate to chose Mg as the reference element for defining a degree of condensation. However, because of a similar abundance of Mg and Si, an equally appropriate choice for the reference element would be Si. Generally the choice of a reference element for defining condensation degrees is to some extent arbitrary and one can chose that one which is the most convenient for the problem under consideration.

$$\varepsilon_k P_{\mathrm{H}} - \sum_{\substack{\text{all solids } j \\ \text{with element } k}} \nu_{j,k} f_j \varepsilon_{j,\mathrm{ref}} P_{\mathrm{H}} = \sum_{\substack{\text{all molecules } i \\ \text{with element } k}} \nu_{i,k} p_i, \tag{19}$$

in order to satisfy the condition set by the abundance of the element in the mixture (stoichiometric conditions). P_{H} is the fictitious partial pressure of all H nuclei if they where present as free atoms.[3] On the l.h.s. the quantity $\varepsilon_{j,\mathrm{ref}}$ denotes the abundance of the element with respect to which the degree of condensation f_j of solid species j is defined, and $\nu_{j,k}$ the number of atoms of element k per atom of the key element of species j.[4] The quantity $\nu_{i,k}$ at the r.h.s. are the number of atoms of element k contained in molecule i.

For the molecules one introduces the law of mass-action, Eq. (17), into the r.h.s. of (19). If there are totally K elements in the mixture from which L solids might be formed, one has a system formed by the K (19) and the L equations (18) for the K partial pressures of the free atoms and the L degrees of condensation of the solids. A solution of this system has to be found in such a way that for each of the solids either $a = 1$ and $f > 0$ or $f = 0$ and $a < 1$.

3.1.3 Minimizing the Gibbs Function

For given p and T in chemical equilibrium the Gibbs free enthalpy

$$G = \sum_i n_i \mu_i \tag{20}$$

takes its absolute minimum subject to the constraints

$$\sum_i n_i \nu_{ik} = n_k, \tag{21}$$

where μ_i is the chemical potential of species i, n_i its number of moles in the mixture, ν_{ik} the number of atoms of element k in species i and n_k the number of moles of the elements k forming the mixture. The composition of a mixture can also be determined by solving this minimization problem. Algorithms for solving the set of equations are described in detail in Smith and Missen [12].

[3] In case of element mixture No. 4 of Table 1 one has to use He as reference element for definition of abundances ε. The modifications required to all equations in that case are obvious.

[4] For example: If j refers to Al_2O_3 (corundum) and we define the degree of condensation f for corundum with respect to Al, and if k refers to oxygen, then one has in the contribution from corundum to the l.h.s of the equation for oxygen $\nu_{j,k} = 3/2$, since in the chemical formula there is 1.5 oxygen atom per aluminium atom. In the contribution to the equation for Al one has $\nu_{j,k} = 1$ because Al is the reference element for corundum.

3.2 Sources of Data

The free enthalpy ΔH_f° of formation of one mole of a substance in the standard state (usually $T = 298.15\,\mathrm{K}$ and $p = 1\,\mathrm{bar}$) from the elements in their reference states and the entropy S° can be obtained from a number of compilations. From these data

$$\Delta G_f^\circ = \Delta H_f^\circ - T S^\circ \tag{22}$$

is calculated for a substance and for the free atoms from which it is formed. The ΔG for the formation of the substance from free atoms follows by (8).

Extensive tabulations for ΔH_f° and S° are the JANAF tables[5] (Chase [13], Barin [14] and Saxena et al. [15]) which cover all the data presently needed for calculations of gas-solid-mixtures in circumstellar shells and protoplanetary accretion discs. Additional data on solids may be found in Kubaschewski and Alcock [16]. Convenient polynomial approximations for the temperature dependence of ΔG for the formation of many solids and gases of astrophysical interest from free atoms are published in Sharp and Huebner [17].

3.3 Solution of the Problem

The problem can be solved numerically in different ways. For pure molecular equilibria this is a standard problem of stellar physics. The calculation of complex solid-gas-mixtures, however, is a rather new problem for astrophysics, which only recently came up in the context of modelling Brown Dwarf atmospheres and protostellar accretion discs. In planetary physics and in the context of laboratory investigations of meteorites, the problem of calculating the composition of solid-gas-mixtures in matter with a cosmic element mixture has been studied already much earlier (Grossman [18]). The method of choice depends on the degree of information required. General multi-purpose methods for calculating equilibria in gas-solid-mixtures are mostly based on the minimization of the Gibbs free energy function $G(P, T, n_j)$ of the whole mixture (cf. Sect. 3.1.3). Such methods are extensively described in Smith and Missen [12]. A brief description of the Gibbs energy minimization method is also given in Saxena et al. [15]. Such methods are to be preferred for complex mixtures where a big number of solids have to be checked for their possible condensation.

In many astrophysical problems one only needs to know the most abundant condensates either because only these are of importance, for instance for the purpose of model calculations for accretion discs or circumstellar shells, or because less abundant solid components are (presently) not observable. Some preliminary information on the possible condensates can readily be obtained by first assuming no

[5] also available at: `http://webbook.nist.gov/chemistry/form-ser.html`

condensates to be present and calculating the molecular composition of the gas phase. The partial pressures of the free atoms taken from this solution can be used to calculate the quantities a by means of (18). If the resulting numerical values of a satisfy $a < 1$, the corresponding solids cannot be formed. If they satisfy $a \geq 1$, they may condense and the solids with the highest values of $a \geq 1$ are the possible candidates for condensation.

Figure 4 shows an example of such a calculation for solar system abundances (cf. Table 1) for a sequence of temperatures and a fixed total pressure of $P = 5 \times 10^{-9}$ bar representative for the dust formation zone of stellar winds (cf. Fig. 5). Obviously solid Fe, forsterite Mg_2SiO_4 and enstatite $MgSiO_3$ are the possible candidates for condensation. Enstatite will form despite of its lower activity because olivine alone cannot take up all the available Si and Mg in the standard cosmic element mixture. Other Si bearing compounds will not be formed because of low activities. At about 700 K the activity of FeS becomes higher than the activity of solid Fe. At low temperatures part of the Fe will take up all the available S.

Of course, such preliminary conclusions require verification by explicit calculations of equilibrium compositions. Such qualitative considerations are helpful, however, to isolate from the vast number of possible candidates for condensation the few ones that are likely candidates.

Another possibility is to determine in advance the stability limits of the condensates (cf. Fig. 5), for instance by the kind of considerations in Gail [19], Gail and Sedlmayr [20], Sharp and Wasserburg [21]. Then for each particular P-T-combination one knows the mixture of solids present in this state and one knows the particular system of equations which has to be solved for this state. This is useful for model calculations where equilibria have to be calculated for a very big

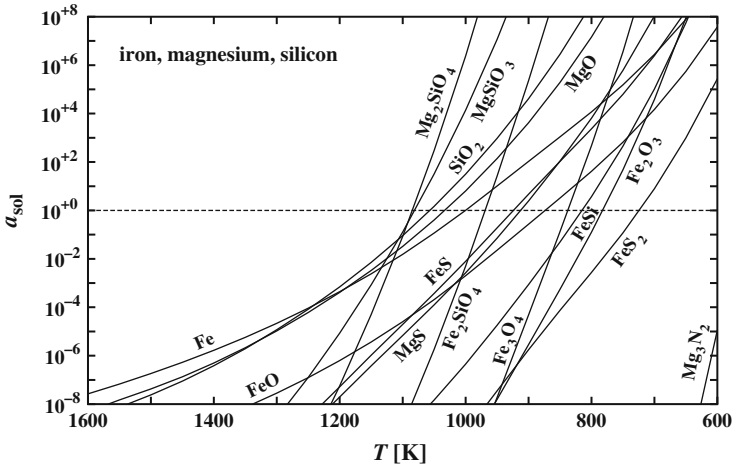

Fig. 4 Pseudo-activities a for a number of solid Si-Mg-Fe compounds calculated from (18) for a sequence of temperatures and a pressure of $P = 5 \times 10^{-9}$ bar representative of the dust formation zone in stellar winds

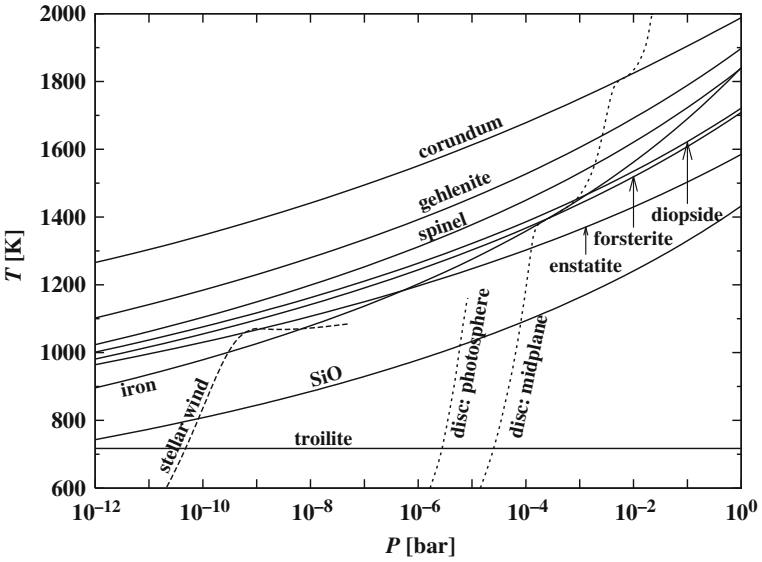

Fig. 5 Stability limits in the $P - T$ plane of the minerals formed by the most abundant refractory elements Si, Mg, Fe, Al, Ca and of Ti and Zr in a Solar System element mixture. The *dotted lines* are $P - T$ trajectories corresponding to a stellar wind (*left*) of an AGB-star with a mass-loss rate of $10^{-5}\,\mathrm{M}_\odot\,\mathrm{year}^{-1}$ and to the photosphere at $\tau = \frac{2}{3}$ (*middle*) and the midplane of a stationary protoplanetary accretion disk (*right*) of a solar like protostar with an accretion rate of $10^{-7}\,\mathrm{M}_\odot\,\mathrm{year}^{-1}$

number of P-T-combinations. In this case it is necessary to reduce the number of equations and number of terms within them to the smallest possible number for saving computer time.

3.4 Results for Some Element Mixtures

Calculations of the composition of solid-gas-mixtures for different purposes and different element mixtures have frequently been performed in the past. The first such calculation for determining the possible condensates in circumstellar dust shells covering the observed C/O abundance variations between M and C stars was that of Gilman [22] while for the primitive solar nebula the first complete calculations of the equilibrium mixture where the seminal papers of Larrimer [23] and Grossman [18]. There have been a number of such calculations preceding that of Gilman, Larrimer and Grossman and there followed numerous other calculations. Some papers of a more general type are for instance Lattimer et al. [24], Saxena and Eriksson [25], Sharp and Huebner [17], Sharp and Wasserburg [21], Lodders and Fegley [26–28] ([27] contains a bibliography on condensation calculations for stellar problems), Glassgold [29], Ebel and Grossman [30], Krot et al. [31], Davis and Richter [32].

As an example for condensation in the standard cosmic element mixture Fig. 5 shows stability limits for the most important minerals formed from Mg, Si, Fe, Al, and Ca. These are the main dust components that are expected to be formed in chemical equilibrium. Additionally the upper stability limits of Ti and Zr compounds are shown, which are not abundant enough to form important dust components, but which may be important for the formation of seed nuclei for growth of dust grains formed by more abundant elements.

Another example is the carbon-rich element mixture. The upper stability limits of the most important minerals formed from C, Si, Mg, Fe, Al, Ca, and Ti are shown in Fig. 6. These are the main dust components that are expected to be formed in chemical equilibrium in a carbon-rich stellar outflow. TiC is not an abundant dust species in such outflows because of the low Ti abundance, but presolar carbon grains are frequently observed to contain in their centre nm-sized TiC particles that obviously served as growth centres for carbon grain formation (see "The Most Primitive Material in Meteorites" by Ott, this volume).

As a third example Fig. 7 shows the upper stability limits of the most abundant condensates in a mixture where the elements C, N, O evolved into isotopic equilibrium according to the CNO-cycle (mixture (3) in Table 1). The abundances of C and O drop below the abundances of Mg, Fe, and Si (cf. Fig. 2), but the mixture stays oxygen rich in the sense that $\varepsilon_O > \varepsilon_C$. Such material is encountered in the outflow of WN stars. Less extreme versions of this element mixture are ejected during the outbursts of LBV stars. If such stars form dust, the dust will have a rather unusual composition since neither the oxygen rich minerals of M stars nor the mixture of carbon dust and carbides as in C stars can be formed. Instead solid iron and iron-silicon alloys are probably the dominant dust components. The composition of the dust is

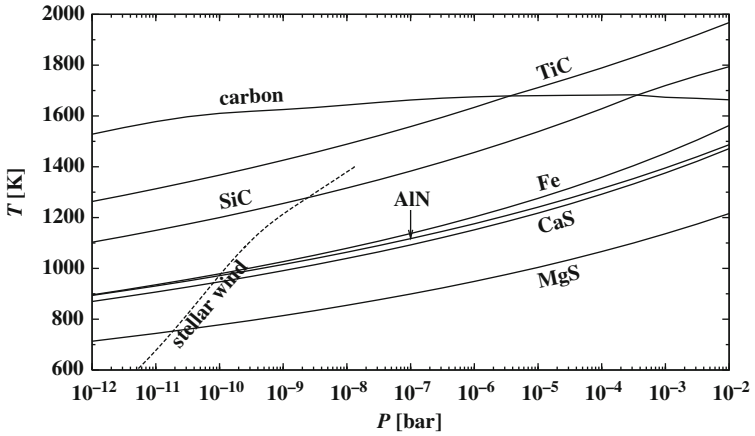

Fig. 6 Stability limits in the $P - T$ plane of the minerals formed by the most abundant refractory elements C, Si, Mg, Fe, Al, Ca and of Ti in a carbon-rich element mixture (C/O = 1.2). The *dashed line* is a $P-$ trajectory corresponding to a stellar wind model with mass-loss rate of $10^{-5}\,M_\odot\,\mathrm{year}^{-1}$

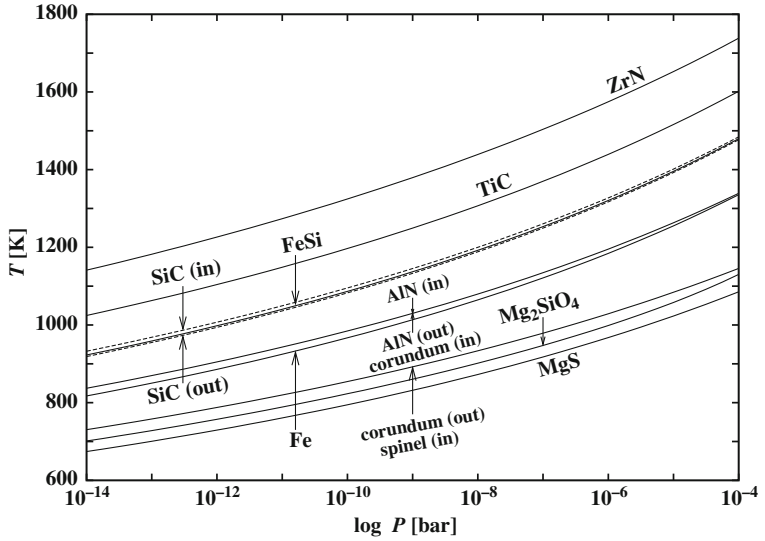

Fig. 7 Stability limits in the $P - T$ plane of the minerals formed by the most abundant refractory elements C, Si, Mg, Fe, Al, Ca and of Ti and Zr in a CNO-cycle processed material

similar to that expected to form in S stars where ε_C nearly equals ε_O (Ferrarotti and Gail [33]).

Results for the composition of carbon-rich mixtures may be found in may of the papers on equilibrium condensation, especially in Lodders and Fegley [26, 27], Sharp and Wasserburg [21] and Lattimer et al. [24].

3.5 Solid Solutions

Some of the minerals existing in circumstellar shells and in protoplanetary accretion discs form solid solutions. Especially this holds for the important silicate dust components and the iron in the standard cosmic element mixture:

- Olivine with composition $Mg_{2x}Fe_{2(1-x)}SiO_4$ is a solid solution formed from the end members forsterite Mg_2SiO_4 and fayalite Fe_2SiO_4.
- Pyroxene with composition $Mg_xFe_{1-x}SiO_3$ is a solid solution formed from enstatite $MgSiO_3$ and ferrosilite $FeSiO_3$.
- Iron forms a solid solution with Ni.

From the less abundant Al-Ca-minerals the minerals

- gehlenite ($Al_2Ca_2SiO_7$) and åkermanite ($MgCa_2Si_2O_7$) form a solid solution which is known as melilite.

There are a number of other solid solutions bearing less abundant elements and the abundant solid solutions contain additional minor solution components (e.g.

Saxena and Eriksson [25], Ebel and Grossman[30]). In view of the rather limited accuracy of present day model calculations only the most abundant solid solutions and their most abundant solution components need to be considered. The theory of solid solutions with applications to minerals of interest for astrophysics is described for instance in Saxena [25, 34], Saxena et al. [15]. Useful information can be obtained also from, e.g., Schmalzried and Navrotsky [35], Schmalzried [36], Philpotts [37], Putnis [38].

In an ideal binary solid solution A_xB_{1-x} of A and B with mole fractions x and $1-x$, respectively, there is no change in the enthalpy due to mixing, but the entropy changes by the entropy of mixing (e.g. Atkins [11])

$$\Delta S = -nR\,(x\ln x + (1-x)\ln(1-x))\,. \tag{23}$$

Here n is the number of moles of mixing sites per mole of the solid solution. For a solid solution like that of Fe and Ni one has one mole of lattice sites over which the Fe and Ni atoms may be distributed in one mole of the solid solution, i.e., $n = 1$ in this case. For olivine there are two moles of mixing sites per mole of SiO_4^{4-} tetrahedrons in the solid solution over which the Mg^{2+} and Fe^{2+} cations may be distributed, i.e., $n = 2$ in this case.

Since for the solid solution one has $\Delta G = \sum_i x_i G_i$ according to (8), Eq. (23) implies that the chemical potential of a component in an ideal solid solution is (e.g. Putnis [38])

$$\mu_i(p,T) = \mu_i(p_0,T) + nRT\ln x_i\,, \tag{24}$$

where x_i is the mole fraction of the solution component i. The activity a_i of component i in an ideal solid solution, as defined by (6), equals x_i. For non-ideal solid solutions one defines

$$\mu_i(p,T) = \mu_i(p_0,T) + nRT\ln\gamma_i x_i \tag{25}$$

with some activity coefficient γ_i describing deviations from ideality. γ_i has to be determined experimentally. The results for binary solutions often can be fitted by an expression of the type (unsymmetric Margules formulation, cf. Putnis [38])

$$RT\ln\gamma_1 = x_2^2\,[\,W_{12} + 2x_1\,(W_{21} - W_{12})\,] \tag{26}$$

and the same for γ_2 with indices 1 and 2 interchanged. The interaction parameters W_{ij} for some astrophysical important solid solutions are given in Table 2.

For the astrophysically important silicates olivine and orthopyroxene the deviations from ideality are quite small and they may be assumed to form ideal solid solutions, but this not admitted for nickel-iron or melilite.

Table 2 Parameters for the Margules formulation (26) of the activity coefficients for some astrophysical important binary solid solutions

Mineral	Component 1	Component 2	W_{12} (kJ/mole)	W_{21} (kJ/mole)	Sources
Olivine	Forsterite	Fayalite	4. 500	4. 500	Saxena et al. [15], Wood and Kleppa[39]
Pyroxene	Enstatite	Ferrosilite	0 for $T > 873$ $13.1 - 0.015\,T$ else	0 for $T > 673$ $3.37 -$ $0.005\,T$ else	Saxena et al. [15]
Pelilite	Gehlenite	Åkermanite	24.2881	0.5021	Saxena et al. [15]
Nickel-iron	Iron	Nickel	−10.135	−3.417	Saxena and Eriksson [25]

3.5.1 Formation of Nickel-Iron

As example consider the formation of nickel-iron (first considered for Solar System conditions by Grossman [18]). For the reactions

$$\mathrm{Ni} \longrightarrow \mathrm{Ni(in\ nickel-iron)(s)}\ , \quad \mathrm{Fe} \longrightarrow \mathrm{Fe(in\ nickel-iron)(s)}$$

of formation of solid Ni and Fe as components of the solid solution nickel-iron from the free atoms one has according to (18) the equilibrium conditions

$$a_{\mathrm{Ni}} = x_{\mathrm{Ni}}\gamma_{\mathrm{Ni}} = p_{\mathrm{Ni}}\,\mathrm{e}^{-\Delta G(\mathrm{Ni})/RT} \tag{27}$$

$$a_{\mathrm{Fe}} = (1 - x_{\mathrm{Ni}})\gamma_{\mathrm{Fe}} = p_{\mathrm{Fe}}\,\mathrm{e}^{-\Delta G(\mathrm{Fe})/RT}. \tag{28}$$

Here x_{Ni} is the mole fraction of Ni in the solid solution, and $\Delta G(\mathrm{Ni})$ and $\Delta G(\mathrm{Fe})$ are the change of free enthalpy in the formation of the pure solids Ni and Fe, respectively, from free atoms, and p_{Ni} and p_{Fe} are the partial pressures of the free atoms in units of standard pressure p_0. Condensation of nickel-iron is essentially independent of all other condensation processes. Since Ni and Fe exist in the gas phase only as free atoms the stoichiometric equations (19) can be written as

$$(1 - f_{\mathrm{Ni}})\,\varepsilon_{\mathrm{Ni}}\,P_{\mathrm{H}} = p_{\mathrm{Ni}} \tag{29}$$

$$(1 - f_{\mathrm{Fe}})\,\varepsilon_{\mathrm{Fe}}\,P_{\mathrm{H}} = p_{\mathrm{Fe}}, \tag{30}$$

where f_{Ni} and f_{Fe} are the fractions of Ni and Fe, respectively, condensed into nickel-iron. In terms of f_{Ni} and f_{Fe} one has

$$x_{\mathrm{Ni}} = f_{\mathrm{Ni}}\varepsilon_{\mathrm{Ni}}/\left(f_{\mathrm{Ni}}\varepsilon_{\mathrm{Ni}} + f_{\mathrm{Fe}}\varepsilon_{\mathrm{Fe}}\right). \tag{31}$$

The relation of P_{H} to the total pressure P is

$$P = \left(\frac{1}{2} + \varepsilon_{\mathrm{He}}\right) P_{\mathrm{H}}, \tag{32}$$

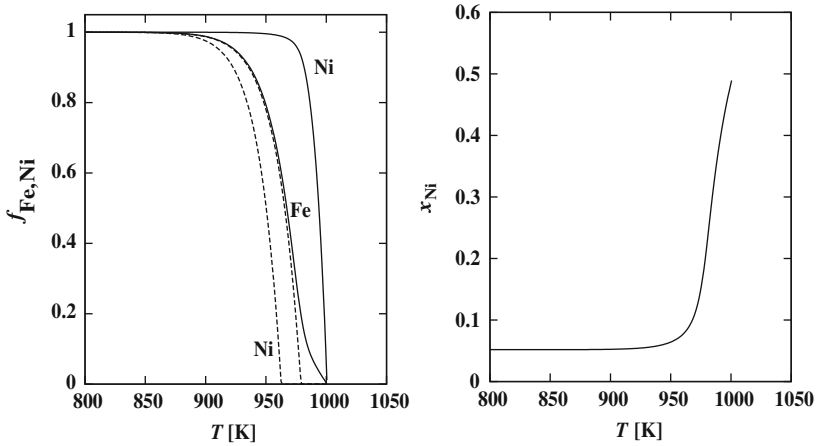

Fig. 8 Condensation of iron and nickel at total pressure $P = 10^{-10}$ bar (stellar wind). *Left part:* Fraction of the total Fe and Ni condensed into nickel-iron (*full lines*) and separate condensation of the pure substances (*dashed lines*) if the formation of the solid solution would not be possible. *Right part:* Mole fraction x_{Ni} of Ni in the nickel-iron

since hydrogen is completely associated to H_2. For given T and P Eqs. (27), (28), (29), (30), and (31) uniquely determine the composition and abundance of nickel-iron.

A representative result is shown for conditions typically encountered in circumstellar dust shells ($P = 10^{-10}$ bar) in Fig. 8. Note that adding some Ni to the iron increases the condensation/vaporization temperature of nickel-iron by about 20 K as compared to that of pure iron. Results for protoplanetary discs, where typically one has $P = 2 \times 10^{-3}$ bar in the region of dust vaporization, are similar, except that nickel-iron vaporizes at about $T = 1\,505$ K.

Note that below $T \approx 720$ K part of the iron forms FeS (cf. Fig. 5) in chemical equilibrium.

3.5.2 Iron Content of Silicates

Two particular important examples for solid solutions as dust components in circumstellar dust shells and in accretion discs are the solid solutions olivine and pyroxene. These solid solutions seem to have first been considered for Solar System conditions by Blander and Katz [40] and in more detail by Grossman [18]. See also Saxena and Eriksson [25]. The mole fractions of the iron bearing end members in these solution series is of special observational relevance for circumstellar dust (e.g. "The Mineralogy of Interstellar and Circumstellar Dust in Galaxies" by Molster et al.,, this volume, Molster et al. [41–43]).

The condensation of olivine, pyroxene, and iron is calculated for instance as follows: The equilibrium conditions for the formation of the solution components of olivine and pyroxene according to (18) are

$$a_{\rm fo} = (x_{\rm fo}\gamma_{\rm fo})^2 = p_{\rm Mg}^2 p_{\rm Si} p_{\rm O}^4 \, {\rm e}^{-\Delta G_{\rm fo}/RT} \tag{33}$$

$$a_{\rm fa} = (x_{\rm fa}\gamma_{\rm fa})^2 = p_{\rm Fe}^2 p_{\rm Si} p_{\rm O}^4 \, {\rm e}^{-\Delta G_{\rm fa}/RT} \tag{34}$$

$$a_{\rm en} = x_{\rm en}\gamma_{\rm en} = p_{\rm Mg} p_{\rm Si} p_{\rm O}^3 \, {\rm e}^{-\Delta G_{\rm en}/RT} \tag{35}$$

$$a_{\rm fs} = x_{\rm fs}\gamma_{\rm fs} = p_{\rm Fe} p_{\rm Si} p_{\rm O}^3 \, {\rm e}^{-\Delta G_{\rm fs}/RT}, \tag{36}$$

where $\Delta G_{\rm fo}$, $\Delta G_{\rm fa}$, $\Delta G_{\rm en}$, and $\Delta G_{\rm fs}$ are the partial free enthalpies of the formation of one mole of the pure components forsterite, fayalite, enstatite, and ferrosilite from free atoms, respectively. The γ's are the activity coefficients, that for most purposes can be set to unity. Additionally one has the mass action laws for the formation of nickel-iron as just before since at higher pressures solid iron coexists with the silicates (cf. Fig. 5).

At the pressures and temperatures of interest, where condensed silicates exist, all H is associated to H_2, all C is bound in CO, nearly all Si not bound in solids is bound in SiO, and all O not bound in CO, SiO and solids is bound in H_2O. The set of stoichiometric equations (19) in its simplest form for the condensation of olivine, pyroxene and solid iron is

$$\left(\varepsilon_{\rm O} - \varepsilon_{\rm C} - \left(4f_{\rm ol} + 3f_{\rm py}\right)\varepsilon_{\rm Si}\right) P_{\rm H} = p_{\rm H_2O} + p_{\rm SiO} \tag{37}$$

$$\left(\varepsilon_{\rm Mg} - \left[2(1-x_{\rm fa})f_{\rm ol} + (1-x_{\rm fs})f_{\rm py}\right]\varepsilon_{\rm Si}\right) P_{\rm H} = p_{\rm Mg} \tag{38}$$

$$\left((1-f_{\rm ir})\,\varepsilon_{\rm Fe} - \left[2x_{\rm fa}f_{\rm ol} + x_{\rm fs}f_{\rm py}\right]\varepsilon_{\rm Si}\right) P_{\rm H} = p_{\rm Fe} \tag{39}$$

$$(1 - f_{\rm ol} - f_{\rm py})\varepsilon_{\rm Si}\, P_{\rm H} = p_{\rm SiO}. \tag{40}$$

The equilibrium conditions are

$$(1-x_{\rm fa})^2 = p_{\rm Mg}^2\, p_{\rm Si}\, p_{\rm O}^4\, {\rm e}^{-\Delta G({\rm fo})/RT} \tag{41}$$

$$x_{\rm fa}^2 = p_{\rm Fe}^2\, p_{\rm Si}\, p_{\rm O}^4\, {\rm e}^{-\Delta G({\rm fa})/RT}. \tag{42}$$

$$1 - x_{\rm fs} = p_{\rm Mg}\, p_{\rm Si}\, p_{\rm O}^3\, {\rm e}^{-\Delta G({\rm en})/RT} \tag{43}$$

$$x_{\rm fs} = p_{\rm Fe}\, p_{\rm Si}\, p_{\rm O}^3\, {\rm e}^{-\Delta G({\rm fs})/RT}. \tag{44}$$

$$1 = p_{\rm Fe}\, {\rm e}^{-\Delta G({\rm ir})/RT}. \tag{45}$$

Here $f_{\rm ol}$ denotes the fraction of Si condensed into olivine, $x_{\rm fa}$ the mole fraction of fayalite Fe_2SiO_4 in the solid solution $Mg_{2(1-x_{\rm fa})}Fe_{2x_{\rm fa}}SiO_4$, $f_{\rm py}$ the fraction of Si condensed into pyroxene, $x_{\rm fs}$ the mole fraction of ferrosilite $FeSiO_3$ in the solid solution $Mg_{1-x_{\rm fs}}Fe_{x_{\rm fs}}SiO_3$, and $f_{\rm ir}$ the fraction of Fe condensed into solid iron. Additionally one has the laws of mass action for the molecules H_2O and SiO and Eq. (32) for the total pressure. An extension of the system to a more complex gas phase chemistry is straight forward.

Equations (37)–(45) form a set of nine equations for the nine unknowns $p_{\rm O}$, $p_{\rm fe}$, $p_{\rm Mg}$, $p_{\rm Si}$, $f_{\rm ol}$, $x_{\rm fa}$, $f_{\rm py}$, $x_{\rm fs}$, and $f_{\rm ir}$ which may be solved for instance by Newton-Raphson iteration, or one uses for the solution of the system one of the multi-purpose methods described in Smith and Missen [12]. The solution is subject to the restrictions that

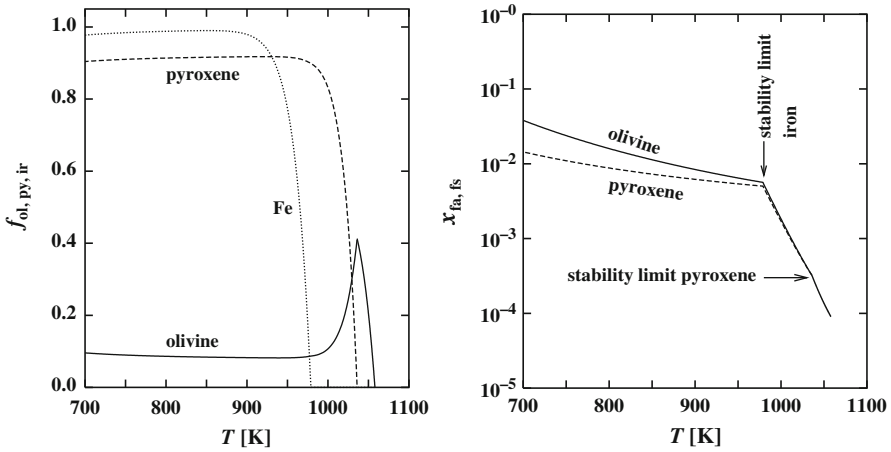

Fig. 9 Condensation of olivine, pyroxene and solid iron at total pressure $P = 10^{-10}$ bar, representative for the condensation zone in stellar winds. *Left part:* Fraction of the Si condensed into olivine and pyroxene and fraction of Fe condensed into solid iron. *Right part:* Mole fractions $x_{\rm fa}$ and $x_{\rm fs}$ of fayalite and ferrosilite in olivine and pyroxene, respectively

$$0 \le f_{\rm ol} \le 1\ , \quad 0 \le f_{\rm py} \le 1\ , \quad 0 \le f_{\rm ir} \le 1\ . \tag{46}$$

Representative results for the composition of olivine and pyroxene are shown in Fig. 9 for conditions encountered in the condensation zone of circumstellar dust shells, and in Fig. 10 for conditions in the dust vaporization region in protoplanetary accretion discs. The iron content of the silicates is very low for temperatures $T > 700$ K in chemical equilibrium, in fact they are essentially pure forsterite and

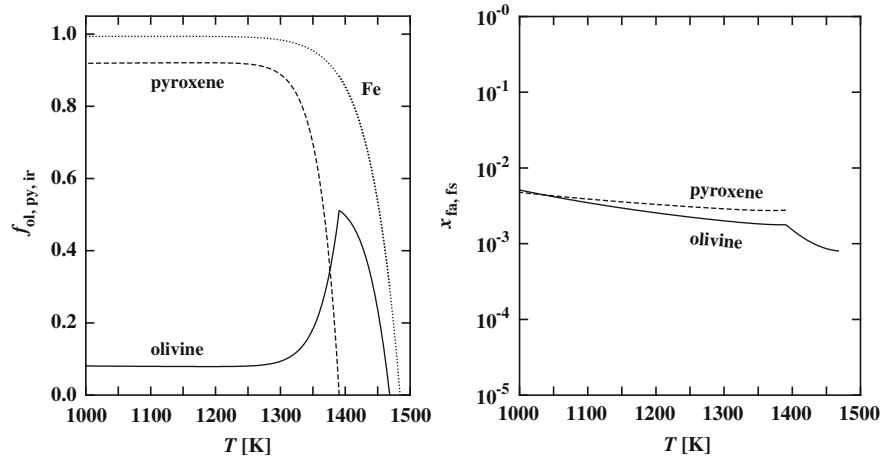

Fig. 10 Similar as Fig. 9, but for a pressure of $P = 2 \times 10^{-3}$ bar representative for the dust vaporization zone in protoplanetary accretion discs

enstatite. At much lower temperatures ($T \lesssim 600\,\mathrm{K}$) the iron content of the silicates in a chemical equilibrium mixture rapidly increases with decreasing temperature, but equilibration is prevented in circumstellar shells and protoplanetary discs at such low temperatures by slow cation diffusion (cf. Sect. 5.2).

4 Dust Growth Processes

4.1 Characteristic Scales

The evaporation and growth of an ensemble of dust grains is determined by two basically different processes: By the processes which remove or add material from the gas phase from or to the surface of a grain, and by transport processes in the gas phase by which material for the growth of particles is supplied or the material evaporated from grains is carried away. They are characterized by a number of length and time scales and dimensionless numbers.

4.1.1 Characteristic Length Scales

There are three different length scales for the problem. The first one is the mean free path length of the gas particles with respect to collisions with H_2

$$\lambda_p = 1/n_p\sigma_p. \tag{47}$$

σ_p is an average collision cross-section for gas phase species which for order of magnitude estimates may be approximated by $\sigma_p = 10^{-15}\,\mathrm{cm}^2$, and n_p is the number density of H_2. The second important length scale is the particle size a. From a and λ_p one defines the dimensionless Knudsen number

$$N_{\mathrm{Kn}} = \lambda_p/a. \tag{48}$$

$N_{\mathrm{Kn}} \to 0$ or $N_{\mathrm{Kn}} \to \infty$ correspond to the limit cases where either the interaction of a grain with the ambient gas can be treated in the hydrodynamic limit or has to be treated by the methods of the theory of rarefied gas dynamics, respectively. Numerically we have

$$N_{\mathrm{Kn}} = 10^9(10^{10}\mathrm{cm}^{-3}/n_p)\,(1\,\mu\mathrm{m}/a). \tag{49}$$

In the dust formation zone of circumstellar shells we have $n_p \approx n_{\mathrm{H}_2} = 10^{10}$–$10^5\,\mathrm{cm}^{-3}$ and $a < 1\,\mu\mathrm{m}$. The Knudsen number always is very large in this case. In protoplanetary accretion discs we have $n_p \approx 10^{15}$–$10^{13}\,\mathrm{cm}^{-3}$ in the regime between the region of dust evaporation and ice evaporation. The Knudsen number satisfies $N_{\mathrm{Kn}} \gg 1$ only for small particles with $a \lesssim 1\,\mathrm{mm}$.

The third important length scale is the inter-grain distance

$$d_{\mathrm{gr}} = 1/n_{\mathrm{gr}}^{1/3}, \tag{50}$$

where n_{gr} is the particle density of grains. From d_{gr} and λ_p we define a second dimensionless Knudsen number

$$N_{\mathrm{Kn,gr}} = \lambda_p / d_{\mathrm{gr}}. \tag{51}$$

The limit cases $N_{\mathrm{Kn,gr}} \to 0$ or $N_{\mathrm{Kn,gr}} \to \infty$ correspond to the cases where either one has only one grain within the sphere with radius λ_p around this grain (case B in Fig. 11) or there are a lot of other grains within this sphere of influence (case A in Fig. 11), respectively. Either the grains are well isolated from each other and only weakly interact by the slow transport processes (e.g. for matter, momentum) via the gas phase (case B), or the particles strongly interact by means of direct particle exchange (case A), respectively. Figure 11 illustrates the two limit cases.

Obviously, in case A all grains "see" changes in the gas phase concentration of species consumed or liberated by particle growth or evaporation, respectively, in the same way and immediately. There are no local concentration reductions or enhancements around a particle. In case B, however, growth or evaporation results in locally reduced or increased concentrations of growth species around a dust grain, which only slowly adjust to the average concentrations in the gas phase by the slow diffusion process.

For an order of magnitude estimate we assume the dust grains to have uniform sizes a and to consume all atoms of some element with abundance ε (by number, relative to H). Then we have

$$\frac{4\pi}{3} a^3 n_{\mathrm{gr}} = V_0 \epsilon N_{\mathrm{H}}. \tag{52}$$

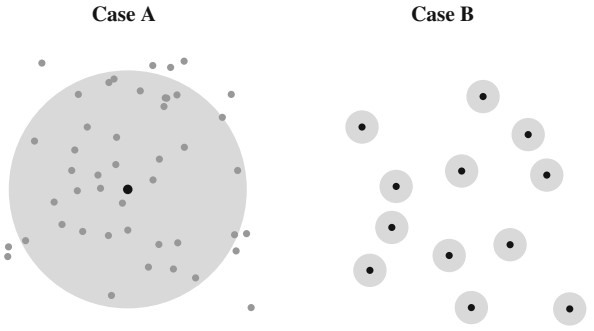

Fig. 11 The two limit cases for grain growth and evaporation. *Case A*: $N_{\mathrm{Kn,gr}} \gg 1$, the sphere of influence (indicated by a *gray circle*) with radius λ around one grain (indicated by the *big black dot*) contains many other dust grains. *Case B*: $N_{\mathrm{Kn,gr}} \ll 1$, the spheres of influence of the different grains are well separated

The quantity V_0 denotes the volume of one formula unit of the condensate in the solid

$$V_0 = Am_{\rm H}/\varrho_{\rm gr}, \tag{53}$$

where A is the atomic weight of one formula unit and $\varrho_{\rm gr}$ the mass density of the solid. $N_{\rm H}$ is the fictitious number density of H nuclei, if all hydrogen atoms are present as fee atoms

$$N_{\rm H} = \varrho/(1 + 4\epsilon_{\rm He})m_{\rm H}. \tag{54}$$

At temperatures where dust exists, we have $N_{\rm H} = 2n_{\rm H_2}$. It follows

$$N_{\rm Kn,gr} = \frac{1}{an_p^{2/3}}\sigma_p \left(\frac{3V_0\epsilon}{2\pi}\right)^{1/3}. \tag{55}$$

Using numbers for olivine grains from Tables 1 and 3 we obtain numerically

$$N_{\rm Kn,gr} = 2.3 \times 10^3 \ (1\,\mu{\rm m}/a) \left(10^{10}\,{\rm cm}^{-3}/n_p\right)^{2/3}. \tag{56}$$

In the growth zone of circumstellar shells we usually have $n_p < 10^{10}\,{\rm cm}^{-3}$ and $a < 1\,\mu$m, hence $N_{\rm Kn,gr} \gg 1$, which corresponds to case A in Fig. 11. In protoplanetary discs, however, particle densities are high (10^{13}–$10^{15}\,{\rm cm}^{-3}$) and dust particles may become much bigger than $1\,\mu$m. The limit case $N_{\rm Kn,gr} \gg 1$, case A in Fig. 11, is valid in protoplanetary discs only if grains remain smaller than about $1\,\mu$m. For bigger grains case B of Fig. 11 applies.

4.1.2 Characteristic Time Scales

There is a characteristic timescale associated with the diffusion of gas phase species through the gas phase

Table 3 Some quantities important for calculating dust growth or evaporation for abundant dust components. Data for ϱ and A from the CRC-handbook (Lide [50]). For α see text

Dust species	ϱ g cm^{-3}	A	V_0 cm^3	α
Quartz	2.648	60.085	3.80×10^{-23}	0.05
Iron	7.87	55.845	1.19×10^{-23}	0.9
Forsterite	3.21	140.694	7.33×10^{-23}	0.1
Fayalite	4.30	203.774		
Enstatite	3.19	100.389	5.26×10^{-23}	
Ferrosilite	4.00	131.93		
Olivine			7.55×10^{-23}	0.1
Pyroxene			5.35×10^{-23}	0.1
Silicon monoxide	2.13	44.09	3.46×10^{-23}	0.02

$$t_{\rm diff} = \lambda_p^2 / D \tag{57}$$

where D is the diffusion coefficient which can be approximated by $D \approx \lambda_p v_{p,\rm th}$, where $v_{p,\rm th} = \left(kT/m_p\right)^{1/2}$. This time is of the order of magnitude of the time required for the development of a stationary sphere of concentration enhancement or reduction by particle evaporation or growth, respectively, around a particle at rest with respect to the gas. For longer periods, particle transport towards or away from a grain is determined by a stationary diffusion current. Numerically we have

$$t_{\rm diff} = 0.5 \left(10^{10}\,{\rm cm}^{-3}/n_p\right)(1000\,{\rm K}/T)\ \ [{\rm s}]. \tag{58}$$

In many cases external forces drive a motion of dust grains through the gas with a drift velocity $v_{\rm dr}$. The characteristic time scale associated with this process is

$$t_{\rm dr} = \lambda_p / v_{\rm dr}. \tag{59}$$

From the two time scales $t_{\rm diff}$ and $t_{\rm dr}$ one defines the dimensionless Mach number

$$Ma = t_{\rm diff}/t_{\rm dr} = v_{\rm dr}/v_{p,\rm th}. \tag{60}$$

In the limit case $Ma \to 0$ the drift of the grain through the gas is so slow that diffusion of vapour species towards or away from the grain relaxes to a stationary state. In the opposite limit $Ma \to \infty$ vapour transport towards or away from the grain is determined by the motion of the grain through the gas. For circumstellar shells one has $Ma \approx 1$ (except for the smallest, just nucleated grains) but in this case also case A of Fig. 11 holds, in which case diffusion anyhow does not play any role. For protoplanetary discs the grain drift velocity relative to the gas remains smaller than $v_{p,\rm th}$ for grain sizes $a \lesssim 10\,{\rm cm}$, cf. Fig. 3 of Weidenschilling and Cuzzi [44], for instance. Thus, for grain sizes between $\approx 1\,\mu{\rm m}$ and $\approx 10\,{\rm cm}$ the transport of vapour species during growth or evaporation towards or away from a particle may be regulated by diffusion through the gas phase. Bigger particles are ventilated by their motion through the gas and diffusion is unimportant.

4.2 Growth of Dust Grains

The simplest growth process for dust grains is that where the chemical composition of the condensate is the same as that of the vapour, as for instance in the case of the condensation of iron atoms into solid iron or of H_2O molecules into ice. This is *homomolecular* growth, in contrast to *heteromolecular* growth where the vapour has a different chemical composition from that of the solid. Homomolecular growth simply requires a step by step addition of the basic molecule to the solid, heteromolecular growth necessarily is a complicated process which requires the reaction of several gas phase species at the surface of the solid to form the basic building block of the condensate. From the abundant cosmic minerals only iron forms

by homomolecular growth. All silicate compounds and all aluminium and calcium compounds decompose on evaporation and, thus, grow by heteromolecular growth processes.

4.2.1 Homomolecular Growth

We start with homomolecular growth as the most simple case and assume that the growth is not diffusion limited and the particles are at rest with respect to the gas. The rate at which particles hit the surface per unit area and time according to a classical result of the kinetic theory of gases is

$$R_{\rm coll} = n\sqrt{kT/2\pi m}. \tag{61}$$

n is the particle density of the growth species and m its mass. If α denotes the probability that a collision results in the deposition of the growth species onto the grain, the growth rate per unit surface area is given by

$$J^{\rm gr} = \alpha R_{\rm coll} = \alpha n\sqrt{kT/2\pi m}. \tag{62}$$

The growth or sticking coefficient α has to be determined by laboratory experiments.

The evaporation rate of a grain is given by

$$J^{\rm vap} = \alpha' R_{\rm coll} = \alpha' n' \sqrt{kT_{\rm d}/2\pi m} \tag{63}$$

with an evaporation coefficient α'. n' refers to the particle density of the growth species in chemical equilibrium between the gas phase and the condensate and is given by the vapour pressure $p_{\rm eq}$ as

$$n' = p_{\rm eq}/kT_{\rm d}. \tag{64}$$

From detailed balancing arguments one finds $\alpha = \alpha'$, but for non-equilibrium growth this does not necessarily hold. Since usually only one, if ever, of these coefficients is known one always assumes $\alpha = \alpha'$. Note that the temperature $T_{\rm d}$ in (63), the internal temperature of the grains, needs not to be the same as the temperature T in (62), the kinetic temperature of the gas phase.

The number N of basic building blocks forming a grain increases with time as

$$\frac{{\rm d}N}{{\rm d}t} = \oint_{\mathcal{A}} dA \left(J^{\rm gr} - J^{\rm vap}\right). \tag{65}$$

The integration is over the surface of a grain. For particles at rest with respect to the gas the rates $J^{\rm vap}$, $J^{\rm gr}$ usually are different for different crystal facets. In view of the many uncertainties of the present state of the theory of cosmic dust formation it is not desirable to treat the detailed growth of crystals with their specific crystal

shapes. Thus, one introduces average evaporation and growth rates and writes

$$\frac{\mathrm{d}N}{\mathrm{d}t} = \mathcal{A}\left(J^{\mathrm{gr}} - J^{\mathrm{vap}}\right), \tag{66}$$

where $\mathcal{A}$ is the total surface area of the grain. If the grains are spherical with radius a then $NV_0 = \frac{4\pi}{3}a^3$ and $\mathcal{A} = 4\pi a^2$. V_0 is defined by (53). Then

$$\frac{\mathrm{d}a}{\mathrm{d}t} = V_0\left(J^{\mathrm{gr}} - J^{\mathrm{vap}}\right). \tag{67}$$

If the growth and evaporation rate are determined by (62) and (63) the equation takes the form

$$\frac{\mathrm{d}a}{\mathrm{d}t} = V_0\alpha\sqrt{\frac{kT}{2\pi m}}\left(n - \frac{p_{\mathrm{eq}}}{kT}\right) = V_0\,\alpha\,\left(p - p_{\mathrm{eq}}\right)/\sqrt{2\pi mkT} \tag{68}$$

which is a variant of the Hertz-Knudsen equation.

4.2.2 Heteromolecular Growth

Most substances of astrophysical interest grow by heteromolecular processes since the nominal molecule corresponding to the chemical formula of the solid does not exist. The magnesium silicate forsterite Mg_2SiO_4, for instance, in a hydrogen rich environment requires for its formation a net reaction of the kind

$$2\mathrm{Mg} + \mathrm{SiO} + 3\mathrm{H_2O} \longrightarrow \mathrm{Mg_2SiO_4}(s) + 3\mathrm{H_2O}, \tag{69}$$

since Mg, SiO and H_2O are the only abundant species in the gas phase from which forsterite can be formed. In such cases there often exist a *rate determining reaction* which rules the whole growth process. For forsterite experimental results (see below) indicate that the addition of SiO from the gas phase determines the rate of forsterite growth. In such cases (68) also describes the growth of dust grains by heteromolecular growth where p refers to the gas phase partial pressure of the least abundant molecule involved in the rate determining reaction and p_{eq} is its partial pressure in chemical equilibrium.

Consider the formation of some solid D from gas phase species A, B, C, ...

$$i\mathrm{A} + j\mathrm{B} + k\mathrm{C} + \ldots \longrightarrow l\mathrm{D(s)} + m\mathrm{E} + n\mathrm{F} + \ldots \tag{70}$$

where E, F, ... are some reaction products, and let the reaction with gas phase species A be the rate determining step for formation of D. The activity of solid D according to (18) is

$$a_{\mathrm{sol}} = \frac{p_{\mathrm{A}}^i p_{\mathrm{B}}^j p_{\mathrm{C}}^k \cdots}{p_{\mathrm{E}}^m p_{\mathrm{F}}^n \cdots} \mathrm{e}^{\Delta G/RT}. \tag{71}$$

For the equilibrium pressure $p_{\rm eq}$ in (68) one has to take the value of $p_{\rm A}$ calculated from (71) by letting $a_{\rm sol} = 1$. Then $p_{\rm eq}/p = p_{\rm A,eq}/p_{\rm A} = 1/a_{\rm sol}^{1/i}$ and (68) changes into

$$\frac{{\rm d}\,a}{{\rm d}\,t} = V_0 \alpha \sqrt{\frac{kT}{2\pi m}} \left(n - \frac{p_{\rm eq}}{kT}\right) = V_0\,\alpha\; p \left(1 - \frac{1}{a_{\rm sol}^{1/i}}\right) / \sqrt{2\pi m k T}. \tag{72}$$

This shows that the activity $a_{\rm sol}$, calculated according to (71), rules the growth or the evaporation of the solid in a non-equilibrium mixture of gases and solids: If $a > 1$ the solid condenses, if $a < 1$ the solid evaporates. Calculations of activities of possible candidates for condensation like that shown in Fig. 4 help to find out the possible non-equilibrium condensates.

For homomolecular growth the activity $a_{\rm sol}$ in (72) is equivalent to the conventional supersaturation ratio.

If the transport of gas phase material to and from the grain is limited by diffusion (case B in Fig. 11), the local concentration at the surface of a particle is fixed by the vapour pressure. One has to solve the stationary diffusion problem for this case in order to determine the rate at which particles arrive at or leave from the surface of the grain. This problem is discussed, for instance, in textbooks on cloud physics (e.g. Pruppacher and Klett [45]).

4.2.3 Laboratory Condensation Experiments

Experimental investigations of condensation of cosmic dust analogs have been performed for Mg-Fe-Si condensates by Rietmeijer and Nuth [46], for Fe-Si condensates, by Rietmeijer et al. [47], and for Al-Si-condensation by Rietmeijer and Karner [48]. These experiments give some hints on the composition and structure of grains forming in cosmic element mixtures, but unfortunately the experiments are performed under conditions that are not directly comparable to cosmic conditions. Condensation experiments performed under more realistic conditions are discussed in Toppani et al. [49].

4.3 Condensation Coefficients

The evaporation or condensation coefficients α have to be determined from laboratory experiments. A number of such experiments have been performed during the last decade and α is now known for the abundant dust minerals, though with an only moderate accuracy in most cases.

Olivine: This material evaporates congruently, which means that the residue has the same composition as the starting material (Nagahara et al. [51]), only the last residues contain some fraction of silica SiO_2 (Nagahara et al. [52]). The evaporation of forsterite in vacuum has been studied by Hashimoto [53]. The evaporation coefficient α derived by Hashimoto for the evaporation reaction

$$Mg_2SiO_4(s) \longrightarrow 2Mg + SiO + O_2 + O \tag{73}$$

is between 0.09 and 0.16 in the experimental temperature regime 1,600–1,890℃. Similar results are obtained in Wang et al. [54]. The composition of the vapour of forsterite has been determined by mass spectrometry of the outflow from a Knudsen cell by Nichols and Wasserburg [55] and from a Langmuir configuration by Nichols et al. [56]. In both cases the composition of the vapour is found to be in accord with the evaporation reaction (73). A new determination of the condensation coefficient by Inaba et al. [58] gave $\alpha = 0.18$ at 1,700℃. In all experiments it is assumed that there is no difference between the condensation and evaporation coefficient. A typical value of the condensation/evaporation coefficient is 0.1 ± 0.05, which is given in Table 3.

Evaporation of olivine in the presence of hydrogen is studied by Nagahara and Ozawa [59, 60] for pressures of H_2 between 10^{-9} and 10^{-3} bar at a temperature of 1,700℃. Below 10^{-6} bar the evaporation rate is found to be independent of the H_2 pressure and similar to the vacuum evaporation rate found by Hashimoto [61], above 10^{-6} bar the evaporation rate increases with H_2 pressure (in bar) as

$$J^{\mathrm{vap}} = (1.72\, P^{1.19} + 9.87) \times 10^{-7} \tag{74}$$

in units $\mathrm{g\,cm^{-2}\,s^{-1}}$. They interpreted their results as a superposition of free evaporation according to (73) at low pressures and chemisputtering with H_2 according to the reaction

$$Mg_2SiO_4(s) + 3H_2 \longrightarrow 2Mg + SiO + 3H_2O \tag{75}$$

at higher pressures. Based on this reaction they determined a condensation coefficient α. At low H_2 pressures α roughly is constant $\alpha = 0.06$. At higher pressure it increases up to about 0.2. A typical value is $\alpha = 0.1$, the same value as determined from vacuum evaporation. The results of Nagahara and Ozawa [59, 60] are criticized by Hashimoto [61].

The evaporation of forsterite in protoplanetary discs and the relation between vacuum evaporation and evaporation in H_2 gas has been discussed by Tsuchiyama et al. [62].

Pyroxene: Enstatite evaporates incongruently with forsterite as residue forming a surface layer on enstatite (Tachibana et al. [63, 64]). Tachibana et al. [64] find that during the early phases the thickness of the forsterite evaporation residual layer grows linear with time, implying that the initial forsterite layer is porous and the evaporation is controlled by surface reactions. During the later phases of evaporation a constant thickness layer evolves which is diffusion controlled. The layer thickness at the transition from surface reaction to diffusion controlled growth of the forsterite residual layer is not reported, but can be estimated from the figures to occur at a layer thickness of about 5 μm thickness. Below this layer thickness the growth rate of the forsterite residual layer thickness is given by (Tachibana et al. [64])

$$k = 6.9 \times 10^2 \, \mathrm{e}^{-43540/T} \ \mathrm{cm\,s^{-1}}. \tag{76}$$

Note that part of the forsterite layer first formed from enstatite later evaporates again, i.e., the true rate for increase of layer thickness is given by the difference between the rate of forsterite formation, Eq. (76), and the rate of decrease by forsterite evaporation.

A detailed study on enstatite evaporation in vacuum and in H_2 gas has been performed by Tachibana et al. [65].

Silica: The evaporation coefficients for SiO_2 reported in the literature are small. Landolt-Börnstein [66] gives 0.02–0.04 in the temperature region 1,429–1,460℃. Hashimoto [53] finds an evaporation coefficient of 0.01 at about 1,600℃. All these experiments are conducted at much higher temperatures than those encountered in circumstellar shells or protoplanetary discs in the region of dust formation or evaporation. The measurements of Mendybaev et al. [67] on the kinetics of SiO_2 evaporation are conducted at lower temperatures an in the presence of H_2. Ferrarotti and Gail [68] derived a value of $\alpha = 0.07$ at 1,000 K from the results. A value of $\alpha = 0.05$ is probably a typical value for the condensation/evaporation coefficient of SiO_2. This is the value given in Table 3.

Iron: The evaporation coefficient of iron is 0.8–1.0 in the temperature region 1,020–1,440℃ (Landolt-Börnstein [66]). In a new determination Tachibana et al. [69] obtained $\alpha = 0.83$–0.92 at temperatures between 1,170 and 1,360℃. A typical value of the condensation/evaporation coefficient of iron is 0.9 which is given in Table 3.

Silicon monoxide: Silicon monoxide is a solid material with unclear structure. It is prone to decomposition in Si-nanoclusters embedded in a SiO_2 matrix. The material is speculated to be the first condensate in oxygen rich stellar outflows. Its thermodynamic properties and growth coefficient have recently been redetermined with a substantial revision downward (Ferguson and Nuth [70]; Klevenz [71]). The evaporation coefficient at low temperature is found to be $\alpha = 0.02 \pm 0.1$.

4.4 Nucleation Theory

Dust formation in many cases is a two step process which starts with the formation of tiny seed nuclei from the gas phase and proceeds by growth to macroscopic sized grains via precipitation of condensable material from the gas phase onto the seed nuclei. The seed nuclei need not to be formed from the same material as the grains that finally emerge from the process. The formal theory of nucleation and its application to astrophysical problems is discussed, e.g., in Salpeter [72], Draine [73], Gail and Sedlmayr [74], Patzer et al. [75], Yamamoto et al. [76]. The main problem in astrophysical problems is to determine the nature of the seed nuclei, since this determines the onset of dust formation.

For the problem of dust formation in carbon-rich environments the rich data bases developed for the purposes of modelling terrestrial flames allowed a modelling of

the basic mechanisms of carbon dust nucleation. The first attempt to model carbon dust nucleation from the gas phase by Keller [77] was followed by the more detailed treatments of Frenklach and Feigelson [78] and especially by Cherchneff et al. [79]. The investigations of presolar dust grains (Bernatowicz et al. [80]) have shown that carbon dust in some (but not all) cases grows on seed nuclei of metal carbides like TiC, ZrC, MoC or solid solutions of these carbides. An overview over the problem is given by Sedlmayr and Krüger [81]. Recent major progress is the calculation of nucleation in WC stars by Cherchneff et al. [82] and in supernova ejecta by Clayton et al. [83].

Dust nucleation in oxygen-rich environments remains an unsolved problem up to now. The present state with respect to nucleation is described in Gail and Sedlmayr [20, 84]. The possible candidates for nucleation seem to be clusters of the types Al_nO_m and Ti_nO_m and at high pressures possibly Fe_n, but no definite conclusion with respect to the nature of the nucleation species is possible at present since the data with respect to cluster structures, bond energies, vibrational frequencies, and reaction rates required for calculating the cluster formation process are not yet available. These have to be determined by quantum mechanical calculations. Some progress for Ti_nO_m clusters has recently been made by Jeong et al. [85] and for Al_nO_m clusters by Chang et al. [86, 87], Patzer et al. [88] and more calculations are currently under way.

5 Dust Processing

For dust formed in oxygen-rich environments there arise some complications in determining the composition and properties of the dust mixture because some of the oxides form solid solutions with variable compositions which may change their composition by solid diffusion or they may undergo solid-state chemical reactions. Additionally the optical properties of amorphous and crystalline oxides are considerably different and one has to determine the degree of crystallinity of such materials. For dust material formed in carbon-rich or other chemically diverse environments there seems to be presently no need for considering such complications.

5.1 Annealing

The dust formed under astrophysical conditions in most cases has an amorphous lattice structure, where the basic building blocks of the minerals, e.g. the SiO_4–tetrahedra in the silicates, show a disordered arrangement in the solid. In some cases, however, if the material is heated for sufficiently long times to high temperatures, internal rearrangement processes are activated by which the material evolves into the regular crystalline lattice structure (annealing). For instance, annealing is thought to be responsible for the observed crystalline dust component in cometary dust or in meteoritic matrix material (see Sect. 7.8).

5.1.1 Annealing of Amorphous Olivine and Orthopyroxene

Annealing has been studied in the laboratory for the most important dust components formed in an oxygen-rich environment by Hallenbeck et al. [89], Brucato et al. [90], Hallenbeck and Nuth [91], Fabian et al. [92], Thompson and Tang [93].

Fabian et al. [92] studied annealing of enstatite glass, of smokes obtained by laser ablation of forsterite and enstatite targets, and of nano-sized silica particles. The materials have been annealed at temperatures between 1,000 K and 1,121 K for different durations. The evolution of spectral IR absorption features associated with the development of a crystalline structure have been monitored and the characteristic annealing time τ was determined. From this, the activation energy E_a for annealing was derived from

$$\tau^{-1} = \nu_{\rm vib}\, {\rm e}^{-E_a/kT} \ . \tag{77}$$

$\nu_{\rm vib}$ is a characteristic vibration frequency, which is taken to be $\nu_{\rm vib} = 2 \times 10^{13}\,{\rm s}^{-1}$ (Lenzuni et al. [94]). The results obtained for E_a show a marked scatter and some temperature dependence. Average values given by Fabian et al. [92] are shown in Table 4.

Brucato et al. [90] formed amorphous pyroxene grains by laser ablation of natural enstatite and the structural changes during annealing are monitored by the evolution of the IR spectrum. The activation energy for annealing, again, is determined from relation (77). Converting to the same $\nu_{\rm vib}$ as used in Fabian et al. [92], they obtained an activation energy $E_a/k = 47,300\,{\rm K}$, significantly higher than that of Fabian et al. [92]. The difference is probably due to the different composition and structure of the samples.

Hallenbeck et al. [89] produced amorphous magnesium silicate smokes by vapour condensation. The dust has been annealed at temperatures between 1,000 K and 1,300 K and the IR spectra were monitored as function of the annealing time. Contrary to the experiments of Fabian et al. [92] and Brucato et al. [90] they found after initial rapid annealing a stall phase without significant change of the absorption spectrum followed later by further evolution towards crystallinity. Such a stall phase has also been detected in the annealing experiment by Thompson and Tang [93], who prepared their samples as precipitates from reaction of $MgCl_2$ and Na_2SiO_2 in water. Probably the different annealing behaviour is due to the different composition and structure of the samples. Activation energies for annealing have not been derived

Table 4 Activation energies for annealing of some silicate dust components

Mineral	Structure	E_a [K]	Temperature range [K]	References
Forsterite	Smoke	39, 100	1,000–1,120	[92]
Enstatite	Smoke	42, 040	1,000–1,120	[92]
Enstatite	Glass	40, 100–42,300	1,000–1,120	[92]
Quartz	Smoke	49, 000	1,000–1,120	[92]
Pyroxene	Smoke	47, 300	1,070	[90]

by Hallenbeck et al. [89], so unfortunately their results can not directly be used in model calculations for the evolution of the dust properties.

Annealing in protoplanetary discs occurs at lower temperatures than that for which laboratory studies are performed because of the much longer timescales available. Application of the laboratory data to astrophysical problems requires extrapolation to much lower temperatures. Whether this is admitted or not is not known.

5.1.2 Growth of Crystallized Regions

Crystallization usually is a two step process which starts with the formation of growth centres and then proceeds by a local rearrangement of the lattice building blocks at the border between the crystallized and non-crystalline region, by which the crystallized region expands into its amorphous environment.

The growth of a crystallized region starting from some growth centre, can be described in the most simple case by an equation of the type

$$\frac{\mathrm{d}\, V_{\mathrm{cr}}}{\mathrm{d}\, t} = 6 V_0^{\frac{1}{3}} V_{\mathrm{cr}}^{\frac{2}{3}} \nu_{\mathrm{vib}} \mathrm{e}^{-E_a/kT} \tag{78}$$

(Gail [19]). Similar equations have been used by Kouchi et al. [95] and Sogawa and Kozasa [96]. V_{cr} is the volume of the crystallized region. V_0 is defined by (53). The characteristic timescale for the crystallization can be defined by

$$\tau_{\mathrm{cry}} = V_{\mathrm{cr}} \left| \mathrm{d} V_{\mathrm{cr}} / \mathrm{d} t \right|^{-1} . \tag{79}$$

The run of τ_{cry} for the silicate dust species olivine, orthopyroxene, and quartz are shown in Fig. 12.

The timescale τ_{cry} becomes shorter than the timescale for radial mixing and transport in protoplanetary discs at about 800 K for olivine and orthopyroxene (or about 950 K using data from Hallenbeck et al. [89]). Above this temperature these two dust species rapidly crystallize, if crystallization starts on pre-formed growth centres. Quartz crystallizes for $T \gtrsim 900$ K.

In stellar winds τ_{cry} becomes shorter than the timescale for cooling of the outflowing gas between about 900 K and 850 K. Dust formed above about 900 K will have a crystalline structure because any initial disorder of whatsoever origin will rapidly be annealed. Dust formed below about 800 K will be amorphous if the initial growth process results in a disordered material, because the disorder in the lattice structure later cannot be healed up.

If growth of crystalline regions within a dust grain starts from more than one growth centre, then the growth regions from some instant on come into contact. Growth then only proceeds into the remaining amorphous part of the grain volume and there result different crystallized regions in the grain. This situation is sketched in Fig. 13. The simple growth equation (78) then cannot be used for the late phases of crystallization, if crystallisation starts at more than one growth centre and the crystallized regions start to come into contact. If there are several growth centres the

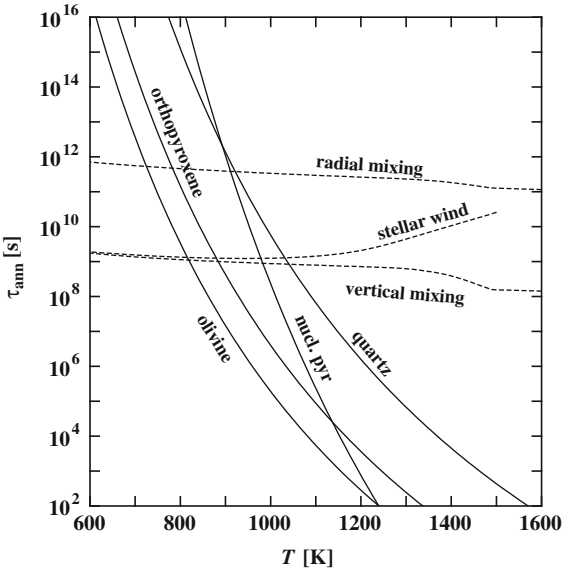

Fig. 12 Characteristic time scales for annealing of a 0.1 μm dust grain and time required for formation of growth centres (nucleation) in enstatite (*Full lines*). Data for the activation energy from Fabian et al. [92]. For comparison, the time scales for radial and vertical transport processes (mixing) in protoplanetary discs and the hydrodynamic timescale r/v for a stationary stellar wind model are shown as *dashed lines*

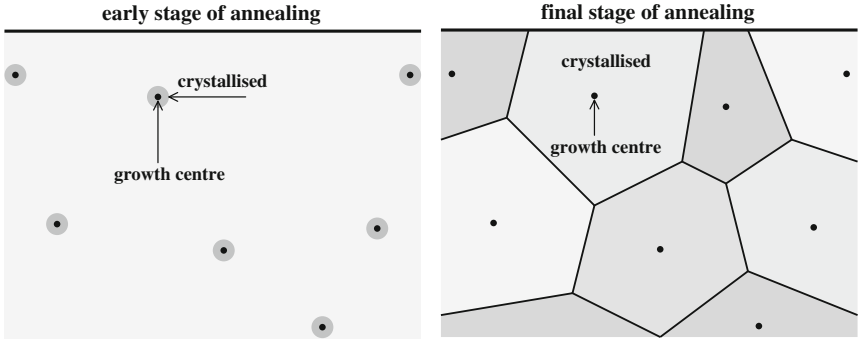

Fig. 13 Schematic sketch of annealing of an amorphous material into a crystalline material. It is assumed that growth centres form at random inside the volume. *Left:* Early stage, where only small crystallized regions have grown around the centres. *Right:* Late stage, when the whole volume is crystallized

problem of overlap can be handled by means of the Avrami-Johnson-Mehl model (e.g. Carter [98]). Also, if growth centres preferentially form at surfaces, as it was observed by Fabian et al. [92], the growth cannot be treated in the simple approximation (78).

The average degree of crystallization $x_{\rm cr}$ of a grain can approximately be determined from the solution of (78) by

$$x_{\rm cr} = \min\left(V_{\rm cr}(t)\zeta_{\rm cr}/V_0\ ,\ 1\right). \tag{80}$$

Here $\zeta_{\rm cr}$ denotes the number of growth centres per Si nucleus. According to this definition of $\zeta_{\rm cr}$ the quantity $V_0/\zeta_{\rm cr}$ is the average volume of the amorphous material available for each growth centre, into which the crystallized region may expand (Gail [99]).

The growth centres may already pre-exist in the amorphous material or they have to be formed by a nucleation process. The nucleation of growth centres for crystallization of circumstellar dust on the basis of classical nucleation theory was studied by Kouchi et al. [95] and by Sogawa and Kozasa [96], Kozasa and Sogawa [100].

Some experimental hints on the formation of seed nuclei for crystallization in enstatite can be found in Fig. 2 of Fabian et al. [92], from which one reads off an induction time required for the formation of seed nuclei of about 235 h at 1,080 K and about 18 h at 1,121 K. This can be fitted by

$$\tau_{\rm nuc} = 2.62 \times 10^{-25}\,{\rm e}^{75\,870/T}\ {\rm s}. \tag{81}$$

The time required for the formation of crystallization centres in amorphous enstatite is shown in Fig. 12. If crystallization requires the nucleation of growth centres, the temperature required for onset of crystallization in protoplanetary discs will be shifted from 800 K to about 900 K. Since the timescale for crystallization, Eq. (79), is shorter than $\tau_{\rm nuc}$, the formation of the first growth centre is followed by complete crystallization.

5.2 Solid Diffusion

Diffusion is a transport of matter within a mixture (solution) driven by concentration gradients. The temperature dependence of the diffusion coefficient can usually be approximated by the Arrhenius form

$$D = D_0\,{\rm e}^{-Q/RT}. \tag{82}$$

R is the gas constant. The frequency factor D_0 and the activation energy Q have to be determined for each material by laboratory experiments.

Solid diffusion of the different constituents within the dust minerals is important because it determines to a large extent the composition of growing or vaporizing dust species, the rate of solid chemical reactions, and the existence and extent of internal composition gradients within dust grains. Counterdiffusion of the main components forming a substance, which changes its local composition, is called *interdiffusion*. Generally interdiffusion of species in a composite material tends to homogenize any internal composition gradients within grains, but diffusion in solids involves signif-

icant activation energy barriers and does not operate, or operates only incompletely, at low temperatures.

Diffusive transport of matter in solids may occur by three major path's: by *volume diffusion* through the grain lattice, by *surface diffusion* across a grain surface, and by *grain boundary diffusion*. The slowest process is volume diffusion. It requires the existence of point defects in the solid (e.g. vacant lattice sites or interstitial atoms). Diffusion along grain-grain boundaries, if such exist like in fine-grained polycrystalline material, is much easier. It requires the existence of line or surface defects like, e.g., dislocations or internal grain boundaries. Matter transport across free surfaces or via the gas phase usually is fast. Here we consider volume diffusion, since this is responsible for homogenization of composition differences within microcrystallites and for solid reactions.

A brief general discussion of the basic principles of solid diffusion in silicate minerals and glasses is given by Freer [101]. Extensive compilations of data for diffusion in minerals are given by Freer [101] and Brady [102].

5.2.1 Intrinsic and Extrinsic Diffusion

The lattice defects required for solid diffusion have two significantly different contributions: either they are permanently present resulting from impurity ions, dislocations, grain boundaries and so on, or they are created spontaneously as pairs of vacancies and interstitial ions by thermal excitation at high temperatures. Diffusion mediated by this kind of defects usually requires higher activation energies than diffusion mediated by impurity ions and other pre-existing defects, since additionally to the activation energy for migration the activation energy for defect creation has to be overcome. Hence, there exist two regions with different temperature dependencies and quite different values of the diffusion coefficient, the region of *intrinsic* diffusion at high temperature and the region of *extrinsic* diffusion at low temperature. In an Arrhenius plot of the diffusion coefficient the transition from intrinsic to extrinsic diffusion is characterized by the occurrence of a kink. This is illustrated in the right part of Fig. 14.

Obviously, the diffusion coefficient corresponding to intrinsic diffusion is a property of the material under consideration and, in principle, at a given temperature is the same for all particles formed by the same material. The extrinsic diffusion coefficient, however, depends on the history and formation conditions of a particle and may be grossly different for different specimens of the same material.

Since timescales available for diffusion, both under circumstellar shell or protoplanetary disk conditions, are rather long compared to laboratory measurement conditions, diffusion effects in cosmic objects become important already at a much lower temperature ($<1,000\,\mathrm{K}$) than in the laboratory. For astrophysical applications one needs diffusion data for rather low temperatures where possibly diffusion is dominated by extrinsic diffusion. One has therefore to be cautious in applying laboratory measured diffusion coefficients obtained for intrinsic diffusion to astrophysical problems.

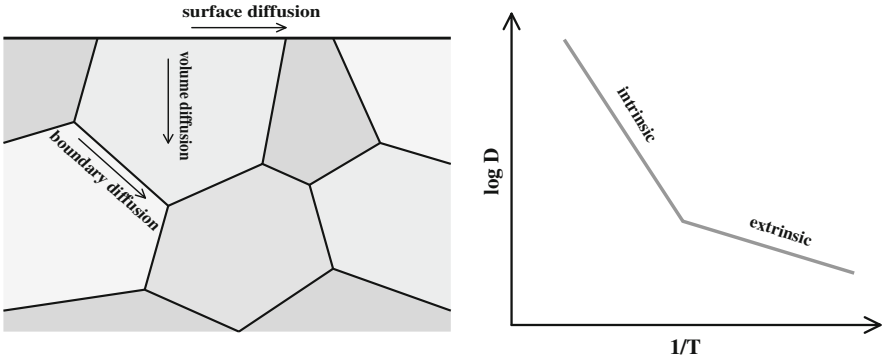

Fig. 14 *Left:* The different diffusion modes in a solid. *Right:* Temperature dependence of diffusion data showing extrinsic and intrinsic regimes

5.2.2 Interdiffusion of Mg and Fe in Olivine

The interdiffusion of the Mg^{++} and Fe^{++} cations in the magnesium-iron silicates olivine and orthopyroxene is of particular importance because these minerals form the dominating dust species in the standard cosmic element mixture. The exchange of Mg and Fe between olivine, orthopyroxene, and iron and its diffusional transport within grains determines the chemical composition of the dust mixture in circumstellar shells and protoplanetary discs.

Diffusion of Mg and Fe in olivine with particular emphasis on astrophysical or geophysical applications has been studied in the laboratory several times (Buening and Buseck [106], Misener [107], Morioka [108, 109], Chakraborty et al. [110], Chakraborty [103]). Especially the older studies of Buening and Buseck [106] seemed to indicate an intrinsic-extrinsic diffusion transition. The most recent and more consistent determination of Mg-Fe-interdiffusion in olivine by Chakraborty [103] yields much lower diffusion coefficients than older determinations and show no indications for a change from intrinsic to extrinsic diffusion. It is argued by Chakraborty that true intrinsic diffusion is unlikely to be observable for olivine and that the observed interdiffusion of Fe and Mg over the whole experimental temperature regime is determined by the presence of Fe^{+++} impurities, i.e., extrinsic diffusion dominates. Extrapolation of the results to lower temperatures seems to be uncritical in this case.

For olivine with composition $Fo_{86}Fa_{14}$ Chakraborty finds $D_0 = (5.38 \pm 0.89) \times 10^{-5}\,\mathrm{cm^2\,s^{-1}}$ and $Q = 226 \pm 18\,\mathrm{kJ/mole}$. The diffusion coefficient of olivine depends considerably on the fayalite concentration and this may be approximated by an exponential law (Buening and Buseck [106], Misener [107])

$$D_0(x) = D_0(0)\,\mathrm{e}^{-\alpha x}, \tag{83}$$

where x is the mole fraction of forsterite in olivine. Values of α for a number of cations are compiled in Morioka [109]. Chakraborty [103] finds essentially the same

Table 5 Diffusion coefficients for cation interdiffusion for some important dust materials: $D = D_0 \exp\{-T_0/T - \alpha x\}$

Mineral	Cations	D_0 [cm^2/s]	T_0 [K]	α	Temperature range [K]	References
Olivine	Fe-Mg	2.0×10^{-2}	27,180	6.91	1,250–1,570	[103]
Pyroxene	Fe-Mg	1.1	43,300	–	1,020–1,170	[104]
Melilite	Al-Si	$9.3 \times 10^{+1}$	50,510	3.34	1,470–1,620	[105]

dependence of D_0 on x as the previous studies. For $T = 1,000$℃ one finds from Fig. 4 of that paper a value of $\alpha = 3 \ln 10$. Since the study of Chakraborty seems to be the most reliable one, we choose this value for α. Then one finds for olivine $D_0(0) = 2.0 \times 10^{-2}\,\mathrm{cm}^2\,s^{-1}$. The data are listed in Table 5.

The activation energy for Mg-Fe interdiffusion in olivine is much lower than the activation energy for annealing (cf. Tables 4 and 5). Internal gradients in the Fe/(Mg+Fe) concentration within dust grains are erased already at a lower temperature than disorders in the lattice structure.

The role of Mg-Fe-cation interdiffusion in olivine evaporation is studied by Ozawa and Nagahara [111].

5.2.3 Interdiffusion of Mg and Fe in Pyroxene

The Mg-Fe interdiffusion in orthopyroxene minerals seems to be less well studied. Some laboratory data on Mg self-diffusion are reported by Schwandt et al. [104]. A detailed study on Fe-Mg interdiffusion in natural specimens of orthopyroxene was performed by Klügel [112]. There are no experimental data over an extended temperature regime. The results of Klügel [112] seem to indicate (Fig. 7 of the paper) that the data of Schwandt et al. [104] for Mg tracer diffusion can be taken as representative also for Mg-Fe interdiffusion in orthopyroxene. The frequency factor of the coefficient of Mg self-diffusion in crystallographic (100) direction in orthopyroxene with composition $\mathrm{En_{88}Fs_{12}}$ according to Schwandt et al. [104] is $\log D_0 = 0.04 \pm 2.48$ (D in units cm^2 s^{-1}) and the activation energy is 360 ± 52 kJ/mole. These data are listed in Table 5. The rather low temperature for which D was experimentally determined makes it rather unlikely that the results refer to intrinsic diffusion, i.e., extrapolation of the diffusion coefficient to lower temperatures probably is admitted. Most likely the diffusion coefficient depends on the enstatite-ferrosilite mixing ratio in orthopyroxene similar to the case of olivine, but no experimental results are available.

The activation energy for Mg-Fe interdiffusion in olivine seems to be somewhat higher than the activation energy for annealing (cf. Tables 4 and 5), but the difference is probably within the experimental errors.

5.2.4 Interdiffusion of Al and Si in Melilite

The interdiffusion of Al + Al vs. Mg + Si in melilite, a solid solution between gehlenite ($\mathrm{Ca_2Al_2SiO_7}$) and åkermanite ($\mathrm{Ca_2MgSi_2O_7}$), is important for the evolution of the Al-Ca dust component, since melilite is one of the important Ca-Al compounds formed in the oxygen-rich element mixture.

The interdiffusion process in this material is quite complex since it requires paired diffusion of $Al^{3+} + Al^{3+}$ versus $Mg^{2+} + Si^{4+}$ because of charge balancing. This results in a complex composition dependence of the diffusion coefficient as found by Nagasawa et al. [105]. For astrophysical applications only the gehlenite rich melilite mixture is of interest. The activation energy Q for mixtures with composition $Ge_{100} - Ge_{50}$ found by Nagasawa et al. [105] is 420 ± 50 kJ/mole. The frequency factor depends on the mole fraction x of gehlenite in the solution as in (83) if $x > 0.5$. For $x < 0.5$ the dependency is quite different. The frequency factor $D_0(0)$ in (83) can be determined from Fig. 2 of Nagasawa et al. [105] as $D_0(0) = 92.7$ for the gehlenite rich mixture ($x < 0.5$) and a coefficient α for (83) of 3.34. The temperature interval in the laboratory experiments of Nagasawa et al. [105] covers the temperature region where gehlenite may be formed in protoplanetary discs. No substantial extrapolation of the laboratory results is required in this case. The data are listed in Table 5.

Figure 15 shows the characteristic diffusion time

$$\tau_{\text{diff}} = a^2/D \tag{84}$$

for dust grains of radius $a = 0.1\,\mu$m for the different materials. For comparison the figure also shows the characteristic timescales for radial and vertical mixing in protoplanetary discs for a stationary disk model and the characteristic hydrodynamic time scale r/v for a stationary wind model.

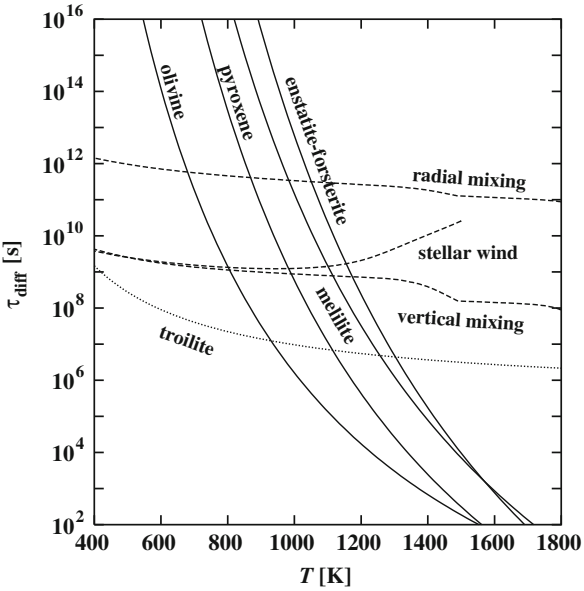

Fig. 15 *Full lines:* Characteristic timescales for solid inter-diffusion of cations in 0.1 μm dust grains. For olivine and orthopyroxene a 10% iron content is assumed, for melilite a 10% content of åkermanite. *Dashed lines:* Time scales for radial and vertical transport processes are as in Fig. 12. *Dotted line:* Troilite formation from iron by reaction with H_2S at total gas pressure of 10^{-3} bar

5.3 Chemical Reactions

There are a number of chemical reactions between the gas phase and the solids and between solids that are important for the evolution of the dust mixture, especially in the case of protoplanetary discs. Only a few of these reactions seem to have been studied in the laboratory.

5.3.1 Enstatite Formation from Olivine

Since olivine is stable up to higher temperatures than pyroxene (cf. Fig. 5), but pyroxene is the dominant component at low temperatures, a solid state chemical reaction is required for conversion of forsterite into enstatite and vice versa. An experimental study of the formation of enstatite rims on forsterite in a Si-rich gas has been performed by Imae et al. [113] (see Table 6). The vapour from thermal vaporization of cristobalite ($SiO_2 \rightarrow SiO + O_2$) reacted with a forsterite crystal and formed a layer of stoichiometric enstatite which covered the forsterite. A parabolic rate law

$$x^2 = kt \tag{85}$$

was observed for the growth of an enstatite layer of thickness x. This indicates that the reaction is controlled by diffusion through the enstatite layers. A model is favoured, that growth occurred by Si^{4+} and $2Mg^{2+}$ counterdiffusion via grain boundary diffusion. The experimental results for the rate constant k are fitted by

$$k = k_0\, \mathrm{e}^{-Q/RT} \tag{86}$$

with $Q = 505 \pm 188\,\mathrm{kJ/mole}$ and $\log k_0 = 3.6 \pm 5.6$ where k_0 is in units cm^2/s. The results are obtained at rather high temperatures between 1,450 K and 1, 820 K. Since the basic diffusion mechanism controlling the solid reaction seems to be grain boundary diffusion, the data probably can be extrapolated to lower temperatures. The formation of a forsterite layer on entstatite during enstatite evaporation is studied by Tachibana et al. [65].

The reaction kinetics of formation of enstatite as a reaction rim from forsterite and quartz was studied by Milke et al. [114]. They determined a rather high activation energy of $426 \pm 34\,\mathrm{kJ\,mol}^{-1}$.

Table 6 Rate coefficients for the formation of reaction rims: $k = k_0 \exp\{-T_0/T\}$

Minerals	k_0 [cm^2/s]	T_0 [K]	Temperature range [K]	Reference
Enstatite-forsterite	4.0×10^3	60, 730	1,450–1,820	[113]

5.3.2 Formation of Troilite

At temperatures below about 720 K the iron reacts with H_2S molecules from the gas phase to form the sulphide FeS (cf. Fig. 5). This reaction has been studied in great detail in the laboratory by Lauretta et al. [115], which also give references to the preceding studies on FeS formation. Lauretta et al. found a linear growth kinetics for FeS layers on Fe up to a layer thickness of $\approx 30\,\mu$m and a parabolic growth kinetics controlled by diffusion of Fe^{2+} through FeS above $30\,\mu$m. Iron grains in protoplanetary accretion discs prior to the planetary formation stage probably are smaller than $10\,\mu$m (Kerridge [116]) and the linear growth rate has to be applied. They determined for this case a rate coefficient for the formation of FeS from solid Fe of $k_f = 5.6 \times \exp(-3,360/T)$ in units gram FeS per cm^2, hour, and atm and $k_r = 10.3 \times \exp(-11,140/T)$ for the reverse reaction. The reaction timescale in a gas of total pressure $P = 10^{-3}$ bar and solar abundance is shown in Fig. 15.

A more recent study of FeS reduction by H_2 has been performed by Tachibana and Tsuchiyama [117]. Because of the big specimens used in their experiments the results are not applicable for very small dust grains.

5.3.3 Formation of Magnetite

At temperatures below about 380 K in chemical equilibrium the iron metal would be converted under protoplanetary disk conditions into magnetite (Fe_3O_4). The kinetics of the formation of magnetite from iron has been studied by Hong and Fegley [118]. They found much slower conversion of iron into magnetite than of iron into troilite. The oxidation reaction was studied at standard pressure and no dependence of the rate constant on H_2 and H_2O pressures has been determined, so unfortunately it is not possible to use the results in model calculations at the much lower pressures in accretion discs and circumstellar shells.

5.3.4 Reduction of Silicates by H_2

The reduction of silicates by hot H_2 gas was studied by Allen et al. [119].

6 Circumstellar Dust Shells

Dust is formed in late stages of stellar evolution by stars from almost the whole range of initial stellar masses on the main sequence. Here we discuss the formation of the most abundant minerals in circumstellar shells with an oxygen-rich element mixture. We do not consider the soot formation problem in carbon-rich environments and we do not consider the problem of formation of secondary dust components formed from Al and Ca (see Fig. 5 for the most stable Al-Ca-compounds). Al bearing dust grains have been found as presolar grains (cf. Nittler

et al. [120]), but presently nothing seems to be known on the condensation kinetics of such dust materials.

6.1 Predictions of Dust Composition by Equilibrium Calculations

Low and intermediate mass stars reach the upper part of the AGB as M-stars with the slight modifications of their initial element abundances by first and second dredge up processes (mixture (1) in Table 1) where they start to experience severe mass-loss by a dust driven wind. After the onset of thermal pulsing the products of He-burning are mixed during the "third dredge-up" from the core into the stellar envelope and the carbon abundance increases in discrete steps after each pulse (e.g. Groenewegen et al. [121]; Herwig [1]), while the oxygen abundance essentially remains unchanged.

Stars with initial masses $M_* \lesssim 1.5\,\mathrm{M}_\odot$ have lost most of their envelope and evolve off from the AGB towards the stage where they excite a planetary nebula (PN) before the carbon abundance in their envelope exceeds that of oxygen (e.g. Groenewegen et al. [121]), and stars with initial masses less than about $1\,\mathrm{M}_\odot$ even do not suffer third dredge-up. All these stars remain M-stars during their whole AGB evolution.

Stars with initial masses in the range $1.5 \lesssim M_* \lesssim 4$–$5\,\mathrm{M}_\odot$ (the limits depend somewhat on metallicity) suffer several thermal pulses and increase their carbon abundance in the envelope from an initial C/O abundance ratio of about 0.3 after first and second dredge-up, to a value of $\mathrm{C/O} > 1$ where carbon is more abundant than oxygen. The star then becomes a C-star and remains to be so until the star evolves off from the AGB towards the PN-stage.

Stars with initial masses between 4–5 $\mathrm{M}_\odot$ and $8\,\mathrm{M}_\odot$ most likely experience "hot bottom burning". These stars do not become carbon stars (cf. Lattanzio and Forestini [122]). They develop a strong N overabundance instead.

If during the stepwise increase of the carbon abundance in the envelope the C/O abundance ratio is close to unity, the star appears as of spectral type S (Scalo and Ross [123]) where the chemistry is different from both that of M and of C stars. For stars with initial masses in the region $1.5 \lesssim M_* \lesssim 2\,\mathrm{M}_\odot$, however, the C/O ratio increases in a few and rather big steps from $\mathrm{C/O} < 1$ to $\mathrm{C/O} > 1$ and the intermediate state of $\mathrm{C/O} \approx 1$ of an S star probably is skipped in most cases (Groenewegen et al. [121]).

The chemistry in the stellar envelope and the spectral appearance of the stars is completely different for each of the three different carbon to oxygen abundance ratios $\mathrm{C/O} < 1$, $\mathrm{C/O} \approx 1$, and $\mathrm{C/O} > 1$. This also holds for the chemical composition of the dust formed in their dust shells.

Massive stars from the region of initial masses $8 \lesssim M_* \lesssim 25\,\mathrm{M}_\odot$ reach the RGB (Schaller et al. [3]) before they explode as supernovae and form dust during their evolutionary stage as Red Supergiant. The element mixture in their atmospheres in this stage corresponds to that of M stars on the AGB (e.g. Schaller et al. [3]).

6.1.1 M Stars

From chemical equilibrium condensation calculations it is known that for the standard cosmic element mixture the most abundant refractory elements Si, Mg, Fe form the silicates olivine ($Mg_{2x}Fe_{2(1-x)}SiO_4$) and pyroxene ($Mg_xFe_{1-x}SiO_3$) (cf. Fig. 5) and solid nickel-iron (cf. Fig. 8). The iron content of the silicates in chemical equilibrium at high temperatures is small, as is demonstrated in Fig. 9. Their composition corresponds to nearly pure forsterite Mg_2SiO_4 and enstatite $MgSiO_3$. Observationally it is found from infrared observations of circumstellar dust shells around M stars that silicates are the dominating dust species (see "The Mineralogy of Interstellar and Circumstellar Dust in Galaxies" by Molster et al., this volume). Usually the lattice structure is not crystalline but amorphous and they seem to form with significant iron content, i.e., the dust has olivine-like or pyroxene like composition with x being significantly smaller than unity. Only in stars with very high mass-loss rate one observes condensation of certain fractions of crystalline silicates, that are indeed found to be iron poor, as it is predicted from equilibrium calculations. Additionally a number of minor dust components, in particular Al-compounds and some oxides not existing in chemical equilibrium, are detected by their spectral signatures (see "The Mineralogy of Interstellar and Circumstellar Dust in Galaxies" by Molster et al., this volume).

The abundance ratio of Mg/Si of Pop I stars shows some scatter between different stars (cf. Fig. 1) and only marginally exceeds unity in the Solar System (Lodders et al. [8]). The stability regions of the different equilibrium condensates with varying Mg/Si abundance ratio for a pressure typical for the condensation zone in a stellar wind is shown in Fig. 16. For Mg/Si abundance ratios exceeding unity one expects forsterite and enstatite to be the main silicate dust compounds, for Mg/Si abundance ratios less than unity quartz (SiO_2) additionally becomes a stable condensate, which is absent from the mixture for $\varepsilon_{Mg}/\varepsilon_{Si} > 1$ since in the latter case the magnesium silicates can bind all Si and Mg. Current data on stellar Mg and Si abundances do

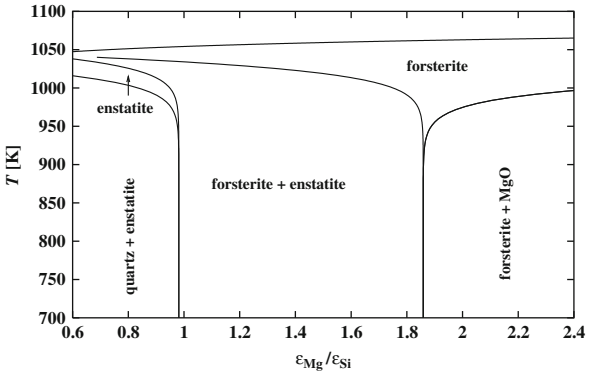

Fig. 16 Stability limits of the abundant magnesium and silicate compounds at $P = 10^{-10}$ bar for varying abundance ratios of magnesium to silicon. The picture shows the regions of existence of the different condensates in chemical equilibrium (Ferrarotti and Gail [68])

not exclude Mg/Si < 1 in some fraction of stars. For other elements of interest for dust formation (Fe, Al, Ca) the scatter in element abundances seems to be too small to cause variations in the type of dust mixture.

6.1.2 S Stars

Chemical equilibrium calculations for determining the stable condensates for varying C/O abundance ratios at the transition from M to C stars ($\varepsilon_C/\varepsilon_O \approx 1$) have been performed by Ferrarotti and Gail [33] and Lodders and Fegley [26]. The main characteristics of the chemistry at the transition is the lack of oxygen and carbon which prevents the formation of silicates and oxides at one hand and of carbon dust and carbides on the other hand. The most abundant refractory elements according to equilibrium calculations form solid iron and FeSi (cf. Fig. 17). The magnesium would condense in chemical equilibrium as MgS (not shown in Fig. 17) at temperatures below about 800 K and probably is of no interest for circumstellar condensation in S stars.

6.1.3 C Stars

The equilibrium chemistry of the carbon-rich mixture is discussed at length by e.g. Lodders and Fegley [26, 27], Sharp and Wasserburg [21]. The upper stability limits of condensed phases formed in this case are shown in Fig. 6. The main condensed phases formed from the abundant elements are carbon dust, SiC, and MgS. These have been detected by their infrared emission from circumstellar dust shells (see "The Mineralogy of Interstellar and Circumstellar Dust in Galaxies" by Molster et al., this volume). Also solid iron (or FeC_3) might be formed, but observationally nothing is known about this. The condensation of carbon dust is not treated in detail in this contribution since it is not a mineral.

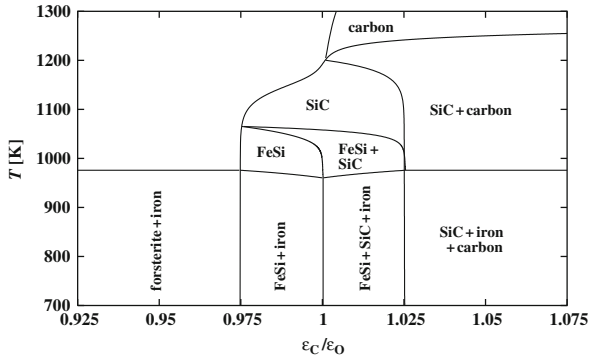

Fig. 17 Stability limits of the abundant condensates at the transition from M over S to C stars for varying carbon to oxygen abundance ratios and a pressure of $P = 10^{-10}$ bar. The picture shows the regions of existence of the different condensates in chemical equilibrium (Ferrarotti and Gail [68])

6.1.4 CNO Processed Element Mixture

In material having burned hydrogen via the CNO-cycle and having reached equilibrium of C, N, and O isotopes the abundance of C and O drop below that of the abundant dust forming elements Si, Fe, and Mg (cf. Fig. 2), but the mixture remains oxygen rich (mixture (3) in Table 1). Insufficient amounts of O and C are available to form oxides or carbides. In this respect the chemistry in this mixture bears some similarities with that of S-stars. The stability limits of the most stable condensates formed from this mixture are shown in Fig. 7. Solid iron and Fe-Si-alloys are expected to be the most abundant dust components formed from this mixture. The chemical equilibrium dust composition with respect to Fe and Si for this mixture is shown in Fig. 18.

Such kind of dust may be formed in the rare cases where Luminous Blue Variables form dust or during post-AGB evolution after a late thermal pulse (cf. Blöcker [124]).

6.2 Non-equilibrium Dust Formation

In stellar outflows the dust forms in a rapidly cooling and rapidly diluted environment. Under these conditions the chemistry in such shells does not evolve into an equilibrium state. Dust formation in stellar outflows is a time dependent problem which must be calculated by solving the equations for the time dependent condensation kinetics.

6.2.1 Timescales

The dust formation problem is governed by three characteristic timescales.

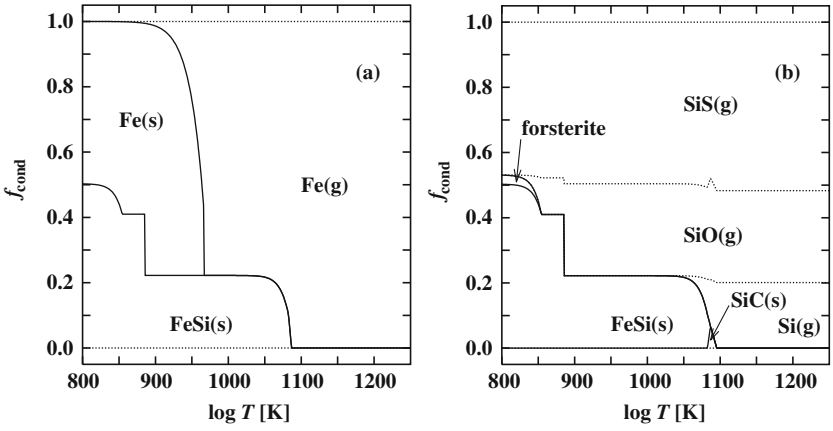

Fig. 18 Distribution of the dust forming elements Fe, Si in chemical equilibrium between solids and the gas phase for CNO-cycle processed material at $P = 10^{-10}$ bar

Growth timescale: The growth of grains is determined by (72). The essential growth species are a few abundant molecules from the gas phase which usually carry nearly all atoms of an element which is essential for the formation of a dust species. In the oxygen-rich element mixture for instance the abundant dust species olivine and pyroxene are formed from SiO, Fe, and Mg, and from H_2O as oxidizing agent. If the growth species are not yet substantially consumed by grain growth one has for the particle density n of the rate determining growth species

$$n = \varepsilon \dot{M}/4\pi r^2 v(1+4\epsilon_{\rm e})m_{\rm He}, \tag{87}$$

if we assume for simplicity a stationary outflow. Here ε is the abundance of the element forming the essential growth species. The characteristic timescale for particle growth up to size a_d is (Eq. 72)

$$\tau_{\rm gr} = \frac{a_d}{|\dot{a}_d|} = \frac{a4\pi r^2 v(1+4\epsilon_{\rm He})m_{\rm H}}{V_0 \alpha v_{\rm th} \varepsilon \dot{M}(1-a_{\rm sol}^{-1/i})}. \tag{88}$$

Using the relation $4\pi R_*^2 \sigma T_{\rm eff}^4 = L_*$ and introducing numerical values for forsterite from Table 3 one obtains numerically

$$\tau_{\rm gr} = 1.8\times 10^8 \frac{1}{1-a_{\rm sol}^{1/i}} \frac{0.1}{\alpha} \frac{v}{c_T} \frac{r^2}{(4R_*)^2} \frac{L_*}{10^4 {\rm L}_\odot} \frac{1}{\dot{M}_{-5}} \left(\frac{2500{\rm K}}{T_{\rm eff}}\right)^4 {\rm sec}. \tag{89}$$

c_T is the isothermal sound velocity of the gas and $\dot{M}_{-5}$ the mass-loss-rate in units $10^{-5}\,{\rm M}_\odot\, year^{-1}$. $a_{\rm sol}$ is the activity.

Cooling timescale: Assuming for simplicity a grey temperature structure $T \propto r^{-1/2}$ in the dust-forming region we obtain for the time required by a gas parcel to cool by ΔT

$$\tau_{\rm cool} = 2(r/v)\ (\Delta T/T). \tag{90}$$

For the hydrodynamic expansion timescale we have

$$\tau_{\rm exp} = \frac{r}{v} = 1.8\times 10^8 \frac{c_T}{v} \frac{r}{R_*}\ {\rm sec}. \tag{91}$$

The isothermal sound velocity c_T at 1,000 K is about $2\,{\rm km\,s^{-1}}$.

At the onset of condensation ($a_{\rm sol} = 1$ at this point) the wind enters the condensation zone with a rather low velocity which is of the order of the sonic velocity. The time required for cooling by 10 K according to (90) is 3.7×10^6 s which is short compared to the growth time (89) of 1.8×10^8 s at $r = 4R_*$ and $v = c_T$. A decrease in T by 10 K typically increases the activities $a_{\rm sol}$ of the dust materials of interest by factor of about 10 (cf. Fig. 4). Short after the onset of dust growth the evaporation

term ($\propto 1/a^i_{\rm sol}$) in the growth equation becomes negligible because of significant cooling without significant depletion of the gas phase from condensable material.

From (90) one infers that during the time required for dust grains to grow to their final size of about 0.1 μm the gas in the stellar wind cools by several 100 K.

Acceleration timescale: After significant amounts of dust from the most abundant refractory elements are condensed the gas is rapidly accelerated by radiation pressure on grains. Neglecting pressure effects, the velocity increase between two radii r_1 and r_2 is

$$v_2^2 - v_1^2 = 2GM_*(\Gamma - 1)\int_{r_1}^{r_2} dr/r^2 = 2GM_*(\Gamma - 1)\ (r_2 - r_1)/(r_2 r_1) \qquad (92)$$

where

$$\Gamma = f\kappa\, L_*/4\pi cGM_* = 0.77 \times f\,\kappa\,\frac{L_*}{10^4 L_\odot}\,\frac{M_\odot}{M_*} \qquad (93)$$

is the ratio of radiative acceleration to gravitational attraction. κ is the mass extinction of the dust, which is about 20 at $T_{\rm eff} = 2,500$ K (e.g. Fig. 10 in Ferarotti and Gail [33]), and f is the fraction of the condensible material condensed into grains. Starting from about sonic velocity $c_T \ll v$ at r_1 yields $v^2 \approx (\Gamma - 1)v^2_{\rm esc}\ \Delta r/r$. The time $\tau_{\rm acc}$ required for a gas parcel to move from r_1 to r_2 can be approximated by $\tau_{\rm acc} = 2\Delta r/v$ which yields

$$\tau_{\rm acc} \approx \frac{2}{\Gamma - 1}\,\tau_{\rm exp}\, v^2/v^2_{\rm esc}. \qquad (94)$$

Since Γ usually is of the order of 2–5the time required to accelerate the wind material to its final expansion velocity of $v \approx v_{\rm esc}(4R_*)$ is of the same order as the growth timescale $\tau_{\rm gr}$ if $\dot{M} \approx 10^{-5}\,{\rm M}_\odot\ year^{-1}$.

The increase of v from c_T to the supersonic outflow velocity increases the growth timescale by a factor of about 10 compared to its initial value. The further growth of grains is strongly slowed down from this point on. Due to the further increase of $\tau_{\rm gr} \propto r^2$ (cf. Eq. (89)) during the outward motion of a gas parcel the grain growth essentially ceases by rapid dilution of the wind material after acceleration of the wind to strongly supersonic outflow velocities.

For mass-loss rates exceeding about $\dot{M} \approx 10^{-5}\,{\rm M}_\odot\ year^{-1}$ one has $\tau_{\rm gr} \le \tau_{\rm acc}$ and the condensation of the condensable material into grains will be more or less complete. For mass loss rates $\dot{M} < 10^{-5}\,{\rm M}_\odot\ year^{-1}$ condensation is incomplete because $\tau_{\rm gr} > \tau_{\rm acc}$ and grain growth is suppressed before condensation is complete.

At low mass loss rates $\dot{M} < 10^{-5}\,{\rm M}_\odot\ year^{-1}$ one has to be aware that only part of the material is condensed and one has bigger to much bigger gas to dust ratios than in the ISM!

In this estimate it is assumed that sufficient dust condenses to accelerate the wind material to supersonic velocities which requires a sufficiently high mass-loss rate. This problem is discussed in Gail and Sedlmayr [125].

6.2.2 Non-equilibrium Condensation

As we have seen, in a stellar wind the gas cools by several 100 K from the onset of condensation until either all condensible material is consumed or further growth is suppressed by rapid dilution. This has the consequence that for a less stable condensed phase, that can be formed from the same growth species as some more stable dust material that is just growing by collecting material from the gas phase, the activity $a_{\rm sol}$ also increases above unity during rapid cooling because the more stable dust species had not sufficient time to collect all the growth species from the gas phase. From this point on such less stable materials may also start to condense from the gas phase, though they would not be present in a chemical equilibrium state.

The evolution of the activities of two possible condensates competing for the same growth species from the gas phase during cooling is shown schematically in Fig. 19:

- $\tau_{\rm cool} \ll \tau_{\rm gr}$: For very rapid cooling (left part) condensation is completely suppressed because of strong dilution of wind material.
- $\tau_{\rm cool} \gg \tau_{\rm gr}$: For very slow cooling (right part) only one of the two competing components is formed as in chemical equilibrium because the more stable material consumes all the condensable material. The activity of the more stable material first increases to unity and remains constant from that point on. The activity of the thermodynamic less stable material remains always less than unity.
- $\tau_{\rm cool} \approx \tau_{\rm gr}$: During rapid cooling (middle part), growth cannot take place with the shift of the equilibrium state with decreasing temperature. The activity of

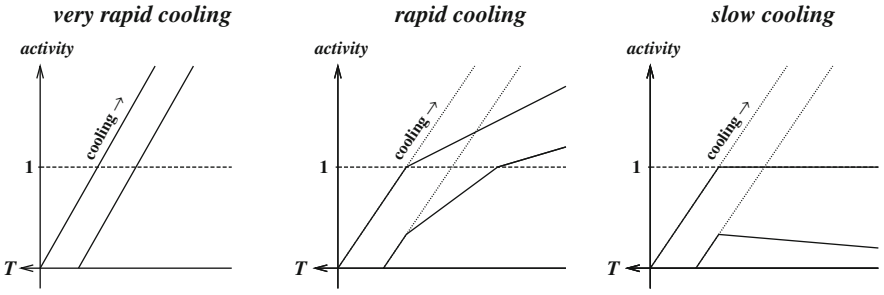

Fig. 19 Schematic evolution of the activities of two competing substances that can be formed from the same gas phase material during cooling. *Left:* Cooling is so rapid that essentially no condensation occurs. *Middle:* Rapid cooling where the more stable substance has not consumed the condensable material at the instant where the less stable material starts to condense. *Right:* Cooling is so slow that the system always is close to chemical equilibrium. The less stable material never condenses because its activity always remains < 1

the more stable material exceeds unity since the growth rate of the condensed phase is less that rate of increase of activity. For this reason the activity of the less stable material also exceeds unity from some point on and this material also starts to condense

In the rapid cooling environment of stellar outflows one obtains a non equilibrium dust mixture which represents some *frozen-in transient state* of the chemical system on its evolution towards chemical equilibrium that, however, never can be attained.

An inspection of Fig. 4 shows that for the standard oxygen-rich element mixture this particular case is relevant for quartz (SiO_2) and magnesiumoxide (MgO). These two solids do not exist in chemical equilibrium in the oxygen-rich element mixture because all Mg and Si condenses into the thermodynamically more stable magnesium silicates. Because of rapid cooling in a stellar outflow, however, they become stable before olivine and pyroxene formation have consumed all of the material from which solid SiO_2 and MgO can be formed. Hence quartz and MgO is expected to form as separate dust components in this case (Gail and Sedlmayr [126]; Ferrarotti and Gail [68]). More precisely, since MgO forms a solid solution with $Fe_{1-\delta}O$ ($\delta \ll 1$) one obtains magnesio-wüstite $Mg_xFe_{1-x-\delta}O$ as dust component in oxygen-rich dust shells (Ferrarotti and Gail [127]), which, in fact, has been found in observations (Posch et al. [128]).

The appropriate tool for studying this type of non-equilibrium condensation due to rather rapid cooling is the activity-temperature diagram that is shown for the particular case of condensation from the oxygen rich element mixture in Fig. 4. One readily reads off from this diagram which solids are expected to be the most stable ones which first start to condense (those with the highest activities) and which are the secondary products which do not exist in chemical equilibrium but are formed during rapid cooling. These are those for which activities cross the border $a = 1$ within a temperature difference ΔT to the onset of condensation of the first abundant condensate for which $\tau_{\rm cool}(\Delta T)$ defined by (90) equals $\tau_{\rm acc}$:

$$\Delta T \approx \frac{1}{2} T \tau_{\rm acc}/\tau_{\rm exp}. \tag{95}$$

This difference ΔT amounts to about 200–300 K at $\dot{M} \approx 10^{-5}\,{\rm M}_\odot\, year^{-1}$ and may be different for different cooling rates.

Model calculations for non-equilibrium condensation require to solve the set of growth equations of the type (72) for each of the possible condensates simultaneously with the equations for the consumption of gas phase material and the equations of the stellar wind. The set of equations to be solved is discussed in Gail and Sedlmayr [126] and Ferrarotti and Gail [33, 68]. Solutions have been obtained so far only for the case of oxygen rich element mixtures and the case of S-Stars.

While the dust growth problem for the most abundant minerals in circumstellar shells in principle can be treated realistically since many of the data required for the calculation have been determined in the laboratory during the last two decades (see

Sects. 4 and 5), realistic model calculations presently are seriously hampered by our ignorance with respect to the nucleation processes in oxygen-rich environments.

6.2.3 Fe Content of Olivine and Pyroxene

Besides the well known amorphous silicates in circumstellar shells of oxygen-rich stars a crystalline silicate component has been detected in the infrared spectra of many late type stars with circumstellar dust shells. The observation shows that the crystalline dust component has a low iron content (see "The Mineralogy of Interstellar and Circumstellar Dust in Galaxies" by Molster et al., this volume). A low iron content of the silicates is characteristic for a dust mixture where silicate dust has equilibrated with solid iron.

Figure 20 shows the degree of condensation of olivine and pyroxene and the mole fraction of the iron rich end-member of the solid solution series if it is assumed that iron does not condense. In this case the partial pressure of Fe atoms in the gas phase is not fixed to the low vapour pressure of iron but remains high. Comparison with Fig. 9 shows that a low iron content of olivine and pyroxene formed in a stellar wind can only be expected if silicate condensation runs into completion already at temperatures $T \gtrsim 950\,\mathrm{K}$ where the vapour pressure of the iron rich component is high and the iron content of silicates is low despite of a high partial pressure of Fe in the gas phase. If the condensation process in the outflow extends to much lower temperatures, there is no preference for iron-poor silicates. One mainly obtains Fe-rich silicates, mainly of olivine composition, due to incomplete condensation of iron, the pressure of Fe atoms in the gas phase much exceeds the vapour pressure

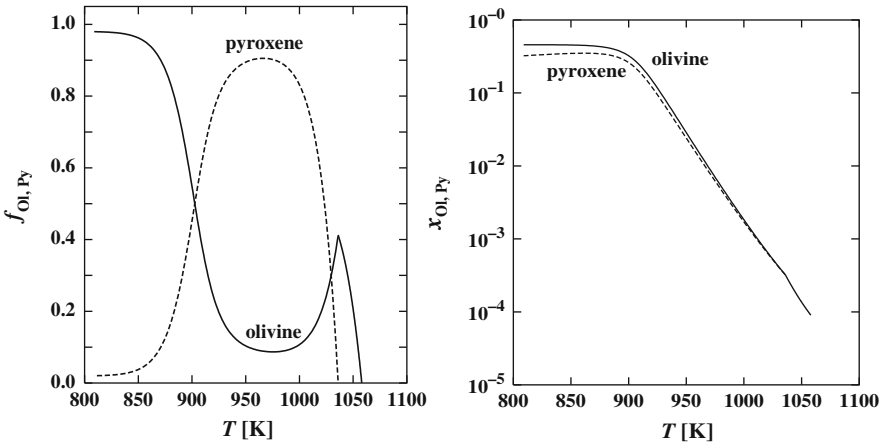

Fig. 20 Condensation of olivine and pyroxene in chemical equilibrium at total pressure $P = 10^{-10}$ bar, representative for the condensation zone in stellar winds. The condensation of solid iron is suppressed. *Left part:* Fraction of the Si condensed into olivine and pyroxene. *Right part:* Mole fractions x_{fa} and x_{fs} of the iron bearing end members fayalite and ferrosilite in olivine and pyroxene, respectively

of iron. Only if the Fe partial pressure is buffered by solid iron one gets iron poor silicates and mainly enstatite.

7 Dust in Protoplanetary Accretion Discs

This section considers the dust component of the material in protostellar and protoplanetary accretion discs and its evolution. We restrict our considerations to the early evolutionary phases of such discs before the onset of planet formation, when the disk material consists of a well mixed gas-dust mixture.

A precise knowledge of the composition, structure and extinction properties of the dust is important for calculating the structure and evolution of such discs as the dust extinction determines their temperature structure, the presence or absence of convection, the shielding of the discs interior from ionizing radiation from the outside and so on. Also the determination of the nature of the raw material from which later planetesimals and planets are formed requires an as precise knowledge as possible of the composition and structure of the dust.

The dust mixture probably is very complex; it consists of a big number of different compounds from the elements heavier than He, mainly compounds of the rock forming elements Si, Fe, Mg, Al, Ca, and Na with O, of Ni-Fe-alloy, and of carbonaceous compounds, but also numerous minerals of the less abundant elements are present (cf. Rubin [129]). For reasons of cosmic element abundance the most abundant dust components are compounds of Si, Mg, Fe and O, metallic iron or FeS, and carbon dust. They also dominate the extinction of the disk material. For the purpose of constructing models of protoplanetary discs it suffices to concentrate on the few most abundant dust species. Other dust components are important in other respects, but have no significant influence on the disk structure and evolution.

In the following we outline the basic problems which have to be solved in order to arrive at a self-consistent description of the evolution of protoplanetary discs during their early evolution, when the raw material for formation of planetesimals and planetary bodies is fabricated. Some reviews on this topic are, e.g. Cuzzi et al. [130], Wooden et al. [131]. For the related problem of ice formation see, e.g. Dodson-Robinson et al. [132].

7.1 Dust Mixture in the Outer Disk

Analysis of infrared emission from accretion discs around young stellar objects have not yet given conclusive results for the dust mixture in the outermost parts of accretion discs that are not affected by mixing with material from inner parts of the disk and therefore represent the pristine material of the Solar Nebula. Pollack et al. [133] have therefore attempted to derive the composition of the dust by carefully discussing the question which types of dust, formed from the most abundant dust forming elements (C, N, O, Mg, Si, and Fe), can be expected to exist in the

Table 7 Composition of the dust mixture in the outer regions of a protoplanetary accretion disk according to Pollack et al. [133], and fraction of the most abundant elements condensed into the different dust species. x denotes the mole fraction of the pure magnesium silicate end members of the solid solution series forming the magnesium-iron-silicates olivine and pyroxene, respectively

Dust	Composition	Mg	Fe	Si	S	C	x
Olivine	$Mg_{2x}Fe_{2(1-x)}SiO_4$	0.83	0.42	0.63			0.7
Pyroxene	$Mg_xFe_{1-x}SiO_3$	0.17	0.09	0.27			0.7
Quartz	SiO_2			0.10			
Iron	Fe		0.10				
Troilite	FeS		0.39		0.75		
Kerogen	HCNO					0.55	

parent molecular cloud cores, from which stars are formed, and in the cool outer parts of the resulting protostellar and protoplanetary accretion disks. They arrived at the conclusion that there exists a multicomponent mixture of several kinds of dust species, which is dominated most likely by the few species listed in Table 7.

The silicates have an amorphous lattice structure since dust in molecular clouds shows no indications for the existence of a crystalline component. The lattice structure of quartz probably also is amorphous, though from observations nothing is known about its structure. The solid iron and the troilite probably are solid solutions with Ni or NiS, respectively. The nature of the carbon dust component is not clear. The model of Pollack et al. [133] assumes kerogen, a carbon-rich substance containing also significant amounts of H, N, and O. This is the carbonaceous material found in the matrix of carbonaceous chondrites. It is unclear in which respect it resembles or differs from carbonaceous material in the ISM.

Less abundant dust components should also be present but are not considered in the model of Pollack et al. [133] because of their unimportance for the extinction of disk matter.

The model certainly is an only very crude estimate of the composition of the dust input of an accretion disk from its parent molecular cloud, but no better model is presently available and it seems to be grossly in accord with what is known from infrared observations (e.g. Watson [134]).

7.2 Dust Metamorphosis

Viscous torques in the accretion disk induce a slow inward migration of the disk material by which the material is transported from the cold outer disk toward increasingly warmer zones. Additionally, turbulent mixing in the convectively unstable parts of the disk intermingles material from different disk regions. At sufficiently high temperature, solid diffusion and annealing processes are activated in the dust grains which tend (i) to ex-solve impurities from the grain lattice and (ii) to form a regular crystalline lattice structure (Duschl et al. [135]; Gail [19]; Hallenbeck et al. [89]; Fabian et al. [92]). The grain material develops from the dirty and amorphous composition, which is responsible for the observed extinction

properties of interstellar grains, to a more clean and crystalline lattice structure. The basic chemical composition of individual grains as given in Table 7, however, is not changed by these processes. The assemblage of minerals, forming the dust mixture, essentially remains preserved at this stage, since there operate only *intra-grain* transport processes by solid diffusion, but no *inter-grain* transport processes via the gas phase.

This change in the lattice structure of the dust grains occurs in the region where the timescale for solid diffusion and annealing roughly equals the timescale for radial inward migration of the disk material. The model calculations in Gail [99] and Wehrstedt and Gail [136] have shown this to occur at about 800 K for glassy silicates (cf. also Fig. 12). If the structure of the silicate dust is more similar to that of the smokes prepared in the annealing experiments of Hallenbeck et al. [89] one determines from the data in Hallenbeck et al. [91] a somewhat higher annealing temperature of about 950 K (cf. Gail [99]). At temperatures above the annealing temperature the grains have a crystalline lattice structure, which at the same time increases their stability against evaporation.

At a temperature significantly higher than that required for annealing, transport processes between the surfaces of different grains via the gas phase start to operate (evaporation and re-condensation). Since the ISM dust mixture of the outer disk contains dust species, which have been formed in chemically such diverse environments as circumstellar shells of AGB-, RSG-, WC-stars, ejecta of supernovae, or by destruction of ISM dust by shocks and subsequent re-condensation in the ISM (cf. Draine [137]; Tielens [138]; Zhukovska and Gail [10]), the mineral components of the ISM-mixture are thermodynamically unstable for the element mixture of the protoplanetary disk material. The *inter-grain* transport processes via the gas phase tend to remove the thermodynamically less stable condensed components from the ISM mineral mixture in favour of the thermodynamically most stable materials. This change in the dust composition occurs in the zone where the timescale for this kind of chemical metamorphism is comparable with the timescale of radial inward migration of the disk material. Inside of this zone, the composition of the mineral assemblage corresponds to a chemical equilibrium state.

Figure 21 gives a schematic sketch of the dust metamorphosis in a protostellar disk and the processes involved.

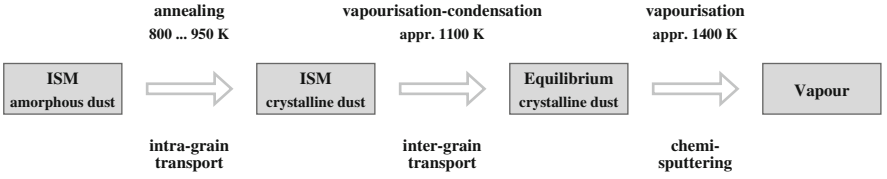

Fig. 21 Main processes responsible for the conversion of the interstellar silicate dust mixture into a chemical equilibrium dust mixture and for its final destruction

7.3 Dust Mixture in the Inner Disk

The mineral mixture existing in chemical equilibrium for standard cosmic element abundances and the stability limits against evaporation/decomposition of the most abundant minerals in a chemical equilibrium mixture are shown in Fig. 5. The main components of the mixture are

- *forsterite* with composition Mg_2SiO_4,
- *enstatite* with composition $MgSiO_3$,
- *solid iron* which forms a solid solution with all the available Ni,
- *troilite* with composition FeS which forms a solid solution with NiS.

If the Mg/Si abundance ratio in extrasolar protoplanetary disk is at the lower end but within the observed range of scattering of Mg/Si ratios in stars, also quartz (SiO_2) may be an abundant component of the equilibrium mixture (cf. Fig. 16). The frequency of such cases increases with decreasing metallicity (Ferrarotti and Gail [68]).

All condensates in the inner disk are solids; pressure and temperature conditions in the disk generally do not allow for the existence of melts.[6]

There are two significant differences in the chemical composition between the equilibrium mineral mixture in the inner disk and the ISM dust mixture in the outer disk proposed by Pollack et al. [133]. First, since the average element mixture of the disk is oxygen rich there exists no carbon dust in the equilibrium mixture. The carbon dust is destroyed during the evolution towards the equilibrium mixture. Second, the silicate dust components olivine and pyroxene in the ISM bear a significant fraction of the iron-silicates fayalite or ferrosilite, respectively, while in chemical equilibrium the silicates are nearly iron free and can assumed to be essentially pure forsterite and enstatite (cf. Fig. 10). Additionally, in most cases quartz is absent from the equilibrium mixture.

The lattice structures of the silicates in both cases also are completely different. The ISM dust has an amorphous lattice structure (Kemper et al. [139]) and a considerable fraction of impurities is build into the lattice. In chemical equilibrium, however, the substances are crystalline and the concentration of impurities solved in the solids is small.

7.4 The Three Main Dust Mixtures

The transport, diffusion, annealing, evaporation, and re-condensation processes in a protoplanetary accretion disk result in the existence of *three significantly different dust mixtures in the inner, middle and outer part of the accretion disk:*

[6] The existence of chondrules in meteoritic material shows, however, that by local, not yet understood processes, some part of the disk matter was flash-heated to temperatures above the melting point.

1. Amorphous dust with a strong non-equilibrium composition in the cold outer parts of the disk (ISM dust),
2. crystalline dust with chemical equilibrium composition in the innermost parts of the disk down to the evaporation limits of the solids, and
3. a mixture of processed dust from the outer regions. with non-equilibrium composition, and the chemical equilibrium mineral mixture from the innermost zone in some inner part of the disk.

Carbon dust is not part of the second mixture; the chemical equilibrium mixture of condensed phases in an oxygen-rich element mixture is free of carbon dust.

For the first mixture, the isotopic mixture of the elements and the abundances of impurities in individual grains may be very different for grains that basically have the same chemical composition, since the grains preserved the vastly different isotopic and elemental compositions of their formation sites. In meteorites they correspond to the presolar grains if they are from stellar sources. The grains of the third mixture are already processed. They probably lost all or nearly all of their noble gas contents by outgassing at high temperatures. Also the isotopic anomalies of their impurities may partially be erased by internal diffusion and exchange processes with the gas phase. In meteorites, this dust component will hardly be recognized as grains of interstellar origin. The second component is home-made dust of the accretion disk. The isotopic compositions of individual grains correspond to the average isotopic mixture of the Solar System (or of other accretion discs) after complete homogenisation.

The opacities of these dust mixtures are strongly different, the opacity of the equilibrium mixture being lower than that of the ISM mixture by a factor of more than ten. The reason is that (i) the carbon in the ISM mixture accounts for nearly one half of the total opacity, that (ii) the opacity of crystalline material usually is much lower than that of amorphous material, and that (iii) iron poor silicates have a lower opacity than iron rich silicates. A realistic modelling of the structure and evolution of protoplanetary accretion discs needs to include in the model computations the gradual change in dust composition and lattice structure

- from the ISM mixture of grains of interstellar origin, encountered in the cool outer parts of the disk,
- through the intermediate non-equilibrium mixture,
- into the chemical equilibrium mixture existing in the warm inner parts of the disk.

7.5 Disk Models

Presently almost all model calculations of disk structure are based on approximations where accretion disks are treated as quasi-stationary structures that slowly evolve under the action of viscous torques that are themselves based on parameterisations. The theory is described in Lin and Papaloizou [140], some basic results can

be found in, to give only a few examples, Ruden and Lin [141], Bell et al. [142, 143], Huesco and Guillot [144], Wehrstedt and Gail [145].

Most model calculations use the one-zone approximation where disks (i) are assumed to be rotationally symmetric and mirror-symmetric with respect to an equatorial plane, and (ii) the disk structure is averaged with respect to the direction vertical to the equatorial plane. Such kind of models describe the (averaged) radial structure of accretion disks and have been applied with considerable success to study basic properties of disks and their evolution. They describe the radial mass-distribution by the surface density Σ, the vertically integrated local mass-density. The evolution of the surface density is determined by an equation of the diffusion type

$$\frac{\partial \Sigma}{\partial t} = -\frac{1}{2\pi r}\frac{\partial}{\partial r}\dot{M} \tag{96}$$

$$\dot{M} = -6\pi\sqrt{r}\,\frac{\partial}{\partial r}\,\nu\sqrt{r}\,\Sigma. \tag{97}$$

Here ν is the viscosity that is frequently parameterised by $\nu = \alpha c_s h$, c_s is the isothermal velocity of sound, $h = c_s\Omega^{-1}$ is the scale-height of the disk, and $\Omega = (GM_*/r^3)^{1/2}$ is the Keplerian rotation velocity at distance r from the centre, and α (typically 10^{-3}–10^{-2}) is the parameter of the viscosity parameterisation. This has

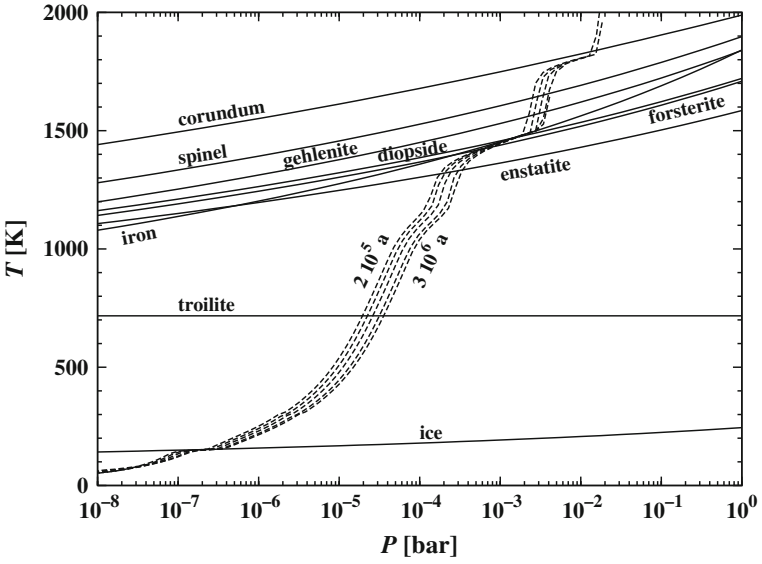

Fig. 22 The temperature-pressure stratification at the midplane in a model of a thin Keplerian α-disc in the one-zone approximation around a star with $M = 1\,\mathrm{M}_\odot$. *Dashed lines:* Snapshots of the radial disk structure of a time dependent model at 2×10^5, 5×10^5, 1×10^6, 2×10^6, and 3×10^6 year (from left to right). *Full lines:* Stability limits of the indicated condensed phases

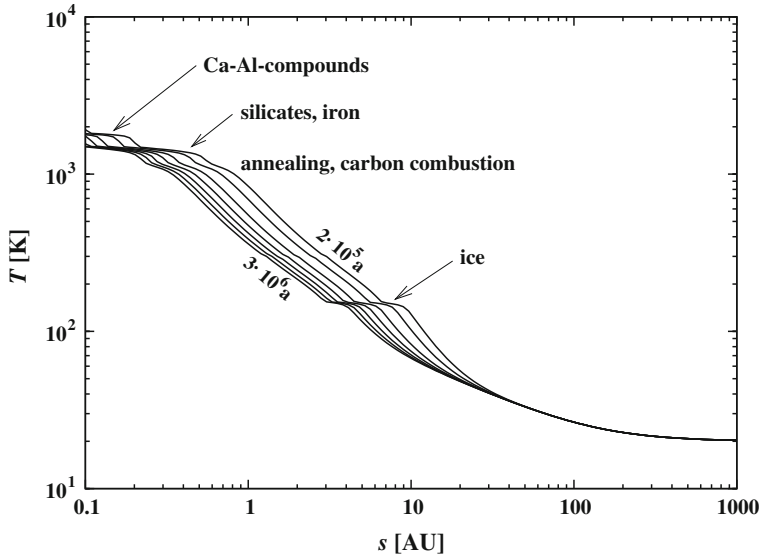

Fig. 23 Midplane temperature stratification in a model of a thin Keplerian α-disk in the one-zone approximation around a star with $M = 1\,\mathrm{M}_\odot$. Snapshots at 2×10^5, 5×10^5, 1×10^6, 2×10^6, and 3×10^6 year (from *top* to *bottom*). Suspicious temperature structures are related to disappearance of certain important sources of opacity; these are indicated. The temperature for $r > 20\,\mathrm{AU}$ drops rather slowly due to disk flaring

to be augmented by an equation for the temperature in the equatorial plane of the disk (details are described in the papers cited above).

We show some results of model calculations for a disk around a solar-type star with viscosity parameter $\alpha = 3 \times 10^{-3}$ for the period from 2×10^5 to 3×10^6 years. This covers roughly the period of time during which (i) accretion discs have lost already most of their initial mass to the star and are of sufficiently low mass to be gravitationally stable, and (ii) massive planets have not yet formed. By formation of Jupiter-mass planets the disk structure and properties change strongly and are no more described by the simple kind of accretion disk models considered here. The first one or two million years of accretion disk evolution are the crucial period where the composition of the dust material is fixed that forms the raw material from which planetesimals and later planets form in the accretion disk.

Figure 22 shows the variation of pressure and temperature in the midplane of protoplanetary accretion discs and stability limits of abundant condensed phases in chemical equilibrium for Solar System element abundances. The variation of temperature with distance r from the star is shown in Fig. 23. There are some conspicuous features in the thermodynamic structure of a disk which result from the vaporisation or destruction of one of the mayor opacity sources. This acts like a thermostat that counteracts any temperature increase by a reduction of opacity. This intimate coupling between dust properties and disk structure requires a self-

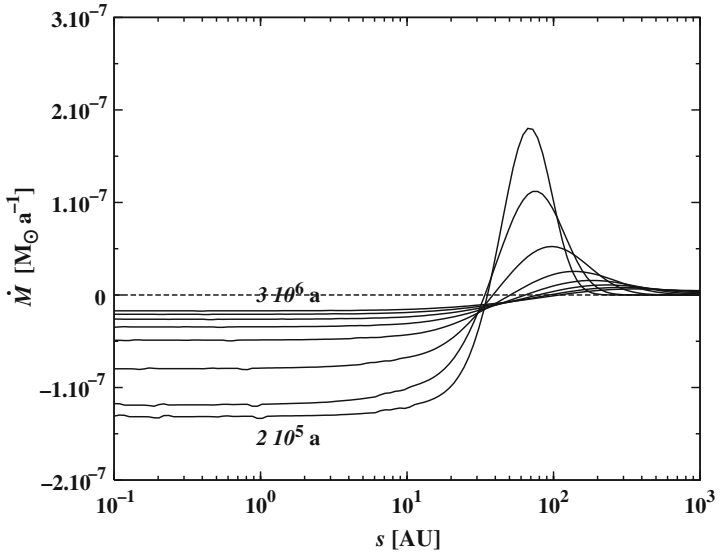

Fig. 24 Radial variation of mass-accretion rate in models of a thin Keplerian α-disk in the one-zone approximation around a star with $M = 1\,\mathrm{M}_\odot$. Snapshots at 2×10^5, 5×10^5, 1×10^6, 2×10^6, and 3×10^6 year (from *bottom* to *top*)

consistent calculation of dust abundances, dust properties, and of disk structure. This has been done in the model calculations shown in the figures.

Figure 24 shows the radial variation of the mass-accretion rate $\dot{M}$ that describes the matter transport in an accretion disk due to angular momentum transport. In the inner part of the disk one has a slow inflow of matter. At the same time the angular momentum of this material is transported outward by viscous torques. In the outer part of the disk one has an outflow of matter because this material takes up the angular momentum of the material in the inner part of the accretion disk that migrates toward the star. As is readily seen the mass-accretion rate rapidly approaches a radial constant value from the innermost region out to about 20–30 AU. In this region the disk evolves in a quasi-stationary fashion ($\partial \Sigma / \partial t \approx 0$).

Figure 25, left part, shows the radial variation of the radial component of the velocity, v_r, defined by

$$\dot{M} = 2\pi r \Sigma v_r . \tag{98}$$

The velocity v_r is slow and because of its slowness only material from the inner $r \approx 30\,\mathrm{AU}$ of the accretion disk moves into the innermost part $r \lesssim 1\,\mathrm{AU}$ during the few million years lifetime (Haisch [146]) of an accretion disk. Material farther out does not contribute to the matter from which planets formed in our Solar System.

These models can be extended to two-dimensional models by reconstructing from one-zone models their vertical structure. This is possible because disks are in almost perfect hydrostatic equilibrium in the vertical direction during all phases

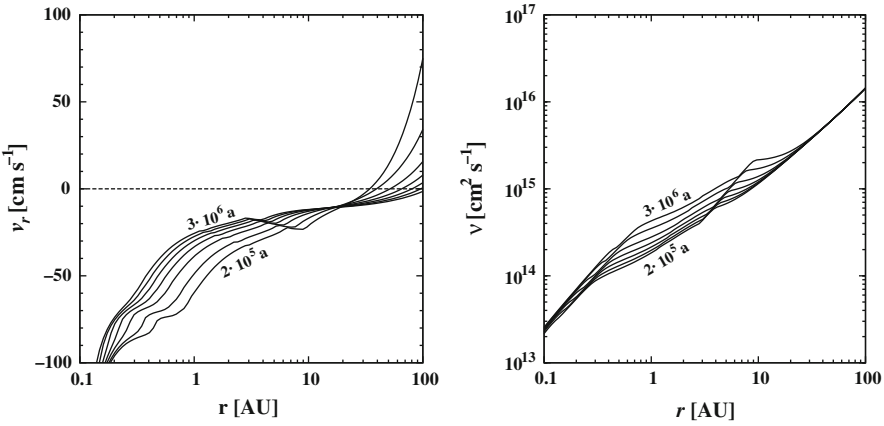

Fig. 25 Radial variation of radial accretion velocity (*left*) and viscosity ν (*right*) in a model of a thin Keplerian α-disk in the one-zone approximation around a star with $M = 1\,\mathrm{M}_\odot$. Snapshots at 2×10^5, 5×10^5, and between 1×10^6 and 3×10^6 year in steps of 0.5×10^6 year

of their evolution where (i) they are stable against gravitational instabilities, (ii) they are thin in the sense that their vertical scale-height h at some radial distance r is small, $h \ll r$, and if (iii) planets have not yet formed. Neglecting curvature effects, one constructs a plane-parallel "stellar atmosphere" model at each distance r by integrating the hydrostatic equation and the equation for the vertical energy transport. The model is constructed such that it fits to the surface density Σ of the one-zone model (cf., e.g., Bell et al. [143]; Huesco and Guillot [144] or Wehrstedt and Gail [145] for details). This approximation is called the (1+1)-dim approximation. It is frequently used if questions are studied that require to know the vertical disk structure. True 2D or 3D hydrodynamic disk models that solve all the basic equations of physics (hydrodynamics, gravitation, radiative transfer, chemistry) with valid numerical methods and that have sufficient spatial resolution remain to be constructed.

In the following some details of the evolution of the dust in protoplanetary discs are discussed and results for thin Keplerian disk models are shown. We concentrate on the Solar System since for this we know some details of its early evolution.

7.6 Flow Structure in the Accretion Disk

There exist extended meridional circulation currents in accretion discs that transport matter between widely separated regions of the disk. These flows are superposed on the general accretion flow in the disk and on the local turbulent flow pattern responsible for viscous angular momentum transport (magneto-hydrodynamic instabilities, convection). They result in modifications of the composition of the dust mixture. This kind of flow is found in hydrodynamic models of flows in accretion disks (e.g. Kley and Lin [147]; Keller and Gail [148]; Tscharnuter and Gail [149]) and was

studied in analytic approximations (e.g. Urpin [150]; Różyczka et al. [151]; Regev and Gitelman [152]; Takeuchi and Lin [153]) and numerically (Ciesla [154]).

Analytic studies start from equations where it is assumed that averaging over local turbulent flow structures is already performed. Time dependence in the resulting equations is neglected since after averaging only the long-term disk evolution remains. In the approximation of thin disks ($\varepsilon = (h/r) \ll 1$) one neglects terms of order higher than ε^2. In lowest order one recovers the equations for the (1+1)-dim disk models. In the next order one obtains equations (in cylindrical coordinates r, z, ϕ) for the r, z, and ϕ-component of the velocity (Keller and Gail [148]). These describe slow circulation currents that are driven by temperature gradients and a slight mismatch in the radial momentum equation between centrifugal acceleration on one hand side and pressure and gravitational forces on the other hand side which do not completely cancel because of different z-dependencies. The velocity components are (Takeuchi and Lin [153]; Keller and Gail [148])

$$v_\phi = \left[1 - \frac{3}{4}\left(\frac{z}{r}\right)^2 + \frac{r^2}{2GM_*\varrho}\frac{\partial p}{\partial r}\right] v_\mathrm{K} \tag{99}$$

$$v_r = \left[\frac{1}{r\rho}\frac{\partial}{\partial r} r^3 \varrho\, \nu \frac{\partial}{\partial r}\frac{v_\phi}{r} + \frac{r}{\varrho}\frac{\partial}{\partial z}\varrho\nu\frac{\partial v_\phi}{\partial z}\right]\frac{2}{v_\mathrm{K}}, \tag{100}$$

$$v_z = -\frac{1}{r\rho}\int_0^z \frac{\partial}{\partial r} r\varrho\, v_r \,\mathrm{d}z, \tag{101}$$

where v_K is the Keplerian velocity of revolution

$$v_\mathrm{K} = \sqrt{GM_*/r}. \tag{102}$$

For p, ϱ, and ν one uses the results of (1+1)-dim model calculations.

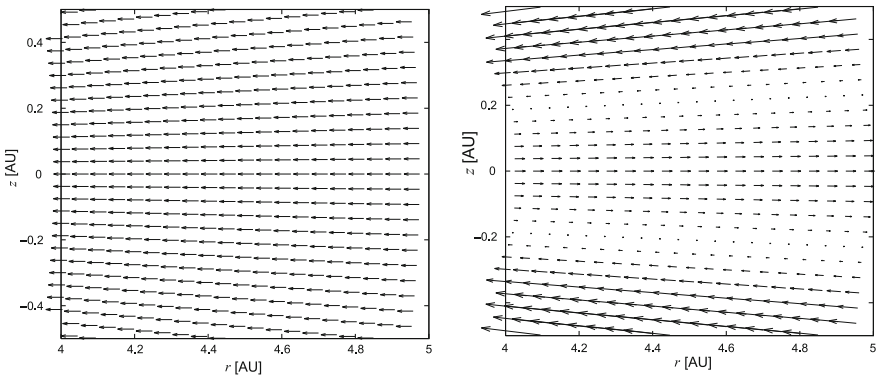

Fig. 26 Structure of accretion flows for a section of an accretion disk. *Left:* Inflow corresponding to the general accretion flow. *Right:* Accretion flow with superposed circulation currents. Close to the midplane one observes a net *outflow*, at higher layers an *inflow*. After averaging in vertical direction, there results a net inflow of mass (from Keller and Gail [148])

Figure 26 shows for a section of a simplified (1+1)-dim model the accretion flow structure. The left part shows the general accretion flow corresponding to the zero-order result of one-zone models, where one has inflow of matter at all heights z above the midplane. The right part of the figure shows the flow structure if the additional slow meridional circulation flow, Eqs. (99), (100), and (101), is added to the zero-order inflow. The structure of the resulting accretion flow turns out to be layered, with *outflow* close to the midplane of the disk and *inflow* at higher layers. The total mass accretion rate is the same as is calculated in one-zone models, but there is also a net outflow of matter that transports matter from warm inner regions of accretion disks to cold outer regions.

The radial velocity component can be approximated for $r \gg R_*$ by (Keller and Gail [148])

$$v_r = \frac{\nu}{r}\left(3 - \frac{5}{2}\lambda - \frac{1}{2}(9 - 5\lambda)\frac{z^2}{h^2}\right) \tag{103}$$

where

$$\lambda = -\frac{\partial \ln T}{\partial \ln r}$$

and T is the temperature in the midplane of the disk. The layered flow structure exists in regions of the disk where for $z = 0$ one has $v_r > 0$, i.e., where $\lambda < 6/5$. Inspection of Fig. 23 shows that this is realised over most part of the disk. The validity of the approximate solutions (99), (100), (101), (102), and (103) requires, however, that the disk evolves in a quasi-stationary fashion which is satisfied in the radius range between 0.1 and 30 AU. At larger distances the disk structure is time dependent and the flow structure has to be determined from hydrodynamic models.

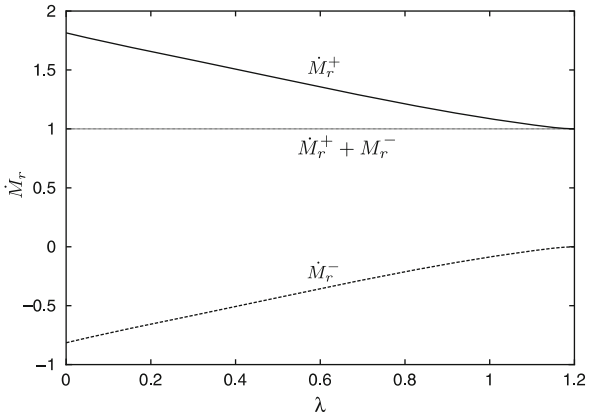

Fig. 27 Inflow and outflow rates $\dot{M}_r^-$ and $\dot{M}_r^+$, respectively, at radii $r \gg R_\star$ in units of the mean accretion rate $\dot{M}_r$, derived from standard one-zone disk models. The net mass flux rate is $\dot{M}_r^- + \dot{M}_r^+ = \dot{M}_r$ (from Keller and Gail [148])

Table 8 In- and outflow rates for typical values of λ and at large radii $r \gg R_*$

λ	1	0.75	0.62
$\dot{M}_r^-/\dot{M}_r$	−0.087	−0.250	−0.344
$\dot{M}_r^+/\dot{M}_r$	1.087	1.250	1.344

The total mass-outflow rate close to the midplane, $\dot{M}_r^-$, and mass-inflow rate in the upper layers, $\dot{M}_r^+$, are

$$\dot{M}_r^- = -2\pi r\, 2 \int_0^{z_0} \mathrm{d}z\, \varrho v_r \ , \quad \dot{M}_r^+ = -2\pi r\, 2 \int_{z_0}^{\infty} \mathrm{d}z\, \varrho v_r , \tag{104}$$

where z_0 is the height z where v_r changes sign. This can be evaluated analytically (Keller and Gail [148]) and some results are shown in Fig. 27 and Table 8. The total mass-accretion rate $\dot{M}_r = \dot{M}_r^+ + \dot{M}_r^-$ equals the mass-loss rate as determined in the one-zone approximation. For a typical average value of $\lambda \approx 3/4$ in the range $r < 30\,\mathrm{AU}$ (cf. Fig. 23) the ratio of the mass-outflow rate to the mass-inflow rate is $|\dot{M}_r^-/\dot{M}_r^+| \approx 0.2$. There results a significant transport of matter outwards.

Superposed on this flow is the local turbulent flow structure from convection or the magneto-rotational instability (whatever drives accretion). This results in a local mixing of material in vertical direction. The layered structure of the accretion flow therefore does not necessarily result in a layered composition of disk matter.

In 3-dimensional extensions the flow field of accretion disks should additionally show large vortices superposed on the large-scale meridional circulations that are due to the baroclinic instability (Klahr and Bodenheimer [97]; Klahr [155]).

7.7 The Advection–Diffusion–Reaction Equation

The basic equation describing the metamorphosis of the dust mixture in protoplanetary accretion discs is the combined equation

- for advection of disk material by the accretion process, by large scale circulation currents, and by particle drift,
- for radial and vertical inward and outward mixing of matter by turbulent flows,
- and for chemical reactions between dust grains and gas phase species, and for processes like annealing that occur within grains.

Before we start to explicate how this equation looks like, we introduce first some important simplifications.

7.7.1 Dust Grains and Dust Aggregates

The dust particles in an accretion disk do not exist as individual dust grains of a single dust material (possibly with some inclusions of other materials like in the case of GEMS, see “The Astromineralogy of Interplanetary Dust Particles” by Bradley, this

volume). They are members of bigger units of agglomerated particles consisting of many many sub-units of tiny particles of all dust species present in an accretion disk, bound together by rather weak attractive forces, e.g. by van der Waals attraction, or by sticky coatings, e.g. by tar-like material as it is observed for IDPs (see "The Astromineralogy of Interplanetary Dust Particles" by Bradley, this volume). We consider here an early evolutionary phase of the accretion disk where the agglomeration process has not yet proceeded so far that the dust has strongly settled toward the midplane of the disk and rapid formation of planetesimals commences which locks most of the dust material into km-sized compact bodies. The rapid growth to large bodies starts if particle sizes exceed about $10\,\mu$m, i.e., we assume that the agglomerated particles are generally smaller than this.

If we talk about dust grains, we mean in the following the small sub-units of the bigger agglomerated particles. The atoms in these sub-units are held together by strong chemical bonding and the dust grains mainly consist of a single condensed phase. They are usually of a rather compact geometric shape without voids or handles, cf. the figures in the chapter "The Astromineralogy of Interplanetary Dust Particles" by Bradley (this volume), and this is taken as justification for approximating their true shape by spheres. We denote the bigger agglomerated particles composed from the elementary dust particles also as dust aggregates. It is assumed that the composition of the dust aggregates with respect to the different species j of dust particles (on average) is the same for all aggregates.

During the early phase of dust evolution in accretion discs it is assumed that the dust aggregates form rather open, fluffy structures resulting from cluster-cluster aggregation. In such highly porous structures most of the sub-units forming the dust aggregates are exposed to the gas phase as if they are freely suspended in the gas, only a small fraction is shadowed by other dust particles in the aggregate. With respect to interactions with the gas phase the particles can be treated as if they exist as isolated particles that are not members of a bigger unit. Matter exchange between different grains, then, is most easily achieved via the gas-phase. This kind of matter exchange is not limited to dust particles from the same dust aggregate. Additionally, the members of a dust aggregate may exchange material with other dust particles from the *same* dust aggregate by surface diffusion. Usually transport of material via the gas-phase, if this is possible, is more rapid than transport via surface diffusion and for the following considerations diffusional transport across the surface is neglected.

Another possibility for particles in a dust aggregate, which does not exist for single isolated dust grains, is to coalesce at elevated temperatures by surface diffusion with contacting particles of either the same material, or of a different material for which solid solution formation is possible. This sintering process has not yet been studied for dust in accretion discs and therefore it is presently not possible to judge whether this is important.

In the following the chemically or physically different dust species are denoted by a lower index j. The dust particles of a species j may have different sizes and shapes. It is assumed that they are of spherical shape and for the purpose of describing the frequency distribution of their radii a set of fixed grain radii a_i is defined for

each of the different substances j. The dust grains then are grouped into different segments i that comprise all grains with radii between a_i and a_{i+1}. The number density of grains having radii within $[a_i, a_{i+1}]$ is divided by the number density of hydrogen nuclei n. The resulting quantity, the number of dust grains of species j with radii between a_i and a_{i+1} per hydrogen nucleus, i.e., the concentration of grain of species j in radius segment i, is denoted by $c_{j,i}$.

7.7.2 Transport-Reaction Equation

The equation for time evolution of the concentration $c_{j,i}$ by advection, diffusion, and evaporation or condensation of dust grains is the continuity equation. Written for concentrations it is given in cylindrical coordinates, and assuming axial symmetry, by

$$\frac{\partial c_{j,i}}{\partial t} + v_{r,j,i}\frac{\partial c_{j,i}}{\partial r} + v_{z,j,i}\frac{\partial c_{j,i}}{\partial z} = \frac{1}{rn}\frac{\partial}{\partial r} rnD_{j,i}\frac{\partial c_{j,i}}{\partial r} + \frac{1}{n}\frac{\partial}{\partial z} nD_{j,i}\frac{\partial c_{j,i}}{\partial z} + R_{j,i}, \quad (105)$$

where n is the number density of hydrogen nuclei (in practice $= 2n_{\mathrm{H}_2}$), $v_{r,j,i}$ and $v_{z,j,i}$ are the radial and vertical velocity components of the dust grains, respectively, and $D_{j,i}$ is the diffusion coefficient. The rate term $R_{i,j}$ describes the evaporation or condensation processes or other chemical or physical processes that change the concentration $c_{j,i}$.

The dust grains in protoplanetary discs are members of dust aggregates. Equation (105) does not describe the size distribution of the aggregates; this requires a separate equation – the coagulation equation – for describing the evolution of aggregate sizes, which is not our topic.

The velocities $v_{r,j,i}$ and $v_{z,j,i}$ of the dust grains are the superposition of the corresponding components of the gas velocity and the relative drift velocity of the dust particles. If the drift of particles relative to the gas-phase is considered, one has to observe that they are members of a dust aggregate and not really free particles. All members of a dust aggregate move with the same velocity[7] and this velocity is determined by the size and mass of the dust aggregate. One has to use for all dust particles, irrespective of their kind j and membership in some size segment i, the drift velocity of the dust aggregate which they are members of. Since it is not to be expected that the (average) composition of dust aggregates depend on their size, one can average Eq. (105) with respect to aggregate sizes, i.e., one has to use average drift velocities of dust aggregates in Eq. (105). Because we suppose that dust aggregates are at most of a size of several μm, the frictional coupling to the gas is strong and particle drift is negligible. The velocity components $v_{r,j,i}$ and $v_{z,j,i}$ in

[7] Rotation of dust aggregates is neglected.

Eq. (105) are in this case the velocity components of the carrier gas into which the dust aggregates are embedded. These were discussed in Sect. 7.6.

Correspondingly, the diffusion of the dust particles is determined by the diffusion of the dust aggregates. The dominating process is mixing by the small-scale random velocities in turbulent flows (due to convection or magneto-rotational instabilities in accretion disks). Due to strong frictional coupling of small dust grains to the gas they are carried around by these flows which macroscopically results in a diffusion-like transport of the aggregates. For the diffusion coefficient $D_{j,i}$ one has to use, for the same reasons as in the case of particle drift, for all dust grains the same diffusion coefficient obtained from averaging with respect to the aggregate sizes. This diffusion coefficient is assumed to be given by

$$D = \frac{\nu}{Sc}, \tag{106}$$

where ν is the kinematic viscosity of the disk matter (see Sect. 7.5) and Sc the Schmidt number (e.g. Gail [99]; Wehrstedt and Gail [145]), typically of order O(1). For some further discussions on the value of Sc see, e.g., Johansen et al. [57, 156]; Turner et al. [157]; Pavlyuchenkov and Dullemond [158].

Numerical values for ν for the Solar Nebula are shown in Fig. 25. The relation between D and ν is only qualitatively correct, but a physical theory for a consistent calculation of D from first principles is still missing. In principle the diffusion coefficient may be different for vertical and radial diffusion, but in view of the uncertainties with respect to the precise value of D this is neglected.

7.7.3 Timescales

The spatial and temporal distribution of some dust species j in an accretion disk is determined by the characteristic timescales for drift, diffusion, and for chemical reactions or physical changes. To begin with, the timescale $\tau_{\rm diff}$ of diffusion of some tracer over distances of the order $\Delta\ell$ is

$$\tau_{\rm diff} = \Delta\ell^2/D. \tag{107}$$

Numerical values for the Solar Nebula are shown in Figs. 12 and 15. Since $\tau_{\rm diff}$ scales quadratically with $\Delta\ell$, the timescale for mixing material in the vertical direction is about a factor of 100 shorter than the timescale for mixing in the radial direction since the disk height h varies approximately as $h \approx 0.1\,r$. There is a strong tendency to homogenise the composition of the disk material in the vertical direction. This tendency can be counteracted only if temperature dependent chemical process operate over shorter timescales than vertical mixing and maintain vertical compositional inhomogeneities. This holds, for instance, for evaporation or condensation of dust in the disk, which operates on rather short timescales and drives the mineral mixture into chemical equilibrium.

The timescale for transport by radial flows in the accretion disk is

$$\tau_{\rm hyd} = \Delta\ell / v_r . \tag{108}$$

The radial flow in the disk is layered with outflow close to the midplane and inflow at higher layers. Close to the midplane one has $v_r = 3\nu/r$ (see Eq. (103)) and, hence, $\tau_{\rm diff} \approx 3\tau_{\rm hyd}$. This means that radial transport of matter by outflow close to the midplane is more efficient then mixing of matter from inner to outer regions by diffusion. At higher layers of the disk one has inflow and diffusive mixing outward in this region requires upstream diffusion which is generally inefficient and enables mixing only over limited distances (Morfill and Völk [159]). Superposed on the radial transport is the more rapid vertical diffusional mixing that intermingles material from the inflowing and outflowing layers. Realistic studies of mixing processes require to consider the layered 2-D structure of the accretion flow (or, if possible, the 3-D structure including vortex flows, see Klahr and Bodenheimer [97]; Klahr [155]; Boss [160, 161]).

7.7.4 One-Zone Approximation

Because vertical mixing tends to homogenize the composition of disk material in the vertical direction one may refrain from considering the detailed vertical structure and average the continuity equation over the vertical direction. In this one-zone approximation, Eq. (105) for the concentrations changes to (e.g. Gail [99]; Wehrstedt and Gail [145])

$$\frac{\partial c_{j,i}}{\partial t} + v_r \frac{\partial c_{j,i}}{\partial r} = \frac{1}{rhn} \frac{\partial}{\partial r} rhnD \frac{\partial c_{j,i}}{\partial r} + R_{j,i}, \tag{109}$$

where $c_{j,i}$, v_r, D, and $R_{j,i}$ are all vertically averaged quantities. The quantity n is the midplane density of hydrogen nuclei and the disk height h enters[8] because the surface density $\sigma = \int n(r,z){\rm d}z$ of hydrogen nuclei, that enters during the averaging process, is replaced by $\sigma = 2hn$.

7.7.5 Reaction Rates

The term $R_{j,i}$ in Eq. (105) describes the gain and loss processes for dust grains of species j within radius segment i. For grain growth and evaporation the gains and losses for each species (j,i) are given by (Gail [99])

$$R_{j,i} = \begin{cases} \left(\dfrac{c_{j,i+1}}{\Delta a_{i+1}} - \dfrac{c_{j,i}}{\Delta a_i} \right) \left| \dfrac{{\rm d}a_{j,i}}{{\rm d}t} \right| & \text{if } \dfrac{{\rm d}a_{j,i}}{{\rm d}t} < 0 \\ \left(\dfrac{c_{j,i-1}}{\Delta a_{i-1}} - \dfrac{c_{j,i}}{\Delta a_i} \right) \dfrac{{\rm d}a_{j,i}}{{\rm d}t} & \text{if } \dfrac{{\rm d}a_{j,i}}{{\rm d}t} > 0 \end{cases} , \tag{110}$$

where ${\rm d}a/{\rm d}t$ is given by an equation of the type (66), and $\Delta a_i = a_{i+1} - a_i$.

[8] In Gail [99] the factor h was missing.

For gas-phase species there also holds an equation of the type (109). The rate terms in this case refer to chemical reactions with other gas phase species. If they are involved in reactions with grains there is an additional rate term corresponding to consumption from or injection into the gas phase by grain growth or destruction processes, respectively:

$$R_m = \sum_j \sum_r \nu_{j,r,m} (J_j^{\mathrm{ev}} - J_j^{\mathrm{gr}}) \mathcal{A}_j . \tag{111}$$

The summation is over all dust species j, which are involved in reactions with molecule m and over all relevant reactions r. $\nu_{j,r,m}$ is the number of molecules m injected into or removed from the gas phase in reaction r with dust species j,

$$\mathcal{A}_j = 4\pi \sum_i a_i^2 c_{j,i} \tag{112}$$

is the total surface area of all particles of dust species j per hydrogen nucleus, and J_j^{ev}, J_j^{gr} are the evaporation or growth current densities for grains of species j as defined in Sect. 4.2.

Equation (109) for all dust species j and grain radii i and for the relevant gas phase species have to be solved simultaneously with the equations for the disk structure and evolution. Results for stationary disk models are described in Gail [99, 162] and for time dependent models in Wehrstedt and Gail [136, 145]; Tscharnuter and Gail [149].

7.8 Annealing

Annealing of the amorphous silicate grains of interstellar origin in protostellar discs and its implications for the disk structure is discussed in Duschl et al. [135], Gail [19, 99, 162] and Wehrstedt and Gail [136, 145].

In the model calculations [99, 136] the annealing process is modeled by solving Eq. (78) for the growth around each growth centre and defining the average degree of crystallization by (80). It is shown how this simple model can be used to determine the distribution function of the degrees of crystallization for an ensemble of dust grains. One defines a grid $0 \le x_i \le 1$ ($i = 1, \ldots, I$) of totally I discrete degrees of crystallization for the dust grains. The gain and loss term in the advection–diffusion–reaction Eq. (109) for the concentration c_i of grains with a degree of crystallization between x_i and x_{i+1} is shown in [99] to be given by

$$R_i = \left(\frac{c_{i-1}}{x_i - x_{i-1}} - \frac{c_i}{x_{i+1} - x_i} \right) \frac{\mathrm{d}\, V_{\mathrm{cr}}^{\frac{1}{3}}}{\mathrm{d}\, t} \tag{113}$$

where V_{cr} is defined by (78).

The rate term depends strongly on temperature because it contains an exponential factor $\exp(-E_a/kT)$. Averaging with respect to the vertical temperature distribution results, except for some factor O(1), in an exponential factor depending on the mid-plane temperature. Annealing occurs almost exclusively close to the mid-plane because temperature is highest there.[9] However, since matter is more rapidly mixed in vertical direction than transported in radial direction, there does not develop a vertical gradient in the degree of crystallinity of dust; mixing enforces an essentially homogenous dust composition in vertical direction. For this reason the problem of annealing can be treated by a vertically averaged transport-reaction equation.

A solution of the system of differential Eq. (109) with the appropriate boundary conditions (all grains amorphous in the cold disk, all grains are crystalline in the warm inner part of the disk) then yields the probability distribution c_i for the different degrees of crystallization from which the average degree of crystallization x_{cr} can be determined.

Calculations have been performed for stationary disk models by Gail [99], for time dependent models by Wehrstedt and Gail [136], and for simple semi-analytic disk models and assuming only two states (either crystalline or amorphous) by Bockelée-Morvan et al. [163]. Some results are shown in Fig. 28 for a stationary disk

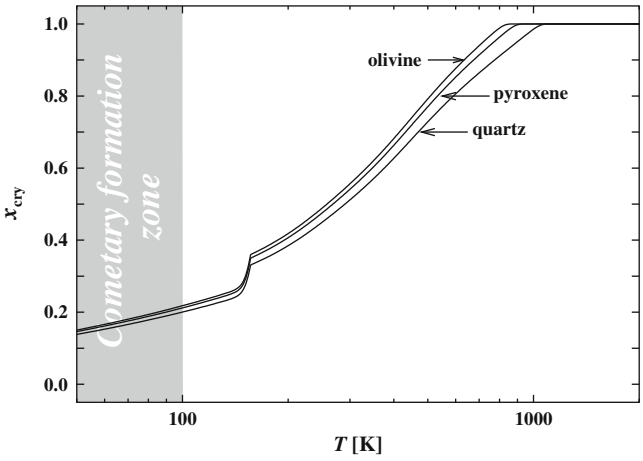

Fig. 28 Variation of the average degree of crystallization x_{cry} of the grains of interstellar origin due to annealing and radial mixing of crystallized grains as function of the midplane temperature T in a protoplanetary accretion disk. Stationary disk model with accretion rate $\dot{M} = 10^{-7}\,M_\odot\,year^{-1}$. The feature at about 150 K is due to the temperature plateau in the region of water ice evaporation (cf. Fig. 23). The grey shaded area roughly indicates the zone where cometary nuclei are expected to be formed

[9] Dust temperatures may also be high in high layers of the disk photosphere where the dust is irradiated by the proto-star, but this region contains a negligible fraction of the total surface density $\Sigma(r)$.

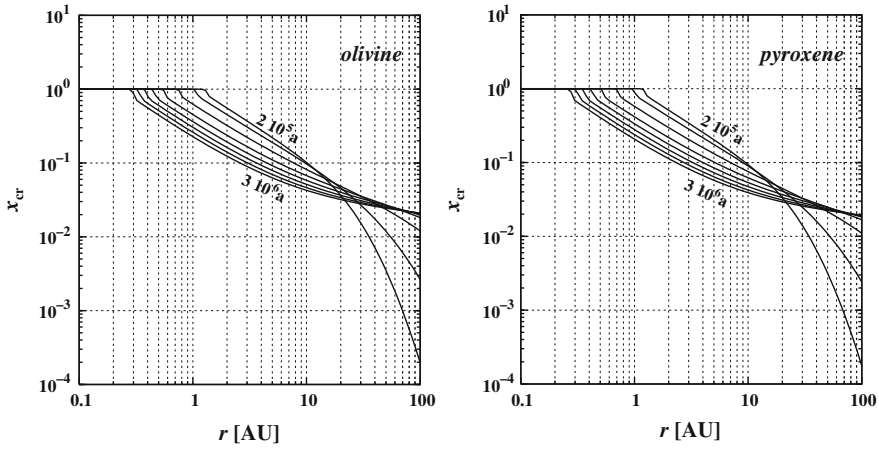

Fig. 29 Radial and temporal variation of the degree of crystallisation x_{cr} of olivine and pyroxene grains due to annealing and radial mixing of crystallized grains for a time dependent disk model. Snapshots at 2×10^5, 5×10^5, and between 1×10^6 and 3×10^6 year in steps of 0.5×10^6 year. According to the model calculation crystalline dust is mixed into fairly distant outer regions of the disk during its evolution

model and in Fig. 29 for a time dependent model which confirm the expectations based on Fig. 12: Annealing temperatures of about 800 K for olivine and pyroxene dust grains, and at about 900 K for quartz grains. The low average annealing temperature found in the calculations is important in so far, as dust destruction processes by evaporation occur at a much higher temperature. Both processes, crystallisation and evaporation, occur in different zones.

An important result of the model calculations is that crystalline dust, formed at about 800 K, is transported into cool outer parts of the disk by diffusion and flows, even into the region beyond 10 AU (the grey shaded area in Fig. 28), where it may be incorporated into the planetesimals formed in the cold outer disk. Probably this mechanism is responsible for the considerable fraction of crystalline silicates observed to exist in cometary nuclei (e.g. Wooden et al. [164, 165]).

Calculations of the degree of crystallization of dust in protostellar discs based on the results of Hallenbeck et al. [89, 91] have not yet performed. A rough estimate (Gail [99]) is that crystallization occurs at about 950 K for their amorphous silicate material. Also in this case crystallization occurs at significantly lower temperature than the evaporation of the silicate dust.

7.9 Evaporation of the Interstellar Dust Component

Accretion moves the dust material of interstellar origin into warm inner disk regions where the dust starts to evaporate. It is important to note that the pristine silicate

dust components olivine, orthopyroxene, and possibly silica are not stable in an environment with Solar System element abundances:

(1) Quartz does not exist in chemical equilibrium in such an environment because the vapour pressure of SiO molecules is much higher for quartz than for olivine and pyroxene. In an equilibrium state the silicon is condensed in forsterite and enstatite, and not in quartz.
(2) The interstellar olivine and pyroxene are assumed to have a rather high Fe/(Fe+Mg) ratio (cf. Table 7), while in chemical equilibrium the iron content is low (cf. Fig. 10). Since the upper stability limit of the iron-magnesium silicates considerably decreases with increasing iron content, the iron rich interstellar silicates are unstable with respect to evaporation and re-condensation of their material into the iron poor silicates forsterite and enstatite and into solid iron.

The details of the evaporation mechanism of theses dust components in the inner disk depend on the degree of mixing in the disk:

1. If silicate material with equilibrium composition (forsterite + enstatite) from the inner disk region is mixed into the zone where the ISM-silicates start to evaporate, the gas phase pressure of SiO (and Mg) in the evaporation zone of the ISM-silicates is *buffered* by the low vapour pressure of the forsterite-enstatite mixture.
2. If, on the other hand, no outward mixing of material from the inner zone occurs, the partial pressure of SiO (and Mg) in the gas phase is determined by the evaporation of the ISM-silicates itself.

The mode of conversion to an equilibrium mixture in the second case is different from the case where equilibrium grains are already present and act as buffer for the

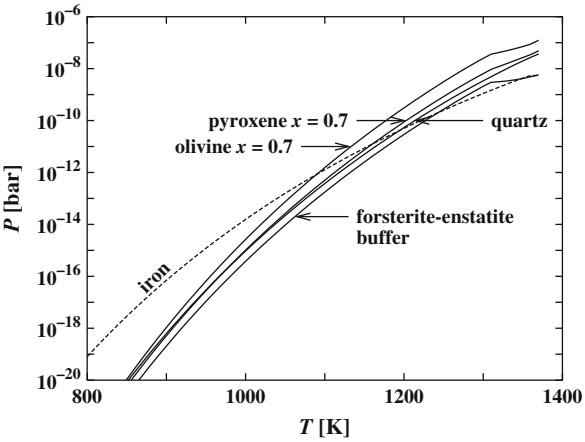

Fig. 30 Partial pressure of SiO in chemical equilibrium between the indicated solid silicon compounds and the hydrogen rich gas phase. The total pressure is $P = 10^{-4}$ bar. The dashed line shows the vapour pressure of iron

vapour pressure. Since mixing seems to be important in protoplanetary discs, only the first case needs to be considered.

Due to annealing at lower temperature the silicates have a crystalline lattice structure at the instant when they start to evaporate. This allows to use thermodynamic data of crystalline silicates for calculating their evaporation, which are well defined contrary to the thermodynamic data of amorphous materials. Figure 30 shows the partial pressures of SiO molecules in a state of chemical equilibrium between gas and solids with respect to the following reactions:

$$\begin{aligned} \mathrm{Mg}_{2x}\mathrm{Fe}_{2(1-x)}\mathrm{SiO}_4 + 3\mathrm{H}_2 &\longrightarrow 2x\mathrm{Mg} + 2(1-x)\mathrm{Fe} + \mathrm{SiO} + 3\mathrm{H}_2\mathrm{O} \\ \mathrm{Mg}_{x}\mathrm{Fe}_{(1-x)}\mathrm{SiO}_3 + 2\mathrm{H}_2 &\longrightarrow x\mathrm{Mg} + (1-x)\mathrm{Fe} + \mathrm{SiO} + 2\mathrm{H}_2\mathrm{O} \\ \mathrm{SiO}_2 + \mathrm{H}_2 &\longrightarrow \mathrm{SiO} + \mathrm{H}_2\mathrm{O}. \end{aligned}$$

They are calculated for a typical pressure of $P = 10^{-4}$ bar in the zone where silicate destruction occurs (cf. Fig. 22), and a composition of olivine and pyroxene of $x = 0.7$ (cf. Table 7). Figure 30 shows that the vapour pressures of the iron rich silicates and quartz exceeds the vapour pressure of the forsterite-enstatite buffer by at least a factor of three. If evaporation and growth is not limited by diffusion in the gas phase (case A in Fig. 11) all material evaporated off from the grains of interstellar origin will precipitate on forsterite, enstatite, and on solid iron with only negligible re-condensation on the interstellar grains. The exchange of material between instellar dust and the disk made dust is schematically depicted in Fig. 31

Since only evaporation needs to be considered in the rate term (110) of Eq. (109) for calculating the local abundance and size spectrum of the olivine, orthopyroxene, and quartz grains of interstellar origin, one has for instance for olivine (Eq. 68)

$$R_{\mathrm{ol},i} = \left(\frac{c_{j,i-1}}{\Delta a_{i-1}} - \frac{c_{j,i}}{\Delta a_i} \right) \alpha_{\mathrm{ol}} v_{\mathrm{th,SiO}} \frac{p^{\mathrm{ol}}_{\mathrm{SiO,eq}}}{kT}, \tag{114}$$

and similar terms for the other silicates. Terms of a similar structure appear as source terms in the equations for the evaporation products Mg, Fe, SiO, H_2O. Olivine, for

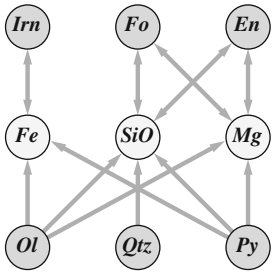

Fig. 31 Exchange of material between the different dust components (denoted by obvious abbreviations) and the vapour species (Fe, Mg, SiO) if the partial pressure of SiO is buffered by the presence of forsterite and enstatite. The exchange with the H_2O reservoir is not shown

instance, contributes the following source terms to Eq. (109) for SiO, Mg, Fe and H_2O

$$R_{\rm SiO} = \alpha_{\rm ol} v_{\rm th,SiO} \frac{p^{\rm ol}_{\rm SiO,eq}}{kT} \mathcal{A}_{\rm ol}, \quad R_{\rm Mg} = 2x R_{\rm SiO} \\ R_{\rm Fe} = 2(1-x) R_{\rm SiO}, \qquad R_{\rm H_2O} = 3 R_{\rm SiO}, \tag{115}$$

and corresponding terms occur for the other silicates. For iron one has additional terms from evaporation and condensation of solid iron as source and sink terms:

$$R_{\rm Fe} = \alpha_{\rm ir} v_{\rm th,Fe} \frac{p^{\rm ir}_{\rm Fe,eq} - p_{\rm Fe}}{kT} \mathcal{A}_{\rm ir} \, . \tag{116}$$

From the solution of Eq. (109) one obtains $\mathcal{A}_j$ for the dust species and from this the local production rates for Mg, Fe, SiO, and H_2O by dust evaporation which allows to calculate the local abundance of the elements Mg, Fe, Si, and O not bound in interstellar dust grains.

7.10 Conversion of Silicates into the Equilibrium Mixture

The characteristic timescales for transport and mixing in protoplanetary discs are so big that dust growth or evaporation occurs under near-equilibrium conditions (Duschl et al. [135]) and the deviation of the gas phase abundance from the equilibrium vapour pressure is very small. The fraction of the refractory elements condensed into solids can, therefore, be calculated in lowest order approximation by

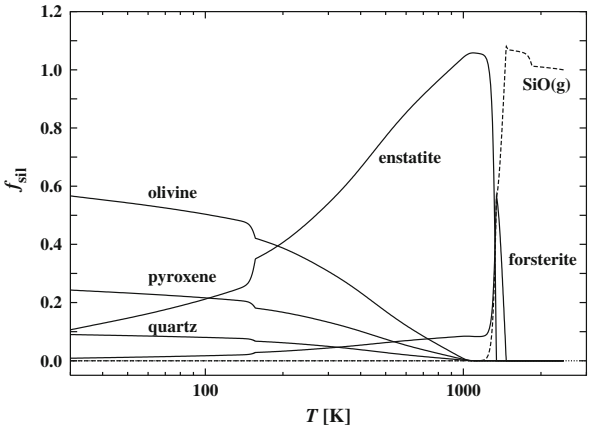

Fig. 32 Radial variation of the fraction of Si condensed into the individual Si-bearing condensates (*full lines*) and the fraction of Si bound in SiO molecules (*dashed line*) for a stationary disk model with $\dot{M} = 1 \times 10^{-7}\,{\rm M}_\odot year^{-1}$ and a protostar of $1\,{\rm M}_\odot$. The abundances are normalized to the interstellar Si abundance

simply assuming chemical equilibrium. This has been done in the past by extensive calculations of condensation sequences (Sect. 3.4). For more accurate model calculations for the composition of the dust material in protoplanetary discs the set of kinetic Eqs. (105) or (109) for condensation, evaporation, and annealing has to be solved for all dust and gas-phase species.

Figure 32 shows the fraction of the Si bound into olivine, orthopyroxene, and quartz, as calculated from the solutions of (109) for these dust species, as function of the midplane temperature in a stationary disk model that assumes as initial composition of the dust mixture the Pollack et al. [133] model for the abundant dust species. The last ISM grains evaporate according to the model calculation at about 1,100 K. At this temperature they are already completely crystallized (cf. Fig. 28) and their vapour pressure can and has to be calculated for crystalline materials. Further, by interdiffusion all spatial compositional inhomogeneities with respect to the cations Fe^{2+} and Mg^{2+} within silicate grains are erased for $T \gtrsim 700$ K for olivine and $T \gtrsim 900$ K for pyroxene (cf. Fig. 15). If the grains arrive in the evaporation zone (cf. Fig. 15) the silicate grains can be assumed to be homogeneously composed.

The deviations of the gas phase partial pressures of the vapour compounds of the silicates, i.e., SiO, Mg and Fe,[10] are very small and forsterite and enstatite essentially are in chemical equilibrium with the gas phase. The fraction of Si bound in

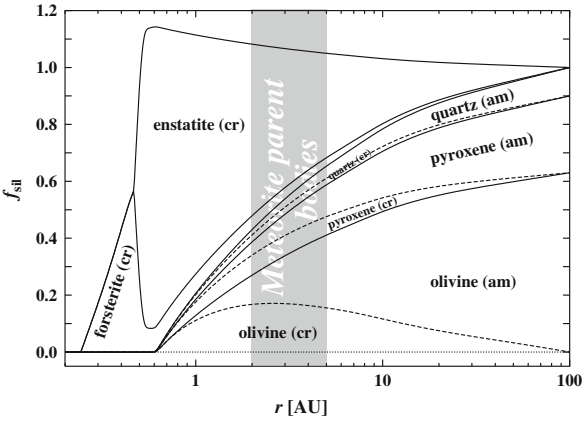

Fig. 33 Cumulative representation of the distribution of the silicon condensed into dust between the different silicate dust components (interstellar and equilibrium ones) within the protoplanetary disk, and the fraction of amorphous (am) and crystalline (cr) interstellar silicates. The equilibrium dust components forsterite and enstatite are always crystalline. The total Si abundance is normalized to the interstellar Si abundance. An enhancement of the Si abundance in the region of evaporation of the interstellar silicates is due to diffusive mixing effects. The *grey shaded area* roughly indicates the region where the parent bodies of meteorites are located. Stationary disk model with an accretion rate $\dot{M} = 1 \times 10^{-7}\,M_\odot\,\mathrm{year}^{-1}$ and a protostar of $1\,M_\odot$

[10] H_2O in any case is so abundant that abundance variations with varying degree of condensation of the silicates can be neglected.

Table 9 Composition of the silicate mixture at 3 and 20 AU in a stationary protoplanetary disk model with $\dot{M} = 1 \times 10^{-7}\,\mathrm{M}_\odot\,\mathrm{year}^{-1}$. The numbers are fractions of the silicon contained in the different dust species. "cr" and "am" denote crystalline or amorphous dust, respectively

r	Olivine		Forsterite	Pyroxene		Enstatite	Quartz	
AU	cr	am	cr	cr	am	cr	cr	am
3	0.159	0.158	0.037	0.067	0.070	0.458	0.023	0.027
20	0.073	0.469	0.010	0.031	0.202	0.129	0.011	0.076

forsterite and enstatite in this case also is shown in Fig. 32. One also readily sees that the region of evaporation of the equilibrium dust components forsterite and enstatite is well separated from the region where the interstellar silicates evaporate. These processes operate in different regions of the disk.

Figure 33 shows in a cumulative representation the distribution of the Si between the different silicate dust species at different radii, calculated for a stationary accretion disk model. This is the mixture of silicate dust species from which the planetesimals are formed. Note the local enrichment of Si by diffusive mixing effects in the region where the interstellar silicates evaporate.

Table 9 shows the composition of the silicate mixture at 3 AU and 20 AU. These radii are roughly representative for the regions where the parent bodies of meteorites and the cometary nuclei, respectively, have been formed in our Solar System. The results presently are obtained on the basis of a rather crude modeling of the accretion disk (one-zone approximation, stationary, α-disk) and cannot be considered as completely realistic, but they probably outline the trends for the composition of the silicate mineral mixture in an accretion disk:

- A high fraction of equilibrated silicate dust from the warm inner region and a rather high degree of crystallization in the zone where the parent bodies of meteorites are formed.
- Mostly interstellar dust with an admixture of up to about 20% annealed interstellar dust and equilibrated dust from the warm inner disk region in the zone where cometary nuclei are formed.

These trends are in accord with what is observed for dust from comets (e.g. Wooden et al. [164, 165]). For meteoritic matrix material the predicted fraction of enstatite in the mixture seem to be somewhat high compared to forsterite, but the general trends fits with the observed composition of the matrix material of primitive meteorites (e.g. Scott et al. [166], Brearley et al. [167], Buseck and Hua [168]). The somewhat high pyroxene content in the present model calculation results from the assumption of complete chemical equilibrium between forsterite and enstatite, which possibly cannot be attained because of the slow forsterite-enstatite conversion (cf. Fig. 15).

Figure 34 shows corresponding results for the radial distribution of the mass-fractions of different dust species and of ice for two different stages of the time-dependent evolution of an accretion disk around a solar-like protostar corresponding to instants of 5×10^5 year and 1×10^6 year. They correspond to the mixture of

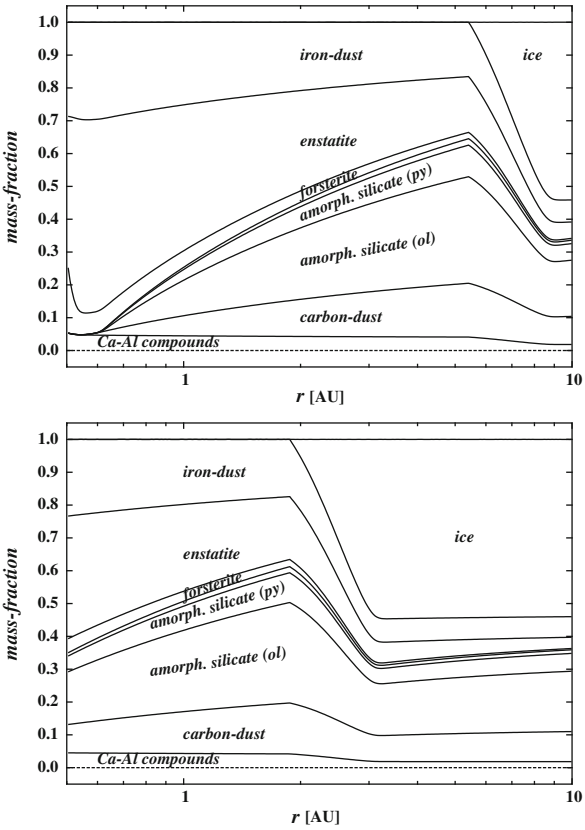

Fig. 34 Radial variation of the pristine composition of planetesimals formed by agglomeration of dust, if planetesimal formation starts about 0.5 Ma (*top*) or 1 Ma (*bottom*) after formation of the proto-sun

dust species entering the planetesimals if planetesimal formation commences at the respective instants. This determines the composition of the raw material of planetary bodies that later form from the swarm of planetesimals.

7.11 Processing of Other Dust Components

At temperatures below $\approx$ 720 K part of the solid iron in the protoplanetary accretion disk reacts with H_2 to form FeS. The kinetics of this process was discussed by, e.g., Fegley and Prinn[169] and Fegley [170]. It has been studied in the laboratory and discussed in detail by Lauretta et al. [115] and by Tachibana and Tsuchiyama [117]. Figure 15 shows the reaction timescale for conversion of a 0.1 μm iron grain into FeS at a pressure of 10^{-3} bar and Solar System abundances, calculated from the linear reaction kinetics rate coefficient of Lauretta et al. [115]. For small grains (size

$\lesssim 10\,\mu$m) the reaction is fast enough that the abundance of FeS can be assumed to be as in chemical equilibrium. No model calculation results for the radial distribution of the thickness of FeS rims on Fe grains in an accretion disk are presently available.

The kinetics of formation of magnetite is discussed in Fegley [170], Hong and Fegley [118] and of other materials in Fegley [170].

According to equilibrium calculations there exist several dust components bearing Al and Ca that are stable in different regions of the p-T-plane (cf. Fig. 5). If condensates from different zones of the disk are intermingled by mixing and transport processes, dust components moved from their stability region into a zone where they are unstable and start to convert into the locally stable species. No experimental data for the processes by which the different species are converted into each other (e.g. corundum to gehlenite, corundum to spinel, gehlenite to diopside) seem to be available at present.

8 Concluding Remarks

In this contribution we have discussed some problems related to the formation and evolution of mineral mixtures in circumstellar dust shells and protoplanetary accretion discs. We have seen that numerous experimental investigations have been undertaken during the last twenty years to study a lot of processes that are important for condensation, evaporation, and for chemical and physical processing of cosmic dust. Many phenomenological coefficients entering the basic equations describing such processes now are determined thanks to these experimental efforts. This enables more realistic model calculations for the abundant magnesium-iron-silicates and for the iron dust component than those which were possible in the past, where such coefficients usually had simply to be guessed.

On the theoretical side much progress has been achieved during the last years in modelling the structure and evolution of protoplanetary accretion discs in 1, 2 and even 3 spatial dimensions. Combining such calculations with realistic modelling of the composition and evolution of the dust component in discs will certainly dramatically improve our understanding of the early history of our Solar System and generally of the early stages of the evolution of planetary systems.

For circumstellar dust shells there is an urgent need for combining time dependent hydrodynamical calculations of stellar winds with multi-component dust formation models in order to obtain realistic models for oxygen rich AGB stellar winds.

There remain, however, important deficiencies in our knowledge. For the important group of Al-Ca-compounds no such type of laboratory measurements of dust evaporation or growth and of dust processing are available as for the magnesium-iron-silicates. This probably results from the much higher temperatures required for such experiments for the more refractory Ca-Al-compound than for the silicates. Technical improvements in the high temperature experimental equipment will hopefully improve this situation in the near future.

The main shortcoming in the whole field, however, is our only rudimentary knowledge (or better, our ignorance) of the basic processes responsible for dust nucleation. More theoretical and experimental efforts are required to solve this fundamental problem.

Acknowledgments This work has been performed as part of the projects of the special research programmes SFB 359*"Reactive flows, diffusion and transport"* and SFB 439 *"Galaxies in the Young Universe"* and the Forschergruppe 759 *"The formation of planets. The critical first growth phase"* which are supported by the Deutsche Forschungsgemeinschaft (DFG).

References

1. Herwig, F.: Annu. Rev. Astron. Astrophys. **43**, 435 (2005) 62, 102
2. Boothroyd, A.I., Sackmann, I.-J.: Astrophys. J. **510**, 232 (1999) 64
3. Schaller, G., Schaerer, D., Meynet, G., Maeder, A.: Astron. Astrophys. Suppl. **96**, 269 (1992) 64, 102
4. Meynet, G., Maeder, A., Schaller, G., Schaerer, D., Charbonnel, C.: Astron. Astrophys. Suppl. **103**, 97 (1994) 64, 65
5. Anders, E., Grevesse N.: Geochim. Cosmochim. Acta **53**, 197 (1989) 64
6. Grevesse, N., Noels, A.: Cosmic abundances of the elements. In: Prantzos, N., Vangioni-Flam, E., Cassé, M. (eds.) Origin and Evolution of the Elements, pp. 15–25. Cambridge University Press, Cambridge (1993) 64
7. Soubiran, C., Girard, P.: Astron. Astrophys. **438**, 139 (2005) 65
8. Lodders, K., Palme, H., Gail, H.-P.: Abundance of the elements in the solar system. In: Landolt-Börnstein New Series, Astronomy and Astrophysics, Springer Verlag, Berlin (2009) 64, 103
9. Tielens, A.G.G.M.: The destruction of interstellar dust. In: Greenberg, J.M., Li, A. (eds.) Formation and Evolution of Solids in Space, pp. 331–375. Kluwer, Dordrecht (1999) 66
10. Zhukovska, S.V., Gail, H.-P., Trieloff, M.: Astron. Astrophys. **479**, 453 (2008) 66, 113
11. Atkins, P.W.: Physical Chemistry, 5th edn. Oxford University Press, Oxford (1994) 67, 68, 77
12. Smith, W.R., Missen, R.W.: Chemical Reaction Equilibrium Anaysis: Theory and Algorithms. Wiley, New York, NY (1982) 67, 71, 72, 80
13. Chase, M.W.: NIST-JANAF thermochemical tables. 4th edn. J. Phys. Chem. Ref. Data, Monograph No. 9 (1998) 72
14. Barin, I.: Thermochemical Data of Pure Substances, vols. I and II, 3rd edn. VCH Verlagsgesellschaft, Weinheim (1995) 72
15. Saxena, S.K., Chatterjee, N., Fei, Y., Shen, G.: Thermodynamic Data on Oxides and Silicates. Springer, Heidelberg (1993) 72, 77, 78
16. Kubaschewski, O., Alcock, C.B.: Metallurgical Chemistry, 5th edn. Pergamon Press, Oxford (1983) 72
17. Sharp, C.M., Huebner, W.F.: Astrophys. J. Suppl. **72**, 417 (1990) 72, 74
18. Grossman, L.: Geochim. Cosmochim. Acta **36**, 597 (1972) 72, 74, 78, 79
19. Gail, H.-P.: Astron. Astrophys. **332**, 1099 (1998) 73, 93, 112, 127
20. Gail, H.-P., Sedlmayr, E.: Dust formation in M stars. In: Hartquist, T.W., Williams, D.A. (eds.) The Molecular Astrophysics of Stars and Galaxies, pp. 285–312. Oxford University Press, Oxford (1998) 73, 91
21. Sharp, C.M., Wasserburg, G.J.: Geochim. Cosmochim. Acta **59** 1633 (1995) 73, 74, 76, 104
22. Gilman, R.C.: Astrophys. J. **155**, L185 (1969) 74
23. Larimer, J.W.: Geochim. Cosmochim. Acta **31**, 1215 (1967) 74
24. Lattimer, J.M., Schramm, D.N., Grossman, L.: Astrophys. J. **219**, 230 (1978) 74, 76

25. Saxena, S.K., Eriksson, G.: Chemistry of the formation of the terrestrial planets. In: Saxena, S.K. (ed.) Chemistry and Physics of Terrestrial Planets, pp. 30–105. Springer, New York, NY (1986) 74, 77, 78, 79
26. Lodders, K., Fegley, B., Jr.: Meteoritics **30**, 661 (1995) 74, 76, 104
27. Lodders, K., Fegley, B., Jr.: Condensation chemistry of carbon stars. In: Bernatowicz, T.J., Zinner, E.K. (eds.) Astrophysical Implications of the Laboratory Study of Presolar Materials, pp. 391–423. American Institute of Physics, New York, NY (1997) 74, 76, 104
28. Lodders, K., Fegley, B., Jr.: Condensation chemistry of circumstellar grains. In: Le Bertre, T., Lèbre, A., Waelkens, C. (eds.) Asymptotic Giant Branch Stars, pp. 279–289. ASP, San Francisco, CA (1999) 74
29. Glassgold, A.E.: Annu. Rev. Astron. Astrophys. **34**, 241 (1996) 74
30. Ebel, D.S., Grossman, L.: Geochim. Cosmochim. Acta **64**, 339 (2000) 74, 77
31. Krot, A., Fegley, B., Jr., Lodders, K., Palme, H.: Meteoritical and astrophysical constraints on the oxidation state of the solar nebula. In: Mannings, V., Boss, A.P., Russel, S.S. (eds.) Protostars and Planets IV, pp. 1019–1054. University of Arizona Press, Tucson, AZ (2000) 74
32. Davis, A.M., Richter, F.M.: Condensation and evaporation of solar system materials In: Davis, A.M. (ed.) Treatise on Geochemistry, vol. 1, p. 407. Elsevier, Amsterdam (2003) 74
33. Ferrarotti, A.S., Gail, H.-P.: Astron. Astrophys. **382**, 256 (2002) 76, 104, 107, 109
34. Saxena, S.K.: Thermodynamics of Rock-Forming Crystalline Solutions. Springer, Berlin (1973) 77
35. Schmalzried, H., Navrotsky, A.: Festkörperthermodynamik. Verlag Chemie, Weinheim (1975) 77
36. Schmalzried, H.: Chemical Kinetics of Solids. Wiley-VCH, Weinheim (1995) 77
37. Philpotts, A.R.: Principles of Igneous and Metamorphic Petrology. Prentice Hall, Englewood Cliffs, NJ (1990) 77
38. Putnis, A.: An Introduction to Mineral Sciences. Cambridge University Press, Cambridge (2001) 77
39. Wood, B.J., Kleppa, O.J.: Geochim. Cosmochim. Acta **45**, 534 (1981) 78
40. Blander, M., Katz, J.L.: Geochim. Cosmochim. Acta **31**, 1025 (1967) 79
41. Molster, F.J., Waters, L.B.F.M., Tielens, A.G.G.M., Barlow, M.J.: Astron. Astrophys. **382**, 184 (2002) 79
42. Molster, F.J., Waters, L.B.F.M., Tielens, A.G.G.M.: Astron. Astrophys. **382**, 222 (2002) 79
43. Molster, F.J., Waters, L.B.F.M., Tielens, A.G.G.M., Koike, C., Chihara, H.: Astron. Astrophys. **382**, 241 (2002) 79
44. Weidenschilling, S.J., Cuzzi, J.N.: Formation of planetesimals in the solar nebula. In: Levy, E.H., Lunine, J.I. (eds.) Protostars and Planets III, pp. 1031–1060. University of Arizona Press, Tucson, AZ (1993) 85
45. Pruppacher, H.R., Klett, J.D.: Microphysics of Clouds and Precipitation. Reidel, Dordrecht (1978) 88
46. Rietmeijer, F.J.M., Nuth, J.A., III: Astrophys. J. **527**, 395 (1999) 88
47. Rietmeijer, F.J.M., Nuth, J.A., III, Karner, J.M.: Phys. Chem. Chem. Phys. **1**, 1511 (1999) 88
48. Rietmeijer, F.J.M., Karner, J.M.: J. Chem. Phys. **110**, 4554 (1999) 88
49. Toppani, A., Libourel, G., Robert, F., Ghanbaja, J.: Geochim. Cosmochim. Acta **70**, 5035 (2006) 88
50. Lide, R.D.: CRC Handbook of Chemistry and Physics, 76th edn. CRC Press, Boca Raton, FL (1995) 84
51. Nagahara, H., Kushiro, I., Mysen, B.O.: Geochim. Cosmochim. Acta **58**, 1951 (1994) 88
52. Nagahara, H., Kushiro, I., Mysen, B.O., Mori, H.: Nature **331**, 516 (1988) 88
53. Hashimoto, A.: Nature **347**, 53 (1990) 88, 90
54. Wang, J., Davis, A.M., Clayton, R.N., Hashimoto, A.: Geochim. Cosmochim. Acta **63**, 953 (1999) 89
55. Nichols, R.H., Jr., Wasserburg, G.J.: Lunar Planet. Sci. Conf. **XXVI**, 1047 (1995) 89
56. Nichols, R.H., Jr., Grimley, R.T., Wasserburg, G.J.: Meteorit. Planet. Sci. **33**, A115 (1998) 89

57. Johansen, A., Klahr, H., Mee, A.J.: Mon. Not. R. Astron. Soc. **370**, L71 (2006) 125
58. Inaba, H., Tachibana, S., Nagahara, H., Ozawa, K.: Lunar Planet. Sci. Conf. **XXXII**, 1837 (2001) 89
59. Nagahara, H., Ozawa, K.: Meteoritcs **29**, 508 (1994) 89
60. Nagahara, H., Ozawa, K.: Geochim. Cosmochim. Acta **60**, 1445 (1996) 89
61. Hashimoto, A.: Meteorit. Planet. Sci. **33**, A65 (1998) 89
62. Tsuchiyama, A., Tachibana, S., Takahashi, T.: Geochim. Cosmochim. Acta **63**, 2451 (1999) 89
63. Tachibana, S., Tsuchiyama, A., Nagahara, H.: Lunar Planet. Sci. Conf. **XXIX**, 1539 (1998) 89
64. Tachibana, S., Tsuchiyama, A., Nagahara, H.: Lunar Planet. Sci. Conf. **XXXI**, 1588 (2000) 89
65. Tachibana, S., Tsuchiyama, A., Nagahara, H.: Geochim. Cosmochim. Acta **66**, 713 (2002) 90, 100
66. Landolt-Börnstein, Schäfer, K. (ed.) Zahlenwerte und Funktionen, vol. 5b. Springer Verlag, Heidelberg (1968) 90
67. Mendybaev, R.A., Beckett, J.R., Grossman, L., Stolper, E.: Lunar Planet. Sci. Conf. **XXIX**, 1871 (1998) 90
68. Ferrarotti, A.S., Gail, H.-P.: Astron. Astrophys. **371**, 133 (2001) 90, 103, 104, 109, 114
69. Tachibana, S., Nagahara, H., Ozawa, K.: Lunar Planet. Sci. Conf. **XXXII**, 1767 (2001) 90
70. Ferguson, F.T., Nuth, J.A., III: J. Chem. Eng. Data **53**, 2824 (2008) 90
71. Klevenz, M.: Thesis, University of Heidelberg (2009) 90
72. Salpeter, E.E.: Astrophys. J. **193**, 579 (1974) 90
73. Draine, B.T.: Astrophys. Space Sci. **65**, 313 (1979) 90
74. Gail, H.-P., Sedlmayr, E.: Astron. Astrophys. **206**, 153 (1988) 90
75. Patzer, A.B.C., Gauger, A., Sedlmayr, E.: Astron. Astrophys. **337**, 847 (1998) 90
76. Yamamoto, T., Chigai, T., Watanabe, S., Kozasa, T.: Astron. Astrophys. **380**, 373 (2001) 90
77. Keller, R.: Polyaromatic hydrocarbons and the condensation of carbon in stellar winds. In: Legér, A., d'Hendecourt, L., Boccara, N. (eds.) Polycyclic Aromatic Hydrocarbons and Astrophysics, pp. 387–397. Reidel, Dordrecht (1987) 91
78. Frenklach, M., Feigelson, E.D.: Astrophys. J. **341**, 372 (1989) 91
79. Cherchneff, I., Barker, J.R., Tielens, A.G.G.M.: Astrophys. J. **401**, 269 (1992) 91
80. Bernatowicz, T.J., Cowsik, R., Gibbons, P.C., Lodders, K., Fegley, B., Jr., Amari, S., Lewis, R.S.: Astrophys. J. **472**, 760 (1996) 91
81. Sedlmayr, E., Krüger, D.: Formation of dust particles in cool stellar outflows. In: Bernatowicz, T.J., Zinner, E.K. (eds.) Astrophysical Implications of the Laboratory Studies of Presolar Material, pp. 425–450. American Institute of Physics, New York, NY (1997) 91
82. Cherchneff, I., Le Teuff, Y.H., Williams, P.M., Tielens, A.G.G.M.: Astron. Astrophys. **357**, 572 (2000) 91
83. Clayton, D.D., Deneault, E.A.-N., Meyer, B.S.: Astrophys. J. **562**, 480 (2001) 91
84. Gail, H.-P., Sedlmayr, E.: Faraday Discuss. **109**, 303 (1998) 91
85. Jeong, K.S., Chang, Ch., Sedlmayr, E., Sülzle, D.: J. Phys. B **33**, 3417 (2000) 91
86. Chang, C., Patzer, A.B.C., Sedlmayr, E., Sülzle, D.: Eur. Phys. J. D **2**, 57 (1998) 91
87. Chang, Ch., Patzer, A.B.C., Sedlmayr, E., Steinke, T., Sülzle, D.: Chem. Phys. Lett. **324**, 108 (2000) 91
88. Patzer, A.B.C., Chang, C., Sedlmayr, E., Sülzle, D.: Eur. Phys. J. D **6**, 57 (1999) 91
89. Hallenbeck, S.L., Nuth, J.A., III, Daukantas, P.L.: Icarus **131**, 198 (1998) 92, 93, 112, 113, 129
90. Brucato, J.R., Colangeli, L., Mennella, V., Palumbo, P., Bussoletti, E.: Astron. Astrophys. **348**, 1012 (1999) 92
91. Hallenbeck, S.L., Nuth, J.A., III, Nelson, R.N.: Astrophys. J. **535**, 247 (2000) 92, 113, 129
92. Fabian, D., Jäger, C., Henning, Th., Dorschner, J., Mutschke, H.: Astron. Astrophys. **364**, 282 (2000) 92, 94, 95, 112
93. Thompson, S.P., Tang, C.C.: Astron. Astrophys. **368**, 721 (2001) 92
94. Lenzuni, P., Gail, H.-P., Henning, Th.: Astrophys. J. **447**, 848 (1995) 92
95. Kouchi, A., Yamamoto, T., Kozasa, T., Kuroda, T., Greenberg, J.M.: Astron. Astrophys. **290**, 1009 (1994) 93, 95
96. Sogawa, H., Kozasa, T.: Astrophys. J. **516**, L33 (1999) 93, 95

97. Klahr, H.H., Bodenheimer, P.: Astrophys. J. **582**, 869 (2003) 122, 126
98. Carter, G.: Philos. Mag. **79**, 2773–2784 (1999) 94
99. Gail, H.-P.: Astron. Astrophys. **387**, 192 (2001) 95, 113, 125, 126, 127, 128, 129
100. Kozasa, T., Sogawa, H.: Formation of crystalline silicate around oxygen-rich AGB stars. In: Le Bertre, T., Lèbre, A., Waelkens, C. (eds.) Asymptotic Giant Branch Stars, pp. 239–244. ASP, San Francisco, CA (1999) 95
101. Freer, R.: Contrib. Mineral. Petrol. **76** 440 (1981) 96
102. Brady, J.B.: Diffusion data for silicate minerals, glasses and liquids. In: Ahrens, Th.J. (ed.) Mineral Physics and Crystallography, A Handbook of Physical Constants, pp. 269–290. American Geophysical Union, Washington, DC (1995) 96
103. Chakraborty, S.: J. Geophys. Res. **102**, 12 317 (1997) 97, 98
104. Schwandt, C.S., Cygan, R.T., Westrich, H.R.: Contrib. Mineral. Petrol. **130**, 390 (1998) 98
105. Nagasawa, H., Suzuki, T., Ito, M., Morioka, M.: Phys. Chem. Miner. **28**, 706 (2001) 98, 99
106. Buening, D.K., Buseck, P.R.: J. Geophys. Res. **78**, 6852 (1973) 97
107. Misener, D.J.: Cationic diffusion in olivine to 1400℃ and 35 kbar. In: Hoffman, A.W., Giletti, B.J., Yoder, H.S., Yund, R.A. (eds.) Geochemical Transport and Kinetics, pp. 117–129. Carnegie Institute of Washington, Washington, DC (1974) 97
108. Morioka, M.: Geochim. Cosmochim. Acta **44**, 759 (1980) 97
109. Morioka, M.: Geochim. Cosmochim. Acta **45**, 1573 (1981) 97
110. Chakraborty, S., Farver, J.R., Yund, R.A., Rubie, D.C.: Phys. Chem. Miner. **21**, 489 (1994) 97
111. Ozawa, K., Nagahara, H.: Geochim. Cosmochim. Acta **64**, 939 (2000) 98
112. Klügel, A.: Contrib. Mineral. Petrol. **141** 1 (2001) 98
113. Imae, N., Tsuchiyama, A., Kitamura, M.: Earth Planet. Sci. Lett. **118**, 21 (1993) 100
114. Milke, R., Dohmen, R., Becker, H.-W., Wirth, R.: Contrib. Mineral. Petrol. **154**, 519 (2007) 100
115. Lauretta, D.S., Kremser, D.T., Fegley, B., Jr.: Icarus **122**, 288 (1996) 101, 135
116. Kerridge, J.F.: Icarus **106**, 135 (1993) 101
117. Tachibana, S., Tsuchiyama, A.: Geochim. Cosmochim. Acta **62**, 2005 (1998) 101, 135
118. Hong, Y., Fegley, B., Jr.: Meteorit. Planet. Sci. **33**, 1101 (1998) 101, 136
119. Allen, C.C., Morris, R.V., Lauer, H.V., Jr., McKay, D.S.: Icarus **104**, 291 (1993) 101
120. Nittler, L.R., Alexander, C.M.O., Gao, X., Walker, R.M., Zinner, E.: Astrophys. J. **483**, 475 (1997) 102
121. Groenewegen, M.A.T., van den Hoek, L.B., de Jong, T.: Astron. Astrophys. **293**, 381 (1995) 102
122. Lattanzio, J., Forestini, M.: Nucleosynthesis in AGB stars. In: Le Bertre, T., Lèbre, A., Waelkens, C. (eds.) IAU Symposium 191: Asymptotic Giant Branch Stars, pp. 31–40. ASP, San Francisco, CA (1999) 102
123. Scalo, J.M., Ross, J.E.: Astron. Astrophys. **48**, 219 (1976) 102
124. Blöcker, T.: Astrophys. Space Sci. **275**, 1 (2001) 105
125. Gail, H.-P., Sedlmayr, E.: Astron. Astrophys. **177**, 186 (1987) 108
126. Gail, H.-P., Sedlmayr, E.: Astron. Astrophys. **347**, 594 (1999) 109
127. Ferrarotti, A.S., Gail, H.-P.: Astron. Astrophys. **398**, 1029 (2003) 109
128. Posch, Th., Kerschbaum, F., Mutschke, H., Dorschner, J., Jäger, C.: Astron. Astrophys. **393**, L7 (2002) 109
129. Rubin, A.E.: Meteorit. Planet. Sci. **32**, 231 (1997) 111
130. Cuzzi, J.N., Ciesla, F.J., Petaev, M.I., Krot, A.N., Scott, E.R.D., Weidenschilling, S.J.: Nebular evolution of thermally processed solids: reconciling models and meteorites. In: Krot, A.N., Scott, E.R.D., Reipurth, B. (eds.) Chondrites and the Protoplanetary Disk. ASP Conf. Ser. vol. 341, pp. 732–773. ASP, San Francisco, CA (2005) 111
131. Wooden, D., Desch, S., Harker, D., Gail, H.-P., Keller, L.: Comet grains and implications for heating and radial mixing in the protoplanetary disk. In: Reipurth, B., Jewitt, D., Keil, K. (eds.) Protostars and Planets V, pp. 815–833. University of Arizona Press, Tucson, AZ (2007) 111
132. Dodson-Robinson, S.E., Willacy, K., Bodenheimer, P., Turner, N.J., Beichman, C.A.: Icarus **200**, 672 (2009) 111

133. Pollack, J.B., Hollenbach, D., Beckwith, S., Simonelli, D.P., Roush, T., Fong, W.: Astrophys. J. **421**, 615 (1994) 111, 112, 114, 133
134. Watson, D.M.: Mineralization, grain growth and disk structure: observations of the evolution of dust in protoplanetary disk. In: Henning, Th., Gruen, E., Steinacker, J. (eds.) Cosmic Dust – Near and Far. ASP Conf. Ser., vol. 414, pp. 77–98. ASP, San Francisco, CA (2009) 112
135. Duschl, W.J., Gail, H.-P., Tscharnuter, W.M.: Astron. Astrophys. **312**, 624 (1996) 112, 127, 132
136. Wehrstedt, M., Gail, H.-P.: Astron. Astrophys. **385**, 181 (2002) 113, 127, 128
137. Draine, B.: Evolution of interstellar dust. In: Blitz, L. (ed.) The Evolution of the Interstellar Medium. ASP Conf. Proc. vol. 12, p. 193. ASP, San Francisco, CA (1990) 113
138. Tielens, A.G.G.M.: Astrophys. J. **499**, 267 (1998) 113
139. Kemper, F., Vriend, W.J., Tielens, A.G.G.M.: Astrophys. J. **609**, 826 (2004) 114
140. Lin, D.N.C., Papaloizou, J.: On the dynamical origin of the solar nebula. In: Black, D.C., Matthews, M.S. (eds.) Protostars and Planets II, pp. 981–1072. University of Arizona Press, Tucson, AZ (1985) 115
141. Ruden, S.P., Lin, D.N.C.: Astrophys. J. **308**, 883 (1986) 116
142. Bell, K.R., Lin, D.N.C.: Astrophys. J. **427**, 987 (1994) 116
143. Bell, K.R., Cassen, P.M., Klahr, H.H., Henning, Th.: Astrophys. J. **486**, 372 (1997) 116, 119
144. Huesco, R., Guillot, T.: Astron. Astrophys. **442**, 703 (2005) 116, 119
145. Wehrstedt, M., Gail, H.-P.: Radial mixing in protoplanetary accretion disks VII. 2-dimensional transport of tracers. (arXiv:0804.3377v1) (2008) 116, 119, 125, 126, 127
146. Haisch, K.E., Jr., Lada, E.A., Lada, C.J.: Astrophys. J. Lett. **553**, L153–L156 (2001) 118
147. Kley, W., Lin, D.N.C.: Astrophys. J. **397**, 600 (1992) 119
148. Keller, Ch., Gail, H.-P.: Astron. Astrophys. **415**, 1177 (2004) 119, 120, 121, 122
149. Tscharnuter, W.M., Gail, H.-P.: Astron. Astrophys. **463**, 369 (2007) 119, 127
150. Urpin, V.A.: Sov. Astron. **28**, 50 (1984) 120
151. Różyczka, M., Bodenheimer, P., Bell, K.R.: Astrophys. J. **423**, 736 (1994) 120
152. Regev, O., Gitelman, L.: Astron. Astrophys. **396**, 623 (2002) 120
153. Takeuchi, T., Lin, D.N.C.: Astrophys. J. **581**, 1344 (2002) 120
154. Ciesla, F.J.: Icarus **200**, 655 (2009) 120
155. Klahr, H.H.: Astrophys. J. **606**, 1070 (2004) 122, 126
156. Johansen, A., Klahr, H.: Astrophys. J. **634**, 1353 (2005) 125
157. Turner, N.J., Willacy, K., Bryden, G., Yorke, H.W.: Astrophys. J. **639**, 1218 (2006) 125
158. Pavlyuchenkov, Y., Dullemond, C.P.: Astron. Astrophys. **471**, 833 (2007) 125
159. Morfill, G.E., Völk, H.-J.: Astrophys. J. **287**, 371 (1984) 126
160. Boss, A.P.: Astrophys. J. **616**, 1265 (2004) 126
161. Boss, A.P.: Earth Planet. Sci. Lett. **268**, 102 (2008) 126
162. Gail, H.-P.: Astron. Astrophys. **413**, 571 (2004) 127
163. Bockelée-Morvan, D., Gautier, D., Hersant, F., Huré, J.-M., Robert, F.: Astron. Astrophys. **384**, 1107 (2002) 128
164. Wooden, D.H., Harker, D.E., Woodward, C.E., Butner, H.M., Koike, C., Witteborn, F.C., McMurtry, C.W.: Astrophys. J. **517**, 1034 (1999) 129, 134
165. Wooden, D.H., Butner, H.M., Harker, D.E., Woodward, C.E.: Icarus **143**, 126 (2000) 129, 134
166. Scott, E.R.D., Barber, D.J., Alexander, C.M., Hutchinson, R., Peck, J.A.: Primitive material surviving in chondrites: matrix. In: Kerridge, J.F., Matthews, M.S. (eds.) Meteorites and the Early Solar System, pp. 718–745. University of Arizona Press, Tucson, AZ (1988) 134
167. Brearley, A.J., Scott, E.R.D., Keil, K., Clayton, R.N., Mayeda, T.K., Boynton, W.V., Hill, D.H.: Geochim. Cosmochim. Acta **53**, 2081 (1989) 134
168. Buseck, P.R., Hua, X.: Annu. Rev. Earth Planet. Sci. **21**, 255 (1993) 134
169. Fegley, B., Jr., Prinn, R.G.: Solar nebula chemistry: implications for volatiles in the solar system. In: Weaver, H.A., Danly, L. (eds.) The Formation and Evolution of Planetary Systems, pp. 171–205. Cambridge University Press, Cambridge (1989) 135
170. Fegley, B., Jr.: Space Sci. Rev. **92**, 177 (2000) 135, 136

The Mineralogy of Interstellar and Circumstellar Dust in Galaxies

F.J. Molster, L.B.F.M. Waters, and F. Kemper

Abstract Dust in space is ubiquitous and is part of the cycle of matter in galaxies. The observed properties of dust change as a function of the astrophysical environment in which it is found. Dust can therefore be used as a tracer and probe of the physical and chemical conditions where it is detected. We present an observational overview of interstellar and circumstellar dust using spectroscopy at infrared wavelengths. Thanks to the contributions made by space-based infrared spectrographs, a large observational database of dust in space is now available. In this review, we focus on the identification of solid state resonances at these wavelengths, and present an inventory of dust species in different astrophysical environments. The picture that emerges is that of a very rich circumstellar dust mineralogy, while the interstellar medium shows only a limited amount of species. The implications for our understanding of dust processing in different astrophysical environments are also discussed.

F.J. Molster (✉)
Nederlandse Organisatie voor Wetenschappelijk Onderzoek (NWO), Anna van Saksenlaan 51, 2593 HW Den Haag, The Netherlands; Nederlandse Onderzoekschool Voor Astronomie (NOVA), Leiden Observatory, Niels Bohrweg 2, 2333 CA Leiden, The Netherlands
e-mail: molster@strw.leidenuniv.nl

L.B.F.M. Waters
Astronomical Institute "Anton Pannekoek", University of Amsterdam, Kruislaan 403, 1098 SJ Amsterdam, The Netherlands; Instituut voor Sterrenkunde, Katholieke Universiteit Leuven, Celestijnenlaan 200D, B-3001 Heverlee, Belgium
e-mail: rensw@astro.uva.nl

F. Kemper
Jodrell Bank Centre for Astrophysics, The Alan Turing Building, School of Physics and Astronomy, The University of Manchester, Manchester M13 9PL, UK
e-mail: f.kemper@manchester.ac.uk

Molster, F.J. et al.: *The Mineralogy of Interstellar and Circumstellar Dust in Galaxies*. Lect. Notes Phys. **815**, 143–201 (2010)
DOI 10.1007/978-3-642-13259-9_3

1 Introduction

Interstellar space is not empty, but filled with gas – mostly hydrogen – and small solid particles, referred to as *dust*. The presence of small interstellar dust particles was first deduced in the early part of the twentieth century from the reddening of the colours of stars with a similar spectral type. Starlight was found to be polarized, which can be explained if some of the light is scattered by non-spherical aligned dust particles in the line of sight. The properties of reflection nebulae can be understood if they contain small solid particles. Studies of interstellar extinction and its wavelength dependence have resulted in constraints on the gas to dust ratio in the interstellar medium (ISM), the size distribution of interstellar grains, and to some extent their chemical composition, see Li and Greenberg [1] for an excellent review.

The ubiquitous presence of dust became even more evident with the advent of infrared astronomy around 1960, and in particular with the far-IR all-sky survey carried out with the IRAS satellite in 1983. The infrared wavelength range is where the bulk of the thermal emission from dust grains, heated by optical and ultraviolet starlight, is emitted. Some galaxies contain so much dust that they emit more than 90% of their energy at infrared wavelengths! The study of dust impacts on our understanding of the physics and chemistry of the ISM, the star formation process, and on the last phases in the life of stars.

Thermal emission from dust has been detected from a wide variety of regions in our and in external galaxies, ranging between the densest molecular clouds to the diffuse low-density clouds at high galactic latitude, and even from intergalactic clouds. IR excess emission from stars is often a strong indication for the presence of *circumstellar* dust. Indeed, stardust is found around stars of a wide variety of mass, luminosity and evolutionary state. This dust can be related to their infancy, i.e. the star- and planet formation process, or it can be due to episodes of mass loss that stars experience at various epochs during their life. There is a strong relation between the dust produced by stars during their life, dust in the ISM and dust in molecular clouds and star forming regions. Stars are believed to be the main dust factories in galaxies. The *life cycle* of dust, from their production by stars, their life in the ISM and their incorporation into new generations of stars and planets is one of the central themes of astromineralogy.

Perhaps the most powerful tool in the field of observational astromineralogy is infrared spectroscopy of the vibrational resonances in the solid. The IR spectral region contains most of the relevant resonances of abundant species. These resonances provide information about chemical composition, size, shape, lattice structure, abundance and temperature of the grains. The resonances can be studied in absorption against bright background sources (stars) or in emission.

Infrared spectroscopy of dust in space started around 1970 with the detection of broad emission bands in the mid-infrared wavelength region using ground-based telescopes. These bands were attributed to amorphous silicates and polycyclic aromatic hydrocarbons (PAHs). Large contributions to infrared spectroscopy were made by the NASA Kuiper Airborne Observatory (KAO) and by the Low Resolution Spectrometer (LRS) on board IRAS, which operated between 8 and 23 μm.

A landslide of new results in the field of astromineralogy has resulted from observations made with the Short Wavelength Spectrometer (SWS [2]) and Long Wavelength Spectrometer (LWS [3]) on board of the Infrared Space Observatory (ISO [4]). These two instruments provided an uninterrupted spectral coverage between 2 and 200 μm with a resolution $\lambda/\Delta\lambda$ between 150 and 2,000. The Spitzer Space Telescope [5], operated by NASA, whose cryogenic mission lasted from August 2003 until May 2009 has added a huge database of infrared spectra in the 5–40 μm wavelength range, using the Infrared Spectrograph [IRS; 6]. The Japanese AKARI satellite [7] was operational between May 2006 and August 2007 has carried out an all-sky survey in the 1.7–180 μm wavelength range and has also carried out spectroscopic observations. In this review we will mostly use ISO and Spitzer data to illustrate the presence of minerals in space.

This chapter describes our current understanding of the composition of interstellar and circumstellar dust as derived from infrared spectroscopy. We concentrate on refractory materials and restrict the discussion to solids, leaving out ices and large molecules such as PAHs.

2 Observations and Identification

Apart from the dust in our own solar system, which can be collected and analyzed in situ or brought back to the laboratories on earth, all other dust grains can only be studied via their influence on electromagnetic radiation. In principle there are three ways in which dust interacts with light; it can absorb, scatter and emit radiation; in general it will do all three at the same time. Since the amount of absorption, scattering and/or emission depends on the grain shape, size, composition and the wavelength of the light, it allows us to get quite accurate information about the properties of the dust present outside our solar system. The main characteristic dust bands lie in the infrared region, where most of the vibrational and translational bands are found. In the remainder of this section we will therefore discuss the infrared properties of cosmic dust grains.

2.1 The Identification of Solids in Space

The identification of solids using astronomical spectra of interstellar and circumstellar dust requires laboratory data of astrophysically relevant samples whose properties are determined at the relevant temperatures. Ideally, "real" samples of stardust or interstellar dust should be used for this purpose, but such materials are either not available or extremely rare, and at any rate difficult to handle. Materials that could be used in this context are lunar samples, meteorites and Interplanetary Dust Particles (IDPs). However, it is by no means evident that these materials are indeed representative. An exception could be the IDPs of cometary origin, such as used by Bradley et al. [8] for amorphous silicates and by Keller et al. [9] for FeS.

Alternatively, laboratory samples of natural (i.e. found on Earth) and of synthetic minerals are a useful starting point to compare to the astronomical spectra. Of course, the simplest and most abundant minerals found in the solar system are the prime candidates to use. However, it should be kept in mind that the local conditions in space can be very different from those that prevailed during the formation of the solar system, resulting in the formation of minerals that are rare in the solar system.

There are several methods to obtain the spectral properties of materials; examples are absorption-, reflection-, emission- and Raman-spectroscopy. The most frequently used methods for astronomical purposes are reflection and absorption (also referred to as transmission) spectroscopy. The absorption spectra of very small particles ($<1\,\mu$m) turn out to be very helpful for identification purposes and to obtain relative strength ratios of the features. Apparently the size and shape of the particles after grinding down is a good analogue for, but not necessarily similar to, the material that has been found around stars. For all the identification purposes in the rest of this section we have used absorption spectra. However, for modelling purposes, where not only the absorption but also the scattering is important, it is necessary to know the complete optical constants of the materials. Since the shape distribution of the laboratory samples is often not well characterized, absorption spectra are less helpful to determine the optical properties. Reflection spectra, although less convenient for identification purposes, are preferred to derive the optical constants.

In Fig. 1 we show the infrared spectrum of MWC 922, together with the (calculated) emissivity of forsterite at 90 K, roughly the temperature of the forsterite around MWC 922 [10]. It is clear that the grain shape is of great importance in the position and width of the features. For forsterite, the Mie calculations (0.1 μm

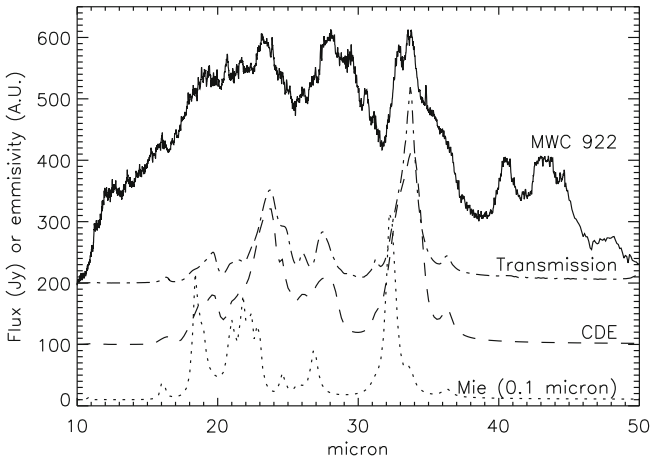

Fig. 1 The spectrum of MWC 922 compared with the emissivities of forsterite at 90 K derived directly from transmission spectra [*dashed dotted line* 12], and calculated for two different grain shape distributions; Mie calculations of 0.1 μm spheres (*dotted line*) and a continuous distribution of ellipsoids (CDE; *dashed line*). The optical constants used for these calculations are derived from reflection measurements [13, 14]

spheres) clearly differ from the positions measured in transmission for the same material. The Continuous Distribution of Ellipsoids (CDE) gives already a much better fit, although the features seem to be a little too broad. The best match to the astronomical data is given by the absorption spectra. This indicates that the grain shapes of ground down grains used for transmission are probably a better analogue for the actual shape distribution of astronomical grains than spherical or ellipsoidal grains.

Probably the most reliable laboratory measurements of the optical properties of small dust particles can be obtained by using free-floating samples, since this avoids the difficulty of correcting for matrix effects to derive the optical constants. Reference [11] shows that important effects for strong resonances in, e.g. forsterite can occur, in particular for the wavelength of the resonances.

The detailed interpretation of the presently available astronomical spectra requires (full) radiative transfer calculations using optical constants measured in the laboratory and assumptions about the source geometry, and the composition, abundance, size, and shape of the grains. The laboratory spectra should have a large wavelength coverage (preferably from the UV to the mm wavelengths) and with relatively high spectral resolution ($\frac{\lambda}{\Delta\lambda} \geq 200$ for the infrared) and should be of chemically and structurally well characterized materials with an appropriate grain size (and shape). Unfortunately, only in recent years such thorough studies of cosmic dust analogues have become available, while many older studies are difficult to use due to only partial wavelength coverage and/or poor sample characterization. This can lead to some confusion in the literature as to the assignment of some bands to certain minerals. Nevertheless, even in those cases where samples have been properly characterized, disturbing differences still remain (see Fig. 2). Useful laboratory measurements of well qualified materials include amorphous [15] and crystalline silicates [12, 16–18], oxides [19], metallic iron [20], metal sulfides [21], carbon bearing minerals like amorphous carbon [22], SiC [23, 24], TiC [25] and carbonates [26], sometimes also measured at different temperatures [27–31].

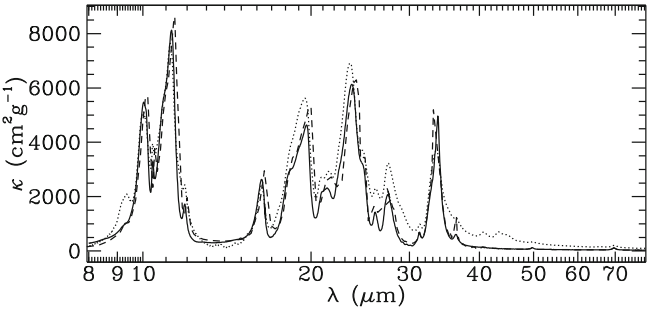

Fig. 2 The mass absorption coefficients of forsterite derived from different laboratory measurements by Koike et al. [12, *solid line*], Jäger et al. [17, *dotted line*], Koike et al. [16, *dashed line*]. Note that the Jäger et al. data have been multiplied by a factor 2 to match the other measurements. Figure taken from [32]

As shown in Fig. 1, there are still problems to convert the optical properties in a realistic way to absorption and scattering efficiencies. These properties can only be exactly calculated for a restricted set of regular shapes (spheres, ellipsoids, needles etc.), while in nature dust particles do not have these regular shapes. Although CDE nicely reproduces the spectra in the case of forsterite, there are still quite some problems with this approach. First of all, CDE is not suitable for all materials (see e.g. [9]) and secondly it assumes that all particles are significantly smaller than the wavelength considered. Several methods exist to calculate the optical properties of irregular grains (like the discrete dipole approximation (DDA) [33, 34] and T(ransition)-matrix method [35, 36]), however these methods often require long calculation times to calculate even a single grain, not to mention whole grain populations, and is not applicable to all sets of optical constants (especially not when very strong resonances are involved). In recent years the introduction of new methods, e.g. the gaussian random spheres approximation [37] and the hollow spheres approach [38] have provided access to more complex grain shapes and sizes. However, even with the restricted set of shapes one can get a reasonable estimate of the kind, amount and location of the circumstellar dust [e.g. 39–41].

Besides grain size and grain shape effects, also the temperature influences the shape and position of the features. Laboratory experiments show that optical constants are temperature dependent. Lowering the temperature will result in narrowing and shifting of most features [see e.g. 27–30]. As the bond length decreases, the energy of the associated phonon mode increases, and therefore the infrared peak shifts to shorter wavelengths (see Fig. 3). This phenomenon can be used to estimate

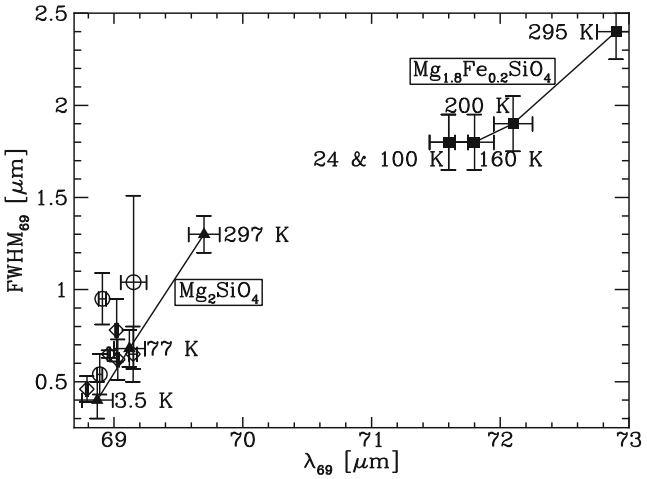

Fig. 3 The observed FWHM and peak wavelength of the 69.0 μm feature in the spectra of the dust around stars (*open diamonds* for the sources with a disk and *open circles* for the sources without a disk) and in the laboratory at different temperatures (*filled triangles* – forsterite [Fo_{100}; 29], and *filled squares* – olivine [Fo_{90}; 28]). The temperatures are indicated at each point, and within the resolution the 24 K and 100 K for Fo_{90} are similar. Note that the measurements were not corrected for the instrumental FWHM ($\approx$ 0.29, for the ISO observations, and 0.25 and 1.0 μm for the laboratory observations of respectively Fo_{100} and Fo_{90}). Figure taken from [10]

the temperature of the dust species [42]. Despite all this, optical constants have often only been measured at room temperature.

The precise mineralogical composition is also very important. Laboratory measurements of several samples in the same solid solution series with slightly different compositions allow us to determine the composition of the minerals with reasonable accuracy. The spectral resolution of ISO allows us for example to see the difference between Fe-rich, Fe-poor and Fe-free silicates of the same solid solution series (see e.g. Fig. 3). The purity and characterization of the laboratory samples is therefore very important for an accurate description of the dust found around other stars.

Alternatively, it is possible to derive empirical dust properties from astronomical observations covering a wide wavelength range. For example, in this way optical constants for amorphous ("astronomical") silicates have been constructed [43, 44]. However, since we do not have a sample of the material, their exact composition has remained unclear. Nevertheless, this approach has proven very practical in many studies of interstellar dust. Of course, it should not be forgotten that for a long time the spectral resolution of the astronomical observations lacked the quality needed for detailed investigations of the dust properties. This changed when ISO, and later also Spitzer spectra became available. These data do allow for detailed investigations of the circumstellar and interstellar dust composition.

3 Observational Astromineralogical Results

In Table 1 we have listed the dust species which were found spectroscopically in astrophysical environments. Note that for most dust species this is based on the identification of only one (strong) feature. In the case of the amorphous and crystalline silicates, $MgAl_2O_4$, FeS and the nano-diamonds more than one band could be attributed to these species. Most of the Solar system materials have been analyzed by other means than spectroscopy (e.g. chemically, TEM), and the identification of the different dust species for the Solar system is therefore very robust.

3.1 Dust Produced in O-rich Environments

3.1.1 Amorphous Silicates

Amorphous silicates are the most abundant grain species in interstellar space, and are responsible for the broad bands at about 9.7 (see Fig. 4) and 18 μm. These are seen in absorption against bright background sources (such as the galactic centre or proto-stellar cores), and in emission or self-absorption in many oxygen-rich cool red giants and supergiants. The 9.7 μm band is due to the Si—O stretch resonance, while the 18 μm band is caused by the Si—O—Si bending mode in the SiO_4 tetrahedron.

Both resonances unfortunately show only a minor dependence on chemical composition of the material, as several laboratory studies have shown [e.g. 15]. Therefore, it is difficult to derive strong constraints on, e.g. the Fe/Mg ratio or on inclu-

Table 1 Overview of the presence of the different dust species in astronomical environments

		Young stars				AGB		pAGB		PNe					
	ISM	PS	TT	Her	SS	O	C	O	C	O	C	WD	Mass. stars	SN	EG
O-rich dust															
Amorphous silicates	√	√	√	√	√	√	√	√		√	√	√	√	√	√
Crystalline silicates			√	√	√	√	√	√	√	√	√		√		√
Proto-Mg-silicates														√	
Carbonates		√:			√					√					
Al_2O_3					√	√							√	√:	
$MgAl_2O_4$					√	√									
SiO_2			√	√	√			√:	√:	√:				√	
[Mg,Fe]O		√:		√:	√	√							√:		
C-rich dust															
Carbonaceous dust	√				√		√		√		√				
SiC	√				√		√		√		√				√
TiC					√				√		√				
(nano-)diamonds				√	√				√						
C-glass														√:	
Other dust species															
MgS	√:						√		√		√				√
FeS				√:	√						√			√:	
Si														√:	
Metallic Fe					√	√								√:	

√: indicates an insecure or dubious detection.

ISM = interstellar medium; PS = proto stars; TT = T-Tauri stars; Her = Herbig Ae/Be stars; SS = solar system material, IDPs and meteortites; (p)AGB = (post) asymptotic giant branch star; PNe = planetary nebulae; O = O-rich; C = C-rich; WD = White dwarf; Mass stars = massive stars (e.g. Luminous Blue Variables, Wolf Rayet stars); EG = Extra Galactic detections.

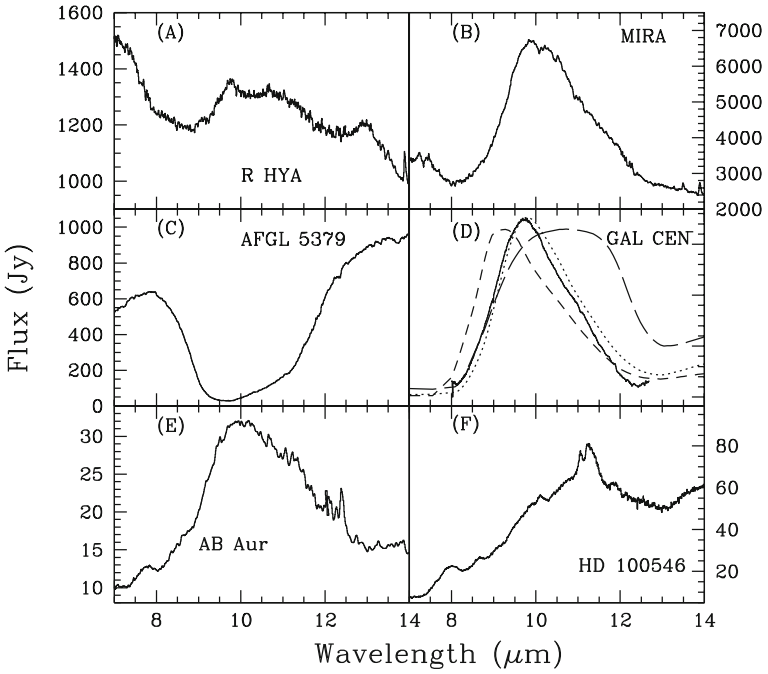

Fig. 4 Examples of 10 μm amorphous silicate band shapes in different astronomical environments. (**a**) R Hya, a low mass loss AGB star with a 10 μm band dominated by simple oxides and a minor amorphous silicate contribution, (**b**) Mira, an AGB star showing a strong amorphous silicate band very similar in shape to that seen in the ISM, (**c**) the OH/IR star AFGL 5379, an AGB star with very high mass loss rate showing a strong amorphous silicate absorption, (**d**) the galactic centre 10 μm silicate band shape (*solid line*) which is observed in absorption, but shown in emission here to illustrate the band shape, and compared to laboratory samples of 0.1 and 2 μm amorphous olivines (*dotted* and *long-dashed lines*, respectively) and small pyroxene grains (*short dashed line*), (**e**) the Herbig Ae/Be star AB Aur, and (**f**) the Herbig Ae/Be star HD 100546, whose silicate band shows prominent contributions from polycyclic aromatic hydrocarbons and from crystalline silicates

sions such as Ca and Al. Based on analysis of the temperature of dust condensing in the outflows of late-type stars, Jones and Merrill [45] suggested that the amorphous silicates should have a substantial opacity in the near-IR, requiring the addition of metals like iron. This can be either as cations into the lattice or as metal grains incorporated into a silicate grain. This is often referred to as "dirty silicates", meaning amorphous (or glassy) silicates with unknown composition and/or inclusions. Draine and Lee [43] introduced "astronomical silicates" to describe *empirically* the absorption and emission properties of interstellar silicates from observations, without detailed composition determination. A similar approach was used by Pegourie [46], Ossenkopf [44] and Suh [47], all using infrared spectra of M-giants. While these empirically derived optical constants are practical in fitting spectra, they do not provide more insight into the chemical composition of amorphous silicates.

More recent studies try to improve on this situation by using optical constants from well characterized materials to fit the astronomical spectra of amorphous silicates [e.g. 15, 41, 48–50]. The first and the latter two studies conclude that amorphous silicates in evolved cool giants are well represented by an olivine stoichiometric ratio ($[Mg, Fe]_2SiO_4$), but that an additional source of opacity is needed in the 3–8 μm wavelength range. Kemper et al. [41] show for OH 127.8+0.0 and Harwit et al. [51] for VY CMa that a good fit can be achieved with small metallic Fe particles. We note that Harwit et al. [51] used spherical grains and needed much more Fe than was available compared to cosmic abundances, while Kemper et al. [41] used a continuous distribution of ellipsoids and remained within the atomic mass budget of Fe. This would imply the Fe particles are not spherical.

The 10 and 20 μm spectral regions in oxygen-rich AGB stars show a considerable spread in the peak position and width of the 10 and 20 μm bands (see Fig. 4). Part of these variations can be attributed to the size and possibly shape changes of the particles, but also the presence of other dust components, such as simple oxides (see Sect. 3.1) or a change in silicate composition has been observed. While amorphous silicates in evolved stars [e.g. 52] may have an olivine stoichiometric ratio, amorphous silicates around young stars appear however to be more similar to pyroxene [$[Mg, Fe]SiO_3$; 49]. Such a change may be due to the impact of supernova shock waves, which will alter the Si/O ratio by sputtering [52]. Lisse et al. [53] find a correlation between the systems evolutionary age of dusty disks and the olivine over pyroxene ratio. Indicating a change from a pyroxene-like stoichiometric ratio for the very young systems [54] to an olivine-like stoichiometric ratio for the amorphous silicates for the dust disks around white dwarfs [55, 56].

Possibly the best analogue for the amorphous silicates in the ISM and around young stars are the GEMS (Glasses with embedded metals and sulfides) found in IDPs that are believed to come from comets (see "The Astromineralogy of Interplanetary Dust Particles" by Bradley, this volume). Their properties show many similarities with the amorphous silicates in the ISM [8]. An infrared spectroscopic analysis of the composition of interstellar silicates observed in the direction of the galactic centre indeed shows that these interstellar silicates are Mg-rich and Fe-poor, with $Mg/(Fe + Mg) \approx 0.9$, consistent with glassy silicates in GEMS [38]. The Mg-rich and Fe-poor nature of interstellar silicates has also been derived from X-ray absorption and scattering analysis [57]. However, there are also differences reported, e.g the (Mg+Si)/Si ratio in the silicates in the galactic centre sightline is 1.5, while in GEMS it can have a wide range but averages at about 0.7 [38].

3.1.2 Crystalline Silicates

Crystalline silicates are the highly ordered counterparts of the amorphous silicates. For a long time the crystalline silicates were only known to be present on earth, in solar system comets [58, 59], IDPs [60, 61], in the dust disk of β-Pictoris [62, 63], and suggested in the disks of T-Tauri stars [64]. A crystalline olivine feature was also reported in the polarized 10 μm spectrum of AFGL2591 [65]. In all these cases

the crystalline silicates were found by infrared spectro(polari)metry around 10 μm, except for the IDPs that were found with the aid of transmission electron microscopy in a laboratory, and later confirmed by infrared spectroscopy [e.g. 61, 66].

In hindsight, we can understand why crystalline silicates were only discovered to be ubiquitous after ISO was launched. Before ISO the main observational MIR/FIR window was around 10 μm. In this wavelength range the crystalline silicates are either overwhelmed by emission from the much more abundant and warmer amorphous silicates, and/or simply too cold to show any detectable feature. The (relatively) low temperature of the crystalline silicates suppresses the intrinsically strong crystalline silicate features around 10 μm. Thanks to the extended wavelength range (up to 200 μm) of the spectrographs on board ISO, the composition of the cold dust could be studied in detail for the first time. The IRS on board Spitzer has significantly increased the database of infrared spectra, giving a much more complete overview. At present, crystalline silicates have been found around young stars with a wide range in mass [e.g 6, 67–74] comets [e.g. 58, 75–77], and evolved stars [e.g. 78, 79] but not convincingly so in the interstellar medium. It should be noted that crystalline silicates were not only found in the outflows of oxygen-rich evolved stars, but also around stars that show clear evidence of a carbon-rich chemistry. The presence of the crystalline silicates in these environments has likely to do with previous mass loss episodes. We will discuss the properties of the crystalline silicates in what follows.

The sharp infrared features [see e.g. 17, for an assignment of the bands of forsterite] of the crystalline silicates allow a quite accurate identification of the crystalline materials. The two most abundant crystalline silicates that have been found are forsterite (Mg_2SiO_4) and enstatite ($MgSiO_3$, which can have a monoclinic and orthorhombic crystallographic structure, called respectively clino and ortho-enstatite). A fit to the continuum subtracted spectrum of MWC 922 with only these two species can be found in Fig. 5. The infrared spectra of ortho and clino-enstatite are very similar, only at wavelengths beyond of 40 μm clear differences in the absorption spectra become visible (see Fig. 5). A comparison of the strength of the individual features of ortho and clino-enstatite shows that around most stars the abundance is about equal. For some stars, with very high mass loss rates, ortho-enstatite may be more abundant than clino-enstatite [10].

Besides the above mentioned Mg-silicates, there is also evidence for Ca-pyroxenes such as diopside [80]. In Fig. 6, we show the spectrum of the planetary nebula NGC6302, which shows a rather broad emission bump around 60 μm. Both diopside and crystalline water ice have a rather broad feature near the peak of this 60 μm band. However, the observed 60 μm band is broader than the individual H_2O ice and diopside bands, while a sum of both materials gives a satisfactory fit the 60 μm region (note that the addition of the carbonate dolomite improves the fit even further; however see also Posch et al. [31] who studied low temperature carbonate dust spectra). Unfortunately, the low abundance of diopside in combination with blending of the short wavelength diopside bands with those of forsterite and enstatite make it hard to unambiguously identify diopside based on only the shorter wavelength bands. This implies that we can only clearly identify this material in

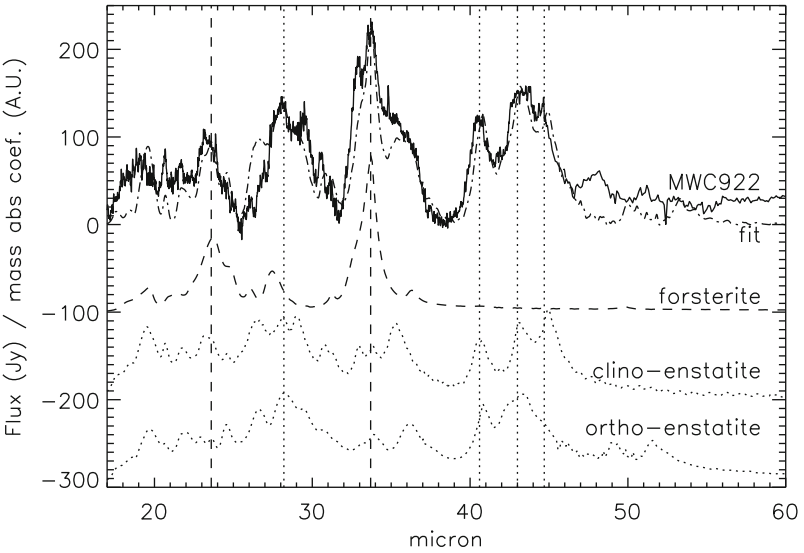

Fig. 5 The continuum subtracted spectrum of MWC 922 [*solid line*; 101], compared with the calculated emission spectrum of forsterite (at 90 K; *dashed line*), and clino and ortho-enstatite (at 100 K; *dotted line*). The temperatures have been derived by Molster et al. [10], when they were fitting the continuum subtracted spectrum with only forsterite and enstatite (50% ortho and 50% clino enstatite). The fit is shown as the dashed-dotted line. The vertical lines denote the diagnostic features of forsterite (*dashed lines*) and enstatite (*dotted lines*)

systems which have very cool dust (T $<$ 100 K), such as OH/IR stars and planetary nebulae.

We now turn to the chemical composition of the crystalline silicates, focusing on the olivines and pyroxenes. Their chemical composition can be rather accurately determined because the wavelength and strength of the bands are very sensitive to differences in the Fe/Mg ratio. Laboratory studies show that a simple relation exists between the position of the crystalline silicate bands and the Fe/Mg ratio in the lattice. The peak position shift in the frequency space due to the inclusion of Fe goes roughly linear with the percentage of [FeO] in the silicate [17].

$$100 * x/\Delta\nu \;=\; -1.8 \quad \text{for olivines } (Mg_{(2-2x)}Fe_{2x}SiO_4) \text{ and} \tag{1}$$

$$100 * x/\Delta\nu \;=\; -1.5 \quad \text{for pyroxenes } (Mg_{(1-x)}Fe_xSiO_3), \tag{2}$$

with $0 \leq x \leq 1$ and $\Delta\nu = \nu_x - -\nu_0$ where ν_x and ν_0 are respectively the wavenumber of the feature for composition x and $x = 0$. This implies that the shift in the wavelength domain is proportional to λ^2 and therefore clearest at the longest wavelengths. Therefore it is difficult to determine the exact Mg/Fe ratio from observations limited to only the 10 micron region.

Focusing on the 69 μm band, Fig. 3 shows the evidence for the high Mg/Fe ratio of the crystalline olivines in the outflows of evolved stars. In fact the data is even

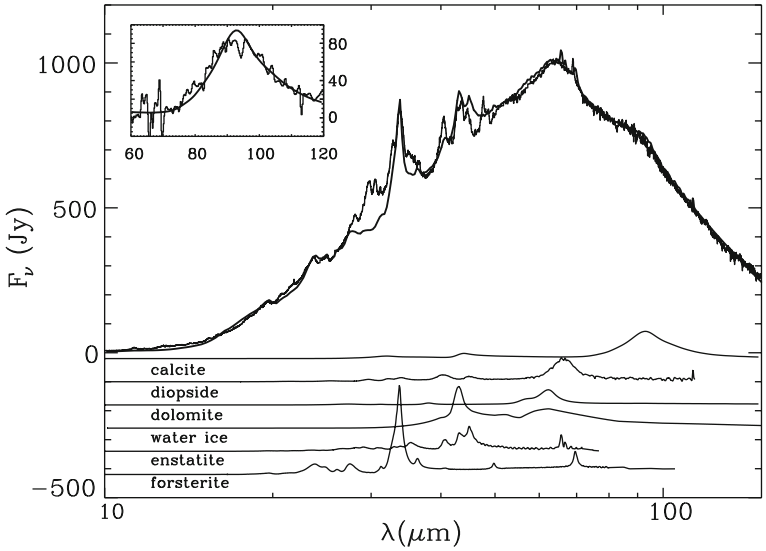

Fig. 6 Model fit to the ISO spectrum of the planetary nebula NGC6302. The thin line represents the observed spectrum. The thick line represents an optically thin dust model fit, consisting of amorphous olivine, metallic iron, forsterite, enstatite, H_2O-ice, diopside, calcite and dolomite. All contributions, except the featureless contributions from metallic iron and the amorphous olivine, are included in the bottom part of the figure. The inset shows the observed spectrum (*thin line*) and the model fit (*thick line*) from 60–120 μm, where the contributions of all species except calcite, are subtracted from both the observations as well as the model, therefore showing only the observed calcite feature. Figure taken from [26]

consistent with the absence of iron in the matrix (i.e. forsterite). It is also clear that the forsterite crystals are rather cold. A similar result holds for the pyroxenes based on the 40.5 micron feature. The crystalline pyroxenes found in the dusty winds of evolved stars invariably show evidence for very Mg-rich crystals (enstatite).

The determination of the exact chemical composition of the crystalline silicates around young stars using the 69 μm band is severely hampered by lack of data; only few high quality ISO spectra are available of the proto-planetary disks around young stars; more data are available for the dust envelopes of proto-stars. To date, there is only one young star for which a 69 micron feature has been found (HD 100546) and even that one is rather noisy [81]. The characteristic features of crystalline silicates are found at wavelengths below 45 μm, especially in the 10 μm complex region. The absence of the 69 μm feature in the spectra of most young stars may have several causes. The abundance of crystalline silicates may be too low, or the temperature of the crystalline silicates may be too high (a lower temperature will result in a stronger and narrower feature, and a lower temperature will also relatively enhance the 69 μm feature with respect to other IR-features). It is also possible that there is some Fe in the matrix, which will also weaken the 69 μm feature [16, 17]. Finally, the low 60–70 μm flux of many young stars inhibits the detection of the weak 69 μm band. However, the short wavelength crystalline silicate bands in young stars (and

in Hale-Bopp) do point to a low Fe content, which may be as low as in the evolved stars. This is also the case for most of the high-quality Spitzer IRS spectra of dusty disks surrounding young stars. These spectra can be well fitted assuming forsterite and enstatite [e.g. 82].

Due to the large number of bands available for analysis, an independent determination of the temperature of the different species of crystalline silicates can be made. It is interesting to note that in evolved stars the crystalline silicates are usually cooler than the amorphous ones [10]. This indicates that these two types of grains are not in thermal contact, and either they are spatially distinct, or they have significantly different optical properties, which leads to different equilibrium temperatures. The temperature difference can be explained in a straightforward way if we consider differences in the Fe/Mg ratios of co-spatial amorphous and crystalline silicates. As has been shown, the crystalline silicates are very Fe-poor. In contrast, it has been argued that amorphous silicates contain Fe, either in the matrix or as a metal inclusion, in order to reach the observed temperatures of these grains in circumstellar dust shells [41, 44, 45]. Adding a modest amount of iron already increases the opacity in the near-IR significantly [15]. Radiative transfer modelling shows that, if one assumes that the amorphous silicates have Fe/Mg $\approx$ 1 and that the crystalline silicates have no Fe, the temperature differences are explained by the difference in near-IR opacity. Both the amorphous and crystalline silicates can then be co-spatial [e.g. 39, 40].

Radiative transfer calculations can be used to constrain the abundance of crystalline silicates in different environments. The abundance of crystalline silicates in the winds of evolved stars is typically of the order of 10% or less. From simple modelling of the infrared spectra it has been deduced that enstatite is roughly three times as abundant as the forsterite in these outflows [10]. It should be noted that the derived abundances depend on the laboratory spectra used in the analysis. Using different sets of lab data sometimes changes the abundances by a factor two! The above mentioned values for the abundances are only derived for evolved stars with a relatively high mass loss rate. Crystalline silicates have not been found around low mass-loss-rate stars [78, 83]. This might be a temperature effect. Indeed, Kemper et al. [84] show that the temperature difference between the crystalline and amorphous silicates, will cause the emission from the crystalline silicates to be overwhelmed by the warm amorphous silicates in the low mass-loss-rate stars. In some peculiar objects, likely as a result of binary interaction, the crystalline silicate abundance can be very high, up to 75% of the small grains [85].

The abundance of crystalline silicates in Hale-Bopp has been estimated by several authors [86–88]. The derived abundance of crystalline silicates ranges between more than 90% [86] and about 7% [88] of the total dust mass. These studies use different Fe contents for the silicates and different grain size and shape distributions. Since the presence of Fe also reduces the strength of the features of crystalline olivine significantly [see e.g. 17], the abundance of the crystalline silicates in this comet remains uncertain. For other comets only spectra of the 10 μm region are available. This limits the determination of the abundance very much because it is

very sensitive to the temperature of the different dust components, which is very difficult to obtain from a small wavelength range (8–13 μm).

Up to now we do not have strong evidence for the presence of crystalline silicates in the ISM. From the absorption profiles of proto-stars an upper limit of about 2% for the abundance of crystalline forsterite has been derived [49]. Kemper et al. [89] find an upper limit of 2.2% using ISO observations of the line of sight towards the galactic centre. Cesarsky et al. [90] suggest that several emission bands in the ISO spectra of the Orion nebula may be due to crystalline silicates. We note however that the peak position, shape and width of the bands seen in Orion differ from those of crystalline silicates in other environments. In addition, PAH emission bands may complicate the situation. If the bands seen by Cesarsky et al. [90] are indeed crystalline silicates, these would have to be of a different composition from those seen elsewhere. We conclude that so far no convincing evidence has been found for the presence of crystalline silicates in the ISM.

The abundance of crystalline silicates in the dust surrounding young stars has been derived using both ground-based and space-based infrared spectroscopy. The space-based observations cover a wide wavelength range thus allowing a measurement of the abundance of crystalline silicates over a wide range of temperatures (and so distance from the star). Mid-infrared interferometric observations have spatially resolved some dusty proto-planetary disks allowing for a direct measurement of the spatial distribution of the dust. It should be kept in mind that the crystalline silicate abundances have been derived using simplified assumptions about the geometry of the disk and dust grain properties such as size, shape and chemical homogeneity. The derived abundances only relate to the small grains in the disk surface, except in the case of debris disks that can safely be assumed to be optically thin and so probe the whole disk (but still only the small grain component).

Ground-based spectral surveys in the 10 μm atmospheric window of Herbig Ae/Be and T Tau stars show a crystalline silicate dust fraction between 5 and 20–30% [91, 92], with a wide range in the relative abdundance of forsterite and enstatite. Van Boekel et al. [91] show a relation between the abundance of forsterite and silica (SiO_2), which may indicate thermal annealing of amorphous grains as source of crystalline silicates. Spatially resolved mid-infrared observations of disks surrounding nearby Herbig Ae/Be stars and T Tau stars show that crystalline silicate abundances are high in the inner disk and tend to decrease further out, consistent with thermal annealing and/or gas-phase condensation in the inner disk regions [93, 94]. The crystallinity in the innermost disk regions can reach very high values, up to 100%.

ISO and Spitzer spectra of proto-planetary disks show that there is a wide range in the strength of the crystalline silicate bands in the 15–45 μm wavelength range [e.g. 72–74, 81, 88, 95, 96]. This implies large star to star differences in the abundance and radial distribution of crystalline silicates in the upper layers of these disks. The abundances of cold ($T < 100$–200 K) crystalline silicates derived for some stars significantly exceeds 10%, which implies efficient radial mixing or a local formation process. An interstellar origin of these cold crystals is ruled out since their

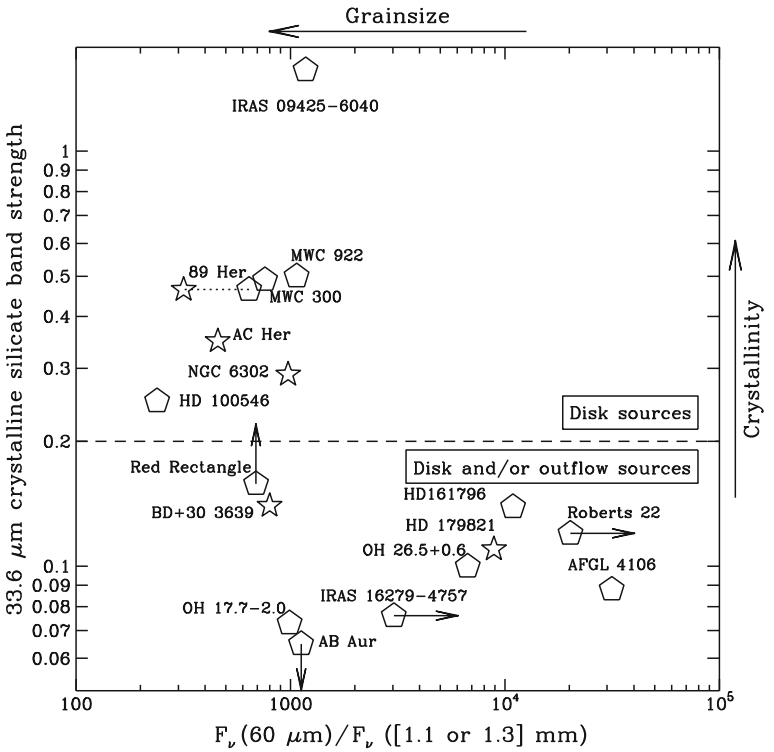

Fig. 7 Correlation between the IRAS 60 μm over 1.1 mm (*stars*) or 1.3 mm (*pentagons*) flux ratio and crystalline silicate band strength, measured from the crystalline forsterite band at 33.6 μm ($[F_{33.6\,\mu\mathrm{m\ peak}} - F_{\mathrm{cont}}]/F_{\mathrm{cont}}$). The selected sources have dust colour temperatures above $\approx$ 100 K, so that the Planck function peaks at wavelengths shorter than 60 μm. The emptiness of the upper right corner of this diagram is an indication that the presence of highly crystalline dust is correlated with disks and grain-growth. All stars above the line $(F_{33.6\,\mu\mathrm{m\ peak}} - F_{\mathrm{cont}})/F_{\mathrm{cont}} = 0.2$ have relatively small 60 μm over mm-flux ratios and have indications for the presence of a disk (e.g. by direct imaging and/or the spectral energy distribution). The stars below this line are predominantly normal outflow sources, without any evidence for a disk, although exceptions exist (e.g. Roberts 22). NGC 6302 and BD+30 3639 have been shifted by a factor 2 along the *x*-axis since it is estimated that only half of the mm continuum flux is due to dust emission while the other half is due to free-free emission. Figure taken from [97]

abundance is far above the upper limit of 2.2% set for crystalline silicates in the interstellar medium [89].

The ISO observations suggest that a relation may exist between the abundance of crystalline silicates and the *geometry* of the circumstellar dust shell. Figure 7 shows the correlation between the strength of the 33.6 micron feature (attributed to forsterite) and the IRAS 60 μm/mm flux ratio. The first value gives an indication of the abundance ratio between amorphous and crystalline silicates in the dust, while the second ratio is a rough indication of the average grain size. It is interesting to note that those sources which seem to have a large abundance of crystalline silicates,

also show evidence for the presence of a disk-like structure [97] and for grain coagulation. It should be added that the opposite is not true, if stars do have a disk (and large grains) it does not automatically imply that they have a high fraction of crystalline silicates. Whether the crystallization of amorphous silicates is related to grain coagulation, or that we are simply dealing with two different processes, which both require long timescales has not yet been established (see also Sect. 4).

3.1.3 Carbonates

Many studies have searched for carbonates ([Ca, Mg, Fe, . . .]CO_3) in the solar system and interstellar space (see Kemper et al. [98] for an overview). The strongest mid infrared (MIR) band of carbonates is around 6.8 μm and is due to the C═O stretching mode. Other relatively strong MIR features are found near 11 and 14 μm and are caused by respectively the out of plane and in-plane bending modes of C═O. The features found beyond 25 μm are due to a translation of the metal cations and represent motions perpendicular and parallel to the plane of the carbonate anions [99]. So far, searches for the MIR features have not been successful: while many objects show spectral bands in the 6.8 and 11–14 μm region, these bands have all been attributed to other species.

Barlow [100] discovered an emission band in NGC 6302 ranging from 88–98 μm. A similar band has been found in NGC 6537 [101]. Kemper et al. [26] showed that these bands are evidence for the presence of carbonates in these two planetary nebulae. This claim was strengthened by the presence of an emission band at 65 μm (see Fig. 6). The 92 μm band is attributed to calcite ($CaCO_3$), which gives a very good match between laboratory data and ISO observations. The 65 μm band seen in the ISO spectra is a blend and has contributions from diopside and crystalline H_2O ice. The analysis of Kemper et al. [26] showed that the inclusion of dolomite ($CaMg(CO_3)_2$) substantially improves the fit in the 60–70 μm region (however, see also [31]). The low temperature and the low abundance of the carbonates prevents any detection of the carbonate features in the 5–15 μm region. Calcite and dolomite are also the two most abundant carbonates in the solar system.

In the spectrum of NGC1333-IRAS4, a young protostar, there is some evidence for a band at 90 μm, which is rather similar the $CaCO_3$ band [102]. Since the material in the vicinity of this protostar presumably has only experienced typical interstellar medium conditions it might imply that, if the identification can be confirmed, carbonates are also present in the ISM.

3.1.4 Al_2O_3

The presence of corundum (Al_2O_3) has been inferred from mid-infrared IRAS-LRS spectra of oxygen-rich red giants, that show a broad 11 μm feature [e.g. 103]. This band is often found to co-exist with the 9.7 μm amorphous silicate Si—O stretch, and tends to be seen in stars with weak dust emission. Cami showed that ISO spectra of low mass loss red giants show a broad 11 μm band consistent with amorphous alumina-oxide [104] (see Fig. 8).

Recent work of Verhoelst et al. [105] shows that Al_2O_3 seems to be present around the massive star Betelgeuse between the silicate dust formation zone and the stellar atmosphere. They propose that corundum might act as nucleation core for the silicate grains.

A narrow dust feature at 13 μm was discovered in the IRAS-LRS spectra of bright M Mira variables [107], which has been attributed to γ-Al_2O_3 [108]. However, more detailed studies showed that γ-Al_2O_3 does not provide a satisfactory match to the band [109]; attempts to improve the match using α-Al_2O_3 were successful, if a continuous distribution of ellipsoids is assumed as particle shape. However a second band of α-Al_2O_3 near 21 μm has not been detected, suggesting that α-Al_2O_3 cannot be the carrier of the narrow 13 μm band.

The discovery of presolar Al_2O_3 in meteorites [110–113], whose isotopic composition points to oxygen-rich red giants as their origin, supports the spectroscopic identification of Al_2O_3 in the mid-IR spectra of red giants. Dust nucleation models for oxygen-rich outflows from cool giants based on thermodynamic considerations predict Al_2O_3 to be one of the first condensates [114]. However, detailed quantum mechanical calculations show that homogeneous nucleation of molecular Al_2O_3 from the gas phase is unlikely in these environments [115]. The Al_2O_3 grains, which bear isotopic evidence of a formation around an AGB stars and found in meteorites, are likely formed via grain surface reaction in an AGB wind [116].

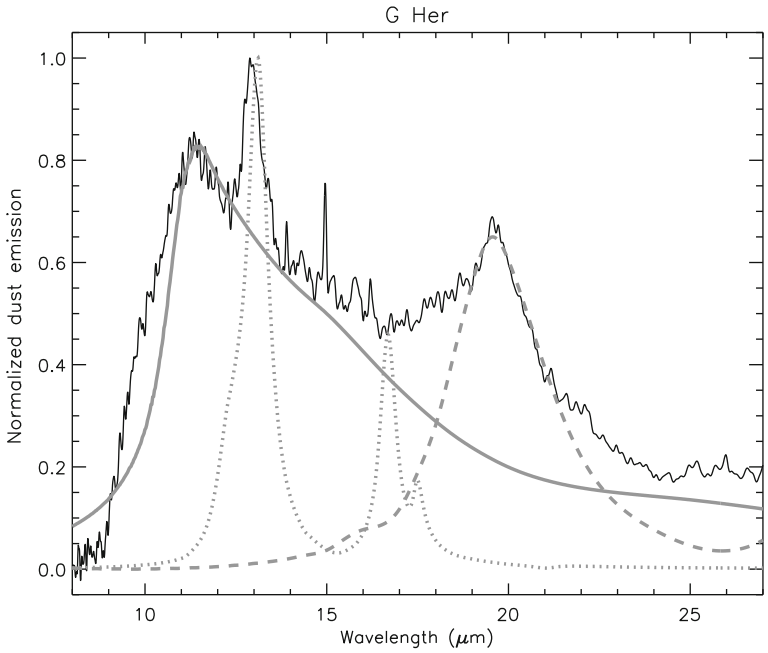

Fig. 8 The continuum subtracted spectrum of the AGB star G Her, with possible identifications of the emission bands. The grey solid line represents amorphous Al_2O_3, the dotted line spinel, and the dashed line $Mg_{0.1}Fe_{0.9}O$. See also [106]. Figure taken from [104]

Al_2O_3 has not been detected in the diffuse interstellar medium. This may prove difficult given the strong amorphous silicate 9.7 μm resonance.

3.1.5 $MgAl_2O_4$

Posch et al. [106] suggest (annealed) spinel ($MgAl_2O_4$) as the carrier of the 13 micron feature detected in spectra of oxygen-rich red giants. Speck et al. [117] raised doubts about this identification and proposed SiO_2 as the carrier. However, SiO_2 should have a very strong feature around 9 μm, which is not observed. Fabian et al. [118] seem to settle the dispute with the discovery of two other bands (around 16.8 and 32 μm) which can also be attributed to spinel.

Spinel presolar grains have been found in meteorites [119, 120], and, as with Al_2O_3, is predicted to be a condensate in the winds of oxygen-rich stars. The 13 μm band has not been detected in the diffuse ISM, suggesting it is not produced in large quantities by red giants, or that it does not survive long in the ISM.

3.1.6 [Mg,Fe]O

$Mg_xFe_{1-x}O$ shows a fairly broad resonance which shifts from about 16.5 to 19 μm as x varies from 1 to 0 [19]. In addition, the band shape and strength depend strongly on grain shape. These properties make it difficult to identify this simple oxide spectroscopically. Cami [104] and Posch et al. [121] propose that the broad 19.5 μm band seen in low mass loss red giants is due to spherical $Mg_xFe_{1-x}O$ grains with $x \approx 0.1$. Molster et al. [39] show that the 18 μm amorphous silicate band cannot account for all emission in the 20–28 μm spectrum of AFGL 4106. An additional broad dust band near 23 μm is inferred and a continuous distribution of ellipsoids (CDE) of FeO particles has been proposed as its carrier [39]. Similarly, Bouwman et al. [122] suggest *non-spherical* FeO grains to account for additional emission in the 23 μm region of Herbig Ae/Be stars. In contrast Demyk et al. [49] find that *spherical* inclusions of FeO improve the fit to the dust absorption profile around the protostars RAFGL7009S and IRAS19110 + 1045 to the 18 μm band. Keller et al. [9] suggest that the 23 μm band in the spectra of young stars is not due to FeO with a CDE distribution, but more likely to FeS and that the assumption of a CDE shape distribution seem to fail for Fe-oxides. The reason for the failure of this assumption is likely related to the fact that Fe-oxides have a cubic crystal symmetry. Therefore the crystal will not grow in a preferred direction and the shape of the particle will be more spherical like. So, we conclude that there is some evidence for the presence of spherical $Mg_xFe_{1-x}O$ grains (with $x \approx 0.1$) in dust shells surrounding evolved stars, but a firm theory to explain the existence of only this stoichiometric ratio is still lacking.

3.1.7 SiO_2

Silica shows bands at approximately 8.6 and 20.5 μm. An analysis of ISO spectra of young stars suggests that a small fraction of the silicate dust in the disks surrounding

Herbig Ae/Be stars is SiO_2 [123]. This material could be formed by annealing of amorphous silicates. Natta et al. [124] analyse the 10 μm silicate band in T Tauri stars, and find evidence for a ≈ 9 μm contribution by SiO_2. The analysis of Bouwman et al. [123] shows that the temperature of the silica is roughly equal to that of the crystalline silicates. Since silica has a very low opacity in the UV to NIR this phenomenon is best explained if the crystalline silicates and the silica are in thermal contact.

Molster et al. [32] found a relative sharp band at 20.5 μm in many oxygen-rich evolved stars. They tentatively attributed this band to silica. However, it should be noted that the width of this feature is considerably narrower than in the laboratory spectra of silica. This could be a temperature effect, since the laboratory spectra were taken at room temperature, while the silica around these evolved stars is likely much cooler. It would be useful to measure laboratory spectra of crystalline SiO_2 at low temperature. For glassy SiO_2 there is no large influence of the temperature on the width of the feature [27].

A detailed analysis of Spitzer spectra of T Tau stars by [125] shows clear evidence for the presence of crystalline silica. Comparison with laboratory data suggests the silica in these disks is dominated by cristobalite (with some trimydite), which may from due to high temperature annealing of amorphous silicates. Rapid cooling of these grains is required in order to retain their high-temperature polymorph structure.

Lisse et al. [126] find evidence for the presence of tektite in the spectrum of HD 172555, and interpret this as evidence for a hypervelocity ($>10\,km\,s^{-1}$) impact between large rocky planetesimals in the circumstellar disk.

3.1.8 Metallic Fe

The presence of metallic Fe cannot be demonstrated on the basis of the detection of an infrared resonance, because there are no infrared active vibrational modes known in this material. Nevertheless, evidence for its presence in oxygen-rich dust shells surrounding evolved stars has been found on the basis of the high near-IR opacity that metallic Fe particles provide [41, 51]. Radiative transfer models of dust shells around M supergiants and AGB stars using only laboratory opacities of silicates fail to reproduce the 3–8 μm spectral region. The inclusion of metallic Fe particles results in a satisfactory fit. The shape of these particles is very likely non-spherical. To produce enough opacity a spherical shape requires more iron than is available on cosmic abundance grounds. It is not clear from these models in what form the metallic Fe particles are included in the dust: they may be individual particles or they may be inclusions in amorphous silicates as is found in GEMS.

3.2 Dust Produced in C-rich Environments

3.2.1 Carbonaceous Dust

Amorphous carbon does not have a clear spectroscopic signature in the infrared. Its presence is mostly based on the need for an extra source of opacity in the spectra of

carbon stars. Graphite would also have a very similar spectrum. However, a narrow feature at 11.52 μm, which is predicted for graphite, has not been found in carbon-rich stars. This places an upper limit of 3% on the solid carbon being in the form of small graphite particles [127]. Also the slope of the SED at the long wavelength side points to amorphous carbon instead of graphite, which would produce a steeper decline.

Graphite is often suggested as the carrier of the 2175 Å extinction feature [128]. Small (radii ≤150 Å) graphite grains can reproduce the feature and part of the UV extinction. However, it should be noted that up to now, apart from this feature no other signature of graphite has been found in the ISM, also no source has yet been identified that could account for the production of graphite. According to Draine [129] only 15% of the carbon in the ISM has to be in graphite grains to explain the 2175 Å feature. It is unclear if the present day observations can already put such an upper limit on its abundance. Part of the popularity of graphite arises from the fact that graphite is one of the few carbonaceous materials that is well characterized and for which good laboratory optical constants are available [131].

Graphite grains have been found in meteorites [132], however they are not alike the grains, required to explain the 2175 Å feature. The inferred ISM graphite grains are very small well crystallized and abundant, while the graphite grains found in meteorites are much larger, with radii in the range of 1–5 μm [133], and often contain scales of poorly graphitized carbon. It is therefore likely that meteoritic graphite grains and interstellar "graphite" particles responsible for the 2175 Å feature are unrelated.

In many carbon-rich stars there is emission found between 3–4 and 11–17 μm, which is indicative for vibrationally excited C—H bonds. A closer look reveals emission from H-atoms bound to sp^2 and sp^3 sites [134, 135]. The combination of these two bonds together with the emission plateau from 6–9 μm is found in hydrogenated amorphous carbon (HAC), which is also known as $a\text{-}C\text{:}H$ or diamond-like amorphous carbon. On earth this material has been very well studied (see Robertson for a review [136]), but the exact structure of the HACs in circumstellar environments is still not well known. Hony et al. [137] show that HAC grains in radiative equilibrium do not explain the features found in HD 56126. However, these authors suggest that transiently heated small HAC grains with a H/(H + C) ratio of 0.35 may explain the observed features.

An infrared absorption feature at 3.4 μm, characteristic of dust in the diffuse ISM, is normally attributed to C—H stretching vibrations of aliphatic hydrocarbons [138, 139].

3.2.2 Nano-Diamonds

It has long been assumed that nano-diamonds are presolar and formed in interstellar shocks [140], in the atmospheres of carbon stars, and/or in supernovae. The discovery of an anomalous Xe-HL component associated with the nano-diamonds in primitive meteorites gave strong support for a supernova origin of these grains [141–143]. However, their bulk $^{13}C/^{12}C$ composition is solar and only 1 in 10^6 nano-diamonds contains a Xe atom. Since it is not (yet) possible to measure the

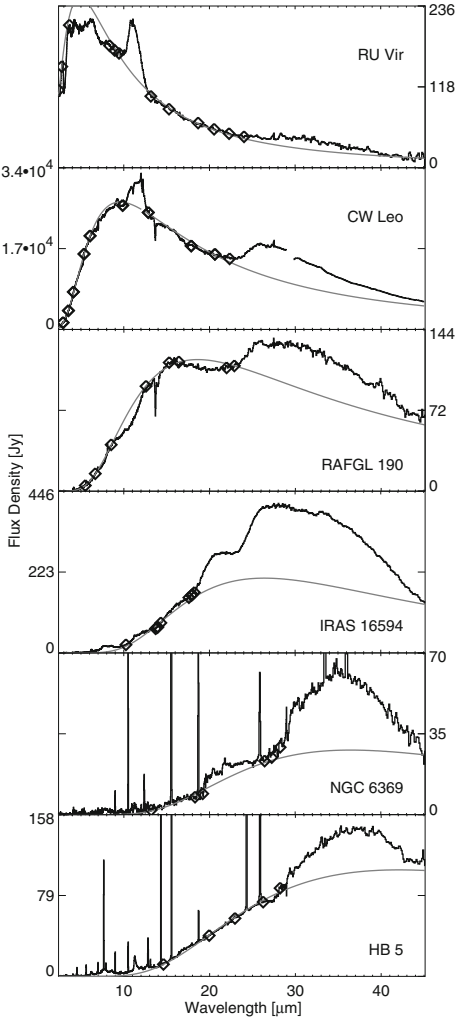

Fig. 9 Overview of ISO spectra of carbon-rich stars, post-AGB stars and planetary nebulae [130]. The 11.3 μm band is prominently in emission in RU Vir and CW Leo and is in absorption in RAFGL 190. The 30 μm MgS band is present in all objects, but shifts its position from about 26 to 35 μm going from AGB to planetary nebula. The emission lines in the spectra of NGC 6369 and HB 5 are due to ionized gas in the AGB remnant

isotopic composition of a single nano-diamond, the origin of (most of) these grains is not clear. The lack of very strong isotopic anomalies, as for instance seen in SiC or Al_2O_3, has precluded a firm identification with a particular stellar birth site for these grains (see also the contributions in this book).

A study by Guillois et al. [144] showed that, while pure diamonds have no infrared-active single phonons, hydrogenated nano-diamonds do show spectral structure in the 3–4 μm wavelength region. They propose that an emission band seen in a small number of stars at 3.53 μm (and two weaker ones at 3.43 and 3.41 μm) can be attributed to C—H bonds in hydrogenated nano-diamonds. So far, the 3.53 μm band has been identified in only five objects: the young stars HD 97048 [145], Elias I [146] and MWC 297 [147], and in the (peculiar) post-AGB stars HR 4049 [148]

and HD 52961 [149]. These stars, while in vastly different evolutionary phases, all have a circumstellar disk with dust temperatures exceeding 1000 K, and have a hydrogen-rich atmosphere. Laboratory studies suggest that high temperatures and pressures are required to form nano-diamonds, consistent with the conditions that prevail in the sites where they have been identified.

Van Kerckhoven et al. [150] suggest an in situ formation of the nano-diamonds in the five objects with 3.53 μm emission, which of course opens the possibility that (part of) the nano-diamonds in the solar system were formed by the same process. This notion has gained support by the recent finding that cometary IDPs have a much lower abundance of nano-diamonds than the primitive meteorites do [151], suggesting a gradient in the abundance of nano-diamonds in the proto-solar cloud. Such a gradient could naturally result from the production in the inner solar system of nano-diamonds and their inclusion in proto-planetary bodies.

3.2.3 MgS

A broad emission band near 30 μm was first noted in the spectra of three carbon-rich evolved stars [152]. Later studies showed that the 30 μm band is present in objects ranging from mass-losing carbon stars to post-AGB stars and planetary nebulae [e.g. 130, 153–157]. MgS has been tentatively detected in KAO spectra of the galactic centre [158] and it may be present in the peculiar massive star η Car (P. Morris, private communication).

MgS has been suggested for the identification of this feature [159]. Based on the optical constants derived by Begemann et al. [21] a single resonance at 26 μm is predicted for spherical grains. This feature shifts and broadens significantly if grain shape effects are taken into account. Transmission spectra taken by Nuth et al. [160] show a strong and broad band around 36 μm. The strength of the observed emission has cast some doubt on this identification (some objects emit about 30% of their light in the 30 μm band). Begemann et al. [21] convincingly demonstrate that MgS is the most likely candidate to cause the 30 μm band in IRC+10216.

ISO spectroscopy has shown that the 30 μm band shows considerable variations in strength, and width. In addition, the peak position varies from 26 to about 35 μm [155, 157, 161] (see Fig. 9). This led to the suggestion that the band is caused by two dust components whose relative strengths vary between sources [157]. However, Hony et al. [130] show that the shift in peak position of the feature can be understood as a temperature effect: the large intrinsic width of the band causes the peak to shift to longer wavelengths as it is weighed with black bodies with decreasing temperature. Both the width and the peak position change systematically as the temperature of the underlying continuum changes, corresponding to an evolution from the asymptotic giant branch to the planetary nebula phase [130]. A weaker band near 26 μm remains visible in some AGB stars after the strong MgS contribution is removed. This component is tentatively identified with spherical homogeneous MgS particles [130] (Fig. 10).

MgS is expected to condense in a carbon-rich environment [162]. However, sulfur is found to be only marginally depleted from the gas-phase in the diffuse ISM

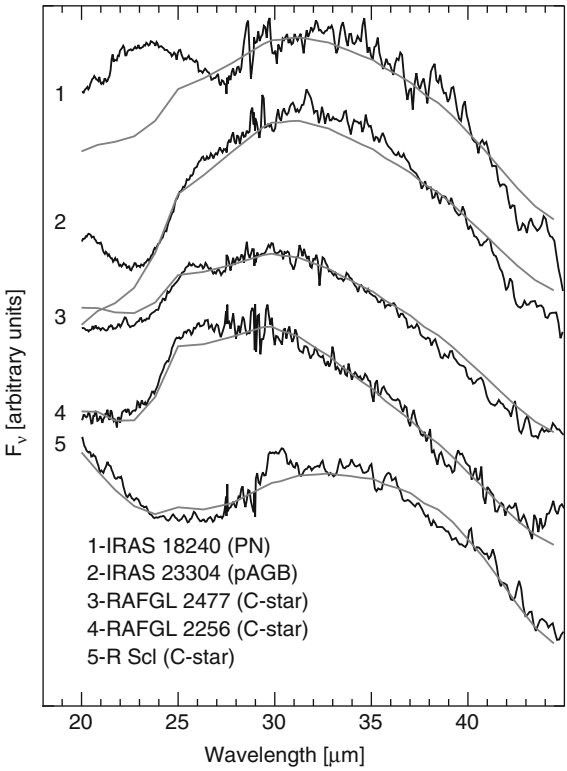

Fig. 10 Model fits to the 30 μm band using a CDE shape distribution for MgS grains and a varying MgS temperature to account for the shift in band position. Taken from [130]

[163] which suggests that MgS cannot be a major source of sulfur in the diffuse ISM. MgS is unlikely to survive in the oxygen-rich environment which the ISM is believed to be. In meteorites no presolar MgS grains have been found so far.

3.2.4 The 21 μm Feature

A prominent emission band near 21 μm was first noted by Kwok et al. [164] in the IRAS-LRS spectra of a small group of carbon-rich post-AGB stars. These objects became known in the literature as the "21 μm sources"; some 15 have been found to date. ISO-SWS spectra show that the band is actually peaking at 20.1 μm [165], however it is still referred to as the 21 μm band (Fig. 11). The band shape hardly varies between sources. Evidence for the presence of the 21 μm feature has also been found in two carbon-rich planetary nebulae [166]. This shows that the carrier can survive the harsh conditions that prevail in such objects. So far the 21 μm band has not been seen in carbon-rich AGB stars, which indicates that its carrier is either not produced until the very end of the AGB, or that its excitation requires optical and/or UV photons.

Various identifications for the carrier of the band have been suggested (e.g. SiS_2 [167, 168]; nano-diamonds [169]), none of these however provided a convincing

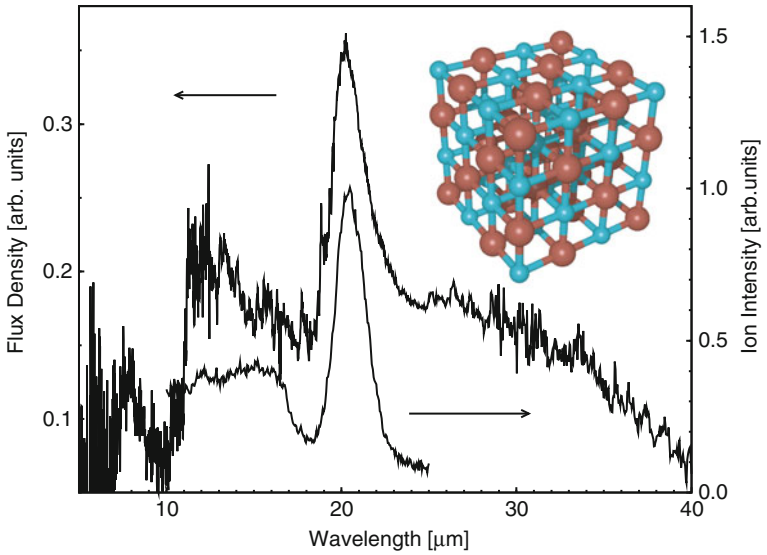

Fig. 11 The emission spectrum of the post-AGB object SAO 96709, taken by the ISO satellite (*upper curve*, left axis) and the wavelength spectra of the TiC nano-crystal recorded in the laboratory (*lower curve*, right axis). Also shown is a pictorial representation of a typical ($4 \times 4 \times 4$ atom) TiC nano-crystal. The small spheres are carbon atoms, and the large spheres are Titanium atoms. Figure taken from [25]

fit. Recently, it has been suggested that TiC nano-clusters could be the carrier of the band [25]. This identification is inspired by the remarkable similarity between the laboratory spectra of TiC nano-particles (both in peak position and in width and shape of the band), and by the presence of TiC inclusions in presolar amorphous carbon grains [170], that can be traced to carbon-rich AGB stars. A detailed analysis of the strength of the 21 μm band in the post-AGB star HD 56126 led Hony et al. [137] to the conclusion that the TiC identification may not be tenable unless the nano-particles absorb optical and near-UV light from the star very efficiently. Speck and Hofmeister[171] suggest SiC nano-particles as a carrier. While this identification would relax the abundance problems encountered with TiC nano-particles, it also predicts a prominent 11.2 μm band which is not observed.

3.2.5 SiC

Silicon Carbide (SiC) was suggested to be part of the ISM by Friedemann [172]. It was first identified in the mid-IR spectra of carbon-rich AGB stars [173], following the detection of an 11.2 μm emission band in these objects [174]. Early spectral surveys of the SiC band were carried out by, e.g. Forrest et al. [175] and Cohen [176]. There is considerable variation in the wavelength of the peak, ranging between 11.2 and 11.7 μm, [e.g. 177–179], while the full width at half maximum of the band is

about 1.3–2.0 μm. The band is commonly observed in mass-losing AGB stars as well as in post-AGB stars and some planetary nebulae [e.g. 130, 176, 180, 181].

SiC is predicted to be a high-temperature condensate in the outflows of carbon stars [e.g. 182]. Kozasa et al. [183] suggest that SiC grains form by homogeneous nucleation, and that these grains develop an amorphous carbon mantle as they move out in the envelope. For high mass loss rates the amorphous carbon may dominate, suppressing the SiC spectral signature. More recent observations of SiC in extreme carbon stars however revealed a self-absorbed SiC band [130, 181, 184], showing that even at these high mass loss rates SiC remains detectable.

Presolar SiC grains have been identified in meteorites [185]. The isotopic ratios of noble gases extracted from bulk, as well as isotopic ratio $^{12}C/^{13}C$ found in individual grains strongly points to carbon stars as their main production site, while novae and supernovae may be other sources of interstellar SiC grains [e.g. 186]. All presolar SiC grains have a cubic lattice structure (so-called β type SiC). In contrast, the SiC seen in carbon stars has long been attributed to hexagonal or α-SiC, but recently doubts have arisen whether or not the shape of the 11.3 μm resonance of SiC allows a discrimination between both types [187]. Interestingly, some presolar SiC grains have diameters in excess of 10 μm [143, and references therein] which is difficult to understand in the context of grain formation in AGB winds.

The detection of SiC in the diffuse ISM is difficult given the proximity of the strong amorphous silicate band at 9.7 μm [188]. An analysis of the line of sight to the galactic centre has shown evidence for interstellar SiC at an abundance of 3% [38]. More lines of sight must be investigated to establish the distribution of SiC in the interstellar medium.

3.3 Questionable Identifications

3.3.1 FeSi

Ferrarotti et al. [189] propose an identification of an emission band in the ISO-LWS spectrum of AFGL 4106 at 47.5 μm with FeSi. Their chemical condensation calculations show that FeSi will only be formed in the outflows of stars with a C/O ratio near unity [189]. However, this band has been seen in many oxygen-rich (C/O <1) dust shells [32, 100] but to our knowledge it is not prominent in S-type (C/O ≈ 1) AGB stars. Finally, this mineral is expected to show an additional band at 32 μm, which has not been found so far. We conclude that the identification of FeSi is not yet very convincing.

3.3.2 Hydrous Silicates

Layer lattice silicates have been found in solar system material collected on earth, like the Murchison meteorite and in IDPs [61, 66, 190]. The spectra of comets are less clear. The presence of hydrous silicates in space has been suggested based on the shape of the 10 μm silicate feature in some comets [58, 66, 191], but a definite

answer could not been given yet. Still, hydrous silicates seem to be a well established component in IDPs and in other bodies found in the inner solar system, however they have not been detected convincingly in interstellar space. Malfait et al. [192] find a prominent, broad emission band near 100 μm in the ISO-LWS spectrum of the young intermediate mass star HD 142527, which they attribute to the hydrous silicate montmorrilonite based on laboratory data [193, 194]. This identification is supported by the presence of very strong crystalline H_2O ice bands at 43 and 60 μm in HD 142527. However, a large abundance of 15% of hydrous silicates is required to fit the ISO spectrum [192]. It is not clear what could cause such a high abundance of hydrous silicates in this object.

3.3.3 FeS

Although FeS is a solid which is predicted to condense in the winds of carbon-rich red giants, until recently it has eluded detection outside the solar system. In contrast, FeS is abundant in meteorites and in IDPs. In fact, FeS carries the bulk of sulphur in the solar system. Hony et al. [137] have suggested the presence of FeS in the ISO spectra of two carbon-rich planetary nebulae, by means of emission in the 23 μm band. They also find evidence for weaker bands of FeS (troilite) at 33, 38 and 44 μm, albeit much weaker than expected on the basis of laboratory spectra. Laboratory spectra of different kinds of FeS (such as pyrite (FeS_2), troilite (FeS) and pyrrhotite ($Fe_{1-x}S$)) all show a broad emission band at approximately 23 μm. At longer wavelengths, these materials show large differences in their spectra. Hony et al. [137] suggest that in space different kinds of FeS coexist, weakening the spectral signature of individual species at the longer wavelengths, but keeping the prominent FeS band near 23 μm.

FeS has also been suggested in the ISO spectra of some young intermediate-mass Herbig Ae/Be stars [9], on the basis of a 23 μm excess. This 23 μm excess matches the 23 μm band seen in laboratory spectra of FeS taken from IDPs [9]. We note that Spitzer spectra of proto-planetary disks do not yet confirm the presence of FeS.

4 Life-Cycle of Dust

The rich mineralogy of refractory dust species that has been described in the previous sections reflects the equally rich diversity in physical and chemical conditions that prevail in space. Observations show that the *circumstellar* mineralogy is by far the richest, when compared to the interstellar one. Indeed, a disappointingly small number of interstellar dust species have been identified unambiguously by means of infrared spectroscopy. This may seem surprising since it is generally accepted that stars are the dominant dust production sites in galaxies. While observational selection effects may play a role (interstellar dust has low temperatures and is usually detected in absorption, circumstellar dust is detected in emission and absorption), the paucity of detected dust species in interstellar space is probably real and suggests that the composition of interstellar dust is not merely a sum of stellar dust production

rates of the different circumstellar dust species: dust is (strongly) processed in the interstellar medium, and seems to reach a fairly homogeneous composition with only a few dominant species.

Most dust forms either in the slowly expanding wind of low mass evolved stars ($M < 8M_{\odot}$) and the massive red supergiants, or in the expelled layers after a supernova (SN) explosion. After being expelled into the harsh ISM, it is exposed to many destructive processes [195]. On the other hand dust also forms in these environments, and because of the totally different formation conditions, different dust species than the ones which entered the ISM will form. Eventually, the dust will end up in a star forming region. Here the dust will either be accreted onto the proto-star, "survive" as a planet (esimal), or be expelled back into the ISM, via a bipolar outflow.

In this section we will discuss the dust (trans-)formation and destruction processes based on astronomical observations and their comparison with laboratory measurements. For a more comprehensive review of the dust processes in outflows and disks we refer to the chapter by Gail in this book.

4.1 Dust Formation in Evolved Stars

There are two main classes of evolved stars that produce significant amounts of dust: (i) the evolved low-mass stars, with their slow expanding winds during the AGB phase, and (ii) the high-mass stars that go through a red supergiant phase during which they have a stellar wind with properties somewhat similar to those of the low-mass AGB stars. There are also some rare, unstable massive stars, called Luminous Blue Variables, that produce some dust. Below we discuss the dust formation in AGB stars; a similar description holds for the red supergiants.

The numerous AGB stars in our galaxy make it easy to study the dust formation in their slowly expanding winds. Based on the C/O ratio in their atmosphere, one can distinguish three types of objects: The oxygen-rich ($C/O < 1$) M-type stars, the carbon-rich ($C/O > 1$) C-stars and the S-type stars that have $C/O \approx 1$. The type of dust that forms in the outer atmosphere of cool evolved stars depends significantly on the C/O ratio of the gas from which the dust condenses. When this ratio is larger than unity, all oxygen will be trapped in the very stable CO molecule and carbon containing dust will form. On the other hand when this ratio is smaller than unity (which is the case when a star is born) all carbon atoms will be trapped in CO and the remaining oxygen will determine the dust properties, silicates and oxides will form. The type of dust that forms not only depends on the molecular and atomic abundances of the gas from which it condenses, but also on the local physical conditions that prevail (such as temperature, pressure, UV radiation, presence of seed particles). We note that the supergiants only have oxygen-rich members.

4.1.1 Oxygen-Rich Stars

In M giants with low mass loss rates ($\dot{M} < 10^{-7}M_{\odot}/yr$) the dominant dust species that form are simple metal oxides [104, 121]; amorphous silicates are not prominent

in the spectra. The low density in the wind likely prevents the formation of relatively complex solids like the silicates, because that requires multiple gas–solid interactions. It is not clear at present whether these simple oxides also form in the innermost regions of AGB winds with higher mass loss rates.

The most abundant dust species in the winds of oxygen-rich stars with intermediate and high mass loss rates are the silicates. The formation of silicates is not well understood. Homogeneous silicate dust formation directly from the gas phase is not possible, it requires first the formation of condensation seeds. It is logical to search for high temperature condensates that can form through homogeneous nucleation that could serve as condensation seeds for other materials. Gail and Sedlmayr [196] propose that in O-rich winds TiO_2 (rutile) clusters can act as condensation nuclei for silicates. Quantum mechanical calculations seem to confirm this possibility [197]. However, no evidence has been found yet for the presence of rutile in the spectra of outflows of evolved stars; probably the low gas-phase abundance of titanium prevents detection.

Another high temperature condensate that could serve as a seed for the formation of other materials is crystalline Al_2O_3, also because it has been associated with the 13 μm feature. However, the 13 μm feature is likely not due to crystalline Al_2O_3 (see Sect. 3.1.4). Detailed quantum mechanical calculations show that homogeneous nucleation of molecular Al_2O_3 from the gas phase is very unlikely in a circumstellar environment [115]. The detected amorphous Al_2O_3 and the meteoritic evidence for the formation of Al_2O_3 in the winds of AGB stars, likely result from reactions in a grain mantle [116]. In stars with very high mass loss rate, ZrO_2 clusters may form in large enough quantities to play a role as seed particle [198]. Again, no spectroscopic evidence of its existence around evolved stars has been found so far.

One of the main discoveries of ISO in the field of solids in space has been the detection of crystalline silicates in the outflows of AGB stars with high mass loss rates. It should be kept in mind that the abundance of crystalline silicates compared to the amorphous silicates is modest, typically 10–15%, and only in very special cases the crystalline silicates dominate. Dust nucleation theories are now challenged to explain the co-existence and difference in properties of crystalline and amorphous silicates in AGB stars: (i) crystalline silicates are Fe-poor, amorphous ones contain Fe in some form, (ii) crystalline and amorphous silicates have different temperatures and thus are separate populations of grains. “Partially crystalline” grains do not seem to exist, which can be explained from a thermodynamic point of view: thermal crystallisation timescales are a steep function of temperature, and it requires extreme fine-tuning in the thermal history of a particle to observe it partially crystalline.

Although the crystalline lattice structure is energetically the most favorable state for silicates, the observations show that most of the silicate grains are amorphous or glassy. This requires an explanation. First of all, some threshold energy has to be overcome before an amorphous silicate will crystallize. At temperatures above 1,000 K the crystallization takes place on a timescale of seconds to hours, while below 900 K it will take years to more than a Hubble timescale [199]. If silicate dust condenses much quicker than the crystallization timescale, it will be amorphous. This implies that if the silicates form or quickly cool off below 900 K, they will

remain amorphous. Since the majority of the silicates that forms is amorphous, this may imply a formation below the glass temperature.

An alternative theory assumes that the silicates condense as crystals but their crystal structure will get destroyed in time. Tielens et al. [200] propose a scenario to explain the difference between crystalline and amorphous silicates by this destruction mechanism. They propose that gas phase Fe diffuses into the Mg-rich crystals around 800 K (which is for all practical purposes below the crystallization temperature) and destroys the crystal structure during its intrusion. In this scenario all grains would form crystalline and only later the bulk would turn amorphous as Fe is adsorbed. Very high spatial resolution far-IR observations of the dust around AGB stars should indicate if there is indeed a rather sudden decrease of the crystalline silicate abundance in the dust shell at a temperature of roughly 800 K.

Finally, the velocity difference between dust and gas particles can be high enough for destruction and sputtering. E.g., for silicate grains the velocity difference with a helium atom should be about 30 km/s for sputtering, and these velocities are not unlikely [201]. Colliding crystalline silicate grains might be heated high enough to become a melt or even evaporate. In the first case, the very quick cooling timescale (depending on the grain size), might result in amorphous silicates. It remains difficult however to explain the different opacities for amorphous and crystalline silicate grains in this scenario.

As mentioned above, the crystalline olivines and pyroxenes formed in the winds of AGB stars with high mass loss are Fe-free [10]. Interestingly, it is also the Fe-free olivines and pyroxenes that are the first silicates that are expected to condense. This will take place at temperatures where they will crystallize very quickly. Thermodynamic calculations show that the Fe-containing silicates will condense at a somewhat lower temperature, and since there is no evidence for Fe-containing crystalline silicates, they apparently remain amorphous. A possible explanation for this phenomenon is that as soon as some dust forms, radiation pressure will accelerate the dust (and through the drag-force also the gas) and the material will quickly be pushed to cooler regions. So, only the very first condensed silicates, the Fe-free silicates, might have a chance to crystallize, while the later condensed silicates (the Fe-containing silicates) are formed in an environment where the annealing timescale is much longer than the accretion timescale. We should note here that it is not clear that a ferromagnesiosilica will condense at all from the gas-phase. Gas phase condensation experiments of a Fe-Mg-SiO-H_2-O_2 vapor show only condensates of a magnesiosilica and of a ferrosilica composition but not of a ferromagnesiosilica composition (see Fig. 12).

While in most cases crystalline silicate dust is only a minor component in circumstellar dust shells, there are some evolved stars with a very high abundance of crystalline silicates. Remarkably, these always have a disk-like dust distribution [97]. Because the temperature in these disks is well below the annealing temperatures of amorphous silicates, Molster et al. [97] suggested that a low-temperature crystallization process is responsible for the higher fraction of crystalline silicates. Several processes were discussed by Molster et al. [97], but no conclusive answer could be given. Recently, partial crystallization at room temperature due to electron

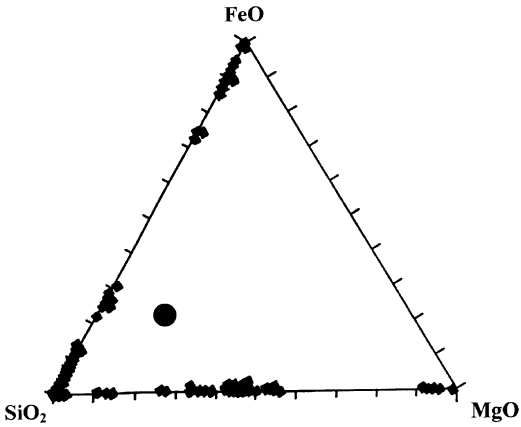

Fig. 12 Ternary diagram MgO-FeO-SiO_2 (oxide wt%) with the chemical compositions of gas to solid condensed grains from a Fe-Mg-SiO-H_2-O_2 vapor. The "average bulk solid" composition (*the big dot*) is roughly the gas phase composition which might have been somewhat less SiO_2-rich. Figure taken from [202]

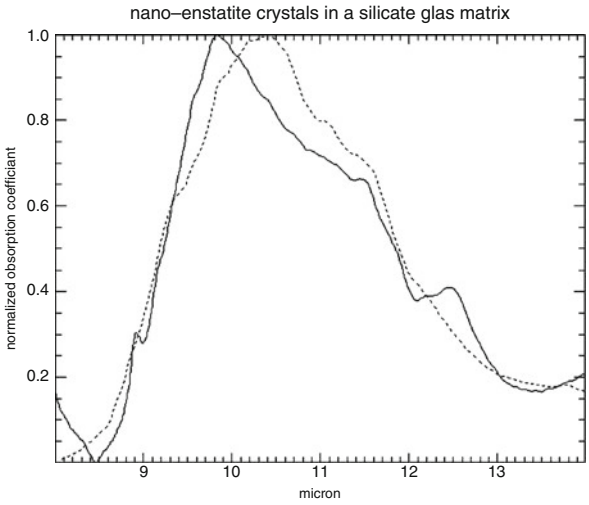

Fig. 13 The infrared absorption spectrum of an amorphous silicate smoke before (*dashed line*) and after (*solid line*) a 10 min irradiation by the electron beam of a transmission electron microscope. Note the upcoming of the spectral features

irradiation has been detected (Fig. 13 and [203]). Although this is a promising effect, there are still open questions. It is not sure that this process can create highly crystalline material in sufficient quantities. Investigations are still necessary to find out whether the particles can become completely crystallized or will simply become partially amorphous and partially crystalline. Note, that electron irradiation only causes local crystallization unlike thermal crystallization, which acts on the whole grain at the same time. Observations indicate that the amorphous and crystalline silicates are two different grain populations which are not in thermal contact [10] and it is unclear that this can be achieved by this process. Finally, the compositional implications (with or without Fe) of this process are also not well studied yet.

Theoretical calculations predict that in both oxygen-rich as well as carbon-rich stars metallic Fe can condense [198]. At lower temperatures it can react with both

oxygen as well as sulfur to form respectively FeO and FeS. Although there is a tentative detection of FeO in AFGL4106 [39], the lack of detailed features of FeO makes this identification subject to discussion and others identify the applicable feature with FeS [9]. In principle one would expect that at lower temperatures FeS would react further to form FeO in oxygen-rich environments. However, it is very likely that in the outflows of these stars the temperature and density of the dust particles drop so rapidly that equilibrium reactions simply freeze out and do not take place anymore.

The presence of carbonates around two planetary nebulae [26] shows that the normal assumed dust formation processes are not always applicable. The enormous amount of small carbonate grains (50 $M_{\oplus}$) in NGC6302 cannot be explained by aqueous alteration, as is observed on Earth (and probably on Mars). These conditions are unlikely to exist in the circumstellar environment of evolved stars. Kemper et al. note that in both objects with carbonates there is also evidence for crystalline silicates as well as abundant crystalline H_2O ice [26]. The carbonate formation mechanism may involve a mobile H_2O-ice layer including CO_2 which reacts with the silicate core on which the ice was deposited, possibly via the intermediate formation of hydrous silicates. This reaction however is unlikely to occur at the temperatures a which the ice can exist (below 100 K). Also the non-detection of hydrous silicates makes this scenario unlikely. The lack of hydrous silicates also hampers a second theory, that assumes that gas phase H_2O will react with silicates to form hydrous silicates, which transform further to carbonates by a reaction with gas phase CO_2. Alternatively, the carbonates may form near the surface of mass-losing AGB stars from gas-phase condensation of CaO in the presence of H_2O and CO_2. Kemper et al. favour this latter mechanism. This latter formation path has been seen in laboratory condensation experiments [204].

Rietmeijer (private comm.) suggested that the formation of carbonates proceeds via the so called weathering cycle. Due to a bombardment of energetic particles the rim of diopside will be amorphized and the lighter elements will be sputtered away [e.g. 205]. This will result in an excess of Ca. Together with CO_2 from the gas phase the rim will decompose into diopside and calcite or even dolomite. Note that diopside has been detected in these environments in contrast to the hydrous silicates.

The detection of carbonates in the circumstellar environment of evolved stars opens the possibility that *some* solar system carbonates found in primitive bodies as IDPs and the most primitive meteorites may not have formed by aqueous alteration and might even have an interstellar origin. It is clear however that the origin of the carbonates in many meteorites can most naturally be explained by aqueous alteration, as evidenced by the structure of the meteoritic matrix.

Around some oxygen-rich PNe and LBVs a small amount of PAHs have been detected together with some obvious oxygen-rich components like crystalline silicates. The origin of these carbon-rich molecules in these oxygen-rich environments is still not well understood. These stars, especially the LBVs, are not expected to have experienced a period in which the C/O ratio in their envelope was above 1. Probably the dissociation of CO (by the UV radiation field) produce some free carbon which might react with other C-atoms to form benzene rings.

After formation, dust grains in stellar outflows travel away from the star towards lower density and temperature. The grains continue to collide with gas, and, in high density winds, also grain-grain collisions (with all its consequences) can be important. The gas-grain interaction can lead to further grain growth, and to the condensation of ices (in particular H_2O ice) if conditions are favourable.

4.1.2 Carbon Stars

In carbon stars (where the C/O ratio of the gas is higher than 1) carbon-rich dust species form. One of the first detected species was SiC [173]. There is still some debate about the exact crystal structure (see Sect. 3.2.5) but the SiC itself is undisputed. SiC is rather stable and forms already at relatively high temperatures, so it is therefore the expected grain to form when both Si and C are very abundant and oxygen is not.

TiC, a high temperature condensate, is often suggested to be the seed particle for dust forming processes in carbon-rich environments. Because of its low abundance it is only expected to form in significant amounts in a high density environment, which are found in the atmospheres of evolved stars at the (very) end of the AGB. This would fit with the proposal that the 21 μm feature is due to TiC, and this feature is only seen in post-AGB (directly after the huge mass loss at the end of the AGB) stars and two PN.

The chemical composition of photospheres of carbon stars and some of the physical parameters characterizing the inner stellar winds are very similar to the conditions encountered in the combustion of hydrocarbons in the laboratory. Indeed, acetylene, C_2H_2, is the dominant carbon-bearing molecule after CO in the photospheres of carbon stars [206]. The typical temperature of carbon stars (2,500 K) are also found in flames rich in acetylene which are efficient sources of amorphous carbon particles in the form of soot. This natural link was used by several people to apply the well studied combustion chemistry to the modelling of the formation of amorphous carbon grains in C-stars [207]. The formation of amorphous carbon (soot) can be divided into two steps, the nucleation phase and the condensation phase. The nucleation phase starts with the formation of benzene (C_6H_6). The addition of acetylene to an aromatic radical, the subsequent extraction of hydrogen and the second addition of an acetylene molecule, resulting in the closure of another ring, leads to the growth of the PAH-molecule. When enough large aromatic molecules are formed, condensation products will (simultaneously) form. Condensation, the growth of planar species into 3-D solid (amorphous carbon) grains, is initiated by the formation of PAH dimers, where the aromatics are linked by van der Waals forces. The growth to amorphous carbon particles then proceeds through coagulation of condensation products of PAH molecules, deposition of carbon via acetylene surface reactions and surface condensation of free PAH molecules on the grain [208].

There exists a small group of carbon-rich AGB stars, which show the clear presence of amorphous and/or crystalline silicate dust in their infrared spectra. It is thought that in these cases the silicates are the remnants of a previous mass loss

phase, during which the star was still oxygen-rich. The current theory assumes that these silicates are then stored (due to binary interaction) in a circum-stellar/binary disk. While the star evolved further and became carbon-rich the old (oxygen-rich) dust remained present around the evolved star [209]. Another case are the Wolf-Rayet [WC] central stars of planetary nebulae, a poorly understood class of PNe, with little or no H in their atmospheres, while the ejecta are C-rich and H-rich. ISO discovered that besides the known PAH features, also crystalline silicates are present [210–212]. Two different scenarios are proposed to explain the nature of these objects. One theory explains the chemical dichotomy by a thermal pulse either at the very end of the AGB or young PN phase [late AGB thermal pulse; 213], or when the star is already on the cooling track [very late thermal pulse; 214]. The H-rich and O-rich layers may be removed due to efficient mixing and subsequent nuclear burning, or by extensive mass loss, exposing processed layers to the surface. The model has both statistical and timing problems, however. Such late pulses only occur at the right moment to cause a [WC] star for a small fraction of AGB stars, and in many cases the star would already be carbon rich. The other theory solves this by storing the oxygen-rich material in a longer-lived reservoir. This is seen in objects such as the Red Rectangle, where a circumbinary disk has formed capturing earlier mass loss [215]. A fairly large fraction of the known galactic post-AGB stars may be binaries in which oxygen-rich dust was stored in a circum-binary disk [216], however most of these do not show evidence for carbon-rich dust. Accretion from a disk on the star, as is also expected to have taken place in the case of the Red Rectangle [217], may lead to the [WC] phenomenon, but this is highly speculative. The discovery of a disk around CPD-56°8032 [218] makes the disk storage mechanism more attractive. But this leaves the relation between disk and [WC] star open: there is no evidence for binarity in such stars. It should be emphasized that no information is yet available about the distribution of the O-rich and C-rich dust components. High spatial resolution infrared observations may reveal the location of the different dust components and might help in distinguishing between the two theories [see e.g. 219, 220].

4.1.3 S Stars

S stars, with their C/O ratio close to one, normally show a rather flat SED without many dust features. This has long been interpreted as evidence for the presence of carbonaceous dust. Since, the mass loss rates for those stars were based on the 60 micron flux, the assumption about the presence of carbonaceous dust resulted in rather low mass loss rates for these stars. However, recently Ferraroti and Gail [198] calculate that the two most likely dust components that form are solid Fe and FeSi, which both also have a rather flat spectrum, without prominent features. Furthermore, if the presence of these two materials can be confirmed, it would also bring the empirical dust mass loss rates (based on the 60 μm opacity) and the gas to dust ratio much closer to the values derived for M and C-stars.

4.2 Dust Formation in Supernovae

Unfortunately, little is known about the dust production rate in SNe. The best studied object is the supernova remnant Cas A. However the obtained infrared spectra are not always conclusive. Arendt et al. [221] show a reasonable fit with proto-silicates to the SWS spectrum of an area centered on a fast moving knot (position N3) in the supernova remnant of Cas A. Douvion et al. [222] reject this identification based on an SWS spectrum taken very close to position N3, which shows many similarities (but is not exactly equal). They fit their spectrum with a mixture of three dust species ($MgSiO_3$, SiO_2 and Al_2O_3) with each having two different temperatures together with some synchrotron emission. The presence of amorphous $MgSiO_3$ was predicted by Kozasa et al. [223] and fitted the ISOCAM spectra reasonably well [224]. Recently, Rho et al. [225] fitted the spectra of several regions of Cas A. They came to the conclusion that there are three distinct ejecta dust populations, based on the shape of the spectrum. However, we would like to note that like in all these publications, rather artificial temperatures (all dust species have different temperatures, which are not directly related to opacity differences), the arbitrary dust sizes and the more or less one feature identifications, leave room for alternative interpretations. Therefore, most of our knowledge about dust production in SNe is still based on the analysis of presolar grains, which due to their isotopic anomaly could be traced back to a supernova explosion. Selection effects make it impossible to deduce the dust production rate from these data. In addition, the large differences in physical and chemical conditions between AGB winds and SN ejecta make it difficult to assume similarities in the types of dust that may condense in SN ejecta. Nevertheless, based on these isotopic measurements in general one can say that nano-diamonds, corundum, SiC, etc. do form after a supernova explosion (but none of them has been spectroscopically identified yet).

For completeness we mention here that also some novae are shown to produce dust during the eruption [e.g. 226].

4.3 The Processing of Dust in the ISM

The average lifetime of a silicate dust grain in the ISM is roughly 4×10^8 years, while the replenishment rate of ISM dust is about 2.5×10^9 years [195]. This means that interstellar dust grains are destroyed and re-formed about six times before finally entering a star forming region to be incorporated into a new generation of stars. Thus, new grains must be formed in the ISM. Below, we discuss dust formation and destruction mechanisms that may occur in the ISM.

4.3.1 Dust Formation

The dust formation process in the ISM is not clear, however it seems inevitable that it takes place in the dark molecular clouds, where high densities prevail. The C/O

ratio in the ISM is in general smaller than unity, which normally would result in the formation of oxygen-rich material. However, in diffuse clouds the interstellar radiation field easily dissociates the CO molecule. Thus, especially in the diffuse ISM the formation of carbon-rich dust cannot be excluded. In the dark molecular clouds a rather complex chemistry is taking place, which might also result in the formation of carbon-rich dust without a C/O ratio larger than 1, but not much is known about this process.

The most important difference between the dust formation process in the interstellar medium and the dust around stars is the temperature and density of the gas. Around stars dust forms at temperature of about 1,000 K, while in the ISM dust temperatures between 10 and $\approx$ 100 K are found. These low temperatures are far below any annealing point, therefore the grains formed in the ISM will be amorphous. This is consistent with the fact that no crystalline silicates have been found in the ISM.

From depletion pattern differences between cool clouds in the Galactic disk and warm clouds in the galactic halo, it seems that the dust that forms in the ISM has an olivine stoichiometric ratio [227]. Note that this does not imply that they are olivines.

For carbon rich dust the situation is even more complicated, based on the fact that with the exception of SiC no conclusive spectroscopic identification has been made for the carbon dust component in the ISM. For many SiC particles found in meteorites it has been proven that they come from carbon stars or supernovae. They must therefore have resided in the ISM before they got incorporated in the collapsing cloud from which the solar system formed. Analysis of the line of sight to the galactic centre led [38] to conclude that SiC is present at an abundance of 3%, or 9–12% of the Si is in SiC. This exceeds the upper limit found by Whittet et al. [188], who found an upper limit of the amount of Si in SiC in the ISM of 5% of that in silicates. More lines of sight must be investigated to establish the presence and distribution of SiC in the interstellar medium. Tang and Anders deduce from ^{21}Ne isotopes in SiC grain in C2 chondrites that the lifetime [228] of these grains is only 40 million years. This is remarkably short compared to the estimated lifetime of a grain in the ISM (400 million years). Interestingly enough this 40 million years, is roughly equal to the oxidation time-scale for diffuse interstellar clouds. One can therefore argue that oxidation will selectively destruct the SiC grains [188] in the ISM.

Very small graphite particles have been proposed as the carrier of the 2175 Å feature [128], but its formation site is not well known. Amorphous carbon has been proposed to form around carbon stars and interstellar shock waves might provide the energy to convert it to graphite. According to Tielens et al. [140] only 5% of the very small carbon grains (maximum size about 100 Å) will be converted to diamonds, while the rest would likely become graphitic C. This process might be the source of very small graphitic grains.

Sandford et al. [229] show that the C—H stretching band shows a linear correlation with the visual extinction, except for the direction towards the galactic center. This behaviour is remarkably similar for the Si—O stretching band. This similarity suggests that the silicates, responsible for the Si—O stretch, and the aliphatic hydro-

carbons, responsible for the 2950 cm^{-1} (3.4 μm) C—H stretch may be coupled, perhaps in the form of a silicate core, organic mantle grain. If true, those mantles might provide a good shielding for the destruction processes in the ISM. This will likely alter the life-cycle of the silicate dust, especially the destruction rate. How they are formed is still unclear, but the carbonaceous mantles found around IDPs (see "The Astromineralogy of Interplanetary Dust Particles" by Bradley this volume), might result from a similar kind of process and can provide a better understanding of the core mantle grains in the ISM.

The 90 μm band in NGC1333-IRAS4 attributed to $CaCO_3$, sheds (if confirmed) new light on the formation of carbonates. The material in the vicinity of this protostar presumably has only experienced typical interstellar medium conditions and thus a gas-phase condensation mechanism for the carbonates, as suggested by Kemper et al. [26] for the planetary nebulae, seems implausible. Ceccarelli et al. [102] suggest that the low-temperature mechanism, considered by Kemper et al. may be more likely. Alternatively, the carbonates around evolved stars may have survived their residence in the ISM.

4.3.2 Dust Destruction

The harsh conditions that prevail in the ISM can result in the destruction or modification of interstellar dust. Interstellar shocks may shatter grains into smaller fragments, thus changing the grain size distribution by producing more small grains. The ISM is a destructive place for the crystalline silicates. We observe these grains in the outflows of evolved stars, but not along lines of sight through the ISM. The exact abundance of the crystalline silicates brought into the ISM by stars is not known yet. This depends on how much cold crystalline silicates are hidden in the warm amorphous silicate profiles. But the lack of crystalline silicate features in the ISM, makes it plausible that the crystalline silicates are destroyed or amorphized in the ISM.

In fact both processes are expected to occur in the ISM. It has been suggested that the amorphization might be due to a bombardment of the crystal structure by energetic radiation as will take place in the ISM. If the temperatures are below the crystallization temperatures there will be not enough internal energy to overcome the threshold energy necessary to fix the faults in the crystal. This is the situation in the harsh environment of the ISM, where energetic particles can destroy the matrix, and the low temperatures prevent repairs of these defects. However, Day [230] shows that MeV protons hardly have any influence on the crystalline silicates and electron irradiation might even make grains more crystalline [203].

It seems that the destructive power in the ISM mainly comes from SN shock waves. These have a different influence on the particles depending on their size and composition. Laboratory experiments of irradiation by He^+ ions, resembling supernova shock waves through the ISM, show that the small crystalline silicates are likely amorphized in the ISM [52]. Although there is a limited penetration depth, only the first micron will be completely amorphized, and larger grains might therefore survive complete amorphization, but they will suffer more from sputtering and

evaporation in these shocks [195]. So, in the end it is not expected that the silicate grains, especially the crystalline ones, will survive a long stay the ISM.

The final structure of silicates exposed to He^+ irradiation shows some resemblance with the GEMS in IDPs ("The Astromineralogy of Interplanetary Dust Particles" by Bradley, this volume). In this respect it is also interesting to note that sometimes inside a GEMS a so-called relict forsterite grain is found, which shows evidence for heavy irradiation damage, much more than what is expected during their stay in the solar nebula. Furthermore, these irradiation experiments showed that O and Mg are preferentially sputtered away from the first 100 nm of the test samples. This might explain the evolution of the amorphous silicate dust which looks more like an amorphous olivine around the evolved stars and more like an amorphous pyroxene around young stars [52]. A similar selective sputtering, but then by solar wind irradiation has been observed in solar system material [231].

4.4 Dust Processing in Star-Forming Regions

Without doubt the solar system is the best evidence available for the dramatic changes in dust composition that occur during star and planet formation. The vast literature on the mineralogy of solar system objects, ranging from planets to IDPs demonstrates that large differences exist between the properties of solids in the solar system and in interstellar space. In recent years it has become evident that these differences also exist for dust in primitive solar system objects such as comets. Clearly, understanding these differences is one of the main challenges of the field of star- and planet formation.

4.4.1 Molecular Cloud Dust

Evidence is accumulating that dust in molecular clouds has different properties compared to dust found in the diffuse ISM. This is shown in Fig. 14 where the near-IR extinction E(J-K) is plotted against the optical depth of the 9.7 μm amorphous silicate absorption band, measured against bright background stars. The sightlines dominated by diffuse interstellar dust show a clear correlation between E(J-K) and $\tau_{9.7}$, while the molecular cloud sightlines show much larger E(J-K) for a given $\tau_{9.7}$ when E(J-K) exceeds a value of about 1.5 (see e.g. [232, 233]). The line of sight to the galactic center shows the opposite effect. The near-IR extinction is dominated by carbonaceous dust, while $\tau_{9.7}$ is due to amorphous silicates. Therefore a possible interpretation of Figure 14 is changes in the relative abundance of carbonaceous and silicate dust, for instance in the line of sight towards the galactic center. However, this seems unlikely for the diffuse and molecular sightlines. Grain growth has been suggested as an alternative. However, variations in the shape of the 9.7 μm silicate band are modest; there is a small difference at the short wavelength side of the band, possibly consistent with a higher abundance of pyroxene in molecular clouds (Fig. 14). The relatively small changes in silicate band strength are remarkable and

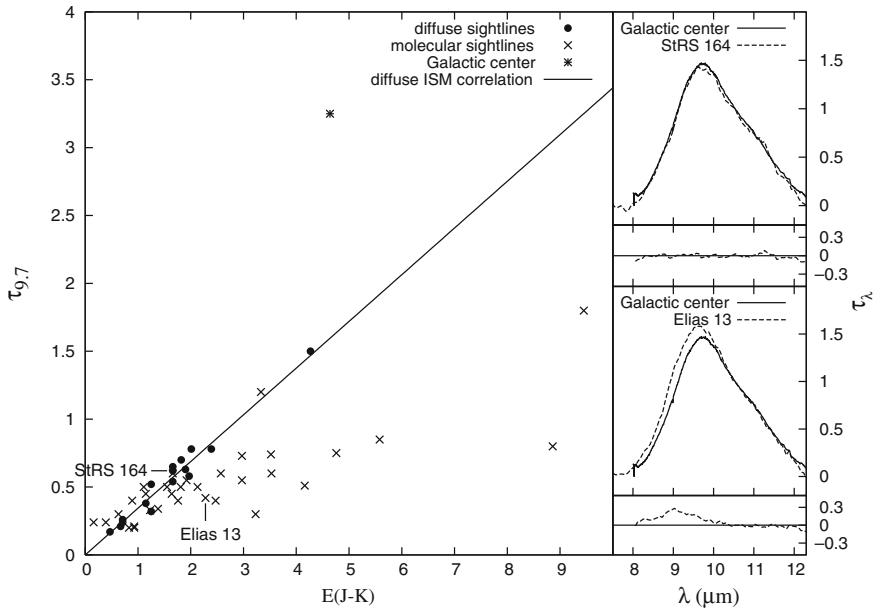

Fig. 14 Comparison of near-IR extinction and optical depth in the 9.7 μm amorphous silicate band for different lines of sight in the galaxy. The right-hand panels show (i) the normalized silicate band shapes towards the galactic center and the diffuse ISM line of sight towards the background star StRS 164 (*upper right*) and the difference between these two band shapes; and (ii) the molecular cloud line of sight Elias 13 (*lower right*) and the galactic center, and their difference. Figure adapted from van Breemen et al. (in preparation)

set limits on grain growth as a cause for the different behaviour of dust in molecular clouds and the diffuse ISM.

4.4.2 Proto-Planetary Disks

Astronomical observations of planet-forming disks around young stars also begin to reveal evidence for processing of dust. For instance, infrared spectroscopy and millimeter observations of disks surrounding Herbig Ae/Be and T Tauri stars suggest that grains in proto-planetary disks have coagulated into sizes up to cm, and probably to even substantially larger bodies that escape spectroscopic detection. Substantial changes in the composition of the gas also occur, both through freeze-out onto grains as well as through chemical reactions. Some of these reactions occur on the surface of the grains, and require irradiation with UV photons from the newly born proto-star.

Apart from an increase in average size, infrared spectroscopy has also shown that the composition of dust in proto-planetary disks changes in time [53] and significantly differs from the dust in the ISM. Probably the clearest example of the last is the crystallization of the amorphous silicates in the disks surrounding young

low- and intermediate mass stars. There is no convincing evidence for the presence of crystalline silicates in the ISM. The crystalline silicates found around young stars therefore have to be formed in situ. They will be formed both by gas-phase condensation, as well as by annealing of amorphous silicates, as is also seen in our own solar system [234]. Both processes will take place close to the young star. This seems to be supported by the observations. The strength of crystalline silicate bands as a function of wavelength can be used to derive the radial distribution of crystalline silicates. In most young stars there are indications for the presence of crystalline silicates, but only in the 10 μm region. This implies that the crystalline silicates are indeed hot and close to the star [e.g. 95, 123]. A conclusion that is further strengthened by interferometric observations of proto-planetary disks, which indeed show that the inner disk is more crystalline than the outer regions [93, 94].

The gas phase condensation process will produce very Fe-poor crystalline silicates, similar to what has been found around evolved stars, while the annealing process will very likely produce Fe-containing crystalline silicates. Because the amorphous silicates will in general not have the same stoichiometric ratio as the annealed crystals, some remainder material is expected to form. The presence of silica in the dust emission spectra of young stars supports this scenario. This material is transparent at optical wavelengths and will normally be very cold relative to the other minerals. The fact that the silica features in the 10 μm region are detected, indicates that silica is much warmer than expected. It should therefore be in thermal contact with the other minerals, as is expected when it is a remainder of annealing of amorphous silicates [123].

Nebular shocks have been suggested as an alternative mechanism to provide the temperatures necessary for annealing of the amorphous silicates in the proto-solar nebula at larger distances [235]. Although this mechanism fails to explain some of the aspects of the crystalline silicates in the solar system, and will therefore not be applicable to all crystalline silicates found, it cannot be excluded as a competing mechanism. Shock heating, together with radial mixing, may explain the presence of cold crystalline silicates seen in proto-planetary disks. Shocks might also play a role in the disks surrounding evolved stars.

Interestingly, crystallization through flash heating resulting from a stellar flare may play an important role in magnetically active young low mass stars [236]. In the young solar type star EX Lupi crystalline silicates were found to form following a stellar flare. The abundance of crystalline silicates in the disk surface layers may thus vary on relatively short timescales.

A spectacular result of the ISO mission has been the remarkable similarity between the spectral appearance of the solar system comet Hale-Bopp [75] and that of the Herbig Ae/Be star HD 100546 [81]. In both objects the emission bands of crystalline silicates, as usual Fe-poor, stand out (Fig 15). The origin of the high abundance of crystalline silicates in both objects is not clear. In HD 100546 the abundance of forsterite increases with distance from the star [88], which is not expected in the case of radial mixing of annealed silicates [235, 237, 238]. Bouwman et al. [88] propose a local production of small forsterite grains as a result of the collisional destruction of a large parent body.

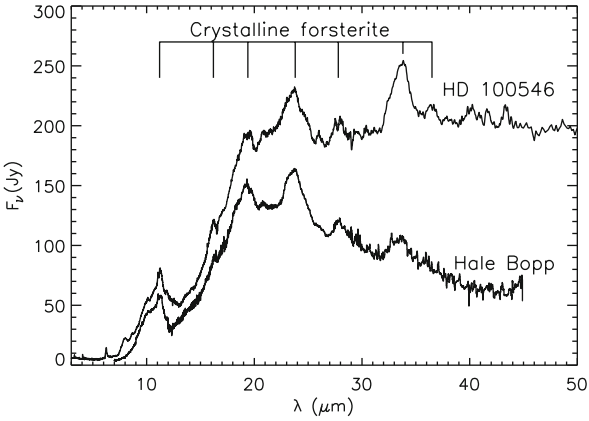

Fig. 15 The ISO SWS spectra of Hale-Bopp [75] and HD 100546 [81]. The crystalline forsterite features are indicated

The IRS on board Spitzer has provided a very large data set of disk spectra showing that grain processing and crystallization are a common phenomenon for young stars with a wide range of mass (Fig. 16). These disk spectra map the geometry of the disk such as their flaring angle and the presence of disk inner holes and disk gaps.

Clearly, grain processing is driven by the physical and chemical conditions in the disk, such as radial and vertical mixing, and planet formation and is much less a function of stellar mass. Many theoretical studies have been performed to better understand the processing of gas and dust in proto-planetary disks. For instance, Gail [241] applies a thorough thermal equilibrium calculation to the dust mixture in a proto-stellar accretion disk. He takes into account the disk structure, opacity and the chemical compositions and abundances of the major dust species. His calculations show that substantial dust processing can occur in the inner regions of the accretion disks surrounding proto-stars, and that radial mixing can result in a substantial abundance of crystalline silicates in the outer disk regions.

Most considerations about the formation of crystalline silicates come from theory. However, also laboratory experiments sometimes shed new light on this subject. There are indications that the width of some features are an indication of the internal structure of a crystal, and therefore of their formation history. Molster et al. [10] remark the differences in band shape between the laboratory spectra of a single forsterite crystal and an annealed amorphous forsterite. They compare these band shapes to those of some characteristic bands seen in the spectra of evolved and young stars. The evolved stars, with freshly made stardust, show a band shape which fits better that of the single crystal. This may be expected, since gas-phase condensation would naturally lead to particles with a single crystal structure. On the other hand, the spectrum of HD 100546 shows a resemblance to that of the annealed sample. This is an indication that the forsterite in HD 100546 has stacking faults. Both fractionation of a differentiated body (as proposed by Bouwman et al. [88] for HD 100546), as well as annealing of amorphous silicates (as seem to occur around many other young stars) will lead to stacking faults in the forsterite crystal

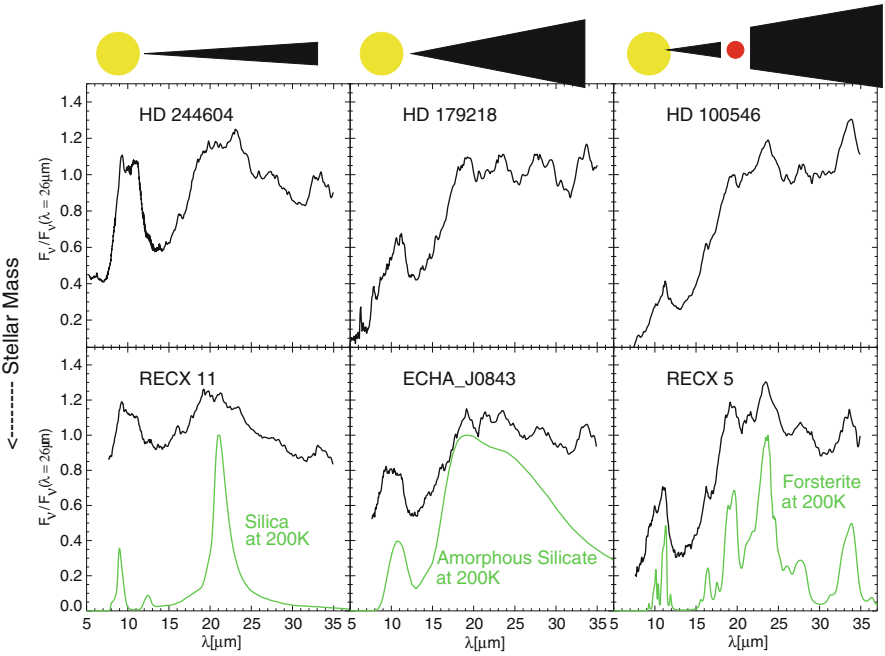

Fig. 16 Spitzer IRS spectra of proto-planetary disks surrounding young stars. The top row panels are intermediate mass (2–3 $M_\odot$) Herbig Ae/Be stars (Juhász et al. [294]), while the bottom row are those of low mass stars in the 8 million years old η Cha cluster (0.7, 0.2 and 0.2 $M_\odot$ for RECX11, ECHA–J0843 and RECX5, respectively, [239, 240]. The pictographs on top show a possible geometry of the disks plotted in the different columns. Also shown are the dust opacities of silica, amorphous silicate and forsterite at 200 K. The strong 33.6 μm forsterite band indicates the presence of cold crystalline silicate, indicative of substantial processing at large distance from the star. This process occurs in disks surrounding stars with a wide range of mass

and is therefore in agreement with the observations. Murata et al. [242] compare the spectra of two evolved stars with the spectra of single crystal enstatite and enstatite with several stacking faults. Their conclusion is that for those two objects, which both are assumed to have a disk and not a normal outflow, the fit to the spectra is better if they use enstatite with stacking faults than if they use the single crystals. It is important to stress however, that there are other effects that can influence the band shapes, such as blends with other dust species, and grain size and grain shape effects.

The presence of carbonates in evolved stars shows that there may exist alternative formation mechanisms for these materials, which has implications for the use of carbonates to reconstruct the early history of the solar system: although there is much evidence that most carbonates in the solar system are formed by aqueous alteration, this does not automatically have to be true for *all* carbonates.

Solid FeS is abundant in IDPs and primitive meteorites, but not be confirmed outside the Solar system. In the solar system, virtually all sulfur in primitive bodies is found as FeS, suggesting an extremely efficient formation mechanism. Since sulfur

is not depleted significantly from the gas-phase in the diffuse interstellar medium, this implies that the sulfur depletion occurs at some point during the star formation process, eventually leading to the formation of solid FeS. Since even in IDPs sulfur is locked up in FeS, it seems that the formation of this solid must have occurred very early in the collapse of the proto-solar cloud. Perhaps a gas-phase-solid reaction between metallic Fe and H_2S is responsible. However, this reaction only occurs at temperatures above 400 K, which seems difficult to reconcile with the low temperature conditions that prevailed in the outer regions of the proto-solar cloud. We note that analysis of Spitzer spectra of proto-planetary disks so far has not shown evidence for the presence of FeS, and so we consider the identification by Keller et al. [9] as unconfirmed and the formation process in the early Solar system as a still open question.

The discovery that most nano-diamonds are formed in the accretion disks of young stars and are not presolar ("The Astromineralogy of Interplanetary Dust Particles" by Bradley, this volume), opens the question about their (trans)formation. It was long accepted that the nano-diamonds in meteorites came from the ISM and should therefore be quite abundant. However, the lack of features in the ISM and the apparent increase of the abundance of nano-diamonds towards the inner solar system ("The Astromineralogy of Interplanetary Dust Particles" by Bradley, this volume) have caused some doubt to this statement. If nano-diamonds are very abundant in the ISM, it would imply that these diamonds were very easily formed via chemical vapor deposition in interstellar or circumstellar environments [i.e. 141] or via shock processing in interstellar shocks [140]. The problem is that pure nano-diamonds have no or only very weak features in the IR. They will only become detectable when they are hydrogenated [144]. And up to now only in five sources these features have been detected, two post-AGB star (HR 4049 and HD 52961) and three Herbig Ae/Be stars (Elias 1, HD 97048 and MWC 297) [144, 150]. The key question has now become are nano-diamonds only formed in special places, or are they only visible in special environments. The 5 known sites where the nano-diamonds have been found give a clue about this. All stars have a relatively hot circumstellar disk and at least four of them also an oxygen-rich gas chemistry, which is obvious for the three Herbig Ae/Be stars and more surprising for HR 4049 [104]. The fifth, HD 52961, has a circumbinary disk with very metal poor gas, and no obvious oxygen-rich gas chemistry has been reported. Chang et al. [243] showed that the formation of diamond crystals is facilitated by both high temperatures and the presence of oxygen. Also the formation timescales in a disk are much longer, compared to normal outflows, due to the storage of dust in a disk. Hydrogenation, necessary to detect the otherwise (almost) IR-inactive nano-diamonds, should also be possible in a carbon dominated environment. Furthermore, the size distribution of the nano-diamonds in meteorites is log-normal, which points to a growth process in a circumstellar environment and not to fractionation as is expected when the grains would have resided in the ISM [244]. Combining all this information, it seems that it is the special environment in which these diamonds are made, instead of a special environment necessary to detect them. The formation of nano-diamonds is facilitated by the presence of carbonaceous dust together with an oxygen-rich gas

chemistry, long storage times and high temperatures. Interestingly enough, these were also the conditions in the inner solar system. The most likely formation mechanism is the shock-heating of carbonaceous material in the proto-stellar accretion disk. The almost complete coverage of IDPs by a carbonaceous layer (see e.g. [245] and "The Astromineralogy of Interplanetary Dust Particles" by Bradley, this volume) indicates that although the overall C/O ratio is below one, a carbon based chemistry can take place in these environments.

5 Dust in Extragalactic Environments

Studies of the mineralogy of the interstellar and circumstellar environment can be extended to extragalactic environments. Physical conditions in external galaxies are often markedly different from what is found in our own Milky Way. For instance, differences in the star formation rate give rise to either an older or younger stellar population and hence differences in the UV radiation field; Extragalactic environments may be at a different stage in their galactic chemical evolution and thus show a different metallicity; the gas or stellar density might be lower; or the galaxy may host an active galactic nucleus (AGN) or quasar. All these effects can in principle process grains in different ways than what is seen in the Galaxy, or even give rise to the formation of grains not usually seen in the Milky Way. Although some work on extragalactic mineralogy has already been done prior to Spitzer, with the advent of Spitzer Space Telescope, extragalactic astromineralogy has really taken off. The unprecedented sensitivity of the IRS allows the study of individual stars and clouds in local group galaxies, and in integrated light has expanded our view on astromineralogy.

5.1 Local Group Galaxies

5.1.1 The Magellanic System

The Milky Way's neighbours in the local group, the Large Magellanic Cloud (LMC) and the Small Magellanic Cloud provide a good compromise between distance and size, in order to study the mineralogy of dust. They are the nearest reasonably sized galaxies, with the LMC at $\sim$50 kpc [246], and the SMC at $\sim$60 kpc [247], which allows for studies of individual objects and their mineralogy using Spitzer. The sub-solar metallicity in both the LMC and SMC – $Z \approx 0.3 - 0.5 Z_{\odot}$ [e.g. 248] and $Z \approx 0.2 Z_{\odot}$ [e.g. 249], respectively – expands parameter space for exploration of interstellar and circumstellar dust processing. The dust-to-gas mass ratios are lower with respect to what is seen in the Milky Way, resulting in substantially higher ambient UV fields than the Solar neighbourhood, affecting physical processes in the ISM and circumstellar environments. In the LMC, the shape of the interstellar extinction curve in the UV appears to not depend on metallicity, thus constraining the differences between Galactic and LMC grain properties, although large variations exist between environments in the LMC [250]. In the SMC, only a

limited number (5) of measurements of the interstellar extinction curve exist, and no definitive conclusion on the shape of the interstellar extinction curve can be drawn, although it appears that the SMC extinction curve has properties similar to those seen in starburst galaxies [251].

5.1.2 Oxygen-Rich Dust in Early-Type Objects

Prior to the launch of Spitzer, the number of infrared spectroscopic observations of objects outside the Milky Way good enough to draw conclusions on the astromineralogy, was very limited. Among the pioneering work was the study by Voors et al. [252] who have obtained 2–45 μm spectroscopy of R71, a luminous blue variable in the LMC, using the ISO-SWS. The spectrum of R71 exhibits the signature of crystalline enstatite at 23 μm, making this the first detection of extragalactic crystalline silicates. Voors et al. [252] argue that the dust composition in R71 is consistent with what is found for Galactic analogues, such as NML Cyg. Using the 8–13 μm window visible from the ground, Dijkstra et al. [253] studied the appearance of the 10 μm silicate feature in M stars in the LMC, as a function of mass loss parameters. They found that the mineralogy was either pure silicate, or a silicate/Al_2O_3 mix, where the Al_2O_3 fraction decreases with increasing wind density, conforming expectations from dust condensation models.

The extragalactic mineralogical landscape became much more clear when Spitzer was pointed at the LMC. IRS spectroscopy of two B[e] hypergiants (R126 and R66) reveal the presence of silicate dust, where R66 also shows a very rich crystalline silicate spectrum and evidence for a dual chemistry with the presence of PAHs [254]. These sources are very similar. Both are known to have disks – as is confirmed by the shape of the SED in the infrared – which may provide a suitable environment for crystallization. It remains unclear why the silicates around R66 are highly crystalline, while the crystalline features in the spectrum of R126 appear to be absent. Crystalline silicates are also commonly found in the circumstellar disks of RV Tau stars in the LMC [see Fig. 17; 255].

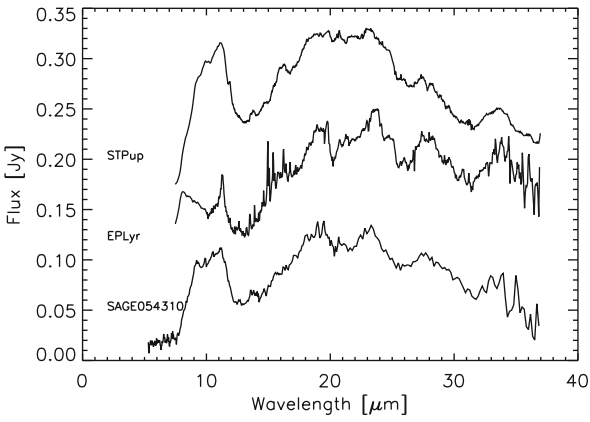

Fig. 17 Spitzer IRS spectra of disks surrounding evolved binary stars in the galaxy (ST Pup and EP Lyr [256]) and a related source in the LMC (SAGE054310). Prominent crystalline silicate bands are visible suggesting grain processing has occurred in a similar way as observed in the disks surrounding young stars. Figure adapted from [255]

Additional LMC sources exhibiting crystalline and amorphous silicates are reported by Zijlstra et al. [257], who find one AGB star (IRAS 05003–6712) showing the characteristic features of enstatite and forsterite in a sample of otherwise carbon-rich AGB stars, and by Sloan et al. [258], who have observed an unusually shaped 10 μm resonance in Mira HV 2310, potentially due to a mix of amorphous silicates and alumina (Al_2O_3). Sloan et al. [258] speculate that perhaps an iron-containing crystalline olivine may be required to explain the observed shift, although unfortunately the 20% spacing in compositions used in laboratory spectroscopy is too coarse to give a conclusive answer.

5.1.3 Carbon-Rich Dust in the Late Stages of Stellar Evolution

A consequence of the fact that early LMC and SMC observations were limited to the tip of the AGB, is that due to dredge-up of carbon, many of the AGB stars have indeed developed into carbon-stars by the time they enter the phase of high mass-loss [257]. This more easily occurs than at Solar metallicities, due to the lower initial oxygen-abundance in the stellar atmospheres. [257] have made an initial inventory of the spectral features in a sample of 27 carbon stars in the LMC. The spectra are remarkably uniform in their appearance, showing only dust features due to SiC (in all sources), and MgS (in about 2/3 of the sources) on top of an amorphous carbon continuum, with no significant variation in feature shape (see Fig. 18 for example carbon star spectra). The waxing and waning of the features as a function of spectral index, seems to indicate that MgS condenses on top of the SiC. A similar study was performed for the SMC [259]. These results were confirmed by Lagadec et al. [260], who expanded the sample with another 14 carbon stars from the lower metallicity environment in the SMC, showing that at the SMC metallicity, the onset of MgS condensation occurs at even higher spectral indices, and hence higher mass loss rates. The peak strength of the SiC feature decreases with decreasing metallicity, which can be understood as an effect of the changing SiC/amorphous carbon ratio. At low metallicities, less Si is available for the formation of SiC, while the carbon is produced by the carbon stars themselves. Indeed, this trend has been used to estimate the metallicity of carbon-stars in the Sagittarius Dwarf Spheroidal Galaxy, and a value close to solar metallicity was found, consistent with previous metallicity determinations for this galaxy [261]. On the extreme end of this trend is the recent discovery by Sloan et al. [262], showing that in an ultra-low metallicity galaxy, dust formation around carbon stars may still occur in the form of amorphous carbon from the dredge-up products, but that there is virtually no presence of SiC.

Another category of carbon-stars are the extreme AGB stars, with very dense winds, just prior to the formation of a post-AGB star. In the Galaxy, such objects are often OH/IR stars, with strong silicate absorptions [e.g. 264], but in low metallicity environments like the LMC, these objects have long become carbon rich. The first example of this class is IRAS 04496–6958, which shows very deep molecular bands due to C_2H_2, but also SiC at 11.3 μm in absorption [265]. This seems to

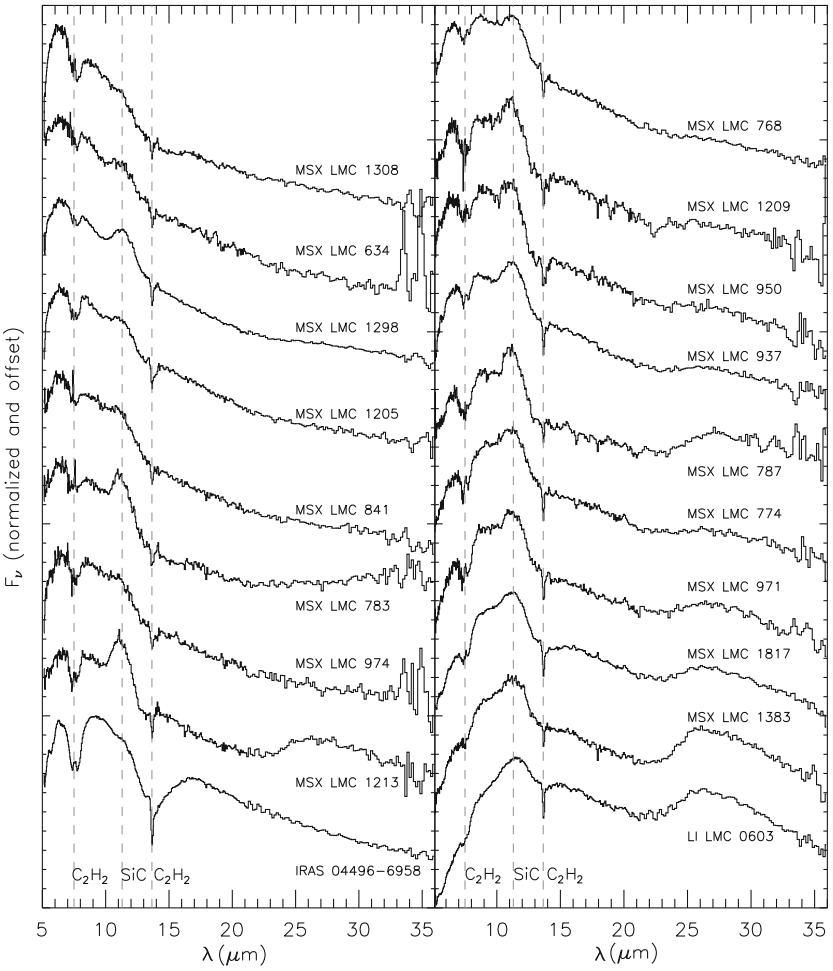

Fig. 18 Example of carbon star spectroscopy from the LMC. These spectra are ordered by increasing spectral index. The positions of the molecular bands due to C_2H_2 are indicated by the dashed lines, as well as the SiC dust features. The MgS feature around 30 μm is apparent as a broad bump at the red part of the spectrum. Figure taken from [263]

indicate a significant column density of dust and molecular gas, although its spectral energy distribution appears to be too blue for a heavily embedded object. Figure 19 shows the spectrum of IRAS 04496–6958 in comparison with some Galactic objects showing SiC absorption. A further seven extremely reddened carbon stars showing evidence for SiC in absorption, and MgS in emission are found by Gruendl et al. [266].

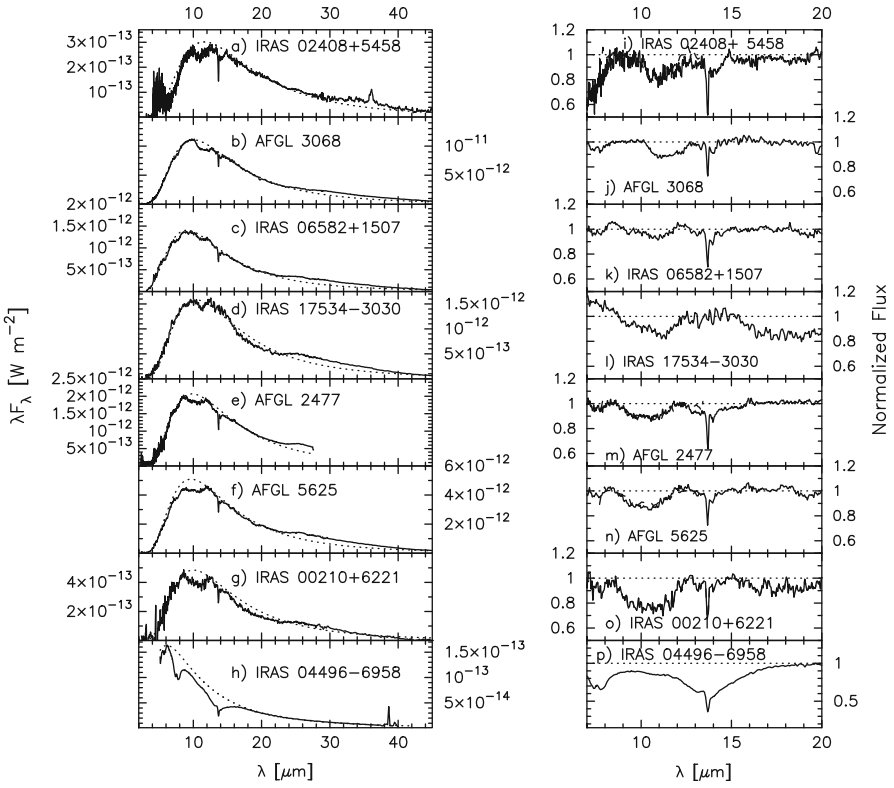

Fig. 19 *Left panel:* Comparison of the Spitzer IRS spectrum of IRAS 04496-6958 (*bottom left*) with a sample of Galactic extreme carbon stars observed with ISO-SWS. In each panel a blackbody fit (*dotted line*) to the data (*solid line*) is shown. *Right panel:* Continuum-divided spectra (*solid lines*) of the same sample of objects. Figure taken from [265]

5.1.4 PNe and SNe, the Final Stages

The prevalence of the carbon-rich phase in stellar evolution is supported by evidence from IRS observations of Planetary Nebulae (PNe). Stanghellini et al. [267] have observed 41 PNe in both Magellanic clouds, and which are previously observed using HST. Roughly half of the spectra show solid state features, mostly carbon-rich species. In a few cases, grain growth is observed through broadening of the 11.3 μm SiC feature. Only two LMC objects and one SMC object show clear detections of oxygen-rich dust, in particular crystalline silicates. Generally, the occurrence of dust in PNe is less frequent than what is observed in the Galaxy.

Amongst high mass stars, silicate dust is commonly found, however. A detailed study of supernova remnant N132D by Tappe et al. [268] included IRS observations and a strong feature at ∼20 μm due to amorphous silicates. The observations were taken of part of the shell and a fast-moving knot. The IRS spectrum of recent SN 1987A is dominated by emission from silicate dust, with a few atomic lines [269]. The shape of the residuals, after the amorphous silicate emission was

accounted for, is speculated to be due to crystalline silicate emission, although no constraints are set on the crystalline fraction.

5.2 Active Galaxies

Spectroscopic evidence of the presence of silicates in AGN emerged only recently by observing resonances at 9.7 and 18 μm [e.g. 270], initially only in absorption. Emission features were detected towards several quasars a few years later [e.g. 271–274].

Seyfert 2 galaxies are very suitable to study the silicate dust mineralogy in the torus as the bright nucleus is partially obscured by the torus, but not by the dust in the host galaxy. A well-studied case is NGC 1068. Jaffe et al. [275] find that while the overall silicate profile in NGC 1068 is consistent with the Galactic ISM silicate feature [e.g. 89], the dust in the innermost parts of the galaxy has a different composition, which may be aluminum-rich silicates. Using long-slit spectroscopy, the spatial distribution of dust in this relatively nearby AGN can be studied: with LWS on Keck I it was found that the variations in the silicate profile seen across NGC 1068 were consistent with two dust populations with different properties [276]. The dust population in the ionization cone may have on average larger grains than the dust in the torus, as the smaller grains are preferentially destroyed. For a small sample of Seyfert 2 galaxies the 9.7 μm profile could be fitted with the profile from μ Cep silicate, representing the ISM silicate [277], although one of the objects shows substructure at 11 μm potentially due to crystalline silicates.

When the silicate features are seen in emission, more variation in spectral appearance is observed. Two low-ionization nuclear emission-line region AGNs show a silicate 9.7 μm feature that deviates from the typical ISM silicate, namely M81 [278] and NGC 3998 [272]. In the latter case the feature is observed to be shifted to longer wavelengths, and also appears to be broader than the ISM silicate. The authors hypothesize that crystallization may have occurred, causing the peak to shift to around 11 μm. Li et al. [279] explain the same effects by modelling the amorphous silicates as porous particles. In case of M81, no good carrier has been identified.

A rich mineralogy was observed in quasar PG2112+059 [280] showing the presence of silicates through emission features, which are blended with the spectral signature of oxides such as alumina and periclase, as well as crystalline silicates and PAHs (see Fig. 20).

These authors clearly see this dust population separate from the dust in the torus, and speculate that it may be formed in the wind rising of the accretion disk. Indeed, dust formation may occur in these environments [281], and are predicted to produce dust masses up to 10^7 $M_\odot$. The presence of the highly refractory corundum, the crystalline silicates and and the less refractory MgO and amorphous silicates indicates that the wind of PG2112+059 has an inhomogeneous temperature and density structure [280], which is consistent with the dust formation model proposed by [281], who suggest that expanding clouds of varying density and size in the wind provide the conditions required.

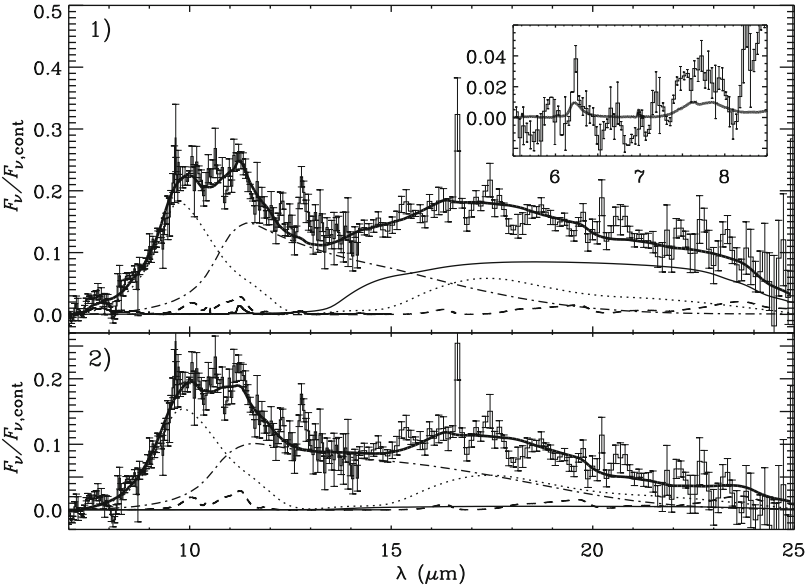

Fig. 20 Two alternative fits (*thick solid lines*) to the 8–25 μm (rest wavelength) spectral features (histograms with errorbars) seen in PG 2112 + 059, based on two extreme choices of continuum. The fits are composed of amorphous olivine (*dotted line*), forsterite (*dashed line*), alumina (Al_2O_3; *dash-dotted line*), MgO (*dash-triple-dotted line*), and the mean interstellar PAH spectrum (solid line; only in panel 1). The inset in panel 1 shows the strength of PAH features expected in the 5.5–8.5 μm range for a radiation field comparable to that of the Galaxy. Figure taken from [280]

Apart from PG2112+059 crystalline silicates in AGN have only reliably been detected in ULIRGs. In Fig. 21 an example is given where the crystalline silicates have been found in absorption [282]. In a larger sample of 77 ULIRGs, 12 were identified as containing crystalline silicates, with crystalline fractions ranging from 7–13%, using the same definition of crystallinity as used by Kemper et al. [89]. Spoon et al. [282] reject the possibility that the crystallization is due to processing by the AGN, and hypothesize that the crystalline silicates are produced by massive stars originating from the starburst.

The presence of dust is not limited to the local universe, but is ubiquitous throughout the observable universe. Large quantities of dust are clearly present even at early times: submm and far-infrared observations of quasar host galaxies at $z \sim 6$, at a time that the universe is less than 1 Gyr old, show evidence for 10^{8-9} $M_\odot$[283, 284]. Unfortunately, the mineralogy of the dust in these distant galaxies in the infant universe cannot be studied using infrared spectroscopy, with the current generation of telescopes, but the UV extinction curves for a $z = 6.2$ quasar and GRB 050904 ($z = 6.29$) are not consistent with those locally [285, 286], but are similar to what is seen in more nearby AGN [287], suggesting that local AGN analogs exist, and can be used to study the overall dust properties.

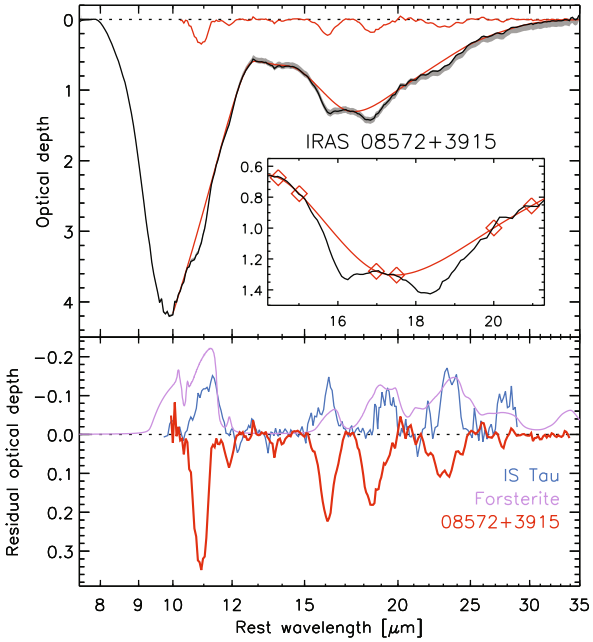

Fig. 21 *Top panel:* Optical depth spectrum of IRAS 08572 + 3915 (black). The gray shading on the spectrum indicates the effect of a different choice of local continuum on the resulting optical depth profile; The smooth thin line is a spline fit to the amorphous silicate profile, ignoring the narrow substructure near 11, 16, 19, and 23 μm. The residual spectral structure, shown at the top of this panel, is too strong to be attributed to imperfections in the fitting method. The features at 11, 16, 19, and 23 μm are attributed to forsterite. *Top panel inset:* Close-up of the 1,421 m range, demonstrating the prescribed placement of spline pivots at 14.5, 15.0, 17.0, 17.5, 20.0, and 21.0 μm. *Bottom panel:* Residual optical depth spectrum of IRAS 08572 + 3915 (negative peaks) is compared to the residual crystalline silicate emissivity of the disk around the young star IS Tau (noisy positive peaks) and the opacity profile of forsterite (smooth positive peaks). The last two spectra have both been scaled by arbitrary factors. Figure taken from [282]

6 Conclusions and Future Directions

Astromineralogy has gained a tremendous momentum with the launch of the Infrared Space Observatory. The spectral resolution of this satellite was perfect for the study of dust at infrared wavelengths. Where IRAS opened the infrared studies at wavelengths up to 23 μm, ISO opened the electromagnetic spectrum beyond 23 μm for systematic investigations. Some pioneering work in this wavelength region was already done by KAO, but the much improved sensitivity of ISO and its wide wavelength coverage allowed much more detailed studies. The legacy of the Spitzer Space Telescope and its Infrared Spectrograph lies in the huge database of high quality spectra it has provided covering many astrophysical environments, ranging from our solar system to distant quasars. Harvesting the IRS legacy has only begun, and much has still to be unravelled.

The future of observational astromineralogy looks bright: the Herschel satellite [288], successfully launched in May of 2009, will provide many new spectra of dusty objects in the 55–200 μm wavelength range. The MIRI [289] imaging spectrograph of the James Webb Space Telescope [290], planned for launch in 2014, will take spectra in the 5–28 μm range with unprecedented sensitivity. And for the even more distant future, the Japanese SPICA mission [291] is a cooled telescope with a 3.5 m primary mirror planned to provide full spectral coverage in the 5–200 μm wavelength range.

With respect to the spatial resolution, Matisse [292] with the VLTI and METIS [293] with the E-ELT will bring (very) high spatial resolution observations at infrared wavelengths. This will allow us to study the dust composition as a function of distance to the central object like young stars with planetary disks, evolved stars with their outflows and AGN's with their torus. This will put tight constraints on dust formation, evolution and destruction models.

Undoubtedly these new missions and instruments will add to our knowledge of the cycle of dust in galaxies, and its role in the formation of stars and planetary systems!

Acknowledgments We would like to thank Sacha Hony, Jan Cami, Jeroen Bouwman, Jolanda van Breemen, Clio Gielen, Henrik Spoon and Frans Rietmeijer for the supply of several figures and Sacha Hony also for the careful reading of the manuscript. We thank Chiyoe Koike, John Bradley, and our colleagues in Amsterdam, Groningen, Leuven and Jena for the numerous discussions about dust in space and in the laboratory. This overview would not have been possible without the help of ADS and Simbad.

References

1. Li, A., Greenberg, J.M.: In dust we trust: an overview of observations and theories of interstellar dust. In: Pirronello, V., Krelowski, J., Manicò, G. (eds.) Solid State Astrochemistry, pp.37–84. Kluwer Academic Publishers, Dordrecht (2003). ISBN 1-4020-1558-5 144
2. de Graauw, T., et al.: Astron. Astrophys. **315**, L49–L54 (1996) 145
3. Clegg, P.E., et al.: Astron. Astrophys. **315**, L38–L42 (1996) 145
4. Kessler, M.F., et al.: Astron. Astrophys. **315**, L27–L31 (1996) 145
5. Werner, M.W., et al.: Astrophys. J. Suppl. **154**, 1–9 (2004) 145
6. Houck, J.R., et al.: Astrophys. J. Suppl. **154**, 18–24 (2004) 145, 153
7. Murakami, H., et al.: Publ. Astron. Soc. Jpn. **59**, 369–376 (2007) 145
8. Bradley, J.P., et al.: Science **285**, 1716–1718 (1999) 145, 152
9. Keller, L., et al.: Nature **417**, 148–150 (2002) 145, 148, 161, 169, 174, 185
10. Molster, F.J., Waters, L.B.F.M., Tielens, A.G.G.M., Koike, C., Chihara, H.: Astron. Astrophys. **382**, 241–255 (2002) 146, 148, 153, 154, 156, 172, 173, 183
11. Tamanai, A., Mutschke, H., Blum, J., Meeus, G., Astrophys. J. **648**, L147–L150 (2006) 147
12. Koike, C., Tsuchiyama, A., Suto, H.: The spectra of crystalline silicates in infrared region. In: Proceedings of the 32nd ISAS Lunar and Planetary Symposium, pp. 175–178 (1999) 146, 147
13. Servoin, J.L., Piriou, B.: Phys. Status Solidi (B) **55**, 677–686 (1973) 146
14. Scott, A., Duley, W.W.: Astrophys. J. Suppl. **105**, 401–405 (1996) 146
15. Dorschner, J., Begemann, B., Henning, T., Jäger, C., Mutschke, H.: Astron. Astrophys. **300**, 503–520 (1995) 147, 149, 152, 156
16. Koike, C., Shibai, H., Tuchiyama, A.: Mon. Not. R. Astron. Soc. **264**, 654–658 (1993) 147, 155

17. Jäger, C., et al.: Astron. Astrophys. **339**, 904–916 (1998) 147, 153, 154, 155, 156
18. Chihara, H., Koike, C., Tsuchiyama, A., Tachibana, S., Sakamoto, D.: Astron. Astrophys. **391**, 267–273 (2002) 147
19. Henning, T., Begemann, B., Mutschke, H., Dorschner, J.: Astron. Astrophys. Suppl. **112**, 143–149 (1995) 147, 161
20. Ordal, M.A., Bell, R.J., Alexander, R.W., Newquist, L.A., Querry, M.R.: Appl. Opt. **27**, 1203–1209 (1988) 147
21. Begemann, B., Dorschner, J., Henning, T., Mutschke, H., Thamm, E.: Astrophys. J. Lett. **423**, L71–L74 (1994). 147, 165
22. Koike, C., et al.: Astrophys. J. **446**, 902–906 (1995) 147
23. Borghesi, A., Bussoletti, E., Colangeli, L., Orofino, V., Guido, M.: Infrared Phys. **26**, 37–42 (1986) 147
24. Pegourie, B.: Astron. Astrophys. **194**, 335–339 (1988) 147
25. von Helden, G., et al.: Science **288**, 313–316 (2000) 147, 167
26. Kemper, F., et al.: Nature **415**, 295–297 (2002) 147, 155, 159, 174, 179
27. Henning, T., Mutschke, H.: Astron. Astrophys. **327**, 743–754 (1997) 147, 148, 162
28. Mennella, V., et al.: Astrophys. J. **496**, 1058–1066 (1998) 147, 148
29. Bowey, J.E., et al.: Mon. Not. R. Astron. Soc. **325**, 886–896 (2001) 147, 148
30. Chihara, H., Koike, C., Tsuchiyama, A.: Publ. Astron. Soc. Jpn. **53**, 243–250 (2001) 147, 148
31. Posch, T., Baier, A., Mutschke, H., Henning, T.: Astrophys. J. **668**, 993–1000 (2007) 147, 153, 159
32. Molster, F.J., Waters, L.B.F.M., Tielens, A.G.G.M.: Astron. Astrophys. **382**, 222–240 (2002) 147, 162, 168
33. Purcell, E.M., Pennypacker, C.R.: Astrophys. J. **186**, 705–714 (1973) 148
34. Draine, B.T.: Astrophys. J. **333**, 848–872 (1988) 148
35. Barber, P.W., Yeh, C.: Appl. Opt. **14**, 2864–2872 (1975) 148
36. Mishchenko, M.I., Travis, L.D., Mackowski, D.W.: J. Quant. Spectrosc. Radiat. Transf. **55**, 535–575 (1996) 148
37. Muinonen, K., et al.: J. Quant. Spectrosc. Radiat. Transf. **55**, 577–601 (1996) 148
38. Min, M., et al.: Astron. Astrophys. **462**, 667–676 (2007) 148, 152, 168, 178
39. Molster, F.J., et al.: Astron. Astrophys. **350**, 163–180 (1999) 148, 156, 161, 174
40. Hoogzaad, S.N., et al.: Astron. Astrophys. **389**, 547–555 (2002) 148, 156
41. Kemper, F., de Koter, A., Waters, L.B.F.M., Bouwman, J., Tielens, A.G.G.M.: Astron. Astrophys. **384**, 585–593 (2002) 148, 152, 156, 162
42. Bowey, J.E., et al.: Mon. Not. R. Astron. Soc. **331**, L1–L6 (2002) 149
43. Draine, B.T., Lee, H. M.: Astrophys. J. **285**, 89–108 (1984) 149, 151
44. Ossenkopf, V., Henning, T., Mathis, J.S.: Astron. Astrophys. **261**, 567–578 (1992) 149, 151, 156
45. Jones, T.W., Merrill, K.M.: Astrophys. J. **209**, 509–524 (1976) 151, 156
46. Pegourie, B., Papoular, R.: Astron. Astrophys. **142**, 451–460 (1985) 151
47. Suh, K.: Mon. Not. R. Astron. Soc. **304**, 389–405 (1999) 151
48. Guertler, J., Henning, T.: Astrophys. Space Sci. **128**, 163–175 (1986). 152
49. Demyk, K., Jones, A.P., Dartois, E., Cox, P., D'Hendecourt, L.: Astron. Astrophys. **349**, 267–275 (1999) 152, 157, 161
50. Demyk, K., Dartois, E., Wiesemeyer, H., Jones, A.P., d'Hendecourt, L.: Astron. Astrophys. **364**, 170–178 (2000) 152
51. Harwit, M., et al.: Astrophys. J. **557**, 844–853 (2001) 152, 162
52. Demyk, K., et al.: Astron. Astrophys. **368**, L38–L41 (2001) 152, 179, 180
53. Lisse, C.M., Chen, C.H., Wyatt, M.C., Morlok, A.: Astrophys. J. **673**, 1106–1122 (2007) 152, 181
54. Lisse, C.M., et al.: Icarus **187**, 69–86 (2007) 152
55. Jura, M., Farihi, J., Zuckerman, B., Becklin, E.E.: Astron. J. **133**, 1927–1933 (2007) 152
56. Jura, M., Farihi, J., Zuckerman, B.: Astron. J. **137**, 3191–3197 (2009) 152
57. Costantini, E., et al.: Astron. Astrophys. **444**, 187–200 (2005) 152
58. Hanner, M.S., Lynch, D.K., Russell, R.W.: Astrophys. J. **425**, 274–285 (1994) 152, 153, 168
59. Hanner, M.S.: Composition and optical properties of cometary dust. In: ASP Conf. Ser. 104: IAU Colloq. 150: Physics, Chemistry, and Dynamics of Interplanetary Dust, p. 367 (1996). 152

60. MacKinnon, I.D.R., Rietmeijer, F.J.M.: Rev. Geophys. **25**, 1527–1553 (1987) 152
61. Bradley, J.P., Humecki, H.J., Germani, M.S.: Astrophys. J. **394**, 643–651 (1992) 152, 153, 168
62. Knacke, R.F., et al.: Astrophys. J. **418**, 440–450 (1993) 152
63. Fajardo-Acosta, S.B., Knacke, R.F.: Astron. Astrophys. **295**, 767–774 (1995) 152
64. Cohen, M., Witteborn, F.C.: Astrophys. J. **294**, 345–256 (1985) 152
65. Aitken, D.K., Smith, C.H., James, S.D., Roche, P.F., Hough, J.H.: Mon. Not. R. Astron. Soc. **230**, 629–638 (1988) 152
66. Sandford, S.A., Walker, R.M.: Astrophys. J. **291**, 838–851 (1985) 153, 168
67. Sitko, M., Lynch, D.K., Russel, R.W.: Astron. J. **120**, 2609–2614 (2000) 153
68. Waelkens, C., et al.: Astron. Astrophys. **315**, L245–L248 (1996) 153
69. Forrest, W.J., et al.: Astron. Astrophys. **154**, 443–447 (2004) 153
70. Apai, D., et al.: Science **310**, 834–836 (2005) 153
71. Furlan, E., et al.: Astrophys. J. **621**, L129–L132 (2005) 153
72. Kessler-Silacci, J., et al.: Astrophys. J. **639**, 275–291 (2006) 153, 157
73. Bouwman, J., et al.: Astrophys. J. **683**, 479–498 (2008) 153, 157
74. Sargent, B. A. et al., Astrophys. J. Suppl. **182**, 477–508 (2009). 153, 157
75. Crovisier, J., et al.: Science **275**, 1904–1907 (1997) 153, 182, 183
76. Kelley, M.S., et al.: Astrophys. J. **651**, 1256–1271 (2006) 153
77. Lisse, C.M., et al.: Science **313**, 635–640 (2006) 153
78. Waters, L.B.F.M., et al.: Astron. Astrophys. **315**, L361–L364 (1996) 153, 156
79. Sloan, G.C., et al.: Astrophys. J. **686**, 1056–1081 (2008) 153
80. Koike, C., et al.: Astron. Astrophys. **363**, 1115–1122 (2000) 153
81. Malfait, K., et al.: Astron. Astrophys. **332**, L25–L28 (1998) 155, 157, 182, 183
82. Watson, D.M.: Mineralization, grain growth, and disk structure: observations of the evolution of dust in protoplanetary disks. In: Henning, Th., Grün, E., Steinacker, J. (eds.) Cosmic Dust-Near and Far. ASP Conference Series. vol. 414, pp. 77–98 ASP, San Francisco, CA (2009). 156
83. Cami, J., de Jong, T., Justtannont, K., Yamamura, I., Waters, L.B.F.M.: Astrophys. Space Sci. **255**, 339–340 (1997) 156
84. Kemper, F., Waters, L.B.F.M., de Koter, A., Tielens, A.G.G.M.: Astron. Astrophys. **369**, 132–141 (2001) 156
85. Molster, F.J., et al.: Astron. Astrophys. **366**, 923–929 (2001) 156
86. Wooden, D.H., et al.: Astrophys. J. **517**, 1034–1058 (1999) 156
87. Brucato, J.R., Colangeli, L., Mennella, V., Palumbo, P., Bussoletti, E.: Planet. Space Sci. **47**, 773–779 (1999) 156
88. Bouwman, J., de Koter, A., Dominik, C., Waters, L.B.F.M.: Astron. Astrophys. **401** 577–592 (2003) 156, 157, 182, 183
89. Kemper, F., Vriend, W.J., Tielens, A.G.G.M.: Astrophys. J. **609**, 826–837 (2004) 157, 158, 191, 192
90. Cesarsky, D., Jones, A.P., Lequeux, J., Verstraete, L.: Astron. Astrophys. **358**, 708–716 (2000) 157
91. van Boekel, R., et al.: Astron. Astrophys. **437**, 189–208 (2005) 157
92. Honda, M., et al.: Astrophys. J. **646**, 1024–1037 (2006) 157
93. van Boekel, R., et al.: Nature **432**, 479–482 (2004) 157, 182
94. Ratzka, T., et al.: Astron. Astrophys. **471**, 173–185 (2007) 157, 182
95. Meeus, G., et al.: Astron. Astrophys. **365**, 476–490 (2001) 157, 182
96. Merín, B., et al.: Astrophys. J. **661**, 361–367 (2007) 157
97. Molster, F.J., et al.: Nature **401**, 563–565 (1999) 158, 159, 172
98. Kemper, F., et al.: Astron. Astrophys. **394**, 679–690 (2002) 159
99. Hellwege, K.H., et al.: Z. Phys. **232**, 61 (1970) 159
100. Barlow, M.J.: Astrophys. Space Sci. **255**, 315–323 (1997) 159, 168
101. Molster, F.J., Waters, L.B.F.M., Tielens, A.G.G.M., Barlow, M.J.: Astron. Astrophys. **382**, 184–221 (2002) 154, 159
102. Ceccarelli, C., et al.: Astron. Astrophys. **395** L29-L33 (2002) 159, 179

103. Stencel, R.E., et al.: Astrophys. J. Lett. **350**, L45–L48 (1990) 159
104. Cami, J.: Ph.D. Thesis, University of Amsterdam, The Netherlands (2002) 159, 160, 161, 170, 185
105. Verhoelst, T., et al.: Astron. Astrophys. **447**, 311–324 (2006) 160
106. Posch, T., et al.: Astron. Astrophys. **352**, 609–618 (1999) 160, 161
107. Vardya, M.S., et al.: Astrophys. J. Lett. **304**, L29–L32 (1986) 160
108. Onaka, T., et al.: Astron. Astrophys. **218**, 169–179 (1989) 160
109. Begemann, B., et al.: Astrophys. J. **476**, 199–208 (1997) 160
110. Huss, G.R., Hutcheon, I.D., Wasserburg, G.J., Stone, J.: Lunar Planet. Sci. Conf. **23**, 29–33 (1992) 160
111. Hutcheon, I.D., Huss, G.R., Fahey, A.J., Wasserburg, G.J.: Astrophys. J. Lett. **425**, L97–L100 (1994) 160
112. Huss, G.R., Fahey, A.J., Gallino, R., Wasserburg, G.J.: Astrophys. J. Lett. **430**, L81–L84 (1994) 160
113. Nittler, L.R., Alexander, C.M.O., Gao, X., Walker, R.M., Zinner, E.K.: Nature **370**, 443 (1994) 160
114. Gail, H.-P., Sedlmayr, E.: Dust formation in M stars. In: Hartquist, T.W., Williams, D.A. (eds.) The Molecular Astrophysics of Stars and Galaxies, pp. 285–312. Oxford University Press, Oxford (1998) 160
115. Patzer, A.B.C., Chang, C., Sedlmayr, E., Sülzle, D., Eur. Phys. J. D **6**, 57–62 (1999) 160, 171
116. Jeong, K.S., Winters, J.M., Sedlmayr, E.: Dust formation in oxygen-rich circumstellar shells around long-period variables. In: Le Bertre, T., Lèbre, A., Waelkens, C. (eds.) Asymptotic Giant Branch Stars, Proceedings of IAU Symposium 191, vol. 191, pp. 233–238. (1999) 160, 171
117. Speck, A.K., Barlow, M.J., Sylvester, R.J., Hofmeister, A.M.: Astron. Astrophys. Suppl. **146**, 437–464 (2000) 161
118. Fabian, D., Posch, T., Mutschke, H., Kerschbaum, F., Dorschner, J.: Astron. Astrophys. **373**, 1125–1138 (2001) 161
119. Nittler, L.R., Alexander, C.M.O., Gao, X., Walker, R.M., Zinner, E.: Astrophys. J. **483**, 475–495 (1997) 161
120. Choi, B.-G., Huss, R.H., Wasserburg, G.J., Gallino, R.: Science **282**, 1284–1289 (1998) 161
121. Posch, T., Kerschbaum, F., Mutschke, H., Dorschner, J., Jäger, C.: Astron. Astrophys. **393**, L7–L10 (2002) 161, 170
122. Bouwman, J., de Koter, A., van den Ancker, M.E., Waters, L.B.F.M.: Astron. Astrophys. **360**, 213–226 (2000) 161
123. Bouwman, J., et al.: Astron. Astrophys. **375**, 950–962 (2001) 162, 182
124. Natta, A., Meyer, M.R., Beckwith, S.V.W.: Astrophys. J. **534**, 838–845 (2000) 162
125. Sargent, B.A., et al.: Astrophys. J. **690**, 1193–1207 (2009) 162
126. Lisse, C.M., et al.: Astrophys. J. **701**, 2019–2032 (2009) 162
127. Martin, P.G., Rogers, C.: Astrophys. J. **322**, 374–392 (1987) 163
128. Mathis, J.S., Rumpl, W., Nordsieck, K.H.: Astrophys. J. **217**, 425–433 (1977) 163, 178
129. Draine, B.: On the interpretation of the λ2175Å feature. In: Allamandola, L.J., Tielens, A.G.G.M. (eds.) Interstellar Dust, Proceedings of IAU Symposium 135, vol. 135, pp. 313–327. Kluwer, Dordrecht (1989) 163
130. Hony, S., Waters, L.B.F.M., Tielens, A.G.G.M.: Astron. Astrophys. **390**, 533–553 (2002) 164, 165, 166, 168
131. Sandford, S.A.: Meteorit. Planet. Sci. **31**, 449–476 (1996) 163
132. Amari, S., Anders, A., Virag, A., Zinner, E.: Nature **345**, 238–240 (1990) 163
133. Zinner, E., Amari, S., Wopenka, B., Lewis, R.S.: Meteoritics **30**, 209–226 (1995) 163
134. Buss, R.H., et al.: Astrophys. J. Lett. **365**, L23–L26 (1990) 163
135. Kwok, S., Volk, K., Bernath, P.: Astrophys. J. Lett. **554**, L87–L90 (2001) 163
136. Robertson, J.: Mater. Sci. Eng. **R37**, 129–281 (2002) 163
137. Hony, S., Tielens, A.G.G.M., Waters, L.B.F.M., de Koter, A.: Astron. Astrophys. **402**, 211–218 (2003) 163, 167, 169
138. Sandford, S.A., et al.: Astrophys. J. **371**, 607–620 (1991) 163
139. Pendleton, Y.J., et al.: Astrophys. J. **437**, 683–696 (1994) 163

140. Tielens, A.G.G.M., et al.: Astrophys. J. Lett. **319**, L109–L113 (1987) 163, 178, 185
141. Lewis, R.S., Ming, T., Wacker, J.F., Anders, E., Steel, E.: Nature **326**, 160–162 (1987) 163, 185
142. Lewis, R.S., Anders, E., Draine, B.T.: Nature **339**, 117–121 (1989) 163
143. Anders, E., Zinner, E.: Meteoritics **28**, 490–514 (1993) 163, 168
144. Guillois, O., Ledoux, G., Reynaud, C.: Astrophys. J. Lett. **521**, L133–L36 (1999) 164, 185
145. Blades, J.C., Whittet, D.C.B.: Mon. Not. R. Astron. Soc. **191**, 701–709 (1980) 164
146. Whittet, D.C.B., McFadzean, A.D., Geballe, T.R.: Mon. Not. R. Astron. Soc. **211**, 29P–31P (1984) 164
147. Terada, H., Imanishi, M., Goto, M., Maihara, T.: Astron. Astrophys. **377**, 994–998 (2001) 164
148. Geballe, T.R., Noll, K.S., Whittet, D.C.B., Waters, L.B.F.M.: Astrophys. J. Lett. **340**, L29–L32 (1989) 164
149. Oudmaijer, R.D., Waters, L.B.F.M., van der Veen, W.E.C.J., Geballe, T.R.: Astron. Astrophys. **299**, 69–78 (1995) 165
150. Van Kerckhoven, C., Tielens, A.G.G.M., Waelkens, C.: Astron. Astrophys. **384**, 568–584 (2002) 165, 185
151. Dai, Z.R., Bradley, J.P., Joswiak, D.J., Brownlee, D.E., Genge, M.J.: Lunar and Planetary Institute Conference Abstracts, vol. 33, p. 1321 (2002) 165
152. Forrest, W.J., Houck, J.R., McCarthy, J.F.: Astrophys. J. **248**, 195–200 (1981) 165
153. Omont, A., et al.: Astrophys. J. **454**, 819–825 (1995) 165
154. Jiang, B.W., Szczerba, R., Deguchi, S.: Astron. Astrophys. **344**, 918–922 (1999) 165
155. Szczerba, R., Henning, T., Volk, K., Kwok, S., Cox, P.: Astron. Astrophys. **345**, L39–L42 (1999) 165
156. Hrivnak, B.J., Volk, K., Kwok, S.: Astrophys. J. **535**, 275–292 (2000) 165
157. Volk, K., Kwok, S., Hrivnak, B.J., Szczerba, R.: Astrophys. J. **567**, 412–422 (2002) 165
158. Chan, K., et al.: Astrophys. J. **483**, 798–810 (1997) 165
159. Goebel, J.H., Moseley, S.H.: Astrophys. J. Lett. **290**, L35–L39 (1985) 165
160. Nuth, J.A., Moseley, S.H., Silverberg, R.F., Goebel, J.H., Moore, W.J.: Astrophys. J. Lett. **290**, L41–L43 (1985) 165
161. Waters, L.B.F.M., et al.: ISO observations of AGB and post-AGB stars. In: The Universe as Seen by ISO, UNESCO, Paris, France, 20–23 October 1998, ESA SP-427, vol. 1, pp. 219–228 (1999) 165
162. Lattimer, J.M., Schramm, D.N., Grossman, L.: Astrophys. J. **219**, 230–249 (1978) 165
163. Savage, B.D., Sembach, K.R.: Annu. Rev. Astron. Astrophys. **34**, 279–330 (1996) 166
164. Kwok, S., Volk, K.M., Hrivnak, B.J.: Astrophys. J. Lett. **345**, L51–L54 (1989) 166
165. Volk, K., Kwok, S., Hrivnak, B.J.: Astrophys. J. Lett. **516**, L99–L102 (1999) 166
166. Hony, S., Waters, L.B.F.M., Tielens, A.G.G.M.: Astron. Astrophys. **378**, L41–L44 (2001) 166
167. Goebel, J.H.: Astron. Astrophys. **278**, 226–230 (1993) 166
168. Begemann, B., Dorschner, J., Henning, T., Mutschke, H.: Astrophys. J. Lett. **464**, L195–L198 (1996) 166
169. Hill, H.G.M., Jones, A.P., D'Hendecourt, L.B.: Astron. Astrophys. **336**, L41–L44 (1998) 166
170. Bernatowicz, T.J., et al.: Astrophys. J. **472**, 760–782 (1996) 167
171. Speck, A.K., Hofmeister, A.M.: Lunar and Planetary Institute Conference Abstracts, vol. 33, p. 1155 (2002) 167
172. Friedemann, C.: Astron. Nachr. **291**, 177–186 (1969) 167
173. Gilra, D.P.: Dust particles and molecules in the extended atmospheres of carbon stars. Proceedings of IAU Symposium 52: Interstellar Dust and Related Topics, vol. 52, pp. 517–528 (1973) 167, 175
174. Hackwell, J.A.: Astron. Astrophys. **21**, 239–248 (1972) 167
175. Forrest, W.J., Gillett, F.C., Stein, W.A.: Astrophys. J. **195**, 423–440 (1975) 167
176. Cohen, M.: Mon. Not. R. Astron. Soc. **206**, 137–147 (1984) 167, 168
177. Baron, Y., Papoular, R., Jourdain de Muizon, M., Pegourie, B., Astron. Astrophys. **186**, 271–279 (1987) 167
178. Willems, F.J.: Astron. Astrophys. **203**, 51–70 (1988) 167

179. Goebel, J.H., Cheeseman, P., Gerbault, F.: Astrophys. J. **449**, 246–257 (1995) 167
180. Treffers, R., Cohen, M.: Astrophys. J. **188**, 545–552 (1974) 168
181. Speck, A.K., Barlow, M.J., Skinner, C. J.: Mon. Not. R. Astron. Soc. **288**, 431–456 (1997) 168
182. Gilman, R.C.: Astrophys. J. Lett. **155**, L185–L187 (1969) 168
183. Kozasa, T., Dorschner, J., Henning, T., Stognienko, R., Astron. Astrophys. **307**, 551–560 (1996) 168
184. Justtanont, K., Yamamura, I., de Jong, T., Waters, L.B.F.M.: Astrophys. Space Sci. **251**, 25–30 (1997) 168
185. Bernatowicz, T., et al.: Nature **330**, 728–730 (1987) 168
186. Huss, G.R., Lewis, R.S.: Geochim. Cosmochim. Acta **59**, 115–160 (1995) 168
187. Mutschke, H., Andersen, A.C., Clément, D., Henning, T., Peiter, G.: Astron. Astrophys. **345**, 187–202 (1999) 168
188. Whittet, D.C.B., Duley, W.W., Martin, P.G.: Mon. Not. R. Astron. Soc. **244**, 427–431 (1990) 168, 178
189. Ferrarotti, A., Gail, H.-P., Degiorgi, L., Ott, H.R.: Astron. Astrophys. **357**, L13–L16 (2000) 168
190. Rietmeijer, F.J.M., MacKinnon, I.D.R.: J. Geophys. Res. Suppl. **90**, 149–155 (1985) 168
191. Bregman, J.D., et al.: Astron. Astrophys. **187**, 616–620 (1987) 168
192. Malfait, K., Waelkens, C., Bouwman, J., de Koter, A., Waters, L.B.F.M.: Astron. Astrophys. **345**, 181–186 (1999) 169
193. Koike, C., Hasegawa, H., Hattori, T.: Astrophys. Space Sci. **88**, 89–98 (1982) 169
194. Koike, C., Shibai, H.: Mon. Not. R. Astron. Soc. **246**, 332–336 (1990) 169
195. Jones, A.P., Tielens, A.G.G.M., Hollenbach, D.J., Astrophys. J. **469**, 740–764 (1996) 170, 177, 180
196. Gail, H.-P., Sedlmayr, E.: Chemistry and physics of molecules and grains in space. Faraday Discuss. **109**, 303–320 (1998). 171
197. Jeong, K.S., Sedlmayr, E., Winters, J.M.: Circumstellar dust shells around oxygen-rich long-period variable stars. In: Astronomische Gesellschaft Meeting Abstracts, vol. 17, p. 30 (2000). 171
198. Ferrarotti, A.S., Gail, H.-P.: Astron. Astrophys. **382**, 256–281 (2002) 171, 173, 176
199. Hallenbeck, S.L., Nuth, J.A., Daukantas, P.L.: Icarus **131**, 198–209 (1998) 171
200. Tielens, A.G.G.M., Waters, L.B.F.M., Molster, F.J., Justtanont, K.: Astrophys. Space Sci. **255**, 415–426 (1997) 172
201. Simis, Y.J.W.: Ph.D. Thesis, Leiden Observatory, The Netherlands (2001) 172
202. Rietmeijer, F.J.M., Nuth, J.A., Karner, J.M.: Astrophys. J. **527**, 395–404 (1999) 173
203. Carrez, P., Demyk, K., Leroux, H., Cordier, P.: Meteorit. Planet. Sci. **36**(Suppl.), A36 (2001) 173, 179
204. Toppani, A., et al.: Nature **437**, 1121–1124 (2005) 174
205. Bradley, J.P.: Science **265**, 925–929 (1994) 174
206. Gail, H.-P., Sedlmayr, E.: Astron. Astrophys. **206**, 153–168 (1988) 175
207. Cherchneff, I., Barker, J.R., Tielens, A.G.G.M.: Astrophys. J. **401**, 269–287 (1992) 175
208. Cherchneff, I., Cau, P.: The chemistry of carbon dust formation. Proceedings of IAU Symposium 191: Asymptotic Giant Branch Stars, vol. 191, pp. 251–259 (1999) 175
209. Yamamura, I., Dominik, C., de Jong, T., Waters, L.B.F.M., Molster, F.J.: Astron. Astrophys. **363**, 629–639 (2000) 176
210. Waters, L.B.F.M., et al.: Astron. Astrophys. **331**, L61–L64 (1998) 176
211. Cohen, M., et al.: Astrophys. J. Lett. **513**, L135–L138 (1999) 176
212. Cohen, M., Barlow, M.J., Liu, X.-W., Jones, A.F.: Mon. Not. R. Astron. Soc. **332**, 879–890 (2002) 176
213. Zijlstra, A.A., et al.: Astron. Astrophys. **243**, L9–L12 (1991) 176
214. Iben, I.: Astrophys. J. **277**, 333–354 (1984) 176
215. Waters, L.B.F.M., et al.: Nature **391**, 868–871 (1998) 176
216. Van Winckel, H.: Annu. Rev. Astron. Astrophys. **41**, 391–427 (2003) 176
217. Waters, L.B.F.M., Trams, N.R., Waelkens, C.: Astron. Astrophys. **262**, L37–L40 (1992) 176
218. De Marco, O., Barlow, M.J., Cohen, M.: Astrophys. J. Lett. **574**, L83–L86 (2002) 176
219. Chesneau, O., et al.: Astron. Astrophys. **455**, 1009–1018 (2006) 176
220. Deroo, P., et al.: Astron. Astrophys. **450**, 181–192 (2006) 176

221. Arendt, R.G., Dwek, E., Moseley, S.H.: Astrophys. J. **521**, 234–245 (1999) 177
222. Douvion, T., Lagage, P.O., Pantin, E.: Astron. Astrophys. **369**, 589–593 (2001) 177
223. Kozasa, T., Hasegawa, H., Nomoto, K.: Astron. Astrophys. **249**, 474–482 (1991) 177
224. Douvion, T., Lagage, P.O., Cesarsky, C.J.: Astron. Astrophys. **352**, L111–L115 (1999) 177
225. Rho, J., et al.: Astrophys. J. **673**, 271–282 (2008) 177
226. Evans, A.: Formation and evolution of dust in novae. Proceedings of IAU Colloquium 122: Physics of Classical Nova, pp. 253–263 (1990) 177
227. Jones, A.P.: J. Geophys. Res. **105**, 10257–10268 (2000).
228. Tang, M., Anders, E.: Astrophys. J. Lett. **335**, L31–L34 (1988) 178
229. Sandford, S.A., Pendleton, Y.J., Allamandola, L.J.: Astrophys. J. **440**, 697–705 (1995) 178
230. Day, K.L.: Mon. Not. R. Astron. Soc. **178**, 49P–51P (1977) 178
231. Bradley, J.P.: Meteoritics **29**, 447 (1994) 179
232. Chiar, J.E., Tielens, A.G.G.M.: Astrophys. J. **637**, 774–785 (2006) 180
233. Chiar, J.E., et al.: Astrophys. J. **666**, L73–L76 (2007) 180
234. Molster, F.J., Bradley, J.P.: Meteorit. Planet. Sci. Suppl. **36**, A140–A141 (2001) 180
235. Harker, D.E., Desch, S.J.: Astrophys. J. Lett. **565**, L109–L112 (2002) 182
236. Ábrahám, P., et al.: Nature **459**, 224–226 (2009) 182
237. Nuth, J.A., Hill, H.G.M., Kletetschka, G.: Nature **406**, 275–276 (2000) 182
238. Bockelée-Morvan, D., Gautier, D., Hersant, F., Huré, J.-M., Robert, F.: Astron. Astrophys. **384**, 1107–1118 (2002) 182
239. Lawson, W.A., Lyo, A.-R., Muzerolle, J.: Mon. Not. R. Astron. Soc. **351**, L39–L43 (2004) 182
240. Bouwman, J., et al.: Astrophys. J. **653**, L57-L60 (2006) 184
241. Gail, H.-P.: Astron. Astrophys. **332**, 1099–1122 (1998) 184
242. Murata, K., et al.: Astrophys. J. **698**, 1903–1906 (2009) 183
243. Chang, C.P., Flamm, D.L., Ibbotson, D.E., Mucha, J.A.: J. Appl. Phys. **63**, 1744–1748 (1988) 184
244. Daulton, T.L., Eisenhour, D.D., Bernatowicz, T.J., Lewis, R.S., Buseck, P.R.: Geochim. Cosmochim. Acta **60**, 4853–4872 (1996). 185
245. Brownlee, D.E., Joswiak, D.J., Bradley, J.P., Gezo, J.C., Hill, H.G.M.: Lunar and Planetary Institute Conference Abstracts, vol. 31, p. 1921 (2000) 185
246. Feast, M., Publ. Astron. Soc. Pac. **111**, 775–793 (1999). 186
247. Hilditch, R.W., Howarth, I.D., Harries, T.J.: Mon. Not. R. Astron. Soc. **357**, 304–324 (2005) 186
248. Westerlund, B.E.: The Magellanic Clouds. Cambridge University Press, Cambridge (1997) 186
249. Rolleston, W.R.J., Venn, K., Tolstoy, E., Dufton, P.L.: Astron. Astrophys. **400**, 21–30 (2003) 186
250. Misselt, K.A., Clayton, G.C., Gordon, K. D.: Astrophys. J. **515**, 128–139 (1999) 186
251. Gordon, K.D., Clayton, G.C.: Astrophys. J. **500**, 816–824 (1998) 186
252. Voors, R.H.M., Waters, L.B.F.M., Morris, P.W., Trams, N.R., de Koter, A., Bouwman, J.: Astron. Astrophys. **341**, L67–L70 (1999) 187
253. Dijkstra, C., Speck, A.K., Reid, R.B., Abraham, P.: Astrophys. J. Lett. **633**, L133–L136 (2005) 187
254. Kastner, J.H., Buchanan, C.L., Sargent, B., Forrest, W.J.: Astrophys. J. Lett. **638**, L29–L32 (2006) 187
255. Gielen, C.: Ph.D. Thesis, Institute of Astronomy, K.U. Leuven, Belgium (2009) 187
256. Gielen, C., et al.: Astron. Astrophys. **490**, 725–735 (2008) 187
257. Zijlstra, A.A., et al.: Mon. Not. R. Astron. Soc. **370**, 1961–1978 (2006) 187
258. Sloan, G.C., et al.: Astrophys. J. **638**, 472–477 (2006) 188
259. Sloan, G.C., et al.: Astrophys. J. **645**, 1118–1130 (2006) 188
260. Lagadec, E., et al.: Mon. Not. R. Astron. Soc. **376**, 1270–1284 (2007) 188
261. Lagadec, E., et al.: Mon. Not. R. Astron. Soc. **396**, 598–608 (2009) 188
262. Sloan, G.C., et al.: Science **323**, 353–355 (2009) 188
263. Leisenring, J.M., Kemper, F., Sloan, G.C.: Astrophys. J. **681**, 1557–1573 (2008) 188
264. Sylvester, R.J., et al.: Astron. Astrophys. **352**, 587-599 (1999) 189
265. Speck, A.K., et al.: Astrophys. J. **650**, 892–900 (2006) 188
266. Gruendl, R.A., et al.: Astrophys. J. **688**, L9–L12 (2008) 188, 190

267. Stanghellini, L., et al.: Astrophys. J. **671**, 1669–1684 (2007) 189
268. Tappe, A., Rho, J., Reach, W.T.: Astrophys. J. **653**, 267–279 (2006) 190
269. Bouchet, P., et al.: Astrophys. J. **650**, 212–227 (2006) 190
270. Imanishi, M., Ueno, S.: Astrophys. J. **535**, 626–631 (2000) 190
271. Siebenmorgen, R., Haas, M., Krügel, E., Schulz, B.: Astron. Astrophys. **436**, L5–L8 (2005) 191
272. Sturm, E., et al.: Astrophys. J. **629**, L21–L23 (2005) 191
273. Hao, L., et al.: Astrophys. J. **625**, L75–L78 (2005) 191
274. Shi, Y., et al.: Astrophys. J. **653**, 127–136 (2006) 191
275. Jaffe, W., et al.: Nature **429**, 47–49 (2004) 191
276. Rhee, J.H., Larkin, J.E.: Astrophys. J. **640**, 625–638 (2006) 191
277. Roche, P.F., Packham, C., Aitken, D.K., Mason, R.E.: Mon. Not. R. Astron. Soc. **375**, 99–104 (2007) 191
278. Smith, H.A., et al.: Bull. Am. Astron. Soc. **41**, 238 (2009) 191
279. Li, M.P., Shi, Q.J., Li, A.: Mon. Not. R. Astron. Soc. **391**, L49–L53 (2008) 191
280. Markwick-Kemper, F., Gallagher, S.C., Hines, D.C., Bouwman, J.: Astrophys. J. **668**, L107–L110 (2007) 191
281. Elvis, M., Marengo, M., Karovska, M.: Astrophys. J. **567**, L107–L110 (2002) 191, 192
282. Spoon, H.W.W., et al.: Astrophys. J. **638**, 759–765 (2006) 191
283. Priddey, R.S.: Mon. Not. R. Astron. Soc. **344**, L74–L78 (2003) 192, 193
284. Beelen, A.: Astrophys. J. **642**, 694–701 (2006) 192
285. Maiolino, R., et al.: Nature **431**, 533–535 (2004) 192
286. Stratta, G., Maiolino, R., Fiore, F., D'Elia, V.: Astrophys. J. **661**, L9–L12 (2007) 192
287. Maiolino, R., et al.: Astron. Astrophys. **365**, 28–36 (2001) 192
288. Pilbratt, G.L.: EAS Publications Series **35**, 15–31 (2009) 192
289. Wright, G.S., et al.: SPIE Conference Series **7010** (2008) 194
290. Gardner, J.P., et al.: Space Sci. Rev. **123**, 485–606 (2006) 194
291. Swinyard, B., et al.: Exp. Astron. **23**, 193–219 (2009) 194
292. Lopez, B., et al.: Science with the VLT in the ELT Era. In: Astrophysics and Space Science Proceedings, pp. 353–357. Springer, The Netherlands (2009) 194
293. Brandl, B.R., et al.: SPIE Conference Series **7014** (2008) 194
294. Juhász, A., et al.: Astrophys. J. (2010, in press) 194

The Mineralogy of Cometary Dust

M.S. Hanner and M.E. Zolensky

Abstract Cometary dust is a heterogeneous mixture of unequilibrated olivine and pyroxenes, amorphous silicates, Fe-Ni sulfides, and minor amounts of oxides and other minerals. While forsterite (Mg_2SiO_4) and enstatite ($MgSiO_3$) are the most common silicate minerals, both the olivine and pyroxenes also show a wide range in Mg/Fe in at least some comets. Carbon in the dust is enriched relative to CI chondrites; a significant fraction of the carbon is in the form of organic refractory material. The return of the particulate sample from ecliptic comet 81P/Wild 2 has opened up a new window for revealing the dust mineralogy at a level of detail not previously possible. The most interesting result from the Wild 2 sample to date is the discovery of refractory calcium aluminum-rich inclusions (CAI) similar to those found in primitive meteorites; chondrule fragments are also present.

Comets formed in the outer parts of the solar nebula where temperatures remained low enough so that interstellar grains could have survived. The small glassy silicates in comets may indeed be interstellar grains. The CAI and the widespread, abundant crystalline silicates must have condensed in the hot inner solar nebula; their presence in comets is evidence for strong radial mixing in the solar nebula. The preponderance of Mg-rich silicates has a natural explanation in the condensation sequence; they are the first to condense in a hot gas and only react with iron at lower temperatures.

This review discusses the mineralogy of cometary dust determined from infrared spectroscopy, in situ Halley measurements, IDPs, and the captured particles from comet Wild 2.

M.S. Hanner (✉)
University of Massachusetts, Amherst, MA 01003, USA
e-mail: mhanner@astro.umass.edu

M.E. Zolensky
NASA Johnson Space Center, Houston, TX 77058, USA
e-mail: Michael.E.Zolensky@nasa.gov

Hanner, M.S., Zolensky, M.E.: *The Mineralogy of Cometary Dust*. Lect. Notes Phys. **815**, 203–232 (2010)
DOI 10.1007/978-3-642-13259-9_4

1 Introduction

Comets contain some of the most primitive material surviving from the early solar system. The comets we see today come from two reservoirs. The Oort Cloud, at heliocentric distance, $r \sim 10^4$–10^5 AU, is the source of the nearly isotropic comets (new and long-period comets). The nearly isotropic comets formed in the region of the giant planets, and were dynamically scattered to the Oort Cloud, as described by [1]. The ecliptic comets, with their shorter periods and low inclination orbits, have migrated inward from the Kuiper Belt region beyond Neptune. Several dynamical classes are recognized in the Kuiper Belt. The Scattered Disk consists of those objects on orbits that could have encountered Neptune on its present orbit at least once during the past 4 Gyr [2]. The classical Kuiper Belt contains objects on orbits that have not interacted with Neptune in the past 4 Gyr. It is further divided into "cold" objects with orbital inclinations less than 4 degrees and "hot" objects with orbital inclinations up to 30 degrees or more. A smaller resonant population includes objects in mean motion resonances with Neptune, such as the Plutinos (2:3 resonance). Ecliptic comets are thought to be supplied primarily by the Scattered Disk, based on numerical simulations by [3, 4]. However, Volk and Malhotra [5] concluded that the number of ecliptic comets from the scattered disk and from the classical Kuiper Belt could be comparable; the scattered disk is a more efficient source, but the classical Kuiper Belt contains more objects. Which source dominates depends on the uncertain extrapolation of the size distribution down to km-sized objects for the scattered disk and Kuiper Belt respectively.

Dynamical simulations indicate that the scattered disk objects formed initially at $r < 30$ AU and were scattered outward by Neptune [3, 6]. Whether the classical Kuiper Belt objects formed in their present location is still under debate; the required mass is far larger than the current mass of the Kuiper Belt. The "hot" Kuiper Belt may represent objects in the disk of planetesimals at $r \sim 20 - 35$ AU that had a history of close encounters with Neptune as it migrated outward through the planetesimal disk [7]. Reference [8] has proposed that the dynamically "cold" population formed at $r < 35$ AU and were "pushed" outward by the 2:1 mean motion resonance with Neptune during Neptune's final migration to its present orbit.

To summarize, dynamical simulations by a number of authors predict that the 4 giant planets formed in a more compact arrangement and the disk of planetesimals extended to about 30–35 AU. The giant planets migrated to their present orbits via energy and momentum exchange with the disk of planetesimals, in the process scattering icy planetesimals into the region of the Kuiper Belt.

Thus, all comets that approach the inner solar system today most likely formed between 5 and 35 AU in the solar nebula. This region of the solar nebula was cold enough that pre-existing interstellar grains, organic material and even interstellar ices could have been incorporated into the growing comet nuclei. Was the solar nebula composition uniform across this wide region? What was the extent of radial mixing of material formed in the warm inner solar nebula? What fraction of the material retained in comets is presolar? Studying compositional differences among comets in their ices, organic material, and refractory grains will help to answer these questions.

In 1950, comet nuclei were first described as icy conglomerate objects a few km in size, whose activity is due primarily to the sublimation of water ice [9]. Over the past 60 years, remote sensing from Earth and several spacecraft flybys, beginning with 1P/Halley in 1986, have filled in our picture. Nuclear diameters range from a few hundred meters to Hale-Bopp's $\sim$ 40 km nucleus [10]. The small fragments detected as sun-grazing comets [11] and the observed cases of nucleus fragmentation, such as comet Shoemaker-Levy 9 [12], which was torn apart during a close pass by Jupiter in 1992, indicate that the internal strength of at least some comet nuclei is low, consistent with a collisional history.

In most comets, outgassing appears to be confined to perhaps 10% of the surface, based on the spacecraft images of comet P/Halley [13], P/Borrelly [14], 81P/Wild 2 [15], and 9P/Tempel 1 [16]. The rest of the surface is covered with dark, non-volatile material. While water is the dominant sublimating ice, some comets are enriched in more volatile species, such as CO, and display activity at large heliocentric distances. Many other molecules have been detected at the 0.1–5% level [17–19]

Solid particles are entrained in the outflowing gas to form a dust coma. The dust detectors on board the Halley probes in 1986 detected particle masses from 10^{-16} to 10^{-3} g [20]. Small particles are dispersed by solar radiation pressure, while large particles (mm-cm sized) form dust trails along the cometary orbit [21, 22]. Although micron-sized particles contribute much of the observed scattered light and thermal emission from the dust coma, most of the particulate mass is contained in the large particles, based on the measured Halley dust mass distribution and the mass distribution derived from infrared observations of dust trails.

Mineralogy of cometary dust can be studied remotely via infrared spectroscopy of the dust coma. Additionally, interplanetary dust particles (IDPs), if their cometary origin can be inferred, allow detailed study of particle structure and mineralogy. Of course, in situ sampling and sample return provide far more detailed compositional and mineralogical information for specific comets. In this regard, the return of the Stardust 81P/Wild 2 dust sample in January 2006 has been a major milestone. This review will discuss and compare the mineralogy determined from infrared spectroscopy, IDPs, and the laboratory analysis of captured particles from comet Wild 2.

2 Mineralogy from Infrared Spectroscopy

Although sample return and in situ experiments can provide detailed analysis for a few comets, only Earth-based observations are possible for most comets. Mid-infrared spectroscopy is the best tool for remotely assessing the mineralogy of comet dust, documenting the differences among comets, and comparing to similar spectroscopy of interstellar and circumstellar dust. Small silicate particles in the optically thin dust coma will generate the characteristic 10 and 16–35 μm spectral features in emission. The 10 μm feature lies within the 8–13 μm atmospheric window and ground-based spectra are now available for a number of comets.

Ever since the first 8–13 μm spectra of comet P/Halley, it has been recognized that crystalline silicates are a significant component of cometary dust [25, 23]. These

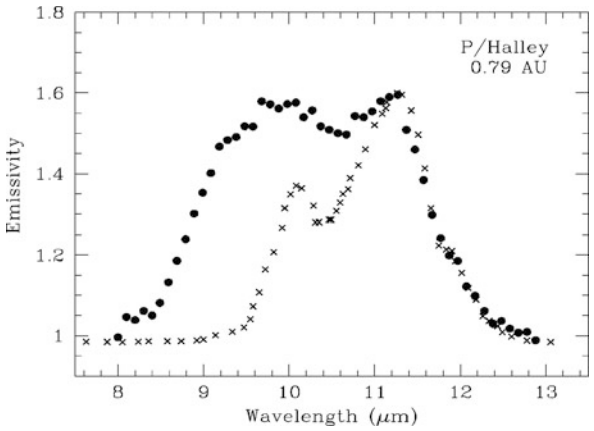

Fig. 1 Olivine feature in comet 1P/Halley. *filled circles*: spectrum from [23] divided by a 360 K blackbody; *crosses*: measured relative emissivity of ground forsterite (Mg-olivine) from [24]

spectra clearly indicated the presence of crystalline olivine from its distinctive peak at 11.2 μm (Fig. 1). The wavelength of the peak is indicative of Mg-rich olivine (forsterite). It is also evident from Fig. 1 that other silicate minerals must be present to explain the full width of the feature. However, uncertainty in the correction for the telluric ozone feature near 9.5 μm made 9–10 μm spectral structure in these spectra uncertain.

The bright comet (C/1995 O1) Hale-Bopp exhibited one of the strongest silicate features ever seen in a comet. The dust coma was observed in the infrared from 4.6 AU preperihelion through perihelion at $r = 0.93$ to 3.9 AU postperihelion, and a number of 8–13 μm spectra were obtained [26–29]. The high signal/noise in these spectra have enabled the silicate mineralogy to be determined. Moreover, full 16–40 μm spectra of Hale-Bopp were acquired for the first time by the SWS instrument on board ESA's Infrared Space Observatory (ISO).

The SWS spectrum taken when the comet was at 2.8 AU from the Sun before perihelion is presented in Fig. 2 [30, 31]. All of the major spectral peaks correspond to those of forsterite [32]. Minor structure is attributed to crystalline pyroxene [29].

A typical 8–13 μm spectrum near perihelion is shown in Fig. 3. One sees maxima at 9.2, 10.0, and 11.2 μm and minor structure at 10.5 and 11.9 μm. These peaks appear consistently in spectra taken with 4 different instruments over several months under a wide range of observing conditions. The 11.2 μm olivine peak is similar to that seen in comet Halley; the 11.9 μm shoulder is also due to olivine. The 9.2 μm maximum is evidence of pyroxene grains. The broad maximum in the spectrum near 10 μm can be produced by glassy or amorphous olivine; crystalline olivine may also contribute. The overall width of the silicate feature, its relatively flat top from 10 to 11 μm, and the structure near 10.5 μm are most likely due to crystalline pyroxene. Crystalline pyroxenes display considerable variety in their spectral shapes. Pyroxene-rich IDPs tend to have a broad feature with peaks in the 10–11 μm region [33] and a few have a peak near 9.3 μm as well [34]. The orthorhombic orthoenstatite measured by [24] exhibited a narrow feature sharply peaked at 9.9 μm.

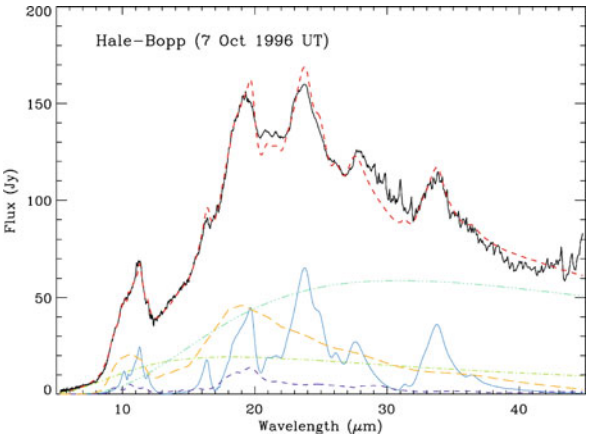

Fig. 2 ISO/SWS spectrum of comet Hale-Bopp at 2.8 AU compared with a dust model. Solid curve: SWS spectrum; dashed curve: best-fit emission model. The components comprising the model are shown in the lower curves: forsterite, orthopyroxene, amorphous pyroxene, and smooth blackbody curves for $T = 280\,\mathrm{K}$ and $T = 165\,\mathrm{K}$. The major spectral peaks are due to forsterite (*from* [30])

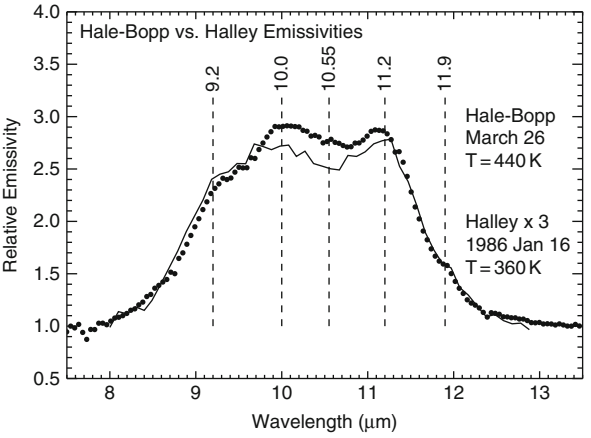

Fig. 3 The silicate feature in Hale-Bopp (*filled circles*) [27] and P/Halley (*line*) [23]. Each spectrum has been divided by a blackbody at the temperature shown and the Halley spectrum has been multiplied by 3. (*from* [27])

To produce a strong emission feature, silicate particles must have radii of order 1 μm or smaller. Larger particles will display a strong feature only if they are very porous aggregates, such that the individual small constituent grains radiate essentially independently [35, 36].

Several authors have modelled the Hale-Bopp silicate spectra, using various mixtures of crystalline and amorphous olivine and pyroxene [28, 29, 34, 37–41]. The strength of an emission feature produced by a small grain will depend on its emissivity and temperature. The emissivity is a function of grain size, shape and porosity, as well as composition and crystal structure. The temperature of a silicate particle in the comet coma is controlled by the balance between absorption of solar radiation and infrared emission and will vary with grain size, Mg/Fe ratio, and contact with absorbing material. To determine quantitative results for the relative abundance of various silicate minerals, all of these parameters have to be modelled for each grain

component. The underlying quasi-blackbody continuum is usually modelled with small warm carbonaceous grains. One small consolation for this complexity is that the dust coma is optically thin.

The most extensive modelling was carried out by [40], who explicitly included porosity among the fitting parameters. Measured emissivities were adopted for the crystalline components and Mie theory was applied to compute emissivities for the amorphous components. A wide wavelength range is needed to constrain the grain temperatures; the SWS spectrum was used at 2.8 AU preperihelion and 3–18 μm photometry together with 8–13 μm spectra were used near perihelion. The authors find crystalline olivine to be the dominant silicate mineral, not surprising given the strong peaks in Fig. 2. The crystalline pyroxene abundance increased near perihelion, as the 9.3 μm peak became more pronounced. The mass ratio of crystalline to amorphous silicates increased from ∼1.5 at 2.8 AU to ∼3.7 near perihelion. The grain size distribution steepened as the comet approached perihelion, with relatively more submicron-sized grains and higher porosity. These smaller and/or fluffier grains were more pronounced in jets [28] and may have been dredged up from deeper layers below the nucleus surface, or they could result from particle fragmentation and loss of organic refractory mantles.

Reference [41] applied their dust model from 9P/Tempel (described below) to the SWS spectrum of Hale-Bopp. They found that they could achieve an acceptable fit with the same compositional mix as that in 9P/Tempel, including minor amounts of sulfides, hydrated silicates, PAHs, and carbonates. In contrast to 9P/Tempel, no Fe-olivines were evident in Hale-Bopp.

Hale-Bopp and P/Halley are both Oort Cloud comets. Other Oort Cloud comets with similar silicate features include Levy (C/1990 K1) [42], Bradfield (C/1987 P1) [42], Mueller (C/1993 A1) [43], Hyakutake (C/1996 B2), and C/2002 V1 NEAT [44, 45]. The 8–13 μm spectrum of comet Mueller is fit exactly by the same silicate model used to fit Hale-Bopp by Hayward et al. [28], although the ratio of small silicates to featureless absorbing material is somewhat lower. The dynamically new Oort Cloud comet C/2001 Q4 NEAT also exhibited a strong silicate feature; thermal emission models indicate the same relative mineral abundances as in Hale-Bopp, although Q4 had a somewhat larger mean grain size [46].

The 8–13 μm spectra of four other new comets discussed in [42] are puzzling; each has a unique, and not understood, spectrum. Comet Austin (1990 V) showed a feature 20% above the continuum with a maximum near 9 μm while Okazaki-Levy-Rudenko (1989 XIX) displayed a 20% feature with a broad maximum at 11–11.5 μm.

In contrast to the Oort Cloud comets, ecliptic comets generally show broad weak 10 μm emission ∼20% above a black-body continuum, once thermal emission from the nucleus has been accounted for. A recent review is given by [47]. The absence of strong silicate emission in the short-period comets could be explained either by a difference in the dust composition between Oort Cloud and ecliptic comets or by a lack of submicron-sized particles in the coma. Short-period comets have generally been outgassing during many orbits in the inner solar system and the smaller or more fluffy particles may have preferentially been expelled over time, leaving a lag

deposit of larger and more compact particles on the surface. Perhaps it is these larger particles that are now being entrained in the outflowing gas.

Any debate that ecliptic comets, as a class, have a different composition was effectively ended by the Deep Impact mission to comet 9P/Tempel 1 in 2005. One of the goals of the Deep Impact mission was to examine whether the composition of the dust and gas released from beneath the surface differed from the material in the ambient coma [16]. A 370 kg impactor was released by the spacecraft and impacted the surface at 10.3 km/s, creating a crater and releasing a large cloud of debris. Several infrared spectra of the ejecta cloud were obtained from ground-based telescopes and from the Spitzer Space Telescope [48, 49]. These spectra left little doubt that the sub-surface dust composition of 9P/Tempel 1 is very similar to that of the Oort Cloud comets.

Spitzer spectra of Tempel 1 are shown in Fig. 4 [48]. The pre-impact spectrum (lowest curve) shows broad 8–12 μm and 15–20 μm emission ∼20% above the continuum, while the impact spectrum displays the strong, structured silicate features typical of Oort Cloud comets. The impact spectrum is very similar to the spectrum of Hale-Bopp (upper curve)

Lisse et al. [48] have modelled the Spitzer impact spectrum by testing emissivity models for more than 80 candidate mineral species, folded into modelled temperature, size distribution, and porosity of the grains. The authors used the chi-squared value of the fit as the criterion for accepting any new species into the model. Their final model includes 15 components. In addition to the expected crystalline and amorphous olivine and pyroxenes, they find that hydrated silicates account for 8%

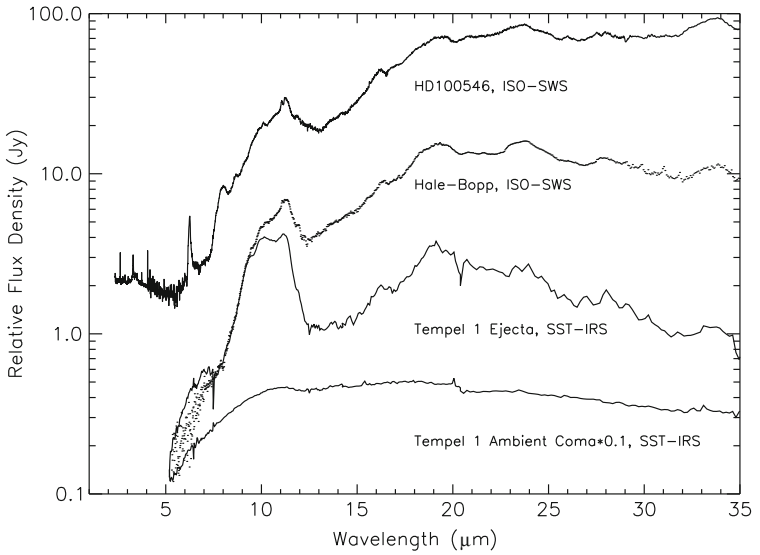

Fig. 4 Comparison of the Spitzer spectrum of comet P/Tempel 1 ejecta following DI impact with the quiescent spectrum of the Tempel 1 dust coma, the ISO spectrum of Hale-Bopp, and the spectrum of Herbig AeBe star HD100546. (*from* [48])

of all silicates, carbonates contribute ~5% of the grain surface area, and PAHs are present. Residual emission at 27–30 μm is attributed to sulfides. While forsterite was the major olivine mineral, Fe-rich fayalite was also detected and Fe-rich pyroxene was more abundant than Mg-rich pyroxene.

Carbonate grains and PAHs have emission features in the 5–7 μm spectral region. Woodward et al. [50] analyzed the 5.5–7.5 μm Spitzer spectrum of comet C/2003 K4 LINEAR at $r = 1.76$ AU preperihelion. After the ν_2 band of water was modeled and fit to the spectrum, no evidence of PAH emission at 6.2 μm or carbonate emission at 7 μm was seen. A similar analysis of the 5.5–7.5 μm Tempel 1 Spitzer spectrum was reported by [51]. Again, no PAH 6.2 μm emission was present after fitting the water bands, although some residual emission remained and 7 μm carbonate emission was not ruled out. Thus, identification of carbonates or PAHs in 5–7.5 μm spectra of comets depends critically on the modeling of the water bands.

In summary, then, at least one ecliptic comet has a small-particle composition similar to that observed for a number of Oort Cloud comets, suggesting that the broad weak silicate emission typically seen in ecliptic comets is likely due to larger or more absorbing particles from the nucleus surface. During the temporal evolution of the Deep Impact ejecta, infrared observers noted that the changing continuum flux indicated that the fastest ejecta material, from the original nucleus surface, was primarily dark amorphous carbon grains, mixed with amorphous olivine [49].

Despite the recent advances, remote spectroscopy does have limitations. Disadvantages of IR spectroscopy for inferring comet dust mineralogy are (1) the quantitative abundance determinations may not be unique, because of the large number of modelling parameters and (2) the micron and sub-micron sized grains producing the emission features may represent only a small fraction of the total mass of solid material released from the comet. The modelling is more uncertain when only ground-based 8–13 μm spectra are available, because the grain temperatures are not well constrained. Complete 5–40 μm spectra are necessary to interpret fully the silicate mineralogy and the presence of minor components.

3 In Situ Sampling

The first in situ measurements of dust composition were obtained during comet P/Halley's perihelion passage in 1986. The two Soviet Vega missions and the European Space Agency's Giotto mission sent to fly past comet Halley each carried an impact ionization time of flight mass spectrometer to measure the elemental composition of the dust [52, 53]. All together, the composition was recorded for about 5,000 particles in the mass range 10^{-16}–10^{-11} g. Although the total mass of material measured was only a few nanograms, it was sampled over tens of thousands of km in the coma along three spacecraft tracks. These experiments are described further in the chapter by Mann and Jessberger.

The sampled particles are divided into three main types: mass spectra dominated by the major rock-forming elements, Mg, Si, Ca, Fe; mass spectra consisting pri-

marily of the light elements H,C,O,N, the "CHON" particles; and mixed spectra containing both the rock and CHON elements. If we define mixed particles as having a ratio of carbon to rock-forming elements between 0.1 and 10, then ∼50% of the particles are mixed and ∼25% are rock and CHON respectively [54]. At some level, however, the CHON and rocky material are mixed down to the finest submicron scale in all particles [55]. The bulk abundances of the major rock-forming elements are solar (chondritic) within a factor of ∼2 [56, 57]. (Conversion of the mass spectra to relative elemental abundances depends on the ion yields, which are uncertain by at least a factor of 2 because of the impossibility of calibrating the instrument at the flyby speed of ∼70 km/s). The CHON elements, especially C,H,N, are enriched relative to CI-chondrites, classifying the cometary material as more "primitive" than the carbonaceous chondrite meteorites.

The rocky material displays a wide range in Fe/Mg, but a narrow range in Si/Mg [57, 58]. The range in Fe/Mg is distinctly different from that of primitive meteorites. Mg-rich (Fe-poor) silicates comprise at least 40% and maybe ≥60% of the rocky particles [56]. Iron is present in other minerals including metals (1–2%), iron oxide (≤1%) and iron sulfides (∼10%) [59].

Isotopic ratios are solar, within the measurement uncertainties, with the exception of $^{12}C/^{13}C$, which displays a wide range [56, 60]. While low ratios (^{13}C enrichment) are uncertain due to noise of uncertain origin, definite ^{12}C enrichments, up to $^{12}C/^{13}C$ ∼5000 have been identified, indicative of presolar nucleosynthesis products.

4 Interplanetary Dust Particles of Probable Cometary Origin

The submicron grain size, high Mg/Fe ratio, and mix of crystalline and non-crystalline olivine and pyroxenes inferred from infrared spectroscopy and the Halley sampling have no counterpart in any meteoritic material, with the exception of the anhydrous chondritic aggregate interplanetary dust particles (IDPs). These are fine-grained heterogeneous aggregates having chondritic abundances of the major rock–forming elements; they comprise a major fraction of the IDPs captured in the stratosphere [61, 62] ("The Astromineralogy of Interplanetary Dust Particles" by Bradley, this volume). Typical grain sizes within the aggregates are 0.1–0.5 μm; micron-sized crystals, primarily forsterite and enstatite, are also present. These aggregate IDPs are thought to originate from comets, based on their porous structure, small grain size, high carbon content, and relatively high atmospheric entry velocities. The entry velocities are deduced mainly by measurement of noble gas concentrations [63]. The match between the mineral identifications in the Hale-Bopp spectra and the silicates seen in the anhydrous IDPs strengthens the link between comets and this class of IDPs.

Thus, the dust composition and physical structure of chondritic aggregate IDPs can be used to augment our understanding of the nature and origin of cometary dust. These IDPs are a mixture of crystalline and non-crystalline silicate particles embedded in dark, carbon-rich matrix material. Their aggregate structure suggests

that the larger particles in comets are aggregates of small grains, with a range of porosities.

The mineralogy of the anhydrous chondritic IDPs can be described as consisting of matrix, coarse-grained phases and Glass with Embedded Metal and Sulfides (GEMS) [62] ("The Astromineralogy of Interplanetary Dust Particles" by Bradley, this volume). The coarse-grained phases are mainly (1) olivine, with a Mg/Fe composition ranging from Fo_{50-100}, and a pronounced peak at almost pure forsterite, Fo_{99}; (2) low-Ca pyroxene, with a Mg/Fe composition ranging from enstatite fraction En_{50-100} and a peak at En_{99}, and occasionally having a whisker or plate morphology [64]; and (3) troilite and pyrrhotite [65]. Olivine crystals sometimes have significant concentrations of CaO (<0.2 wt%), MnO (<0.7 wt%) and Cr_2O_3 (<0.3 wt%). Low-Ca pyroxenes can also carry significant MnO (<2.6 wt%) [66]. Many accessory phases are found, including plagioclase (principally anorthite), Ca-phosphates, and high-Ca pyroxenes diopside (including the high-Ti variety formerly known as fassaite), pigeonite and augite [62].

Matrix phases consist of all the aforementioned minerals plus spinel, magnetite, kamacite, taenite, chromite, magnéli phases (Ti_nO_{2n-1}, $n = 4, 5, 6$), silica, bismuth, tin oxide, and poorly-characterized nanometer-sized organic phases [62].

The dominant form of non-crystalline silicates in the chondritic aggregate IDPs are the GEMS, submicron glassy Mg-silicate grains with embedded nanometer FeNi and Fe sulfide crystals [67] ("The Astromineralogy of Interplanetary Dust Particles" by Bradley, this volume). The GEMS show evidence of exposure to large doses of ionizing radiation, such as eroded surfaces, oxygen enrichment, gradients in Mg/Si ratio decreasing outward from the center, and formation of reduced FeNi metal, pointing to exposure in the interstellar medium prior to their incorporation into comets. They are frequently embedded in carbon-rich material having high D/H ratios, also indicative of an interstellar origin. Infrared spectra of GEMS-rich IDP samples resemble the cometary spectra, while spectra of individual GEMS reveal a single broad peak between 9.3 μm (pyroxene-type) and 10 μm (olivine-type) [68]. The FeNi inclusions provide sufficient absorption of solar radiation to heat a GEMS grain in a cometary coma to a temperature close to that of a blackbody.

There are also rare refractory IDPs, whose entry velocities have not been measured. They appear to be finer-grained analogues of meteoritic calcium aluminum-rich inclusions (CAI) [69, 70]. These refractory IDPs have been ignored for 20 years, but now that CAI have been located among the Wild 2 samples (see below), they are of considerable interest as being of potentially cometary origin.

5 Mineralogy of the Wild 2 Sample

Thanks to the Stardust mission, we can now perform mineralogical and petrographic analyses of particles derived directly from the Jupiter-family comet 81P/Wild 2. Stardust, one of NASA's Discovery series, was designed to capture cometary dust particles during a close flyby of Wild 2 at 1.86 AU from the sun. The spacecraft penetrated the inner dust coma to a distance of 235 km from the nucleus, capturing

particles within hours of their release from the nucleus. Dust collection was accomplished using $2 \times 4 \times 3$ cm tiles of low-density silica aerogel, with a graded density from <0.01 g/cm^3 at the surface to 0.05 g/cm^3. The collector was returned to Earth on January 15, 2006, safely stowed inside the sample return capsule. The collector tray was scanned optically to identify track locations, then some of the 132 aerogel tiles were removed for study. During the first year, captured particles in these tiles were examined by the Preliminary Examination Team (PET), using a variety of analysis techniques [71]. The samples are curated at Johnson Space Center; even now, 3 years after sample return, only a fraction of the tracks and terminal particles have been analyzed.

Pre-flight laboratory experiments demonstrated that compact 10–100 μm particles can be captured into aerogel intact at the flyby velocity of 6.1 km/s. Impacting particles leave a carrot-shaped track of damaged aerogel, with the terminal particle lodged at the end. More fluffy aggregate particles are likely to fragment upon impacting the aerogel, with the fragmented grains lining the aerogel track.

All of the captured Wild 2 particles have been modified in various ways by the capture process, in which cometary "particles" punched into the silica aerogel, making various types of tracks, and disaggregating into "grains" distributed along the tracks [71, 72].

Three types of tracks were evident: long tapered tracks ending with a terminal particle; bulbous cavities with one or more narrow tracks extending below the "bulb"; and bulbous cavities with no associated narrow tracks (Fig. 5)[73]. All particles that may have been loose aggregates disaggregated into individual components with the larger, denser components penetrating more deeply into the aerogel, making thin tracks with terminal grains. Individual grains experienced heating effects that ranged widely from excellent preservation to melting; such behavior was expected [74–76]. It appears that the material deposited along track walls experienced the greatest heating, while the denser grains outran the heated areas as they penetrated deeper into the aerogel (Kyoko Okudaira, personal communication 2007). This differential collection heating introduced a serious bias into the survival of different portions of the Wild 2 particles: the coarser-grained portions of the particles have a higher survival rate than the finer-grained portion. Most results to date have been obtained from only the coarser-grained portions of captured particles; only in a few instances thus far have we seen the true mineralogy of the finest-grained materials. Here and there accumulations of the finest-grained materials firmly attached to coarser grains survived to the end of tracks and are available for analysis. Also, fine-grained materials located in the upper portions of some tracks mysteriously survived intact. Thus, our understanding of the finest-grained materials from Wild-2 is very incomplete, and only will be revealed in full by future work. Readers should understand that the conclusions reached in this review may only pertain to the fraction of Wild-2 minerals coarser grained than 1 μm.

Researchers have by now harvested Wild 2 grains from approximately 140 separate particle capture tracks, and have obtained a rudimentary understanding of the mineralogy of approximately half of these samples [72, 77]. Of these best-studied tracks, ~33% are dominated by olivine grains (Tracks 1, 22, 26, 43, 57, 68, 71, 77),

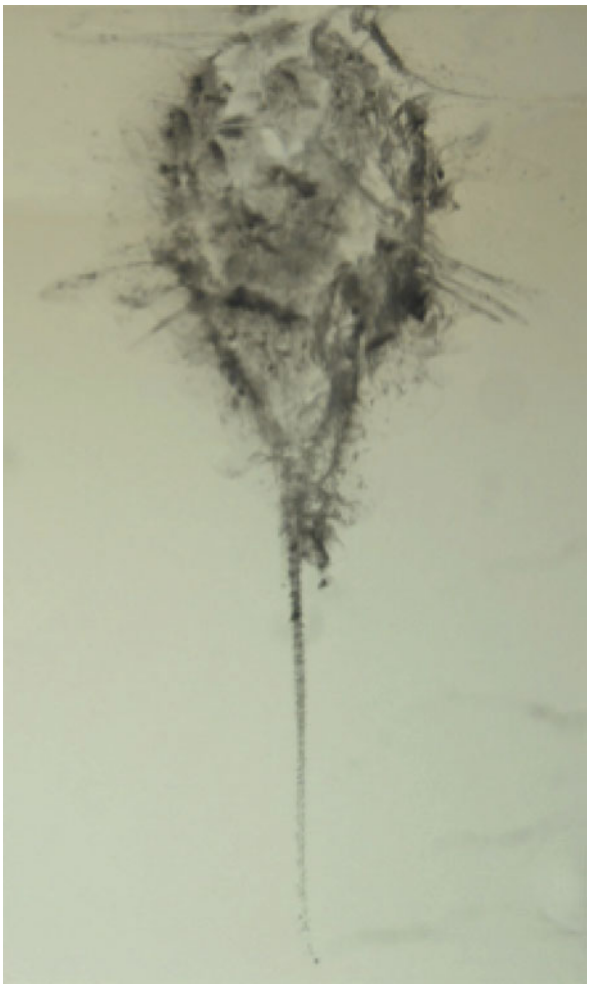

Fig. 5 Example of a track (C054-T3) in the Wild 2 aerogel collector. showing bulbous upper cavity with narrow tracks of terminal grains branching from it

∼24% by low-calcium pyroxene (Tracks 17, 20, 24, 27, 32, 41, 69), ∼10% by a fairly equal amount of olivine and pyroxene (Tracks 5, 10, 35), and the remaining ∼33% are dominated by other minerals, mainly Fe-Ni sulfides. These results suggest that crystalline materials are abundant in Wild 2. Figure 6 shows 4 examples of terminal particles.

The recovered Wild 2 samples are mixtures of crystalline and amorphous materials. Analytical Electron Microscopy (AEM) analysis of grains from the upper, often bulb-shaped, portions of tracks show that they typically have widely varying compositions, but are frequently similar to chondrites for most elements except Si, even in severely heated and melted regions [72, 80–82]. The crystalline grains observed

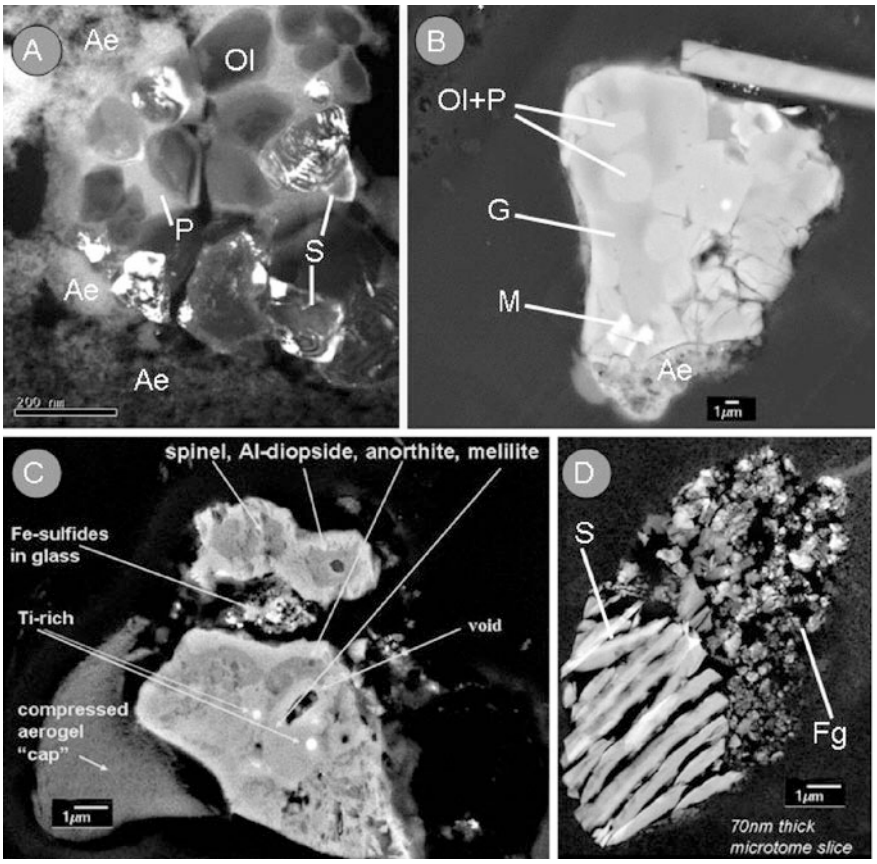

Fig. 6 (**a**) Bright field TEM image showing an olivine (Ol) and low-Ca pyroxene (P) dominated grain with Fe-Ni sulfide (S). Enclosing aerogel (Ae) is also apparent. Individual olivine and low-Ca pyroxene crystallites are surrounded by amorphous matrix (which may or may not have been produced during capture) (after [77]). (**b**) Bright field TEM image of a microporphyritic, chondrule-like object dominated by olivine and low-Ca pyroxene (Ol+P) within aluminosilicate glass (G), with accessory Fe-Ni metal (M) (after [78]). (**c**) Refractory, CAI grain containing calcium-, aluminium-, and titanium-rich phases (after [72]). (**d**) Fe sulphide (S) crystal attached to residual fine-grained Wild-2 phases (Fg) with a bulk chondritic composition, which contain well-preserved cometary organic phases (after [79])

within the upper portions of individual tracks are almost always sub-micrometer in grain size. These observations suggest that the materials captured in the upper portions of the tracks are, in general, much finer grained than the material at the end of the slender, so-called stylus tracks that almost always project from the bulb-like upper tracks. AEM of very small craters on the aluminum foil also reveals crystalline olivine, pyroxene and sulfides derived from separate submicrometer components within micrometer-size particles [83]. The craters in aluminum foils frequently are multilobed, indicating that the impacting particles were aggregates [73, 83]. Syn-

chrotron X-Ray Fluorescence (SXRF) analyses [80], suggest that 40–100% of the collected grains' mass is found in the upper portions of the tracks, and up to 60% is represented by the track terminal grains (on average).

Thus our current model for the structure of the captured grains is one of very fine-grained (sub-micrometer), loosely-bound aggregates with a bulk chondritic composition, with most aggregates also containing one or more much larger individual crystals (most commonly) of olivine, pyroxene and Fe-Ni sulfides.

Out of the several hundred tracks we have thus far carefully photodocumented, only 2 appear to have no visible terminal grains. This finding indicates that practically all collected cometary particles contained some of these larger grains, which probably served to nucleate the cometary particles at the earliest stage of accretion. This view is supported by some of the larger crater morphologies observed on the Stardust Al foils, which have a multilobe appearance rather than being simple hemispherical craters, and which can contain diverse sub-grain compositions [73, 83]. This physical structure is consistent with several chondritic materials, including chondritic interplanetary dust particles [62, 84].

One problem we face in writing this review is deciding how to organize the mineralogical description. If the Wild-2 grains were mainly similar to one another then the best approach would be to describe each mineral in turn. We will in fact do this to some degree. However, it is now clear that many of the captured particles to some degree possessed rather unique mineralogies, expressing varied formation locations and conditions. Thus it is also appropriate to provide some grain by grain descriptions.

5.1 Olivine and Low-Calcium Pyroxene

Olivine and pyroxene are thus present in the majority of Wild 2 particles, with observed grain size ranging from submicrometer to over 10 μm. Both low- and high-calcium pyroxenes are present among the Wild 2 grains, with the former being dominant. Wild 2 olivine has an extremely wide composition range, from Fo_{4-100} with a pronounced frequency peak at Fo_{99} [77]. The presence of significant Fe-rich olivine and lack of a peak at equilibrated olivine compositions ($\sim Fo_{40-60}$) suggests that composition changes due to capture heating have been insignificant in the coarse-grained (>0.2 μm) component en masse [74–76, 85–87], and also that these grains were never significantly thermally metamorphosed. Wild 2 olivines include some with very elevated MnO, Al_2O_3 and Cr_2O_3 contents, up to 6.45, 0.71 and 1.46 wt%, respectively [72]. About 1/4 of these Mn- and Cr-rich olivines contain $\ll$1% FeO. Olivines with enrichments in these elements have been reported in carbonaceous chondrites, micrometeorites, and chondritic IDPs, though they are rare [62, 66, 88–90]. The wide Mg-Fe composition range of Wild 2 olivine is similar to that for anhydrous chondritic IDPs. However, the range of these olivine compositions is also similar to that found in the matrix of the chondrites Murchison (CM2), and Orgueil (CI1), which have experienced significant-to-pervasive aqueous alteration. The presence of the pronounced peak in forsterite seen in the CMs could

be due to the preferential survival of Mg-rich olivine during aqueous alteration, a well- known phenomenon since Fe-rich olivine is significantly more susceptible to dissolution, and alteration than Mg-rich olivine [91]. The olivine analyses alone, however, do not demonstrate whether comet Wild 2 ever hosted liquid water. The enhanced abundance of Mg-rich olivine has a natural explanation in the condensation sequence from a hot gas in the solar nebula, as described in Sect. 6, and it is detected spectroscopically in circumstellar dust ("The Mineralogy of Interstellar and Circumstellar Dust in Galaxies" by Molster et al., this volume). Nevertheless, the resemblance of Wild 2 olivine to CI and CM chondrite matrix olivine with pronounced forsterite peaks suggests that a more detailed search for possible aqueous alteration products should be undertaken.

In some cases Synchrotron X-ray Diffraction (SXRD) or Selected Area Electron Diffraction (SAED) patterns reveal Wild 2 low-calcium pyroxenes to be orthoenstatite, requiring slow cooling, but in the majority of cases we have only EDX analyses and are not yet certain whether we have ortho- or clinopyroxene [81, 82]. The composition range displayed by the low-calcium pyroxene is also very extensive, from En_{52} to En_{100}, with a significant frequency peak centered at En_{95} [77]. Low-calcium pyroxene usually coexists with olivine in the Wild 2 grains, but the Mg/Fe ratios for coexisting phases are not always similar. For example, Track 17 contains olivine in the range Fo_{55-69}, while associated low-calcium pyroxene is En_{52-96}. The extreme compositional range of low-Ca pyroxene is again similar to the anhydrous chondritic IDPs, and significantly broader than that observed in most chondrites, including Murchison and Orgueil. It should be possible to measure compositional profiles across the boundaries of adjacent olivine and low-calcium pyroxene crystals and between olivine and metal grains, to determine the extent of Mg and Fe zoning, which will yield the thermal histories of these assemblages. This is particularly important since the Wild-2 grains have experienced such diverse formation histories.

5.2 Unusual Pyroxene Compositions

References [81, 92] report results of a transmission electron microscopy (TEM) study of a pyroxene-bearing terminal particles, which contain lamellar intergrowths of pigeonite and diopside on the (001) plane. This microstructure is typical for an igneous process and formation by exsolution during cooling. Width and wavelength of the lamellae indicate a cooling rate within the range 10–100° C/h, in close agreement with those of chondrules or lava from an asteroidal igneous rock. References [81, 82, 92, 93] describe an abundance of diopside in the Wild 2 grains which is far beyond what is normally found in chondritic IDPs or unequilibrated chondrites. Some of this diopside could have resulted from thermal metamorphism, but the available information is inconclusive. Reference [93] reported a high abundance of Na+Cr-rich silicate phases in half of the tracks they have investigated. They found high-Ca pyroxenes including diopside, augite and pigeonite with high Na and Cr contents, and one occurrence of the sodic and chromium-rich amphibole

richterite. The high Na, Cr and sometimes higher Mn contents of these pyroxene appears to be in excess of what has been reported from chondrites; it is unknown how these compositions compare to pyroxene in chondritic IDPs [77]. Joswiak et al. [93] have suggested that these minerals formed through metamorphism at high pressure, which would require the rapid formation and early destruction of a large (500–1,000 km diameter) parent body. There is some support for the idea that there are such large busted up Kuiper Belt Objects [94]. However, Joswiak et al. [93] point out that these pyroxenes could also have formed from condensation from a fractionated nebular gas reservoir which had been enriched in volatile components by partial evaporation of preexisting solids, or through magmatic processes at low pressures.

5.3 Fe-Ni Sulfides

Sulfides are the only mineral group found in all extraterrestrial materials. Fe-Ni sulfides are also ubiquitous in the Wild 2 grains, grading from sulfides which apparently melted during collection and separated into a mixture of sulfide and metal [72, 81, 82], all the way to apparently unmodified FeS and pentlandite ($(Fe, Ni)_9S_8$) grains. Several coarse Wild 2 grains are dominated by FeS or pentlandite. We refer here to troilite (stoichiometric FeS) and pyrrhotite ($Fe_{1-x}S$) collectively as "FeS" because the exact stoichiometry and structure is still unknown for most Wild 2 samples. Many Wild 2 sulfides have compositions close to stoichiometric FeS, with less than 2 atom% Ni. To date, fewer than 5 pentlandite grains have been found among the Wild 2 grains, suggesting that this mineral is not abundant. The complete lack of compositions between FeS and pentlandite (with intermediate solid solution compositions) suggests (but does not require) that FeS and pentlandite formed as crystalline species, i.e. did not form as amorphous phases, which later became annealed [95]. The remaining Wild 2 Fe-Ni-S bearing phases (approximately half analyzed so far) have compositions that trend from FeS directly towards the Fe apex of the Fe-Ni-S ternary diagram. SAED patterns for these phases show the presence of two different lattices: strong maxima for a Fe-Ni sulfide phase and a much finer pattern consistent with kamacite [81, 82]. These phases are almost certainly a result of capture heating, and their presence can be used to gauge the degree of capture modification of the enclosing Wild 2 grains.

The few verified pentlandite crystals in Wild 2 tracks are intriguing since this phase is frequently an indicator of low-temperature metamorphism under oxidizing conditions, and/or aqueous alteration [65, 96]. So far we have not observed tochilinite, which is a hallmark of the hydrated CM2s and a few hydrous chondritic IDPs [97, 98]. Ni-rich sulfides are not found in totally anhydrous chondritic IDPs, but are found in IDPs that experienced aqueous alteration, and are abundant in carbonaceous chondrites that are aqueously altered. Therefore, at face value the presence of these few Ni-rich sulfides suggests that some Wild 2 particles could have experienced a limited degree of aqueous alteration.

5.4 High-Temperature Mineral Assemblages (Rocks)

A major surprise of the Stardust Mission has been the rather abundant (few percent) occurrence of high temperature mineral assemblages, most notably refractory element-rich aggregates, which are identical to meteoritic calcium aluminum rich inclusions (CAI) [72, 99, 100] and aggregates with obvious magmatic origins which are identical to chondrules from carbonaceous chondrites [78]. The best studied CAI (from Track 25) consists mainly of anorthite, gehlenite, spinel and diopside. Crystals of orbornite (TiN), (V,Ti)N, and Fe-Ni metal are sitting within all phases except diopside. The metals grains contain inclusions of platinum-group elements, and Mo, W alloys. All of the minerals in the CAI require high formation temperatures, especially the nitrides, which would have condensed in the nebula at 1600–2000K, depending upon the local oxygen fugacity [101]. It should be possible to measure compositional profiles across the boundaries of spinel within silicates to determine the extent of Mg zoning, which will elucidate one portion of the thermal history of the Wild 2 CAI. The oxygen isotope composition of the Wild 2 CAI is along the trend defined by carbonaceous chondrite CAI [99, 100].

At least 8 Wild 2 grains have now been found to be identical to chondrules from carbonaceous chondrites [78, 92]. These chondrule-like Wild 2 grains are characterized by (1) igneous porphyritic or poikilitic textures suggestive of partial melting at high temperatures; (2) presence of glass formed during rapid cooling, which is directly in contact to silicates; and (3) dominant occurrence of Mg-rich olivine and low-Ca pyroxene with minor amounts of rounded Fe-metal inclusions suggestive of crystallization under reducing conditions in space. One grain consists of a myrmekitic intergrowth of nepheline, olivine, augite, plagioclase, and a Ca phosphate, which must also be igneous in origin [77]. Compared with average meteorite porphyritic chondrules, the crystal size of olivine in Wild 2 chondrule-like objects (mostly 2–10 μm) is much smaller. But some chondrites, such as the ALH-85085 CH chondrite, have similarly fine-grained chondrules [102]. Major element abundances of olivine, pyroxene, and mesostasis glass in the chondrules-like particles are within the range of compositions defined by a majority of meteorite chondrules [78]. However, the range of oxygen isotope ratios of these particles spans the entire range observed for chondrules in carbonaceous chondrites. None of the data plot on or above the terrestrial mass fractionation line, which clearly resolves these particles from ordinary and rumuruti chondrites and enstatite chondrite objects [78]. Therefore, the chondrules-like objects in Wild 2 are most similar to type I and II olivine-pyroxene chondrules in carbonaceous chondrites. Spectroscopic studies suggest that carbonaceous chondrites came from asteroids located mainly at the mid to outer asteroid belt, whereas ordinary and enstatite chondrites are from the inner asteroid belt [103]. Therefore, Wild 2 chondrule-like objects appear to have a strong genetic relation with chondrules in the outer asteroid belt.

Since the oxygen isotope compositions of these Wild-2 CAI and chondrules-like objects are identical to the meteorite analogues, these objects probably formed within the inner solar system (assuming the Sun was the heat source for their formation) as opposed to some other stellar system. The ^{16}O-richest composition of Wild

2 chondrule-like objects is $-49.7 \pm 0.9‰ \delta^{18}O$ and that of the Wild 2 CAI [6] is $-41.6 \pm 1.3‰$ in $\delta^{18}O$, suggesting that both sampled a common oxygen reservoir during formation, probably the Sun [78, 99]. This in turn requires that some solar system wide dynamic process was operating to carry inner solar system solids (CAI and chondrules) out to the comet assembly region.

5.5 Non-crystalline Silicates

It is also fundamentally important to determine the nature of any amorphous cometary silicates that may be present in the Wild 2 samples. We know from infrared spectroscopy that glassy or amorphous silicates are present in comets. In the chondritic aggregate IDPs of probable cometary origin, GEMS comprise over 50% of the volume [104]. It was anticipated that GEMS would be prevalent in the Wild 2 sample. Distinguishing small (0.1–0.5 μm) GEMS from the silica aerogel that melted during particle impact has proven to be difficult, however. Reference [81] presented a detailed study of the material along a number of track walls; they describe a silica-rich matrix where cometary material has mixed with melted aerogel. Fe-Ni and Fe-Ni-S inclusions are present, as are localized regions of high Mg abundance, along with minor anounts of Ca, Al, Fe. If one assumes CI abundances, then cometary material constitutes about 10% of the mix.

Although the metal and sulfide inclusions are reminiscent of GEMS, Ishii et al. [104] have concluded that these inclusions formed during the impact process: In contrast to the IDPs, the GEMs-like material has very low Mg abundance. Moreover, this material is generally found along tracks having a terminal FeS particle. Similar material, including reduced Fe-Ni inclusions, has been produced in laboratory experiments when FeS particles were accelerated into silica aerogel, leading to the conclusion that most of the GEMS-like material is a byproduct of the impact process. On the other hand, nanometer scale compositional mapping has identified Mg-rich domains within the molten aerogel, of a size and composition consistent with GEMS [81, 105]. Thus, there are hints that cometary GEMS are present in the sample, but well-camoflaged within the aerogel.

5.6 Low-Temperature Phases

No direct evidence of phyllosilicates has yet been seen in any Wild 2 samples [72]. Despite the fact that significant heating and structural modification accompanied collection of many grains in the aerogel, we should have seen characteristic compositions, grain morphologies, and lattice fringes of phyllosilicates had they been present, even if they had been thermally modified [74, 76, 87]. During heating, phyllosilicates lose interlayer water and OH, and interlayer lattice fringes collapse in a characteristic manner. Eventually, a neoformed anhydrous silicate is formed, generally orthopyroxene or olivine. The neoformed silicates retain the flaky morphologies of the original phyllosilicates, however, and so are still rec-

ognizable as transformed phyllosilicates. We have observed this phenomenon in naturally-heated (metamorphosed) carbonaceous chondrites [85, 98, 106, 107]. References [108, 109] launched phyllosilicates (serpentine and cronstedtite) into aerogel at velocities of 4 and 6.1 km s^{-1}, and saw preservation of a significant fraction. Additional evidence that some phyllosilicates would have survived capture is presented by the partial survival of scattered, delicate, low temperature phases among the Wild 2 samples – fine-grained, organic rich phases rich in deuterium and ^{15}N excesses [110, 111]. These fine-grained materials survived capture in the aerogel with minimal heating when attached to larger, more refractory grains. Phyllosilicates would have behaved similarly.

Rare and tiny crystals of calcite and Fe-Mg carbonate have been reported from three Wild 2 grains, so, although they are present, it is clear that carbonates are exceedingly rare in the Wild 2 samples [112, 113]. In metamorphosed carbonaceous chondrites carbonates devolatilize to hydroxides or oxides [114]. We have also observed the devolatilization products of carbonates within hydrous IDPs that have been seriously heated during atmospheric entry [115]. Ca-Mg-Fe carbonates in these IDPs boil down to Ca-Mg-Fe hydroxides and finally oxides. Thus, it is possible that carbonates were more abundant in the Wild 2 particles before capture and capture heating, but this is not yet known.

Thus the lack of phyllosilicates, and rarity of carbonates among the ~100 Wild 2 grains we have so far well characterized suggests that they could not have composed more than a few percent of the more coarse-grained fraction of captured Wild 2 sample. However, it is also true that for the most part only the most coarse-grained objects at the end of capture tracks have been analyzed to a significant degree during Stardust PET, and that these have for the most part been incompletely characterized (only "exciting" grains like the CAI particle have received detailed analysis so far). It is also likely that phyllosilicate-rich (and other OH-bearing phases) grains, if ever present among captured Wild 2 particles, would have been deposited along the walls of bulb tracks as well as at track termini. These wall grains have been little studied during PET. Therefore more thorough characterization of bulb wall grains as well as the terminal grains will be necessary to definitively determine whether Comet Wild 2 dust was ever exposed to aqueous alteration. If phyllosilicates had dominated the mineralogy of the captured samples, we would probably have seen strong evidence of this already. But if aqueous alteration has affected much less than half of the comet materials we would probably have missed it during sample PET. A critical question we must address in future work is: Did Wild 2 ever support liquid water, and if so to what extent?

6 Origins of Cometary Silicates

We have seen that cometary dust is a heterogeneous unequilibrated mixture of minerals, including grains that must have formed at high temperatures and grains that formed at low temperatures. These various components do not necessarily share

a common origin. The temperatures in the outer solar nebula where comet nuclei accreted were too cold for significant processing of dust particles. Thus, pre-existing interstellar grains could have survived in this environment. Particles that condensed or were thermally processed in the warm inner solar nebula were transported to the colder outer regions. For an extensive discussion of comet dust origins and processing see [116].

6.1 Amorphous Silicates

The glassy silicate grains (GEMS) described in Sect. 4 appear to constitute the major fraction of the non-crystalline silicates in cometary IDPs. The evidence is quite strong that these are interstellar grains, based on their morphology and inferred high radiation dose. The physical and chemical properties of GEMS are similar to those inferred for interstellar grains. For example, the FeNi metal beads have sufficient paramagnetism to align a GEMS grain in the interstellar magnetic field to the extent needed to explain observed interstellar polarization [117, 118]. The infrared spectra of GEMS are consistent with spectra of silicates in interstellar sources [68]. Some GEMS are embedded in organic refractory material having non-solar nitrogen isotopic ratios and deuterium enrichment.

A few GEMS display oxygen isotopic anomalies identifying them as presolar; however, most appear to have solar oxygen isotopic ratios [119, 120]. Thus, any scenario for their origin has to account for both the high radiation dosage and solar isotopic abundances. Moreover, some GEMS contain relict crystals of forsterite or FeS and the overall shape of the GEMS grain retains the shape of that relict crystal, indicating that, originally, the GEMS grain was a single crystalline grain [121].

The radiation damage in the GEMS requires a high fluence of very energetic ions. Reference [122] has proposed that the GEMS condensed as crystalline grains in the outflows from massive stars in OB associations. Subsequently, they were accelerated by supernova shocks within the superbubble and were bombarded by hot gas atoms. These high-velocity encounters with gas atoms destroyed the crystal structure to a depth corresponding to the encounter velocity and implanted atoms into the grain. Because the oxygen atoms were implanted from the gas phase, most GEMS are isotopically homogeneous.

High velocity jets from protostars represent another possible environment where small dust grains are accelerated and are impacted by gas atoms at high relative velocity and then are dispersed into the ISM [123].

6.2 Crystalline Silicates

Crystalline silicates are widespread in both Oort Cloud and ecliptic comets; thus, they must have been widespread in the region of comet formation. Furthermore, the crystalline grains in Wild 2 are large, up to ten micrometers or more. The cometary crystalline silicates are Mg-rich, the dominant minerals being forsterite

and enstatite, whereas the amorphous silicates have a larger range in Fe/Mg content. These facts have to be explained by any model for their origin.

Crystalline silicates are known to form in the envelopes around evolved stars. Forsterite and also enstatite have been detected in the spectra of some evolved stars [124] ("The Mineralogy of Interstellar and Circumstellar Dust in Galaxies" by Molster et al., this volume). However, these grains are efficiently destroyed in interstellar shocks and spectral signatures of crystalline silicates are not seen in the interstellar medium. References [125, 126] set a conservative upper limit of 2.2% to the degree of crystallinity in the diffuse interstellar medium toward the galactic center. Most protostellar sources show no evidence of crystalline silicates. Only in late stage Herbig Ae/Be stars and T Tauri stars do the spectral peaks of crystalline mineral grains appear [127, 128] ("The Mineralogy of Interstellar and Circumstellar Dust in Galaxies" by Molster et al., this volume). The ISO spectrum of HD100546, for example, is remarkably similar to that of Hale-Bopp [129]. The β Pictoris debris disk is another example of crystalline silicates [130]. Some of these systems are thought to have developed a population of comets that are the source of the dust [131, 132]. The lack of crystalline grains in the ISM, their appearance at late stages of protostellar evolution, and the presence of abundant large (compared to IS grains) crystalline grains in the Stardust samples, lead to the conclusion that the crystalline grains in comets must have formed in the inner solar nebula.

Crystalline silicate grains can form by direct condensation from the vapor phase at $T = 1{,}200$–$1{,}400$ K. The Mg minerals forsterite and enstatite are predicted from thermodynamic models to be the first to condense in a hot gas and only react with Fe at lower temperatures [133]. Enstatite whiskers, rods, and platelets found in aggregate IDPs of likely cometary origin have growth patterns, such as axial screw dislocations, that indicate direct vapor phase condensation from a hot gas [134]. In the model presented by [133]) (see also [116]), initially amorphous interstellar grains with a mixed Fe-Mg composition migrate inward in the solar nebula. When their temperature reaches ~900 K, the grains anneal. With further heating, the process of grain evaporation, gas phase transport, and recondensation produces grains with an equilibrium composition appropriate to the prevailing temperature, pressure, and gas phase composition. At temperatures of 1,200–1,400 K, the model predicts that forsterite, enstatite and metallic iron are the equilibrium products for low water vapor content (low oxygen fugacity). Thus, high-temperature condensation is a natural explanation for the preponderance of Mg-rich silicates in the comet dust.

Turbulent diffusion and large-scale circulation currents could provide the means to transport the high-temperature condensates outward to the region of comet formation; the Stardust results have stimulated renewed interest in modelling this process ([133, 135], "Formation and Evolution of Minerals in Accretion Disks and Stellar Outflows" by Gail, this volume). Reference [136] applied 2-D modelling and showed that outward diffusion of materials at the midplane of a turbulent disk is more efficient than previous 1-D models predicted. The X-winds described by [137] are another possible means of transporting grains outward.

How can one explain the Fe-rich crystalline silicate grains found in the Wild 2 sample? Icy grains and icy planetesimals may have migrated inward in the solar

nebula. As they evaporated, localized regions of high water vapor content would have been created; in such environments, Fe-rich crystalline silicates are predicted to form [116, 138].

6.3 CAI and Chondrules

The presence of calcium and aluminum-rich inclusions (CAI) in the Wild 2 dust is of particular interest. All of the minerals in the CAI require high temperature formation, up to 1,600–2,000 K [101]. They are thought to be the earliest condensates in the hot inner solar nebula. Their appearance in Wild 2 is further evidence for efficient radial transport. Previously, these materials were found only in primitive meteorites. It is not known how far from the sun Wild 2 formed. The CAI, chondrules, and other minor constituents resembling the composition of carbonaceous chondrites might suggest that Wild 2 formed in the inner part of the icy planetesimal range, closer to 5 than 35 AU.

7 Discussion and Conclusions

The return of the Wild 2 dust sample was widely anticipated as "ground truth" to confirm (or not) the conclusions about comet dust composition from spectroscopy, the Halley probes, and comparison with the anhydrous chondritic aggregate IDPs. In general, a consistent picture of the major dust mineralogy emerges from the infrared spectra, the Wild 2 analysis, and the "rock" component of the Halley measurements.

Silicates constitute the most abundant material; they are present in both crystalline and amorphous (or glassy) form and include both olivine and pyroxene mineralogy. Terminal particles studied to date in the Wild 2 sample are approximately 33% olivine, 24% low-calcium pyroxene, about 10% equal amounts of olivine and pyroxene, and about 33% other minerals, mainly Fe-Ni sulfides. Cometary silicates are Mg-rich. The full 8–40 μm spectrum of Hale-Bopp was dominated by forsterite emission peaks; enstatite peaks were also detected. It is notable that Mg-silicates predominate over the size range from ∼0.1 μm (Halley particles) to ∼10 μm or more (Wild 2 terminal particles). However, the silicates also display a wide range in Mg/Fe, with some Wild 2 particles having Mg/Fe ∼1. Anhydrous IDPs show a similar wide range in Fe content.

The detection of calcium aluminum-rich inclusions in the Wild 2 collection was a new and interesting discovery. These very refractory grains are thought to be the very earliest condensates in the inner solar nebula. Chondrule fragments were also found, raising questions as to the extent that the nucleus of Wild 2 resembles chondritic meteorite parent bodies.

Cometary infrared spectra also show the broader emission bands of amorphous silicates. GEMS (Glass with Embedded Metal and Sulfides) are a major component of the chondritic aggregate IDPs of likely cometary origin. The relative abundance of glassy (or amorphous) silicates in Wild 2 dust may never be known, however,

because of the difficulty in distinguishing between bona fide amorphous cometary grains and molten aerogel. This fact also makes it difficult to compare Wild 2 and the IDPs. The coarse-grained matrix material in the IDPs is similar to that in the Wild 2 sample except that the enstatite whiskers and platelets seen in the IDPs appear to be rare or absent among the Wild 2 particles. However, GEMS comprise ~50% of the volume in these IDPs and they are not yet definitively detected along the particle tracks in the aerogel.

No direct evidence of phyllosilicates has yet been found in the Wild 2 dust; we conclude they could not represent more than a few percent of the coarse-grained fraction of Wild 2 dust. The fine-grained material lining the "bulb" and track walls has not yet been as thoroughly studied, however. More thorough characterization of this material will be required to decide whether Wild 2 cometary material was ever exposed to aqueous alteration. No distinctive infrared feature of phyllosilicates is evident in cometary spectra. The Spitzer Tempel 1 spectrum of the material released following Deep Impact is probably the most sensitive existing comet spectrum. The best model fit to the spectrum (defined by chi-squared test) included 8% hydrated silicates [48]; this result has to be considered tentative because of the large number of modelling parameters.

There is considerable evidence that cometary dust includes a component of organic refractory material. Already in 1982 [139] it was proposed that interstellar silicate grains possess organic refractory mantles as a result of UV photoprocessing in the diffuse interstellar medium following deposition of icy mantles in cold molecular clouds. Comet Halley's dust contains a high abundance of CHON material, usually in combination with silicates. Significant clustering of subgroups (e.g., [H,C], [H,C,O]) within the CHON classification indicated variable composition of the organic refractory component [140]. The anhydrous chondritic IDPs contain several percent carbon, at least some of it in an organic phase. The carbon is distributed throughout the IDP as a matrix surrounding the mineral grains. Organic refractory material is present along the tracks in the Wild 2 collected sample; the reader is referred to [79, 111] for a detailed description.

Not only are small crystalline grains widespread in comets, but abundant large (up to $\sim 10\,\mu$m) silicate grains are present in at least one comet. These grains most likely formed by direct vapor phase condensation in the hot inner solar nebula. The Mg-silicates are predicted by thermodynamic models to be the first to condense in a hot gas, providing a natural explanation for the high relative abundance of Mg-silicates in cometary dust, as well as in circumstellar silicates. Where the Fe-silicates in comets formed is not so clear. Reference [138] proposed that the Fe-silicates formed in regions of higher oxygen fugacity in the inner solar nebula when icy bodies migrated inward and vaporized. If so, Fe-silicates may have formed at a later stage than the Mg-silicates and may have different abundance in comet nuclei depending on when and where a particular comet nucleus formed [116]. Reference [41] concluded that Hale-Bopp had less Fe-silicates than Tempel 1, based on model fits to the spectra. Aqueous alteration in the parent bodies is another possibility for producing Fe-silicates, although phyllosilicates should also be present in this case and they have not been detected in Wild 2 sample analysis to date.

The presence in comets of refractory CAI as well as crystalline silicates demonstrate that large-scale mixing took place in the solar nebula during the epoch of comet formation. Since any given comet could have formed anywhere between 5 and 35 AU, we cannot use our present knowledge to determine radial gradients in the solar nebula composition. The possible differing Mg/Fe range in silicates from different comets is intriguing.

It is estimated that ∼1200 particles larger than 1 μm were captured during the Wild 2 flyby. Only a small fraction of these have been analyzed to date. We can expect new discoveries as further measurements are carried out over the next several years.

Our next opportunity to sample cometary dust will be ESA's Rosetta mission currently on its way to rendezvous with comet P/Churymov-Gerasimenko. The payload includes instruments to perform a variety of in situ analyses of dust particles collected at low velocity within the coma (See "The In-Situ Study of Solid Particles in the Solar System" by Mann and Jessberger, this volume).

Acknowledgments M.Z. acknowledges support from the NASA Stardust Data Analysis Program.

References

1. Dones, L., Weissman, P.R., Levison, H.F., Duncan, M.J.: Oort cloud formation and dynamics. In: Festou, M.C., Keller, H.U., Weaver, H.A. (eds.) Comets II, pp. 153–174. University of Arizona Press, Tucson, AZ (2004) 204
2. Morbidelli, A., Brown, M.E.: The Kuiper belt and the primordial evolution of the solar system. In: Festou, M., Keller, H.U., Weaver, H.A. (eds.) Comets II, pp. 175–191. University of Arizona Press, Tucson, AZ (2004) 204
3. Duncan, M.J., Levison, H.F.: A disk of scattered icy objects and the origin of Jupiter family omets. Science **276**, 1670–1672 (1997) 204
4. Duncan, M., Levison, H.F., Dones, L.: Dynamical evolution of ecliptic comets. In: Festou, M., Keller, H.U., Weaver, H.A. (eds.) Comets II, pp. 193–204. University of Arizona Press, Tucson, AZ (2004) 204
5. Volk, K., Malhotra, R.: Reassessing the classical Kuiper belt as a source of the Jupiter family comets. Bull. Am. Astron. Soc. **40**, 481 (2008) 204
6. Charnoz, S., Morbidelli, A.: Coupling 2dynamical and collisional evolution of small bodies II. Forming the Kuiper belt, the scattered disk and the Oort cloud. Icarus **188**, 468–480 (2007) 204, 220
7. Gomes, R.S.: The origin of the Kuiper belt high-inclination population. Icarus **161**, 404–418 (2003) 204
8. Levison, H.F., Morbidelli, A.: The formation of the Kuiper belt by the outward transport of bodies during Neptune's migration. Nature **426** 419–421 (2003) 204
9. Whipple, F.L.: A comet model: I. The acceleration of comet Encke. Astrophys. J. **111**, 375–394 (1950) 205
10. Weaver, H.A., Lamy, P.L.: Estimating the size of Hale-Bopp's nucleus. Earth Moon Planets **79**, 17–33 (1999) 205
11. Sekanina, Z.: Secondary fragmentation of the Solar and Heliospheric Observatory sungrazing comets at very large heliocentric distances. Astrophys. J. Lett. **542**, L147–L150 (2000) 205
12. Sekanina, Z., Hanner, M.S., Jessberger, E.K., Fomenkova, M.N.: Cometary dust. In: Grün, E., Gustafson, B.A.S., Dermott, S., Fechtig, H. (eds.) Interplanetary Dust. Springer, Heidelberg (2001) 205

13. Keller, H.U., Delamare, W.A., Huebner, W.F., et al.: Comet P/Halley's nucleus and its activity. Astron. Astrophys. **187**, 807–823 (1987) 205
14. Soderblom, L.A., Boice, D.C., Britt, D.T., Brown, R.H., Buratti, B.J., Hicks, M.D., et al.: Observations of comet 19P/Borrelly from the miniature integrated camera and spectrometer (MICAS) aboard deep space 1 (DS1). Bull. Am. Astron. Soc. **33**, 1087 (2001) 205
15. Brownlee, D.E., Horz, F., Newburn, R.L., Zolensky, M., Duxbury, T.C., Sandford, S., et al.: Surface of young Jupiter family comet 81P/Wild 2: view from the Stardust spacecraft. Science **304**, 1764–1769 (2004) 205
16. A'Hearn, M.F.,et al.: Deep impact: excavating comet tempel 1. Science **310**, 258–264 (2005) 205, 209
17. Crovisier, J., Bockelee-Morvan, D.: Remote observations of cometary volatiles. Space Sci. Rev. **90**, 19–32 (1999) 205
18. Irvine, W.M., Schloerb, F.P., Crovisier, J., Fegley, B., Mumma, M.J.: Comets: a link between interstellar and nebular chemistry. In: Mannings, V., Boss, A.P., Russell, S.S., (eds.) Protostars and Planets IV, pp. 1159–1200. University of Arizona Press, Tucson, AZ (2000) 205
19. Bockelee-Morvan, D., Crovisier, J., Mumma, M.J., Weaver, H.A.: The composition of cometary volatiles. In: Festou, M.C., Keller, H.U., Weaver, H.A. (eds.) Comets II, pp. 391–423. University of Arizona Press, Tucson, AZ (2004) 205
20. McDonnell, J.A.M., Lamy, P.L., Pankiewicz, G.S.: Physical properties of cometary dust. In: Newburn, R.L., Neugebauer, M., Rahe, J. (eds.) Comets in the Post Halley Era, pp. 1043–1073. Kluwer, Dordrecht (1991) 205
21. Sykes, M.V., Walker, R.G.: Cometary dust trails. Icarus **95**, 180–210 (1992) 205
22. Reach, W.T., Sykes, M.V., Lien, D., Davies, J.K.: The formation of Encke meteoroids and dust trail. Icarus **148**, 80–94 (2000) 205
23. Campins, H., Ryan, E.: The identification of crystalline olivine in cometary silicates. Astrophys. J. **341**, 1059–1066 (1989) 205, 206, 207
24. Stephens, J.R., Russell, R.W.: Emission and extinction of ground and vapor-condensed silicates from 4 to 14 microns and the 10 micron silicate feature. Astrophys. J. **228**, 780–786 (1979) 206
25. Bregman, J.H., Campins, H., Witteborn, F.C., Wooden, D.H., Rank, D.M., Allamandola, L.J., Cohen, M., Tielens, A.G.G.M.: Airborne and groundbased spectrophotometry of comet P/Halley from 5–13 μm. Astron. Astrophys. **187**, 616–620 (1987) 205
26. Davies, J.K., Geballe, T.R., Hanner, M.S., Weaver, H.A., Crovisier, J., Bockelee-Morvan, D.: Thermal infrared spectra of comet Hale-Bopp at heliocentric distances of 4 and 2.9 AU. Earth Moon Planets **78**, 293–298 (1999) 206
27. Hanner, M.S., Gehrz, R.D., Harker, D.E., Hayward, T.L., Lynch, D.K., Mason, C.C., Russell, R.W., Williams, D.M., Wooden, D.H., Woodward, C.E.: Thermal emission from the dust coma of comet Hale-Bopp and the composition of the silicate grains. Earth Moon Planets **79**, 247–264 (1999) 206, 207
28. Hayward, T.L., Hanner, M.S., Sekanina, Z.: Thermal infrared imaging and spectroscopy of comet Hale-Bopp (C/1995 O1). Astrophys. J. **538**, 428–455 (2000) 206, 207, 208
29. Wooden, D.H., Harker, D.E., Woodward, C.E., Butner, H., Koike, C., Witteborn, F.C., McMurty, C.W.: Silicate mineralogy of the dust in the inner coma of comet C/1995 O1 (Hale-Bopp) pre- and post-perihelion. Astrophys. J. **517**, 1034–1058 (1999) 206, 207
30. Crovisier, J., Brooke, T.Y., Leech, K., et al.: The thermal infrared spectra of comets Hale-Bopp and 103P/Hartley 2 observed with the Infrared Space Observatory. In: Sitko, M.L., Sprague, A.L., Lynch, (eds.) Thermal Emission Spectroscopy and Analysis of Dust, Disks, and Regoliths. ASP Conf. Series, vol. 196, pp. 109–117. ASP, San Francisco, CA (2000) 206, 207
31. Crovisier, J., Leech, K., Bockelee-Morvan, D., Brooke, T.Y., Hanner, M.S., Altieri, B., Keller, H.U., Lellouch, E.: The spectrum of comet Hale–Bopp (C/1995 O1) observed with the Infrared Space Observatory at 2.9 astronomical units from the sun. Science **275**, 1904–1907 (1997) 206
32. Koike, C., Shibai, H., Tuchiyama, A.: Extinction of olivine and pyroxene in the mid- and far-infrared. Mon. Not. R. Astron. Soc. **264**, 654–658 (1993) 206

33. Sandford, S.A., Walker, R.M.: Laboratory infrared transmission spectra of individual interplanetary dust particles from 2.5 to 25 microns. Astrophys. J. **291**, 838–851 (1985) 206
34. Wooden, D.H., Butner, H.M., Harker, D.E., Woodward, C.E.: Mg-rich silicate crystals in Comet Hale-Bopp: ISM relics or solar nebula condensates? Icarus **143**, 126–137 (2000) 206, 207
35. Greenberg, J.M., Hage, J.I.: From interstellar dust to comets: a unification of observational constraints. Astrophys. J. **361**, 260–274 (1990) 207
36. Hage, J.I., Greenberg, J.M.: A model for the optical properties of porous grains. Astrophys. J. **361**, 251–259 (1990) 207
37. Brucato, J.R., Colangeli, L., Mennella, V., Palumbo, P., Bussoletti, E.: Silicates in Hale-Bopp: hints from laboratory studies. Planet. Space Sci. **47**, 773–779 (1999) 207
38. Colangeli, L., Mennella, V., Brucato, J.R., Palumbo, P., Rotundi, A.: Characterization of cosmic materials in the laboratory. Space Sci. Rev. **90**, 341–354 (1999) 207
39. Galdemard, P., Lagage, P.O., Dubreuil, D., Jouan, R., Masse, P., Pantin, E., Bockelee-Morvan, D.: Mid-infrared spectro-imaging observations of Comet Hale-Bopp. Earth Moon Planets **78**, 271-277 (1999) 207
40. Harker, D.E., Wooden, D.H., Woodward, C.E., Lisse, C.M.: Grain properties of Comet C/1995 O1 (Hale-Bopp). Astrophys. J. **580**, 579–597 (2002) 207, 208
41. Lisse, C.M., Kraemer, K.E., Nuth, J.A., Li, A., Joswiak, D.: Comparison of the composition of the Tempel 1 ejecta to the dust in Comet C/Hale-Bopp 1995 O1 and YSO HD100546. Icarus **191**, 223–240 (2007) 207, 208, 225
42. Hanner, M.S., Lynch, D.K., Russell, R.W.: The 8–13 micron spectra of comets and the composition of silicate grains. Astrophys. J. **425**, 274–285 (1994) 208
43. Hanner, M.S., Hackwell, J.A., Russell, R.W., Lynch, D.K.: Silicate emission feature in the spectrum of comet Mueller 1993a. Icarus **112**, 490–495 (1994) 208
44. Honda, M., et al.: 'The 10 micron spectra of comet C/2002 V1 (NEAT) and C/2001 RX14 (LINEAR). Astrophys. J. **601**, 577–582 (2004) 208
45. Sitko, M.L., Lynch, D.K., Russell, R.W., Hanner, M.S.: 3–14 Micron spectroscopy of comets C/2002 O4 (Honig), C/2002 V1 (NEAT), C/2002 X5 (Kudo-Fujikawa), C/2002 Y1 (Juels-Holvorcem), and 69P/Taylor and the relationships among grain temperature, silicate band strength, and structure among comet families. Astrophys. J. **612**, 576–587 (2004) 208
46. Wooden, D.H., Woodward, C.E., Harker, D.E.: Discovery of crystalline silicates in Comet C/2001 Q4 (NEAT). Astrophys. J. **612**, L77–L80 (2004) 208
47. Kelley, M.S., Wooden, D.H.: The composition of dust in Jupiter family comets inferred from infrared spectroscopy. Planet. Space Sci. **57**, 1133–1145 (2008) 208
48. Lisse, C.M., et al.: Spitzer spectral observations of the Deep Impact ejecta. Science **313**, 635–640 (2006) 209, 225
49. Harker, D.E., Woodward, C.E., Wooden, D.H., Fisher, R.S., Trujillo, C.A.: Gemini-N mid-IR observations of the dust properties of the ejecta excavated from Comet 9P/Tempel 1 during Deep Impact. Icarus **191**, 432–453 (2007) 209, 210
50. Woodward, C.E., Kelley, M.S., Bockelee-Morvan, D., Gehrz, R.D.: Water in Comet C/2003 K4 (LINEAR) with Spitzer. Astrophys. J. **671**, 1065–1074 (2007) 210
51. Bockelee-Morvan, D., Woodward, C.E., Kelley, M.S.: Water, PAHs, and carbonate emission features in Spitzer spectra of comets C/2003 K4 (linear) and 9P/Tempel 1. Bull. Am. Astron. Soc. **39**, 508 (2007) 210
52. Kissel, J., et al.: Composition of comet Halley dust particles from Giotto observations. Nature **321**, 336–338 (1986) 210
53. Kissel, J., et al.: Composition of comet Halley dust particles from Vega observations. Nature **321**, 280–282 (1986) 210
54. Fomenkova, M., Kerridge, J., Marti, K., McFadden, L.: Compositional trends in rock-forming elements of comet Halley dust. Science **258**, 266–269 (1992) 211
55. Lawler, M.E., Brownlee, D.E.: CHON as a component of dust from comet Halley. Nature **359**, 810–812 (1992) 211

56. Jessberger, E.: Rocky cometary particulates: their elemental, isotopic, and mineralogical ingredients. Space Sci. Rev. **90**, 91–97 (1999) 211
57. Jessberger, E., Christoforidis, A., Kissel, J.: Aspects of the major element composition of Halley's dust. Nature **332**, 691–695 (1988) 211
58. Lawler, M.E., Brownlee, D.E., Temple, S., Wheelock, M.M.: Iron, magnesium, and silicon in dust from Comet Halley. Icarus **80**, 225–242 (1989) 211
59. Schulze, H., Kissel, J., Jessberger, E.: Chemistry and mineralogy of Comet Halley's dust. In: Pendleton, Y.J., Tielens, A.G.G.M. (eds.) From Stardust to Planetesimals. ASP Conf. Series, vol. 122, pp. 397–414. ASP, San Francisco, CA (1997) 211
60. Jessberger, E., Kissel, J.: Chemical properties of cometary dust and a note on carbon isotopes. In: Newburn, R.L., Neugebauer, M., Rahe, J. (eds.) Comets in the Post-Halley Era, pp. 1075–1092. Kluwer, Dordrecht (1991) 211
61. Brownlee, D.E.: Cosmic dust: collection and research. Annu. Rev. Earth Planet. Sci. **13**, 147–173 (1985) 211
62. Rietmeijer, F.J.M.: Interplanetary dust particles. In: Papike, J.J. (ed.) Planetary Materials, Reviews in Mineralogy, vol. 36, pp. 2-1–2-95. Mineralogical Society of America, Chantilly, VA (1998) 211, 212, 216
63. Nier, A.O., Schlutter D.J.: The thermal history of interplanetary dust particles in the Earth's stratosphere. Meteoritics **28**, 675–681 (1993) 211
64. Zolensky, M.E., Barrett R.A.: Chondritic interplanetary dust particles: basing their sources on olivine and pyroxene compositions. Meteoritics **29**, 616–620 (1994) 212
65. Zolensky, M.E., Thomas K.: Iron and iron-nickel sulfides in chondritic interplanetary dust particles. Geochim. Cosmochim. Acta **59**, 4707–4712. (1995) 212, 218
66. Klöck, W., Thomas, K.L., McKay, D.S., Palme, P.: Unusual olivine and pyroxene compositions in interplanetary dust and unequilibrated ordinary chondrites. Nature **339**, 126–128 (1989) 212, 216
67. Bradley, J.P.: Chemically anomalous, preaccretionally irradiated grains in interplanetary dust from comets. Science **265**, 925 (1994) 212
68. Bradley, J.P., Keller, L.P., Snow, T.P., Hanner, M.S., Flynn, G.J., Gezo, J.C., Clemett, S.J., Brownlee, D.E., Bowey, J.E.: An infrared spectral match between GEMS and interstellar grains. Science **285**, 1716–1718 (1999) 212, 222
69. Zolensky, M.E.: Refractory interplanetary dust particles. Science **237**, 1466–1468 (1987) 212
70. McKeegan, K.D.: Oxygen isotopes in refractory stratospheric dust particles: proof of extraterrestrial origin. Science **237**, 1468–1471 (1987) 212
71. Brownlee, D.E., the PET Team: Comet Wild 2 under a microscope. Science **314**, 1710–1714 (2006) 213
72. Zolensky, M., et al.: 'Mineralogy and petrology of Comet Wild 2 nucleus samples. Science **314**, 1735–1740 (2006) 213, 214, 215, 216, 218, 219, 220
73. Burchell, M.J., Fairey, S., Wozniakiewicz, P., Brownlee, D.E., Horzm F., Kearsley, A.T., See, T., Tsou, P., Westphal, A., Green, S.F., Trigo-Rodriguez, J.M., Dominguez, G.: Characteristics of cometary dust tracks in Stardust aerogel and laboratory calibrations. Meteorit. Planet. Sci. **43**, 23–40 (2008) 213, 215, 216
74. Barrett R.A., Zolensky M.E., Horz F., Lindstrom D.J., Gibson E.K.: Suitability of silica aerogel as a capture medium for interplanetary dust. Proceedings of the 19th Lunar and Planetary Science Conference, pp. 203–221 (1992) 213, 216, 220
75. Burchell, M.J., Graham G., Kearsley A.: Cosmic dust collection in aerogel. Annu. Rev. Earth Planet. Sci. **34**, 385 (2006) 213, 216
76. Hörz, F., Zolensky M.E., Bernhard R.P., See T.H., Warren J.L.: Impact features and projectile residues in aerogel exposed on Mir. Icarus **147**, 559–579 (2000) 213, 216, 220
77. Zolensky, M., et al.: Comparing Wild 2 particles to chondrites and IDPs. Meteorit. Planet. Sci. **43**, 261–272 (2008) 213, 215, 216, 217, 218, 219
78. Nakamura, T., Noguchi T., Tsuchiyama A., Ushikubo T., Kita N., Valley J., Zolensky M.E., Kakazu Y., Sakamoto K., Mashio E., Uesugi K., Nakano T.: Chondrulelike objects in short-period comet 81P/Wild. Science **321**, 1664–1667 (2008) 215, 219, 220

79. Matrajt, G., Ito, M., Wirick, S., Messenger, S., Brownlee, D., Joswiak, D., Flynn, G., Sandford, S., Snead, C., Westphal, A.: Carbon investigation of two Stardust particles: a TEM, NanoSIMS, and XANES study. Meteorit. Planet. Sci. **43**, 315–334 (2008) 215, 225
80. Flynn, G.J.,et al.: Elemental compositions of comet 81P/Wild 2 samples collected by Stardust. Science **314**, 1730–1733 (2006) 214, 216
81. Leroux, H., Rietmeijer, F.J.M., Velbel, M.A., Brearley, A.J., Jacob, D., Langenhorst, F., Bridges, J.C., Zega, T.J., Stroud, R.M., Cordier, P., Harvey, R.P., Lee, M., Gounelle, M., Zolensky, M.E.: A TEM study of thermally modified comet 81P/Wild 2 dust particles by interactions with the aerogel matrix during the Stardust capture process. Meteorit. Planet. Sci. **43**, 97–120 (2008a) 214, 217, 218, 220
82. Leroux, H., Stroud, R.M., Dai, Z.R., Graham, G., Troadec, D., Bradley, J., Teslich, N., Borg, J., Kearsley, A., Hörz, F.: Transmission electron microscopy of cometary residues from micron-sized craters in the Stardust Al-foils. Meteorit. Planet. Sci. **43**, 143–160 (2008b) 214, 217, 218
83. Kearsley, A.T., Borg, J., Graham, G.A., Burchell, M.J., Cole, M.J., Lerouz, H., et al.: 'Dust from comet Wild 2: interpreting particle size, shape, structure, and composition from impact features on the Stardust aluminium foils. Meteorit. Planet. Sci. **43**, 41–74 (2008) 215, 216
84. Rietmeijer, F.J.M.: The earliest chemical dust evolution in the solar nebula. Chem. Erde **62**, 1–45 (2002) 216
85. Akai, J.: Incompletely transformed serpentine-type phyllosilicates in the matrix of Antarctic CM chondrites. Geochim. Cosmochim. Acta **52**, 1593–1599 (1988) 216, 221
86. Zolensky, M.E., Kinard, W.H.: Results of the LDEF meteoroid and debris special investigation group. Adv. Space Res. **13**, (8)75–(8)85 (1993) 216
87. Barrett, R.A., Zolensky, M.E., Bernhard, R.: Mineralogy of chondritic interplanetary dust particle impact residues from LDEF. Lunar Planet. Sci. **XXIV**, 65–66 (1993) 216, 220
88. Gounelle, M., Devouard, B., Engrand, C., Genge, M., Topani, A., Leroux, H.: TEM study of Antarctic micrometeorites: a preliminary report. Meteorit. Planet. Sci. **37**, A55 (2002) 216
89. Simon, S.B., Grossman, L.: Petrography and mineral chemistry of the Tagish Lake carbonaceous chondrite. Meteorit. Planet. Sci. **38**, 813–825 (2003) 216
90. Weisberg, M.K., Connolly, H.C., Ebel, D.S.: Petrology and origin of amoeboid olivine aggregates in CR chondrites. Meteorit. Planet. Sci. **39**, 1741–1753 (2004) 216
91. Wogelius, R.A., Walther, J.V.: Olivine dissolution kinetics at near surface conditions. Chem. Geol. **9**7, 101–112 (1992) 217
92. Leroux, H., Jacob, D., Stodolna, J., Nakamura-Messenger, K., Zolensky, M.: Igneous Ca-rich pyroxene in comet 81P/Wild 2. Am. Mineral. (93), 1933–1936 (2008c) 217, 219
93. Joswiak, D.J., Brownlee, D.E., Matrajt, G.I.: Surprisingly high abundance of Na and Cr-rich calcic pyroxenes in Stardust tracks. Lunar Planet. Sci. **XXXIX**, Abstract 2177 (2008) 217, 218
94. Brown, M.E., Barkume, K.M., Ragozzine, D., Schaller, E.L.: A collisional family of icy objects in the Kuiper belt. Nature **446**, 294–29 (2007) 218
95. Vaughan, D., Craig, J.: Mineral Chemistry of Metal Sulfides, p. 493 . Cambridge University Press, Cambridge (1978) 218
96. Bullock, E.S., Gounelle, M., Lauretta, D.S., Grady, M.M., Russell, S.: Mineralogy and texture of Fe-Ni sulfides in CI1 chondrites: clues to the extent of aqueous alteration on the CI1 parent body. Geochim. Cosmochim. Acta **69**, 2687–2700 (2005) 218
97. Bradley, J.B., Brownlee, D.E.: An interplanetary dust particle linked directly to CM meteorites and an asteroidal origin. Science **251**, 549–552 (1991) 218
98. Zolensky, M.E., Barrett, R.A., Browning, L.: Mineralogy and composition of matrix and chondrule rims in carbonaceous chondrites. Geochim. Cosmochim. Acta **57**, 3123–3148 (1993) 218, 221
99. Simon, S.B., Joswiak, D.J., Ishii, H.A., Bradley, J.P., Chi, M., Grossman, L., Aléon, J., Brownlee, D.E., Fallon, S., Hutcheon, I.D., Matrajt, G., McKeegan, K.D.: A refractory inclusion returned by Stardust from comet Wild 2. Meteorit. Planet. Sci. **43**, 1861–1877 (2008) 219, 220
100. McKeegan, K., Aléon, J., Bradley, J., Brownlee, D., Busemann, H., Butterworth, A., et al.: Isotopic compositions of cometary matter returned by Stardust. Science **314**, 1724–1728 (2006) 219

101. Ebel, D.S.: Condensation of rocky material in astrophysical environments. In: Lauretta, D., et al. (eds.) Meteorites and the Early Solar System II, pp. 253–277. University of Arizona, Tucson, AZ (2006) 219, 224
102. Grossman, J.N., Rubin, A.E., MacPherson, G.J.: A unique volatile-poor carbonaceous chondrite with implications for nebular agglomeration and fractionation processes. Earth Planet. Sci. Lett. **91**, 33–54 (1988) 219
103. Gaffey, M.J., Bell, J.F., Cruikshank, D.P.: Reflectance spectroscopy and asteroid surface mineralogy. In: Binzel, R.P., Gehrels, T., Matthews, M.S. (eds.) Asteroid II, pp. 98–127. University of Arizona Press, Tucson, AZ (1989) 219
104. Ishii, H.A., Bradley, J.P., Dai, Z.R., Chi, M., Kearsley, A.T., Burchell, M.J., Browning, N.D., Molster, F.: Comparison of comet 81P/Wild 2 dust with interplanetary dust from comets. Science **319**, 447–450 (2008) 220
105. Keller, L.P., Messenger, S.: Relict amorphous silicates in Stardust samples. 71st Annual Meteoritical Society Meeting, Matsue, Japan (2008) 220
106. Akai, J.: Mineralogical evidence of heating events in Antarctic carbonaceous chondrites, Y-86720 and Y-82162. Proceedings of the NIPR Symposium on Antarctic Meteorites, No. 3, pp. 55–68. (1990) 221
107. Zolensky, M.E., Prinz, M., Lipschutz, M.E.: Mineralogy and thermal history of Y-86720, Y-86720 and B-7904. Proceedings of the 16th Symposium on Antarctic Meteorites, Tokyo, 78-2 (1991) 221
108. Okudaira, K., Noguchi, T., Nakamura, T., Sugita, S., Sekine, Y., Yano, H.: Evaluation of mineralogical alteration of micrometeoroid analog materials captured in aerogel. Adv. Space Res. **34**, 2299–2304 (2004) 221
109. Okudaira, K., Yano, H., Noguchi, T., Nakamura, T., Burchell, M.J., Cole, M.J.: Are they really intact? — Evaluation of captured micrometeoroid analogs by aerogel at the flyby speed of Stardust. Lunar Planet. Sci. **XXXVII**, 1832 (2006) 221
110. Cody, G.D., Yabuta, H., Alexander, C.M.O'd, Araki, T., Kilcoyne, A.L.D., The Stardust Pet TEAM: Placing comet 81p/Wild 2 organic particles into context with chondritic organic solids. Lunar Planet. Sci. **XXXVIII**, Abstract 2286 (2007) 221
111. Sandford, S.A., Aléon, J., Alexander, C.M.O.'D., Araki, T., Bajt, S., Baratta, G.A., et al.: Organics captured from comet Wild 2 by the Stardust spacecraft. Science **314**, 1720–1724 (2006) 221, 225
112. Wirick, S., Leroux, H., Tomeoka, K., Zolensky, M., Flynn, G., Tyliszczak, T., Butterworth, A., Tomioka, N., Ohnishi, I., Nakamura-Messenger, K., Sandford, S., Keller, L., Jacobsen, C.: Carbonates found in Stardust aerogel tracks. Lunar Planet. Sci. **XXXVIII**, p.1534 (2007) 221
113. Mikouchi, T., Tachikawa, O., Hagiya, K., Ohsumi, K., Zolensky, M.: Mineralogy and crystallography of comet 81P/Wild 2 particles returned by the Stardust mission. Lunar Planet. Sci. **XXXVIII**, p. 1946 (2007) 221
114. Tonui, E., Zolensky, M.E., Lipschutz, M.E.: Petrography, mineralogy and trace element chemistry of Y-86029, Y-793321 and LEW 85332: aqueous alteration and heating events. Proceedings of the NIPR Symposium on Antarctic Meteorites, No. 15, pp. 38–58 (2002) 221
115. Zolensky, M., Lindstrom, D.J.: Mineralogy of 12 large chondritic interplanetary dust particles. Proceedings of the 19th Lunar and Planetary Science Conference, pp. 161–169 (1992) 221
116. Wooden, D.H.: Cometary refractory grains: interstellar and nebular sources. Space Sci. Rev. **138**, 75–108 (2008) 222, 223, 224, 225
117. Martin, P.G.: On the value of GEMS (glass with embedded metal and sulfides). Astrophys. J. **445**, L63–L66 (1995) 222
118. Goodman, A.A., Whittet, D.C.B.: A point in favor of the superparamagnetic grain hypothesis. Astrophys. J. **455**, L181–L184 (1995) 222
119. Messenger, S., Keller, L.P., Stadermann, F.J., Walker, R.M., Zinner, E.: Samples of stars beyond the solar system: silicate grains in interplanetary dust. Science **300**, 105–108 (2003) 222
120. Keller, L.P., Messenger, S.: Coordinated chemical and isotopic studies of GEMS grains in IDPs. Lunar Planet. Sci. **39**, 2347 (2008) 222

121. Bradley, J.P., Dai, Z.R.: Mechanism of formation of glass with embedded metal and sulfides. Astrophys. J. **617**, 650–655 (2004) 222
122. Westphal, A.J., Bradley, J.P.: Formation of glass with embedded metal and sulfides from shock-accelerated crystalline dust in superbubbles. Astrophys. J. **617**, 1131–1141 (2004) 222
123. Tielens, A.G.G.M., Waters, L.B.F.M., Bernatowicz, T.J.: Origin and evolution of dust in circumstellar and interstellar environments. In: Krot, A.N., Scott, E.R.D., Reipurth, B. (eds.) Chondrules and the Protoplanetary Disk. ASP Conf. Series vol. 341, pp. 605–651. ASP, San Francisco, CA (2005) 222
124. Waters, L.B.F.M., Molster, F.J., de Jong, T., et al.: Mineralogy of oxygen-rich dust shells. Astron. Astrophys. **315**, L361–L364 (1996) 223
125. Kemper, F., Vriend, W.J., Tielens, A.G.G.M.: The absence of crystalline silicates in the diffuse interstellar medium. Astrophys. J. **609**, 826–837 (2004) 223
126. Kemper, F., Vriend, W.J., Tielens, A.G.G.M.: Erratum: the absence of crystalline silicates in the diffuse interstellar medium. Astrophys. J. **633**, 534 (2005) 223
127. Waelkens, C., Waters, L.B.F.M., de Graauw, M.S., et al.: SWS observations of young main-sequence stars with dusty circumstellar disks. Astron. Astrophys. **315**, L245–248 (1996) 223
128. Weinberger, A.J., Becklin, E.E., Schneider, G., Chang, E.I., Lowrance, P.J., Silverstone, M., Zuckerman, B., Hines, D.C., Smith, B.A.: Infrared views of the TW Hydra disk. Astrophys. J. **566**, 409–418 (2002) 223
129. Malfait, K., Waelkens, C., Waters, L.B.F.M., Vandenbussche, B., Huygen, E., de Graauw, M.S.: The spectrum of the young star HD100546 observed with the Infrared Space Observatory. Astron. Astrophys. **332**, L25–L28 (1998) 223
130. Knacke, R.F., Fajardo-Acosta, S.B., Telesco, C.M., Hackwell, J.A., Lynch, D.K., Russell, R.W.: The silicates in the disk of β pictoris. Astron. Astrophys. **418**, 440–450 (1993) 223
131. Grady, C.A., Sitko, M.L., Bjorkman, K.S., Perez, M.R., Lynch, D.K., Russell, R.W., Hanner, M.S.: The star-grazing extrasolar comets in the HD100546 system. Astrophys. J. **483**, 449–456 (1997) 223
132. Weissman, P.R.: The Vega particulate shell: comets or Asteroids. Science **224**, 987 (1984) 223
133. Gail, H.-P.: Radial mixing in protoplanetary accretion disks IV. Metamorphosis of the silicate dust complex. Astron. Astrophys. **413**, 571–591 (2004) 223
134. Bradley, J.P., Brownlee, D.E., Veblen, D.R.: Pyroxene whiskers and platelets in interplanetary dust: evidence of vapour phase growth. Nature **301**, 473–477 (1983) 223
135. Boss, A.P.: Mixing in the solar nebula: implications for isotopic heterogeneity and large-scale transport of refractory grains. Earth Planet. Sci. Lett. **268**, 102–109 (2008) 223
136. Ciesla, F.J.: Outward transport of high-temperature materials around the midplane of the solar nebula. Science **318**, 613–615 (2007) 223
137. Shu, F.H., Shang, H., Glassgold, A.E. , Lee, T.: X-rays and fluctuating X-winds from protostars. Science **277**, 1475–1475 (1997) 223
138. Cuzzi, J.N., Zahnle, K.: Material enhancement in protoplanetary nebulae by particle drift through evaporation fronts. Astrophys. J. **614**, 490–496 (2004) 224, 225
139. Greenberg, J.M.: What are comets made of? A model based on interstellar dust. In: Wilkening, L.L. (ed.) Comets, pp. 131Ů163. University of Arizona Press, Tucson (1982) 225
140. Fomenkova, M.N., Chang, S., Mukhin, L.M.: Carbonaceous components in the comet Halley dust. Geochim. Cosmochim. Acta **58**, 4503–4512 (1994) 225

The In-Situ Study of Solid Particles in the Solar System

I. Mann and E.K. Jessberger

Abstract In-situ measurements of dust from spacecraft can in principle provide information about dust properties at any given place in the solar system and under conditions that are not reproducible on Earth. Already relatively simple in-situ measurements provide information about the properties of dust particles. Measurements of interplanetary dust have shown for the first time the fluffy and porous structure of interplanetary dust as well as the existence of two dust components with distinctly different properties. Experiments during the missions to comet Halley have shown the cometary dust to consist of two major components to about the same amount: a component that is rich in rock-forming elements and a component that is rich in the elements H, C, N and O. The latter component is assumed to consist of refractory organic material. Although the composition of interstellar dust particles is not directly measured yet, their conditions of entry into the solar system reveal the forces that are acting on them. The forces depend on the properties of dust and allow for a comparison to astrophysical models of dust size, composition and structure. In-situ measurements with improved dust detectors are presently carried out and planned for future missions. The scientific return of these future measurements can be greatly enhanced by combining detailed laboratory studies of the physics and functional principles of the detectors.

1 Introduction

The interplanetary medium of our solar system is filled with neutral and charged atoms and molecules as well as with solid dust particles. Dust particles are ejected from comets, generated by mutual collisions of solar system bodies, and emerge

I. Mann (✉)
School of Science and Engineering, Kindai University, Kowakae 3-4-1, Higashi-Osaka, Osaka, 577-8502, Japan
e-mail: mann@kindai.ac.jp

E.K. Jessberger
Institut für Planetologie, Westfälische Wilhelms-Universität, Münster, Wilhelm-Klemm-Str. 10, 48149 Münster, Germany
e-mail: ekj@uni-muenster.de

Mann, I., Jessberger, E.K.: *The In-Situ Study of Solid Particles in the Solar System*. Lect. Notes Phys. **815**, 233–257 (2010)
DOI 10.1007/978-3-642-13259-9_5

from atmosphereless bodies for instance due to volcanic activity, collisions, and impact erosion. The two latter mechanisms produce considerable amounts of dust from asteroids in the inner solar system and presumably from Kuiper belt objects in the outer solar system beyond the giant planets, while dust from comets is one of the major components in the inner solar system. Aside from those dust particles that originate from solar system objects, interstellar dust particles stream through the solar system due to the motion of the Sun relative to the surrounding interstellar medium.

Dust particles are considerably larger than atoms, molecules and ions and opposed to these particles usually show some of the properties of a solid. They are sufficiently large to built up a solid structure which can be heterogeneous. While compared to large solar system bodies, they do not show significant internal processing. As far as their dynamics is concerned, gravitational forces affect them in the same way as large solar system objects, but also radiation pressure and electromagnetic forces act on them as they act on ions. Dust particles bear the properties of their parent bodies and their study reveals different paths and different degrees of processing of solid material from the time of the formation of the solar system.

The detection methods of dust in the solar system are summarized in Fig. 1. At present, information on dust particles is gathered from astronomical observations, from direct measurements of dust from spacecraft, from the detection of particles entering the Earth's atmosphere and from the collection of its fragments or even of the entire particle on Earth. Remote astronomical observations of solar light scattered by dust as well as of the thermal emission reveal the average properties of dust particles along the line of sight of observations and over their entire size spectrum. Among the astronomical observations, thermal emission in many cases characterizes the material composition of dust particles, while, for instance, the polarization of the scattered light provides information on the material, size and structure of the particles. The direct detection of dust particles (i.e. meteoroids) is possible when they enter the Earth's atmosphere. The decelerated meteoroidal material and surrounding atmospheric particles are ionized and produce the observable brightness, i.e. the meteor. Depending on the size, structure and entry conditions, meteoroidal material reaches the ground as meteorites where it can be collected and further studied. For particles of certain sizes entry conditions can be very smooth and they can be collected in the stratosphere, as IDPs (Interplanetary Dust Particles).[1]

Clearly, as seen in Fig. 1, in-situ measurements of cosmic dust from spacecraft cover the size range with the largest number of particles. But still the study with in-

[1] According to the IAU convention bodies that are considerably smaller than an asteroid and considerably larger than an atom or molecule are defined as meteoroids (cf. [1]). Dust particles are micrometeoroids typically of sizes of 100 μm and smaller. In some cases, the term "IDP" is solely used for those Interplanetary Dust Particles (IDPs) that are collected in the stratosphere by high-flying aircrafts. Their typical size ranges from 5 to 50 μm. Cosmic dust particles that are collected in the Arctic or Antarctic Ice or from the sea floor and typically range between 100 and 1, 000 μm are often denoted as Micrometeorites (MMs). Dust particles in interplanetary space that make up the visible and thermal brightness of the Zodiacal light, i.e. mainly dust in the size interval 1–100 μm are often referred to as Zodiacal dust.

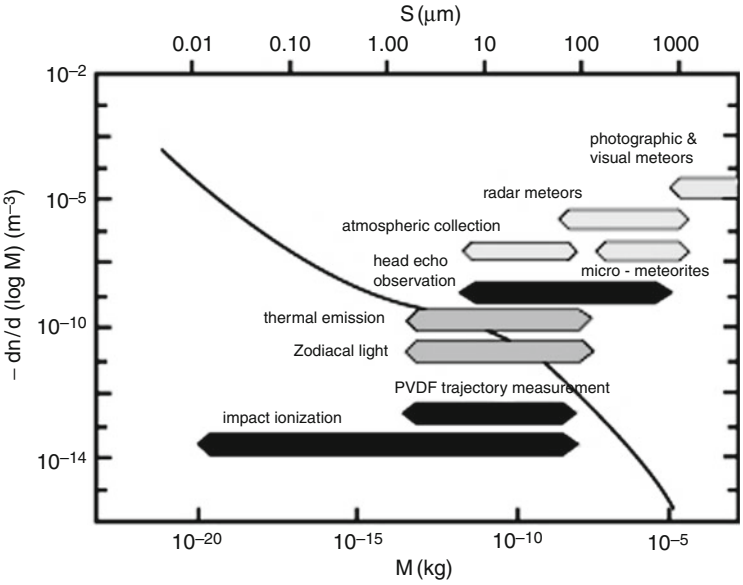

Fig. 1 Detection methods of dust and meteorites in interplanetary space. The solid line denotes the differential number density distribution as function of the mass of particles derived from various measurements at 1 AU as compiled by Grün et al. [2] on the basis of several data sets. The upper axis denotes the size corresponding to the mass scale under the assumption of a bulk density of 3 10^3 kg/m^3. The range of detection is shown for different methods. The observation of meteors [3], the atmospheric collection of IDPs (see "The Astromineralogy of Interplanetary Dust Particles" by Bradley, this volume) and collection of micrometeorites [4] on the ground yield data about near Earth dust and meteorites of sizes beyond several μm. Meteor head-echo measurements directly provide the velocities of entering particles [5]. Thermal emission and visual scattered light measurements of the Zodiacal light describe the dust mainly near the ecliptic between 0.3 and 1.7 AU distance from the Sun and in the size interval from about 1 to 100 μm [6]. Polyvinylidene Fluoride (PVDF) [7] and impact ionization detectors (cf. [8]) measure dust, predominantly of sizes below 100 μm from spacecraft. The in-situ detection of large dust particles in space is limited by the statistics of the low number densities

situ experiments is impeded by the low flux of impacting dust particles, the selection of certain sizes and locally occurring dust fluxes, the limited number of spacecraft carrying dust detectors as well as the experimental limits of the instruments.

The interest in in-situ dust measurements is two-fold: (a) measurements of dust fluxes and sizes as function of time and location reveal the dynamics of dust particles and the underlying physical processes, and (b) in-situ measurements could, in principal, provide direct information on the chemistry, structure and isotopic composition that is not biased by the entry conditions if particles hit the Earth. This article discusses the possibilities of in-situ experiments from the mineralogical point of view in comparison and as complement to the other measurement techniques mentioned above. In the context of astromineralogy the basic issues that should be addressed with in-situ measurements and can be compared to other studies (of IDPs,

astronomical observations, etc.) are properties of interstellar dust and the evolution of interplanetary and cometary dust in the solar system.

"Full information" about dust particles would result from structural, chemical, mineralogical, molecular and isotopic analyses if combined with the orbital parameters. However, even solid interplanetary dust particles that are readily available for laboratory analysis hide behind their small size the wealth of information they potentially contain: A typically 15 μm particle only can be analyzed rather roughly (cf. [9, 10]) and e.g. the radiometric age of not even a single IDP has been obtained! Although the in-situ analysis in space is even limited to much greater extend, we will show that already in-situ detection in terms of dust sizes and flux rates can provide valuable information for restricting the range of parameters of models that are derived from observations. We further discuss results from mass spectrometry measurements performed in-situ in space.

We first describe the basic functional principles of in-situ experiments and indirect dust measurements during previous and on-going space missions. We then will discuss the study of dust properties based on space experiments addressing three specific topics: measurements of the interplanetary dust cloud, in-situ measurements at comets and in-situ measurements of interstellar dust entering the solar system.

2 The Basis of Dust Measurements

A process that is similar to meteor formation takes place when dust particles hit a solid target in space. Momentum is transferred onto the target and, depending on impact speed and mass of the particle, both target and projectile material are mechanically deformed; part of the material is melted and sublimates. The impact process can be distinguished according to three regimes of impact parameters: The scattering and accretion regime, the fragmentation and low vaporization regime, and the volume vaporization regime. The boundaries between these regimes depend on the relative velocity and on the mass of the particles. At relative velocities – between dust and analyzing tool – below about 1 km/s collisions may lead to the accretion or sticking of the colliding particles. At relative velocities 1–50 km/s collisions lead to fragmentation as well as to the ionization of surface materials. At relative velocities beyond 50 km/s the entire particle is destroyed and the produced vapor is ionized (Fig. 2). Many of the former and current space dust experiments are based on the detection of the ionized impact debris (impact ionization detectors). For most spacecraft cruising in interplanetary space (Helios, Ulysses) or on fast flyby trajectories (Giotto, Vega) relative velocities are in a range where impacting particles are partly destroyed. During so-called rendezvous missions, on the other hand, the spacecraft closely follows a solar system body in its orbit. Hence impact speeds are low and impacting particles are accreted at a collection surface without or with few mechanical destruction. An example is the Rosetta mission to comet Churyumov-Gerasimenko (see below).

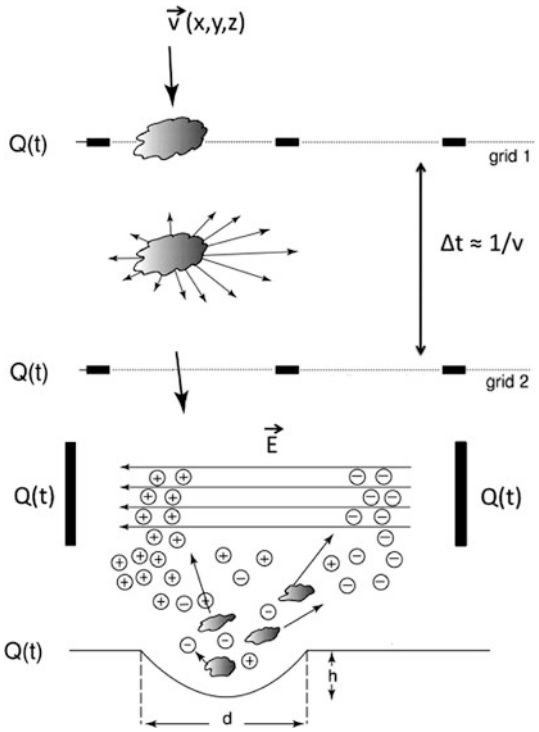

Fig. 2 Schematic view of some of the dust detection mechanisms. The electric surface charge of dust induces a charge pulse when dust particles travel through a system of conductive grids. This allows to derive the travel time of the particle. Particles may be optically detected through a scattered light signal. Upon impact on a solid target the particles transfer momentum and charge onto the target. Both, target and projectile material are mechanically deformed and solid material is ejected. Target and projectile material are heated, partly melted and ionized. Positively and negatively charged particles are separated in an electric field and can be measured. The formation of an ion cloud also causes a light flash

McDonnell [11] gave a summary of the first techniques to measure dust in space. Early experiments detected the momentum transfer associated with a dust impact with microphones. Also the destructed target area can be determined to estimate the size of the impacting particles (see for instance [12, 13]). Moreover, the light flash that is associated with the impact can be measured. For the technical and functional principle of modern instruments we refer to a recent review by Auer [8]. We now shortly describe the different methods of dust detection from spacecraft.

2.1 Impact Ionization Detectors

Impact ionization detectors are based on the fact that the particles are destroyed during the impact: the produced electrons and ions are separately detected as shown

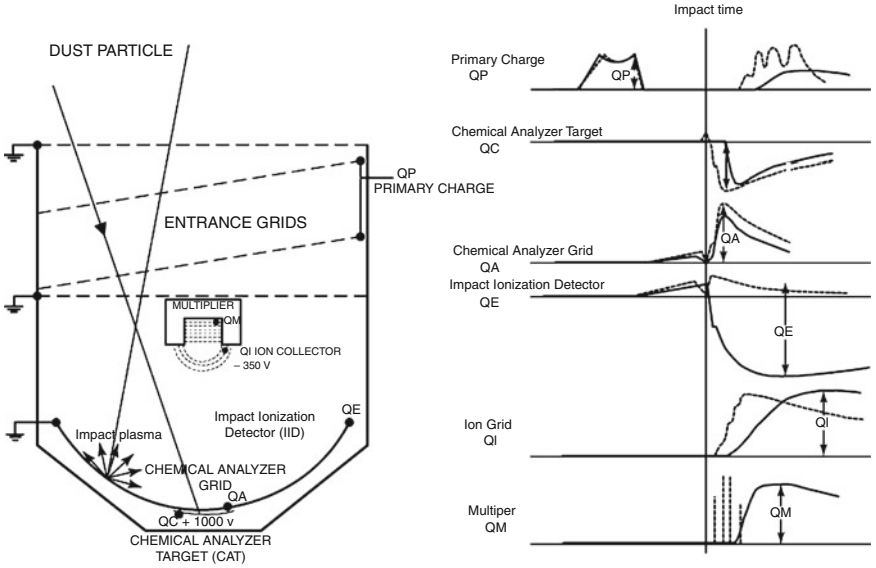

Fig. 3 The impact ionization dust analyzer aboard Cassini [14]. The *left hand side* of the figure show the schematics of the detector, the right hand side shows the different channels of measured signals: The particle velocity is estimated through the sequence of charges that are induced in a system of tilted entrance grids (denoted as primary charge QP on the *right hand side* of the figure) before they impact onto the target plate. The produced ions and electrons are detected at the target plate (QE, QA, QC) and in the ion collector (QI). Ions that are produced are accelerated due to the applied voltage and measured as a function of their flight time at a multichannelplate (QM)

in Fig. 2. Further, time of flight measurement of the produced ions yields the element composition. The principal of impact ionization detectors is demonstrated with the dust analyzer onboard Cassini shown in Fig. 3 [14, 15]. The Cassini experiment predominantly analyses dust in the vicinity of Saturn. Some results concerning

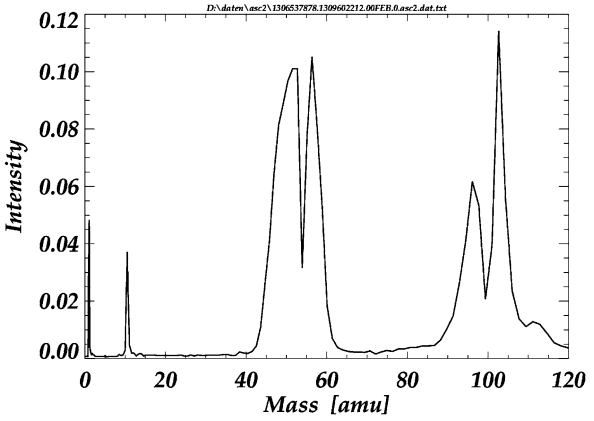

Fig. 4 The first mass spectrum of time-of-flight ion measurements with the Cassini dust analyzer corresponding to channel QM in Fig. 3

interplanetary dust are given below. Figure 4 shows the first time-of-flight spectrum obtained with the Cassini experiment. In this spectrum a broad peak ranges over more than 10 amu and is not resolved. The difference to laboratory mass spectra is obvious. It arises partly from instrumental limitations and partly from the impact ionization process. The detected species originate from a complex ionization, expansion and recombination process that takes place in the dust-plasma cloud that is formed at the high velocity impact. The interpretation in terms of the element compositions of the impacting dust particles is not unambiguous and requires a detailed analysis of the impact ionization process.

2.2 Measurement of Structure and Optical Properties

A combined study of non-optical in-situ measurements and remote optical observations would allow for a close comparison to astronomical observations. Such measurements are potentially applicable to dust components that have small relative velocities to the spacecraft. Giese et al. [16] had pointed out the possibility to measure the light scattered by a single cometary dust particle as it passes through a collimated light beam and suggested the analysis of cometary dust by optical scattering experiments locally from space probes. Due to the required time resolution for optical detection, the method is favorable for dust measurements at small relative velocities. An optical probe experiment was suggested for the European fly-by mission to Comet Halley to measure the local brightness and polarization along the spacecraft trajectory [17]. The proposed experiments were limited by the light sources and detector units that were available for space instrumentation at that time and the instrument aboard GIOTTO used sunlight for illumination [18]. Development of low weight and low power laser elements now allows for using them in space experiments. Laser light scattering instruments are built for the Rosetta mission and will be used to estimate the velocity vector of infalling dust particles (cf. [19]) This points to an important issue of dust measurements from spacecraft: How to obtain orbital information on the detected particles?

2.3 Measurement of Dust Orbits

The impact speed and direction of particles can often only be crudely estimated from the orientation of the spacecraft at the time of the impact. Tuzzolino et al. [7] recently attempted a more specific measurement of a dust particle velocity and impact direction from spacecraft. The Space Dust (SPADUS) instrument aboard the Earth orbiting satellite ARGOS uses Polyvinylidene Fluoride (PVDF) dust sensors combined with a velocity/trajectory system. Dust particles travel through a sandwich of sensor foils where the impact time and location is measured. This allows estimating the impact velocity and direction [7]. It permits the distinction between orbital debris and cosmic dust, as well as the determination of the orbital elements for some of the impacting particles [20]. McDonnell et al. [21] suggested combining aerogel

collection to retrieve samples for analysis with real time detection with a position-sensitive impact sensor in order to achieve a better classification of the samples. We expect the determination of dust orbital parameters to improve for future dedicated dust experiments.

2.4 Indirect Measurements

Aside from these direct dust detections some information on dust properties is also obtained from signals gathered with other space instruments. The charged particles that are produced by dust impact ionization cause a variation of plasma parameters which is typically nonlinear and hence its interpretation is difficult. The radio noise that was detected when the Voyager 1 and 2 spacecraft crossed the Saturn rings was explained with dust as a possible source [22]. During the Uranus ring plane crossing of the Voyager 2 spacecraft the Planetary Radio Astronomy instrument aboard recorded a characteristic intense noise due to the impact ionization of dust particles with sizes $> 1\,\mu m$ [23]. Voyager measurements at planetary rings and ICE (International Cometary Explorer) measurements during the encounter with comet Giacobini-Zinner were used to estimate dust sizes and fluxes [24, 25]. Dust impacts in the milligram range on the Giotto spacecraft were observed to influence the time variation of the measured magnetic field; and simultaneous events were seen in the plasma analyzer and an ion mass spectrometer [26]. The plasma wave measurements onboard Voyager were also used to estimate dust fluxes in the outer solar system [27].

3 In-Situ Measurements of Interplanetary Dust

3.1 Experimental Results

Early in-situ experiments did not measure the element composition of dust, but they allowed already an estimate of parameters like density and structure. An important piece of information obtained from combining the results of in-situ and optical measurements is that a large fraction of dust in the interplanetary medium has a fluffy, porous structure: During the missions of the Helios space probes dust flux measurements could be compared to optical measurements aboard the same spacecraft. The comparison of the local dust number density and local scattered light brightness showed that previous models explaining the Zodiacal light by light scattered primarily at compact dust particles of sizes below $1\,\mu m$ were not valid. Instead, Giese et al. [28] suggested that the main contribution to the zodiacal light originated from particles greater than or equal to $10\,\mu m$ in size. In order to find a consistent description of both flux measurements and optical measurement, they proposed absorbing particles of fluffy structure as an important component of the interplanetary dust cloud. Around the same time the analysis of interplanetary dust samples collected

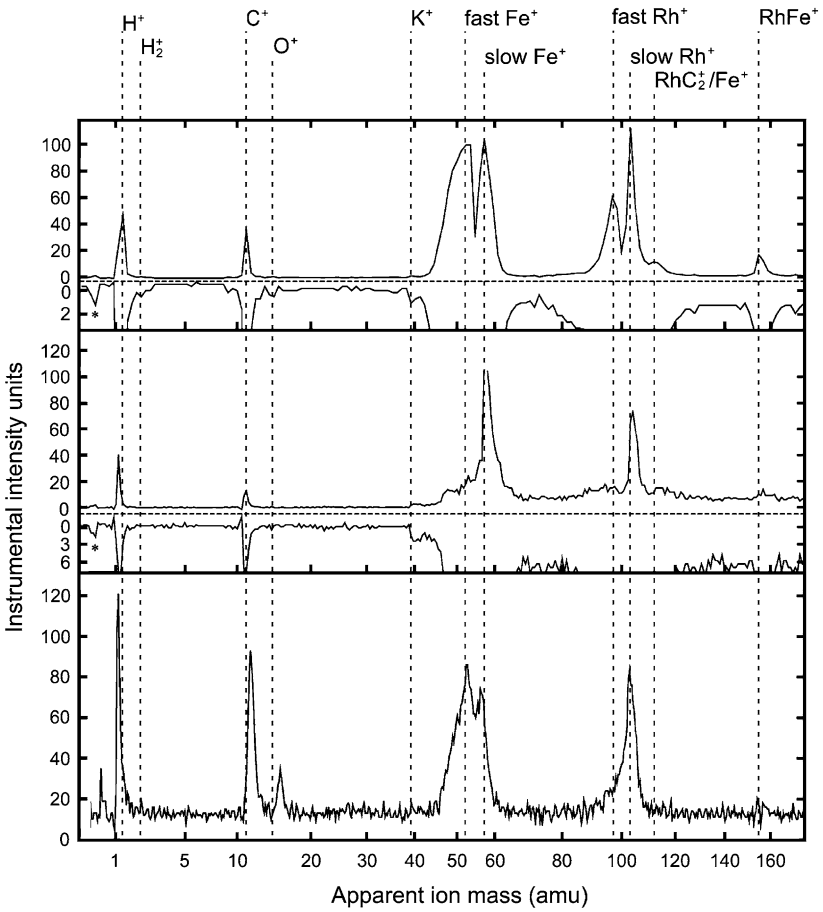

Fig. 5 Time of Flight (TOF) mass spectra generated by interplanetary dust particle impacts on the Cosmic Dust Analyzer (CDA) onboard the Cassini spacecraft (*upper two panels*) and by a 2×10^{-15} kg iron particle on the CDA Flight Spare Unit in the laboratory (*lower panel*). In the upper two panels below the vertical dashed lines the spectra are shown inverted and magnified for clarity. Above the upper panel the ion peaks are identified by the authors as specific ions. The distinction between "fast" and "slow" species of the same ion rests on the fact that both types were not focused into the same TOF slot by a Mamyrian ion mirror as is usual in TOF mass spectrometry. Points marked with asterisks are known instrumental artifacts. Note the striking similarity of the flight and laboratory mass spectra. The slight mass offset in the low ion mass region probably is due to the about a factor of 20 lower energy deposited in the laboratory impact compared to the flight impacts (flight particle speed 10 and 20 km/s, masses of 10^{-14} kg and 10^{-12} kg, respectively, laboratory particle speed 29 km/s and mass 2×10^{-15} kg). The shown figures are adapted from Hillier et al. [32]

from the stratosphere demonstrated that they are fine-grained aggregates of non-volatile building blocks [29, 30]. Today the irregular structure of the interplanetary dust and the high porosity of a fraction of the interplanetary dust are considered established.

Measurements of the Helios missions also indicated the existence of two dust components in the inner solar system between 0.3 and 1 AU [31]: the components have distinctly different densities and orbits and presumably originate from different sources. The measurements, however did not allow for a close analysis of the dust composition.

During cruise to Jupiter, the Cassini dust experiment measured time of flight mass spectra of two interplanetary dust particles (see Fig. 5). Hillier et al. [32] studied the spectra in detail and suggest based on their analyses that the particles are iron-rich. They further conclude that the evidence for silicates is surprisingly small. The estimated size of the particles is in the range of a few micrometer and they were in bound prograde orbits.

3.2 Future Measurements of Interplanetary Dust

While dust measurements in the outer solar system are of interest for studying the interstellar dust that enters the solar system, the measurements in the inner solar system provide more information about the interplanetary dust. Future missions to explore the vicinity of the sun within several solar radii consider dust measurements in order to study the dust interactions with the solar wind plasma [33]. The dust density as well as plasma density and temperature increase near the Sun and dust-plasma interactions are becoming particularly important [34]. Dust measurements in the near solar environment would reveal the dynamics of dust in the time variable solar magnetic field. Even more interesting in terms of dust composition, they provide the opportunity to follow the dust properties under intense solar wind and energetic particle fluxes and the gradual heating of the dust material up to temperatures of about 2,000 K. The thermochemical data suggest that metal silicates contained in the dust, initially decompose into metal oxides and silica and these subsequently either directly sublimate or they form monoxides before they finally sublimate [35].

Aside from that the near solar studies may enhance our knowledge of the carbonaceous dust component. New observations of cometary dust trails show that they eject a larger amount of meteorite fragments than previously assumed [36]. These fragments are a possible source of fresh cometary dust in the inner solar system. The solar wind, then, carries pick up ions from a so-called inner source that is possibly connected to the dust component [37]. During high velocity dust collisions parts of the dust vaporizes and this possibly is the source of the heavy elements within the observed pick-up ions. The observed fraction of carbon among the pick-up ions is possibly generated by cometary dust and this implies that cometary dust contains carbon bearing species that can survive high temperatures in the vicinity of the Sun [38].

4 In-Situ Studies at Comets

4.1 Experimental Results

Among the various types of investigations of cometary dust (see "The Mineralogy of Cometary Dust" by Hanner and Zolensky, this volume), the missions to comet Halley around 1986 allowed for the first time the direct in-situ detection of dust around a comet. Several instruments were used to study dust masses or flux rates [18, 39–42] and several instruments revealed information about dust composition in space [43–45]. Extensive flux measurements were also carried out in early 2004 during the Stardust flyby at comet Wild 2 [46–48]. Measurements during both missions showed that the dust coma of comets is highly variable. Among others, the data suggest the existence of localized dust emission regions on the nucleus, the fragmentation of dust even at large distances from the nucleus, and dust material alteration during the first couple of hours after ejection from the nucleus.

We now concentrate on measurements of the dust composition with mass spectrometry. The results obtained from the measurements of PIA and PUMA $1+2$ onboard GIOTTO and VEGA $1+2$ can be summarized as follows (cf. [43, 44, 49] and references therein): The masses and densities of the detected and analysed individual dust particles range from 10^{-19} to 10^{-14} kg (approximate diameter range 0.02–2 μm) with densities from 0.3 to 3 10^3 kg/m^3. The abundance of small particles below 10^{-17} kg is higher than anticipated. Most of the small particles are rich in the light elements H, C, N, and O. Particles that are abundant in these light elements have a low ratio of mass to volume i.e. low density. The detected particulates are mixtures of two end-member components, dubbed CHON (rich in the elements H, C, N, and O) and ROCK (rich in rock-forming elements as Si, Mg, Fe), respectively. The CHON component is assumed to be refractory organic material while the ROCK component is assumed to comprise silicates, metals, oxides, sulfides and others. Both end-member components do not occur as pure components but are intimately mixed down to the finest scale. CHON- and ROCK-rich particulates each comprise about 25% of the dust while 50% are MIXED. The latter group is defined by the ratio of carbon to any rock-forming element between 0.1 and 10. Several lines of evidence suggest that the refractory organic CHON-component and the ROCK-components are not homogeneously distributed within the impacting dust particles. Notwithstanding, CHON- and ROCK-components are both observed together even in the smallest particles [50].

The bulk abundances of the rock-forming elements in Halley's dust follow solar and chondritic abundances within a factor of two (Fig. 6). With the plausible assumption that the whole comet (dust and ice) has approximately solar composition (with the exception of H and N) an overall dust/ice ratio of 2 was inferred (Fig. 7). The chondritic and solar abundances shown in Figs. 6 and 7 are from Grevesse and Sauval [51] with some corrected values from Holweger [52] included (see Kimura et al. [53] for a detailed discussion). The element abundances of cometary dust are derived from PIA/PUMA data. It should be noted that recently Allende Prieto et al. [54] suggested the photospheric nitrogen abundances were overestimated, so that the

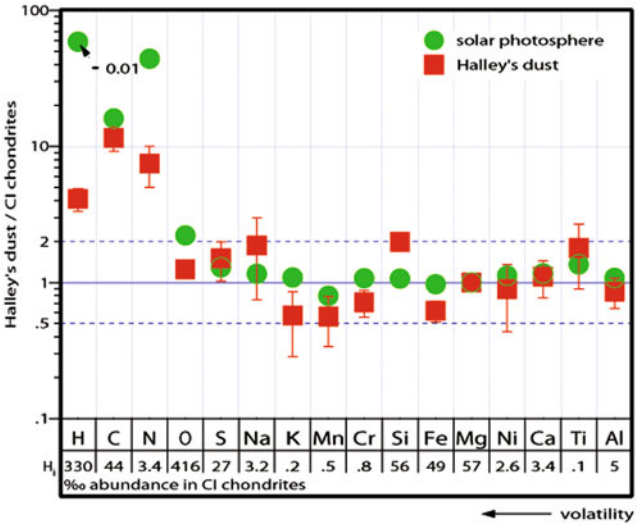

Fig. 6 Mg≡1 normalized element abundances in the dust of comet Halley and the solar photosphere, both relative to the abundances in CI-chondrites. The elements are ordered according to their volatility and recent abundance values were used as explained in the text. The solar hydrogen abundance is multiplied by 0.01. Because of the lack of calibration, Halley's dust data are believed to be certain within a factor two

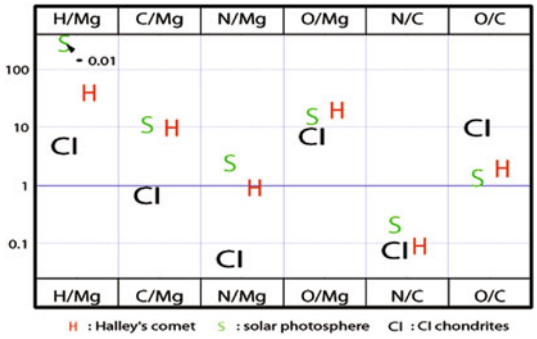

Fig. 7 Element ratios of Halley's comet (H) – dust *and* ice – compared to the same ratios in carbonaceous chondrites (CI) and the solar photosphere (S), obtained from the abundances as in Fig. 6. The solar hydrogen abundance is multiplied by 0.01. The overall similarity of Halley's comet to the solar composition as well as the lesser degree of depletion of non-condensible elements compared to CI-chondrites testify to the more primordial nature of comet Halley

difference between cometary and photospheric nitrogen abundances may originate from observational uncertainties.

Inspecting the variation of the element composition from particle to particle some clues as to the mineralogical composition can be drawn (cf. [55]): Mg/Fe-ratios display a rather wide range, while the variation of the Si/Mg ratios is very limited. At least 40%, maybe more than 60% of the number of analyzed particles are

Mg-rich Fe-poor silicates. About 10% of particles (and therefore the next largest group) are iron- (+nickel)-sulfides while Fe-oxides play only a very minor role (<1%). Particles that are rich in refractory elements and resemble Ca-Al-rich inclusions known from chondrites (possibly the earliest inner-solar-system material formed) or carbonates or sulfates have not been unambiguously identified. The presence of non-equilibrated (high-temperature) minerals like Mg-rich silicates and Fe-sulfides, both formed above ∼600 K, yields evidence that equilibration at low temperatures is too slow a process to have affected the cometary dust particles. It also implies that these minerals after their formation never experienced elevated temperatures during their lifetime within the comet.

As far as the isotopic information is concerned, no significant (i.e. greater than a factor of two) deviation from the normal composition was found for those elements

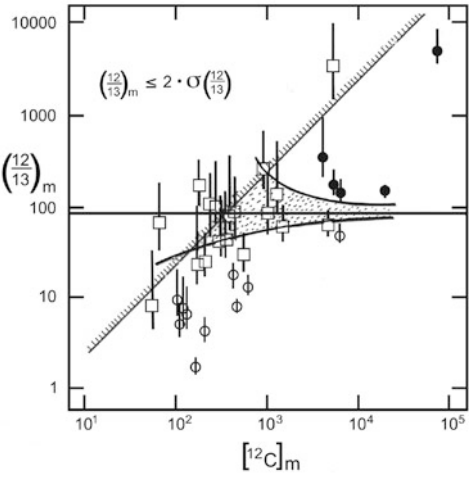

Fig. 8 The carbon isotope ratios for 32 selected high quality time-of-flight mass spectra of cometary dust measured by PUMA-1 onboard Vega-1: shown is the ratio $(12/13)_m$ of the raw signal intensities (=number of recorded ions) at amu = 12 to those at amu = 13 versus the intensity at mass = 12. The intensity at amu = 12 is identified as solely being due to ^{12}C since there are no interfering molecular ions and doubly charged ions have not been observed at all in the PUMA-1 mass spectra. All error bars are based on counting statistics. The vertical line corresponds to the terrestrial $^{12}C/^{13}C$-ratio of 90. Points within the dotted envelope area are within the 2σ error from this normal ratio. The 17 particles (53%), whose (12/13) ratios are shown as *open squares* have normal carbon isotopic composition. In the area to the left of the inclined line the 2σ-ratio uncertainty is larger than the ratio itself. Those data points there are not reliable. The data points below the normal line appear to be ^{13}C-rich (shown as *open circles*). However, the signal intensity at amu = 13 may be enhanced by $^{12}CH^+$ or by noise. Thus, the isotopic carbon composition of these 10 particles (31%) remains open. The *filled circles* above the normal line are derived from low-noise spectra with considerable count rates at amu = 12 as well as at amu = 13 and the ion ratios 12/13 in these 5 particles (16%) safely are identified as true $^{12}C/^{13}C$-ratios. The highest carbon isotopic ratio, $^{12}C/^{13}C = 5,000$, was measured for a particle that is almost pure carbon with a minor rock-element component, further discussion of these data is given in the text

for which it technically would be detectable, like Mg and S. The notable exception, however, is carbon.

The $^{12}C/^{13}C$ ratios of 32 selected cometary dust particles are shown in Fig. 8. They were derived from PUMA-1 measurements onboard Vega-1. The dust has a variable carbon isotopic compositions and only about half of the particles have normal compositions. For one, almost pure carbon particle a $^{12}C/^{13}C$ ratio as high as 5,000 was measured [56]. Similar values were measured in certain presolar graphite grains extracted from carbonaceous chondrites [57]. (See " The Most Primitive Material in Meteorites" by Ott, this volume and Zinner [58], for a discussion of presolar grains.) Besides the extremely high $^{12}C/^{13}C$ ratios also $^{12}C/^{13}C$ ratios below the normal value were measured. They are, however, *strictu sensu* lower limits that may result from noise intensities of unknown origin in the mass spectra. Two conclusions can be drawn from the derived isotopic data: (a) There is no single fixed or typical cometary carbon isotopic composition at least for the case of comet Halley. (b) The presence of the wide range of isotopic compositions of carbon excludes any equilibration processes affecting the carbon carrier during comet formation or later in the comet's history. We further note that such varying carbon isotope ratios have not been measured in the Stardust samples. If this latter result remains during the future studies of Stardust samples it is a further indication that comets are not alike.

4.2 Future Measurements of Cometary Dust

The space mission Stardust allowed for the first time to bring to Earth samples of interstellar and cometary dust and analyses are currently in progress. The hitherto results are discussed in detail in another chapter of this volume.

The space mission Rosetta that was launched in 2003 includes in its scientific payload several instruments designed to better understand the nature of cometary dust. Goals of the measurements cover the determination of the evolution of the dust fluxes and dust dynamics in the coma as well as studies of the dust microstructure and the dust composition. The GIADA experiment (Grain Impact Analyzer and Dust Accumulator, Colangeli et al. [19]) is designed to measure velocity, momentum and direction of the dust flux. The passage of dust through the instrument is detected by laser light scattering, particle momentum by piezoelectric transducers, and mass flux by means of three quartz crystal microbalances. GIADA will be able to detect dust particles in the size range 5–1,000 μm and in the velocity range 0.1–150 m/s. The MIDAS instrument aboard Rosetta is an atomic force microscope (AFM) where a micro–needle scans the surface structure of dust samples collected near the comet [59]. Aside from providing for the first time structural information by three-dimensional imaging of the small dust particles and thus possibly the first direct analysis of cometary mineralogy, MIDAS will also allow to better determine the size distribution of sub–μm cometary dust. While MIDAS relies on the fact that dust particles reach the spacecraft with small relative velocities and are

not destroyed, experiments to study the dust element composition have to apply a destruction mechanism to allow for a composition analysis of the particles. The COSIMA experiment will analyze the element composition of collected dust particles that are ionized with an ion beam [60]. In May 2014 Rosetta will start its approach into orbit about comet Churyumov-Gerasimenko.

5 In-Situ Detection of Interstellar Dust

5.1 Experimental Results

After an early detection of interstellar dust in near-Earth-orbit [61], interstellar dust particles have been positively identified with measurements onboard Ulysses [62] and then with Hiten near Earth and with Galileo and Cassini in interplanetary space. The interstellar dust is distinguished from solar system dust by its impact speed and impact direction (Mann and Kimura [63], and references therein). Especially the long duration and the path of Ulysses where the direction of the interstellar wind flux into the solar system is nearly perpendicular to the Ulysses orbit provided an excellent data set. Moreover, Ulysses allowed for a direct comparison of the dust direction to the direction of the interstellar neutral helium flux measured with a different instrument onboard the same spacecraft [64]. After flight to and flyby at Jupiter, the space probe Ulysses is orbiting the Sun on a nearly polar orbit that is inclined by 79° relative to the ecliptic with a perihelion distance of 1.3 AU and an aphelion distance of 5.4 AU. A set of 1,695 dust impacts detected with the Ulysses sensor has been accumulated between October 1990 and December 1999 [65–67]. The data obtained until 1999 are shown in Fig. 9.

The mass of the particles detected between 1.8 and 5.4 AU ranges from 10^{-20} to 10^{-8} kg [66] which corresponds to radii a, $0.015\,\mu\text{m} < a < 4.1\,\mu\text{m}$ when assuming compact spherical particles and bulk densities of $2 \times 10^3\,\text{kg}\,\text{m}^{-3}$. The detection efficiency of the dust experiment varies with mass and impact speed of particles and the uncertainty of the mass measurement is a factor of 10. Nevertheless, the measured mass distribution allows to draw some conclusions concerning the interstellar dust models that are suggested to explain astronomical observations. The mass distributions of some models that will be compared to the findings of the Ulysses measurements are also shown in Fig. 9.

Figure 9 shows that the Ulysses data, in comparison to interstellar dust models have a deficit in the small particle masses and extend to relatively large masses. Interstellar dust is partly deflected in the boundary region between solar wind and interstellar medium plasma and those particles that enter the solar system are deflected in the solar wind magnetic field [68]. Both deflection mechanisms result from the Lorentz force that is acting on electrically charged particles moving in a magnetic field. They are particularly important for the small particles (masses $m < 10^{-18}$ kg, approximately) with large ratio of charge to mass within the dust distribution. Since 1996 Ulysses detects a reduced impact rate of smaller dust which is explained by the influence of the solar cycle variation [69]. The deflection pro-

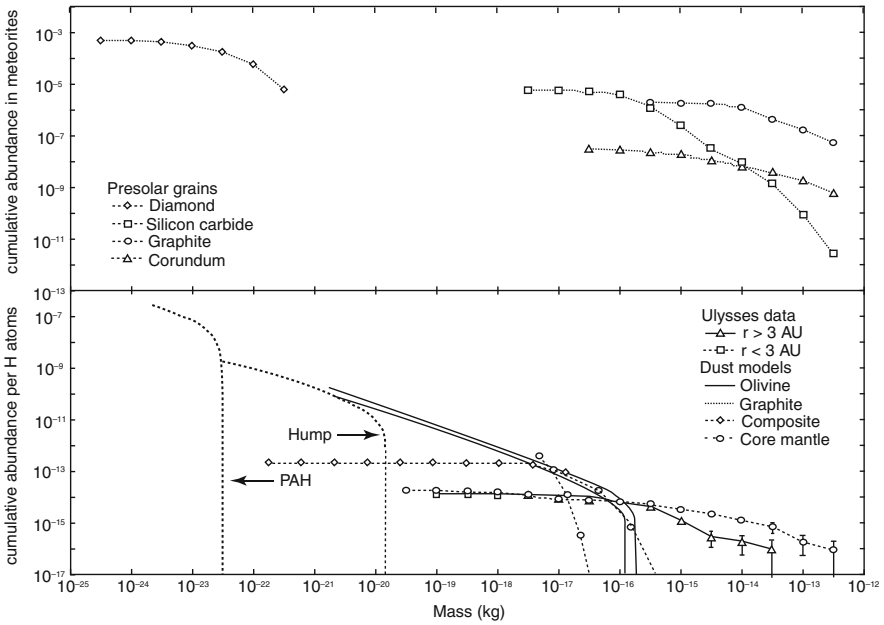

Fig. 9 The upper part of the figure shows the mass distribution of selected presolar grains extracted from meteorites. It shows only a selection of the presolar grains (for the references concerning these data see Mann and Kimura [63]) and may illustrate here that, indeed, dust particles in the size range of the Ulysses data can be present in the interstellar medium. A detailed discussion of presolar grains is given in the chapter "The Most Primitive Material in Meteorites" by Ott, this volume. The lower figure shows Ulysses measurements of interstellar dust and interstellar dust models suggested to explain astronomical observations. The measured flux of interstellar dust is shown separately for the measurements within and beyond 3 AU distance from the Sun. The shown models of interstellar dust are (a) olivine or (b) graphite sub-micrometer particles that follow a power law size distribution; (c) composite dust particles that contain carbon, silicates and oxides; (d) core-mantel particles with a silicate core and organic refractory mantle; (e) very small carbonaceous particles (marked with "hump"); and (f) polycyclic aromatic hydrocarbon (PAH). The two latter model particles lie within a size range that is not accessible to the Ulysses measurements. The other dust models can be discussed in the context of the Ulysses measurements. Both figures show the cumulative distribution

cesses explain the deficit at the small size end, which is preventing us from a detailed comparison to interstellar dust models in this range. Larger particles enter the solar system without significant deflection and are predominantly influenced by solar gravity and radiation pressure when they approach the Sun.

The measurements of larger dust can be discussed in greater detail in comparison to the interstellar dust models, bearing in mind that the Ulysses data provide information about the dust within the local interstellar cloud (LIC) in which the Sun is currently embedded. We here discuss a few representative models. Many models to explain the interstellar extinction (the attenuation of starlight by scattering and absorption of interstellar dust between the star and the observer) suggest a power law size distribution of sub-micrometer particles (see, for instance, Mathis et al. [70],

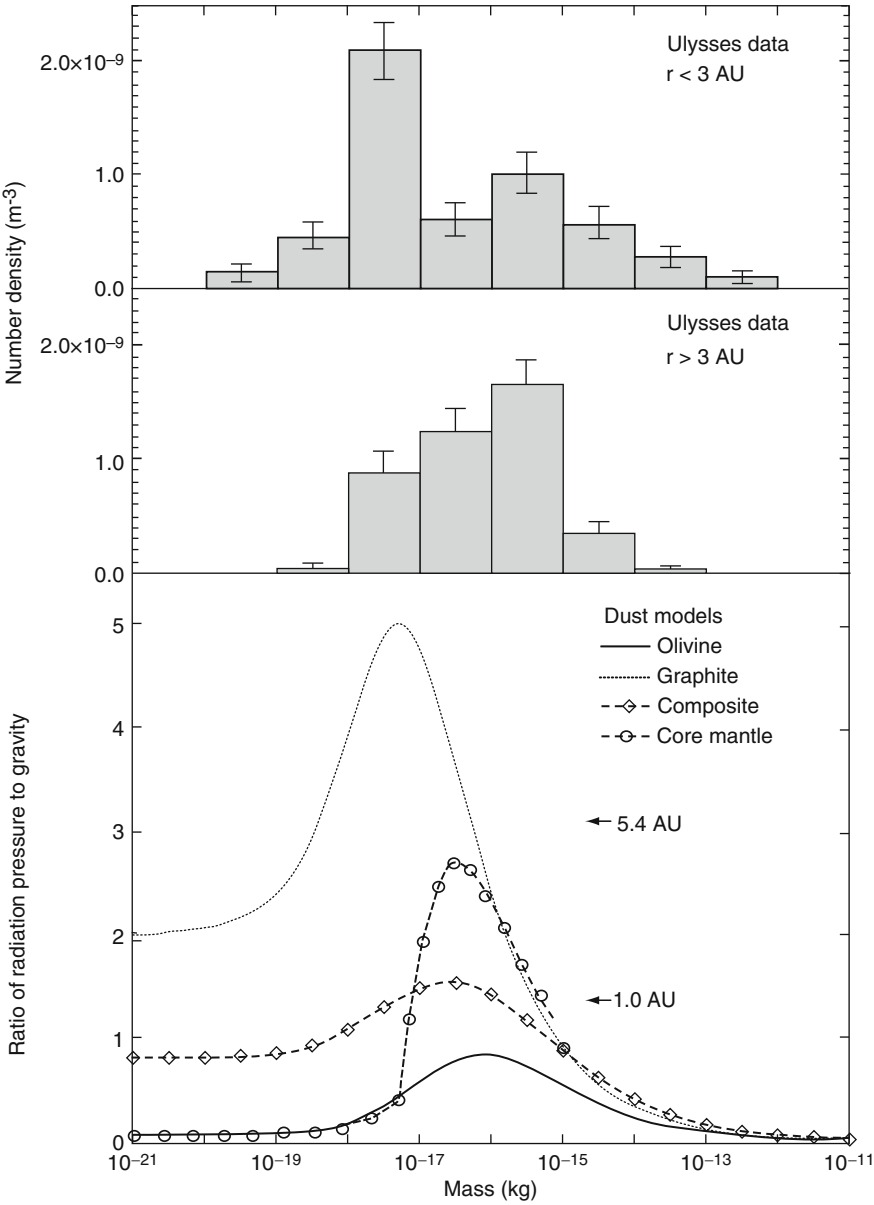

Fig. 10 Number density as function of mass for interstellar dust particles measured aboard Ulysses within and beyond 3 AU are shown in the upper panel of the figure for measurements until 1999. The Ulysses measurements after 1999 confirmed the trend of the data. Measurements within 3 AU show a dip in the mass distribution for $m \approx 10^{-17}$ kg. This dip is caused by radiation pressure repulsion of particles. Measurements within 3 AU also show a slight enhancement in the mass distribution for the most massive particles for which gravitational focussing is important. The lower panel shows the ratio β of radiation pressure force to gravitational force in the same mass interval calculated for different model assumptions of interstellar dust. Marks denote the value $\beta = 3.1$ for

Draine and Lee [71]). In Fig. 9 a power law size distribution as $dn/da \propto a^{-3.5}$ that reproduces extinction data with scattering of olivine (a) or graphite (b) particles is shown. There is a cut-off to larger masses at 10^{-16} kg ($a = 0.25\,\mu$m). Note, however, that larger particles contribute little to the extinction and their number is therefore difficult to determine based on such measurements. A recent model assumes composite dust particles (c) of 0.003–3 μm in size [72] that are produced by coagulation growth. The model accounts, among others, for the abundances of heavy elements in the interstellar medium (ISM). The composite dust contains a (undetermined) carbon compound, silicates, and oxides and is possibly porous. Li and Greenberg [73] described simultaneously the interstellar extinction and its polarization by assuming three types of interstellar dust: large core–mantle particles (d) with a silicate core and an organic refractory mantle, very small carbonaceous particles (e) and small polycyclic aromatic hydrocarbon (PAH) particles (f).

We expect that interstellar dust particles that are not subject to Lorentz force initially form a homogeneous flux into the solar system, so that the mass distribution would be constant with distance from the Sun. The mass distribution of interstellar dust measured at $r < 3$ AU shows a gap around 10^{-17} kg which is not detected at larger distances (see Fig. 10). This gap results from the repelling radiation pressure force acting on particles when they approach the Sun [63, 74]. The flux of more massive particles seems to slightly increase at smaller distances from the sun as would result from gravitational focussing of those dust particles for which solar gravitation force exceeds the radiation pressure force [63].

The gap in the mass distribution can be explained with β–ratios $1.4 < \beta < 3.1$ for $m \approx 10^{-17}$ kg with the ratio of radiation pressure and solar gravitational force

$$\beta = F_{\mathrm{rad}}/F_{\mathrm{grav}} \tag{1}$$

and this allows a comparison of the Ulysses results to interstellar dust models. F_{rad} depends on the size, structure, and material composition of dust particles and can be calculated applying light scattering theory. The results for β from light scattering calculations for the interstellar dust models mentioned above are shown in Fig. 10. The compact interstellar dust models (solid carbon or olivine particles) have radiation pressure forces that are clearly below or above the values that are needed to explain the observed interstellar dust fluxes. The shown values for composite par-

Fig. 10 (continued) dust that is deflected at 5.4 AU and $\beta = 1.4$ for dust that is deflected at 1 AU distance from the Sun. Particles with $\beta > 3.1$ do not reach the Ulysses spacecraft whose orbit has an aphelion of 5.4 AU. The comparison to the interstellar dust models that are shown in Fig. 9 provides the following: (a) The shown calculated values for the compact olivine dust model are $\beta < 1.4$ and for such particles the measured size distribution would not change along the Ulysses orbit. (b) The shown calculated values for the compact graphite dust model are $\beta > 3.1$ and the particles do not approach the Sun close enough to cross the orbit of Ulysses. (c) The composite particle model provides β values close to the minimum required value of 1.4. (d) The β values for core mantle particles lie within the range that is required to explain the Ulysses measurements

ticles and core-mantles particles are closer to conditions for the radiation pressure force that are derived from the Ulysses measurements [63]. These latter models were studied in greater detail ([53, 75], see below).

The in-situ measurements of interstellar dust in the solar system also allow to estimate the mass density of LIC dust and to suggest a model of the LIC dust [53, 75]. The total mass of LIC dust is determined by particles at the large size end of the distribution and therefore the mass density of interstellar dust that is measured within the solar system provides a number of the dust mass density in the LIC. The value derived from the measurements leads to the canonical value of a gas-to-dust mass ratio of 100 for the LIC [53]. It is therefore reasonable to assume that the interstellar dust in the mass range of the Ulysses measurements is coupled to the LIC gas component. Under this condition it is safe to assume that the elements that are underabundant in the gas phase compared to the average element abundances in the Galaxy are condensed onto dust. Hence a model of LIC dust can be constructed that is constrained by the LIC dust-phase element abundances as well as by the radiation pressure force values inferred from the Ulysses measurements. To estimate the dust material composition, the dust compounds are assumed as those that form by condensation in stellar atmospheres: pyroxene, olivine, troilite, kamacite, and corundum and as an organic refractory compound comprising the elements H, C, N, and O. The relative amount of these compounds is chosen to reproduce the element abundances and the radiation pressure force is calculated for particles consisting of these materials. The compounds and their suggested abundance in the dust are listed in Table 1. The model (see [53, 75]) suggests core-mantle particles with a core consisting of Mg-rich pyroxene (enstatite) and Mg-rich olivine (forsterite) with inclusions of troilite, Fe-rich kamacite, and corundum. The silicate consists of more pyroxene than olivine. The core-mantle particles possibly accumulate by

Table 1 Abundances of the elements per million hydrogen atoms and their probable main carriers in dust phases in the local interstellar cloud. The table also shows the abundances in the gas phase. The sum of gas and dust abundances is fixed for each element to the cosmic abundance. The cosmic element abundances are assumed here as those of the solar photosphere. The obtained values slightly vary with the assumed element abundances for the solar photosphere. The gas phase abundances in the local interstellar cloud are derived from observed gas absorption lines assuming a hydrogen ionization fraction of 0.3. This table is adapted from Kimura et al. [75] and a detailed discussion is given there

Element	Compound						Dust	Gas
	Al_2O_3 corundum	FeNi kamacite	Mg_2SiO_4 forsterite	$MgSiO_3$ enstatite	FeS troilite	CHON organic		
C	0	0	0	0	0	222.57	222.57	168.27
N	0	0	0	0	0	38.94	38.94	46.37
O	4.26	0	8.76	82.41	0	165.22	260.65	283.86
Mg	0	0	4.38	27.47	0	0	31.85	2.66
Al	2.84	0	0	0	0	0	2.84	0.11
Si	0	0	2.19	27.47	0	0	29.66	4.70
S	0	0	0	0	10.79	0	10.79	10.59
Fe	0	15.95	0	0	10.79	0	26.74	1.31

coagulation growth. Dust particles with mass smaller than 10^{-17} kg may consist of bare silicates or bare carbonaceous materials .

5.2 Future Measurements of Interstellar Dust

The dust experiment aboard Cassini [14, 15] for a part of the cruising phase was oriented into the direction of the interstellar dust flux in order to obtain the first in-situ measurements of the element composition of interstellar dust in space. Also the Stardust spacecraft was expected, aside from the sample return, to provide in-situ data of interstellar dust [76]. At present no detailed analyses of interstellar dust are reported from these experiments. Dedicated missions to measure the composition of interstellar dust reaching the Earth orbit have been proposed to ESA and NASA several times (see, for instance Grün et al. [77]). Moreover, future missions planned to explore the boundaries of the solar system and the interstellar medium beyond the heliopause with in-situ measurements from spacecraft [78] would overcome the restrictions that entry conditions of interstellar dust into the solar system currently impose on in-situ and laboratory studies of interstellar dust.

6 Discussion

It goes without saying that astromineralogy is based on astronomical observations and is triggered by laboratory studies. Astronomical observations provide information integrated over a large set of particles providing their average properties. They are, however, restricted to a certain size interval of particles and their interpretation is often ambiguous. Collecting samples and bringing them back to Earth, on the other hand, is not only costly, but also limited in the information it provides. Dedicated experiments for the in-situ analyses from spacecraft addressing certain clearly formulated questions are an important complementary tool. Nevertheless, a good physical understanding of the measurement process is essential for deriving reliable information from in-situ analyses of dust from spacecraft. Still this effort is worthwhile. Our discussion of previous in-situ measurements has shown that they reveal information about dust properties – sometimes very unexpected – that is not accessible to other methods of observation.

The progress that in-situ measurements bring for studies of interplanetary, cometary and interstellar dust have been outlined in detail. A further strength of future in-situ measurements lies in their universality as far as the exploration of different “remote” regions in the solar system is concerned and in the fact that space experiments can be especially designed to address certain issues of dust analysis. By in-situ analysis during spacecraft encounter, the detection of ejecta particles for one allows a study of the erosion processes. By means of ejecta particles, information about the composition of the parent body is accessible to spacecraft without the need to actually sample them on their surface. This may prove to be most important

for the study of the many atmosphereless moons of the giant planets as well as of trans-Neptunian objects. The drawback of in-situ measurements from spacecraft is, that they do not (and cannot) reach the level of sophistication of the analytical techniques in the laboratory. All this argues for a strong interdisciplinary approach in astromineralogical studies.

7 Summary

The results derived from in-situ measurements of interplanetary, cometary and interstellar dust demonstrated that in-situ experiments are complementary to other methods of dust measurements and improve our understanding of the material properties of dust. In-situ studies of solar system dust provide access to different stages of the evolution of cosmic matter from interstellar dust, to pristine Kuiper belt and cometary dust, to highly processed asteroidal dust and improve our understanding of the origin and evolution of the solar system. Moreover, the measurements provide information about dust in the local interstellar medium as well as about basic physical processes that occur in cosmic environments. Future studies of cosmic dust need a combined approach from the astronomical, astrophysical, cosmochemical, and mineralogical points of view to enhance the scientific return of space measurements. Important steps in this direction are the design of dedicated space experiments combined with a supporting laboratory program to improve the detailed physical understanding of their functional principles.

Acknowledgements This work has been supportet by the German Aerospace Center DLR (Deutsches Zentrum für Luft- und Raumfahrt) under project (RD-RX /50QP 0403).

References

1. Mann, I.: Meteors. In: Trümper, J. (ed.) Landolt-Börnstein New Series VI/2a. Springer, Berlin (2009) 234
2. Grün, E., Zook, H.A., Fechtig, H., Giese, R.H.: Collisional balance of the meteoritic complex. Icarus **62**, 244 (1985) 235
3. Ceplecha, Z.K., Borovicka, J.I., Elford, W.G., et al.: Meteor phenomena and bodies. Space Sci. Rev. **84**(3/4), 327 (1998) 235
4. Maurette, M., Olinger, C., Michel-Levy, M.C., et al.: A collection of diverse micrometeorites recovered from 100 tonnes of Antarctic blue ice. Nature **351**, 44 (1991) 235
5. Pellinen-Wannberg, A., Westman, A., Wannberg, G., Kaila, K.: Meteor fluxes and visual magnitudes from EISCAT radar event rates: a comparison with cross section based magnitude estimates and optical data. Ann. Geophys. **16**, 1475 (1998) 235
6. Mann, I.: Zodiacal cloud complexes. Earth Planet. Space **50**(6,7), 465 (1998) 235
7. Tuzzolino, A.J., McKibben, R.B., Simpson, J.A., et al.: The space dust (SPADUS) instrument aboard the Earth-orbiting ARGOS spacecraft: I-instrument description. Planet. Space Sci. **49**(7), 689 (2001a) 235, 239

8. Auer, S.: Instrumentation. In: Grün, E., Gustafson, B.A.S., Dermott, S., Fechtig, H. (eds.) Interplanetary Dust, pp. 385–444. Astron. Astrophys. Library, Springer, Berlin, New York, (2001) 235, 237
9. Arndt, P., Bohsung, J., Maetz, M., Jessberger, E.K.: The element abundances in interplanetary dust particles. Meteoritics **31**, 817 (1996) 236
10. Jessberger, E.K., Stephan, T., Rost, D., et al.: Properties of interplanetary dust: Information from collected samples. In: Grün, E., Gustafson, B.A.S., Dermott, S., Fechtig, H. (eds.) Interplanetary Dust. Springer, Berlin, New York (2001) 236
11. McDonnell, J.A.M.: Microparticle studies by space instrumentation. In: McDonnell, J.A.M. (ed.) Cosmic Dust, pp. 337–419. Wiley-Interscience, Chichester, Sussex, England, New York (1978) 237
12. Humes, D.H.: Results of Pioneer 10 and 11 meteoroid experiments - Interplanetary and near-Saturn. J. Geophys. Res. **85**, 5841 (1980) 237
13. Simpson, J.A., Tuzzolino, A.J.: Polarized polymer films as electronic pulse detectors of cosmic dust particles. Nucl. Instrum. Methods Phys. Res. **A236**, 187 (1985) 237
14. Srama, R., Grün, E.: The dust sensor for CASSINI. Adv. Space Res. **20**(8), 1467 (1997) 238, 252
15. Srama, R., Ahrens, T.J., Altobelli, N., et al.: The Cassini cosmic dust analyzer. Space Sci. Rev. **114**(1–4), 465–518 (2004) 238, 252
16. Giese, R.H., Schwehm, G.H., Zerull, R.M.: A concept for analysis of cometary dust by light scattering experiments on future cometary probes. In: Space research XIX, Proceedings of the Open Meetings of the Working Groups on Physical Sciences, Innsbruck 1978, pp. 475–478. Pergamon Press, Oxford (1979) 239
17. Levasseur-Regourd, A.C., Schuerman, D.W., Zerull, R.H., Giese, R.H.: Cometary dust observations by optical in-situ methods. Adv. Space Res. **1**(8), 113 (1981) 239
18. Levasseur-Regourd, A.C., Bertaux, J.L., Dumont, R., et al.: Optical probing of comet Halley from the Giotto spacecraft. Nature **321** (1986) 239, 243
19. Colangeli, L., Lopez-Moreno, J.J., Palumbo, P., et al.: The Grain impact analyser and dust accumulator (GIADA) experiment for the Rosetta mission: design, performances and first results. Space Sci. Rev. **128**, 803 (2007) 239, 246
20. Tuzzolino, A.J., McKibben, R.B., Simpson, J.A., et al.: The space dust (SPADUS) instrument aboard the Earth-orbiting ARGOS spacecraft: II-results from the first 16 months of flight. Planet. Space Sci. **49**(7), 705 (2001b) 239
21. McDonnell, J.A.M., Burchell, M.J., Green, S.F., et al.: APSIS - Aerogel position-sensitive impact sensor: capabilities for in-situ collection and sample return. Adv. Space Res. **25**(2), 315 (1999) 239
22. Aubier, M.G., Meyer-Vernet, N., Pedersen, B.M.: Shot noise from grain and particle impacts in Saturn's ring plane. Geophys. Res. Lett. **10**, 5 (1983) 240
23. Meyer-Vernet, N., Aubier, M.G., Pedersen, B.M.: Voyager 2 at Uranus - Grain impacts in the ring plane. Geophys. Res. Lett. **13**, 617 (1986a) 240
24. Meyer-Vernet, N., Couturier, P., Hoang, S., et al.: Plasma diagnosis from thermal noise and limits on dust flux or mass in comet Giacobini-Zinner. Science **232**, 370 (1986b) 240
25. Tsintikidis, D., Gurnett, D., Granroth, L.J., Allendorf, S.C., Kurth, W.S.: A revised analysis of micron-sized particles detected near Saturn by the Voyager 2 plasma wave instrument. J. Geophys. Res. **99**(A2), 2261 (1994) 240
26. Neubauer, F.M., Glassmeier, K.-H., Coates, A.J., Goldstein, R., Acuna, M.H.: Hypervelocity dust particle impacts observed by the Giotto magnetometer and plasma experiments. Geophys. Res. Lett. **17**, 1809 (1990) 240
27. Gurnett, D.A., Ansher, J.A., Kurth, W.S., Granroth, L.J.: Micron-sized dust particles detected in the outer solar system by Voyager 1 and 2 plasma wave instruments. Geophys. Res. Lett. **24**(24), 3125 (1997) 240
28. Giese, R.H., Weiss, K., Zerull, R.H., Ono, T.: Large fluffy particles - A possible explanation of the optical properties of interplanetary dust. Astron. Astrophys. **65**, 265 (1978) 240

29. Fraundorf, P., Patel, R.I., Freeman, J.J.: Infrared spectroscopy of interplanetary dust in the laboratory.Icarus **47**, 368 (1981) 242
30. Fraundorf, P., Walker, R.M., Brownlee, D.E.: Laboratory studies of interplanetary dust. In: Wilkening, H. (ed.) Comets, pp. 383–409. University of Arizona Press, Tuscon (1982) 242
31. Fechtig, H.: Cometary dust in the solar system. In: Wilkening, H. (ed.) Comets, pp. 370–382. University of Arizona Press, Tuscon, AZ (1982) 242
32. Hillier, J.K., Green, S.F., McBride, N., et al.: Interplanetary dust detected by the Cassini CDA Chemical Analyser. Icarus **190**, 643–654 (2007) 241, 242
33. McComas, D.J., Velli, M., Lewis, W.S., et al.: Understanding coronal heating and solar wind acceleration: the case for in-situ near-Sun measurements. Rev. Geophys. **45**, RG1004 (2007) 242
34. Mann, I., Kimura, H., Biesecker, D.A., et al.: Dust near the Sun. Space Sci. Rev. **110**, 269 (2004) 242
35. Mann, I., Murad, E.: On the existence of silicon nano-dust near the Sun. Astrophys. J. **624**, L125 (2005) 242
36. Ishiguro, M., Watanabe, J., Usui, F., et al.: First detection of an optical dust trail along the orbit of 22P/Kopff. Astrophys. J. **572**(1), L117–L120 (2002) 242
37. Glöckler, G., Geiss, J.: Interstellar and inner source pickup ions observed with SWICS on ULYSSES. Space Sci. Rev. **86**(1/4), 127 (1998) 242
38. Mann, I., Czechowski, A.: Dust destruction and ion formation in the inner solar system. Astrophys. J. **621**, L73 (2005) 242
39. McDonnell, J.A.M., Alexander, W.M., Burton, W.M., et al.: Dust density and mass distribution near comet Halley from Giotto observations. Nature, **321**, 338 (1986) 243
40. Simpson, J.A., Sagdeev, R.Z., Tuzzolino, A.J., et al.: Dust counter and mass analyser (DUCMA) measurements of comet Halley's coma from VEGA spacecraft. Nature **321**, 278 (1986) 243
41. Simpson, J.A., Rabinowitz, D., Tuzzolino, A.J., Ksanfomaliti, L.V., Sagdeev, R.Z.: The dust coma of comet P/Halley - Measurements on the Vega-1 and Vega-2 spacecraft. Astron. Astrophys. **187**(1–2), 742 (1987) 243
42. Utterback, N.G., Kissel, J.: Attogram dust cloud a million kilometers from Comet Halley. Astron. J. **100**, 1315 (1990) 243
43. Kissel, J., Brownlee, D.E., Buchler, K., et al.: Composition of comet Halley dust particles from Giotto observations. Nature **321**, 336 (1986a) 243
44. Kissel, J., Sagdeev, R.Z., Bertaux, J.L., et al.: Composition of comet Halley dust particles from VEGA observations. Nature **321**, 280 (1986b) 243
45. Jessberger, E.K., Christoforidis, A., Kissel, J.: Aspects of the major element composition of Halley's dust. Nature **332**, 691 (1988) 243
46. Tuzzolino, A.J., Economou, T.E., Clarket, B.C., et al.: Dust measurements in the coma of Comet 81P/Wild 2 by the Dust Flux Monitor Instrument. Science **304**, 17760 (2004) 243
47. Green, S.F., McDonnell, J.A.M., McBride, N., et al.: The dust mass distribution of comet 81P/Wild 2. J. Geophys. Res. **109**(E12), CiteID7 E12S04 (2004) 243
48. Tsou, P., Brownlee, D.E., Anderson, J.D., et al.: Stardust encounters comet 81P/Wild 2. J. Geophys. Res. **109** (2004) 243
49. Jessberger, E.K.: On the element, isotopic and mineralogical ingredients of ROCKY cometary particulates. In: Altwegg, K., Ehrenfreund, P., Geiss, J., Huebner, W. (eds.) The Origin and Composition of Cometary Materials. Space Sci. Series of ISSI. Kluwer, Dordrecht. Space Sci. Rev. **90**, 91 (1999) 243
50. Lawler, M.E., Brownlee, D.E.: CHON as a component of dust from Comet Halley. Nature **359**, 6398 (1992) 243
51. Grevesse, N., Sauval, A.J.: Standard solar composition. Space Sci. Rev. **85**(1/2), 161 (1998) 243
52. Holweger, H.: Photospheric abundances: problems, updates, implications. In: Wimmer-Schweingruber, R.F. (ed.) Joint SOHO/ACE Workshop 2001. American Institute of Physics Press, New York, NY. AIP Conf. Proc. **598**, 23 (2001) 243

53. Kimura, H., Mann, I., Jessberger, E.K.: Elemental abundances and mass densities of dust and gas in the local interstellar cloud. Astrophys. J. 582, 846 (2003a) 243, 251
54. Allende Prieto, C., Lambert, D.L., Asplund, M.: A reappraisal of the solar photospheric C/O ratio. Astrophys. J. **573**, L137 (2002) 243
55. Schulze, H., Kissel, J., Jessberger, E.K.: Chemistry and mineralogy of Comet Halley's dust. From Stardust to Planetesimals. Symposium held as part of the 108th Annual meeting of the ASP held at Santa Clara, California 24–26 June 1996. In: Pendleton, Y.J., Tielens, A.G.G.M. (with the editorial assistance of Savage, M.L.) (eds.) ASP Conference Series, vol. 122, pp. 397–414. ASP, San Francisco, CA (1997) 244
56. Jessberger, E.K., Kissel, J.: Chemical properties of cometary dust and a note on carbon isotopes. In: Newburn, R., Neugebauer, M., Rahe, J., (eds.) Comets in the Post-Halley Era, pp. 1075–1092. Springer, Heidelberg (1991) 246
57. Amari, S., Anders, E., Virag, A., Zinner, E.: Interstellar graphite in meteorites. Nature **345**, 238 (1990) 246
58. Zinner, E.: Stellar nucleosynthesis and the isotopic composition of presolar grains from primitive meteorites. Annu. Rev. Earth Planet. Sci. **26**, 147 (1998) 246
59. Riedler, W., Torkar, K., Jeszenszky, H., et al.: MIDAS the micro-imaging dust analysis system for the Rosetta mission. Space Sci. Rev. **128**, 869 (2007) 246
60. Kissel, J., Altwegg, K., Clark, B.C., et al.: Cosima high resolution time-of-flight secondary ion mass spectrometer for the analysis of cometary dust particles onboard Rosetta. Space Sci. Rev. **128**, 823 (2007) 247
61. Bertaux, J.L., Blamont, J.E.: Possible evidence for penetration of interstellar dust into the solar system. Nature **262**, 263 (1976) 247
62. Grün, E., Gustafson, B., Mann, I., et al.: Interstellar dust in the heliosphere. Astron. Astrophys. **286**, 915 (1994) 247
63. Mann, I., Kimura, H.: Interstellar dust properties derived from mass density, mass distribution, and flux rates in the heliosphere. J. Geophys. Res. **105**, 10317 (2000) 247, 248, 250, 251
64. Witte, M., Rosenbauer, H., Banaszkiewicz, M., Fahr, H.: The ULYSSES neutral gas experiment – Determination of the velocity and temperature of the interstellar neutral helium. Adv. Space Res. **13**(6), 121 (1993) 247
65. Krüger, H., Grün, E., Landgraf, M., et al.: Four years of Ulysses dust data: 1996–1999. Planet. Space Sci. **49**(13), 1303 (2001) 247
66. Grün, E., Baguhl, M., Divine, N., et al.: Two years of Ulysses data. Planet. Space Sci. **43**, 971 (1995) 247
67. Krüger, H., Grün, E., Heck, A., Lammers, S.: Analysis of the sensor characteristics of the Galileo dust detector with collimated Jovian dust stream particles. Planet Space Sci. **47**, 1015 (1999) 247
68. Czechowski, A., Mann, I.: Penetration of interstellar dust grains into the heliosphere. J. Geophys. Res. **108**(A10), CiteID 8038 (2003) 247
69. Landgraf, M.: Modeling the motion and distribution of interstellar dust inside the heliosphere. J. Geophys. Res. **105**, 10303 (2000) 247
70. Mathis, J.S., Rumpl, W., Nordsieck, K.H.: The size distribution of interstellar grains. Astrophys. J. **217**, 425 (1977) 248
71. Draine, B.T., Lee, H.M.: Optical properties of interstellar graphite and silicate grains. Astrophys. J. **285**, 89 (1984) 250
72. Mathis, J.S.: Dust models with tight abundance constraints. Astrophys. J. **472**, 643 (1996) 250
73. Li, A., Greenberg, J.M.: A unified model of interstellar dust. Astron. Astrophys. **323** 566 (1997) 250
74. Landgraf, M., Baggaley, W.J., Grün, E., Krüger, H., Linkert, G.: Aspects of the mass distribution of interstellar dust grains in the solar system from in situ measurements. J. Geophys. Res. **105**, 10343 (2000) 250
75. Kimura, H., Mann, I., Jessberger, E.K.: Composition, structure and size distribution of dust in the local interstellar cloud. Astrophys. J. **583**, 314 (2003b) 251

76. Brownlee, D.E., Burnett, D., Clark, B., et al.: STARDUST: Comet and interstellar dust sample return mission. In: Gustafson, B.A.S., Hanner, M.S. (eds.) Physics, Chemistry, and Dynamics of Interplanetary Dust. Astronomical Society of the Pacific Conference Series, pp. 223–225. ASP, San Francisco, CA (1996) 252
77. Grün, E., Landgraf, M., Horányi, M., et al.: Techniques for galactic dust measurements in the heliosphere. J. Geophys. Res. **105**, 10403 (2000) 252
78. Liewer, P.C., Mewaldt, R.A., Ayon, J.A., Wallace, R.A.: NASA's interstellar probe mission. In: El-Genk (ed.) Space Technology and Applications International Forum 2000. American Institute of Physics Press, New York, NY. AIP Conf. Proc. **504**, 911 (2000) 252

The Astromineralogy of Interplanetary Dust Particles

J. Bradley

Abstract Some chondritic interplanetary dust particles (IDPs) collected in the stratosphere are from comets. Because comets accreted at heliocentric distances beyond the giant planets, presolar grains or "astrominerals" with solar and non-solar isotopic compositions are expected to be even more abundant in cometary IDPs than in primitive meteorites. Non-solar D/H and $^{15}N/^{14}N$ isotopic enrichments in chondritic IDPs are associated with a carbonaceous carrier. These H and N enrichments are attributed to extreme mass fractionation during chemical reactions in cold (10–100 K), dense interstellar molecular clouds. Enstatite ($MgSiO_3$) and forsterite (Mg_2SiO_4) crystals in IDPs are physically and compositionally similar to enstatite and forsterite grains detected around young and old stars by the Infrared Space Observatory (ISO), and large non-solar oxygen isotopic compositions recently measured in some IDP silicates establish that they are presolar silicates. The compositions, mineralogy, and optical properties of a class of grains in IDPs, known as GEMS, are consistent with those of interstellar "amorphous silicates". Non-solar isotopic compositions measured in several GEMS confirm that they are interstellar silicate grains, one of the fundamental building blocks of solar systems. Submicrometer FeNi sulfide astrominerals like those found in IDPs may be responsible for a broad $\sim$23.5 μm feature observed around protostars and protoplanetary discs by ISO. The first sample of a known comet (81P/Wild 2) was returned to Earth in 2006 by the Stardust mission. Contrary to expectations, the "Wild 2" sample does not resemble "cometary" IDPs and it does not contain abundant astromaterials. Instead, this particular Kuiper Belt comet resembles chondritic meteorites from the asteroid belt, which reinforces the astrophysical significance of IDPs as perhaps the most cosmically primitive materials available for laboratory investigations.

J. Bradley (✉)
Lawrence Livermore National Laboratory, Institute of Geophysics and Planetary Physics, Livermore, CA 94551, USA
e-mail: bradley33@llnl.gov

Bradley, J.: *The Astromineralogy of Interplanetary Dust Particles*. Lect. Notes Phys. **815**, 259–276 (2010)
DOI 10.1007/978-3-642-13259-9_6

1 Introduction

For the purposes of this chapter astrominerals are defined as those presolar mineral grains in primitive meteoritic materials that existed prior to collapse of the solar nebula. These grains may include preserved circumstellar grains, grains formed in supernovae outflows, grains formed or modified within the interstellar medium (ISM), including grains that were present in the presolar molecular cloud. They may have survived either because they were resistant to asteroidal parent body alteration processes within the inner solar system or because they were sequestered in small primitive bodies like comets at much larger heliocentric distances where post-accretional alteration processes were minimal or essentially non existent. Astrominerals can be found in primitive meteorites (carbonaceous chondrites), polar micrometeorites, IDPs and most recently in samples of comet Wild 2.

The carbonaceous chondrites are believed to be derived from the inner main belt of the asteroids located at a heliocentric distance of 2.5–3 astronomical units (AU) [1]. Their mineralogy and petrography indicate that most have experienced significant parent body alteration and that they are composed almost exclusively of minerals formed within the solar system. However, the discovery of trace quantities of surviving presolar grains within the matrices of carbonaceous chondrites shows that at least some astrominerals survived ([2] "The Most Primitive Material in Meteorites" by Ott, this volume). They are indisputably presolar circumstellar astrominerals because their isotopic compositions differ significantly from solar system compositions. Other presolar interstellar astrominerals may have so far escaped identification because they have normal (solar) isotopic compositions [3]. Astrominerals identified in meteorites include diamond, silicon carbide (SiC), titanium carbide (TiC), graphite, corundum, spinel, and silicon nitride [4]. Although none of these astrominerals are cosmically abundant, the presence of some of them (e.g., SiC and TiC) in circumstellar environments has been confirmed by astronomical observations [5–7].

Most of the astrominerals so far identified in carbonaceous chondrites are highly refractory and their abundance decreases with increasing petrologic grade of meteorite ([4, 8] "The Most Primitive Material in Meteorites" by Ott, this volume). Thus it appears that the most robust astrominerals have better survived incorporation into the parent bodies of meteorites. Less robust silicate minerals are abundant in space as evidenced by strong resonances in astronomical infrared (IR) spectra at $\sim$10 and $\sim$18 μm corresponding to the Si—O stretch and Si—O—Si bending mode vibrations in silicates. These features are observed both in absorption and emission along most lines-of-sight [9]. Prior to the discovery of silicate astromaterials in IDPs, failure to find what is arguably the most cosmically abundant type of astromineral ranked among the most perplexing problems confronting meteoriticists and planetary scientists.

Astrominerals are expected to be more abundant in IDPs because IDPs are more chemically and isotopically primitive than carbonaceous chondrites and some of them are from comets [10–13]. Since comets are small bodies located at extreme heliocentric distances they have likely undergone less alteration than asteroids

([14, 15] "The Mineralogy of Cometary Dust" by Hanner and Zolensky, this volume). High D/H enrichments indicate that some IDPs contain organic matter from a presolar molecular cloud [11, 16]. The first hint of surviving silicate astrominerals in an IDP was provided by the observation of a significant ^{16}O enrichment in a CP IDP, the largest "whole rock" ^{16}O enrichment ever observed in any meteoritic material [17]. Silicates are the major carrier of O in IDPs. The presence of silicate astrominerals in IDPs is now well established with the identification of amorphous and crystalline grains with O isotopic compositions clearly indicating that they are presolar astrominerals [18]. Most of these isotopically anomalous grains are amorphous silicates known as GEMS (glass with embedded metal and sulfides) and some are forsterite (Mg_2SiO_4) crystals [19–21]. The GEMS are interstellar "amorphous silicates", one of the fundamental building blocks of solar systems [22].

This chapter discusses the astromineralogy of the anhydrous "chondritic porous" (CP) subset of IDPs. Measured He release temperatures indicate that many of these IDPs enter the atmosphere at speeds $>16\,km\,s^{-1}$ and are therefore probably of cometary origin [23]. IDPs entering the atmosphere at speeds $<16\,km\,s^{-1}$ are more likely of asteroidal origin, although some of these low-speed IDPs may also be cometary [24, 25]. Although all IDPs are pulse heated during atmospheric entry, the survival of solar flare tracks and low-temperature minerals indicates that many of them experience surprisingly little thermal alteration [26–28]. Studies of IDPs are providing exciting new insight about grain formation, processing, and destruction in space, and comparison of their properties with those of dust in space is a key aspect of the new discipline of astromineralogy

2 Specimen Preparation and Analytical Methods

Typical CP IDPs are 5–20 μm in diameter (Fig. 1). They are composed of heterogeneous aggregates of submicrometer-to-nanometer sized crystalline and amorphous grains (Figs. 2, 3, and 4). Analytical studies of IDPs typically require the use of micromanipulators, embedding and thin-sectioning equipment (ultramicrotomes), and analytical instruments offering both high spatial resolution and high sensitivity. Ultramicrotomy is used for preparing electron and optically transparent thin sections of IDPs [29]. Epoxy is the embedding medium of choice but, as ever more challenging analyses are being attempted (e.g., detection of C, N, and organics in IDPs) other embedding media like sulfur are increasingly utilized [30]. Embedding small particles in sulfur is difficult because (molten) sulfur has a much higher surface tension than epoxy. However, it offers a huge advantage in that it can be completely eliminated (by sublimation) after the thin section has been transferred to a transmission electron microscope (TEM) grid. In the absence of epoxy, spectral backgrounds are reduced making it possible to begin to analyze smaller samples and investigate the nature of indigenous C, N, and organic species.

An in-situ acid "nano-etching" procedure has been developed where all minerals within an ultramicrotomed thin-section of an IDP, except those that are sulfides

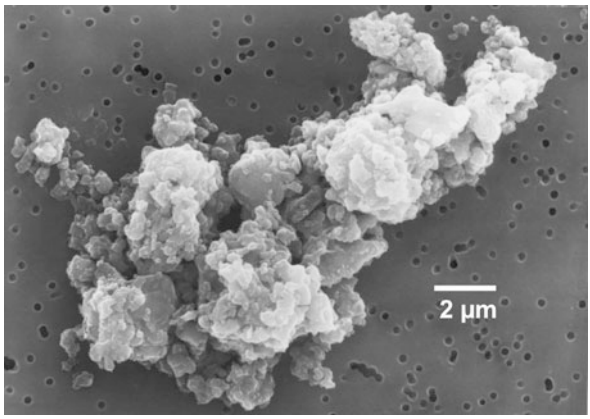

Fig. 1 Secondary electron image of chondritic porous (CP) interplanetary dust particle (IDP) U220B43

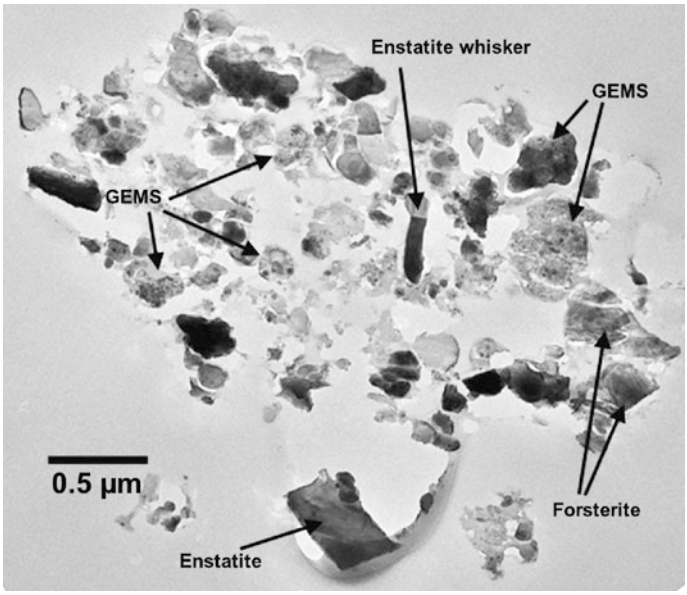

Fig. 2 Brightfield transmission electron micrograph of a thin section of cluster particle U219C3. The three major types of silicate grains found in CP IDPs are GEMS, enstatite, and forsterite

and carbonaceous, are removed [31]. This procedure greatly simplifies the search for acid-resistant astrominerals like nano-diamonds that are otherwise impossible to recognize among other more abundant nanometer-sized minerals (e.g., FeNi metal). The dissolution is carried out by exposing the (gold) TEM grid to triple distilled concentrated hydrofluoric acid (HF). After room temperature etching the grid is rinsed with water and dried. The slices are then characterized in the TEM (Fig. 5).

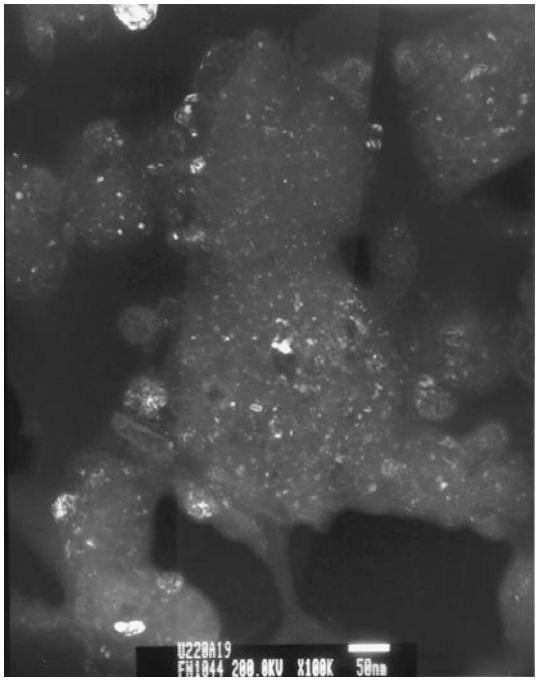

Fig. 3 Darkfield transmission electron micrograph of GEMS (glass with embedded metal and sulfides) in IDP U220A19. The bright inclusions are FeNi metal (see also Fig. 4) and FeNi sulfide crystals that are embedded in Mg-rich silicate glass (uniform *grey matrix*)

The principal instruments used to analyze IDPs are the analytical TEM, ion microprobe, and infrared micro spectrophotometer. A variety of other analytical methods are also applied to IDPs [32–34]. Emerging analytical techniques include scanning transmission X-ray microprobe (STYXM) and X-ray absorption near edge structure (XANES), both of which use a synchrotron radiation source [35–37]. The TEM offers both high image resolution (0.1–0.5 nm) and, in conjunction with focused nanoprobes, high compositional spatial resolution (0.1–0.5 nm) using energy-dispersive X-ray analysis (EDX) and electron energy-loss spectroscopy (EELS). State-of-the-art TEMs are now increasingly configured for compositional mapping of electron transparent thin sections with spatial resolution on a scale of <1 nm using EDX and EELS. New generation SuperSTEM instruments enable compositional mapping with single atomic column spatial resolution. In the future such capabilities may play a key role in the identification of astrominerals through compositional mapping of the ultrafine-grained matrices of IDPs at a whole new level of detail. This may reveal nanoscale petrographic information that has likely been overlooked using conventional brightfield/darkfield imaging and diffraction techniques.

The isotopic compositions of IDPs are measured using secondary ion mass spectroscopy (SIMS). Most measurements have been made on whole particles pressed

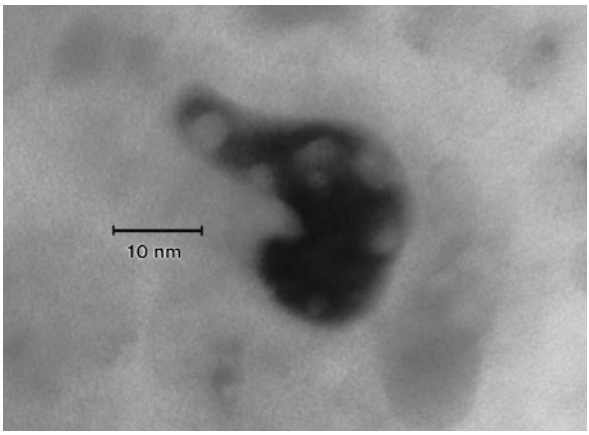

Fig. 4 Brightfield transmission electron micrograph of an FeNi metal grain within GEMS in IDP U220A19. The "polished" morphology and "swiss cheese" microstructure likely result from prolonged exposure to radiation sputtering

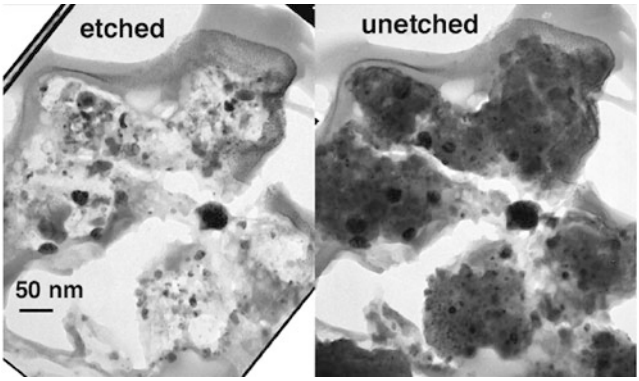

Fig. 5 A GEMS-rich thin section before and after in-situ acid etching. In addition to preserving carbonaceous phases (e.g., organics and nano-diamonds), FeNi sulfides (*dark grains*) are also preserved such that their nanoscale compositions and crystal structures can be measured without interference from other nanophase minerals (e.g., FeNi metal, see Figs. 3 and 4)). See [27]

into gold foils [11, 38], as well as individual grains (enstatite and GEMS) among fragments of an IDP that were crushed and dispersed on a gold substrate [39]. Recently, the first in-situ measurements of submicrometer-sized grains within thin sections of an IDP mounted on a TEM grid were made using the new nanoSIMS [18]. These measurements represent a major breakthrough because they demonstrate that it is possible to first probe the compositions, mineralogy, and petrography of an IDP using TEM and then transfer the specimen to the nanoSIMS for complimentary high-spatial resolution isotope measurements. Already anomalies in H, N, and O have been observed in IDPs using the nanoSIMS, in some cases at levels far above those previously reported. The discovery of preserved presolar interstellar and cir-

cumstellar silicates in IDPs underscores the vital role nanoSIMS is now playing in IDP research [18].

The optical properties of IDPs have been measured in the infrared, visible, and ultraviolet spectral regions [40–43]. Most have been IR transmission measurements in the 2 to 25 μm IR region using microscope spectrophotometers equipped with globar sources [40, 41]. More recently, the high-brightness synchrotron light source has proven to be ideal for spectral microanalysis of IDPs and even subcomponents of IDPs because it provides a ~3 μm diameter IR beam spot more than 100 times brighter than laboratory IR spectrophotometers (equipped with glowbar discharge sources) [44]. Reflectance spectra have been collected from IDPs over the visible 450–800 nm wavelength range [42]. In general chondritic IDPs are spectrally dark objects (<15% reflectivity). Hydrated IDPs that contain layer lattice silicates exhibit spectral characteristics similar to carbonaceous chondrites and main-belt C-type asteroids. Some hydrated IDPs are believed to be of asteroidal origin [28, 45, 46]. In contrast, most anhydrous CP IDPs dominated by enstatite, forsterite, and GEMS exhibit spectral characteristics similar to those of smaller, more primitive solar system objects (e.g., P and D asteroids). Carbon-rich IDPs are spectrally red, with a redness comparable to the comet-like outer asteroid Pholus [42, 47].

3 Astrominerals in IDPs

3.1 Organic Matter

The bulk carbon content of chondritic IDPs is typically 2–5 times higher than in carbonaceous chondrites [48]. The carbon is predominantly amorphous and partially graphitic carbon exhibiting the characteristic ~3.4Å basal spacings, that is common in carbonaceous chondrites, is conspicuously rare in IDPs. The spectral redness of carbon-rich IDPs suggest that they contain organic carbon, which is confirmed by IR spectra that exhibit a pronounced organic C —H stretch feature at ~3.4 μm (Fig. 6) [31].

Some IDPs contain D/H and $^{15}N/^{14}N$ isotopic enrichments that are associated with an organic carrier [49]. The enrichments are attributed to isotope fractionation in cold (10–100 K) dense interstellar molecular clouds where extreme mass fractionation of H and N can occur during chemical reactions. Astronomical measurements of cold clouds show D/H ratios of 10^{-2}–10^{-1} in the coldest clouds, two to three orders of magnitude higher than the solar value (~10^{-4}). Much smaller D/H and $^{15}N/^{14}N$ enrichments observed in meteorites have long been attributed to the partial survival of presolar molecular cloud material that has been diluted and significantly altered by asteroidal parent body processes. However, in some IDPs the magnitudes of the enrichments are far larger and more common, in some cases with D/H values approaching those of molecular clouds, suggesting the complete preservation of molecular cloud material [11, 49].

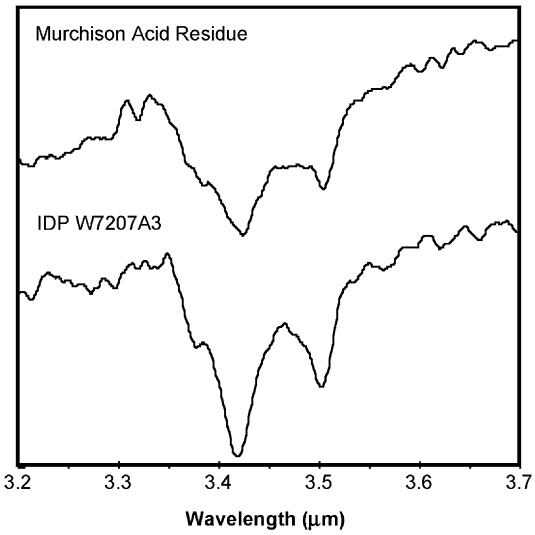

Fig. 6 Comparison of the ~3.4 μm C —H stretch features from Murchison acid residue and a thin section of IDP W7207A3 following in-situ acid dissolution [27]

3.2 Nano-Diamonds

Nano-diamonds are the most abundant type of presolar grains in chondritic meteorites (by over two orders of magnitude) where their average abundance is ~400 ppm [50]. Most nano-diamonds are between 1 and 10 nm in diameter with a lognormal size distribution and an average diameter of ~3 nm [51]. Although the average $^{13}C/^{12}C$ composition of the nano-diamonds is normal (solar), they are widely considered to be presolar astrominerals because of their association with a noble gas carrier, specifically an anomalous Xe-HL component that is consistent with supernovae processes [50]. However, the abundance of Xe is so low that only one nano-diamond in a million contains a Xe atom. Therefore, while at least some nano-diamonds are likely presolar, it remains unclear whether most nano-diamonds in meteorites originated in the solar system or presolar environments [4].

Since chondritic IDPs contain 2–5 times more carbon than carbonaceous chondrites [48], it is possible that they contain even higher abundances of nano-diamonds. Moreover, the abundance of nano-diamonds in IDPs may shed light on their origins for the following reason: if nano-diamonds are presolar astrominerals their abundance is expected to be higher in cometary IDPs because comets originate at extreme heliocentric distances where there is a greater chance of survival. If nano-diamonds formed in the solar system they are expected to be more abundant in meteorites, asteroidal micrometeorites, and asteroidal IDPs because they originate within the inner solar system.

Nano-diamonds in meteorites are isolated from gram-mass samples by a multi-step chemical (acid digestion) process that has been described as “burning down the

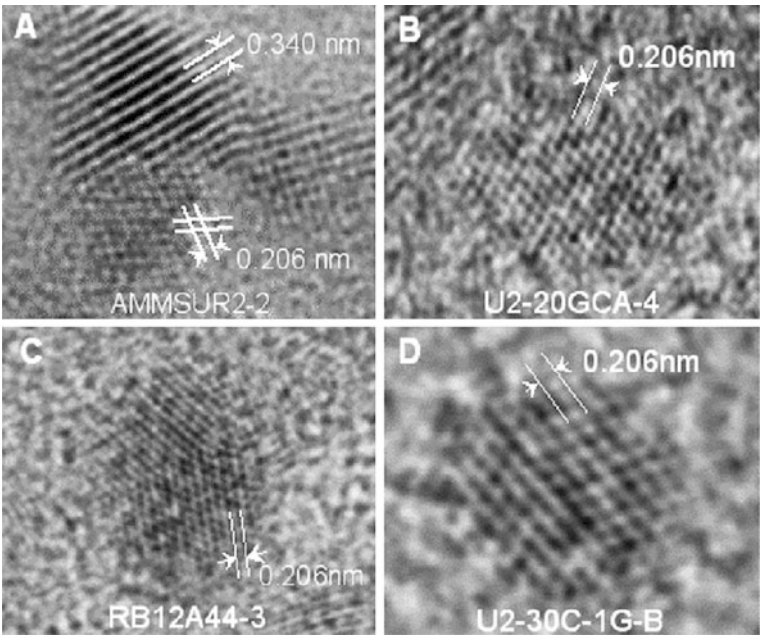

Fig. 7 Lattice-fringe images of nano-diamonds (0.206 nm spacings) in Antarctica micrometeorite AMMSRU2-2 and IDPs U2-20-GCA, RB12A44,and U2-30C-1G-B. See [85]

haystack to find the needle" [2]. Sub-nanogram mass thin sections of IDPs are acid etched in-situ using the simplified procedure described in the previous section [31]. Thin sections of fine-grained matrix from the Murchison (CM) and Orgueil (CI) meteorites, two "CM-like" polar micrometeorites, and nine chondritic IDPs were subjected to the in-situ procedure. Nano-diamonds were identified in the meteorite and micrometeorite thin sections, but in only three of the nine IDPs (Fig. 7). One of the nano-diamond-containing IDPs (RB12A44-3) is mineralogically similar to CM meteorites and is likely an asteroidal particle [28], while another (U2-20GCA-4) is a so-called giant cluster particle. It has been suggested that cluster particles are from asteroids [52], although their mineralogical similarity to cometary IDPs means that they could be derived from comets, asteroids, or both. The other eight particles are typical of cometary IDPs although their atmospheric entry speeds have not been determined. In any case, the apparent absence or depletion of nano-diamonds in most of the IDPs appears to challenge the widely held view that nano-diamonds in meteorites are presolar astrominerals.

3.3 Silicates

Silicates have long been known to be an important constituent of dust in circumstellar environments, the ISM, and solar system comets. The structure of the astronomical 10 and 20 μm Si—O stretch and Si—O—Si bending features indi-

cate that in general, these silicate astrominerals are almost exclusively amorphous (glassy) [9, 53]. This canonical picture of astronomical silicates changed radically when the Infrared Space Observatory (ISO) detected ubiquitous submicrometer crystalline forsterite (Mg_2SiO_4) and enstatite ($MgSiO_3$) around young and old stars and in comet Hale-Bopp [54–56]. The short-wavelength and long-wavelength spectrometers on ISO provided coverage of the mid IR region where the ~10 and ~20 μm "silicate" features are observed and, for the first time, the 20–100 μm region where features due to crystalline silicate minerals occur. More recently the Spitzer Space Telescope has provided even more detail about the nature of the silicate grains around T Tauri stars [57]. Another significant finding is the similarity between the silicate mineralogy of comet Hale-Bopp's dust and dust around the isolated Herbig Ae/Be star HD100546 [15, 58, 59] ("The Mineralogy of Cometary Dust" by Hanner and Zolensky, this volume). Silicate astrominerals were undoubtedly a major component of the dust from which the solar system was formed. ISO provided useful information in the search for crystalline silicate astrominerals in primitive meteoritic materials. The discovery that crystalline circumstellar silicates are Mg-rich, predominantly submicrometer-sized grains greatly simplifies distinguishing presolar silicates from the huge "background" of solar system Mg-Fe silicates in primitive meteoritic materials [54]. There are rare Mg-rich forsterite (and enstatite) grains in chondritic meteorites, some of them exhibiting morphological, compositional, or crystallographic evidence of vapor phase growth, that appear to have survived since the earliest stages of solar system formation [60, 61]. Some "relict" forsterite grains were among the earliest high-temperature solids in the solar nebula and they exhibit ^{16}O enrichments (to 50 parts per thousand) consistent with formation from or mass exchange with an (^{16}O-enriched) reservoir of grains and/or gas [62]. However, most of these grains are much larger than those detected by ISO.

Whilst submicrometer forsterite and enstatite crystals (like those detected by ISO) are exceedingly rare in meteorites and micrometeorites, they are the most abundant crystalline silicates in the fluffy CP class of IDPs [63, 64]. Grain sizes range from 0.05 to 5 μm, although most grains are between 0.1 and 0.75 μm (100–750 nm) in diameter (Fig. 2). The crystalline silicates detected by ISO presumably form by vapor phase growth in stellar outflows, and there is crystallographic evidence that some enstatite grains in IDPs formed by direct gas-to-grain condensation [65]. These crystals exhibit highly unusual whisker and ultrathin platelet morphologies and internal crystallographic defects (axial screw dislocations) that are typical of crystals grown from the vapor phase (Fig. 2). There is also compositional evidence that forsterite and enstatite grains in IDPs grew by direct gas-to-grain condensation from a nebula gas [65]. Low Fe, Mn enriched (LIME) enstatite and forsterite grains in IDPs contain up to 5 wt.% MnO, in contrast to the majority of pyroxenes and olivines in meteorites which contain <0.5 wt.% MnO. It is likely that the high Mn contents reflect condensation from a nebula gas. A measurement of the Mg isotopic composition of a single ~5 μm long enstatite whisker in a CP IDP failed to reveal a significant isotope anomaly [39]. ISO provides little information about the nature of amorphous silicate astrominerals in primitive meteoritic materials. Rare amorphous silicates (glasses) in primitive meteorites are believed to

have formed in the solar system. In contrast, IDPs contain abundant glassy silicates known as GEMS as well as other glassy grains [39, 66, 67]. They are 0.1–0.5 μm glassy spheroids with nanometer-sized FeNi metal and Fe-rich sulfide inclusions. They have aroused much interdisciplinary interest because their properties are similar to the exotic properties that astronomers have inferred for interstellar "amorphous silicates" [68–70]. Although the compositions and mineralogy of GEMS are consistent with interstellar amorphous silicates, rigorously proving that they are presolar required measurement of non-solar isotope abundances. An attempt to detect (Mg) isotope anomalies in individual GEMS was unsuccessful [39], although a high-precision bulk oxygen isotope measurement of a GEMS-rich IDP yielded the highest "whole rock" ^{16}O enrichment yet measured in any chondritic object [17]. Since silicates are the major carrier of oxygen in IDPs, the bulk measurements provided the first hint that GEMS-rich IDPs contain presolar silicates. The presolar interstellar origins of some GEMS has now been rigorously confirmed by measurements of non-solar oxygen isotope compositions using the latest generation nanoSIMS [19–21].

The petrography of GEMS links them to presolar astrominerals. Using EELS, it was shown that nitrogen in a ^{15}N-enriched IDP is localized within a carbonaceous phase that mantles and encapsulates GEMS (Fig. 8) [38]. It is possible that the (isotopically anomalous) mantles were deposited on the GEMS in a presolar molecular cloud environment. A deuterium "hot spot", first identified within an IDP pressed into a gold ion microprobe mount, was subsequently thin-sectioned using

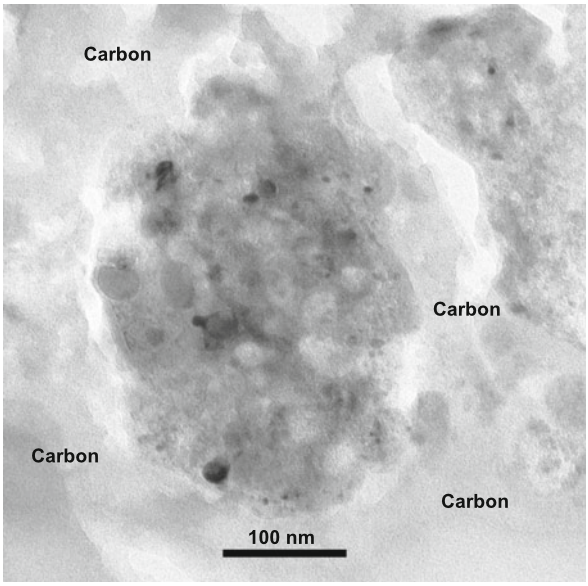

Fig. 8 Brightfield transmission electron micrograph of a GEMS embedded in amorphous carbon material in IDP L2011R11. The remnants of a deeply eroded relict grain with "swiss cheese" microstructure can be seen towards the center of the grain

ultramicrotomy and examined using TEM. The "hotspot" is dominated by poorly ordered organic carbonaceous material with embedded GEMS and Fe-rich sulfides [71].

The IR spectral properties of GEMS provide further insight about their origin(s). GEMS-rich thin sections of IDPs, i.e. sections with GEMS plus submicrometer enstatite and forsterite crystals, exhibit a ~10 μm silicate feature similar to solar system comets and dust around some Herbig Ae/Be stars [44]. Some essentially pure GEMS exhibit an Si—O stretch feature with an absorption minimum at ~9.7 μm, a bandwidth of ~3.5 μm (FWHM), and a pronounced excess or asymmetry on the long wavelength side of the feature. Interstellar silicates also exhibit an Si—O stretch feature with an absorption minimum at ~9.7 μm, a bandwidth of 2.5–3.5 μm (FWHM), and a pronounced excess or asymmetry on the long wavelength side of the feature. These GEMS are the first identified natural silicate to provide such a match, adding to the exotic set of compositional and mineralogical properties required to match those of interstellar amorphous silicates [44, 68–70].

3.4 FeNi Sulfides

FeNi sulfide grains are the major carrier of sulfur in primitive chondritic meteorites and chondritic IDPs [72–74]. They were also identified as a component of comet Halley's dust [75, 76]. Although they are a crystallographically complex group of minerals, sulfides were one of the first minerals identified in IDPs [77–79]. TEM studies have shown that they span an enormous size range (10^{-1}–10^{-4} nm) [10, 73, 80]. Grain morphologies include irregular, hexagonal, rectangular,and rounded shapes, and a variety of different compositions and structures may coexist within a single IDP. Most sulfide grains in IDPs are low-Ni pyrrhotite [78]. Pentlandite, troilite, and sphalerite (ZnS) have also been reported [73, 74, 81].

An Fe-Ni sulfide with a "spinel-like" cubic structure was identified in chondritic IDPs [80]. The composition of this sulfide is similar to those of pyrrhotite and pentlandite, and it is commonly closely associated with hexagonal pyrrhotite. Electron diffraction patterns and high-resolution lattice-fringe images indicate that both minerals are sometimes coherently intergrown on a unit cell scale but, when the spinel sulfide is mildly heated in the electron beam, it transforms into hexagonal pyrrhotite (Fig. 9). Therefore, hexagonal pyrrhotite, the dominant sulfide in IDPs, may be a secondary thermal alteration product of the spinel-like sulfide. All IDPs are pulse heated above 500°C during atmospheric entry [77].

The spinel-like sulfide shows that the sulfide mineralogy of CP IDPs is significantly different from that of the primitive chondritic meteorites. Therefore, it is possible that some or all of the sulfides in IDPs formed in a different kind of environment. A crystallographically similar sulfide was synthesized by low-temperature (<200°C), low-pressure vapor phase growth [82]. There are other indications that the sulfide mineralogy of IDPs differs from that of other meteoritic sulfides. A recent comparative study of sulfides within IDPs and meteorites showed selenium levels in IDPs are 60% higher than those in meteoritic sulfides, implying that "the IDP

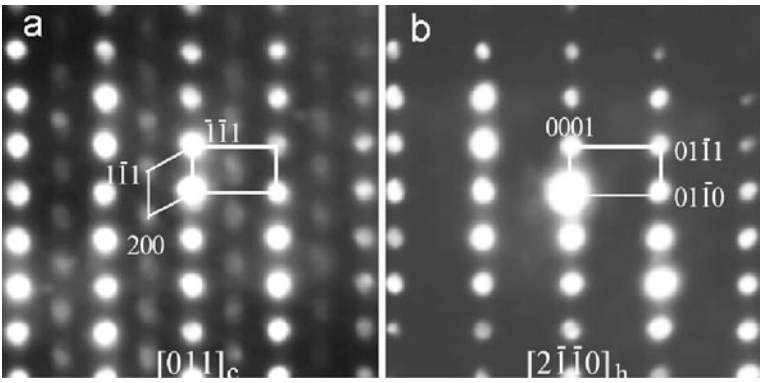

Fig. 9 Time-resolved electron micro-diffraction patterns taken from an FeNi sulfide grain in IDP W7020A-8D. In pattern (**a**), the reflections with strong intensity are indexed as simple hexagonal pyrrhotite (*thick line box*). The extra weak reflections (*thin line box*) are indexed as cubic spinel sulfide. After illumination in the electron beam for several tens of seconds, the weak cubic spinel reflections disappear. See [80]

sulfides are likely to have formed in a different environment than the (Orgueil) meteoritic pyrrhotite" [83].

FeNi sulfides in IDPs may be highly relevant to the field of astromineralogy. We have proposed that sulfides are responsible for a broad ~23 μm feature recently detected around young and old stars by the Infrared Space Observatory (ISO) [84]. Laboratory spectra were obtained from pyrrhotite ($[Fe,Ni]_{1-x}S$) grains in IDPs, as well as pyrrhotite and troilite (FeS) mineral standards using a high-brightness synchrotron light source. All of the sulfides produce a broad Fe-S stretch feature centered at ~23.5 μm similar to the broad 23 μm feature observed in the ISO spectra. Thus Fe sulfide grains may be an important, previously unrecognized component of circumstellar dust. Although S is not significantly depleted from the gas phase in the ISM, it is highly depleted in cold, dense interstellar molecular clouds indicating that it is in solid grains [85–87].

3.5 Grigg-Skjellerup IDPs

In 2003 IDPs were collected in the stratosphere at the time of the comet Grigg-Skjellerup (GS) meteor stream [88]. Although it is not possible to prove that the collected IDPs are from this particular stream, it is clear that their collective properties differ significantly from previous IDP collections. Most of the particles collected are GEMS-rich CP IDPs, and in some cases, are almost exclusively GEMS and carbonaceous matter [89], consistent with the two major types of grains in the ISM. Collectively, the GS IDPs exhibit widespread H, ^{13}C, ^{15}N and O isotope anomalies consistent with preserved molecular cloud material. The number of anomalous sili-

cate grains is the highest ever recorded in any meteoritic material (by ∼100 times) and approaching ∼1% of the total silicate grain population in GS IDPs [90].

4 Astromaterials in Comet 81P/Wild 2

In January 2006, the Stardust mission returned the first samples collected from the coma of a comet to Earth. Less than 1 mg of sample was collected [91, 92]. The samples were largely confined to the 1 to 100 μm size range because larger particles were rare and smaller ones were mostly destroyed during capture into silica aerogel. Surprisingly, the Stardust sample is not the expected mother lode of presolar astromaterials. So far only three isotopically presolar grains have been identified, leading to an estimated abundance of 11 ppm in the "Wild 2" sample, an order of magnitude lower than their abundance in meteorites (100–300 ppm) [93]. However, it possible that limited statistics or even selective destruction of presolar silicates during hypervelocity capture in aerogel are responsible for the low abundance of isotopically anomalous grains [94, 95]. The Wild 2 sample consists predominantly of materials made in the inner solar nebula, as do chondritic meteorites from the asteroid belt. The materials in Wild 2 include high-temperature multi-mineralic "rocks" like chondrule fragments and CAIs [91, 96, 97]. The abundance of presolar astromaterials in the Stardust samples is either less than or similar to their abundance in meteorites [95, 96]. Despite the possible dearth of astromaterials in Comet Wild 2, the Stardust sample proves that materials from throughout the entire solar nebula accretion disk accumulated in the Kuiper Belt. This finding alone is a fundamental milestone in our understanding of the Kuiper Belt (Fig. 10).

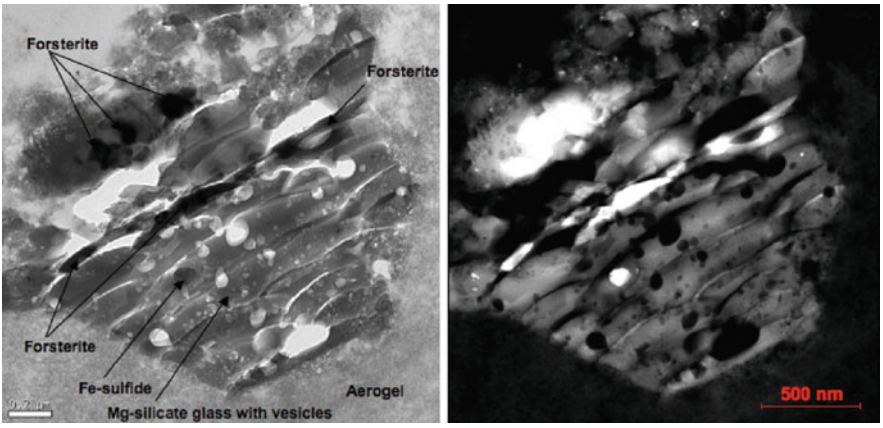

Fig. 10 *Brightfield* and *darkfield* transmission electron micrographs of a Wild 2 grain in an impact track in aerogel. The grains contains enstatite and forsterite as well as iron sulfide inclusions. The forsterite (and sulfide) are crystalline but most of the enstatite is amorphous and vesiculated, presumably a result of hypervelocity capture in aerogel

5 Conclusions

The focus of this chapter has been the anhydrous CP subset of IDPs, some or all of which are likely of cometary origin [23]. Despite the technical difficulties inherent in analyzing tiny nanogram-mass IDPs, a large database of compositional, mineralogical, and isotopic data has been acquired. These data establish that IDPs differ fundamentally from even the most primitive meteorites, micrometeorites and the samples of Comet Wild 2. It is possible and perhaps even likely that the collected CP IDPs include well-preserved aggregates of (presolar) circumstellar and interstellar materials [85]. This conclusion is strengthened by the confirmation that IDPs contain presolar grains, including interstellar "amorphous silicates" and carbonaceous grains that are ubiquitous throughout interstellar space.

Interplanetary dust research may be on the verge of an exciting new era. Techniques for sample micromanipulation have been highly refined, optical and electron-transparent thin-sections are now routinely produced, the compositions, mineralogy and petrography of individual subcomponents of IDPs are determined with sub-nanometer scale resolution, and the isotopic compositions of grains $\leq$100 nm in diameter can now be measured. Synchrotron light sources are being used to measure the optical properties of (thin sections of) IDPs and they are directly compared with those of dust in cometary, interstellar, and circumstellar environments.

Acknowledgments This research is supported by NASA grants NAG5-7450 and NAG5-9797.

References

1. Wetherill, G.W., Chapman, C.R.: Asteroids and meteorites. In: Kerridge, J.F., Matthews, M.S. (eds.) Meteorites and the Early Solar System, pp. 35–70. University of Arizona Press, Tucson, AZ (1988) 260
2. Bernatowicz, T.J., Walker, R.M.: Phys. Today **50**, 26 (1997) 260, 267
3. Bradley, J.P., Sandford, S., Walker, R.M.: Interplanetary dust particles. In: Kerridge, J., Mathews, M.S. (eds.) Meteorites and the Early Solar System, pp. 861–895. University of Arizona Press, Tucson, AZ (1988) 260
4. Hoppe, P., Zinner, E.: J. Geophys. Res. **105**(10), 371 (2000) 260, 266
5. Andersen, A.C., Jäger, J., Mutschke, H., Braatz, A., Clément, D., Henning, Th., Jorgensen, U.G., Ott, U.: Astron. Astrophys. **343**, 933 (1999) 260
6. Mutschke, H., Anderson, A.C., Clément, D., Henning, Th.: Astron. Astrophys. **345**, 187 (1999) 260
7. von Helden, G., Tielens, A.G.G.M., van Heijnsbergen, D., et al: Science **288**, 313 (2000) 260
8. Anders, E., Zinner, E.: Meteoritics **28**, 490 (1993) 260
9. Mathis, J.S.: Rep. Prog. Phys. **56**, 605 (1993) 260, 268
10. Bradley, J.P.: Geochim. Cosmochim. Acta **52**, 889 (1988) 260, 270
11. Messenger, S.: Nature **404**, 968 (2000) 260, 261, 264, 265
12. Schramm, L.S., Brownlee, D.E., Wheelock, M.M.: Meteoritics **24**, 99 (1989) 260
13. Arndt, P., Bohsung, J., Maetz, M., Jessberger, E.K.: Meteorit. Planet. Sci. **31**, 817 (1996) 260
14. Greenberg, J.M.: What are comets made of? In: Wilkening, L.L. (ed.) Comets, pp. 131–162. University of Arizona Press, Tucson, AZ (1982) 261

15. Wooden, D.H., Harker, D.E., Woodward, C.E., Butner, H.M., Koike, C., Witteborn, F.C., McMurty, C.W.: Astrophys. J. **517**, 1034 (1999) 261, 268
16. Clemett, S.J., Maechling, C.R., Zare, R.N., Swan, P.D., Walker, R.M.: Science **262**, 721 (1993) 261
17. Engrand, C., McKeegan, K.D., Leshin, L.A., Bradley, J.P., Brownlee, D.E.: Lunar Planet. Sci. **XXX**, 1690–1691 (1999) 261, 269
18. Messenger, S., Keller, L.P., Walker, R.M.: Lunar Planet. Sci. **XXXIII**, 1887 (2002) 261, 264, 265
19. Floss, C., Stadermann, J.J., Bradley, J.P., Dai, Z.R., Bajt, S., Graham, G., Scott, L.A.: Geochim. Cosmochim. Acta. **70**, 2371 (2006) 261, 269
20. Nguyen, A., Busemann, H., Nittler, L.R.: Lunar Planet. Sci. **XXXVIII**, 2332 (2007) 261, 269
21. Messenger, S., Keller, L.P., Nakamura-Messenger, K.: Lunar Planet. Sci. **XXXVIII**, 2122 (2007) 261, 269
22. Bradley, J.P., Ishii, H.A.: Astron. Astrophys. **486**, 781 (2008) 261
23. Brownlee, D.E., Joswiak, D.J., Schlutter, D.J., Pepin, R.O., Bradley, J.P., Love, S.G.: Lunar Planet. Sci. **XXVI**, 183 (1995) 261, 273
24. Flynn, G.J.: Sources of 10 μm interplanetary dust: possible importance of the Kuiper belt. In: Gustavson, B.Å.S., Hanner, M.S. (eds.) Physics, Chemistry, and Dynamics of Interplanetary Dust. ASP Conference Series, vol. 104, pp. 274–282. ASP, San Francisco, CA (1996) 261
25. Liou, J.C., Zook, H.A.: Lunar Planet. Sci. **XXVII**, 763 (1996) 261
26. Bradley, J.P., Brownlee, D.E., Fraundorf, P.: Science **226**, 1432 (1984) 261
27. Sandford, S.A., Bradley, J.P.: Icarus **82**, 146 (1989) 261, 264, 266
28. Bradley, J.P., Brownlee, D.E.: Science **251**, 549 (1992) 261, 265, 267
29. Bradley, J.P., Brownlee, D.E.: Science **231**, 1542 (1986) 261
30. Bradley, J.P., Keller, L.P., Thomas, K.L., VanderWood, T.B., Brownlee, D.E.: Lunar Planet. Sci. **XXIV**, 173 (1993) 261
31. Brownlee, D.E., Joswiak, D.J., Bradley, J.P., Gezo, J.C., Hill, H.G.M.: Lunar Planet. Sci. **XXXI**, 1921 (2000) 262, 265, 267
32. Zolensky, M.E., Wilson, T.L., Rietmeijer, F.J.M., Flynn, G.J. (eds.): Analysis of Interplanetary Dust. AIP Conference Proceedings, vol. 310, p. 357. American Institute of Physics, New York, NY (1994) 263
33. Zolensky, M.E., Pieters, C., Clark, B., Papike, J.J.: Meteorit. Planet. Sci. **35**, 9 (2000) 263
34. Grün, E., Gustavson, B.Å.S., Dermott, S.F., Fechtig, H. (eds.): Interplanetary Dust, p. 804. Springer, New York, NY (2000) 263
35. Sutton, S.R., Flynn, G.J., Rivers, M., Eng, P., Newville, M., Shea-McCarthy, G., Lanzirotti, A.: Meteorit. Planet. Sci. **34**, A113 (1999) 263
36. Flynn, G.J., Keller, L.P., Jacobsen, C., Wirick, S.: Lunar Planet. Sci. **XXI**, LPI Houston CD-ROM, Abstract #1904 (2000) 263
37. Flynn, G.J., Keller, L.P., Jacobsen, C., Wirick, S.: Meteorit. Planet. Sci. **34**, A36 (1999) 263
38. Keller, L.P., Messenger, S., Bradley, J.P.: J. Geophys. Res. **165**, 10397 (2000) 264, 269
39. Bradley, J.P., Ireland, T.: The search for interstellar components in interplanetary dust particles. In: Gustavson, B.Å.S., Hanner, M.S. (eds.) Physics, Chemistry, and Dynamics of Interplanetary Dust, ASP Conference Series, vol. 104, pp. 274–282. ASP, San Francisco, CA (1996) 264, 268, 269
40. Sandford, S.A., Walker, R.M.: Astrophys. J. **291**, 838 (1982) 265
41. Bradley, J.P., Humecki, H., Germani, M.S.: Astrophys. J. **394**, 643 (1992) 265
42. Bradley, J.P., Keller, L.P., Brownlee, D.E., Thomas, K.L.: Meteorit. Planet. Sci. **31**, 394 (1996) 265
43. Gezo, J.C., Bradley, J.P., Brownlee, D.E., Kaleida, K., Keller, L.P.: Lunar Planet. Sci. **XXX1**, 1816 (2000) 265
44. Bradley, J.P., Keller, L.P., Snow, T.P., Hanner, M.S., Flynn, G.J., Gezo, J.C., Clemett, S.J., Brownlee, D.E., Bowey, J.E.: Science **285**, 1716 (1999) 265, 270
45. Rietmeijer, F.J.M.: Meteorit. Planet. Sci. **31**, 278 (1996) 265
46. Keller, L.P., Thomas, K.L., McKay, D.S.: Geochim. Cosmochim. Acta **56**, 1409 (1992) 265

47. Binzel, R.P.: Icarus **99**, 238 (1993) 265
48. Thomas, K.L., Blanford, G.E., Keller, L.P., Klöck, W., McKay, D.S.: Geochim. Cosmochim. Acta **57**, 1551 (1993) 265, 266
49. Messenger, S., Walker, R.M.: Evidence for molecular cloud material in meteorites and interplanetary dust. In: Astrophysical Implications of the Laboratory Study of Presolar Materials, pp. 545–564. American Institute of Physics, Woodbury, NY (1997) 265
50. Anders, E., Zinner, E.: Meteoritics **28**, 490 (1993) 266
51. Daulton, T.L., Eisenhour, D.D., Bernatowicz, T.J., Lewis, R.S., Buseck, P.R.: Geochim. Cosmochim. Acta **60**, 4853 (1996) 266
52. Thomas, K.L., Blanford, G.E., Clemett, S.J., McKay, D.S., Messenger, S., Zare, R.N.: Geochim. Cosmochim. Acta **59**, 2797 (1995) 267
53. Whittet, D.C.B.: Dust in the Galactic Environment. Institute of Physics, New York, NY (1992) 268
54. Hendecourt, L., Joblin, C., Jones, A. (eds.): Solid Interstellar Matter: The ISO Revolution, p. 315. Les Houches No 11, EDP Sciences, Les Ullis (1999) 268
55. Waters, L.B.F.M., Molster, F.J., de Jong, T., et al.: Astron. Astrophy\s. **315**, L361 (1996) 268
56. Molster, F.J.: Crystalline silicates in circumstellar dust shells. Ph.D. Thesis, University of Amsterdam (2000) 268
57. Werner, M., Giovanni, F., Rieke, G., Roellig, T., Watson, D.M.: Annu. Rev. Astron. Astrophys. **44**, 269 (2006) 268
58. Hanner, M.S., Gehrz, R.D., Harker, D.E., Hayward, T.L., Lynch, D.K., Mason, C.C., Russell, R.W., Williams, D.M., Wooden, D.H., Woodward, C.E.: Earth Moon Planets **79**, 247 (1998) 268
59. Crovisier, J., Leech, K., Bockelee-Morvan, D., Brooke, T.Y., Hanner, M.S., Altieri, B., Keller, H.U., Lellouch, E.: Science **275**, 1904 (1997) 268
60. Steele, I.M.: Geochim. Cosmochim. Acta **50**, 1379 (1986) 268
61. Steele, I.M.: Am. Mineral. **71**, 966 (1986) 268
62. Jones, R.H., Saxton, J.M., Lyon, I.C., Turner, G.: Lunar Planet. Sci. **XXIX**, 1795 (1988) 268
63. Bradley, J.P.: Mg-rich olivine and pyroxene grains in primitive meteoritic materials: comparison with crystalline silicate data from ISO. In: d'Hendecourt, L., Joblin, C., Jones, A. (eds.) Solid Interstellar Matter: The ISO Revolution, pp. 297–315. Les Houches No 11, EDP Sciences, Les Ullis (1999) 268
64. Zolensky, M.E., Barrett, R.: Olivine and pyroxene compositions of chondritic interplanetary dust particles. In: Zolensky, M.E., Wilson, T.L., Rietmeijer, F.J.M., Flynn, G.J. (eds.) Analysis of interplanetary Dust. AIP Conference Proceedings, vol. 310, pp. 105–114. American Institute of Physics, New York, NY (1994) 268
65. Bradley, J.P., Brownlee, D.E., Veblen, D.R.: Nature **301**, 473 (1983) 268
66. Bradley, J.P.: Science **265**, 925 (1994) 269
67. Rietmeijer, F.J.M.: Interplanetary dust particles. In: Papike, J.J. (ed.) Planetary Materials, pp. (2)1–(2)95. Mineralogical Society of America, Washington, DC (1998) 269
68. Flynn, G.J.: Nature **371**, 287 (1994) 269, 270
69. Goodman, A.A., Whittet, D.C.B.: Astrophys. J. **455**, L181 (1995) 269, 270
70. Martin, P.G.: Astrophys. J. **445**, L63 (1995). 269, 270
71. Keller, L.P., Messenger, S., Flynn, G.J., Wirick, S., Jacobsen, C.: Lunar Planet. Sci. **XXXIII**, 1869 (2003) 270
72. Buseck, P.R., Hua, X.: Annu. Rev. Earth Planet. Sci. **21**, 255 (1993) 270
73. Zolensky, M.E., Thomas, K.L.: Geochim. Cosmochim. Acta **59**, 4707 (1995) 270
74. Tomeoka, K., Buseck, P.R.: Earth Planet. Sci. Lett. **69**, 243 (1984) 270
75. Jessberger, E.K., Christoforidis, A., Kissel, J.: Nature **332**, 691 (1988) 270
76. Lawler, M.E., Brownlee, D.E., Temple, S., Wheelock, M.M.: Icarus **80**, 225 (1989) 270
77. Brownlee, D.E.: Interplanetary dust: possible implications for comets and presolar interstellar grains. In: Gehrels, T. (ed.) Protostars and Planets, pp. 134–150. University of Arizona Press, Tucson (1978) 270
78. Fraundorf, P.: Geochim. Cosmochim. Acta **45**, 915 (1981) 270

79. Flynn, G.J., Fraundorf, P., Shirck, J., Walker, R.M.: Proceedings of the 9th Lunar Planetary Science Conference, p. 1187 (1978) 270
80. Dai, Z.R., Bradley, J.P.: Geochim. Cosmochim. Acta **65**, 3601 (2001) 270, 271
81. Love, S.G., Brownlee, D.E.: Icarus **89**, 26 (1991) 270
82. Nakazawa, H., Osaka, T., Sakaguchi, K.: Nature **242**, 13 (1973) 270
83. Flynn, G.J.: Meteorit. Planet. Sci. **35**, A54 (2000) 271
84. Keller, L.P., Bradley, J.P., Molster, F.J., Waters, L.B.F.M., Bouwman, J., Brownlee, D.E., Flynn, G.J., Henning, Th., Mutschke, H.: Nature **417**, 148 (2002) 271
85. Savage, B.D., Sembach, K.R.: Annu. Rev. Astron. Astrophys. **34**, 279 (1996) 267, 271, 273
86. Snow, T.P., Witt, A.N.: Interstellar depletions updated: where all the atoms went. Astrophys. J. **468**, L65 (1996) 271
87. Sofia, U.J., Cardelli, J.A., Savage, B.D.: Astrophys. J. **430**, 650 (1994) 271
88. Flynn, G.J., Lazirotti, A., Sutton, S.R.: Lunar Planet. Sci. **XXXVI**, 1148 (2005) 271
89. Nakamura-Messenger, K., Keller, L.P., Messenger, S., Clemett, S.J., Zolensky, M.E., Palma, R.L., Pepin, R.O., Wirick, S.: Meteorit. Planet. Sci. **43**, A111 (2008) 271
90. Nguyen, A.N., Buseman, H., Nittler, L.R.: Lunar Planet. Sci. **XXXVIII**, 2332 (2007) 272
91. Brownlee, D.E., et al.: Science **314**, 1711 (2006) 272
92. Burnett, D.: Science **314**, 1709 (2006) 272
93. Messenger, S., Joswiak, D., Ito, M., Matrajt, G., Brownlee, D.E.: Lunar Planet. Sci. **XXXX**, 1790 (2009) 272
94. Stadermann, F., Floss, C., Gavinsky, A., Kearsley, A.T., Burchell, M.J.: Lunar Planet. Sci. **XXXX**, 1188 (2009) 272
95. Brownlee, D.E., Joswiak, D., Matrajt, G., Messenger, S., Ito, M.: Lunar Planet. Sci. **XXXX**, 2195 (2009) 272
96. Nakamura, T., Takaaki, N., Tsuchiyama, A., Ushikubo, T., Kita, N.T., Valley, J.W., Zolensky, M.E., Kakazu, Y., Sakamoto, K., Mashio, E., Uesugi, K., Nakano, T.: Science **321**, 1664–1667 (2008) 272
97. Simon, S.B., Joswiak, D.J., Ishii, H.A., Bradley, J.P., Chi, M., Grossman, L., Aléon, J., Brownlee, D.E., Fallon, S., Hutcheon, I.D., Matrajt, G., McKeegan, K.D.: Meteorit. Planet. Sci. **43**, 1861 (2008) 272

The Most Primitive Material in Meteorites

U. Ott

Abstract The most primitive matter known to occur in meteorites are circumstellar condensates. They were originally found as result of the search for the carrier phases of isotopically anomalous noble gases and isolated from the bulk meteorites using harsh chemical treatments. Diamond was the first and may occur with an abundance $>1‰$, but it is not clear what fraction of the observed nanometer-sized diamonds is truly presolar. Others found by this approach consist of thermally and chemically highly resistant materials (graphite, silicon carbide, refractory oxides and silicon nitride) and occur on the sub-ppm to several ten ppm level. Identification of presolar minerals susceptible to chemical treatment became possible with technical developments in secondary ion mass spectrometry allowing searches in the meteorites in situ. Presolar silicates found by this approach occur on an abundance level up to $\sim$200 ppm.

Isotope abundance anomalies are the key feature based on which the presolar nature of a given grain is ascertained. They also allow identifying likely stellar sources for the grains. The major source of SiC, the oxide and the silicate grains are Red Giant/AGB stars, while some ($\sim$1%) of the SiC and all of the silicon nitride grains appear to be linked to supernovae, as are probably the presolar nanodiamonds. Graphite grains come from a number of different stellar sources. The detailed isotopic patterns also allow drawing conclusions about nucleosynthesis and mixing in stars as well as galactic chemical evolution.

Astronomical detection around specific sources, such as in the case of SiC and silicates, would be helpful if it could be achieved also for other grains. Deriving an age for the grains and establishing a detailed history between time of formation in stellar outflows and arrival in what was to become the solar system is a task that remains to be accomplished.

U. Ott (✉)
Max-Planck-Institut für Chemie, Postfach 3060, D-55020 Mainz, Germany
e-mail: ott@mpch-mainz.mpg.de

Ott, U.: *The Most Primitive Material in Meteorites*. Lect. Notes Phys. **815**, 277–311 (2010)
DOI 10.1007/978-3-642-13259-9_7

1 The Most Primitive Material in Meteorites

What is primitive? In a sense, all the material making up the major group of meteorites – the chondrites (∼85% of all falls) – is primitive. All their constituents, including thermally and/or aqueously metamorphosed ones, formed within the first few tens of millions of years after formation of the solar system (e.g., [1, 2]). They thus constitute old material formed 4.5–4.6 Ga ago and essentially unaltered since then – they are primitive. In fact chondritic meteorites, and in particular the subgroup of the carbonaceous chondrites represent the most pristine material that is available for detailed laboratory study in large amounts. Others, less abundantly available materials include interplanetary dust picked up by aircraft in the stratosphere, micrometeorites collected in deep sea sediments/ polar ice (cf. chapter "The In-Situ Study of Solid Particles in the Solar System" by Mann and Jessberger, this volume), and just recently tiny amounts of matter returned by the STARDUST space mission (e.g., [3, 4]).

One of the more astonishing developments in the study of meteorites has been the realization that they contain small amounts of even more primitive material – presolar dust which predates the solar system. These grains the first of which (diamond and silicon carbide) were detected in 1987, formed during the final stages of stellar evolution from material ejected by stars in strong stellar winds or during explosions. Subsequently they survived passage through the interstellar medium and became part of the parcel of gas and dust from which the solar system formed. The grains then survived what violent events there may have been in the early stages of solar system formation and were incorporated into meteorite parent bodies where they spent the following ∼4.5 Ga. Collisions that liberated the meteorites-to-be from their parent bodies and sent them towards Earth made it possible that we can have those presolar grains in the laboratory now where we can investigate them with the full scrutiny of modern analytical techniques (Fig. 1).

The implications of the first decade of laboratory analysis of presolar grains have been the subject of an excellent Conference Book [5] and the reader can find many more details in this book than can be discussed here. Also useful may be the additional study of more recent review articles (e.g., [6–10]) dealing in detail primarily with the isotopic structures of presolar dust grains from meteorites and the inferred stellar sources. A collection of papers on the subject is also contained in the December 2003 Special Issue of *Geochimica et Cosmochimica Acta* (Volume 47, Number 24) dedicated to Robert M. Walker. The most significant advance since the first edition of this book was published has been the identification of presolar silicate grains. This was made possible by progress in analytical techniques, in particular the introduction of the NanoSIMS instrument that allows isotopic mapping of the meteorite in situ on the ∼100 nm scale [11]. Major progress was also made in the field of structural characterization and in putting constraints on the age of the grains.

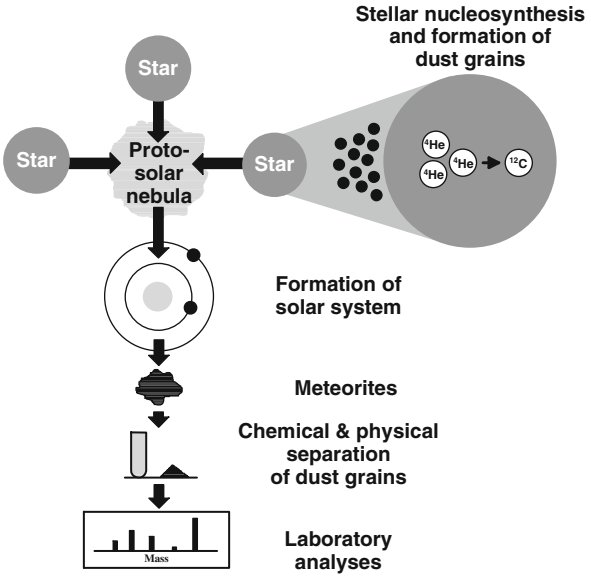

Fig. 1 The path of a circumstellar grain from stellar source to terrestrial laboratory. Sketch courtesy of P. Hoppe, modified from [49]

2 Overview: Identification and Isolation

2.1 Identification

Recognizing presolar grains as such is not a trivial task. Many distinguishing features, even those characteristic for presolar origin, are not unique enough to clearly rule out a more commonplace origin. A case in point is that of the GEMS (Glass with Embedded Metal and Sulfides) found in interplanetary dust particles ([12] "The Astromineralogy of Interplanetary Dust Particles" by Bradley, this volume). Many features, such as amorphous structure, size and non-stochiometry, point to an interstellar origin, but nevertheless there exists general agreement that for confirmation *isotopic* analysis of their constituent elements is required. This task, because of their submicron size, has been impossible with previous analytical equipment. Analyses using the new generation of ion microprobes coming into operation [11] have shown, however, that at least some of them contain material that is of presolar origin [13].

The situation reflects the general agreement that the only reliable indicator of a non-solar-system origin is the isotopic composition of a grain. Elements heavier than and including carbon are produced in stars, and grains forming from matter expelled by a specific star will carry isotopic signatures diagnostic for the

nuclear processes that occurred in this star. A grain of "circumstellar" origin will thus show – relative to solar system isotopic abundances – clear isotope abundance anomalies based upon which it can be recognized. Inter- rather than circumstellar grains, present at the time and place of birth of the solar system, on the other hand, are likely to be isotopically similar to solar system matter. Using the strict isotopic criterion, we may not be able to recognize such material as presolar. Therefore, all the grain types and the features to be discussed below refer to grains of circumstellar origin only, and not to presolar/interstellar grains in general.

It is important to also keep in mind that isotope abundance anomalies have been found in meteorites that have *not* been linked to presolar grains. One type, most conspicuous in the elements in the mass range of iron (Ca, Ti, Cr, Fe, Ni, Zn) is found in calcium-aluminum-rich inclusions (CAIs) in primitive meteorites [14]. These inclusions are macroscopic objects (mm- to cm-size). They may be the first solids that formed within the solar system (e.g., [1, 2]) and anomalies are likely to be due to incomplete homogenization of solar system precursor materials. Anomalies are much smaller than comparable anomalies in true circumstellar grains (e.g., [15]). Other anomalies – in elements that came into the solar system primarily as gas – are also conserved in elements such as hydrogen and nitrogen [16, 17] indicative of the preservation of primitive organics that were a component of the original building blocks of the solar system [18]. In addition, large enhancements of the oxygen isotopes ^{17}O and ^{18}O have been found in as yet ill-defined phases in the matrix of primitive meteorites [19, 20]. The isotopic effects are likely due to high energy particle irradiation during an active phase of the young sun [19] and we will not further discuss them here, concentrating instead on "established" presolar grains that originated as stardust.

2.2 Isolation

A paradigm in the 1960s stated that the planets and other objects in the solar system had formed from "a well-mixed primordial nebula of chemically and isotopically uniform composition" [21] because the assumption was that the nebula had gone through a phase when it was so hot that no solids could survive. However, already then, key evidence to the contrary was evolving: isotopic abundance anomalies were found in the noble gas elements xenon (Fig. 2) and neon that ultimately were traced to the presence of presolar grains. The anomalous xenon first seen by [22] – Xenon-HL in today's nomenclature (e.g., [23]) – is characterized by approximately two-fold enhancement in the abundances of the heaviest (hence H) and lightest (hence L) isotopes; the anomalous neon (Neon-E) first recognized by [24] consists virtually of only one isotope, ^{22}Ne. As we know now, Ne-E occurs in two varieties Ne-E(L) and Ne-E(H) – also named Ne-R and Ne-G these days –, where the former is carried by grains of presolar graphite, the latter by grains of presolar silicon carbide (SiC). Xenon-HL, to the best of our knowledge, is carried by grains of presolar nanometer-sized diamonds.

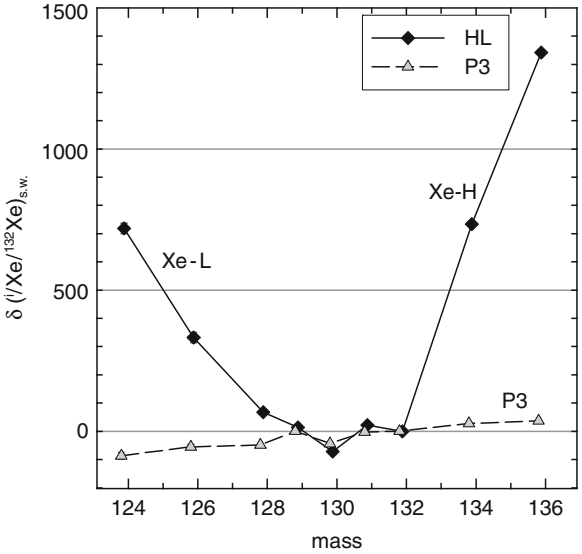

Fig. 2 Composition of xenon in meteoritic nanodiamonds. Xenon HL shows overabundances in light (Xe-L) and heavy (Xe-H) isotopes and indicates a connection to supernovae. The presence of Xe-P3, an isotopically almost normal component of Xe, indicates complexity (cf. also Sect. 3.6). Shown are deviations of isotope ratios $^{i}\mathrm{Xe}/^{132}\mathrm{Xe}$ from solar xenon (in per mill) as inferred from solar wind implanted in lunar material [100]

2.2.1 Isolation of Refractory Grains

It was the search for the carrier phases of noble gases that led, in 1987, to the identification of the first two types of presolar grains, diamond and silicon carbide [25, 26]. Key to the isolation was the realization that they are resistant to acids [27, 28]. Following up on this observation, a kind of "standard recipe" has developed, which is the one described by [29] for their K series separates. In short, the most important steps for isolating the most abundant of the chemically refractory presolar phases (Table 1) involve: (a) dissolving the bulk of the meteorite (silicates and metal) by treatment with hydrofluoric and hydrochloric acid, (b) treatment by, e.g. chromate, to oxidize the more reactive part of the mostly carbonaceous acid residue, (c) colloidal extraction of grains of nano-diamonds, (d) density separation of the non-colloidal part to recover graphite in the light fraction, and (e) treatments of the diamond as well as the heavy part of the non-colloidal fraction with perchloric acid. The latter fraction is, in addition, treated with hot sulfuric acid which dissolves spinels. After this it consists mostly of silicon carbide.

Because the procedure is lengthy and time-consuming, attempts have been made to find shortcuts. For example, accepting loss of graphite, [30] have developed a more aggressive microwave technique which allows isolation of diamonds within one week. Unexpectedly not only graphite, but also silicon carbide was found to be lost in the procedure. Still another modification of the standard procedure where

Table 1 Major types of identified presolar dust grains in meteorites and some of their properties

Mineral	"Typical" abundance [ppm][a]	"Typical" size [μm][a]	Isotopic signatures[b]	Stellar source[c]	Contribution of stellar source[c]
Diamond	~1, 500	~0.0026	Xe-HL	Supernovae	?
Silicon Carbide	~30	~0.1–10	Enhanced ^{13}C, ^{14}N, ^{22}Ne, s-process elements	AGB stars	> 90%
			Low $^{12}C/^{13}C$, often enhanced ^{15}N	J-type C stars (?)	< 5%
			Enhanced ^{12}C, ^{15}N, ^{28}Si; extinct ^{26}Al, ^{44}Ti	Supernovae	~1%
			Low $^{12}C/^{13}C$, low $^{14}N/^{15}N$	Novae	~0.1%
Graphite	~10	~1–10	Enhanced ^{12}C, ^{15}N, ^{28}Si; extinct ^{26}Al, ^{41}Ca, ^{44}Ti	Supernovae, Wolf-Rayet stars (?)	< 80%
			Kr-S	AGB stars	> 10%
			Low $^{12}C/^{13}C$	J-type C stars (?)	< 10%
			Low $^{12}C/^{13}C$; Ne-E(L)	Novae	~2%
Refractory Oxides	~50	~0.1–5	Enhanced ^{17}O, depleted ^{18}O	RGB/AGB stars > 90%	
			Enhanced ^{16}O	Supernovae	~1%
Silicates	~200	~0.1–1	Enhanced ^{17}O, ~normal/depleted ^{18}O	RGB/AGB stars	> 90%
			Depleted ^{17}O, enhanced ^{18}O	Supernovae	< 10%
Silicon Nitride	~0.002	~1	Enhanced ^{12}C, ^{15}N, ^{28}Si; extinct ^{26}Al	Supernovae	100%

[a] Listed size ranges and abundances are from the compilation of [46]. The abundances are reported maximum values from different meteorites. Generally they scale with the matrix fraction of the meteorites and decrease with increasing metamorphism of the host meteorites [156].
[b] Isotopic signatures as well as [c]stellar sources and relative contributions as inferred and listed in [48]. Enhancements and depletions are expressed relative to solar system composition. See also discussion in Chapter 3.

hydrofluoric acid is replaced by other fluorine compounds has been developed by [31].

It is important to keep in mind, though, that even application of the "standard" procedure can lead to significant losses. For example, Russell et al. [32] noted that silicon carbide in sample KJ isolated from the Murchison meteorite by [29] using the standard procedure seemed to be more coarse-grained than SiC in other primitive meteorites. This led [32] to consider the possibility of size-sorting in the solar nebula, but it is almost certain that during preparation of KJ fine-grained SiC was lost (maybe as much as three quarters of all SiC), as shown by analysis of less-processed Murchison acid-resistant residues [30, 33]. Along the same lines, during TEM observations fine-grained SiC was found to be present in non-negligible amounts in diamond samples [34].

2.2.2 Non-chemical Isolation/Identification

Ideally, of course, the grains are extracted using only physical means, avoiding chemical treatments altogether. In fact, [35, 36] succeeded in extracting SiC grains (above a certain size limit) purely physically. Silicon carbide is, of course, a most favorable case, since it is quite distinct from the majority of the meteoritic (mostly silicate) mineral phases and all SiC grains are of presolar origin.

Identification of presolar grains that are not acid-resistant requires a different approach. It has become possible with the introduction of a new generation of ion microprobes (NanoSIMS; [11, 37]) for high-resolution ($\sim$100 nm) ion imaging of the meteorites in situ, i.e. without the actual isolation of grains. The approach finally led to the long awaited detection of pre-solar silicates [38, 39]. Extraction of single silicate (or other) grains identified by in situ searches for further studies, such as TEM observations, is possible using dedicated techniques, but these are hardly applicable on a routine basis (see Sect. 5).

2.3 Overview

An overview on the most abundant of the presolar grain types identified so far is given in Table 1. Among the properties listed are approximate "typical" abundances for the most primitive meteorite types, size, and also characteristic isotopic abundance patterns and inferred stellar sources (see also Sect. 3). A significant contribution is made by the "original presolar" grains, i.e. those that have been found because they carry isotopically anomalous noble gases – diamond, silicon carbide and graphite (Fig. 3). By far most abundant are the nanometer-sized diamonds; this is nominal, however, because in contrast to the typically μm-sized other grains, the nanoadiamonds cannot be analyzed individually and so it is not really known if all or which fraction of them is presolar (cf. Sect. 3.6).

Silicon nitride (Si_3N_4) and the refractory oxides (spinel $MgAl_2O_4$, corundum Al_2O_3, hibonite $CaAl_{12}O_{19}$ and rutile TiO_2) are not known to carry any noble gases, but were discovered due to the fact that they too are resistant to acids and ended up

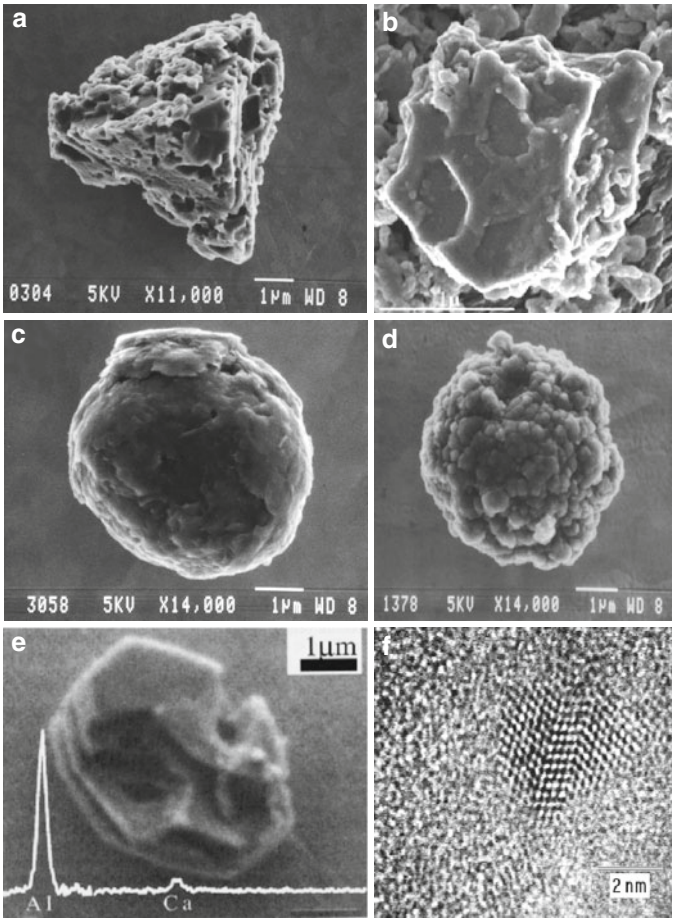

Fig. 3 Images of various types of presolar grains extracted from meteorites: silicon carbide (**a**, **b**), graphite (**c**, **d**), corundum (**e**) by SEM, diamond (**f**) by TEM. The SiC grain shown in (**a**) has been extracted by chemical means, the one shown in (**b**) purely physically. All others have been extracted using chemical treatment [29]. The graphite grains shown represent different morphologies, "onion" (**c**) and "cauliflower" (**d**), cf. Sect. 5. Pictures were provided by S. Amari (**a**, **c**, **d**), T.J. Bernatowicz (**b**), B.-G. Choi (**e**) and F. Banhart (**f**)

in the same residue samples as the silicon carbide grains. Their presolar nature was discovered when grains of these "contaminants" were individually analyzed with the ion microprobe [40–42]. Most abundant among these are spinel and corundum. In contrast to the carbonaceous grains, presolar oxide grains are swamped by isotopically normal oxide grains of solar system origin (cf. [43]). Most were detected only after development of the ion imaging technique for the ion microprobe that allows identifying few candidates among a large number of grains for subsequent detailed analysis.

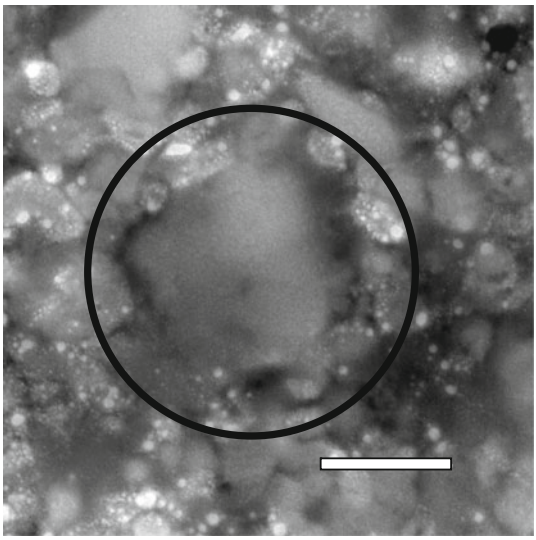

Fig. 4 Presolar silicate grain identified by in situ search using isotopic mapping by NanoSIMS in the Acfer 094 meteorite. Scale bar is 300 nm. Figure courtesy of C. Vollmer

As noted above, application of the ion imaging technique for in situ searches in the meteorites (rather than in spread-out residues) became practical with the high spatial resolution afforded by the new NanoSIMS instrument [11, 37]. Presolar silicates found by this technique (for an example see Fig. 4) amount to ∼200 ppm, which makes them nominally second in abundance among the presolar grains in meteorites. But they may actually surpass the nanodiamonds, if not all of these are presolar.

Finally, tiny grains of heavier carbides (TiC, ZrC) were found within mostly graphite [44] but also SiC grains [45] of presolar origin and therefore must be presolar in origin as well.

3 Isotopic Structures and Stellar Sources

Study of isotopic structures has been the central theme in the investigation of presolar grains in meteorites. Reasons for this are: (a) isotopic analyses are crucial as proof of presolar origin; and (b) they have the potential to answer – in combination with stellar nucleosynthesis theory – the basic question of the stellar sources of the grains. Accordingly the field has been largely dominated by researchers coming from the field of isotopic analyses.

Several excellent reviews have appeared that deal with the subject of isotopic structures and inferred stellar sources of presolar grains in meteorites (recently, e.g., [8–10, 46]). The topic cannot be addressed in the same detail here and the reader is referred to these reviews for more information. An exception is the case of the

nanodiamonds, where the situation is not straightforward and which is only sparingly discussed in existing reviews. They are treated in some detail in Sect. 3.6. The other grains are discussed in the order in which they are listed in Table 1.

3.1 Silicon Carbide

Silicon carbide has been studied in most detail, a fact that has been helped by its abundance, grain size and high content of trace elements. Isotopic analyses were performed on single grains mostly $> 0.5\,\mu m$ by secondary ion mass spectrometry (SIMS) for Si and C as well as abundant (N and Al with up to several wt.%) and other minor elements up to Ti [6, 46–48]. Trace elements were isotopically measured by SIMS [49] and thermal ionization mass spectrometry (TIMS; see [47] for a summary) on aggregates of grains and in single grains by laser-ablation resonance ionization mass spectrometry (RIMS; e.g., [50–53]. Heavy element abundance patterns for single grains have also been measured by SIMS [54] and an overview of the elemental and isotopic abundance patterns in the range of the Rare Earth Elements has been obtained by ICP-MS [55]. Noble gases typically have been determined on grain aggregates, but larger grains have also been measured individually for He and Ne [56, 57].

Practically each grain of SiC analyzed individually has turned out to be of presolar origin, and the variations of isotopic compositions are enormous (Fig. 5; Table 2). The wealth of data has allowed a classification into different categories based on C, N, and Si isotopic compositions. Most abundant (∼90%) are the "mainstream" grains, other types have been named A, B, X, Y, Z (Table 2). For most a rather clear understanding of their stellar origins exists, and for all but the X grains – of likely supernova origin – an origin from Red Giant/AGB carbon stars is highly probable [6, 46, 47]. Arguments are (a) carbon stars provide the necessary chemical environment because the abundance of carbon exceeds that of oxygen; (b) AGB stars are the main contributors of carbonaceous dust to the interstellar medium [58, 59]; (c)

Table 2 Distribution of single SiC grains among subgroups and diagnostic isotopic signatures of the light to intermediate-mass elements (C to Si). From [47], with updates according to [6, 48, 71, 77]

Group	Abundance[a] (%)	$^{12}C/^{13}C$[b]	$^{14}N/^{15}N$[b]	$^{26}Al/^{27}Al$[b]	Si
Mainstream	87–94	10–100	50–20,000	10^{-5}–10^{-2}	Slope ∼1.3–1.4 line
A	2	2–3.5	40–600	10^{-4}–9×10^{-3}	Slope ∼1.3–1.4 line
B	2–5	3.5–10	70–12,000	10^{-4}–5×10^{-3}	Slope ∼1.3–1.4 line
X	1	18–7,000	13–180	up to 0.6	Excess in ^{28}Si(up to 5x)
Y	1–2	140–260	400–5,000	10^{-4}–4×10^{-3}	Slope 0.35 line
Z	0–3	8–180	1,100–19,000	up to 10^{-3}	^{30}Si-rich side of slope ∼1.3–1.4 line

[a] Ranges refer to abundances observed in different size separates.
[b] Approximate ranges.

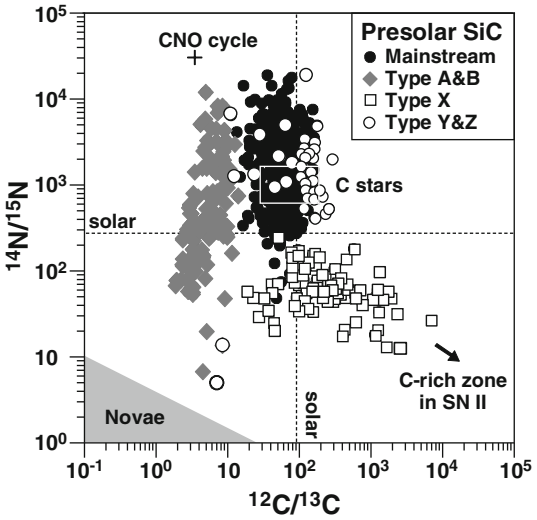

Fig. 5 Carbon and nitrogen isotopic compositions measured in single presolar SiC grains. Solar isotopic compositions are indicated by lines. Most analyses plot in the mainstream field (cf. text and Tables 1 and 2), displaced from normal in a direction indicating the influence of hydrogen burning via the CNO cycle. Also indicated are trends to be expected from novae and supernovae contributions. Graph courtesy of P. Hoppe [162]

AGB stars show in their atmospheres the 11.2 μm emission feature of SiC grains ([60, 61]; Sect. 6); (d) the distribution of $^{12}C/^{13}C$ ratios in singly analyzed SiC grains is similar to that observed for carbon star atmospheres [62]; (e) nucleosynthesis in the He shell produces s-process nuclides as well as Ne dominated by ^{22}Ne, i.e. the observed Ne-E(H) which led to the isolation of presolar SiC [63]. Signatures of the individual subtypes are discussed below.

3.1.1 Mainstream Grains

Mainstream grains range in $^{12}C/^{13}C$ from ~10 to ~100, and from ~50 to ~20,000 in $^{14}N/^{15}N$ (Table 2). Most show the input from hydrogen burning via the CNO cycle, with $^{12}C/^{13}C$ between 40 and 80 (below the solar system value of ~89), and $^{14}N/^{15}N$ between 500 and 5,000, higher than solar. They also contain s-process elements, with a signature similar to that of the "main component" that contributes to the solar system inventory of s-process nuclides [64, 63]. This points to an origin in low-mass (1–3 M_{Sun}) carbon stars in the thermally pulsing asymptotic giant branch (TP-AGB) phase (see also [53, 66]). During this phase, the s-process operates in the He burning shell of the star and the products are brought to the surface by convective mixing in thermal pulses. At the same time Ne-E(H) is produced (also named Ne-**G** because of its association with A**G**B stars; Sect. 2.2 and above). First analyses of single SiC grains seemed to indicate concentration in a few percent of the grains

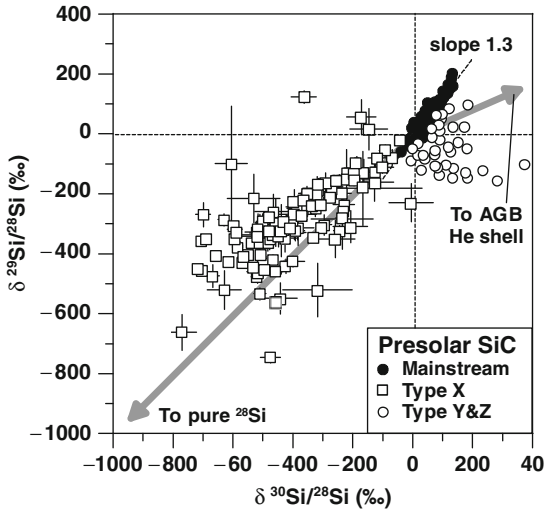

Fig. 6 Si isotopic ratios measured in single single presolar SiC grains. Ratios are shown as δ-values, i.e. deviations from normal values in per mill. In this representation most grains plot within 200‰of normal, close to a line with slope 1.34 (Table 2, see text). X grains of likely supernova origin plot in the lower left showing large relative enhancements of ^{28}Si. Graph courtesy of P. Hoppe [162]

[56], but in a new study [57] found ∼40% of the grains containing Ne-G above their (lower) background.

Silicon isotopes typically show enrichments of the heavy isotopes ^{29}Si and ^{30}Si up to $\sim +200$‰ compared to normal silicon, i.e. $\delta^{29,30}$Si/^{28}Si up to $\sim +200$‰ (Fig. 6). In a plot δ^{29}Si/^{28}Si vs. δ^{30}Si/^{28}Si data points follow an approximately linear relationship with slope ∼1.3–1.4 [6, 9, 46, 47]. The trend is not due to nucleosynthesis in the parent stars, but rather the result of galactic chemical evolution and the fact that the grains derive from a large number of individual stars (e.g., [46, 67, 68].

Also compatible – although details remain to be addressed – are results for the Mg/Al system as well as calcium and titanium [6, 47]. Most grains show detectable excesses of ^{26}Mg, the decay product of ^{26}Al($T_{1/2} = 0.7$ Ma). Inferred ratios for ^{26}Al/^{27}Al at the time of grain formation range from $\sim 10^{-5}$ to $\sim 10^{-2}$. Calcium isotopes were mostly measured on aggregates of grains. Observed are enhancements at ^{42}Ca and ^{43}Ca as expected from s-process contributions, the larger enhancements at ^{44}Ca are likely to be caused by the presence of X grains from supernovae (see below) which carry radiogenic ^{44}Ca from decay of ^{44}Ti($T_{1/2} = 60$ a). In titanium typically lighter and heavier isotopes are enriched relative to the most abundant isotope, ^{48}Ti. As the Si isotopes, the Ti isotopes are influenced by galactic chemical evolution, and variations in Ti and Si isotopes correlate with each other [47]. For recent detailed studies of the case of the Si isotopes and the Si-Ti relation in light of nucleosynthesis in AGB stars and galactic chemical evolution see [69, 70].

3.1.2 A and B Grains

A and B grains are distinguished by their very low $^{12}C/^{13}C$ ratios < 10 (Table 2). The dividing line between the two is the equilibrium value for CNO cycle H burning, with $^{12}C/^{13}C < 3.5$ for grains of type A. The range in $^{14}N/^{15}N$ is from $\sim$40 to $\sim$10, 000, and inferred $^{26}Al/^{27}Al$ at the time of grain formation – as for the mainstream grains – ranges up to 10^{-2} [71]. Also Si and Ti isotopic ratios behave rather similarly as in mainstream grains. The rare A and B grains that have been analyzed for s-process-specific elements suggest that about 2/3 contain overabundances of s-process nuclides, while $\sim 1/3$ do not. The observed features point to an origin from specific types of carbon stars, probably J stars for the s-process rich grains, and possibly "born-again" AGB stars for the s-process poor grains [71].

3.1.3 X Grains

X grains (about 1% of all individually analyzed SiC grains) are clearly distinct from all other types and almost certainly derive from supernovae (Table 2). Ratios $^{12}C/^{13}C$ are typically higher and $^{14}N/^{15}N$ ratios lower than solar (Fig. 5), which is the signature of He burning. More telling even are the Si isotopes that show enormous relative enhancements of ^{28}Si (Fig. 6). These features as well as the huge excesses of ^{26}Mg and ^{44}Ca from decay of ^{26}Al and ^{44}Ti, with inferred $^{26}Al/^{27}Al$ and $^{44}Ti/^{48}Ti$ ratios at the time of grain formation ranging up to $\sim$0.6 and $\sim$0.7, respectively, are diagnostic for an origin as condensates from supernova ejecta [6, 9, 10, 48]. Ti-44, in particular can only be produced in supernovae [6, 9, 72, 73]. To provide suitable conditions for formation of SiC and inclusion of ^{44}Ti in supernovae of type II complex mixing among supernova ejecta material is required and it remains to be seen whether supernovae type II or Ia provide a more suitable environment [6, 74].

An interesting pattern of Mo isotopes has been found in single X grains by RIMS ([51, 75]; Sect. 4). In contrast to the mainstream grains that show the expected s-process signature, molybdenum in SiC grains of type X shows a new pattern that seems best explained as the result of a neutron burst [76], a process intermediate between the traditional s- and r-processes of nucleosynthesis. This process which had originally been invoked in order to explain xenon in presolar diamonds (see Sects. 3.6 and 4) also is thought to occur during the explosion of a supernova. Data for barium in X grains, however, do not so easily fit with the neutron burst scenario [66].

3.1.4 Y and Z Grains

Y and Z grains, like A and B grains, share many properties of the mainstream grains and must have a similar origin. Their abundance is highest among the small grains and decreases with increasing grain size [46, 70]. Characteristic is the difference in Si isotopes ([46, 77]; Table 2): both fall to the ^{30}Si-rich side of the mainstream grains. Y grains have $\delta^{30}Si/^{28}Si > 0$ and $^{12}C/^{13}C > 100$. Z grains, on the other

hand, have always lower than solar $^{29}Si/^{28}Si$ and $^{12}C/^{13}C$, and their deviations in Si from the mainstream grains are larger than for the Y grains. Y grains probably come from low-mass lower-than-solar metallicity AGB stars that experienced strong He shell dredge up [6, 48, 77]. As for the Z grains, the likely source for most of them are low-mass, low-metallicity AGB stars that experienced strong cool bottom processing (Sect. 4) during the Red Giant phase [6, 48, 78], although some fraction with low $^{12}C/^{13}C$ and $^{14}N/^{15}N$ may come from novae [6].

3.2 Graphite

The case of graphite is more complex than that of silicon carbide. Overall $^{12}C/^{13}C$ spans the same wide range of $\sim$2 to$\sim$7, 000 as in SiC, the range in $^{14}N/^{15}N$ is however from $\sim$30 to 700 only, being higher than solar in most grains [6, 79]. The primary parameter based on which the grains can be assigned to one out of four different groups is the carbon isotopic ratio (Fig. 7; [79]), and remarkably there seems to be a correlation with density and morphology: (a) group 3 grains which are characterized by normal $^{12}C/^{13}C$ are of "non-round compact" or "spherulitic aggregate" type; they presumably are condensates from the molecular cloud from which the solar system formed [80]; and (b) among circumstellar grains the relative proportion assigned to each group varies with density and morphology.

Group 1 grains are characterized by $^{12}C/^{13}C$ in the range 2–20, similar to type A and B SiC grains, while group 2 grains with $^{12}C/^{13}C$ between 20 and 80 resemble

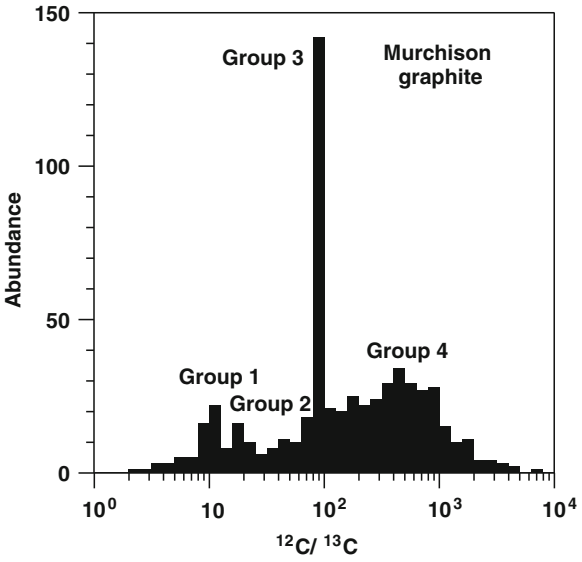

Fig. 7 Distribution of $^{12}C/^{13}C$ ratios measured in single graphite grains (courtesy P. Hoppe, [48]). Based on this ratio four populations can be distinguished

mainstream SiC grains. Group 4 grains are most abundant (∼50%) of all singly analyzed graphite grains) and isotopically light, with $^{12}C/^{13}C > 100$, up to 7,000. With these isotopic features, plus observed excesses of ^{18}O, it is likely that a large fraction of graphite grains derives from massive stars [6]. Considering also the high inferred $^{26}Al/^{27}Al$ ratios (up to 0.15) at the time of grain formation, the fact that most grains show deficits in ^{29}Si and ^{30}Si (similar to type X SiC grains), as well as the large excesses in ^{44}Ca from ^{44}Ti decay (again, as in SiC X grains) and ^{41}K (from ^{41}Ca, $T_{1/2} = 0.1$ Ma), supernovae type II are the primary candidates [6, 48, 81].

However, other sources must have contributed as well. Heavy noble gases measured in grain aggregates show the presence of material that experienced the s-process [82], so some fraction must derive from AGB stars; this is supported by the presence of refractory carbide grains rich in s-process elements within graphite spherules [83]. Finally the presence of Ne-E(L) (=Ne-R; cf. Sect. 2.2) in a small fraction of graphite grains [56, 84] is indicative of contributions from novae. For a specific discussion of the special case of the high density grains see also [85].

3.3 Refractory Oxides

The first identified presolar refractory oxide grains were corundum (aluminum oxide Al_2O_3) grains [40, 41], and the first extensive study and classification was performed by [86]. Other refractory oxides identified in the meantime include spinel ($MgAl_2O_4$), hibonite ($CaAl_{12}O_{19}$) and possibly titanium oxide (TiO_2) [9, 10, 46]. Spinel, which was largely missed in the early work because most of it was dissolved by the chemical isolation procedure of [29] (Sect. 2.2.1), may in fact be more abundant than corundum according to the results from in situ search using the NanoSIMS [39]. Isotopic information on the oxides is more limited compared to graphite and in particular silicon carbide, both because their abundance was low in the initial searches and because of the lower content of interesting trace elements. In addition most grains from the initial work were selected for detailed analysis after ion imaging indicated unusual $^{18}O/^{16}O$ with no initial information on $^{17}O/^{16}O$, so there may be a certain bias in the inferred distribution among different recognized populations.

Oxygen is the isotopically most diagnostic element, with $^{16}O/^{17}O$ ranging [6, 47, 86] from ∼70 to ∼30,000 (0.025 to 11 × solar) and $^{16}O/^{18}O$ from 150 to 50,000 (0.3 to 100× solar). Based on oxygen isotopes four populations have been recognized among the corundum grains ([86]; Fig. 8). Al and Mg have also been analyzed in many grains, while more limited data sets exist for K, Ca and Ti [87]. Inferred $^{26}Al/^{27}Al$ ratios at the time of grain formation show distinct distributions in the different populations, with the highest values (up to ∼0.02) observed in type 1 and 2 grains. Most group 1 and 2 grains have lower than solar $^{16}O/^{17}O$ and higher than solar $^{16}O/^{18}O$ ratios. The composition of the former is similar to ratios observed in the atmospheres of Red Giant and AGB stars (1 to $9M_{Sun}$), which makes these the most likely stellar sources [46, 48]. Group 3 grains may be related to group 1 grains and may originate from Red Giant stars of low mass [46, 48]. Deficiencies

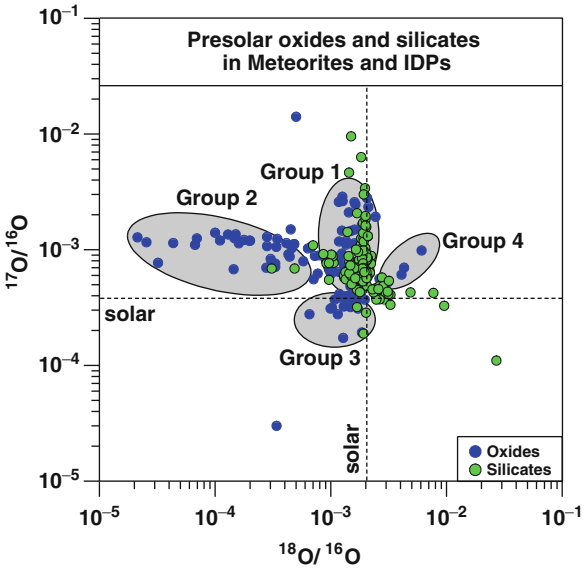

Fig. 8 Oxygen isotopic ratios measured in single presolar oxide and silicate grains. Based on oxygen isotopes most grains can be assigned to one of four groups [46, 86, 91, 92]. Figure courtesy P. Hoppe

of ^{18}O in grains of group 2 are larger than in group 1 grains; their parent stars may have been low mass stars that experienced cool bottom processing during the AGB phase [6, 48, 88]; Sect. 4. Oxygen isotopic signatures of type 4 grains are also compatible with a low-mass AGB star origin [6, 48], but multielement isotopic data obtained by [87] for two grains are more indicative of a single supernova source, where variable amounts from the ^{16}O-rich interior were mixed with outer layer material.

Here, as in many other cases, a complex interplay of variable stellar mass and metallicity, galactic chemical evolution and "new" nucleosynthesis (e.g., cool bottom processing; Sect. 4) is required in order to explain the observations. In addition, three grains analyzed do not fall in any of the four groups and cannot be explained by conventional Red Giant star models. Two of these [89, 90] may come from supernovae, in one case consistent with Ti isotopic data obtained on the same grain [90].

3.4 Silicates

As noted above, presolar silicates were missed during the first one and a half decade of presolar grain research, due to the fact that they were destroyed in the chemical approach used to isolate noble gas-carrying (and other acid resistant) presolar materials. As also noted above, the situation changed only with the advent of a new generation of high-sensitivity, high lateral resolution ion microprobes (NanoSIMS;

[11, 37]) that allowed identification of submicron presolar materials in the meteorites in situ ([38, 39]; Fig. 4). As it stands, silicates are the second-most in abundance of the pre-solar materials identified in primitive meteorites (Table 1), and may actually be first, depending on which fraction of the nanodiamonds is presolar (Sect. 3.6).

Isotopic patterns in silicates resemble those observed previously in presolar refractory oxides (Sect. 3.3) and they can conveniently be placed into the various groups defined by the oxygen isotopes in corundum. Most silicates are enriched in ^{17}O and have close-to-solar or slightly lower $^{18}O/^{16}O$ (group 1). Group 2 grains appear to be rare, but this could be an observational bias [46, 91]. As the oxides, most silicates apparently formed in the winds of Red Giant and AGB stars, with rare contributions from supernovae [46, 92]. Their Si isotopes plot along the same line determined by galactic chemical evolution as the mainstream SiC grains [91, 92].

3.5 Silicon Nitride

As a rule, silicon nitride grains have isotopic signatures similar to those of the silicon carbide X grains [42]. Nitrogen is characterized by low $^{14}N/^{15}N$ (18–100) and silicon by relative enhancements of ^{28}Si, with $\delta^{29}Si/^{28}Si$ ranging down to –200 and $\delta^{30}Si/^{28}Si$ down to –350‰ [6, 48]. Coupled with the high level of radiogenic ^{26}Mg (up to inferred $^{26}Al/^{27}Al$ at grain formation of 0.2) these features clearly indicate formation from supernova ejecta, as for the SiC X grains [6, 46, 48]. Only a single grain of Si_3N_4 has an isotopic composition indicative of an AGB star origin [70].

3.6 The Problems with the Diamonds

The case of the most abundant of the minerals listed in Table 1, the diamonds, is not straightforward (cf. Sect. 2.3). The major problem is that we do not really know how many of them are presolar. A strong argument that a major part is not, comes from the isotopic ratio for the structural element, $^{12}C/^{13}C$. Consisting of on the average about 1,000 atoms only, the diamonds cannot be analyzed individually, and "bulk analyses" of many grains ("aggregates") yields $^{12}C/^{13}C \sim 92$, within the range of isotopic ratios observed in solar system matter, even on Earth. While stellar scenarios can be constructed that result in such a ratio [93], given the large variations observed in stellar atmospheres and other presolar grain types, such a close agreement with "normal" within percent would seem a remarkable coincidence.

Nitrogen is the most abundant trace element in the diamonds, with an abundance close to 1% [94]. The isotopic ratio $^{14}N/^{15}N$ is ~400, i.e. $\delta^{15}N$ is ~ -330‰ relative to the standard, air, value of 3.36×10^{-3} [94]. Is this isotopic ratio anomalous and might it indicate that at least a percent or so of the diamonds are presolar? We do not know for certain at this time, because there are uncertainties about the true $^{14}N/^{15}N$ characteristic for the solar system. For one, "live" solar wind nitrogen measurements by spacecraft have given results compatible within error with the air

value [95]. On the other hand, however, there are several sets of data that suggest significantly higher solar $^{14}N/^{15}N$. This includes measurement of presumably solar wind-implanted nitrogen in lunar grains [96] as well as the re-evaluation of the nitrogen ratio in the Jovian atmosphere [97], which suggests protosolar nitrogen to be "light" with $^{14}N/^{15}N$ possibly as high as ~400. Consistent with this is the recent analysis of osbornite found in a carbonaceous chondrite (CH/CB-like), a titanium nitride thought to be a high temperature solar nebula condensate [98]. Taken together, there are strong hints that nitrogen in macroscopic samples of meteoritic nanodiamonds, like carbon, may be normal after all. Of course, a final conclusion will have to await the final data from the laboratory analysis of solar wind nitrogen collected and brought back by the GENESIS spacecraft [99].

Another complication arises from the noble gases themselves that constituted the evidence for the diamonds' presolar nature in the first place. Diamonds not just contain isotopically anomalous traces like Xe-HL, but also others which are essentially normal in their isotopic composition (Fig. 2). The situation is best studied for xenon [23, 100]: diamonds contain the anomalous xenon (Xe-HL), an approximately normal xenon component (Xe-P3) and a third one that differs from both (Xe-P6). The P6 component has been observed only mixed in variable degrees with the HL component and its endmember (pure) composition is not known. It may be isotopically anomalous or, similar to P3, isotopically close to normal. Taken the isotopic argument for identification of presolar grains (Sect. 2.1) to the extreme, it can be argued that – because the Xe-HL abundance is such that on average one Xe atom occurs per about a million diamonds grains – we can confidently assume only that one out of a million diamonds is of presolar nature. But, of course, Xenon-HL is accompanied by other noble gases. Neon and helium are especially high in abundance, so high that diamonds in fact dominate the helium and neon inventory of many primitive meteorites – i.e. they contribute the major part of what has been called "planetary" helium and neon. Helium occurs in an abundance that a He atom is contained in about every hundredth of the diamond grains. Following the same logic as for Xe, this may indicate that the fraction of presolar diamond grains actually is on the order of percent or more, similar to what one might derive as a limit from nitrogen, if indeed the solar wind has $^{14}N/^{15}N$~400 and diamond nitrogen is isotopically anomalous relative to this value. Interestingly, the abundance level of truly presolar diamond grains inferred from this exercise is quite similar to that for SiC and graphite, but the conclusion is anything but firm.

Information on isotopic anomalies in trace elements other than the noble gases that may help shed light on the issue is sparse. The only convincing case is that of tellurium where [101] identified a Te-H (in analogy to Xe-H) component consisting of the two most neutron-rich isotopes, ^{128}Te and ^{130}Te, only (but not Te-L). The anomaly has been subsequently been confirmed, although the effect was smaller (probably because of dilution with normal matter), by [102], who also observed a barely resolved effect in palladium, with an overabundance of ^{110}Pd of $9 \pm 6‰$. Similarly small and poorly understood effects had been seen before in barium and strontium [103].

Overall, those isotopic anomalies in nanodiamonds that show a clear pattern (Xe, Te) are characterized by overabundances of the most neutron-rich isotopes. This suggests an origin from a kind of rapid neutron capture process, although not the unadulterated standard r-process of nucleosynthesis (Sect. 4). They point to an origin from type II supernovae as the most likely source (e.g., [76, 104–106], where also the simultaneous excesses in the most proton-rich isotopes of Xe (Xe-L) may come from [106, 107], although the situation is less clear. In spite of all the efforts, presently all that these isotopic effects in trace elements indicate is that some fraction of the diamonds is presolar, but we just do not know how large this fraction is.

3.7 Internal Grains

As noted above (Sect. 3.2), graphite grains often contain internal grains composed of carbides of Ti, Mo and Zr and Fe-Ni ([44, 83]; cf. also Sect. 5). Internal grains have also been found inside SiC [45]. Grains of titanium carbide (TiC) in particular are likely to be the host of the often very large enhancements of ^{44}Ca from decay of ^{44}Ti observed in the graphites.

4 Nucleosynthesis Inferred

While general isotopic features observed in presolar grains in many cases clearly point to specific stellar sources, details often point to deficiencies in our understanding of stellar evolution and nucleosynthesis. This naturally concerns mostly the AGB and supernova sources that supply most of the known grains.

Additional information found within the isotopic structures generally falls into one (or several) of the following categories:

(a) quality of nuclear data;
(b) (old) nuclear processes under (new) non-standard conditions;
(c) mixing processes.

In addition, with an ever increasing number of analyzed grains from many stars, it has become obvious that in some cases the initial composition of the parent stars (and, in turn, galactic chemical evolution) is still reflected in the grains. A case in point is the array of mainstream SiC grains – and also the silicates [91, 92] – along the slope ∼1.3–1.4 line in Fig. 6 and the relation between Si and Ti isotopic compositions [67–69, 108]. Notably in this context, the Si isotopic composition of the Z grains together with AGB nucleosynthesis predictions has been used to model the evolution of the ^{29}Si/^{28}Si ratio in the Galaxy as a function of metallicity [69]. Also apparent are isotopic differences in the inherited compositions of parent stars in oxygen [48, 109].

4.1 Mixing in Supernova Ejecta (or New Chemistry?)

Mixing in stars and their ejecta larger than previously expected may be required in several cases. While this also includes Red Giants and AGB stars, the case based on supernova grains (SiC type X, graphite, silicon nitride) is clearest [6, 48]. In type II supernovae, the radionuclide ^{44}Ti, which is the most diagnostic feature, and the observed excesses of ^{28}Si are produced in the innermost zones. The bulk of the grains, however, should have formed from material derived from the outer zones because this is where the abundance of carbon exceeds that of oxygen so that carbonaceous grains can form. As a consequence, if the grains derive from SN type II, outer and inner zones must have mixed and achieved C > O, in spite of the fact that they are separated by a large intermediate region consisting largely of oxygen [6, 7, 48, 110]. If derived from type Ia instead problems in achieving all required conditions simultaneously are quite similar [74, 111] An alternative to extreme mixing may be to invoke a kind of "new chemistry": in the strong radiation field of a supernova formation of the CO molecule may be inhibited thus allowing formation of carbonaceous grains even in an oxygen-rich environment [112].

4.2 Red Giant Light Element Nucleosynthesis

Strong indications for "new kinds" of "old" nucleosynthesis are provided by the oxygen data for the corundum grains. In order to explain them, [113] and [88] had to invoke two processes of hydrogen burning under special conditions. (A) "Hot Bottom Burning" (HBB; [113]) occurs in AGB stars with masses $\geq 4M_{Sun}$ where the convecting envelope is deep enough during interpulse periods to reach the star's hydrogen burning shell. (B) Red Giants of lower mass, on the other hand, experience – following the first dredge-up – "extra mixing" that transports material from the cool bottom of the envelope down to the hydrogen shell where its composition can be modified and from where it can be mixed back into the envelope. This "extra-mixing" process has also been named "Cool Bottom Processing" (CBP; [88]).

4.3 Nuclear Cross Sections

For the light elements the situation is complicated by many contributing factors, so the question of nuclear cross sections has rarely been addressed based on presolar grain data. One case is that of the ^{18}O(p, α)^{15}N reaction where [114] have suggested that the rate may be a factor of ~1,000 higher than commonly assumed, in order to solve the problem of those SiC A and B grains that have both low ^{12}C/^{13}C and low ^{14}N/^{15}N. Another is the case of the Si isotopes in SiC Z grains [69], where the grain data favor the neutron capture cross sections of [115] over those of [116].

The case is more straightforward in the case of the heavy nuclides produced by the s-process, where cross sections can be measured and checked down to precisions

on the percent level. Over a large mass range for neighboring s-process nuclides the approximate relationship

$$N \times \sigma = \text{const.} \quad (1)$$

holds, where N is the abundance of a nuclide manufactured by the s-process and σ its Maxwellian-averaged neutron capture cross section at the relevant temperature (e.g., [116–118]; see also [119]). Discrepancies between this relation where it should hold and observations in presolar SiC have been largely erased whenever the neutron capture cross sections have been re-measured ([6, 47]; but see also [55, 66, 120]).

4.4 Old (and New?) Neutron Capture Processes

Results for the composition of the s-process component in presolar silicon carbide grains have allowed to refine the constraints on physical conditions during the process. Basis for this are nuclide ratios that are affected by branchings in the s-process (i.e. where nuclides are encountered at which there is competition between neutron capture and β-decay). Effective values for neutron density, temperature and electron density can be inferred from the results in the framework of the "classical" model of the s-process (physical parameters held constant, e.g., [47, 117]), but the results of course put also constraints on more realistic "stellar models" [119].

In contrast to the clear signature of the s-process that is seen in the SiC grains, no clear signature of the *rapid* neutron capture process (r-process) has been seen in presolar grains so far. R-process like signatures have been seen in the diamonds (xenon, tellurium) and in SiC grains of type X (molybdenum), but differ from the true r-process in detail (Fig. 9; Sect. 3). The SiC-X Mo data seem well explained by the action of a neutron burst, some kind of neutron capture process intermediate between the canonical s- and r- neutron capture processes [76], however the case of Ba is less convincing [66]. The process does also considerably worse in explaining Xenon-H (the heavy part of Xe-HL) in the nanodiamonds [106], although it was developed specifically for this purpose [105, 121]. Therefore, for the diamonds an alternative "rapid separation" scenario has also been considered [106], which combines the average r-process with separation of stable r-process products from radioactive precursors on a time scale of hours. While the predictions of the model fit the observed Xe-H isotopic pattern [106] and possibly also the tellurium pattern [101, 102], it faces the problem of how to achieve the required separation. One of the processes considered by [106], recoil loss from grains during β-decay seems to be ruled out by an experimental study of recoil effects in nanodiamonds [122]. Possibly an early grain formation process as suggested by [123] for SN Ia – if it also works for SN II, the likely site of the r-process – may do the trick. Volatile species like xenon could be spatially separated from less volatile precursors even if the early grains were quickly destroyed again. Quite clearly, the question of heavy trace elements in diamond and their implications remains open at this time.

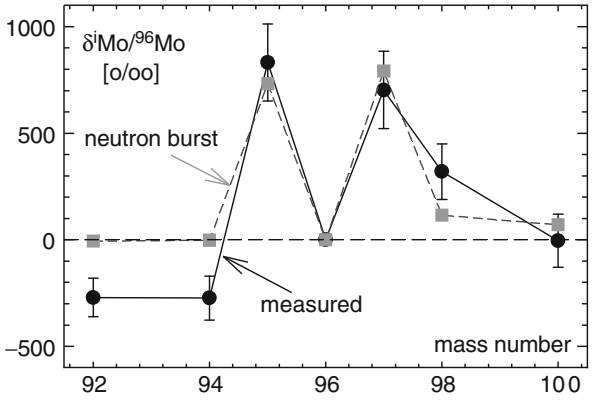

Fig. 9 Molybdenum isotopic composition measured in a single SiC-X grain ([51]; data slightly revised according to A. Davis, pers. commun). Shown are the deviations of isotopic ratios – normalized to the s-process only nuclide ^{96}Mo – from isotopically normal Mo. The composition is largely in agreement with expectations for a mixture of 83% normal Mo and 17% of Mo as produced in a neutron burst [76]

5 Mineralogy and Morphology

The most important fact regarding the mineralogy of the initially identified presolar grains in meteorites was that they were made of minerals – diamond, graphite, silicon carbide, refractory oxides – that are both thermally and chemically highly resistant. They are among the earliest solids formed upon cooling [124] from material expelled from stars, and their high chemical resistance (under the right oxygen fugacity) may have helped their survival in the interstellar medium and the early solar system. Crucial, of course, was that several solids were carrying noble gases that could be used as "beacons" in the search for them (cf. Sect. 2). Finding presolar grains that are acid-soluble and do not carry noble gases, required new techniques like the in-situ search by isotopic imaging using the NanoSIMS [11, 37]. Only with this technical progress has it been possible to find the presolar silicates ([38, 39]; Fig. 4).

5.1 Mineralogy and Morphology

Another simple observation is that generally different grain types have different primary sources: Red Giants for SiC, refractory oxide and silicate grains, supernovae (probably) for diamonds and for silicon nitride, and no single source dominating contributions to graphite in a similar manner. There is, however, generally little information that would allow connecting isotopes with other properties of the grains. One exception is that of the rare (∼1%) X grains of putative supernova origin: they

are distinguished from other SiC grains in that they are commonly observed to be assemblages of smaller (<100 nm) SiC crystals [125], like the supernova silicon nitride grains [126]. Graphite is another exception (Sect. 3.2): (a) only round grains have a non-solar carbon isotope ratio and clearly constitute circumstellar material; (b) grains can be distinguished based on surface features as "onion" or "cauliflower" type (Fig. 3), a distinction reflected also in their trace element contents and interior structure [44] - the "onions" contain cores of graphene or small refractory (Ti, Zr, Mo) carbide grains (Fig. 10); and (c) graphite grains of different density show different relative contributions from the various stellar sources [48, 79].

Returning to silicon carbide, the successful extraction without chemical means of a number of grains has allowed comparing features and it is obvious that the surfaces are etched during chemical isolation (Fig. 3; [35]). However, there is no evidence that the grains are altered otherwise during this process. Early investigations [127] seemed to indicate that all SiC grains were of the β polymorph type, but later work [128] has revealed the presence also of α-SiC. The most detailed study is that of [129, 130], who show that of the many existing polytypes of SiC only two are present, 3C (cubic; β-SiC) and 2H (hexagonal; α-SiC), with the cubic type dominating and a significant occurrence ($\sim$17%) of cases of intergrowth. The

Fig. 10 TEM micrograph of an ultrathin section of an onion-type circumstellar graphite grain. Included in the graphite grain is a TiC subgrain. Figure courtesy of T.J. Bernatowicz

finding that both polytypes are present has partly eliminated another earlier apparent paradox, namely that meteoritic SiC seemed to be of the β type, while spectroscopic observations were interpreted as indicating α-SiC in the atmospheres of carbon stars [61]. More of this apparent puzzle has gone away also with the realization that spectroscopic features of fine-grained SiC may more strongly depend on grain size and shape than on the type of polymorph [131].

Diamonds have been studied in detail in the TEM [34], but their size (average 2.6 nm) does not allow any individual isotopic analysis and the only clear trend associated with morphology is the size dependence of noble gas concentration [132]. Given the rare occurrence of diagnostic trace elements within the diamonds we cannot even be sure that any one of the grains imaged by TEM [34, 133] has been one of circumstellar origin (cf. Sect. 3.6). The microstructural studies favor an origin by a CVD-like process, i.e. formation at low pressure by an isotropic process as opposed to shock transformation from graphitic carbon phases [34].

Major progress has been made since the first edition of this book in the structural characterization of the oxides and the mineralogy and chemical composition of the silicates (e.g., [91, 134], which had not even been identified at the time. In addition to SEM/EDX, Scanning Auger microprobe analysis has been introduced for chemical analysis, because it provides better lateral (down to ~10 nm; [91]) and also depth resolution (it is basically a surface analysis technique) commensurate with the demands of in-situ analysis. Microstructural studies on various grains were performed by TEM after lift-out of electron-transparent grain sections using the focused-ion beam (FIB) technique [135].

A summary of current knowledge about presolar silicate mineralogy and chemical composition is given by [91]. As pointed out by these authors, the specific mineralogy of "stardust" depends on the elemental composition of and physical conditions during grain nucleation and growth of the parent stellar atmospheres. Of the 27 presolar silicates identified at the time roughly comparable numbers (8, 11 and 7) have compositions that are olivine-like, similar to pyroxene and similar in composition to GEMS (glass with embedded metal sulfide as found in interplanetary dust particles ([12] "The Astromineralogy of Interplanetary Dust Particles" by Bradley, this volume; see also Sect. 1). The majority of the grains are crystalline rather than amorphous. Both findings are in contrast to observations of dust shells around evolved stars, where silicates are generally amorphous and more often have a composition that is olivine-like. Also many of the grains are Fe-rich, which may be a primary trait if condensation took place under non-equilibrium conditions [91]. In fact, [136] have found a circumstellar grain with a composition consistent with pure iron oxide in the Acfer 094 carbonaceous chondrite, one of the meteorites richest in presolar silicates.

5.2 Grain Sizes

Grain size is, on the average, ~2.6 nm for the diamonds [34], while the other grains in Table 1 have sizes in the μm range (from few tenths of μm up to ~20 μm; majority submicron). Size distributions have been determined for SiC and graphite by

[29] on grains from the Murchison meteorite. For both graphite and SiC the results can be explained as a sum of log-normal distributions. For SiC, an alternative is a power-law distribution (truncated at the upper and lower end) of the type

$$N = C \times [a \exp(-b)] \tag{2}$$

in the size range from 0.7 to 3.2 μm and $b = 5.7$ for the cumulative distribution.

It is not clear how representative this result is. Earlier work gave some hints that SiC in the Murchison meteorite from which the samples of [29] were derived might be unusually coarse-grained compared to other meteorites [32, 48], but more realistically fine-grained SiC grains seem to have been lost from the SiC sample of [29], presumably during chemical isolation [30, 33]. Taken at face value, nevertheless, the exponent in the distribution of 5.7 is notably different from that in the size distribution for interstellar grains derived by [137] from astronomical observations. It has to be kept in mind, though, that the latter may apply primarily to other types of grains and definitely was derived for a different size range (0.025–0.25 μm). That large sizes are observed in the meteorites, however, is compatible with the sizes of grains that have been observed to enter the solar system today [138].

6 Detection in Space

The detectability in space of those minerals that are present as presolar grains in meteorites is clearly of interest. Where stellar sources have been inferred from isotopic systematics, it will be a welcome confirmation. And where no clear indication exists based on isotopes, detection in space may yield the decisive piece of evidence.

There is little doubt that silicates contribute a substantial fraction of the total mass of interstellar dust ([58, 139], "The Mineralogy of Interstellar and Circumstellar Dust in Galaxies" by Molster et al., this volume). Similarly, the major dust species found in the O-rich dust shells of evolved stars are amorphous silicates [140]. The long-awaited discovery of presolar silicates in meteorites [38, 39] has been a welcome confirmation of the importance of silicates. There are, however, also differences between what has been observed in meteorites so far and what has been inferred from astronomical observation [91]. For one, the majority of the presolar grains in meteorites are crystalline, while silicates in the interstellar medium and around O-rich stars are predominately amorphous. Also the suggested preponderance of silicates with an olivine-like composition ([140]; see also "The Mineralogy of Interstellar and Circumstellar Dust in Galaxies" by Molster et al., this volume) is not reflected in the meteoritic inventory [91]. A possible explanation could lie in a reduced survival probability of amorphous grains [91]. As a matter of fact, reduced survival of amorphous grains has also been invoked as a possible explanation for young ages of (survivor) SiC grains ([141]; Sect. 7.1), but this remains speculative at this time.

Concerning silicon carbide, as pointed out earlier (Sect. 3), the identification of the ∼11.2 μm feature of SiC in carbon star atmospheres [60] even before their

identification in meteorites has been used as major argument for a carbon star origin of most SiC grains. As for the apparent discrepancy (cf. Sect. 5) of α-SiC in C star atmospheres [61] vs. β-SiC in meteorites [127] this has largely disappeared with the recognition that α-SiC is present in meteorites as well [128–130] and that grain size and shape may have a larger influence on details of the feature than the type of polymorph [131].

The diamonds are only weakly – via rare trace elements – linked to a supernova source. As a consequence, much effort has been spent trying to establish what the absorption features are of the meteoritic nanodiamonds, a fact helped by their relatively high abundance (Table 1). However, the many studies [142–146] that have been performed have hardly been conclusive. The major problem is that pure diamonds do not show any absorption in the optical or infrared, so generally features that have been seen are either due to contaminants or to surface groups that – because of the small size – are abundantly attached to the diamonds (cf. [147]). Consequently, features that might be observed in space will depend on the chemical environment (and then might not be specific to diamonds), and what is observed on the meteoritic diamonds in the laboratory depends on the chemical extraction procedure. The latter is abundantly demonstrated by changes observed between various stages of the extraction [146] and the fact that different investigations found different sets of absorption features.

Under these circumstances the only specific features will be those that are caused by the presence of trace elements that are indigenous (rather than surface-correlated) to the diamonds. Nitrogen is the most important case, where in turn the spectroscopic features depend on its configuration, which could be determined via electron paramagnetic resonance (EPR) to occur in the meteoritic nanodiamonds as single atoms [146]. The authors suggest that nanodiamonds of the type found in meteorites should show major nitrogen-related absorption features at 1,130, 1,300 and 1, 344 cm^{-1} (8.85, 7.69 and 7.44 μm; Fig. 11) as well as in the UV at 270 nm [146]. No such features, however, seem to have been reported in the astronomical literature

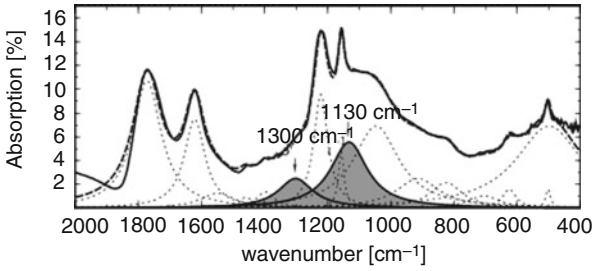

Fig. 11 IR absorption spectra measured on a sample of diamond extracted from the Murchison meteorite. The absorption expected due to nitrogen as single atoms in the diamonds (*gray area*) – probably the only signatures independent from chemical history and current environment – may be present, but are masked by the presence of much larger peaks due to attached surface groups. Figure provided by A. Braatz [146]

[146]. More promising may be a search in emission, and indeed emission features observed in the dusty envelopes of some stars have been interpreted as indicative for the presence of small diamonds [148]. However again, as the absorption features seen in [147], these features are caused by terminal groups at the diamonds' surfaces.

7 Age and History

7.1 Ages

Determination of ages for presolar grains is not straightforward. A major reason is what just characterizes the grains: anomalies in isotope abundances. As a consequence, in the application of long-lived chronometers it is often not clear in what ratio parent and daughter nuclides would have been present at the time of grain formation (the starting composition that then would have changed as a function of time due to radioactive decay). Thorough understanding of nucleosynthesis and mixing in the parent star and/or galactic chemical evolution (which may define the ratios of the nuclides when the parent star formed) would be necessary to overcome this difficulty. An exception may be those "simple" cases, in which stellar nucleosynthesis totally resets the composition. One such process would be an r-process in a supernova which totally resets the distribution of the heavy nuclides. Hence in principle grains like the SiC-X grains might be datable via determination of, e.g. the uranium isotopic ratio, by mass spectrometry or via fission tracks [149]. However, not only will this be a difficult experiment, in addition there is also the problem that the X grains (and the diamonds, for that matter, too) do not show the signature of a simple unadulterated r-process, in lighter elements at least. Instead, the observed pattern is that of a very specific process, the products of which are mixed with some fraction of isotopically (approximately) normal matter (Sect. 4). So interpretation of any obtained results in terms of an age will not be a trivial task. The same approach applied to mainstream SiC rather than X grains, since uranium is produced in the r-process only, would effectively date the time the parent star – and not the grain – was born.

Another approach relies on determining a presolar cosmic ray exposure age that – added to the ∼4.6 Ga age of the solar system – would correspond to the total (absolute) age [150]. Among the known presolar grains the approach is most promising for the SiC mainstream grains, because they are abundant, because some of them are fairly large, and because they contain the right target elements to produce measurable amounts of cosmogenic nuclides (mostly rare noble gas nuclides that can be sensitively determined). Using this approach [150, 151] arrived at presolar cosmic ray exposure ages ranging from ∼10 to ∼100 Ma, increasing with grain size. These results are flawed, however, because recoil losses of the cosmogenic product ^{21}Ne were seriously underestimated [152], and the apparent ^{21}Ne excesses that were attributed to cosmic ray production may predominantly have a nucleosynthetic

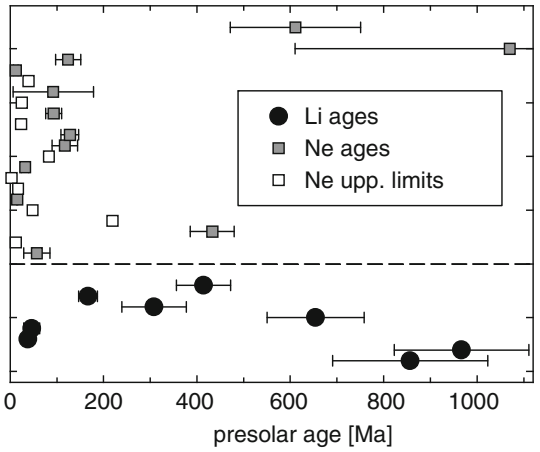

Fig. 12 Presolar cosmic ray exposure ages for large SiC grains from cosmogenic ^{6}Li and ^{21}Ne. Based on preliminary raw data supplied by F. Gyngard and P.R. Heck. See also [153, 155]

origin instead. Losses of xenon isotopes produced by cosmic rays on the abundant trace Ba from ∼μm-sized SiC grains are significantly smaller than those of neon isotopes, on the other hand, and based on cosmogenic Xe an upper, though model-dependent, limit of few tens of Ma was derived by [141].

While these studies were performed on "bulk SiC" samples, i.e. agglomerates of many small grains, more recent work has turned to analyses of single large (∼5–50 μm) grains, where recoil losses are also a lesser problem. Interestingly ages could not only be determined via cosmogenic noble gas isotopes (^{21}Ne, ^{3}He), but also via cosmogenic ^{6}Li. Preliminary results are shown in Fig. 12. Ages based on ^{6}Li are mostly in the range of several hundred Ma [153], similar to the predicted mean lifetime of interstellar grains [154]. On the other hand, only few of the ^{21}Ne (and the usually less certain ^{3}He) ages are that long, being mostly $<$100 Ma instead [155]. It is unclear at present whether the difference between Li and Ne ages (Fig. 12) is a statistical fluke due to small number of analyzed grains or whether it indicates poor knowledge of relevant production rates and/or effects from stellar nucleosynthesis and galactic chemical evolution on the cosmogenic isotopes. Independent of this difference, an inherent problem in the approach is that to find the relevant production rates, which depend on flux and energy spectrum of cosmic rays in the ISM more than 4.6 Ga ago.

7.2 History

There are two things that currently can be said with certainty about the history of the presolar grains in meteorites. One is that many must have formed rather rapidly. This is documented by the signature of extinct radionuclides (Sect. 3) such

as ^{44}Ti($T_{1/2}$ = 60 a) or ^{22}Na($T_{1/2}$ = 2.6 a). The other is that they experienced the same type of metamorphism as the other constituents of their host meteorites. This is shown by the correlation of their abundance with petrologic subtype, with no presolar grains present in types more thermally metamorphosed than type 3.8 chondrites [156]. The sensitivity to thermal metamorphism increases in the order graphite, silicon carbide, diamond [156] and a fine resolution is possible based on the abundance of various noble gas components in the diamonds [157]. Apart from that, those that survived did so largely intact. But the time it took from the stellar sources to the solar system (cf. Sect. 7.1) and the conditions they survived there are poorly defined.

Only in one case, that of the diamonds, a very specific scenario has been suggested for the history of the grains [158]. This scenario is based on the occurrence of multiple components of noble gases ([23]; Fig. 2), the evidence that introduction of trace gases was by ion implantation (e.g., [25, 132]) and results from laboratory simulation experiments (Fig. 13; [158]). In this scenario, after their formation the diamonds were irradiated in a circumstellar environment with trace elements having a supernova isotopic signature, and subsequently heated (up to ∼700°C) which led to loss of part of the implanted atoms. The same diamonds were irradiated again at some later time with trace gases of about normal isotopic composition; or at some other place and time a different population of diamonds was irradiated with this "normal" type material and became subsequently mixed with the ones carrying the "anomalous" matter. After that the diamonds found in the most primitive meteorites did not experience elevated temperatures any more for any significant length of time (e.g., not more than ∼10,000 years at a temperature higher than 100°C or equivalent combinations [120]).The scenario involves a number of assumptions and therefore has to be regarded with some caution, but currently is the only case where a detailed history has been suggested.

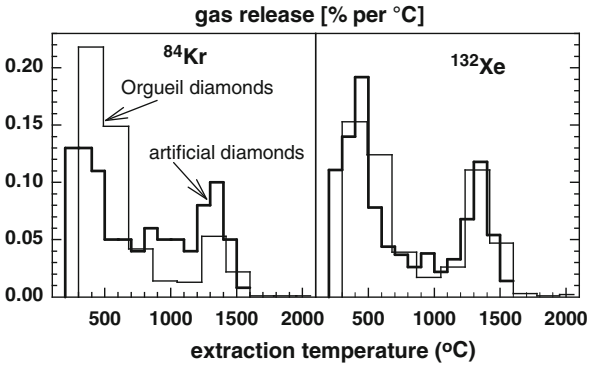

Fig. 13 Differential release upon vacuum pyrolysis of krypton and xenon from diamonds extracted from the Orgueil meteorite [23] compared with the release of gases implanted into artificial terrestrial nano-diamonds [158]. The agreement can be used to construct a history for the interstellar diamonds [158]

Continuing the approach and inferring isotopic mass fractionation from the implantation experiments, the same authors contend that there are excesses of ^{21}Ne due to trapping of recoil cosmogenic Ne produced in ambient silicate material [159] and of ^{3}He whose origin is mostly trapped cosmic rays [160]. Both can in principle be used to determine a ^{21}Ne cosmic ray exposure (CRE) age and a ^{3}He cosmic ray trapping (CRT) age for the diamonds.

The age of the silicon carbide grains, on the other hand, rather than giving a detailed grain history, may be able to teach us something about the history of the Galaxy – provided the short presolar ages based on Ne and Xe are correct. This is because – as pointed out by [141] – short ages would be expected in case of the galactic merger scenario of [161]. This scenario was suggested in order to explain the Si isotopic variations in the SiC mainstream grains (Fig. 6) and calls for a merger of a metal–poor satellite galaxy with the Milky Way 1.5–2.0 Ga before formation of the Solar System causing a starburst. If the low mass AGB host stars of the SiC mainstream grains were formed as a result of this starburst, they would have entered the AGB phase only shortly before Solar System formation and hence dust formed from their outflows would have been young when it entered the forming Solar System. Hence young grain ages would be in support of the galactic merger scenario.

8 Summary

The most primitive material occurring in meteorites are circumstellar condensates several of which occur on the sub-ppm to some 100 ppm level in the most primitive ones: graphite, silicon carbide, silicon nitride, refractory oxides and silicates. Diamond was the first to be detected and may occur in much higher abundance (> per mill), but it is not clear what fraction of the observed nanometer-sized diamonds is truly presolar.

The first of the presently known presolar grain types were found as the result of the search for the carrier phases of isotopically anomalous noble gases: diamond, graphite and silicon carbide are these carriers, and refractory oxides/silicon nitride were found because they followed silicon carbide in the chemical isolation procedure. Detection of silicates and other not chemically refractory grains required a new approach that became possible with instrumental developments in secondary ion mass spectrometry: high resolution (∼100 nm) ion imaging for search in the meteorites in situ. A data base containing by now isotopic data on more than 10,000 presolar grains has been set up by the group at Washington University at http://presolar.wustl.edu/∼pgd/.

Isotope abundance anomalies are the key feature based on which the presolar nature of a given grain is ascertained. Based on this criterion, all of the SiC grains contained in primitive meteorites are presolar, but only a small fraction of oxide and silicate grains. Applying the isotope anomaly criterion has also its limits, as is shown by the case of the nanodiamonds, which consist on the average of ∼1,000 atoms of

carbon only. Requiring – as sometimes is done – that a given grain (which cannot be analyzed singly anyway) that is presolar must carry an atom of anomalous xenon misses a point: in nature there is no such mineral that in bulk contains as much as ∼1% of xenon by weight. In addition xenon would be accompanied by at least some 100 atoms of other elements of the same neutron capture origin, so that such a grain would no longer be anything resembling a diamond any more.

Based on the isotopic features it is possible in many cases to establish likely stellar sources, and the same features also allow drawing conclusions about nucleosynthesis and mixing in stars as well as galactic chemical evolution. The major source of SiC, oxide and silicate grains are RGB/AGB stars, while some (∼1%) of the SiC and essentially all of the silicon nitride grains appear to be linked to supernovae, as are probably the presolar nanodiamonds. Graphite grains come from a number of different stellar sources and the distribution varies with morphology. Astronomical detection around specific sources, such as in the case of SiC and silicates, would be helpful if it could be achieved for all of the presolar grains observed in meteorites. Deriving an age for the grains and establishing a detailed history between time of formation in stellar outflows and arrival in what was to become the solar system remains a task to be accomplished.

Acknowledgments Thanks go to a large number of colleagues in the field for many discussions on topics relating to presolar grains in meteorites. Special thanks go to Peter Hoppe, who also contributed Figs. 1, 5, 6, 7, and 8, and to Sachiko Amari who also supplied Fig. 3a, c, d. Figures 3b and 9 are from T.J. Bernatowicz, Fig. 3e is from B.-G. Choi, Fig. 3f from F. Banhart, Fig. 4 from C. Vollmer and Fig. 11 from A. Braatz.

References

1. Lugmair, G.W., Shukolyukov, A.: Meteorit. Planet. Sci. **36,** 1017 (2001) 278, 280
2. McKeegan, K.D., Davis, A.M.: Early solar system chronology. In: Davis, A.M. (ed.) Meteorites, Comets, and Planets. Treatise on Geochemistry vol. 1, pp. 431–460. Elsevier, Amsterdam (2005) 278, 280
3. Brownlee, D.E., Tsou, P., Anderson, J.D., Hanner, M.S., Newburn, R.L., Sekanina, Z., Clark, B.C., Hörz, F., Zolensky, M.E., Kissel, J., McDonnell, J.A.M., Sandford, S.A., Tuzzolino, A.J.: J. Geophys. Res. E **108**, 8111 (2003) 278
4. Brownlee, D., Tsou, P., Aléon, J., Alexander, C.M.O'D., Araki, T., Bajt, S., Baratta, G.A., Bastien, R., Bland, P., Bleuet, P., et al.: Science **314**, 1711 (2006) 278
5. Bernatowicz, T.J., Zinner, E. (eds.): Astrophysical Implications of the Laboratory Study of Presolar Materials. American Institute of Physics, Woodbury, NY (1997) 278
6. Zinner, E.: Annu. Rev. Earth Planet. Sci. **26**, 147 (1998) 278, 286, 288, 289, 290, 291, 292, 293, 296, 297
7. Nittler, L.R.: Earth Planet. Sci. Lett. **209**, 259 (2003) 278, 296
8. Lodders, K., Amari, S.: Chem. Erde **65**, 93 (2005) 278, 285
9. Zinner, E.K.: Presolar grains. In: Davis, A.M. (ed.) Meteorites, Comets, and Planets. Treatise on Geochemistry, vol. 1, pp. 17–39. Elsevier, Amsterdam (2005) 278, 285, 288, 289, 291
10. Meyer, B.S., Zinner, E.: Nucleosynthesis. In: Lauretta, D.S., McSween, H.Y., Jr. (eds.) Meteorites and the Early Solar System II, pp. 69–108. University of Arizona Press, Tucson, AZ (2006) 278, 285, 289, 291
11. Hoppe, P.: Appl. Surf. Sci. **252**, 7102 (2006) 278, 279, 283, 285, 293, 298

12. Bradley, J.P.: Science **265**, 925 (1994) 279, 300
13. Floss, C., Stadermann, F.J., Bradley, J.P., Dai, Z.R., Bajt, S., Graham, G., Lea, A.S.: Geochim. Cosmochim. Acta **70**, 2371 (2006) 279
14. Lee, T.: Implications of isotopic anomalies for nucleosynthesis. In: Kerridge, J.F., Matthews, M.S. (eds.) Meteorites and the Early Solar System, pp. 1063–1089. University of Arizona Press, Tucson, AZ (1988) 280
15. Ott, U.: Nature **364**, 25 (1993) 280
16. Robert, F., Epstein, S.: Geochim. Cosmochim. Acta **46**, 81 (1982) 280
17. Robert, F.: Science **293**, 1056 (2001) 280
18. Busemann, H., Young, A.F., Alexander, C.M.O'D., Hoppe, P., Mukhopadhyay, S., Nittler, L.R.: Science **312**, 727 (2006) 280
19. Aléon, J., Robert, F., Duprat, J., Derenne, S.: Nature **437**, 385 (2005) 280
20. Sakamoto, N., Seto, Y., Itoh, S., Kuramoto, K., Fujino, K., Nagashima, K., Krot, A.N., Yurimoto, H.: Science **317**, 231 (2007) 280
21. Suess, H.E.: Annu. Rev. Astron. Astrophys. **3**, 217 (1965) 280
22. Reynolds, J.H., Turner, G.: J. Geophys. Res. **69**, 3263 (1964) 280
23. Huss, G.R., Lewis, R.S.: Meteoritics **29**, 791 (1994) 280, 294, 305
24. Black, D.C., Pepin, R.O.: Earth Planet. Sci. Lett. **6**, 395 (1969) 280
25. Lewis, R.S., Tang, M., Wacker, J.F., Anders, E., Steel, E.: Nature **326**, 160 (1987) 281, 305
26. Bernatowicz, T., Fraundorf, G., Tang, M., Anders, E., Wopenka, B., Zinner, E., Fraundorf, P.: Nature **330**, 728 (1987) 281
27. Lewis, R.S., Srinivasan, B., Anders, E.: Science **190**, 1251 (1975) 281
28. Srinivasan, B., Anders, E.: Science **201**, 51 (1978) 281
29. Amari, S., Lewis, R.S., Anders, E.: Geochim. Cosmochim. Acta **58**, 459 (1994) 281, 283, 284, 291, 301
30. Merchel, S., Ott, U., Herrmann, S., Spettel, B., Faestermann, T., Knie, K., Korschinek, G., Rugel, G., Wallner, A.: Geochim. Cosmochim. Acta **67**, 4949 (2003) 281, 283, 301
31. Nittler, L.R., Alexander, C.M.O'D., Tera, F.: Meteorit. Planet. Sci. **36**, A 149 (2001) 283
32. Russell, S.S., Ott, U., Alexander, C.M.O'D., Zinner, E.K., Arden, J.W., Pillinger, C.T.: Meteorit. Planet. Sci. **32**, 719 (1997) 283, 301
33. Huss, G.R., Meshik, A.P., Smith, J.B., Hohenberg, C.M.: Geochim. Cosmochim. Acta **67**, 4823 (2003) 283, 301
34. Daulton, T.L., Eisenhour, D.D., Bernatowicz, T.J., Lewis, R.S., Buseck, P.: Geochim. Cosmochim. Acta **60**, 4853 (1996) 283, 300
35. Bernatowicz, T.J., Messenger, S., Pravdivtseva, O., Swan, P., Walker, R.M.: Geochim. Cosmochim. Acta **67**, 4679 (2003) 283, 299
36. Tizard, J., Lyon, I., Henkel, T.: Meteorit. Planet. Sci. **40**, 335 (2005) 283
37. Ott, U., Hoppe, P., Lugmair, G.W.: New Astron. Rev. **48**, 165 (2004) 283, 285, 293, 298
38. Nguyen, A.N., Zinner, E.: Science **303**, 1496 (2004) 283, 293, 298, 301
39. Mostefaoui, S., Hoppe, P.: Astrophys. J. **613**, L149 (2004) 283, 291, 293, 298, 301
40. Hutcheon, I.D., Huss, G.R., Fahey, A.J., Wasserburg, G.J.: Astrophys. J. **425**, L97 (1994) 284, 291
41. Nittler, L.R., Alexander, C.M.O'D., Gao, X., Walker, R.M., Zinner, E.K.: Nature **370**, 443 (1994) 284, 291
42. Nittler, L.R., Hoppe, P., Alexander, C.M.O'D., Amari, S., Eberhardt, P., Gao, X., Lewis, R.S., Strebel, R., Walker, R.M., Zinner, E.: Astrophys. J. **453**, L25 (1995) 284, 293
43. Virag, A., Zinner, E., Amari, S., Anders, E.: Geochim. Cosmochim. Acta **55**, 2045 (1991) 284
44. Bernatowicz, T.J., Cowsik, R., Gibbons, P.C., Lodders, K., Fegley, B., Jr., Amari, S., Lewis, R.S.: Astrophys. J. **472**, 760 (1996) 285, 295, 299
45. Bernatowicz, T.J., Amari, S., Lewis, R.S.: Lunar Planet. Sci. **XXIII**, 91 (1992) 285, 295
46. Hoppe, P.: Space Sci. Rev. **138**, 43 (2008) 282, 285, 286, 288, 289, 291, 292, 293
47. Hoppe, P., Ott, U.: Mainstream silicon carbide grains from meteorites. In: Bernatowicz, T.J., Zinner, E. (eds.) Astrophysical Implications of the Laboratory Study of Presolar Materials, pp. 27–58. American Institute of Physics, Woodbury, NY (1997) 286, 288, 291, 297
48. Hoppe, P., Zinner, E.: J. Geophys. Res. **105**, 10371 (2000) 282, 286, 289, 290, 291, 292, 293, 295, 296, 299, 3

49. Zinner, E., Amari, S., Lewis, R.S.: Astrophys. J. **382**, L47 (1991) 286
50. Nicolussi, G.K., Davis, A.M., Pellin, M.J., Lewis, R.S., Clayton, R.N., Amari, S.: Science **277**, 1281 (1997) 286
51. Pellin, M.J., Davis, A.M., Lewis, R.S., Amari, S., Clayton, R.N.: Lunar Planet. Sci. **XXX**, #1969 (CD-ROM) (1999) 286, 289, 298
52. Lugaro, M., Davis, A.M., Gallino, R., Pellin, M.J., Straniero, O., Käppeler, F.: Astrophys. J. **593**, 486 (2003) 286
53. Barzyk, J.G., Savina, M.R., Davis, A.M., Gallino, R., Gyngard, F., Amari, S., Zinner, E., Pellin, M.J., Lewis, R.S., Clayton, R.N.: Meteorit. Planet. Sci. **42**, 1103 (2007) 286, 287
54. Amari, S., Hoppe, P., Zinner, E., Lewis, R.S.: Meteoritics **30**, 679 (1995) 286
55. Yin, Q.-Z., Lee, C.-T.A., Ott, U.: Astrophys. J. **647**, 676 (2006) 286, 297
56. Nichols, R.H., Jr., Hohenberg, C.M., Hoppe, P., Amari, S., Lewis, R.S.: Lunar Planet. Sci. **XXIII**, 989 (1992) 286, 288, 291
57. Heck, P.R., Marhas, K.K., Hoppe, P., Gallino, R., Baur, H., Wieler, R.: Astrophys. J. **656**, 1208 (2007) 286, 288
58. Whittet, D.C.B.: Dust in the Galactic Environment, p. 390. Institute of Physics Publishing, Bristol, PA (2003) 286, 301
59. Henning, Th., Salama, F.: Science **282**, 2204 (1998) 286
60. Little-Marenin, I.R.: Astrophys. J. **307**, L15 (1986) 287, 301
61. Speck, A.K., Barlow, M.J., Skinner, C.J.: Mon. Not. R. Astron. Soc. **234**, 79 (1997) 287, 300, 302
62. Alexander, C.M.O'D.: Geochim. Cosmochim. Acta **57**, 2869 (1993) 287
63. Gallino, R., Busso, M., Picchio, G., Raiteri, C.M.: Nature **348**, 298 (1990) 287
64. Ott, U., Begemann, F.: Astrophys. J. **353**, L57 (1990) 287
65. Gallino, R., Raiteri, C.M., Busso, M.: Astrophys. J. **410**, 400 (1993)
66. Marhas, K.K., Hoppe, P., Ott, U.: Meteorit. Planet. Sci. **42**, 1077 (2007) 287, 289, 297
67. Timmes, F.X., Clayton, D.D.: Astrophys. J. **472**, 723 (1996) 288, 295
68. Lugaro, M., Zinner, E., Gallino, R., Amari, S.: Astrophys. J. **527**, 369 (1999) 288, 295
69. Zinner, E., Nittler, L.R., Gallino, R., Karakas, A.I., Lugaro, M., Straniero, O., Lattanzio, J.C.: Astrophys. J. **650**, 350 (2006) 288, 295, 296
70. Zinner, E., Amari, S., Guinness, R., Jennings, C., Mertz, A.F., Nguyen, A.N., Gallino, R., Hoppe, P., Lugaro, M., Nittler, L.R., Lewis, R.S.: Geochim. Cosmochim. Acta **71**, 4786 (2007) 288, 289, 293
71. Amari, S., Nittler, L.R., Zinner, E., Lodders, K., Lewis, R.S.: Astrophys. J. **559**, 463 (2001) 286, 289
72. Woosley, S.E., Weaver, T.A.: Astrophys. J. Suppl. **101**, 181 (1995) 289
73. Timmes, F.X., Woosley, S.E., Hartmann, D.H., Hoffman, R.D.: Astrophys. J. **464,** 332 (1996) 289
74. Clayton, D.D., Arnett, W.D., Kane, J., Meyer, B.S.: Astrophys. J. **486**, 824 (1997) 289, 296
75. Pellin, M.J., Savina, M.R., Calaway, W.F., Tripa, C.E., Barzyk, J.G., Davis, A.M., Gyngard, F., Amari, S., Zinner, E., Lewis, R.S., Clayton, R.N.: Lunar Planet. Sci. **XXXVII**, #2041 (CD-ROM) (2006) 289
76. Meyer, B.S., Clayton, D.D., The, L.-S.: Astrophys. J. **540**, L49 (2000) 289, 295, 297, 298
77. Amari, S., Nittler, L.R., Zinner, E., Gallino, R., Lugaro, M., Lewis, R.S.: Astrophys. J. **546**, 248 (2001) 286, 289, 290
78. Hoppe, P., Annen, P., Strebel, R., Eberhardt, P., Gallino, R., Lugaro, M., Amari, S., Lewis, R.S.: Astrophys. J. **487**, L101 (1997) 290
79. Hoppe, P., Amari, S., Zinner, E., Lewis, R.S.: Geochim. Cosmochim. Acta **59**, 4029 (1995) 290, 299
80. Zinner, E., Amari, S., Wopenka, B., Lewis, R.S.: Meteoritics **30**, 209 (1995) 290
81. Amari, S., Zinner, E., Lewis, R.S.: Astrophys. J. **470**, L101 (1995) 291
82. Amari, S., Lewis, R.S., Anders, E.: Geochim. Cosmochim. Acta **59**, 1411 (1995) 291
83. Croat, T.K., Stadermann, F.J., Bernatowicz, T.J.: Astrophys. J. **631**, 976 (2005) 291, 295
84. Nichols, R.H., Jr., Kehm, K., Brazzle, R., Amari, S., Hohenberg, C.M., Lewis, R.S.: Meteoritics **29**, 510 (1994) 291
85. Jadhav, M., Amari, S., Marhas, K.K., Zinner, E., Maruoka, T., Gallino, R.: Astrophys. J. **682**, 1479 (2008) 291

86. Nittler, L.R., Alexander, C.M.O'D., Gao, X., Walker, R.M., Zinner, E.: Astrophys. J. **483**, 475 (1997) 291, 292
87. Nittler, L.R., Alexander, C.M.O'D., Gallino, R., Hoppe, P., Nguyen, A.N., Stadermann, F.J., Zinner, E.K.: Astrophys. J. **682**, 1450 (2008) 291, 292
88. Wasserburg, G.J., Boothroyd, A.I., Sackmann, I.-J.: Astrophys. J. **447**, L37 (1995) 292, 296
89. Nittler, L.R., Alexander, C.M.O'D., Wang, J., Gao, X.: Nature **393**, 222 (1998) 292
90. Choi, B.-G., Huss, G.R., Wasserburg, G.J., Gallino, R.: Science **282**, 1284 (1998) 292
91. Nguyen, A.N., Stadermann, F.J., Zinner, E., Stroud, R.M., Alexander, C.M.O'D., Nittler, L.R.: Astrophys. J. **656**, 1223 (2007) 292, 293, 295, 300, 301
92. Vollmer, C., Hoppe, P., Brenker, F.E.: Astrophys. J. **684**, 611 (2008) 292, 293, 295
93. Clayton, D.D., Meyer, B.S., Sanderson, C.I., Russell, S.S., Pillinger, C.T.: Astrophys. J. **447**, 894 (1995) 293
94. Russell, S.S., Arden, J.W., Pillinger, C.T.: Meteorit. Planet. Sci. **31**, 343 (1996) 293
95. Kallenbach, R., Geiss, J., Ipavich, F.M., Gloeckler, G., Bochsler, P., Gliem, F., Hefti, S., Hilchenbach, M., Hovestadt, D.: Astrophys. J. **507**, L185 (1998) 294
96. Hashizume, K., Chaussidon, M., Marty, B., Robert, F.: Science **290**, 1142 (2000) 294
97. Owen, T., Mahaffy, P.R., Niemann, H.B., Atreya, S., Wong, M.: Astrophys. J. **553**, L77 (2001) 294
98. Meibom, A., Krot, A.N., Robert, F., Mostefaoui, S., Russell, S.S., Petaev, M.I., Gounelle, M.: Astrophys. J. **656**, L33 (2007) 294
99. Marty, B., Zimmermann, L., Burnard, P.G., Burnett, D.L., Allton, J.H., Wiens, R.C., Heber, V.S., Wieler, R., Bochsler, P., Sestak, S., Franchi, I.A.: Meteorit. Planet. Sci. **43**, A90 294
100. Ott, U.: Noble gases in meteorites – trapped components. In: Porcelli, D., Ballentine, C.J., Wieler, R. (eds.) Noble Gases and Cosmochemistry (Reviews in Mineralogy and Geochemistry), pp. 71–100. Mineralogical Society of America, Washington, DC (2002) 281, 294
101. Richter, S., Ott, U., Begemann, F.: Nature **391**, 261 (1998) 294, 297
102. Maas, R., Loss, R.D., Rosman, K.J.R., DeLaeter, J.R., Lewis, R.S., Huss, G.R., Lugmair, G.W.: Meteorit. Planet. Sci. **36**, 849 (2001) 294, 297
103. Lewis, R.S., Huss, G.R., Lugmair, G.: Lunar Planet. Sci. **XXII**, 807 (1991) 294
104. Heymann, D., Dziczkaniec, M.: Proc. Lunar Sci. Conf. **10**, 1943 (1979) 295
105. Clayton, D.D.: Astrophys. J. **340**, 613 (1989) 295, 297
106. Ott, U.: Astrophys. J. **463**, 344 (1996) 295, 297
107. Heymann, D., Dziczkaniec, M.: Meteoritics **15**, 15 (1980) 295
108. Gallino, R., Raiteri, C.M., Busso, M., Matteucci, F.: Astrophys. J. **430**, 858 (1994) 295
109. Huss, G.R., Fahey, A.J., Gallino, R., Wasserburg, G.J.: Astrophys. J. **430**, L81 (1994) 295
110. Travaglio, C., Gallino, R., Amari, S., Zinner, E., Woosley, S., Lewis, R.S.: Astrophys. J. **510**, 325 (1999) 296
111. Amari, S., Zinner, E., Clayton, D.D., Meyer, B.S.: Meteorit. Planet. Sci. **33**, A10 (1998) 296
112. Clayton, D.D., Liu, W., Dalgarno, A.: Science **283**, 1290 (1999) 296
113. Boothroyd, A.I., Sackmann, I.-J., Wasserburg, G.J.: Astrophys. J. **442**, L21 (1995) 296
114. Huss, G.R., Hutcheon, I.D., Wasserburg, G.J.: Geochim. Cosmochim. Acta **61**, 5117 (1997) 296
115. Guber, K.H., Koehler, P.E., Derrien, H., Valentine, T.E., Leal, L.C., Sayer, R.O., Rauscher, T.: Phys. Rev. C **67**, 026802 (2003) 296
116. Bao, Z.Y., Beer, H., Käppeler, F., Voss, F., Wisshak, K., Rauscher, T.: Atom. Data Nucl. Data **76**, 70 (2000) 296, 297
117. Käppeler, F., Beer, H., Wisshak, K.: Rep. Prog. Phys. **52**, 945 (1989) 297
118. Käppeler, F., Gallino, R., Busso, M., Picchio, G., Raiteri, C.M.: Astrophys. J. **354**, 630 (1990) 297
119. Arlandini, C., Käppeler, F., Wisshak, K., Gallino, R., Lugaro, M., Busso, M., Straniero, O.: Astrophys. J. **525**, 886 (1999) 297
120. Ott, U.: Proc. Indian Acad. Sci. (Earth Planet. Sci.) **107**, 379 (1998) 297, 305
121. Howard, W.M., Meyer, B.S., Clayton, D.D.: Meteoritics **27**, 404 (1992) 297
122. Marosits, E., Ott, U.: Meteorit. Planet. Sci. **41**, A113 (2006) 297
123. Wang, L.: Astrophys. J. **635**, L33 (2005) 297

124. Lodders, K., Fegley, B., Jr.: Meteoritics **30**, 661 (1995) 298
125. Stroud, R.M., Nittler, L.R., Hoppe, P.: Meteorit. Planet. Sci. **39**, A101 (2004) 299
126. Stroud, R.M., Nittler, L.R., Alexander, C.M.O'D.: Meteorit. Planet. Sci. **41**, A168 (2006) 299
127. Virag, A., Wopenka, B., Amari, S., Zinner, E., Anders, E., Lewis, R.S.: Geochim. Cosmochim. Acta **56**, 1715 (1992) 299, 302
128. Daulton, T.L., Lewis, R.S., Amari, S.: Meteorit. Planet. Sci. **33**, A37 (1998) 299, 302
129. Daulton, T.L., Bernatowicz, T.J., Lewis, R.S., Messenger, S., Stadermann, F.J., Amari, S.: Science **296**, 1852 (2002) 299, 302
130. Daulton, T.L., Bernatowicz, T.J., Lewis, R.S., Messenger, S., Stadermann, F.J., Amari, S.: Geochim. Cosmochim. Acta **67**, 4743 (2003) 299, 302
131. Andersen, A.C., Jäger, C., Mutschke, H., Braatz, A., Clément, D., Henning, Th., Jørgensen, U.G., Ott, U.: Astron. Astrophys. **343**, 933 (1999) 300, 302
132. Verchovsky, A.B., Fisenko, A.V., Semjonova, L.F., Wright, I.P., Lee, M.R., Pillinger, C.T.: Science **281**, 1165 (1998) 300, 305
133. Banhart, F., Lyutovich, Y., Braatz, A., Jäger, C., Henning, T., Dorschner, J., Ott, U.: Meteorit. Planet. Sci. **33**, A12 (1998) 300
134. Stroud, R.M., Nittler, L.R., Alexander, C.M.O'D.: Science **305**, 1455 (2004) 300
135. Zega, T.J., Nittler, L.R., Busemann, H., Hoppe, P., Stroud, R.M.: Meteorit. Planet. Sci. **42**, 1373 (2007) 300
136. Floss, C., Stadermann, F.J., Bose, M.: Astrophys. J. **672**, 1266 (2008) 300
137. Mathis, J.S., Rumpl, W., Nordsieck, K.H.: Astrophys. J. **217**, 425 (1977) 301
138. Frisch, P.C., Dorschner, J.M., Geiss, J., Greenberg, J.M., Grün, E., Landgraf, M., et al.: Astrophys. J. **525**, 492 (1999) 301
139. Draine, B.T.: Annu. Rev. Astron. Astrophys. **41**, 241 (2003) 301
140. Demyk, K., Dartois, E., Wiesemeyer, H., Jones, A.P., d'Hendecourt, L.: Astron. Astrophys. **364**, 170 (2000) 301
141. Ott, U., Altmaier, M., Herpers, U., Kuhnhenn, J., Merchel, S., Michel, R., Mohapatra, R.K.: Meteorit. Planet. Sci. **40**, 1635 (2005) 301, 304, 306
142. Lewis, R.S., Anders, E., Draine, B.T.: Nature **339**, 117 (1989) 302
143. Colangeli, L., Mennella, V., Stephens, J., Bussoletti, E.: Astron. Astrophys. **248**, 583 (1994) 302
144. Hill, H., D'Hendecourt, L., Perron, C., Jones, A.: Meteorit. Planet. Sci. **32**, 713 (1997) 302
145. Andersen, A.C., Jørgensen, U.G., Nicolaisen, F.M., Sørensen, P.G., Glejbjøl, K.: Astron. Astrophys. **330**, 1080 (1998) 302
146. Braatz, A., Ott, U., Henning, Th., Jäger, C., Jeschke, G.: Meteorit. Planet. Sci. **35**, 75 (2000) 302, 303
147. Allamandola, L., Sandford, S., Tielens, A., Herbst, T.: Science **260**, 64 (1993) 302, 303
148. Guillois, O., Ledoux, G., Reynaud, C.: Astrophys. J. **521**, L33 (1999) 303
149. Walker, R.M., comm. to Marvin, U.B.: Meteorit. Planet. Sci. **36**, A275 (2001) 303
150. Tang, M., Anders, E.: Astrophys. J. **335**, L31 (1988) 303
151. Lewis, R.S., Amari, S., Anders, E.: Geochim. Cosmochim. Acta **58**, 471 (1994) 303
152. Ott, U., Begemann, F.: Meteorit. Planet. Sci. **35**, 53 (2000) 303
153. Gyngard, F., Amari, S., Zinner, E., Lewis, R.S.: Meteorit. Planet. Sci. **42**, A61 (2007) 304
154. Jones, A.P., Tielens, A.G.G.M., Hollenbach, D.J., McKee, C.F.: The propagation and survival of interstellar grains. In: Bernatowicz, T.J., Zinner, E. (eds.) Astrophysical Implications of the Laboratory Study of Presolar Materials, pp. 595–613. American Institute of Physics, Woodbury, NY (1997) 304
155. Heck, P.R., Gyngard, F., Meier, M.M.M., Avila, J.N., Amari, S., Zinner, E., Lewis, R.S., Baur, H., Wieler, R.: Lunar Planet. Sci. **XXXIX**, #1239 (2008) 304
156. Huss, G.R., Lewis, R.S.: Geochim. Cosmochim. Acta **59**, 115 (1995) 282, 305
157. Huss, G.R., Lewis, R.S.: Meteoritics **29**, 811 (1994) 305
158. Koscheev, A.P., Gromov, M.D., Mohapatra, R.K., Ott, U.: Nature **412**, 615 (2001) 305
159. Huss, G.R., Ott, U., Koscheev, A.P.: Meteorit. Planet. Sci. **43**, 1811 (2008) 306
160. Ott, U., Huss, G.R.: Meteorit. Planet. Sci. **43**, A125 (2008) 306
161. Clayton, D.D.: Astrophys. J. **598**, 313 (2003) 306
162. Hoppe, P.: Nucl. Phys. **A688**, 94c (2001) 287, 288

Laboratory Astrophysics of Cosmic Dust Analogues

T. Henning

Abstract In this chapter, the main techniques for producing and characterizing cosmic dust analogues in the laboratory will be discussed. It will be shown how optical data of astronomically relevant materials can be measured and how such data can be applied to interpret astronomical spectra. The identification of minerals in space from infrared spectroscopy will be summarized.

1 Introduction

The identification of distinct dust components in astronomical spectra requires the knowledge of basic optical data, which have to be provided by laboratory measurements. In contrast to bulk material, solids in space form a system of mostly submicron-sized isolated particles. In dense regions of molecular clouds and in protoplanetary disks grains can coagulate. This process certainly leads to the formation of more complex and inhomogeneous dust aggregates.

Absorption and scattering of light by small particles depend on their shape and size distribution as well as on the material of which they are composed. Surface modes in small particles cause interesting absorption features [1]. Spectra of small metallic particles can show features where none are present in the bulk material. Non-conducting grains display often several features with the wavelength positions and widths depending on both the dielectric function and the shape of the particles. Only spherical particles are characterized by a single resonance, whereas a distribution of shapes leads to broad absorption bands with smaller peak absorption. A condition for the presence of surface modes is a negative value of the real part of the dielectric function. A variety of experimental methods exist to determine the complex dielectric function. In this contribution, we will discuss how such particles can be produced and characterized.

T. Henning (✉)
Max Planck Institute for Astronomy, Königstuhl 17, D-69117 Heidelberg, Germany
e-mail: henning@mpia.de

Henning, T.: *Laboratory Astrophysics of Cosmic Dust Analogues*. Lect. Notes Phys. **815**, 313–329 (2010)
DOI 10.1007/978-3-642-13259-9_8

The dust particles not only absorb light, but also thermally re-radiate energy at infrared and millimetre wavelengths. Therefore, spectral energy distributions of dusty astronomical objects also depend on the temperature of the particles, which is determined by the balance of absorption and re-emission of radiation. Grains of different size and chemical composition will have distinct temperatures. The treatment of radiation transfer through a dusty medium requires the solution of a transfer equation, which complicates the analysis of astronomical spectra [2].

2 What Are Cosmic Dust Analogue Materials?

First constraints on the nature of cosmic grains come from an analysis of abundance patterns, namely the depletion of elements in the interstellar medium with respect to a given reference abundance, and the chemical composition of stellar outflows from evolved stars. Presently, there is a discussion if the solar abundances can be taken as the reference values or if the photospheric abundances of recently formed B stars better represent the interstellar medium [3, 4]. The latter values are about 2/3 of the solar abundances and would impose strong constraints on dust models. In more recent studies, excellent agreement between B-star abundances with recently determined solar values have been obtained [5]. These results still imply rather tight constraints on dust models in terms of carbon abundance.

The potential dust-forming elements can be divided in three major groups [4, 6]:

1. Primary dust-forming elements (abundance $\geq$100 ppm): carbon, oxygen, and nitrogen
2. Abundant dust-forming elements (abundance $\sim$30 ppm): magnesium, silicon, sulphur, iron
3. Minor dust-forming elements (abundance $\sim$3 ppm): aluminium, calcium, sodium, nickel

The abundance values are given relative to 10^6 atoms of hydrogen (ppm). With the exception of sulphur, all these elements are heavily depleted in the cool atomic hydrogen clouds ("diffuse clouds") of the galactic disk [7]. Therefore, the presence of silicon and iron particles, silicates and various metal oxides, carbonaceous grains with various hybridization states, and carbides can be expected in space. The abundant element nitrogen is usually bound to N_2 molecules, but may form nitrides in nitrogen-rich circumstellar environments.

Cosmic dust grains are part of a lifecycle of interstellar matter [8]. New ones form in the outflows of evolved stars. Depending on the chemical composition of these outflows, especially the C/O ratio, different types of grains are produced from the gas phase (cf. contribution by Gail, this volume). The small transition group of S-type stars is characterized by a C/O ratio very close to 1. As a consequence of nucleosynthesis and dredge-up processes during AGB evolution, "oxygen-rich" stars with masses smaller than 4 $M_\odot$ will evolve into carbon stars and the molecular composition of the outflows will change. Other factors influencing the chemical

state of the outflows, apart from the C/O ratio, can be the formation of molecules by grain surface reactions, the dissociation of some of the CO and N_2 molecules by chromospheric UV radiation and the influence of shock chemistry.

In oxygen-rich envelopes, the most abundant elements available for grain formation are O, Fe, Si, Mg, Al, and Ca. Without considering the kinetics of grain formation, we therefore expect the presence of silicates and other oxides (silica, corundum, spinel), iron and silicon grains. Silicates of olivine and pyroxene structure are of special interest. Olivines are solid solutions of forsterite (Mg_2SiO_4) and fayalite (Fe_2SiO_4), whereas pyroxenes are solid solutions of ferrosilite ($FeSiO_3$) and enstatite ($MgSiO_3$). The carbon-rich outflows lead to the production of carbonaceous grains as well as SiC and TiC particles. Si_3N_4, FeSi, and FeS/MgS grains are among other possible circumstellar grain components.

"Stardust" particles are modified during their journey through the interstellar medium by erosion in interstellar shock fronts, UV and ion irradiation, and surface reactions with atomic hydrogen, leading most probably to amorphous materials. In fact, the crystalline fraction of the interstellar silicate grains is less than 2% in mass [9]. This fact could also be explained by the re-formation of cosmic dust in the interstellar medium which is required because stardust is efficiently destroyed by shocks.

In dense and UV-shielded regions such as the cold molecular cloud cores and the interiors of protoplanetary accretion disks, molecular ices form on the grain surfaces and particles grow by mutual collisions. In this paper, I will only deal with refractory materials and not with molecular ices or larger molecules such as carbon chains and polycyclic aromatic hydrocarbons (PAHs).

Laboratory dust analogues should reflect the expected chemical composition of the particles as well as their structural state. Silicates and other oxides, carbonaceous grains, carbides, nitrides, and sulphides are the major material classes which have to be considered. The investigation of "cosmic dust analogues" does not necessarily aim at exactly producing particles with the properties of cosmic dust. It also includes the investigation of bulk matter or thin films prepared for the derivation of the dielectric material functions or the investigation of the annealing behaviour of different materials. Here one should note that some properties of small particles cannot be studied with bulk material. In addition, certain systems may not exist as bulk material at all. This is especially true for carbonaceous particles (e.g. carbon onions and nanotubes) and silicon nanoparticles.

3 Material Production and Characterization

The experimental investigation of cosmic dust analogues is generally based on three major steps: (i) synthesis of the material, (ii) chemical and structural characterization of the samples, and (iii) measurement of the optical properties over a wavelength range as broad as possible. The latter step is far from trivial because it requires different light sources and spectroscopic facilities.

Production methods for refractory solids, applied in laboratory astrophysics, include: laser ablation and thermal evaporation and subsequent condensation in an inert (Ar, He) or reducing (H_2) atmosphere, infrared laser-induced and microwave-induced gas pyrolysis, arc discharges under various atmospheric conditions, burning of hydrocarbons, plasma deposition techniques, and sol-gel reactions in the case of silicatic materials [6, 10]. As an example Fig. 1 shows the Jena laser pyrolysis system which has been used for the production of carbide, nitride, and silicon nanoparticles. Here, one has to keep in mind that "good" cosmic dust analogues may considerably deviate in stoichiometry and crystallinity from materials which are easily available for laboratory analysis. Therefore, dedicated preparative work is often required for producing cosmic dust analogues.

To understand the relation between structural and optical properties of dust grains, they have to be thoroughly characterized. Depending on the material, different methods have been used. Table 1 summarizes the different structural characterization techniques for silicates and their pros and cons. For carbonaceous grains, we refer the reader to the reviews by Henning et al. [11] and Henning and Schnaiter [12]. Here it is especially the hybridization state which is of interest in determining the optical properties of the particles. As examples for the characterization of silicon-based materials, Fig. 2a shows an SEM (scanning electron microsocopy) image of an inhomogeneous silicate of average pyroxene stoichiometry ($Mg_{0.4}Fe_{0.6}SiO_3$) and Fig. 2b some SiO_2 particles. The pyroxene has been produced by melting SiO_2, $MgCO_3$, and $FeC_2O_4 \cdot 6H_2O$ in the right stoichiometric ratio and subsequent slow cooling of the melt [13]. The sample is characterized by phase separation which can be traced by the backscattering electron image. The dark gray phase is a SiO_2 component, the gray phase is made of a Mg-rich pyroxene and the light phase is an Fe-rich pyroxene. The chemical composition of the different phases could be determined by Energy Dispersive X-ray (EDX) analysis. Any determination of optical data of such a sample has to take into account that the measurement is an average over different phases with different optical properties. SEM images can

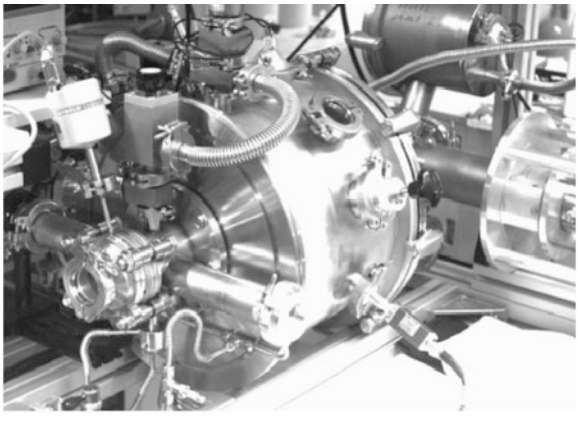

Fig. 1 Jena laser pyrolysis system for the production of small particles

Table 1 Characterization methods for silicate dust analogues

Method	Sensitivity	Pros	Cons
Wet-chemical analysis	Ratio of polyvalent ions	Very accurate	Time-consuming, average over sample
Energy dispersive X-ray analysis	Elemental composition	Check of stoichiometry and purity	No elements lighter than carbon
(HR)TEM	Global ordering	Direct insight into the meso- and macroscopic solid-state structure	"Expensive" search for representative structures
X-ray diffraction	Local ordering	Detailed coordination and bonding study, analysis of crystal phases	Large amounts of material required
X-ray absorption spectroscopy	Local- and medium-sized ordering	Distance of next neighbour and coordination study	
IR spectr.	Local and global ordering	Very sensitive to small structural differences	Difficult to interpret for mixtures

also be used to characterize the morphology of smoke or powder particles. Fig. 2b shows an SEM image of SiO_2 spheres on a surface, containing information on the size, shape, and agglomeration state of grains. These parameters have to be known for the interpretation of spectroscopic measurements.

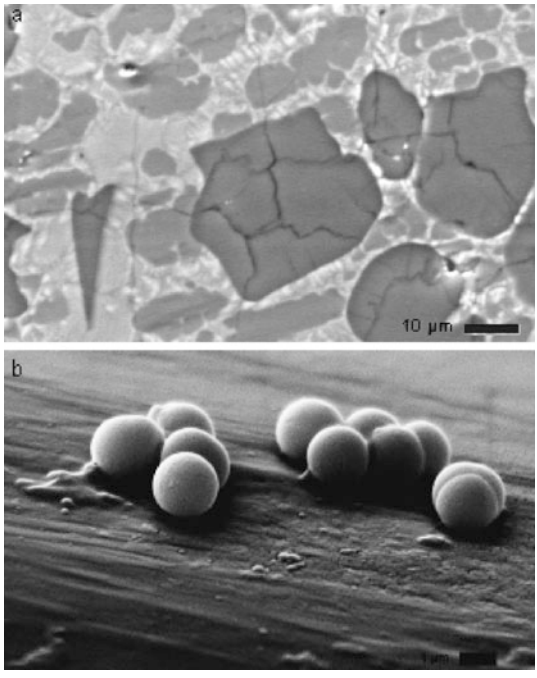

Fig. 2 (**a**) SEM image of an inhomogeneous pyroxene (see text for a discussion). (**b**) Spherical SiO_2 particles on a mineral surface. The average diameter of the spheres is 1 µm

4 Measurement of Optical Properties

The description of the interaction of radiation with small particles requires the knowledge of the frequency-dependent extinction, absorption, and scattering cross sections $C_{\rm ext}$, $C_{\rm abs}$, and $C_{\rm sca}$. These quantities depend on the material properties and the size, shape and agglomeration state of the particles. The fundamental material properties can be described either by the optical constants $m = n + ik$ or the dielectric function $\epsilon = \epsilon_1 + i\ \epsilon_2$, where $\epsilon_1 = n^2 - k^2$ and $\epsilon_2 = 2nk$ are the relations for non-magnetic materials. The optical constants are directly related to the phase velocity and attenuation of plane waves in the material. There are two different approaches for the determination of the optical properties of particles (see Fig. 3):

1. Calculation of cross sections from optical constants. The optical constants are usually determined from transmission measurements on thin films or reflection measurements on bulk materials (strong bands) or transmission measurements

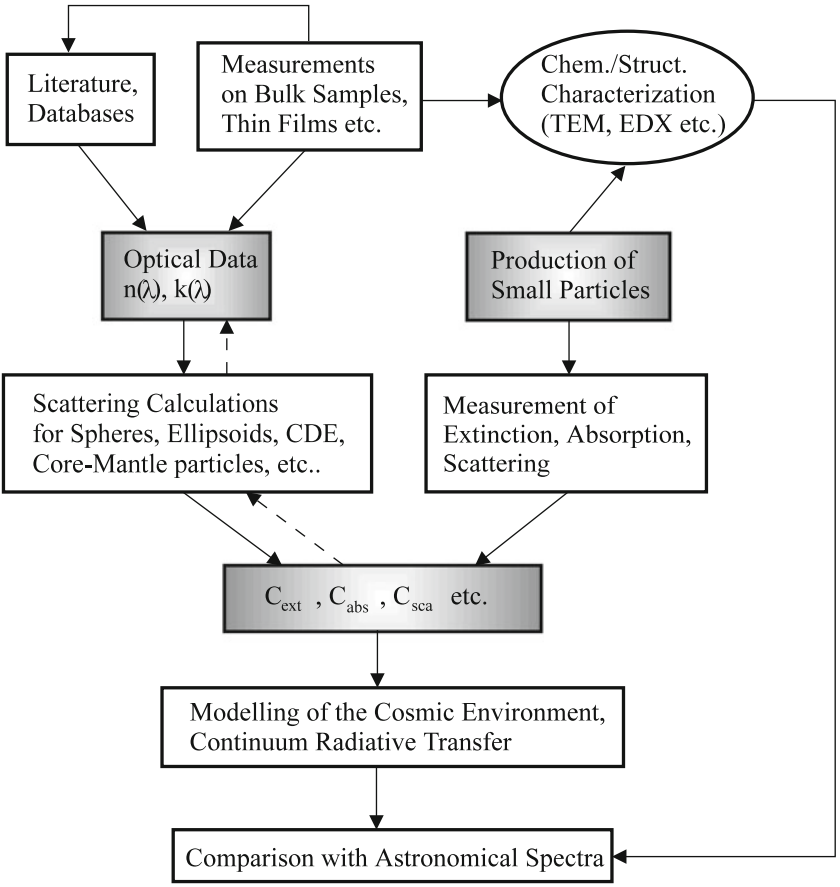

Fig. 3 Different approaches for determining the optical properties of cosmic dust. After [10]

on bulk samples (small k). Reflection spectroscopy works with polished surfaces, using a variety of angles of incidence. A special case of reflection spectroscopy is ellipsometry which is characterized by a measurement of the change of polarization state. Transmission spectroscopy on thin films can be combined with reflection spectroscopy.

The limitation of this approach is the fact that the bulk material may not have the structure of the nano- and microparticles. In addition, the calculation of cross sections from optical constants is not yet possible for complicated grain shapes or agglomerates in regions of strong resonances. In [10] and [14], a short summary of the procedure for calculating cross sections from optical constants is given.

2. Direct measurement of the cross sections on particle samples. This is certainly the way that should be preferred, but also the more complicated approach. One has to produce particles of the desired composition and structure in a narrow size and shape range and has to characterize them by spectroscopy. This is often difficult because conventional infrared spectroscopy (i) uses matrices in which the particles are embedded and (ii) is not able to prevent the agglomeration of primary particles to larger structures. Possibilities to reduce these effects are measurements of isolated particles in argon or neon matrices or direct spectroscopy by intense infrared radiation coming from synchrotron or free-electron laser facilities.

   Furthermore, transmission spectroscopy on a system of small isolated particles can be used to determine optical constants if the size and shape of the particles are known.

   The measurement of an ensemble of isolated particles in a non-disturbing gas environment is also possible if the particles are small enough (a few microns or smaller) to have sufficiently long sedimentation times. An experimental setup consisting of a multi-reflection gas cell attached to an FTIR spectrometer and a commercial brush disperser for aerosol generation has been used to measure IR absorption spectra of a wide variety of silicate and oxide particles. Although these measurements are so far non-quantitative, the experiment allowed, for the first time, to investigate systematically differences of the band profiles between embedded and free particles [15]. In addition, the particles can be retrieved from the aerosol after the measurement and can be characterized by electron microscopy. Therefore, detailed information about the grain morphology is accessible which can be related to the spectra. Such experiments may help to develop realistic theoretical models for the description of optical properties of dust particle ensembles.

The frequency dependence of the optical constants (dispersion relation) is determined by resonances of the electronic system, of the ionic lattice and, at very low frequencies, by relaxation of permanent dipoles. Here, we should note that many crystals, including the astronomically interesting crystalline silicates, show an anisotropy in their optical constants. In these cases, measurements with polarized light along the different axes of the crystal have to be carried out. These measurements require a careful orientation of the crystal and an alignment of the polarizers.

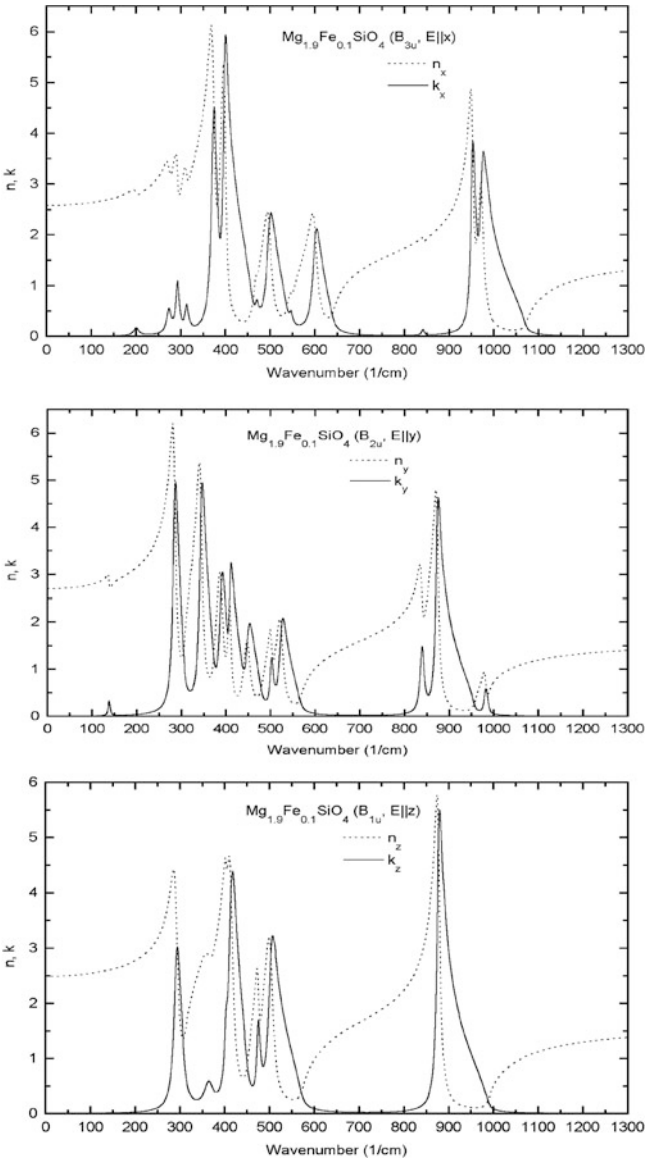

Fig. 4 Complex index of refraction $n + ik$ of an olivine crystal for three different crystallographic orientations. After [27]

An example of such data is given in Fig. 4. In addition, the optical constants of cosmic dust analogues may depend on the temperature, leading to a change of the width and wavelength position of sharp bands of crystalline material or a change of the far-infrared continuum absorption [16–20]. Far-infrared spectra of hydrous silicates have been measured over a broad temperature range, indicating that most

of the bands shift to shorter wavelengths at decreasing temperature and are getting sharper [21].

It should be stressed that optical constants are macroscopic quantities. They loose their meaning for small clusters and molecules. In the transition region from solids to molecules, the introduction of size-dependent optical constants may be a reasonable way to describe the behaviour of the systems. This approach has been used for the description of the confinement of charge carriers to the limited volume of small metallic particles [22].

Compilations of frequency-dependent optical constants of solids can be found in the various editions of the "Handbook of Optical Constants" [23–25]. An electronic database [26], especially dedicated to cosmic dust analogues, can be accessed via the web page http://www.mpia-hd.mpg.de/HJPDOC (Heidelberg-Jena-St. Petersburg Database of Optical Constants).

It has been already mentioned that the absorption and scattering cross sections (or the mass absorption coefficients) not only depend on the optical constants, but also on the shape and size of the particles. This is demonstrated in Fig. 5 where the mass absorption coefficient of forsterite is shown for spheres and two different distributions of ellipsoids. In addition, powder spectra of the small particles and observationally-determined band positions are plotted. It can be seen that the width, shape and position of strong "crystalline" bands depend on the shape of the particles. This effect is much less important for the weaker far-infrared bands, which are practically not influenced by the particle shape. A comparison between mass absorption coefficients and astronomical spectra of optically thin envelopes around evolved stars indicates that both sphere-like particles and ellipsoids elongated along the z-axis are necessary to obtain a convincing band assignment [27].

5 Interpretation of Astronomical Data

The infrared spectral region has been often considered to be the "fingerprint" region for the identification of the chemical composition of cosmic dust particles. Apart from the numerous diffuse interstellar bands (DIBs) at optical wavelengths [29], probably caused by carbon-containing molecules, and the extended red emission (ERE), recently related to silicon nanoparticles [30, 31], the UV/optical wavelength range contains only one strong resonance at 217 nm. This "UV bump" is widely attributed to an electronic transition in carbonaceous grains [11, 12]. An interesting additional fact is that observations show that the UV bump is located between 240 and 250 nm in the spectra of R Coronae Borealis stars – a special class of hydrogen-poor post-AGB stars which eject large amounts of carbon dust at random times [32, 33]. Here, we should note that an alternative ERE carrier could be PAHs or PAH-related materials.

Infrared spectra of solid particles reflect the fundamental vibrations of molecular bonds present in the material as well as the lattice modes of the solid. The broad solid-state bands are easily distinguishable from the rotational-vibrational bands

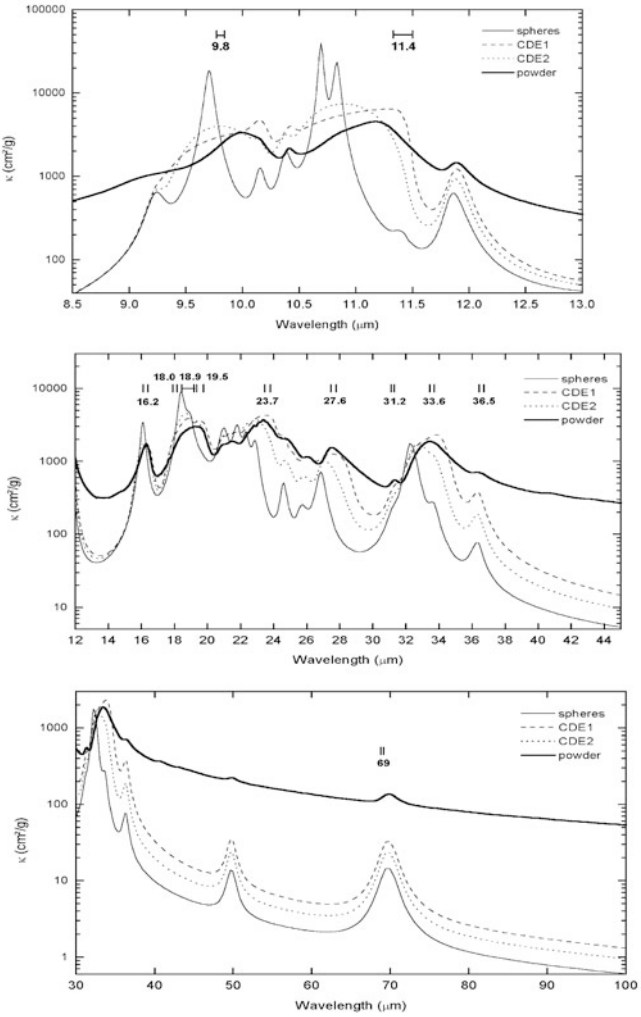

Fig. 5 Mass absorption coefficients of forsterite spheres and two different distributions of ellipsoids (CDE 1 and CDE 2) in vacuum and the Rayleigh limit. In addition, the results of transmission measurements on small particles (diameter $<1\,\mu$m) dispersed in a KBr/PE pellet are shown. Peak positions assigned to forsterite on the basis of ISO spectra from F. Molster [28] have been indicated. After [27]

of gas-phase molecules. A limitation of infrared spectroscopy is the fact that the identification of a specific carrier is difficult if only one band is observed. In addition, complex materials which contain similar molecular species may produce very similar spectra. This is especially true for carbonaceous grains.

Table 2 summarizes identifications of refractory materials based on infrared bands together with some key references which lead to more complete reference

Table 2 Refractory dust components in space

Wavelength (μm)	Component	Sources	References
3.4, 6.85, 7.25	Aliphatic hydrocarbons	C-rich CSE, diffuse ISM[b]	Schnaiter et al. [38], Mennella et al. [39] Pendleton and Allamandola [40]
5.5	Metal carbonyls	Galactic centre	Tielens et al. [41]
10, 18	Silicates[a]		Draine and Lee [42], Ossenkopf et al. [43] and, Henning [34, 35]
11.3	SiC	C-rich CSE[c]	Speck et al. [44, 45] Mutschke et al. [46] Pitman et al. [47]
13	$\alpha - Al_2O_3$ (CDE)	O-rich CSE	Sloan et al. [48], Koike et al. [49], Begemann et al. [50], and DePew et al. [51]
and 17, 32	$MgAl_2O_4$		Posch et al. [52] and Fabian et al. [53]
21 (20.1)	Carbonaceous material, SiS_2	C-rich CSE	Kwok et al. [54], Volk et al. [55], Henning et al. [56], and Begemann et al. [57]
	TiC nanocrystals		von Helden et al. [58]
	SiC/SiO_2		Posch et al. [59]
23	FeO (CDE)	HAEBE stars[d]	van den Ancker et al. [60]
	FeS		Keller et al. [61, 75]
30	MgS	C-rich CSE	Omont et al. [62] Begemann et al. [63] Szczerba et al. [64]
92.6	$CaCO_3$[e]	Planetary nebulae Young stellar objects	Kemper et al. [65] Ceccarelli et al. [66]

[a]Only main features listed; enstatites and forsterites securely identified.
[b]ISM - interstellar medium.
[c]CSE - circumstellar envelopes.
[c]HAEBE stars - Herbig Ae/Be stars.
[e]New laboratory data provided by Posch et al. [67].

lists. We should stress again that the identification based on a single band has to be taken with caution. In the case of the 21 μm feature, SiS_2 is probably not the carrier of the band because it shows a second feature which is not present in spectroscopic data from the *Infrared Space Observatory ISO*. In addition, the identification of FeO should be taken with some caution.

Apart from the components discussed in Table 2, silicates are a widespread component of cosmic dust [6, 34, 35]. Spectroscopic evidence for the presence of amorphous silicates comes from broad bands at 10 and 18 μm which are attributed to Si—O stretching and Si—O—Si bending modes. The depletion of oxygen and silicon is roughly in agreement with these atoms being bound in SiO_4 tetrahedra [36]. The *Infrared Space Observatory ISO* and the *Spitzer Space Telescope* found clear evidence for the presence of crystalline silicates in the disks around brown dwarfs, T Tauri stars, and Herbig Ae/Be stars and the envelopes and disks around evolved

stars. Sharp and distinct features typical of Fe-poor olivines (i.e. Mg_2SiO_4) and pyroxenes (i.e. $MgSiO_3$) could be observed in the 10 μm range and for wavelengths beyond 20 μm (cf. contribution by Molster et al., this volume).

Cosmic dust analogues investigated so far include a wide variety of carbonaceous grains, silicates, metal oxides, carbides, sulphides, and carbonates. We will discuss some of the relevant experimental investigations in the following sections, but will concentrate on infrared studies of carbon- and silicon-based materials. For more complete reviews and extensive compilations of references, the reader is referred to the papers by Colangeli et al. [6] and Henning [34, 35] for silicates, Henning and Mutschke [37] for carbides, and Henning and Schnaiter [12], Henning et al. [11], and Pendleton and Allamandola [40] for carbonaceous solids.

5.1 Carbon-Based Solids

The observation of an absorption band at 3.4 μm along different lines of sight through the galactic diffuse interstellar medium and in some other galaxies provides direct evidence for the presence of hydrogenated carbonaceous grains with aliphatic character. The profile of this band shows substructure at about 3.38, 3.42 and 3.48 μm produced by C—H stretching vibrations in the methyl ($–CH_3$) and methylene ($–CH_2–$) groups. The average $–CH_2–/–CH_3$ ratio is about 2.5. The corresponding C—H deformation modes at 6.85 μm and 7.25 μm could be detected by observations with the Kuiper Airborne Observatory (only at 6.85 μm [41]) and ISO [68]. The structure of the "interstellar" 3.4 μm band is quite similar to the band found in the C-rich protoplanetary nebula CRL 618 [69]. This type of band is completely absent in dense molecular clouds.

The identification of a specific material, producing the features, is not simple because the C—H modes only reflect the local bonding environment and are present in a wide variety of carbonceous materials. Schnaiter et al. [38] produced carbonaceous nanoparticles which reproduced both the 3.4 μm profile and the UV absorption band at 217 nm (see Fig. 6). It would be interesting to find out if these two astronomical features are indeed produced by the same material.

A very comprehensive comparison between astronomical spectra in the 2.5–10 μm range and various laboratory dust analogues has been performed by Pendleton and Allamandola [40]. Their general conclusion is that materials produced by plasma processes reproduce the astronomical data better than ices processed by the irradiation with energetic ions or UV light. The material is characterized by a hydrocarbon, with carbon distributed between aliphatic and aromatic structures and only minor contributions from oxygen and nitrogen. The investigation of UV irradiation of carbonaceous materials and the interaction with atomic hydrogen, expected to occur in the diffuse interstellar medium, led to the proposal that the material is formed in the diffuse medium with an equilibrium value for its degree of hydrogenation [39].

Apart from hydrocarbon particles, SiC (11.3 μm feature) and very tentatively TiC grains (20.1 μm feature) have been identified as a dust component of carbon-rich

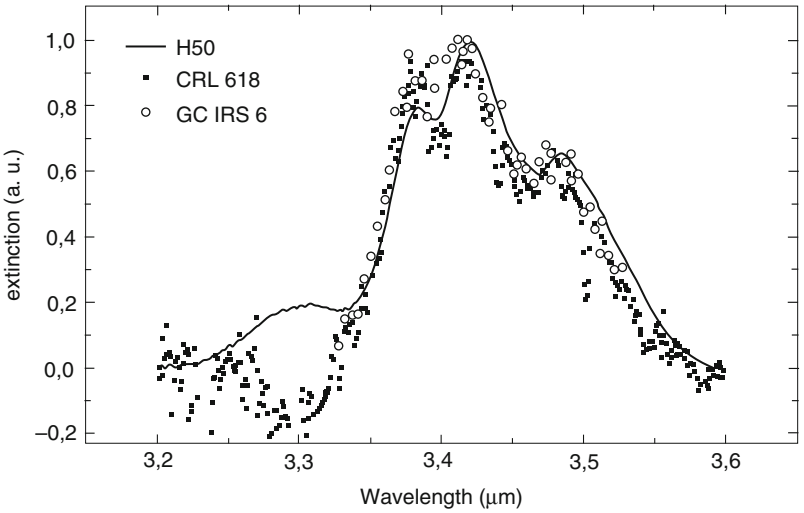

Fig. 6 Comparison of the 3.4 μm feature of the diffuse interstellar medium (*dots*) with measurements on hydrogenated carbon nanoparticles (*solid line*). After [38]

circumstellar envelopes. The identifcation of a specific SiC material as the carrier of the 11.3 μm feature is complicated by the lack of an intrinsic astronomical band shape. This is difficult to obtain because molecular bands and other carbonaceous grains contribute to the measured fluxes. Based on a comparison of ground-based spectra with some laboratory data, it has been concluded that the observed band can be fitted best by β-SiC. However, a detailed laboratory study [46], based on bulk and thin-film optical data, demonstrated that the dielectric functions of the various SiC polytypes should not cause observable differences in the phonon band profile. In addition, this study showed that effects of particle shape and agglomeration state, as well as conductivity introduced by dopants like nitrogen, produce the differences seen in laboratory spectra and are very probably influencing astronomical band profiles. Another feature at about 20.1 μm (21 μm band), observed in the spectra of post-AGB stars, has attracted new attention because high-quality ISO data became available and allowed the derivation of an intrinsic band profile [55]. This profile is very smooth and does not show any substructure due to molecular bands. Titanium carbide clusters or nanocrystals [58] have been proposed as a very good spectroscopic candidate for the explanation of the 20.1 μm feature, but may not be abundant enough to explain the strength of this band.

5.2 Silicates

Spectroscopic evidence for silicates has been found in such different environments as Seyfert galaxies, the galactic centre, disks and envelopes around young stellar objects, circumstellar regions around evolved stars, and also in comets and interplan-

etary dust grains [35, 74]. The broad features, usually observed at 10 and 18 μm, are carried by amorphous silicates, corresponding to Si—O stretching and O—Si—O bending vibrations, respectively. The large width of the bands results from a distribution of bond lengths and angles, typical of the amorphous structure of these solids. The 18 μm band is additionally broadened and generally weaker due to the coupling of the bending mode to the metal-stretching vibrations occurring in this spectral region. The exact position of the Si—O stretching vibration depends on the level of SiO_4 polymerization. As an example, the band is shifted from 9 μm for pure (sub)micron-sized SiO_2 grains to about 10.5 μm for $Mg_{2.2}SiO_{4.4}$ [70]. The 10 and 18 μm features are observed in absorption, self-absorption, and emission depending on the optical depth of the astronomical object.

First evidence for the presence of crystalline silicates in the envelopes of very young massive stars, comets, and β Pictoris-type objects came from the observations of a feature at 11.2 μm (see [13] for references). This feature is typical of crystalline olivine. ISO and Spitzer observations revealed the presence of a wealth of "crystalline" silicate features in the wavelength range between 10 and 70 μm due to metal-oxyen vibrations (cf. chapter by Molster et al., this volume [71–73]). These features are of great diagnostic value and allow a detailed characterization of the mineralogy of crystalline silicates. From the positions of the features, we have strong evidence that Mg-rich olivines and pyroxenes are the major crystalline silicates in space.

Based on laboratory data, forsterite grains have strong bands at 10.0, 11.3, 16.3, 19.8, 23.5, 27.5, 33.5 and 69.7 μm, while enstatite grains have bands at 9.4, 9.9, 10.6, 11.1, 11.6, 18.2, 19.3 and 21.5 μm. Variations in band position and bandwidth are probably related to different dust temperatures and Mg/Fe ratios, the degree of crystallization, and size/shape effects among the particles [34, 35]. All peaks of the olivine series (different Mg/Fe ratios) shift to longer wavlengths with growing iron content [13]. The same trend is visible in the great majority of the bands of the pyroxene series. The mass percentage of FeO is closely related to the wavenumber shift. A fraction of the weaker features observed in the ISO and Spitzer spectra could not yet be identified, which shows the importance of additional investigations of relevant minerals.

6 Conclusions

Laboratory astrophysics, especially the investigation of cosmic dust analogues, has developed from a small field to an integral part of modern astrophysics. The high-quality spectra obtained with the *Infrared Space Observatory* and the *Spitzer Space Telescope* could not have been analyzed without measured optical data of astronomically important materials. Combining detailed analytical characterization with spectroscopic measurements led to a much more comprehensive understanding of the properties of solids in space. New missions such as *Herschel* and the airborne observatory *SOFIA* will extend dust studies to far-infrared wavelengths. The *James Webb Space Telescope* will provide higher sensitivity, allowing to extend dust

spectroscopy to even fainter objects such as disks around low-mass brown dwarfs, exoplanet and brown dwarf atmospheres, and external galaxies.

Acknowledgments I thank my collaborators from the Jena Laboratory Astrophysics Group for many discussions about cosmic dust analogues and Drs. J. Dorschner, J. Gürtler, and H. Mutschke for critically reading of the paper.

References

1. Bohren, C.G., Huffman, D.R.: Absorption and Scattering of Light by Small Particles. Wiley, New York, NY (1983) 313
2. Henning, Th.: Frontiers of radiative transfer. In: Zinnecker, H., Mathieu, R.D. (eds.) The Formation of Binary Stars, IAU Symposium 200, Potsdam, April 10–15, 2000, pp. 567–572. ASP, San Francisco, CA (2001) 314
3. Snow, T.P., Witt, A.N.: Science **270**, 1455 (1995) 314
4. Jones, A.P.: J. Geophys. Res. **105**, 10257 (2000) 314
5. Przybilla, N., Nieva, M.-F., Butler, K.: Astrophys. J. **688**, L103 (2008) 314
6. Colangeli, L., Henning, Th., Brucato, J.R., et al.: Astron. Astrophys. Rev. **11**, 97 (2003) 314, 316, 323, 324
7. Savage, B.D., Sembach, K.R.: Annu. Rev. Astron. Astrophys. **34**, 279 (1996) 314
8. Dorschner, J., Henning, Th.: Astron. Astrophys. Rev. **6**, 271 (1995) 314
9. Kemper, F., Vriend, W.J., Tielens, A.G.G.M.: Astrophys. J. **609**, 826 (2004) 315
10. Henning, Th., Mutschke, H.: Optical properties of cosmic dust analogs. In: Sitko, M.L., Sprague, A.L., Lynch, D.K. (eds.) Thermal Emission Spectroscopy and Analysis of Dust, Disks, and Regoliths, Houston, April 28–30, 1999. ASP Conf. Ser., vol. 196, pp. 253–271. ASP, San Francisco, CA (2000) 316, 318, 319
11. Henning, Th., Jäger, C., Mutschke, H.: Laboratory studies of carbonaceous dust analogs. In: Witt, A.N., Clayton, G.C., Draine, B.T. (eds.) Astrophysics of Dust. ASP Conf. Ser., vol. 309, pp. 603–628. ASP, San Francisco, CA (2004)) 316, 321, 324
12. Henning, Th., Schnaiter, M.: Carbon - From space to the laboratory. In: Ehrenfreund, P., Kochan, H., Krafft, C., Pirronello, V. (eds.) Laboratory Astrophysics and Space Research, pp. 249–278. Kluwer, Dordrecht (1998) 316, 321, 324
13. Jäger, C., Molster, F.J., Dorschner, J., et al.: Astron. Astrophys. **339**, 904 (1998) 316, 326
14. Gustafson, B.A.S., Greenberg, J.M., Kolokolova, L., Yun-lin Xu, Stognienko, R.: Interactions with electromagnetic radiation. In: Grün, E., Gustafson, B.A.S., Dermott, S.F., Fechtig, H. (eds.) Interplanetary Dust, pp. 509–567. Springer, Berlin (2001) 319
15. Tamanai, A., Mutschke, H., Blum, J., Meeus, G.: Astrophys. J. **648**, L147 (2006) 319
16. Agladze, N.I., Sievers, A.J., Jones, S.A., Burlitch, J.M., Beckwith, S.V.W., Astrophys. J. **462**, 1026 (1996) 320
17. Henning, Th., Mutschke, H.: Astron. Astrophys. **327**, 743 (1997) 320
18. Mennella, V., Brucato, J.R., Colangeli, L., Palumbo, P., Rotundi, A., Bussoletti, E.: Astrophys. J. **496**, 1058 (1998) 320
19. Bowey, J.E., Lee, C., Tucker, C., et al.: Mon. Not. R. Astron. Soc. **325**, 886 (2001) 320
20. Chihara, H., Koike, C., Tsuchiyama, A., Publ. Astron. Soc. Jpn. **53**, 243 (2001) 320
21. Mutschke, H., Zeidler, S., Posch, Th., Kerschbaum, F., Baier, A., Henning, Th.: Astron. Astrophys. **492**, 117 (2008) 321
22. Kreibig, U., Vollmer, M.: Optical Properties of Metal Clusters. Springer, Berlin (1995) 321
23. Palik, E.D. (ed.): Handbook of Optical Constants. Academic Press, Orlando, FL (1985) 321
24. Palik, E.D. (ed.): Handbook of Optical Constants II. Academic Press, San Diego, CA (1991) 321
25. Palik, E.D. (ed.): Handbook of Optical Constants III. Academic Press, San Diego, CA (1998) 321
26. Henning, Th., Ilin, V.B., Krivova, N.A., Michel, B., Voshchinnikov, N.V.: Astron. Astrophys. Suppl. **136**, 405 (1999) 321

27. Fabian, D., Henning, Th., Jäger, C., Mutschke, H., Dorschner, J., Wehrhan, O.: Astron. Astrophys. **378**, 228 (2001) 320, 321, 322
28. Molster, F.J., Ph.D. Thesis, University of Amsterdam (2000) 322
29. Herbig, G.H.: Annu. Rev. Astron. Astrophys. **33**, 19 (1995) 321
30. Witt, A.N., Gordon, K.D., Furton, D.: Astrophys. J. **501**, L111 (1998) 321
31. Ledoux, G., Guillois, O., Huisken, F., Kohn, B., Porterat, D., Reynaud, C.: Astron. Astrophys **377**, 707 (2001) 321
32. Drilling, J.S., Hecht, J.H., Clayton, G.C., Mattei, J.A., Landolt, A.U., Whitney, B.A.: Astrophys. J. **476**, 865 (1997) 321
33. Hecht, J.H., Holm, A.V., Donn, B., Wu, C.-C.: Astrophys. J. **280**, 228 (1984) 321
34. Henning, Th.: Cosmic silicates - A review. In: Pirronello, V., Krelowski, J. (eds.) Solid State Astrochemistry, pp. 85–103. Kluwer, Dordrecht (2003) 323, 324, 326
35. Henning, Th.: Cosmic silicate dust. In: Boulanger, F., Joblin, C., Jones, A., Madden, S. (eds.) Interstellar Dust. From Astronomical Observations to Fundamental Studies. EAS. Publ. Ser., pp. 103–114. EDP Sciences, Les Ulis (2009) 323, 324, 326
36. Snow, T.P., Witt, A.N.: Astrophys. J. **468**, L65 (1996) 323
37. Henning, Th., Mutschke, H.: Spectrochim. Acta A **57**, 815 (2001) 324
38. Schnaiter, M., Henning, Th., Mutschke, H., Kohn, B., Ehbrecht, M., Huisken, F.: Astrophys. J. **519**, 687 (1999) 323, 324, 325
39. Mennella, V., Brucato, J.R., Colangeli, L., Palumbo, P.: Astrophys. J. **569**, 531 (2002) 323, 324
40. Pendleton, Y.J., Allamandola, L.J.: Astrophys. J. Suppl. **138**, 75 (2002) 323, 324
41. Tielens, A.G.G.M., Wooden, D.H., Allamandola, L.J., Bregman, J., Witteborn, F.C.: Astrophys. J. **461**, 210 (1996) 323, 324
42. Draine, B.T., Lee, H.M.: Astrophys. J. **285**, 89 (1984) 323
43. Ossenkopf, V., Henning, Th., Mathis, J.S.: Astron. Astrophys. **261**, 567 (1992) 323
44. Speck, A.K., Barlow, M.J., Skinner, C.J.: Mon. Not. R. Astron. Soc. **288**, 431 (1997) 323
45. Speck, A.K., Hofmeister, A.M., Barlow, M.J.: Astrophys. J. **513**, L87 (1999) 323
46. Mutschke, H., Andersen, A.C., Clément, D., Henning, Th., Peiter, G.: Astron. Astrophys. **345**, 187 (1999) 323, 325
47. Pitman, K.M., Hofmeister, A.M., Corman, A.B., Speck, A.K.: Astron. Astrophys. **483**, 661 (2008) 323
48. Sloan, G.C., Levan, P.D., Little-Marenin, I.R.: Astrophys. J. **463**, 310 (1996) 323
49. Koike, C., Kaito, C., Yamamoto, T., Shibai, H., Kimura, S., Suto, H.: Icarus **114**, 203 (1995) 323
50. Begemann, B., Dorschner, J., Henning, Th., et al.: Astrophys. J. **476**, 199 (1997) 323
51. de Pew, K., Speck, A., Dijkstra, C.: Astrophys. J. **640**, 971 (2006) 323
52. Posch, Th., Kerschbaum, F., Mutschke, H., Fabian, D., Dorschner, J., Hron, J.: Astron. Astrophys. **352**, 609 (1999) 323
53. Fabian, D., Posch, Th., Mutschke, H., Kerschbaum, F., Dorschner, J.: Astron. Astrophys. **373**, 1125 (2001) 323
54. Kwok, S., Hrivnak, B.J., Geballe, T.R.: Astrophys. J. **454**, 394 (1995) 323
55. Volk, K., Kwok, S., Hrivnak, B.J.: Astrophys. J. **516**, 99 (1999) 323, 325
56. Henning, Th., Chan, S.J., Assendorp, R.: Astron. Astrophys. **312**, 511 (1996) 323
57. Begemann, B., Dorschner, J., Henning, Th., Mutschke, H., Astrophys. J. **464**, L195 (1996) 323
58. von Helden, G., Tielens, A.G.G.M., van Heijnsbergen, D., et al.: Science **288**, 313 (2000) 323, 325
59. Posch, Th., Mutschke, H., Andersen, A.: Astrophys. J. **616**, 1167 (2004) 323
60. van den Ancker, M.E., Bouwman, J., Wesselius, P.R., Waters, L.B.F.M., Dougherty, S.M., van Dishoeck, E.F.: Astron. Astrophys. **358**, 1035 (2000) 323
61. Keller, L.P., Bradley, J.P., Bouwman, J., et al.: LPI **31**, 1860 (2000) 323
62. Omont, A., Moseley, S.H., Cox, P., et al.: Astrophys. J. **454**, 819 (1995) 323
63. Begemann, B., Dorschner, J., Henning, Th., Mutschke, H., Thamm, E., Astrophys. J. **423**, L71 (1994) 323
64. Szczerba, R., Henning, Th., Volk, K., Cox, P.: Astron. Astrophys. **345**, L39 (1999) 323
65. Kemper, F., Jäger, C., Waters, L.B.F.M., et al.: Nature **415**, 295 (2002) 323

66. Ceccarelli, C., Caux, E., Tielens, A.G.G.M., Kemper, F., Waters, L.B.F.M.: Astron. Astrophys. **395**, L29 (2002) 323
67. Posch, Th., Baier, A., Mutschke, H., Henning, Th.: Astrophys. J. **668**, 993 (2007) 323
68. Chiar, J.E., Tielens, A.G.G.M., Whittet, D.C.B., et al.: Astrophys. J. **537**, 749 (2000) 324
69. Chiar, J.E., Pendleton, Y.J., Geballe, T.G., Tielens, A.G.G.M.: Astrophys. J. **507**, 281 (1998) 324
70. Jäger, C., Dorschner, J., Mutschke, H., Posch, Th., Henning, Th.: Astron. Astrophys. **408**, 193 (2003) 326
71. Bouwman, J., Meeus, G., de Koter, A., et al.: Astron. Astrophys. **375**, 950 (2001) 326
72. Bouwman, J., Henning, Th., Hillenbrand, L.A., et al.: Astrophys. J. **683**, 479 (2008) 326
73. Kessler-Silacci, J., Augereau, J.-C., Dullemond, C.P.: Astrophys. J. **639**, 275 (2006) 326
74. Henning, Th.: Annu. Rev. Astron. Astrophys. **48** (2010) 326
75. Keller, L.P. et al.: Nature **417**, 148 (2002) 323